Conception, synthèse et caractérisations de MOFs à base de porphyrines

Brian Abeykoon

▶ **To cite this version:**

Brian Abeykoon. Conception, synthèse et caractérisations de MOFs à base de porphyrines. Autre. Université de Lyon, 2017. Français. NNT : 2017LYSE1259 . tel-01729322

HAL Id: tel-01729322
https://theses.hal.science/tel-01729322

Submitted on 12 Mar 2018

HAL is a multi-disciplinary open access archive for the deposit and dissemination of scientific research documents, whether they are published or not. The documents may come from teaching and research institutions in France or abroad, or from public or private research centers.

L'archive ouverte pluridisciplinaire **HAL**, est destinée au dépôt et à la diffusion de documents scientifiques de niveau recherche, publiés ou non, émanant des établissements d'enseignement et de recherche français ou étrangers, des laboratoires publics ou privés.

N°d'ordre NNT : 2017LYSE1259

THESE de DOCTORAT
DE L'UNIVERSITE DE LYON
opérée au sein de
l'Université Claude Bernard Lyon 1

Ecole Doctorale N° 206
Chimie de Lyon

Discipline : Chimie

Soutenue publiquement le 30/11/2017, par :
Brian ABEYKOON

Conception, synthèse et caractérisations de MOFs à base de porphyrines

Design, synthesis and characterisation of porphyrin-based Metal Organic Frameworks

Devant le jury composé de :

DOLBECQ Anne	Dir. Recherche CNRS	Univ Versaille St Quentin	Rapporteure
LEMEUNE Alla	Chargée Recherche CNRS	Univ Bourgogne	Rapporteure
DEVIC Thomas	Chargé Recherche CNRS	Univ Nantes	Examinateur
SOROKIN Alexander	Dir. Recherche CNRS	Univ Lyon 1	Président
GOUTAUDIER Christelle	Professeure	Univ Lyon 1	Directrice de thèse
FATEEVA Alexandra	Maître de Conférences	Univ Lyon 1	Co-encadrante

UNIVERSITE CLAUDE BERNARD - LYON 1

Président de l'Université	**M. le Professeur Frédéric FLEURY**
Président du Conseil Académique	M. le Professeur Hamda BEN HADID
Vice-président du Conseil d'Administration	M. le Professeur Didier REVEL
Vice-président du Conseil Formation et Vie Universitaire	M. le Professeur Philippe CHEVALIER
Vice-président de la Commission Recherche	M. Fabrice VALLÉE
Directrice Générale des Services	Mme Dominique MARCHAND

COMPOSANTES SANTE

Faculté de Médecine Lyon Est – Claude Bernard	Directeur : M. le Professeur G.RODE
Faculté de Médecine et de Maïeutique Lyon Sud – Charles Mérieux	Directeur : Mme la Professeure C. BURILLON
Faculté d'Odontologie	Directeur : M. le Professeur D. BOURGEOIS
Institut des Sciences Pharmaceutiques et Biologiques	Directeur : Mme la Professeure C. VINCIGUERRA
Institut des Sciences et Techniques de la Réadaptation	Directeur : M. X. PERROT
Département de formation et Centre de Recherche en Biologie Humaine	Directeur : Mme la Professeure A-M. SCHOTT

COMPOSANTES ET DEPARTEMENTS DE SCIENCES ET TECHNOLOGIES

Faculté des Sciences et Technologies	Directeur : M. F. DE MARCHI
Département Biologie	Directeur : M. le Professeur F. THEVENARD
Département Chimie Biochimie	Directeur : Mme C. FELIX
Département GEP	Directeur : M. H. HAMMOURI
Département Informatique	Directeur : M. le Professeur S. AKKOUCHE
Département Mathématiques	Directeur : M. le Professeur G. TOMANOV
Département Mécanique	Directeur : M. le Professeur H. BEN HADID
Département Physique	Directeur : M. le Professeur J-C PLENET
UFR Sciences et Techniques des Activités Physiques et Sportives	Directeur : M. Y.VANPOULLE
Observatoire des Sciences de l'Univers de Lyon	Directeur : M. B. GUIDERDONI
Polytech Lyon	Directeur : M. le Professeur E.PERRIN
Ecole Supérieure de Chimie Physique Electronique	Directeur : M. G. PIGNAULT
Institut Universitaire de Technologie de Lyon 1	Directeur : M. le Professeur C. VITON
Ecole Supérieure du Professorat et de l'Education	Directeur : M. le Professeur A. MOUGNIOTTE
Institut de Science Financière et d'Assurances	Directeur : M. N. LEBOISNE

Abstract

Porphyrins are important macrocyclic compounds which are prevalent in nature and have been extensively studied by chemists in homogeneous catalysis as enzyme mimics. Incorporating porphyrins in metal-organic frameworks (MOFs) offer an ideal opportunity to obtain material with extended frameworks possessing the same properties as the homogeneous systems. Much work has been done on porphyrinic MOFs but their stability remains a problem and a major limitation for possible wide scale applications. In literature, more stable MOFs have been realised using high valent metal ions in the inorganic building unit (such as Fe^{3+}, Al^{3+}, Zr^{4+}) and/or by using more basic functionalities in the organic linker. However, regarding porphyrinic MOFs, little work is reported with ligands based on functionalities other than carboxylic acid groups. Therefore, our work focused on investigating the reactivity of porphyrinic ligands carrying various functionalities with high valent metal ions. More precisely, we focused on the design, synthesis optimisation and characterisation of such materials. This included studying existing stable carboxylate porphyrinic frameworks with a goal of incorporating new functionalities, which led to new variations of these materials. Our work also demonstrated that the framework topologies observed with carboxylate based porphyrinic ligand can be expanded to other functionalities with the synthesis of a new tetrazolate based porphyrinic MOF. MOF synthesis was also investigated with phenolate functionalised ligands and resulted in the first gallate based porphyrinic MOF reported. The stability of this new material was assessed. This manuscript discusses the synthesis and the characterisation of these MOFs via a combination of experimental techniques (X-ray diffraction, TGA analysis, UV-vis spectroscopy, IR-spectroscopy, sorption studies etc.). The preliminary evaluation of the catalytic activity of some of the MOFs is also described.

Key words:

Metal-organic frameworks, Porphyrin, Gallate porphyrinic ligands, Tetrazolate porphyrinic ligands, Water stability

Résumé

Les porphyrines sont des composés macrocycliques naturels étudiés de manière approfondie en tant que mimétiques enzymatiques ou catalyseurs d'oxydation en milieu homogène. L'incorporation de porphyrines dans des réseaux de polymères de coordination métal-organique (MOFs), qui constituent une famille de composés cristallins poreux connus pour leur diversité structurelle, pourrait conduire à des matériaux constitués de réseaux étendus présentant les mêmes propriétés que les systèmes homogènes. Toutefois de nombreux travaux ont montré que la limitation majeure pour des applications à grande échelle des MOFs est leur stabilité.

La stabilité de ces matériaux peut être accrue en employant des cations métalliques de valence élevée dans l'unité de construction inorganique (tels que Fe^{3+}, Al^{3+}, Zr^{4+}) et / ou en modifiant la fonction coordinante du ligand organique.

Ce travail est relatif à l'étude de la réactivité de ligands porphyriniques portant diverses fonctions coordinantes, avec des ions métalliques de valence élevée. L'influence des paramètres de synthèse et la caractérisation approfondie de ces MOFs ont été réalisées par une combinaison de techniques expérimentales (diffraction des rayons X, analyse thermogravimétrique, spectroscopie UV-vis, spectroscopie infrarouge, études de sorption, etc.). Dans un premier temps, l'étude s'est focalisée sur des MOFs porphyriniques à base de groupements carboxylates stables connus, ce qui a conduit à de nouvelles variantes de ces matériaux. Dans un second temps il est démontré que les topologies des réseaux observées sur un ligand porphyrinique à base carboxylate peuvent être étendues à d'autres fonctionnalités avec la synthèse d'un nouveau MOF à base de tétrazolate. L'amélioration de la stabilité a également été explorée avec des ligands portant des fonctions phénol qui ont abouti à l'élaboration de nouveaux réseaux de coordination. La synthèse et l'étude de stabilité d'un MOF porphyrinique à base de gallate est rapportée. L'évaluation préliminaire de l'activité catalytique de certains des MOFs élaborés est également décrite.

Mots-clés :

MOF, Porphyrine, Gallate, Tetrazolate, Stabilité dans l'eau

Liste des travaux de Brian ABEYKOON

Publications:

1 - *Iron and porphyrin metal-organic framework: Insight into structural diversity, stability and porosity*
A. Fateeva, J. Clarisse, G. Pilet, JM Grenèche, F. Nouard, B. Abeykoon, F. Guegan, C. Goutaudier, D. Luneau, JE. Warren, M. Rosseinsky, T. Devic
Cryst. Growth Des., **2015**, 15, pp. 1819-1826

2 - *Tuning the iron redox state inside a microporous porphyrinic metal-organic framework*
B. Abeykoon, JM Grenèche, E. Jeanneau, D. Chernyshov, C. Goutaudier, A. Demessence, T. Devic, A. Fateeva
Dalton Trans., **2017**, 46, pp. 517-523

3 - *Adaptability of the metal(iii,iv) 1,2,3-trioxobenzene rod secondary building unit for the production of chemically stable and catalytically active MOFs*
G. Mouchaham, B. Abeykoon, M. Gimenez-Marques, S. Navalon, A. Santiago-Portillo, M, Affram, N. Guillou, C. Martineau, H. Garcia, A. Fateeva, T. Devic
Chemical communications, **2017,** 53, 7661-7664.

4 - *Insights into the mechanism of electrocatalysis of the oxygen reduction reaction by a porphyrinic metal organic framework*
M. Lions, J.B. Tommasino, R. Chattot, B. Abeykoon, N. Guillou, T. Devic, A. Demessence, L. Cardenas, F. Maillard, A. Fateeva
Chemical communications, **2017,** 53, 6496-6499.

Colloques:

1 - *Porous MOFs based on metalloporphyrin ligands: rational synthesis and optimization-communication orale*
B. Abeykoon, E. Jeanneau, C. Goutaudier, A. Fateeva
32ème réunion annuelle Groupe Français des Zéolithes, Montagnac (France), 29 mars-01 avril **2016**

2 - *Porous MOFs based on metalloporphyrin ligands: rational synthesis and optimization-poster*
B. Abeykoon, E. Jeanneau, C. Goutaudier, A. Fateeva
The Annual Meeting of the Chemistry Graduate School, Université Claude Bernard Lyon 1, 12 avril **2016**

Acknowledgements

The work presented in the manuscript is not possible without the help of many people and I would like to sincerely thank everybody for their kind assistance and support.

I would like to first thank everyone in the thesis committee, the referees: Dr. Anne Dolbecq and Dr. Alla Lemeune and the guest members: Dr. Alexander Sorokin and Dr. Thomas Devic, for taking time out of their busy schedules and accepting to be part of the jury.

My sincere gratitude goes to my supervisors Dr. Alexandra Fateeva and Professor Christelle Goutaudier, who gave me the opportunity to work on this subject.

This work is not possible at all without the help, supervision and support Alex provided over the years with every aspect of the project. I cannot thank you enough for always being available and assisting me with every difficulty I had. I have learnt a lot from you over these three years and it is not limited to just chemistry. I offer you my most sincere gratitude for providing guidance and being patient during my work and giving me invaluable advice.

I would like to thank Prof. Christelle Goutaudier who helped me immensely during the inevitable tough times and made me successfully navigate through them. Without your kind support and motivation, I would not have been able to finish the project with success and I cannot thank you enough for all your help.

I would like to mention again, Dr. Alexander Sorokin at IRCELYON, who helped me with all the catalytic studies in addition to being part of the jury. Without him, this part of the work is not possible. Thank you for your patience and perseverance with the work. I will not forget the time I spent under your supervision.

My sincere gratitude goes out to Dr. Thomas Devic who supervised my stay at the Institut Lavoisier de Versailles (ILV) where I did all the high throughput synthesis work. Thank you for all the help you gave me and all the effort you put in to the publication and also agreeing to be part of the jury. I also want to mention everyone at ILV, including Dr. Farid Nouar who helped me with my studies during my stay.

I would like to especially thank everyone at LMI for all the support they gave me throughout my thesis. I have to mention Dr. Guillaume Pilet, Dr. Jean-Bernard Tommasino, Prof. Dominique Luneau, Prof. Jacques Jose, Dr. Vincent Salles, Dr. Laurence Bois, Dr. Mathieu Maillard, Prof. Arnaud Brioude, Dr. Bérangère Toury, Dr. Bruno Gardiola and everyone else who helped me during these three

years. I have to especially mention Patricia Combier, Irina Boussin, Elodie Ravis and Corrine Menant for helping me with all the administrative details which were numerous.

I am very grateful to all my colleagues, Djamila, Fred, Angélique, Cécile, Federico, Constance, both the Lauras, Nelly, Victor and everyone else. Thank you very much guys for making the last three years truly enjoyable. Without you this work is not possible. And Djamila, thank you so much for helping me with everything. You were like a sister to me.

I would like to thank Dr. Rodica Chiriac and François Toche who took time out of their busy schedule to help with BET and TGA measurements.

I extend my sincere gratitude to Dr. Erwann Jeanneau and Dr. Ruben Vera for the help they gave me with PXRD and X-ray diffraction studies.

My sincere gratitude goes to Didier Fournier for all the assistance he provided with solid UV-vis analysis and TGA analysis.

I would like to mention Lucie and Oleksandra at IRCELYON. Thank you for helping with all the measurements and analysis work I had to do.

I would sincerely like to thank, Prof. Lyall Hanton, who was my honours supervisor at the University of Otago during my undergraduate studies and Dr. Laurance Beauvais who was my masters supervisor at the San Diego State University for helping me with my chemistry journey. Without your help and support over the years, I would not have reached where I am now.

It is impossible to mention everyone by name, so I would like to thank again everyone else who helped me with my work here. Without their help, how small or big, this work would not have come to fruition.

I would also like to thank all my close friends in Lyon and at La Casa Nostra. I have met many great people over my time here and it is not possible to name each and everyone but you know who you are. Thank you so much for supporting me and being there for me during the last three years. Without your help and support I would not have been able to complete my studies. I will never forget you and the moments we had together.

I have to especially mention, Nanami. Thank you for always being there for me. Without your kind support and ever present positive attitude, I would not have achieved what I did.

Finally, I have to mention my wonderful parents and my sister and my brother. Even though they were miles away they were always there for me and supported me. You guys are the best family anyone could ask for.

Table of Contents

Résumé en Français

1. Introduction

Les 25 dernières années ont vu l'émergence d'une nouvelle classe de solides poreux, les Metal Organic Frameworks (MOFs). Ce sont des matériaux hybrides contenant à la fois des parties organiques et inorganiques, par opposition aux zéolites qui ne contiennent que des composants inorganiques. En choisissant soigneusement ces constituants inorganiques et organiques, il est possible d'élaborer un matériau avec une porosité élevée et des propriétés dédiées.

L'un des plus grands avantages des MOFs est l'infinité de combinaisons possibles de métaux et de ligands organiques ainsi que l'accordabilité et la flexibilité que cela procure. Ainsi, en choisissant des ligands organiques et des nœuds métalliques appropriés, il est possible de concevoir rationnellement les cadres poreux et de contrôler les tailles de pores et les environnements chimiques.[1]

Les porphyrines sont un type de molécules organiques qui peuvent être utilisées comme ligands pour la synthèse de MOFs. Les molécules de porphyrine ont fait l'objet de recherches approfondies dans des domaines tels que la catalyse d'oxydation et les mimétiques enzymatiques dans des systèmes homogènes.[2] Ceci est dû à la prévalence de ces molécules dans la nature. Les MOFs offrent une plate-forme idéale où les propriétés des porphyrines dans des systèmes homogènes peuvent être transférées à des systèmes hétérogènes avec des surfaces et une porosité élevée. De plus, l'incorporation de molécules de porphyrines dans les MOFs permet de séparer les espèces de métalloporphyrines réactives en empêchant leur auto-désactivation.[3]

Structurellement, les porphyrines offrent un ligand idéal pour les MOFs qui est robuste, avec une géométrie plane carrée rigide et des dimensions géométriques relativement grandes qui peuvent conduire à des solides poreux. En tant que ligand, les porphyrines offrent deux sites de liaison potentiels : un site de liaison métallique fonctionnelle à l'intérieur du noyau porphyrine et un site de liaison métallique structurelle à la périphérie avec un groupe fonctionnel de coordination. En outre, ce groupe de coordination peut être modifié en permettant différents environnements de coordination dans les briques inorganiques du MOF résultant.

Robson et al ont été les premiers à rapporter un polymère de coordination à base de porphyrine en 1991[4] et depuis le domaine des solides à base de porphyrines a reçu beaucoup d'attention.[5-6] La plupart des MOFs à base de porphyrines rapportés sont basés sur le groupement de coordination carboxylate avec un métal divalent tels que Zn^{2+}, Ni^{2+}, Co^{2+}, Cu^{2+}.[7-9] Il y a eu très peu de

travaux avec d'autres fonctionnalités de coordination comme par exemple les phénolates et tetrazolates.

- *Les limitations actuelles des MOFs à base de porphyrines*

Le plus grand obstacle avec les MOFs en général est une faible stabilité chimique. La plupart des MOFs basés sur la fonctionnalité coordinante de carboxylate et les ions métalliques divalents tels que Zn^{2+}, Cu^{2+}. Ces MOFs se sont avérés avoir une stabilité chimique limitée, particulièrement en ce qui concerne l'exposition à l'eau.[10] Ceci est dû à l'hydrolyse ou au déplacement du ligand qui se produit en présence d'eau.[11] Comme mentionné précédemment, la plupart des MOFs à base de porphyrines sont construits en utilisant la fonctionnalité coordinante de carboxylate et les ions métalliques divalents. Ainsi, ils partagent les mêmes limitations concernant la stabilité chimique que les MOFs carboxylates généraux. Ceci est un problème majeur car la stabilité dans l'eau est essentielle pour toute utilisation à grande échelle des MOFs car la plupart des applications telles que les procédés de séparation ou la catalyse impliquent une exposition à l'humidité à un certain niveau.

L'importance de la force de liaison métal-ligand sur la stabilité hydrothermique des MOFs a été démontrée dans une étude menée par Low et al.[11] Les auteurs ont étudié la stabilité à la vapeur de divers MOFs en fonction de la température et ont indiqué que des liaisons métal-ligand plus fortes étaient corrélées à une stabilité hydrothermique plus élevée. Une façon d'augmenter la force de la liaison métal-ligand est d'augmenter la charge du métal.[12] L'anion carboxylate peut être considéré comme une base dure; ainsi, la densité de charge accrue d'ions métalliques de valence plus élevée peut conduire à des liaisons M-O plus fortes. L'émergence de MOFs stables à l'eau à base de porphyrines construits avec la fonctionnalité coordinante de carboxylate et des ions métalliques tels que Zr^{4+}, Al^{3+} et Fe^{3+} a démontré cette stabilité chimique élevé.[13-16]

Une autre voie pour augmenter la force de liaison du ligand métallique dans les MOFs est l'utilisation des ligands avec les fonctionnalités coordinantes qui sont plus basiques. Long et al ont suggéré ceci avec leur travail concernant les MOFs qui contenaient des ligands à base d'azolate et la force de la liaison M-L, d'où la stabilité chimique corrélée avec le pKa du ligand utilisé.[17] Ainsi, l'utilisation de fonctionnalités présentant des valeurs de pKa plus élevées que pour le groupe carboxylate (pKa~ 4,76) est une stratégie viable afin d'obtenir des structures stables. Les fonctionnalités coordinantes telles que les catécholates (pK_{a1} ~ 9,5, pK_{a2} ~ 14) et les gallates (pK_{a1} ~ 9,3; pK_{a2} ~ 11; pK_{a3} ~ 14) ont également des valeurs de pKa plus élevées que les groupes carboxylates et peuvent conduire à des MOFs plus stables.[18-19] Cependant, il n'y a eu aucun MOF à base de porphyrines rapporté utilisant la fonctionnalité de gallate et il existe un seul article sur un polymère de coordination construit à partir d'un ligand à base de porphyrine avec la fonctionnalité coordinante

de catécholate. Par conséquent, l'utilisation de fonctionnalités de gallate et de catécholate pour élaborer des MOFs avec une stabilité chimique accrue dans l'eau reste une voie peu explorée.

Plus de 300 structures de MOFs à base de porphyrines sont mentionnées dans la base de données structurelle de Cambridge (estimation à partir du sous-ensemble MOF dans la base de données CSD). Cependant, le nombre de MOFs à base de porphyrines qui ont été rapportés comme étant stables dans l'eau (immergés dans l'eau pendant au moins 24 heures) est limité. Cela met en évidence la difficulté de stabilisation de ces matériaux.

Le but principal de ce travail était en conséquence de concevoir des matériaux poreux fonctionnels stables à base de ligands porphyriniques et d'étudier leurs applications potentielles en catalyse. L'utilisation de matériaux cristallins est indispensable pour mieux appréhender la relation structure-propriété.

Deux stratégies différentes ont été utilisées pour élaborer ces matériaux :

- Étudier les plateformes stables existantes de MOFs à base de porphyrines construites avec le groupement carboxylate (à base de Fe^{3+} et Al^{3+}) et les modifier pour leur conférer de nouvelles fonctionnalités ;
- Explorer la synthèse de nouveaux MOFs en utilisant des ligands à base de porphyrine avec des groupements coordinants moins courants dans la littérature tels que le tétrazolate, le catécholate et le gallate afin d'obtenir des structures plus stables.

Quatre types différents de ligands porphyrines ont été employés lors dans cette thèse (Figure 1). Le chapitre 2 discutera brièvement des propriétés des porphyrines en général et détaillera la synthèse et la caractérisation de ces ligands.

Le chapitre 3 détaille l'étude de deux systèmes de MOFs différents avec des ligands à base de tetra-carboxyphenyl porphyrine (TCPP) et des ions métalliques Fe^{3+} et Al^{3+}. L'objectif était de modifier ces systèmes pour obtenir de nouveaux matériaux avec de nouvelles fonctionnalités potentielles. Le premier système, basé sur Fe^{3+}, a été publié par notre laboratoire et les tentatives faites pour modifier le cadre de ce MOF sont présentées dans la première partie du chapitre. Suite à cela, l'étude de la réactivité de Fe^{3+} avec un ligand TCPP métallé avec le cobalt est présentée. La partie suivante du chapitre détaille les efforts faits pour synthétiser les nouvelles variations d'un MOF basé sur Al^{3+} et présenter les résultats préliminaires de catalyse.

Le chapitre 4 discute de l'article publié par notre groupe sur un nouveau MOF basé sur le ligand porphyrine avec un groupement de coordination tetrazole, H_2TTPP, et Fe^{3+}. Le chapitre

présentera brièvement les MOFs à base de tetrazolate et le potentiel d'obtention de structures étendues avec des propriétés de croisement de spin avec ce ligand.

Le chapitre 5 se concentre sur les systèmes MOFs construits avec deux ligands à base de porphyrine contenant des groupes des phénols, H_{10}-PorphCat et H_{14}-PorphGal. La première partie du chapitre détaille le travail effectué avec H_{10}-PorphCat dans le cadre d'une étude à long terme avec l'Institut Lavoisier de Versailles (ILV). La deuxième partie discute du travail exploratoire effectué avec des ions métalliques à haute valence et H_{14}-PorphGal qui a conduit à la synthèse de structures MOFs à haute stabilité chimique. L'article publié basé sur ce MOF stable est également fourni.

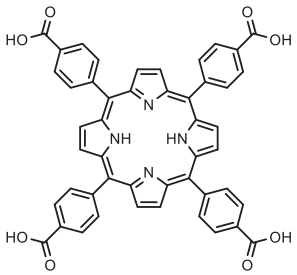

5,10,15,20-Tetrakis(4-carboxyphenyl) porphyrin
(H_2TCPP)

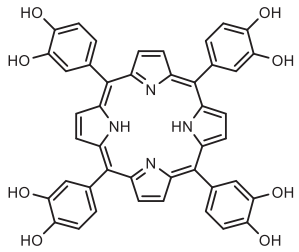

5,10,15,20-Tetrakis(3,4-dihydroxyphenyl)porphyrin
(H_{10}-PorphCat)

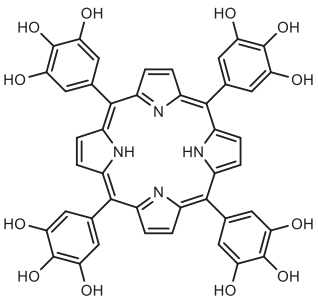

5,10,15,20-tetrakis(3,4,5-trihydroxyphenyl)porphyrin
(H_{14}-PorphGal)

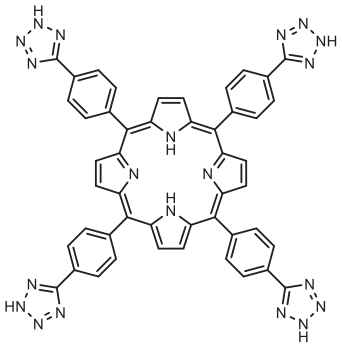

5,10,15,20-tetrakis(4-(2*H*-tetrazol-5-yl)phenyl)
porphyrin
(H_2TTPP)

Figure 1 Les ligands à base de porphyrines étudiés pour la synthèse des MOFs de ce travail.

2. Synthèse des ligands des porphyrines

La méthode Adler a été utilisé pour la synthèse des ligands porphyrines.[20] Ils ont ensuite été isolés et caractérisés par un ensemble de techniques expérimentales (spectrométrie de masse, spectroscopies RMN, UV-vis et IR).

Les ligands de porphyrine métallée au fer, au manganèse et au cobalt avec le groupe fonctionnel de l'acide carboxylique (TCPP) ont été synthétisés avec succès à l'échelle du gramme (3 étapes de synthèse, rendement total de ~ 12%) (Figure 2).

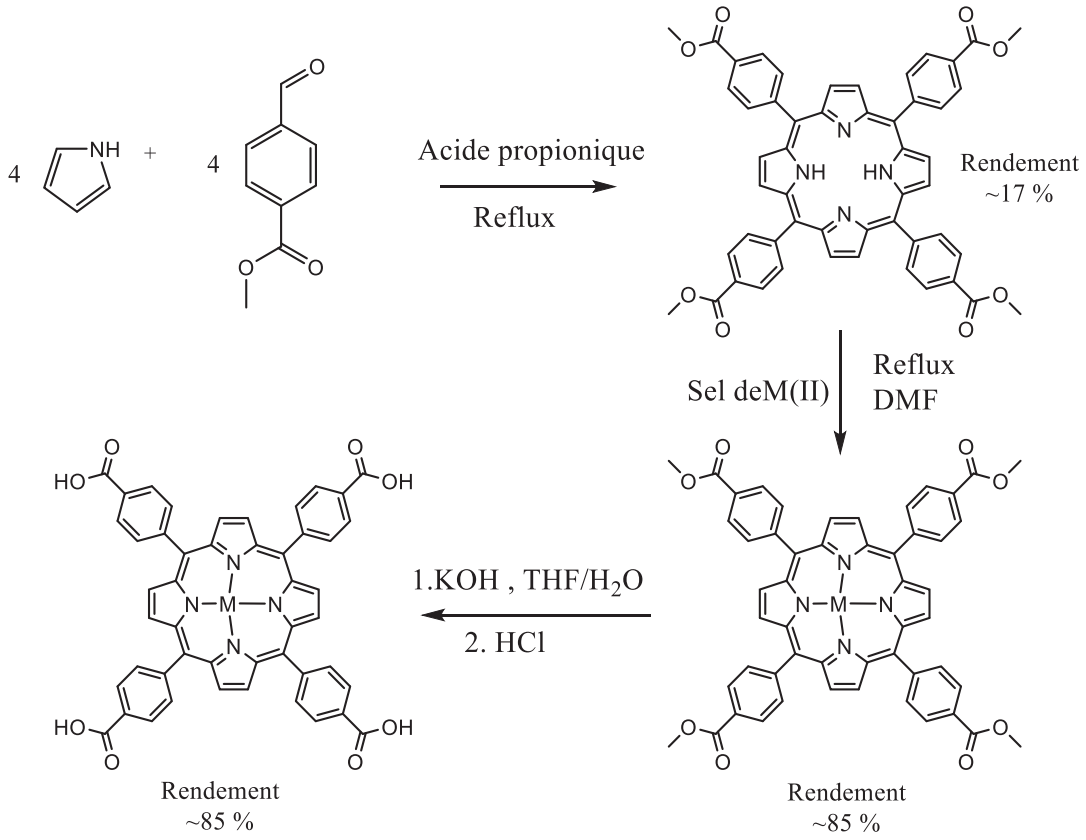

Figure 2 La voie de synthèse générale suivie pour obtenir les ligands de porphyrine à base d'acide carboxylique.

H_{10}-PorphCat avec le groupe fonctionnel du catéchol a été synthétisé à l'échelle du gramme (2 étapes de synthèse, rendement de ~13%) (Figure 3). Le nickel a été inséré avec succès dans $H_2T(OMe)_2PP$ protégé par un groupe méthoxy, et les groupes méthoxy ont ensuite été hydrolysés en utilisant du chlorure de pyridinium pour produire du Ni-H_8-PorphCat avec une faible quantité de démétallation (3 étapes de synthèse, rendement total 9%) (Figure 3).

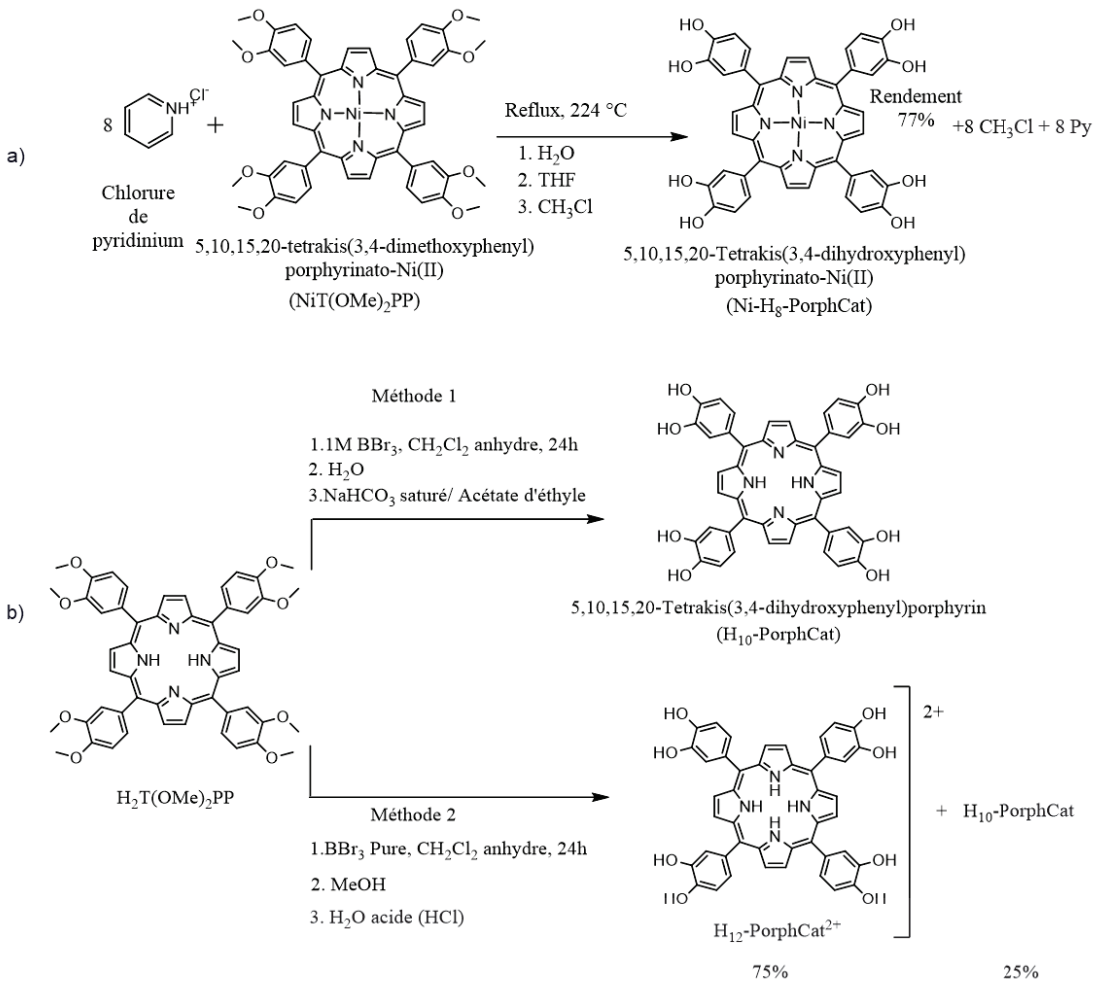

Figure 3 a) Le clivage d'éther de NiT(OMe)$_2$PP avec du chlorure de pyridinium pour obtenir Ni-H$_8$-PorphCat b) Deux procédures de synthèse / méthodes de purification différentes utilisées pour le clivage d'éther des groupes méthoxy de H$_2$T(OMe)$_2$PP en utilisant BBr$_3$. La méthode 2 donne un mélange d'espèces protonées et non protonées.

La porphyrine H$_{14}$-PorphGal fonctionnalisée au gallol a été synthétisée à l'échelle du gramme via la porphyrine intermédiaire H$_2$TtrimPP (Figure 4). Le clivage d'éther du H$_2$TtrimPP en utilisant BBr$_3$ a donné la forme diprotonée du ligand de porphyrine, H$_{16}$-PorphGal-2Br (2 étapes de synthèse, rendement total de ~ 14%).

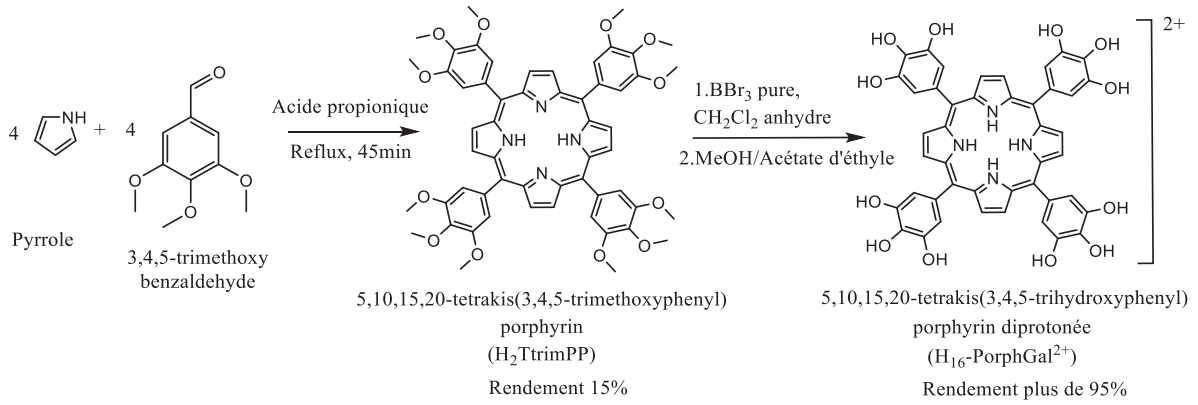

Figure 4 La procédure de synthèse utilisée pour obtenir la 5,10,15,20-tétrakis(3,4,5-trihydroxyphényl)porphyrine (H_{14}-PorphGal). La méthode donne l'espèce dans la forme protonée (H_{16}-PorphGal^{2+}).

H_2TTPP avec le groupe fonctionnel tétrazole a été synthétisé avec succès à l'échelle du gramme via le produit intermédiaire, H_2TCyanoP (2 étapes de synthèse, rendement ~ 5%) (Figure 5).

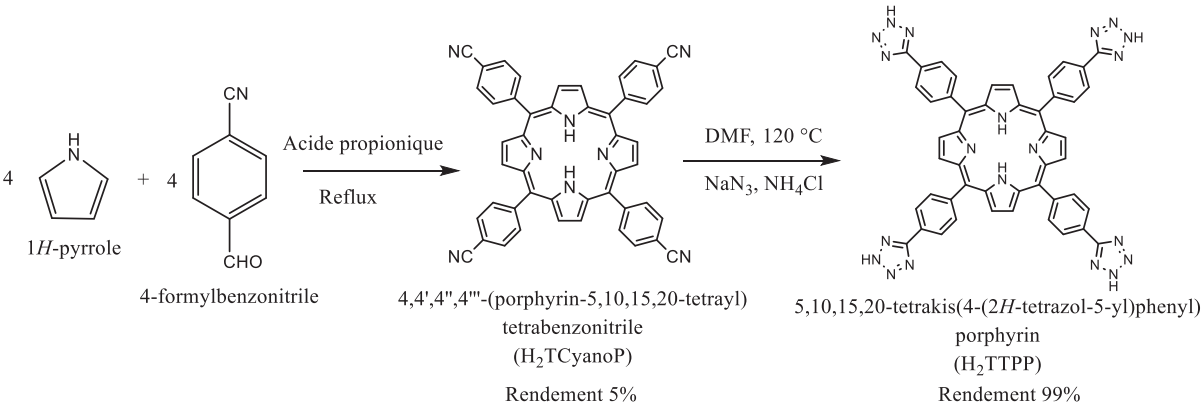

Figure 5 La synthèse de la tétrakis-5,10,15,20(4-(2H-tétrazol-5-yl)phényl)porphyrine (H_2TTPP).

3. Les MOFs à base de porphyrines avec le groupement carboxylate

Les ligands avec la fonctionnalité coordinante carboxylate ont majoritairement étudiés avec des MOFs à base de porphyrines où le ligand plus courant est la tétrakis(4-carboxyphényl)porphyrine, principalement en raison de sa disponibilité commerciale et/ou de sa facilité de synthèse.[5-6, 21] Les études ont montré que l'augmentation de la charge du métal conduit généralement à une amélioration de la stabilité hydrothermique des MOFs à base de carboxylates.[12] L'anion carboxylate peut être considéré comme une base dure ; ainsi, la densité de charge accrue d'ions métalliques de valence plus élevée peut conduire à des liaisons M-O plus fortes. Par conséquent, l'utilisation d'ions métalliques de valence plus élevée tels que Fe^{3+} et Al^{3+} dans la brique inorganique peut conduire à des MOFs à base carboxylate plus stables.

Les composés [Fe^{II}pzTCPP($Fe^{III}OH)_2$] et Al-PMOF {formule chimique [H_2-TCPP($Al^{III}OH)_2$]} publiés par Fateeva et al sont deux MOFs carboxylates à base de porphyrine stables.[15-16] Le travail présenté dans ce chapitre se concentre sur deux sujets principaux. L'un implique l'étude de la réactivité du Fe sur des ligands à base de tétrakis(4-carboxyphényl)porphyrine et l'autre implique l'exploration de la synthèse de matériel Al-PMOF métallé avec Mn^{3+} et Fe^{3+}.

- *Réactivité du Fe avec tétrakis(4-carboxyphényl)porphyrine à base libre*

[Fe^{II}pzTCPP($Fe^{III}OH)_2$] a été synthétisé via la réaction solvothermale du chlorure de fer hydraté et de tétrakis (4-carboxyphényl)porphyrine à base libre (H_2TCPP) en présence de pyrazine.[15] Lorsque les trois composés et le DMF ont réagi, un mélange de deux phases a été obtenu, [Fe^{II}pzTCPP($Fe^{III}OH)_2$] et [Fe^{II}TCPP($Fe^{II}pz)_2$] (Figure 6). Pour obtenir la phase pure du [Fe^{II}pzTCPP($Fe^{III}OH)_2$], une procédure de synthèse en deux étapes a été adaptée. On fait réagir d'abord $FeCl_3.6H_2O$ et H_2TCPP et on isole un solide intermédiaire (Figure 6). Ensuite, on a laissé ce solide réagir avec la pyrazine pour obtenir la phase pure du [Fe^{II}pzTCPP($Fe^{III}OH)_2$]. Dans ce travail, nous avons essayé d'étudier la nature de cette phase intermédiaire car elle pourrait conduire à des informations sur le mécanisme de la formation du MOF. De plus, la possibilité de substituer le ligand pyrazine par d'autres donneurs d'azote a également été étudiée (N-donneurs tels que l'imidazole).

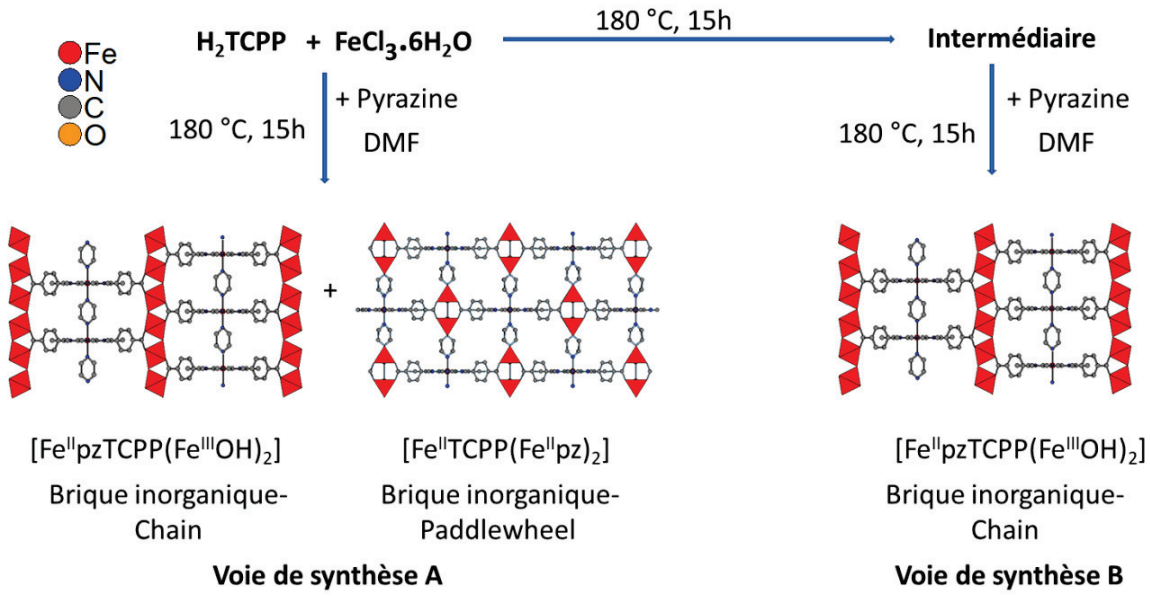

Figure 6 Les voies de synthèse différentes utilisées pour obtenir [Fe^{II}pzTCPP($Fe^{III}OH)_2$].[15] Les hydrogènes sont omis pour plus de clarté.

Au total, 11 réactions ont été tentées pour étudier la nature du produit intermédiaire. La formation d'un gel a été observée dans 6 réactions ce qui a rendu l'analyse difficile. Pour éviter la formation de gel à l'avenir, ce système pourrait être étudié en utilisant des solvants secs dans des conditions anaérobies. L'obtention de monocristaux de qualité suffisante pour les études de diffraction sur monocristal n'a pas été possible (mauvaise qualité cristalline et petite taille).

La substitution de la pyrazine par un N-donneur différent a consisté en 3 tentatives avec l'approche en une seule étape alors que 4 tentatives ont été faites avec l'approche en deux étapes. Les deux approches ont donné des solides qui étaient des polymères de coordination mais des monocristaux de qualité suffisante n'ont pas été obtenus. En outre, 2 tentatives ont été faites pour remplacer la pyrazine dans la structure en utilisant la technique d'échange de ligand assistée par solvant, mais n'ont pas abouti.

Compte tenu du fait que des structures microporeuses ont été obtenues avec le processus de synthèse en une étape, il était pertinent d'étudier l'influence des paramètres température et nature de solvant sur la cristallinité des structures obtenues.

Il semble que la pyrazine ait un effet dans la construction de la structure finale de $[Fe^{II}pzTCPP(Fe^{III}OH)_2]$ à partir du produit intermédiaire. En effet, l'utilisation d'autres ligands donneurs d'azote n'a pas donné lieu à une structure similaire. Cela pourrait être dû à sa taille parfaite dans le cadre et à la capacité d'agir comme un pont entre deux centres Fe^{2+}. Un donneur d'azote intéressant à étudier serait la pipérazine. Même si cette molécule n'est pas aromatique, elle pourrait potentiellement agir comme un ligand pontant avec ses deux atomes d'azotes.

- *Réactivité du Fe avec la tétrakis(4-carboxyphényl)porphyrine métallée au Co*

L'activité photocatalytique et électrocatalytique des porphyrines de cobalt pour la réduction du CO_2 a été bien étudiée.[22-23] L'incorporation de telles métalloporphyrines dans des structures de MOFs stables peut conduire à des catalyseurs hétérogènes stables. Kornienko et al ont démontré les propriétés catalytiques de réduction du CO_2 d'un système MOF à base d'Al-PMOF métallé au cobalt.[24] Cependant, il y a très peu de MOFs stables à base de porphyrines qui ont été basés sur des briques inorganiques contenant du fer.[25] Des briques inorganiques à base de fer trivalent peuvent donner des structures stables comme indiqué dans la section précédente. En plus, la présence de fer dans le bloc de construction inorganique peut être éventuellement exploitée pour renforcer l'activité redox des MOFs.[26]

Durant ce travail, une nouvelle phase a été obtenue à partir de la réaction entre $FeCl_3.6H_2O$ et le ligand TCPP métallé au Co. La résolution de la structure a révélé un nouveau MOF de formule chimique $[CoTCPP(H_2O)_2(Fe^{III}OH)_2]$ (Figure 7). Cependant, la cristallinité de la phase était médiocre et les tentatives répétées pour obtenir des cristaux de meilleure qualité n'ont pas été couronnées de succès.

Deux autres produits polymères de coordination différents ont également été obtenus, l'un à une température isotherme de 190 °C avec du DMF comme solvant et l'autre en utilisant un mélange eau/DMF à 150 °C. A nouveau, l'absence de cristaux de qualité suffisante pour la diffraction des rayons X a entravé l'analyse structurale ultérieure. 4 réactions ont été tentées pour la synthèse de solides obtenus à une température de 190 °C. L'effet du solvant et le programme de chauffage n'ont pas été étudiés. Ainsi, il y a de la place pour une optimisation de synthèse supplémentaire pour ce produit et une analyse plus poussée.

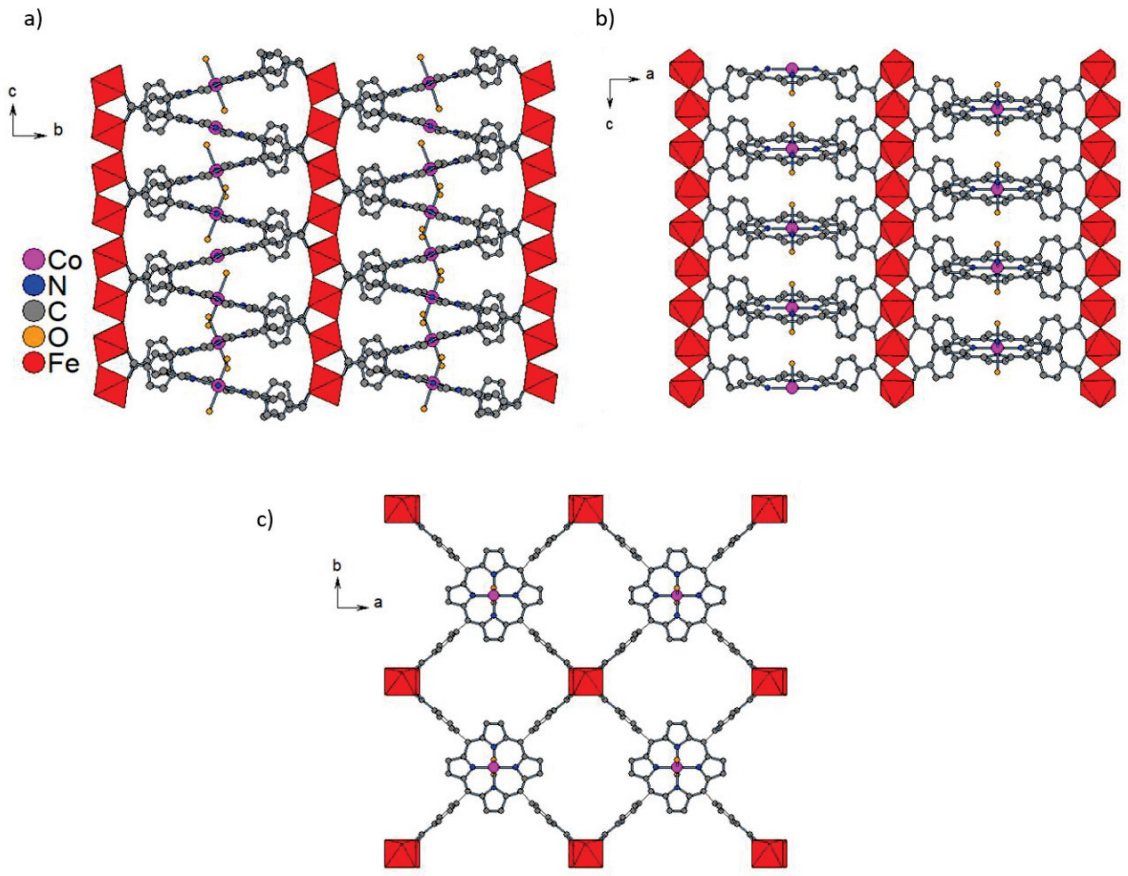

Figure 7 La structure de $[CoTCPP(H_2O)_2(Fe^{III}OH)_2]$. a) le long de l'axe a b) le long de l'axe b c) le long de l'axe c. Les atomes d'hydrogène ont été omis pour plus de clarté.

- *Exploration de la synthèse de matériaux Al-PMOF métallés au Mn^{3+} et Fe^{3+}*

Al-PMOF, [H_2TCPP($Al^{III}OH)_2$] est un MOF stable dans l'eau publié par Fateeva et al.[16] Il a été synthétisé avec un noyau porphyrinique non métallé et des variations Al-PMOF métallés post-synthétiquement avec du zinc divalent,[16] cobalt,[27] et cuivre[28] ont été rapportées. Zn-Al-PMOF a montré une activité photocatalytique vis-à-vis de la production de H_2, Co-Al-PMOF a montré une activité électrocatalytique pour la réduction du CO_2 et Cu-Al-PMOF s'est avéré actif dans la photoréduction du CO_2. Ainsi, le fait d'avoir différents métaux dans le noyau de porphyrine permet d'ajuster la fonctionnalité du matériau. Les métalloporphyrines les plus étudiées sont les porphyrines métallées avec Fe et Mn qui ont été utilisées comme modèles pour imiter le cytochrome P-450 dans l'oxydation catalytique de substrats organiques et comme catalyseurs pour diverses autres réactions d'oxydation.[29-30] Cependant, les Al-PMOFs métallés avec Mn et Fe n'ont pas été rapportés auparavant.

Mn-Al-PMOF a été obtenu avec succès via l'optimisation de paramètres de synthèse pour la réaction solvothermale entre $AlCl_3.6H_2O$ et MnTCPP(OH). Fe-Al-PMOF a été obtenu par optimisation de deux voies de synthèse différentes. La première méthode a exploré la métallation post-synthétique de l'Al-PMOF par le thiocyanate de fer et le Fe-Al-PMOF a été obtenu avec environ 80% d'occupation du Fe dans les noyaux de porphyrine. La deuxième méthode impliquait l'utilisation de FeTCPP(Cl) en tant que ligand de départ et le MOF était obtenu avec une occupation 100% Fe dans les noyaux de porphyrine mais avec une cristallinité inférieure par rapport à la première méthode (Figure 8).

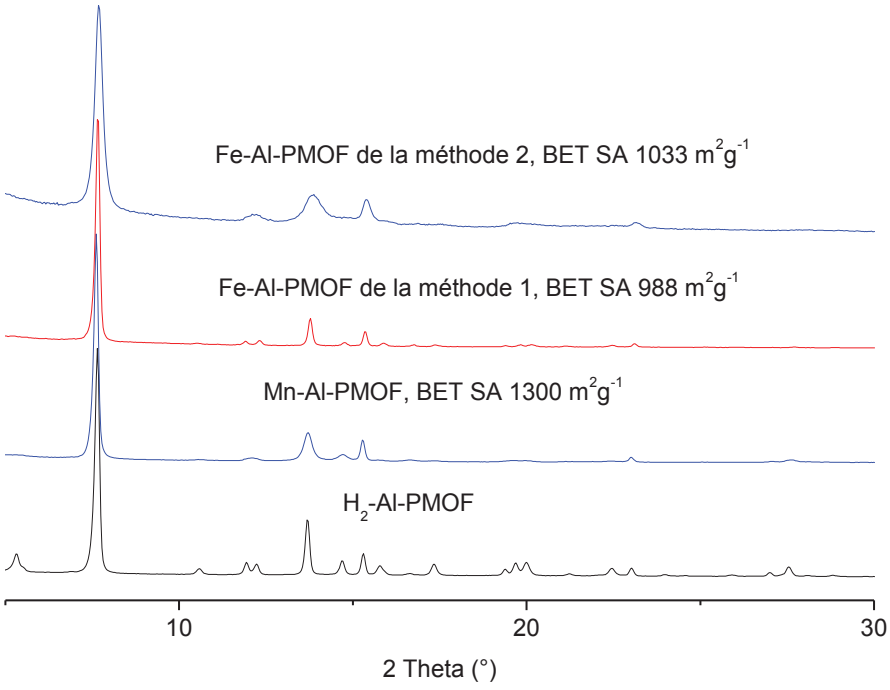

Figure 8 Les données de PXRD comparant pour le Mn-Al-PMOF et les Fe-Al-PMOF préparés à partir des conditions synthétiques optimisées. Les surfaces BET sont indiquées.

- *Evaluation du matériau M-AL-PMOF comme catalyseurs hétérogènes*

Le potentiel des matériaux Al-PMOF métallés au Fe^{3+} et Mn^{3+} en tant que catalyseurs hétérogènes a été exploré avec différents types de réactions. Initialement, l'oxydation de l'hexane, du toluène et du cyclohexène ont été tentées mais des résultats plus prometteurs ont été obtenus pour la formation d'un produit de pyrazoline à partir de diazoacétate d'éthyle (Figure 9).

La formation de ce produit est unique au Fe-Al-PMOF lorsqu'il est comparé à l'état homogène (Figure 10). En outre, le catalyseur est recyclable jusqu'à 5 cycles. Cependant, la désactivation des sites catalytiques au cours des essais catalytiques successifs a été observée.

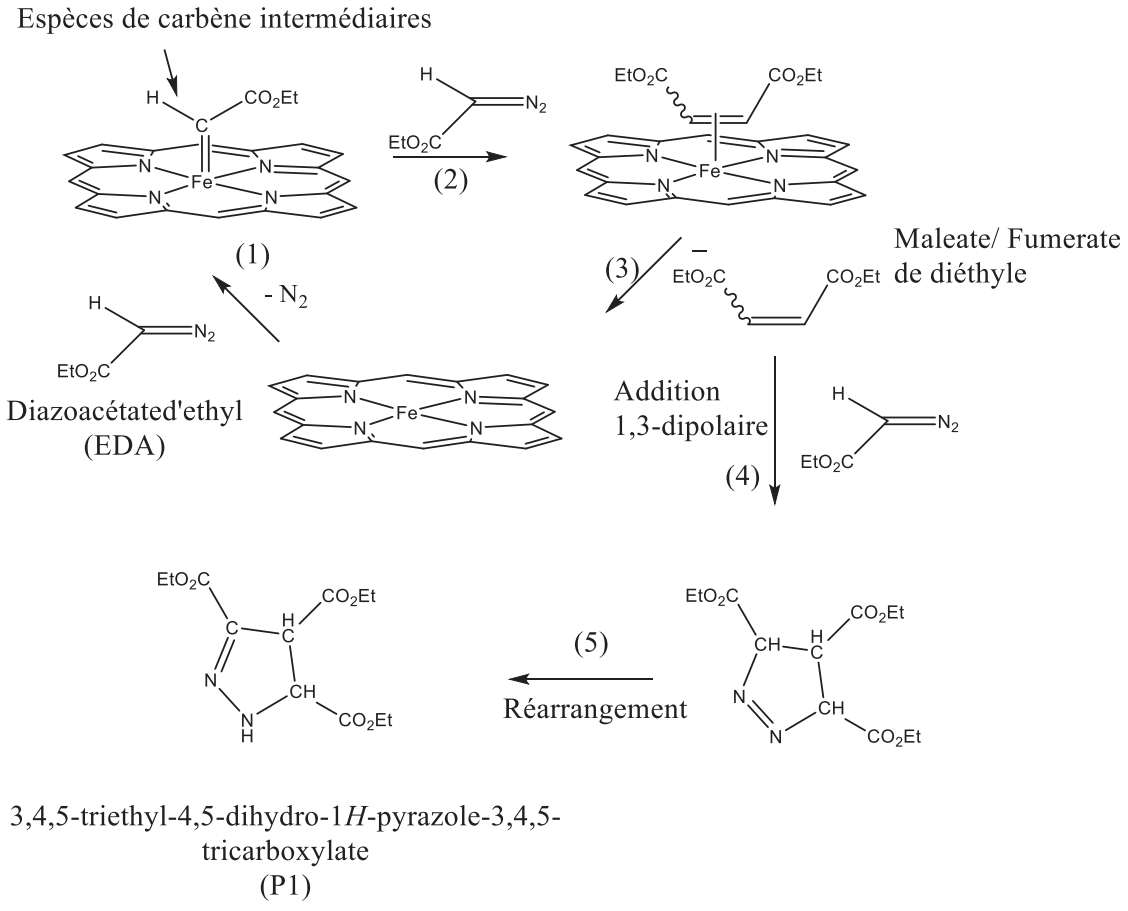

Figure 9 La représentation schématique du mécanisme possible pour la formation des produits dimères et du 3,4,5-triéthyl-4,5-dihydro-1H-pyrazole-3,4,5-tricarboxylate (P1). P1 est formé par l'intermédiaire d'une addition 1,3-dipolaire d'EDA au maléate de diéthyle ou au fumarate (étape 4).

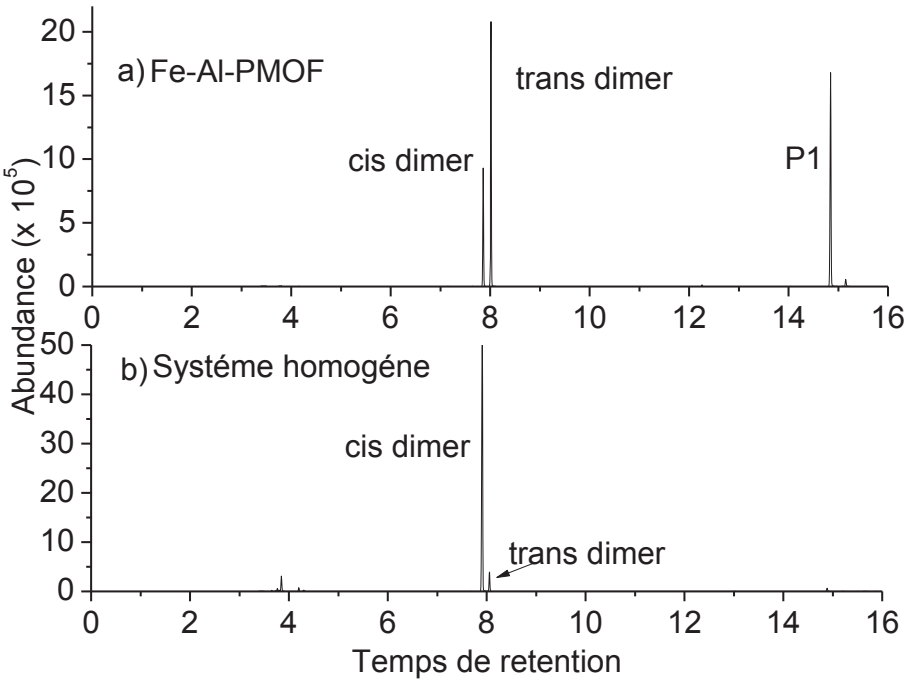

Figure 10 La sélectivité de la réaction du Fe-Al-PMOF avec l'EDA par rapport au système homogène avec FeTesterP(Cl). La réaction a été suivi par GC-MS.

4. Les MOFs à base de porphyrines avec le groupement tetrazolate

Les tétrazoles font partie de la famille des azoles, qui sont des hétérocycles azotés aromatiques à cinq chaînons. Ce sont des donneurs sp^2 hybrides d'azote et ont le même comportement de coordination que les pyridines. Même si les azoles sont généralement connus comme bases (l'azolium est la forme protonée), ils peuvent également être déprotonés pour donner l'ion azolate correspondant.

Il existe de nombreux exemples de polymères de coordination rapportés avec des ligands à base d'azole et la raison de ceci est leur potentiel dans l'application comme matériau de croisement de spin.[31-34] Le croisement de spin est un phénomène observé avec certains composés où il subit un changement d'état de spin lors d'une perturbation externe. Il y a beaucoup de composés à base d'azolate rapportés avec ce comportement mais les composés avec des structures étendues qui montrent une porosité permanente sont rares.[35-37] Ainsi, la motivation de ce travail était d'obtenir un composé à base de Fe-tétrazolate avec des porphyrines et présentant une porosité permanente.

Les études utilisant la synthèse hydrothermale avec $FeCl_3.6H_2O$, H_2TTPP et la pyrazine dans le DMF ont conduit à la synthèse réussie du composé Fe(II)pzTTPP[$Fe(II)_{1-x}DMF_{1-x}Fe(III)_xOH_x$], (x = 0,25 pour échantillon frais). Ce MOF avait une topologie de *fry* où la brique inorganique est constituée d'une chaîne de [FeN_4O] qui est similaire à ce qui a été observé avec un MOF de fer à base de

porphyrine carboxylate rapporté auparavant avec une chaîne inorganique [$FeO_4(OH)$] (Figure 11). La chaîne inorganique contenait à la fois Fe(II) et Fe(III), ce qui a été confirmé par des mesures Mössbauer. Pour obtenir l'équilibre de charge, les ligands pontant OH^- sont remplacés par des molécules de DMF neutres qui ont été confirmées par spectroscopie IR dépendant de la température. Cependant, la structure n'était pas stable à l'air en raison de l'oxydation du Fe(II) en Fe(III) dans la brique inorganique, mais le solide résultant après activation présentait une microporosité intrinsèque. En raison de cette instabilité à l'air, une étude plus poussée des propriétés électrochimiques telles qu'un comportement redox et un croisement de spin n'était pas possible. Potentiellement, des structures plus stables peuvent être obtenues en utilisant un ligand de porphyrine à base de pyrazolate à la place du ligand à base de tétrazolate.[38]

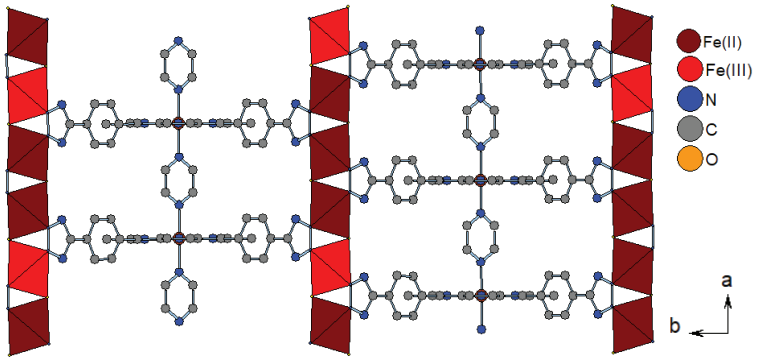

Figure 11 La structure de Fe(II)pzTTPP[$Fe(II)_{1-x}DMF_{1-x}Fe(III)_xOH_x$], vue le long de l'axe c.

5. Les MOFs à base de porphyrines avec les groupements phénolates

Ce chapitre présente le travail effectué sur l'étude de la réactivité de deux porphyrines fonctionnalisées au phénol : 5,10,15,20-tétrakis(3,4-dihydroxyphényl)porphyrine à base de catéchol (H_{10}-PorphCat) et 5,10,15,20-tétrakis(3,4,5-trihydroxyphényl)porphyrine à base de gallol (H_{14}-PorphGal). L'étude concernant la porphyrine fonctionnalisée par le catéchol faisait partie d'un projet à long terme en collaboration avec l'Institut Lavoisier de Versailles (ILV) et portait sur l'optimisation de la synthèse d'une phase MOF de fer conduisant à l'obtention de monocristaux pour l'élucidation structurale. Ce chapitre présente également le travail exploratoire initial effectué en utilisant une porphyrine fonctionnalisée au gallol et divers ions métalliques trivalents. La partie de l'étude concernant la phase MOF obtenue avec des ions de terres rares trivalents a été publiée dans un article fourni dans la section 5.2.2 du chapitre 5 du manuscrit.

- *Etude de la réactivité des ligands à base de catéchol-porphyrine avec Fe(III) pour la synthèse de MOFs*

La force de liaison métal-ligand est l'un des principaux facteurs permettant de déterminer la stabilité chimique des structures MOFs comme mentionné précédemment. Une approche pour augmenter cette force de liaison est d'employer des groupes coordinants plus basiques. Les fonctionnalités 1,2-dihydroxyphényle ou catéchol ont un pKa plus élevé (pK_{a1} ~ 9,5 ; pK_{a2} ~ 14) par rapport au groupe d'acide carboxylique (pKa ~ 4,8). Il y a des MOFs à base de catécholate dans la littérature. Nguyen et al ont rapporté une série des MOFs 3D basés sur le linker triphenylene-2,3,6,7,10,11-hexakis (olate)(THO^{6-}).[18] Un des MOFs de cette série, Fe-CAT-5 [formule chimique Fe (THO)·Fe(SO_4)($DMA)_3$, DMA = diméthylammonium], a montré une stabilité dans l'eau et une conductivité protonique élevée. Cependant, il n'y a qu'un exemple rapporté d'un polymère de coordination basé sur un ligand base à porphyrine fonctionnalisé par le catéchol. Jin et al ont rapporté plusieurs solides cristallins à base de H_{10}-PorphCat avec Cu, Co et Ni divalents.[39] Les structures réelles de ces solides n'ont pas été déterminées car les auteurs étaient intéressés par la synthèse de composites hybrides par thermolyse.

Dans cette partie de la thèse, nous avons étudié la synthèse de MOFs porphyrines basée sur la fonctionnalité des catécholates. C'était la poursuite d'une étude des solides obtenus à l'ILV avec des sels métalliques trivalents et des ligands à base de H_{10}-PorphCat. Le système avec $FeCl_3.6H_2O$, H_{10}-PorphCat, le pyrocatéchol et la pyrazine a été optimisé pour obtenir de meilleurs monocristaux en termes de taille en étudiant l'effet de différents paramètres. Les plus gros cristaux ont été obtenus à partir de la synthèse à 160 °C, avec un rapport réactif de 3: 1: 3: 15 pour le métal: porphyrine: pyrazine: pyrocatéchol et un mélange DMF/eau de 20% / 80% pour le solvant. La taille des monocristaux a été augmentée de 20 µm jusqu'à 140 µm (Figure 12). Ces cristaux ont été analysés par diffraction synchrotronique et le travail relatif à la résolution structurale est toujours en cours.

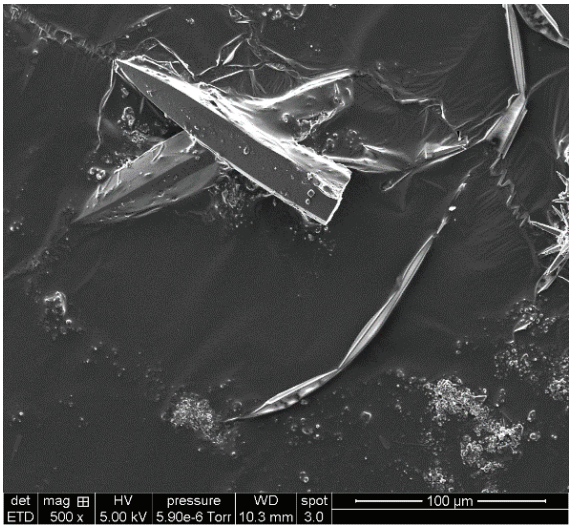

Figure 12 L'Image SEM des cristaux obtenus avec les conditions synthétiques optimisées.

La caractérisation des échantillons globaux synthétisés dans les conditions optimisées a indiqué que ces matériaux possèdent une porosité permanente proche de celle obtenue pour une phase similaire à l'ILV mais la vérification de sa reproductibilité reste à effectuer. Cependant, une analyse précise de la pureté / composition de l'échantillon est difficile sans connaissance de la nature exacte de la structure.

- *Etude de la synthèse de MOFs avec des ligands à base de porphyrine contenant le groupement gallate*

De manière similaire aux groupes de catéchols précédemment décrits, la fonctionnalité 1,2,3-trihydroxyphénol (gallol) a également la capacité de produire des cadres stables en raison de sa basicité élevée (pK_{a1} ~ 9,3 ; pK_{a2} ~ 11 ; pK_{a3} ~ 14).

Il existe quelques MOFs construits avec la fonctionnalité gallate[40-42] mais un seul a été rapporté basé uniquement sur cette fonctionnalité, MIL-163 [formule chimique $Zr(H_2$-TzGal)·x(H_2O)y(DMA), H_6-TzGal= 5,5'-(1,2,4,5-tétrazine-3,6-diyl)bis(benzène-1,2,3-triol), DMA = diméthylamine].[19] Ce matériau a montré une stabilité chimique remarquable même en présence d'espèces coordinantes compétitives, telles que les ions phosphate (solution tampon de phosphate, PBS).

Des tentatives ont été faites pour transposer la topologie du MIL-163 dans une structure en commençant par le ligand à base de porphyrine, 5,10,15,20-tétrakis(3,4,5-trihydroxyphényl) porphyrine (H_{14}-PorphGal) et les sels de zirconium par Mouchaham et al à l'ILV. Ceci a conduit à la synthèse réussie du MIL-173(Zr) [formule chimique $Zr_2(H_6$-PorphGal)$(DMF,H_2O)_n$] qui est le premier MOF à base de porphyrine construit avec cette fonctionnalité. Dans le cadre de la thèse, il a été tenté

d'étendre cette structure aux métaux des terres rares. Ce travail a été effectué en utilisant les installations à haut débit de l'ILV. Cela a donné des composés avec une structure similaire à MIL-173(Zr) avec La^{3+}, Ce^{3+} et Y^{3+}, MIL-173(RE) [formule chimique $RE_2(H_8\text{-PorphGal})(DMF, H_2O)_n$]. En outre, la synthèse avec le Lanthane a donné des monocristaux qui ont été utilisés pour l'élucidation structurelle. Les deux structures contiennent une brique inorganique constituée des chaînes infinies d'octaèdres de ZrO_8 où le Zr/La est relié à quatre unités de porphyrine différentes (Figure 13). A leur tour, les unités de porphyrine sont connectées à huit ions Zr^{4+}/La^{3+} différents. L'équilibre de charge de MIL-173 est obtenu par la présence de protons phénoliques supplémentaires, phénomène courant surdimensionné pour le matériau à base de gallate.

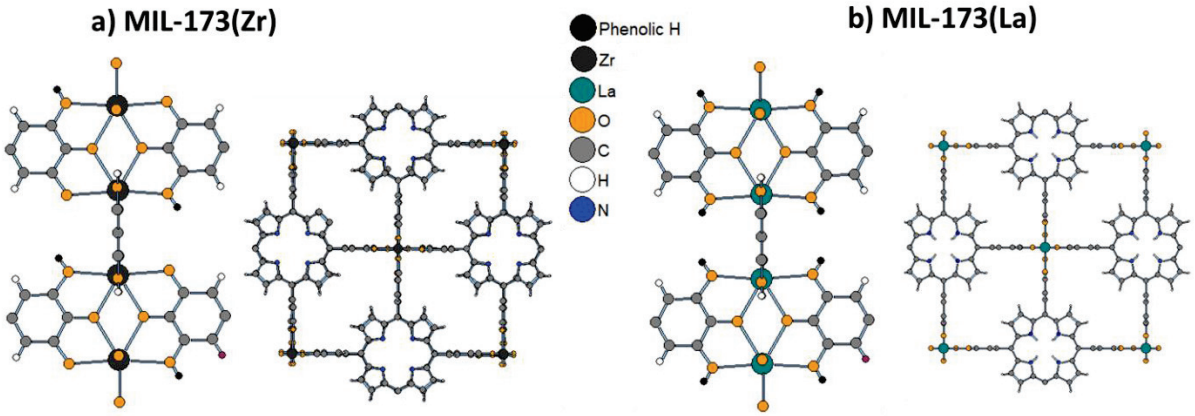

Figure 13 a) La brique inorganique et la structure de MIL-173(Zr). b) La brique inorganique et la structure de MIL-173(La). Il y a des protons phénoliques supplémentaires pour l'équilibre des charges indiqué en noir.

MIL-173(Zr) montre une stabilité exceptionnelle dans l'eau et dans les milieux PBS. Cependant, cette stabilité n'est pas observée pour MIL-173(RE). Cela peut être attribué à la densité de charge plus faible sur les ions RE^{3+} par rapport à l'ion Zr^{4+}.

En outre, MIL-173(Zr) a été métallé post-synthèse avec Co et le matériau résultant montre une activité catalytique hétérogène analogue à l'hème avec de l'oxygène moléculaire comme oxydant. Ainsi, il est possible que la structure de MIL-173(Zr) soit métallée avec différents métaux tels que le fer, ce qui peut conduire à une activité catalytique différente.

L'étude d'autres métaux trivalents a conduit à la synthèse de polymères de coordination basés sur Al^{3+} et In^{3+}. Leurs structures restent inconnues. Une seule température de réaction et le temps d'isotherme ont été étudiés pour la synthèse. Par conséquent, une étude plus approfondie de ces paramètres peut potentiellement produire des monocristaux nécessaires à la résolution de sa structure. Une autre phase 1D a été obtenue dans le cas de In^{3+} en utilisant une teneur en eau plus élevée dans le solvant et la structure a été élucidée par diffraction des rayons X sur monocristal.

Références bibliographiques

1. Zhang, M.; Bosch, M.; Gentle Iii, T.; Zhou, H.-C., Rational design of metal-organic frameworks with anticipated porosities and functionalities. *CrystEngComm* **2014,** *16* (20), 4069-4083.
2. Mansuy, D., A brief history of the contribution of metalloporphyrin models to cytochrome P450 chemistry and oxidation catalysis. *Comptes Rendus Chimie* **2007,** *10* (4–5), 392-413.
3. Chin, D.-H.; La Mar, G. N.; Balch, A. L., Mechanism of autoxidation of iron(II) porphyrins. Detection of a peroxo-bridged iron(III) porphyrin dimer and the mechanism of its thermal decomposition to the oxo-bridged iron(III) porphyrin dimer. *Journal of the American Chemical Society* **1980,** *102* (13), 4344-4350.
4. Abrahams, B. F.; Hoskins, B. F.; Robson, R., A new type of infinite 3D polymeric network containing 4-connected, peripherally-linked metalloporphyrin building blocks. *Journal of the American Chemical Society* **1991,** *113* (9), 3606-3607.
5. Gao, W.-Y.; Chrzanowski, M.; Ma, S., Metal-metalloporphyrin frameworks: a resurging class of functional materials. *Chemical Society reviews* **2014,** *43* (16), 5841-5866.
6. Huh, S.; Kim, S.-J.; Kim, Y., Porphyrinic metal-organic frameworks from custom-designed porphyrins. *CrystEngComm* **2016,** *18* (3), 345-368.
7. Kosal, M. E.; Chou, J.-H.; Wilson, S. R.; Suslick, K. S., A functional zeolite analogue assembled from metalloporphyrins. *Nat Mater* **2002,** *1* (2), 118-121.
8. Burnett, B. J.; Barron, P. M.; Choe, W., Recent advances in porphyrinic metal-organic frameworks: materials design, synthetic strategies, and emerging applications. *CrystEngComm* **2012,** *14* (11), 3839-3846.
9. Gao, W.-Y.; Wojtas, L.; Ma, S., A porous metal-metalloporphyrin framework featuring high-density active sites for chemical fixation of CO2 under ambient conditions. *Chemical communications* **2014,** *50* (40), 5316-5318.
10. Ming, Y.; Purewal, J.; Yang, J.; Xu, C.; Soltis, R.; Warner, J.; Veenstra, M.; Gaab, M.; Müller, U.; Siegel, D. J., Kinetic Stability of MOF-5 in Humid Environments: Impact of Powder Densification, Humidity Level, and Exposure Time. *Langmuir* **2015,** *31* (17), 4988-4995.
11. Low, J. J.; Benin, A. I.; Jakubczak, P.; Abrahamian, J. F.; Faheem, S. A.; Willis, R. R., Virtual High Throughput Screening Confirmed Experimentally: Porous Coordination Polymer Hydration. *Journal of the American Chemical Society* **2009,** *131* (43), 15834-15842.
12. Devic, T.; Serre, C., High valence 3p and transition metal based MOFs. *Chemical Society reviews* **2014,** *43* (16), 6097-6115.
13. Feng, D.; Gu, Z.-Y.; Li, J.-R.; Jiang, H.-L.; Wei, Z.; Zhou, H.-C., Zirconium-Metalloporphyrin PCN-222: Mesoporous Metal–Organic Frameworks with Ultrahigh Stability as Biomimetic Catalysts. *Angewandte Chemie International Edition* **2012,** *51* (41), 10307-10310.
14. Wang, K.; Feng, D.; Liu, T.-F.; Su, J.; Yuan, S.; Chen, Y.-P.; Bosch, M.; Zou, X.; Zhou, H.-C., A Series of Highly Stable Mesoporous Metalloporphyrin Fe-MOFs. *Journal of the American Chemical Society* **2014,** *136* (40), 13983-13986.
15. Fateeva, A.; Clarisse, J.; Pilet, G.; Grenèche, J.-M.; Nouar, F.; Abeykoon, B. K.; Guegan, F.; Goutaudier, C.; Luneau, D.; Warren, J. E.; Rosseinsky, M. J.; Devic, T., Iron and Porphyrin Metal–Organic Frameworks: Insight into Structural Diversity, Stability, and Porosity. *Crystal Growth & Design* **2015,** *15* (4), 1819-1826.
16. Fateeva, A.; Chater, P. A.; Ireland, C. P.; Tahir, A. A.; Khimyak, Y. Z.; Wiper, P. V.; Darwent, J. R.; Rosseinsky, M. J., A water-stable porphyrin-based metal-organic framework active for visible-light photocatalysis. *Angewandte Chemie* **2012,** *51* (30), 7440-4.
17. Colombo, V.; Galli, S.; Choi, H. J.; Han, G. D.; Maspero, A.; Palmisano, G.; Masciocchi, N.; Long, J. R., High thermal and chemical stability in pyrazolate-bridged metal-organic frameworks with exposed metal sites. *Chemical Science* **2011,** *2* (7), 1311-1319.
18. Nguyen, N. T. T.; Furukawa, H.; Gándara, F.; Trickett, C. A.; Jeong, H. M.; Cordova, K. E.; Yaghi, O. M., Three-Dimensional Metal-Catecholate Frameworks and Their Ultrahigh Proton Conductivity. *Journal of the American Chemical Society* **2015,** *137* (49), 15394-15397.

19. Mouchaham, G.; Cooper, L.; Guillou, N.; Martineau, C.; Elkaïm, E.; Bourrelly, S.; Llewellyn, P. L.; Allain, C.; Clavier, G.; Serre, C.; Devic, T., A Robust Infinite Zirconium Phenolate Building Unit to Enhance the Chemical Stability of Zr MOFs. *Angewandte Chemie International Edition* **2015,** *54* (45), 13297-13301.
20. Adler, A. D.; Longo, F. R.; Finarelli, J. D.; Goldmacher, J.; Assour, J.; Korsakoff, L., A simplified synthesis for meso-tetraphenylporphine. *The Journal of Organic Chemistry* **1967,** *32* (2), 476-476.
21. Guo, Z.; Chen, B., Recent developments in metal-metalloporphyrin frameworks. *Dalton Trans.* **2015,** *44* (33), 14574-14583.
22. Grodkowski, J.; Behar, D.; Neta, P.; Hambright, P., Iron Porphyrin-Catalyzed Reduction of CO2. Photochemical and Radiation Chemical Studies. *The Journal of Physical Chemistry A* **1997,** *101* (3), 248-254.
23. Behar, D.; Dhanasekaran, T.; Neta, P.; Hosten, C. M.; Ejeh, D.; Hambright, P.; Fujita, E., Cobalt Porphyrin Catalyzed Reduction of CO2. Radiation Chemical, Photochemical, and Electrochemical Studies. *The Journal of Physical Chemistry A* **1998,** *102* (17), 2870-2877.
24. Kornienko, N.; Zhao, Y.; Kley, C. S.; Zhu, C.; Kim, D.; Lin, S.; Chang, C. J.; Yaghi, O. M.; Yang, P., Metal–organic frameworks for electrocatalytic reduction of carbon dioxide. *J. Am. Chem. Soc* **2015,** *137* (44), 14129-14135.
25. Wang, K.; Feng, D.; Liu, T. F.; Su, J.; Yuan, S.; Chen, Y. P.; Bosch, M.; Zou, X.; Zhou, H. C., A series of highly stable mesoporous metalloporphyrin Fe-MOFs. *Journal of the American Chemical Society* **2014,** *136* (40), 13983-6.
26. Dhakshinamoorthy, A.; Alvaro, M.; Garcia, H., Aerobic oxidation of thiols to disulfides using iron metal-organic frameworks as solid redox catalysts. *Chemical communications* **2010,** *46* (35), 6476-6478.
27. Lions, M.; Tommasino, J. B.; Chattot, R.; Abeykoon, B.; Guillou, N.; Devic, T.; Demessence, A.; Cardenas, L.; Maillard, F.; Fateeva, A., Insights into the mechanism of electrocatalysis of the oxygen reduction reaction by a porphyrinic metal organic framework. *Chemical communications* **2017,** *53* (48), 6496-6499.
28. Liu, Y.; Yang, Y.; Sun, Q.; Wang, Z.; Huang, B.; Dai, Y.; Qin, X.; Zhang, X., Chemical Adsorption Enhanced CO2 Capture and Photoreduction over a Copper Porphyrin Based Metal Organic Framework. *ACS Applied Materials & Interfaces* **2013,** *5* (15), 7654-7658.
29. Mansuy, D., Cytochromes P-450 and model systems: great diversity of catalyzed reactions. In *Pure and Applied Chemistry*, 1994; Vol. 66, p 737.
30. Groves, J. T., The bioinorganic chemistry of iron in oxygenases and supramolecular assemblies. *Proceedings of the National Academy of Sciences of the United States of America* **2003,** *100* (7), 3569-3574.
31. Kahn, O.; Martinez, C. J., Spin-transition polymers: from molecular materials toward memory devices. *Science* **1998,** *279* (5347), 44-48.
32. Kroeber, J.; Audiere, J.-P.; Claude, R.; Codjovi, E.; Kahn, O.; Haasnoot, J. G.; Groliere, F.; Jay, C.; Bousseksou, A., Spin Transitions and Thermal Hysteresis in the Molecular-Based Materials [Fe(Htrz)2(trz)](BF4) and [Fe(Htrz)3](BF4)2.cntdot.H2O (Htrz = 1,2,4-4H-triazole; trz = 1,2,4-triazolato). *Chem. Mat.* **1994,** *6* (8), 1404-1412.
33. Bronisz, R., 1,4-Di(1,2,3-triazol-1-yl)butane as Building Block for the Preparation of the Iron(II) Spin-Crossover 2D Coordination Polymer. *Inorganic Chemistry* **2005,** *44* (13), 4463-4465.
34. Bronisz, R., Tetrazol-2-yl as a Donor Group for Incorporation of a Spin-Crossover Function Based on Fe(II) Ions into a Coordination Network. *Inorganic Chemistry* **2007,** *46* (16), 6733-6739.
35. Salles, F.; Maurin, G.; Serre, C.; Llewellyn, P. L.; Knöfel, C.; Choi, H. J.; Filinchuk, Y.; Oliviero, L.; Vimont, A.; Long, J. R.; Férey, G., Multistep N2 Breathing in the Metal−Organic Framework Co(1,4-benzenedipyrazolate). *Journal of the American Chemical Society* **2010,** *132* (39), 13782-13788.
36. Reed, D. A.; Xiao, D. J.; Gonzalez, M. I.; Darago, L. E.; Herm, Z. R.; Grandjean, F.; Long, J. R., Reversible CO Scavenging via Adsorbate-Dependent Spin State Transitions in an Iron(II)–Triazolate Metal–Organic Framework. *Journal of the American Chemical Society* **2016,** *138* (17), 5594-5602.

37. Sciortino, N. F.; Ragon, F.; Zenere, K. A.; Southon, P. D.; Halder, G. J.; Chapman, K. W.; Piñeiro-López, L.; Real, J. A.; Kepert, C. J.; Neville, S. M., Exploiting Pressure To Induce a "Guest-Blocked" Spin Transition in a Framework Material. *Inorganic Chemistry* **2016,** *55* (20), 10490-10498.
38. Spirkl, S.; Grzywa, M.; Zehe, C. S.; Senker, J.; Demeshko, S.; Meyer, F.; Riegg, S.; Volkmer, D., Fe/Ga-CFA-6 - metal organic frameworks featuring trivalent metal centers and the 4,4[prime or minute]-bipyrazolyl ligand. *CrystEngComm* **2015,** *17* (2), 313-322.
39. Jin, S.; Hill, J. P.; Ji, Q.; Shrestha, L. K.; Ariga, K., Supercapacitive hybrid materials from the thermolysis of porous coordination nanorods based on a catechol porphyrin. *Journal of Materials Chemistry A* **2016,** *4* (15), 5737-5744.
40. Saines, P. J.; Yeung, H. H. M.; Hester, J. R.; Lennie, A. R.; Cheetham, A. K., Detailed investigations of phase transitions and magnetic structure in Fe(iii), Mn(ii), Co(ii) and Ni(ii) 3,4,5-trihydroxybenzoate (gallate) dihydrates by neutron and X-ray diffraction. *Dalton Trans.* **2011,** *40* (24), 6401-6410.
41. Cooper, L.; Hidalgo, T.; Gorman, M.; Lozano-Fernandez, T.; Simon-Vazquez, R.; Olivier, C.; Guillou, N.; Serre, C.; Martineau, C.; Taulelle, F.; Damasceno-Borges, D.; Maurin, G.; Gonzalez-Fernandez, A.; Horcajada, P.; Devic, T., A biocompatible porous Mg-gallate metal-organic framework as an antioxidant carrier. *Chemical communications* **2015,** *51* (27), 5848-5851.
42. Hidalgo, T.; Cooper, L.; Gorman, M.; Lozano-Fernandez, T.; Simon-Vazquez, R.; Mouchaham, G.; Marrot, J.; Guillou, N.; Serre, C.; Fertey, P.; Gonzalez-Fernandez, A.; Devic, T.; Horcajada, P., Crystal structure dependent in vitro antioxidant activity of biocompatible calcium gallate MOFs. *Journal of Materials Chemistry B* **2017,** *5* (15), 2813-2822.

Chapter 1:

An Introduction to Porphyrin Based Metal Organic Frameworks

Table of Contents

1. An introduction to porphyrin based metal organic frameworks

Porphyrinic MOFs have been extensively studied in literature but their chemical stability remains problematic (chapter 1). In this work we explore the possibility of obtaining more stable porphyrinic MOFs by using porphyrinic ligands with various functionalities which were synthesised and characterised (chapter 2). One of the strategies we used in order to reach our goal was to investigate existing stable carboxylate porphyrinic MOF platforms and attempt to modify them to impart new functionalities (chapter 3). The other approach employed was to explore the synthesis of novel MOFs by using porphyrinic ligands with functionalities which are little utilized in literature such as tetrazolate (chapter 4), catecholate and gallate (chapter 5).

This chapter will briefly introduce MOFs and present methods for synthesis optimization and characterisation. Then MOFs based on porphyrinic ligands will be discussed followed by an exhaustive literature study of porphyrinic MOFs based on non-carboxylate linkers. Current limitations of porphyrinic MOFs are also discussed.

1.1. Metal Organic Frameworks

The rational synthesis of porous solids is an on-going challenge in the area of materials science. Porous inorganic materials such as zeolites, which are aluminosilicate minerals made from interlinked tetrahedra of alumina (AlO_4) and silica (SiO_4) have been used widely in industry as catalysts.[1]

Last 25 years have seen the emergence of a new class of porous solids, metal-organic frameworks (MOFs). They are hybrid material containing both organic and inorganic moieties as opposed to zeolites which contain only inorganic components. By carefully choosing these inorganic and organic constituents, material with high porosity and desired properties can be obtained.

The pioneering work for this class of compounds was established by Hoskins and Robson in 1990, with their article regarding the design of 3-dimensional frameworks using octahedral and tetrahedral metal centres linked by “rod-like units”.[2] The term metal-organic frameworks was first coined by Yaghi et al to describe these type of materials.[3] By using 1,3,5-benzenetricarboxylate, pyridine and octahedral Co centres, the authors reported the successful design and synthesis of a layered material that could reversibly and selectively bind aromatic compounds such as benzene.[3] Since then this domain of materials science has grown rapidly.

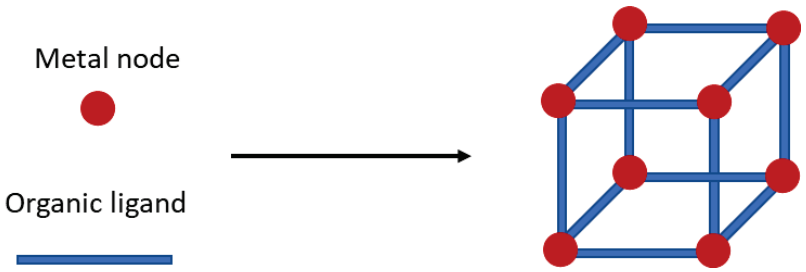

Figure 1-1 Rod and sphere representation of a MOF and its components.

A simple rod and sphere representation can be used to illustrate the modular concept of a MOF. The rods represent the organic backbone of the MOF which are the ligands while the spheres represent the metal nodes (Figure 1-1).

The number of possible organic molecules that can be used as ligands is vast and can have different functionalities for metal coordination. Some of the common coordinative functional groups that have been used successfully in MOF synthesis include carboxylates,[4] phosphonates,[5] pyridyls,[6] pyrazolates,[7] and imidazolates.[8]

The metal nodes represented by the spheres could be a single metal cation or a metal cluster such as $[Zn_4O(CH_3CO_2)_6]$, which is found in the well-known MOF-5.[9] Choice of the metal node plays a vital role in determining the topology of the framework as different connectivities will lead to different framework topologies. Majority of MOFs are based on divalent metals such as Zn^{2+}, Cu^{2}, Cd^{2+}, but recently attention have been given to higher valence metal ions such as Fe^{3+}, Al^{3+} and Zr^{4+} due to them resulting in more stable frameworks, which will be discussed later.[10]

One of the biggest advantages of MOFs is the sheer number of possible combinations of metals and organic ligands available and the tunability and the flexibility it provides. Thus, by choosing suitable organic ligands and metal nodes, it is possible to rationally design the porous frameworks and control the pore sizes and the chemical environments.[11]

1.2. Rational design of MOF

There has been considerable effort made to predict the accessible framework topologies, led by Yaghi et al[12] and Férey et al.[13] A popular approach for rationally designing MOF structures and predict the possible framework is using the concepts of secondary building units (SBU) and reticular synthesis.

SBUs can be defined as basic units present when a MOF structure is deconstructed.[14] They can be thought of being two types, inorganic which contains the metals and organic which contains the organic linker. These two types of SBUs join together to give the overall structure of the framework. The shape of the SBUs are defined by the points they connect to other SBUs (points of extension).

Some common inorganic SBUs found in carboxylate MOFs are shown in Figure 1-2. Certain inorganic SBUs such as chromium acetate cluster and the zinc acetate cluster have also been extended to other functionalities such as azolates (discussed further in chapter 4).[15] [16]

Reticular synthesis in essence is generating a desired topology from the identified compatible SBUs. If the reaction conditions that produce an inorganic SBU with a specific geometry *in situ* is known, in many cases, it is possible to obtain a pre-determined network with the addition of a rigid organic SBU.[12] Wang et al provided an example of this with their porphyrinic MOFs, PCN-601 and PCN-602 (Figure 1-12) which have the same framework topology (described in detail later). The difference is that the latter MOF contains a more spacious ligand which results in larger pores.

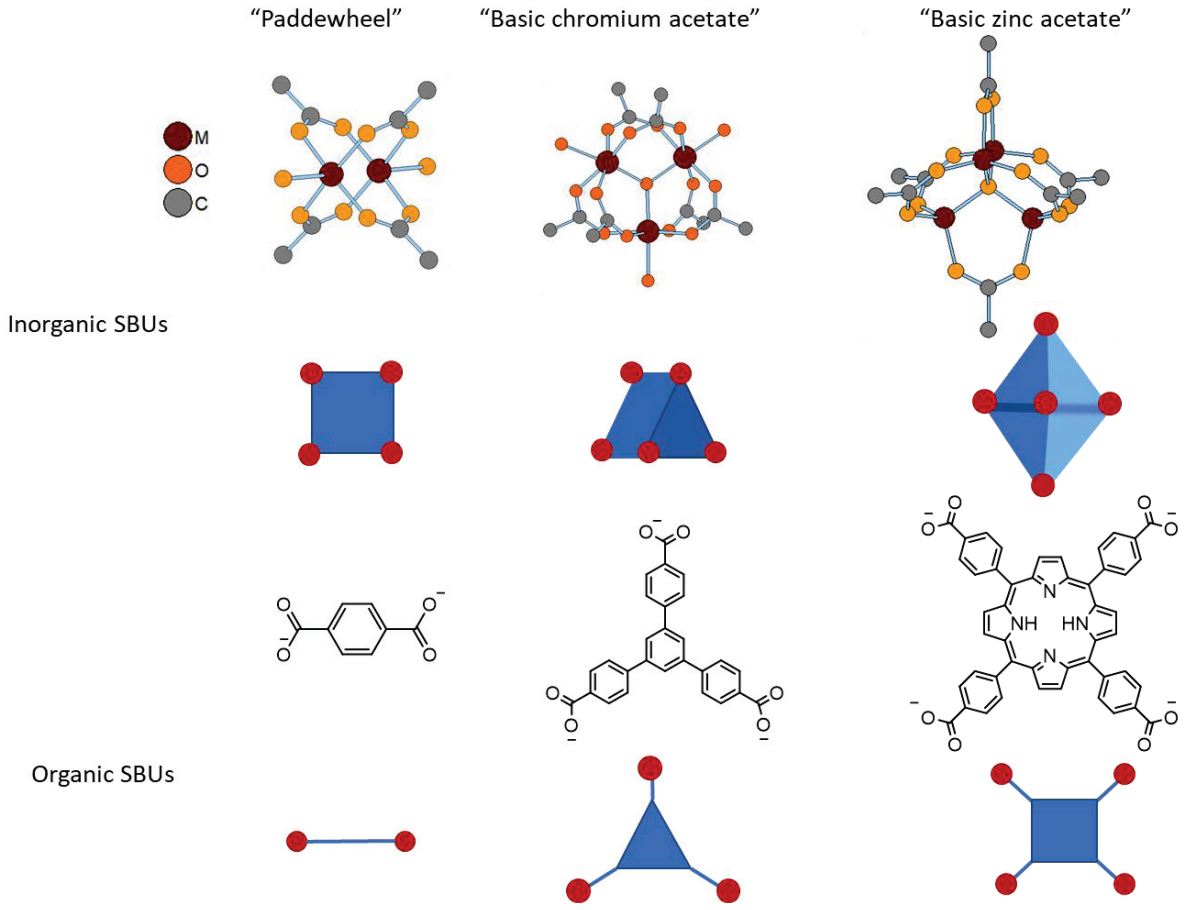

Figure 1-2 Some common SBUs found in carboxylate MOFs. Common named used for the inorganic SBUs are given above the respective structures. Red dots indicate the points where the SBU are linked to another SBU (points of extension).

Reticular synthesis principles work well for rigid organic SBUs and have led to isoreticular series of MOFs with different pore sizes and functionalities such as IRMOF series[9] and UiO MOF series.[17] However, this concept has limitations and can fail when flexibility is introduced to the SBUs as demonstrated by Devic et al.[18] Authors synthesised two frameworks with two different topologies by using two similar tritopic organic SBUs as shown in Figure 1-3. The rigid ligand led to a framework with hexagonal pores with permanent porosity, MIL-103 [La(BTB)(H_2O)·2($C_6H_{11}OH$), BTB= 1,3,5-benzenetrisbenzoate] (Figure 1-3a),[19] while the flexible linker led to a framework with no permanent porosity, MIL-112 [La(**L**)(H_2O)$_2$·2H_2O), L= 4-[3,5-Bis-(1-carbonylmethyl-1*H*-[1,2,3]triazol-4-yl)-phenyl]-[1,2,3]triazol-1-yl acetic acid] (Figure 1-3b).[18] Both the frameworks had similar chain like inorganic SBUs, with a slight difference in the carboxylate coordination modes. In MIL-103 there were two chelating bridging and one bridging carboxylate groups while in MIL-112 there were two chelating bridging and one chelating carboxylate groups. The difference in the topology of the framework was due to the rigidity/flexibility of the linker used. In MIL-103 the linkers have strict C_3-symmetery while in MIL-112 the linkers are T-shaped with different orientations due to the flexibility of the carboxylates around the methylene groups and the presence of the pentagonal triazole rings.

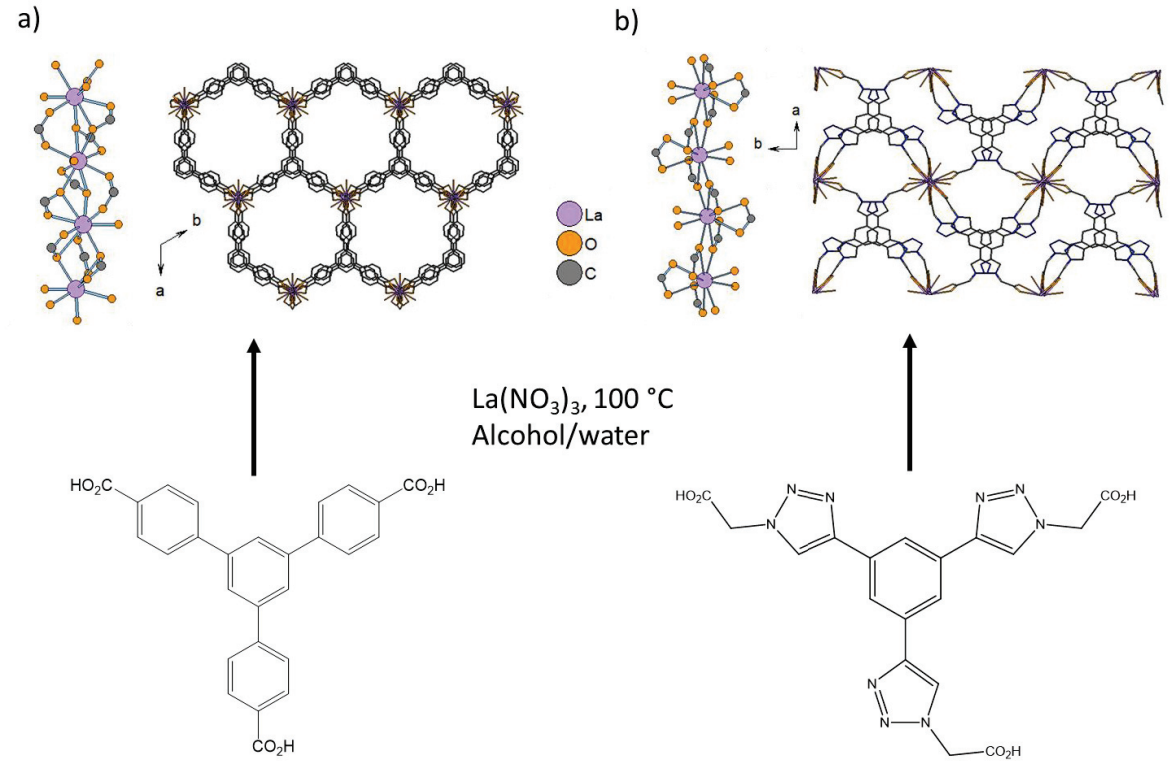

Figure 1-3 Comparison of the network topologies obtained with a rigid and a flexible tritopic ligand a) MIL-103 with [19] b) MIL-112.[18] Hydrogens and solvent molecules are omitted for clarity.

1.3. Synthesis of MOFs

Synthesis methods

Traditional synthesis methods can be divided into two main categories, solvothermal and non-solvothermal. Solvothermal synthesis has become the most commonly used method in MOF chemistry and was used for the work presented in this thesis. It involves reacting the starting materials at or above the boiling temperature of the solvent in a sealed vessel. The autogenous pressure generated helps to enhance the solubility of the starting material as the solvent can be heated above the boiling temperature and promotes the reaction. This method requires special equipment such as autoclaves or sealed containers which can withstand elevated pressures and temperature controlled ovens allowing to set heating and cooling rates.

Non-solvothermal syntheses require classical lab equipment and can be accomplished at room temperature or with conventional heating. Some well-known MOFs, such as HKUST-1,[20] and ZIF-8[8] have been synthesized in this fashion.

Non-traditional methods such as microwave, electrochemical, sonochemical and mechanochemical assisted synthesis have been also reported.[21]

Optimisation of MOF crystallisation process

The formation of MOFs is influenced by many parameters. These can be compositional parameters, such as molar ratios of starting material, concentration of reagents, pH, solvents, and the presence of various additives or it can be process parameters such as reaction time and temperature. These different factors affect not only the topology of the MOF obtained but also the crystal size and phase purity. Thus, the process of optimizing a MOF synthesis often involves the systematic investigation of these parameters in an iterative manner.

Common additives used in MOF synthesis are modulators which can act as monotopic linkers (such as benzoic acid, acetic acid). They can form dynamic bonds with the metal precursor and compete with the linkers for coordination sites which can help to slow down the formation of structural bonds.[22] This can affect the crystal size, crystallinity, porosity and the phase purity of the MOF. Schaate et al reported the successful control of crystal size of UiO-66, which is a Zr_6 cluster based MOF with BDC (1,4-benzene dicarboxylate) as the linker, by varying the amounts of benzoic acid used as a modulator.[23] Increasing the benzoic acid concentration resulted in increased crystal size (Figure 1-4).

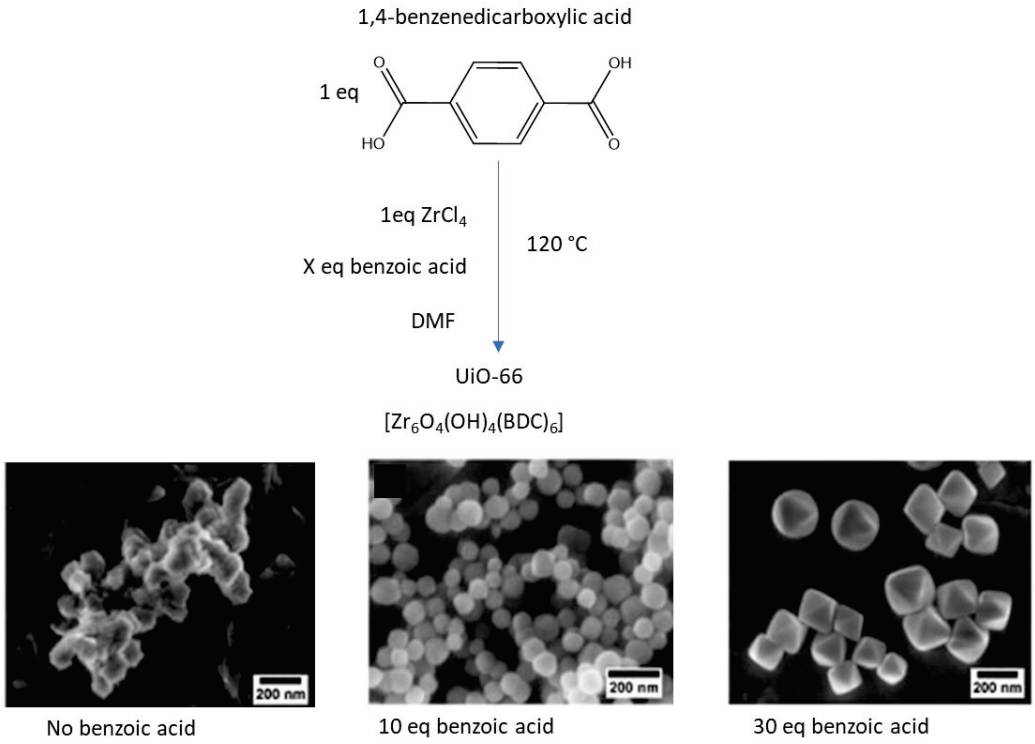

Figure 1-4 Synthesis of UiO-66 using different amounts of benzoic acid leading to different crystal sizes as reported by Schaate et al .[22] SEM images reproduced from the reference 22.

High throughput synthesis methods

As mentioned above there are many process and compositional parameters which influence MOF synthesis and the systematic investigation of these parameters in a serial manner is very time consuming. High throughput synthesis methods can accelerate this process and help the discovery of new MOFs by combining the ideas of parallelisation, miniaturization and automation of screening, which enables generating large amounts of data in a short time scale.[24] With parallelisation, multiple parameters can be investigated at the same time. For example, the two parameters, solvent composition and reactant ratio can be looked at in parallel at the same time for the effect they have on the resultant product as shown in Figure 1-5. The reactions are done in a smaller scale (usually around 0.3-2 mL) in parallel reactors (96, 48 or 24 reactors plates are commonly used). The resultant products are usually analysed and screened via PXRD and optical microscopy to check single crystals formation. These methods require a minimum level of automation at least at the characterisation level to be effective in efficiently analysing the data. Fully automated systems have been reported which includes reactant dispensing (for sample preparation) and purification steps.[25]

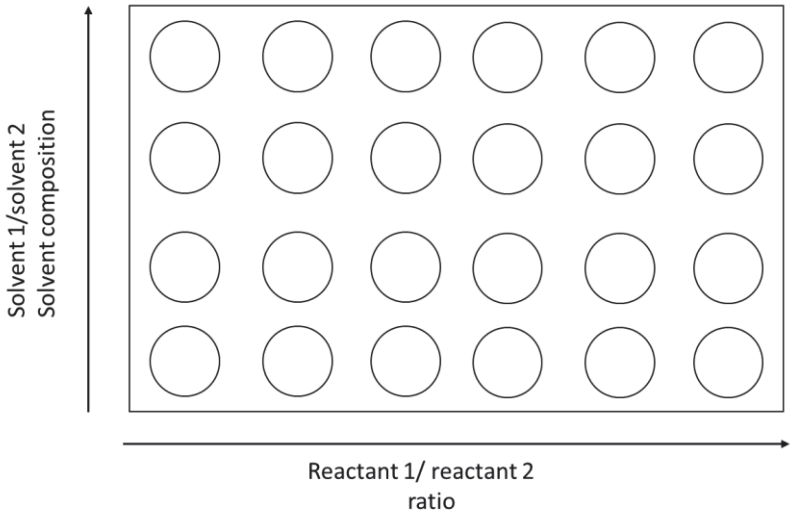

Figure 1-5 An example of a high throughput set up of a 24-reactor plate investigating 2 different reaction parameters in parallel.

Pioneering work on high throughput methods regarding MOF synthesis was reported by the Férey and Yaghi groups. In 2008, Stock and Férey conducted a high throughput study of the system with $FeCl_3$ and 2-amino terephthalic acid, where they looked at the influence of reaction parameters such as molar-ratios, pH, concentration, temperature and solvent.[26] A total of 912 individual reaction mixtures were investigated in 38 high throughput experiments. This led to the identification of the synthesis conditions for three different phases: Fe-MIL-53_NH_2, Fe-MIL-88B_NH_2, and Fe-MIL101_NH_2. Remarkably, all the syntheses conditions were successfully upscaled.

Yaghi et al used a high throughput system to investigate the ZIF (Zeolitic Imidazolate Framework) MOFs based on imidazolate ligands.[27] The authors looked at various reaction parameters such as reactant ratio, solvent and temperature for 9 different ligands and 2 different metal ions (Co^{2+} and Zn^{2+}). 9600 reactions with a reactant volume of 0.3 mL were performed in 100 different experiments which led to the identification of 16 new compounds during this 3-month long study. However, only the synthesis of 7 compounds could be scaled up for bulk analysis which highlights one of the short comings of this technique. The optimised MOF synthesis conditions at a smaller scale do not necessarily translate to the successful synthesis at a higher scale.

During this work, the initial studies regarding the synthesis of the MIL-173(RE) MOF were performed using high throughput methods at the Institut Lavoisier de Versailles in Paris and will be discussed in further detail in chapter 5.

1.4. Characterisation of MOFs

The MOF characterisation techniques used in this work are briefly described in this section.

Single crystal X-ray diffraction

This method relies on the diffraction of X-rays of a fixed wavelength by the lattice of a single crystal with constructive interference according to the Braggs law ($n\lambda=2d\sin\theta$). Braggs law defines the relationship between the wavelength of the electromagnetic radiation, the diffraction angle (θ) and the lattice spacing between two similar parallel planes of atoms(d). The observed diffraction pattern which provides information about the three-dimensional positioning of atoms, can be solved to obtain the structure of this lattice. This is the best method for unambiguous determination of a MOF structure. However, the biggest limiting factor with this technique is obtaining single crystals of sufficient quality for structural elucidation.

Powder X-ray diffraction (PXRD)

PXRD relies on the same principles as the single crystal X-ray diffraction. However, single crystals are not required for this method and is typically performed on the homogenised powdered form of a sample. PXRD relies on the assumption that the powder contains randomly arranged crystallites with statistically significant number of each plane of the crystal structure in the proper orientation to diffract the incident X-rays. Different crystalline material will have a unique powder diffraction pattern which can act as a fingerprint. PXRD is invaluable in MOF chemistry and is useful for rapid and non-destructive determination of bulk crystallinity and the phase purity of the obtained samples by comparing to the simulated patterns of the framework. Furthermore, high resolution PXRD is increasingly used for structural elucidation of MOFs which yield crystals too small for single crystal X-Ray diffraction studies.

Nitrogen adsorption and desorption isotherms and BET surface area analysis

Nitrogen adsorption and desorption isotherms are used to determine the accessible surface area of MOFs. The most common method for determining the surface area is the use of the Brunauer-Emmett-Teller (BET) equation. The method depends on the relationship between the adsorbed volume and pressure at constant temperature, from which the total surface area of the absorbent is determined.

Infrared (IR) spectroscopy

IR spectroscopy relies on the interaction of infrared radiation with matter which corresponds to the vibrational excitation energies. This can give information about the functional groups (such as C=O, -OH) present in a molecule.

UV-vis spectroscopy

In UV-vis spectroscopy, the absorption of the electromagnetic radiation in the UV-vis spectral region by molecules as a function of the wavelength of the incident radiation is measured. The absorption in this region usually corresponds to electronic transitions of molecules with conjugated π bonds (π to π* transitions such as porphyrins) or transition metal complexes (d-d transitions). UV-vis spectroscopy is usually performed in the solution phase but it can also be used to study solid material. In solution phase the transmittance of the radiation is measured as a function of the wavelength while in the solid phase, diffuse (total) reflectance is measured. This method can give information about the concentration of chemical species (Beer-lambert law). It can also indicate the type of species present such as in porphyrins where the absorption maxima changes depending on the metalation of the porphyrin core.

Thermogravimetric analysis (TGA)

In TGA, the change in mass of a sample is measured as a function of temperature which can give information about phase transitions, adsorption/desorption, oxidation/reduction and thermal decomposition of a sample. TGA is used to determine the thermal stability of MOFs and can also be used to calculate their relative purity.

Mössbauer spectroscopy

This technique relies on the emission of gamma radiation from a heavy nucleus (such as of ^{57}Fe) undergoing an energy level transition and gives information about the surrounding electronic and magnetic environment. It is useful with regards to iron containing MOFs and helps to determine the oxidation and the spin state of iron in the framework.

Scanning electron microscopy (SEM) and energy-dispersive X-ray spectroscopy (EDS)

In SEM, a focused beam of high energy electrons is used to study the surface of solid samples which gives information about its morphology. EDS uses the X-rays generated due to the incident electrons to provide information about the chemical composition of the material. SEM is useful studying crystal size and morphology of MOFs. When coupled with EDS, it can also be useful to analyse elemental composition both quantitatively and qualitatively.

1.5. Porphyrinic MOFs

Porphyrin molecules have been extensively researched in areas such as oxidation catalysis and enzyme mimics in homogeneous systems.[28] This is due the prevalence of these molecules in nature as seen in heme groups in enzymes which are responsible for various biological processes (discussed in more detail in chapter 2). MOFs offer an ideal platform where properties of the porphyrins in homogeneous systems can be transferred to heterogeneous systems with high surface areas and

porosity. Furthermore, incorporating porphyrinic moieties in MOFs enables the reactive metalloporphyrin species to be kept apart preventing their self-deactivation.[29]

Structurally, porphyrins offer an ideal ligand for MOFs which is robust with a rigid square planar geometry and relatively large geometrical dimensions that can lead to porous solids. As a ligand, porphyrins offer two potential binding sites. A functional metal binding site within the porphyrin core and a structural metal binding site at the periphery with a coordinating functional group (Figure 1-6). Furthermore, this coordinating group can be changed allowing different coordination environments in the inorganic secondary building units of the resulting MOF.

The functional metal site can be realised either by using metalated porphyrinic ligands as precursors or by post-synthetic metalation of the MOF (Figure 1-6). This paves the pathway to obtain heterobimetallic systems where the metal in the porphyrin core can be changed to obtain varying functionalities (discussed in detail in chapter 3).

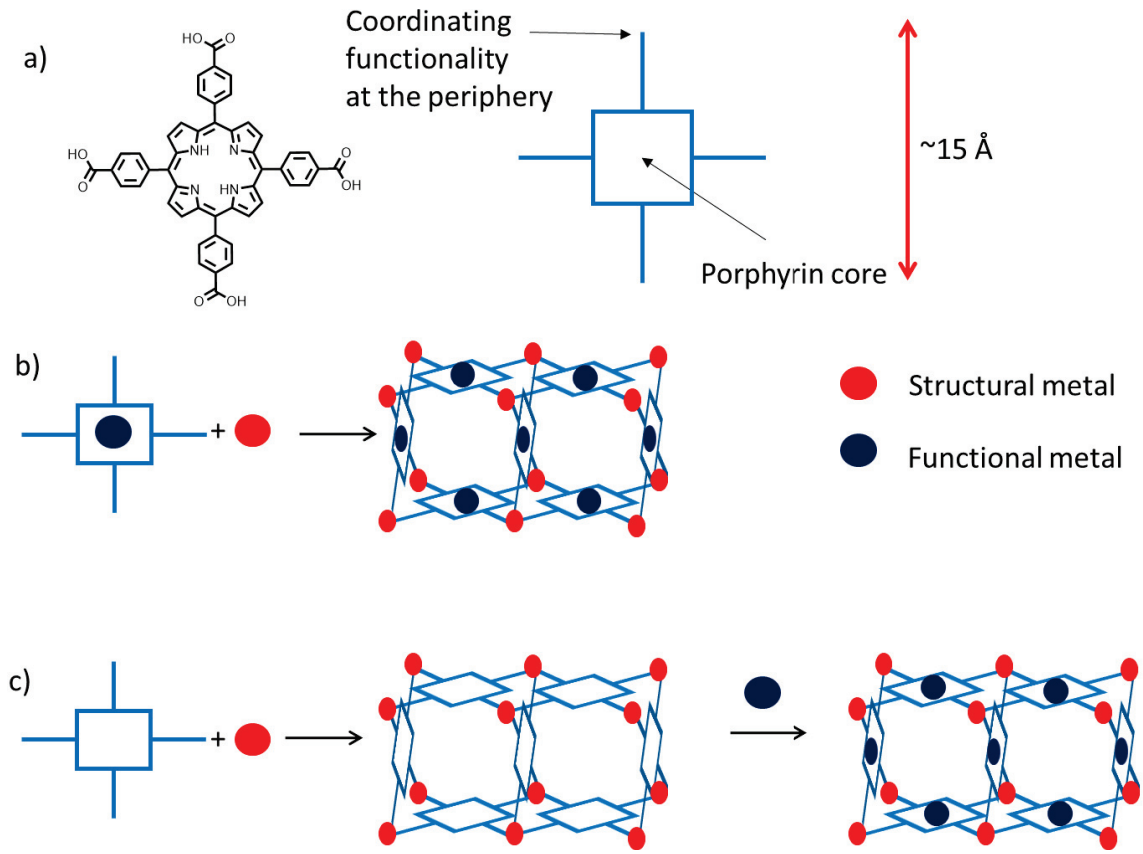

Figure 1-6 a) Schematic representation of a porphyrin ligand b) Synthesis starting with a metalated porphyrin ligand which leads to a heterobimetallic framework. c) Post-synthetic metalation of the porphyrin cores of the framework with a functional metal.

Robson et al were the first to report a porphyrin-based coordination polymer in 1991. The authors reported a three-dimensional framework made from palladium-based tetra pyridyl porphyrin ligands interconnected to cadmium ion nodes, $[Cd_2(NO_3)_2(PdTPyP)]\cdot$hydrate ($H_2$TPyP =5,10,15,20-tetra(pyridin-4-yl)porphyrin).[30] Since then the field of porphyrinic framework solids have received much attention.[31-32] The main groups conducting research in this field are summarised in Table 1-1.

Table 1-1 Main research groups which are currently conducting work on porphyrinic MOFs

Group	Speciality	Published Porphyrinic MOFs
Hupp group Northwestern University, Illinois.	Pillared MOFs with permeant porosity, light harvesting applications	ZnPO-MOF,[33] RPM-MOFs,[34] BOP-MOF,[35] DA-MOF,[36] Hf-NU-1000,[37] NU-902,[38] NU-1102,[39] NU-1104[39]
Zhou group Texas A&M University, Texas	Porous porphyrinic MOFs with high chemical stability	PCN-134,[40] PCN-221,[41] PCN-222,[42] PCN-223,[43] PCN-224,[44] PCN-225,[45] PCN-228,[46]PCN-229,[46] PCN-230,[46] PCN-526, [47] PCN-600,[48] PCN-22,[49], PCN-601,[50] PCN-602,[51] TPMOF-7,[52] SO-PCN[53]
Ma group University of South Florida, Florida	Porphyrinic MOFs for CO_2 capture	MMPF-1,[54] MMPF-2,[55] MMPF-4,[56] MMPF-5,[56] MMPF-6,[57] MMPF-7,[58] MMPF-8,[58] MMPF-9,[59] MMPF-14,[60] , MMPF-18[61]
Zhang group University of Nebraska-Lincoln, Nebraska	Photoactive porphyrinic MOFs	UNLPF-2,[62] UNLPF-10,[63] UNLPF-11,[64] UNLPF-12,[64] UNLPF-13,[65] UNLPF-14,[65] UNLPF-15,[65] UNLPF-16,[65]

Most of the reported porphyrinic MOFs have been based on the carboxylate moiety with divalent metal ions such as Zn^{2+}, Ni^{2+}, Co^{2+}, Cu^{2+} which is a natural extension of the fact that carboxylate based ligands have been the most studied in general MOF chemistry.[59, 66-67] However, the use of other functionalities such as pyrazolate can offer frameworks with enhanced chemical stability due to their increased basicity (discussed further in section 1.7). The next section will present a literature study on porphyrinic MOFs based on non-carboxylate based functionalities which have been reported.

1.6. Porphyrinic MOFs based on non-carboxylate functional groups

This section will look at all the reported MOFs constructed with symmetrical porphyrinic ligands with non-carboxylate functional groups. Only two-dimensional (2D) and three-dimensional (3D) structures were considered. Furthermore, coordination polymers reported where the polymer is extended via axial coordination of metalated cores were not included.

Pyridyl

Pyridyl functionality is the second most studied after the carboxylate functionality with regards to porphyrinic MOFs with 11 different types of 2D and 3D structures reported. In fact, the first porphyrinic MOF reported by Robson et al was synthesized using a porphyrinic ligand with the pyridyl functionality (5,10,15,20-tetra(4-pyridyl)porphyrin, H_2TPyP, Figure 1-7a).[30] This section will look at some recent examples of porphyrinic MOFs built using this functionality.

Table 1-2 Reported porphyrinic MOFs constructed using ligands with pyridyl functionality in literature. Only 2D and 3D MOF frameworks were considered.

Ref Code	Formula	Net type	reference
BAKKIH	$[(PbI_2)(H_2TPyP)]\cdot 4TCE$	2D	[68]
BAKNEG	$[(CdI_2)(H_2TPyP)]\cdot 4TCE$	2D	[68]
NUWCAK	$[Cu(hfacac)_2](CuTPyP)\cdot 6H_2O$	2D	[69]
COPVOU	$Cd(H_2O)_2(Mn^{III}(H_2O)_2TPyP)(PW_{12}O_{40})\}\cdot 10H_2O$	2D	[70]
COPVOA	$Cd(H_2O)_2(Mn^{III}(H_2O)_2TPyP)(PW_{12}O_{40})\}$	2D	[70]
COXXAP	$[(MnCl_2)(H_2TPyP)]\cdot 6TCE$	2D	[71]
FEWGEU	$[(Ag(m\text{-}C_6H_4NH_2Cl)_2)_2(H_2TPyP)](CH_3C_6H_4SO_3)_2$	2D	[72]
QAJBIP	$[Cu_4(CH_3COO^-)_8](CuTPyP)_1]\cdot 4C_6H_4Cl_2$	2D	[73]
TUSGIX	$[Ag_4(H_2TPyP)_3](NO_3)_4$	2D	[74]
TUSGOD	$[Ag_2(H_2TPyP)(NO_3)](NO_3)$	2D	[74]
UFOMAD	$[Pb(NO_3)_2(H_2TPyP)]\cdot C_{60}\cdot 1.5TCE$	2D	[75]
UFOMIL	$[Pb(NO_3)_2(H_2TPyP)]\cdot C_{70}\cdot nCH_2Cl_2\cdot nCH_3OH$	2D	[75]
WUHWIG	$[Cu^{I}_2(phen1)_2(CuTPyP)PF_6]\cdot 4C_6H_4Cl_2$	2D	[76]
DIFKAF	$[(Cu_2(CH_3COO)_4)_2(CuTPyP)\cdot 2CHCl_3]$	2D	[77]
XIHZOE	$HgI_2(H_2T3\text{-}PyP)\cdot C_{60}$	2D	[78]
YIRREY	$[Mn^{II}Cl_2(Mn^{III}TDPAP\text{-}Cl)(DMF)]$	2D	[79]
YIRRAU	$[Cu_3(CuTDPAP)(CH_3COO)_5(HCOO)(CH_3COOH)(H_2O)_3]\cdot CH_3COOH\cdot H_2O$	2D	[79]
YIRQUN	$[Cd_2(H_2TDPAP)(CH_3COO)_4]\cdot DMF\cdot CH_3COOH\cdot 2H_2O$	2D	[79]
CAGKIG	$(CdI_2)(H_2TPyP)$	3D	[80]
CAGKIG01	$(CdI_2)(H_2TPyP)$	3D	[80]
CAGKIG02	$(CdI_2)(H_2TPyP)$	3D	[80]
CAZGIT	$(Cu_2Mo_3O_{11})(CuTPyP)$	3D	[81]
IZULUL	$[Zn_2(H_2O)_4(Sn^{IV}TPyP)(HCOO)_2]\cdot 4NO_3^-\cdot DMF\cdot 4H_2O$	3D	[82]
PIZJEN	$Cu^{I}(Cu^{II}TPyP)\cdot BF_4$	3D	[83]
PUZCUJ	$[Nd(NO_3)_3(H_2O)_2](H_2TPyP)\cdot 3(o\text{-DCB})$	3D	[84]
PUZDAQ	$[Gd(NO_3)_3(H_2O)_2](H_2TPyP)\cdot 3(o\text{-DCB})$	3D	[84]
PUZDEU	$[Tb(NO_3)_3(H_2O)_2](H_2TPyP)\cdot 3(o\text{-DCB})$	3D	[84]
PUZFUM	$[Sm(NO_3)_3(H_2O)_2](H_2TPyP)\cdot 3(o\text{-DCB})$	3D	[84]
RAGBOR	$[(Cu_2V_2O_2(O_3PC_6H_5)_4)(CuTPyP)]\cdot 2H_2O$	3D	[85]

RAGBUX	$[(V_4O_4(O_3PC_6H_5)_4)(NiTPyP)]\cdot 2H_2O$	3D	[85]
SOBTUY	$[Cd_2(NO_3)_2(PdTPyP)]\cdot 8.6H_2O$	3D	[30]
AZIVA	$[CuCl_2(CuTPyP)]\cdot 2.5TCE\cdot 7H_2O$	3D	[86]
UPOSIC	$CdCl_2(H_2T3\text{-}PyP)$	3D	[87]
UPOSOI	$CdCl_2DMF(CdT3\text{-}PyP)$	3D	[87]
XUGSEY	$Zn_2(tcb)(ZnPFDpyP)$	3D	[33]
IBAPIM	$Zn_2(AlTCPP\text{-}OH)(ZnPFDpyP)$	3D	[34]
IBAPOS	$Zn_2(FeTCPP\text{-}Cl)(ZnPFDpyP)$	3D	[34]
IBAPUY	$Zn_2(PdTCPP)(MnPFDpyP\text{-}Cl)$	3D	[34]
IBAQAF	$Zn_2(ZnTCPP)(MnPFDpyP\text{-}Cl)$	3D	[34]
IBAQEJ	$Zn_2(ZnTCPP)(ZnPFDpyP)$	3D	[34]
Not reported	$Zn_2(tcb)(ZnDPEP)$	3D	[36]

TCE = Tetrachloroethane,

$(PW_{12}O_{40})^{3-}$ = phosphomolybdate anion

hfacac = 1,1,1,5,5,5-hexafluoroacetylacetonate

o-DCB= *o*-dichlorobenzene

phen1=dimesityl-(1,10)-phenanthroline

tcb = 1,2,4,5-tetrakis(4-carboxyphenyl)benzene

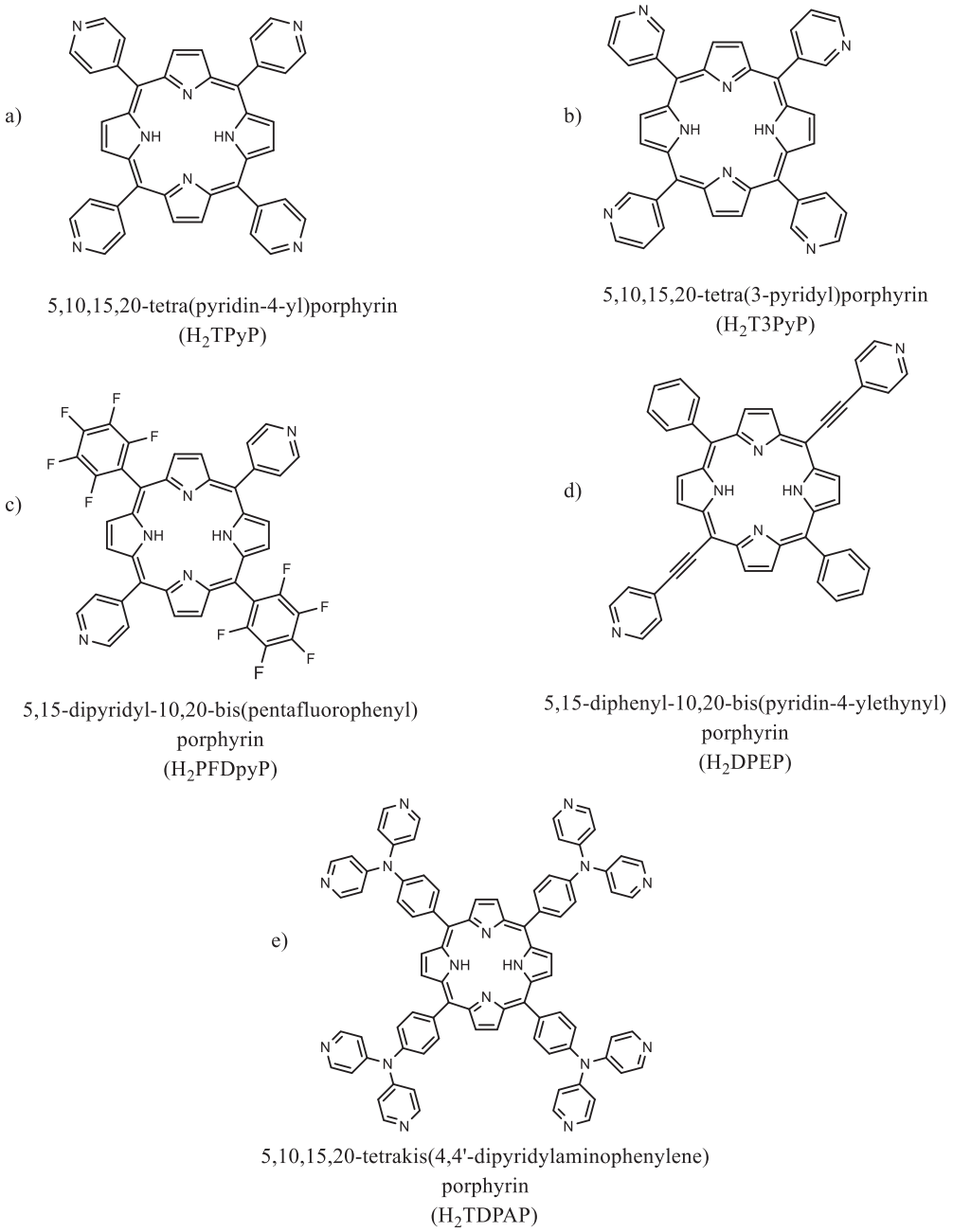

Figure 1-7 Pyridyl based porphyrinic ligands used for the construction of 2D and 3D MOFs

Wu et al. reported a 3D porous MOF, $[Zn_2(H_2O)_4Sn^{IV}(TPyP)(HCOO)_2]\cdot 4NO_3\cdot DMF\cdot 4H_2O$, which has a structure constructed from lamellar networks of tin(IV)-TPyP porphyrin struts linking with Zn nodes in the ab plane (Figure 1-8).[82] The lamellae are linked by formate ions through coordination with Sn^{4+} centres to extend the structure in 3D. The MOF showed photocatalytic activity for the photo-oxygenation of 1,5-dihydroxynaphthalene and sulfides under Xe lamp irradiation with excellent yield (up to 99%).

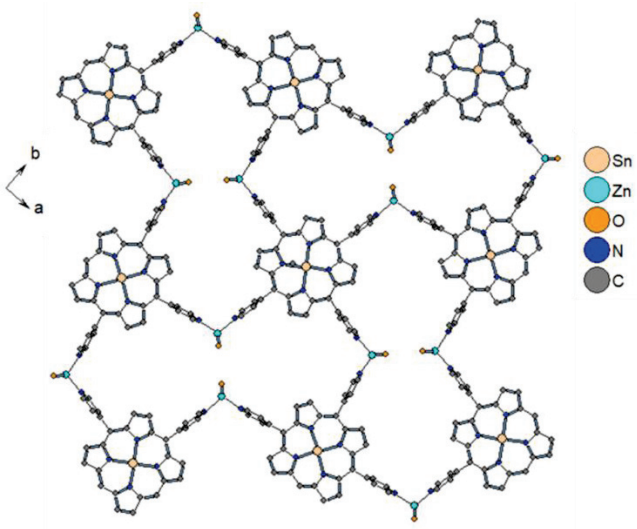

Figure 1-8 The structure of $[Zn_2(H_2O)_4Sn^{IV}(TPyP)(HCOO)_2]\cdot 4NO_3\cdot DMF\cdot 4H_2O$ reported by Wu et al. viewed along the c axis.[82] Hydrogens and solvent molecules are omitted for clarity.

Pyridyl group containing porphyrin ligands have been used to construct 3D pillared MOFs where the N-atoms coordinate to a paddle wheel like SBU at the axial position. Hupp et al. reported a series of robust MOFs with the pyridyl containing ligand, (5,15-dipyridyl-10,20-bis(pentafluorophenyl))porphyrin (H_2PFDPyP) (Figure 1-9). ZnPO-MOF [Zn_2(tcb)(ZnPFDpyP), tcb=1,2,4,5-tetrakis(4-carboxyphenyl)benzene] has Zn paddlewheel SBUs connected to 4 different tcb ligands making 2D layers (Figure 1-9a).[33] These layers are pillared by the ZnPFDPyP at the axial positions of the Zn paddlewheel SBU. Authors reported a gas accessible surface area of ~500 m^2/g for the framework (calculated by applying non-local density functional theory, NLDFT, analysis). ZnPO-MOF showed catalytic activity for the acyl-transfer reaction between *N*-acetylimidazole and 3-pyridyl carbinol which was attributed to the accessible Zn sites in the porphyrin core.

Following the previous work, Hupp et al reported a MOF with the use of the same H_2PFDPyP ligand along with the H_2TCPP [5,10,15,20-tetrakis(4-carboxyphenyl)porphyrin] ligand instead of the tcb (Figure 1-9b).[34] Furthermore, by using metalated varieties for the TCPP and the PFDPyP ligands, MOFs with different metalloporphyrins were obtained. The more spacious ligand led to a higher gas accessible surface area (1000 m^2g^{-1}, calculated by applying NLDFT analysis). Furthermore, one of the MOFs with this latter phase showed catalytic activity towards epoxidation reaction of styrene and hydroxylation of cyclohexane due to the accessible Mn(III) sites in the porphyrin core.

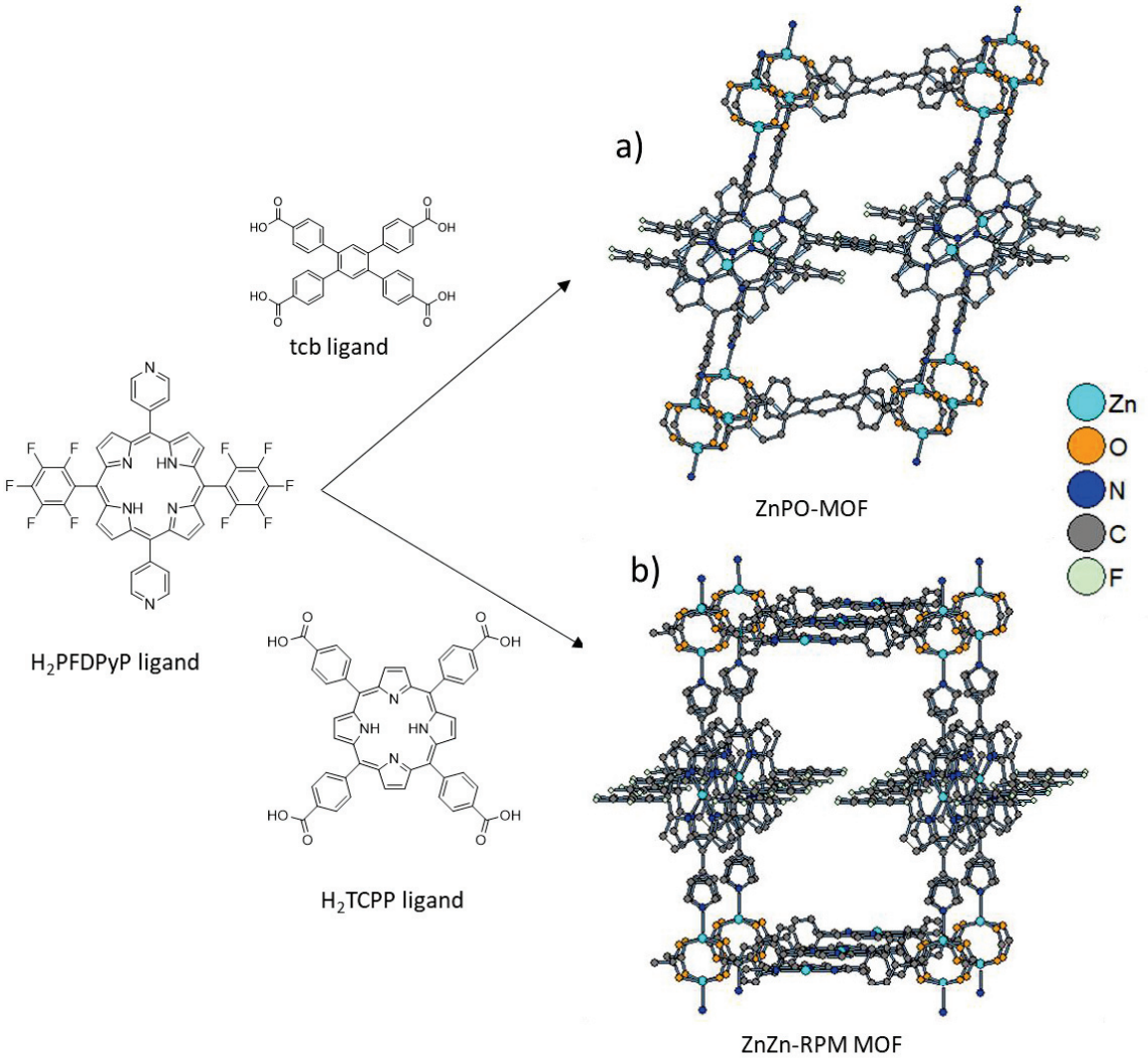

Figure 1-9 Ligands used to synthesise a) ZnPO MOF [33] b) ZnZn-RPM MOF [34] [tcb= 1,2,4,5-tetrakis(4-carboxyphenyl)benzene, H_2TCPP= 5,10,15,20-tetrakis(4-carboxyphenyl)porphyrin, H_2PFDPyP= (5,15-dipyridyl-10,20-bis(pentafluorophenyl))porphyrin]. Hydrogens and solvent molecules are omitted for clarity.

Nitrile

Table 1-3 Reported porphyrinic MOFs constructed using ligands with nitrile functionality in literature. Only 2D and 3D MOF frameworks were considered.

Ref Code	Formula	Net type	reference
PIZJAJ	$Cu^{I}(Cu^{II}TCP)\cdot BF_4$	3D	[83]

Robson et al reported a three-dimensional solid with the PtS topology constructed from copper(II) metalated 5,10,15,20-tetrakis(4-cyanophenyl)porphyrin (CuTCP, Figure 1-10a) which acts as the 4-connected square planar building block and Cu(I) which acts as the tetrahedral metal centre. The network obtained was two-fold interpenetrated and failed to survive removal of solvent molecules. [83]

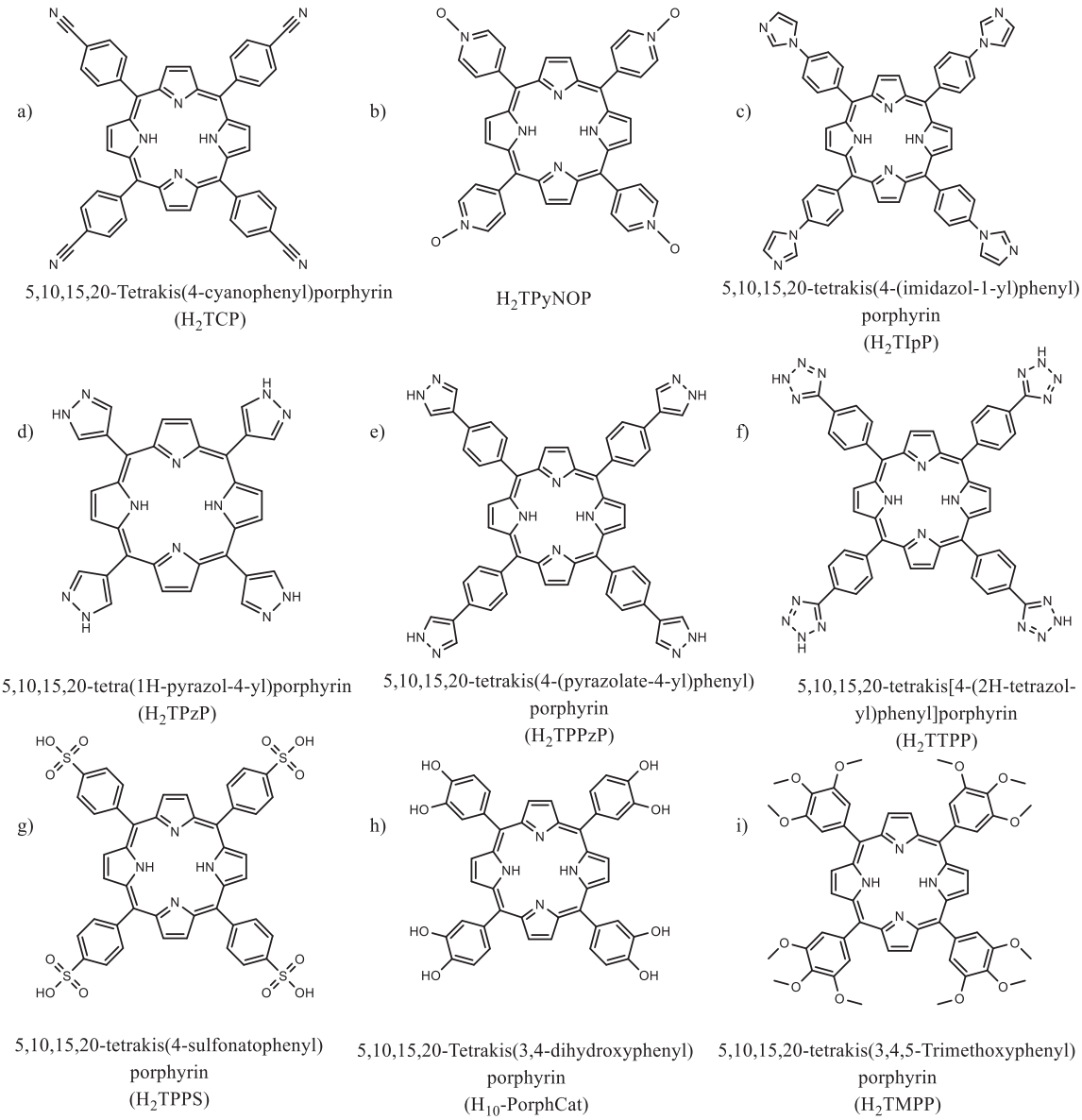

Figure 1-10 Porphyrinic ligands with other functional moieties used in the synthesis of 2D and 3D MOFs.

Pyridyl-N-oxide

Table 1-4 Reported porphyrinic MOFs using ligands with pyridyl-N-oxide functionality in literature. Only 2D and 3D MOF frameworks were considered.

Ref Code	Formula	Net type	reference
NIPNIK	Hg_2Br_4(NiTPyNOP)	3D	[88]

A 3D distorted diamanoid framework, Hg_2Br_4(NiTPyNOP), was reported by Deiters et al, with a Ni metalated pyridyl-N-oxide functionalized porphyrin, NiTPyNOP (Figure 1-10b) and Hg metal nodes. [88]

Imidazolate

Table 1-5 Reported porphyrinic MOFs using ligands with imidazolate functionality in literature. Only 2D and 3D MOF frameworks were considered.

Ref Code	Formula	Net type	reference
KASTIK	$[Cd_2(CdTIpP)(bpdc)_2]\cdot DMA\cdot 9H_2O$	3D	[89]

H_2bpdc = biphenyl-4,4'-dicarboxylic acid, DMA = N,N'-dimethylacetamide

Jiang et al reported a 3D framework, $[Cd_2(CdTIpP)(bpdc)_2]\cdot DMA\cdot 9H_2O$ (H_2TIpP = 5,10,15,20-tetrakis(4-(imidazol-1-yl)phenyl)porphyrin, Figure 1-10c, H_2bpdc= biphenyl-4,4'-dicarboxylic acid, DMA = N,N'-dimethylacetamide), which had a mog (moganite) topology.[89] The porphyrin was metalated during the reaction to afford the 4-connected SBU Cd(II)TIpP. The octahedral Cd(II) ions acted as the 4-connected metal nodes with two different coordinated Cd(II)-TIpP units and two different coordinated $bpdc^{2-}$ anions. The authors did not report the BET surface area, but the framework was intact after activation at 100 °C. The potential of this MOF as a heterogeneous catalyst was demonstrated for the cynanosilylation of aldehydes and ketones with various substrates under solvent-free conditions.

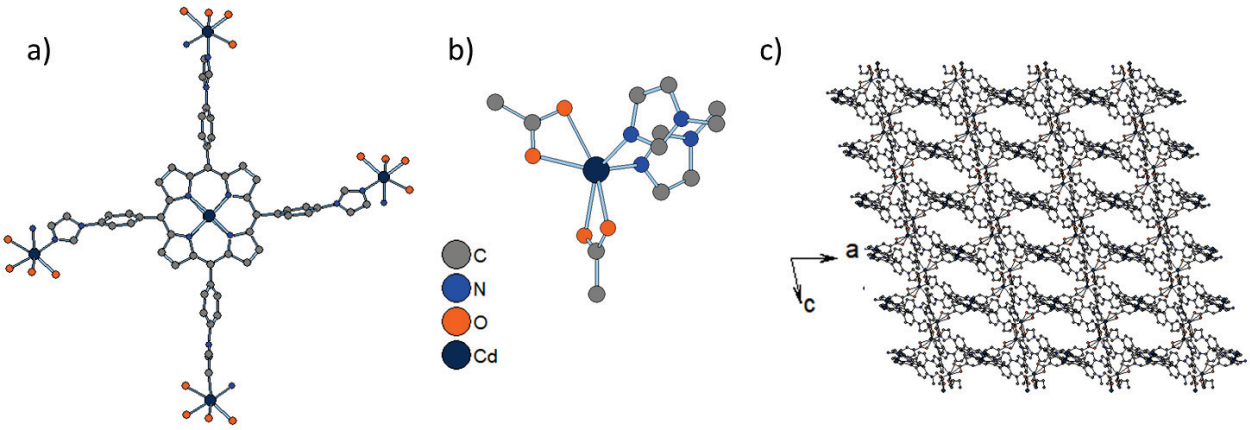

Figure 1-11 a) Coordination of the 4-connected Cd(II)TIpP unit (b) Octahedral coordination at Cd(II) centres to two different Cd(II)TIpP units and two different $bpdc^{2-}$ anions b) 3D framework of $Cd_2(CdTIpP)(bpdc)_2]\cdot DMA\cdot 9H_2O$ viewed along the b axis.[89]

Pyrazolate

Table 1-6 Reported porphyrinic MOFs using ligands with pyrazolate functionality in literature. Only 2D and 3D MOF frameworks were considered.

Ref Code	Formula	Net type	reference
MALMAQ	$[Ni_8(OH)_4(H_2O)_2](NiTPzP)_3$	3D	[50]
BALNAG	$[Ni_8(OH)_4(H_2O)_2](NiTPPzP)_3$	3D	[51]

Wang et al reported the first pyrazolate based porphyrinic MOF, PCN-601. The MOF is constructed from 12-connected $[Ni_8(OH)_4(H_2O)_2(pyrazolate)_{12}]$ nodes and 4-connected 5,10,15,20-tetra(1*H*-pyrazol-4-yl)porphyrin (H_2TPzP, Figure 1-10d) linkers and had a ftw-a topology (Figure 1-12).[50] The structure was determined via high resolution pxrd and Rietveld refinement as single crystals were not obtained. The porous framework had a BET surface area of 1309 $m^2 g^{-1}$ and the porosity was maintained after treatment with saturated NaOH solution at room temperature and at 100 °C for 24 hours. This high stability of the framework is due to the strong coordination bonds between the highly basic pyrazolate group and the metal cluster.

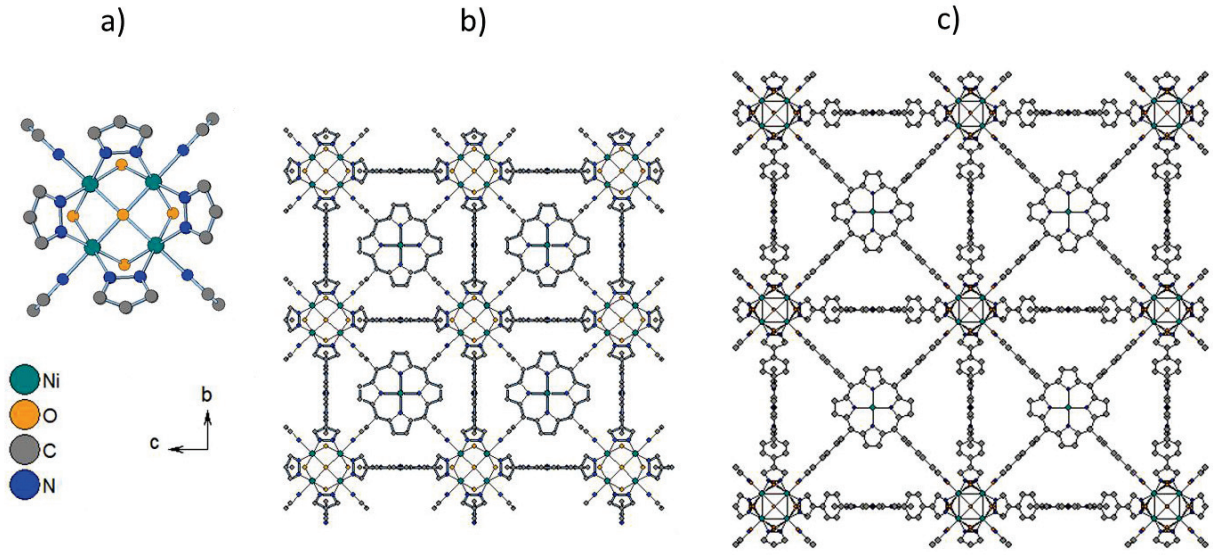

Figure 1-12 a) 12-connected $[Ni_8(OH)_4(H_2O)_2(pyrazolate)_{12}]$ with O_h symmetry b) PCN-601[50] c)PCN-602 [51]. Solvent molecules and hydrogen atoms are omitted for clarity.

In order to increase the pore window size of PCN-601 (~2.1 × 8.0 Å after deducting Van der Waals radii) the authors used an extended version of the ligand: 5,10,15,20-tetrakis(4-(1*H*-pyrazol-4-yl)phenyl)porphyrin (H_2TPPzP, Figure 1-10e) to obtain PCN-602 (Figure 1-12).[51] The new MOF had a larger pore window size of 6.3 × 14.2 Å and a higher BET surface area of 2219 $m^2 g^{-1}$. PCN-602 displayed stability in various solutions such as 1M KF, pH 4 HCl, pH 14 NaOH when exposed for 24

hours. Furthermore, the Mn metalated PCN-602 showed heterogeneous catalytic activity for the C-H bond halogenation of cyclohexane with high yield.

Tetrazolate

Table 1-7 Reported porphyrinic MOFs using ligands with tetrazolate functionality in literature. Only 2D and 3D MOF frameworks were considered.

Ref Code	Formula	Net type	reference
DOZCEC	$[Mn(II)_{4.5}Cl(Mn(III)Cl\text{-}TTPP)_2(H_2O)_4]\cdot(DEF)_{20}\cdot(CH_3OH)_{18}\cdot(H_2O)_{12}$	3D	[90]
UQOFEN	$[Cd_{4.5}Cl(CdTTPP)_2]$	3D	[47]
DAMRER	$[Fe^{II}pzTTPP(Fe^{II}_{1-x}DMF_{1-x}Fe^{III}_xOH_x)]$ (x ≥ 0.25)	3D	[91]

DEF = *N*,*N*'-diethylformamide

There are only three reported porphyrinic MOFs based on the tetrazolate functionality with the ligand, 5,10,15,20-tetrakis(4-(2H-tetrazol-5-yl)phenyl)porphyrin, (H_2TTPP, Figure 1-10f). Two of the reported frameworks, UTSA-57[90] and PCN-526[47] had the same topology with 8-connected $M_4Cl(ttz)_8$ clusters as the inorganic SBU with Mn and Cd as the metals respectively (for charge balance there are Mn^{2+} and Cd^{2+} ions present in the respective frameworks represented by $M_{0.5}$ in the formulae). The third one was obtained during this work; these materials will be further discussed in chapter 4.

Sulfonate

Table 1-8 Reported porphyrinic MOFs using ligands with sulfonate functionality in literature. Only 2D and 3D MOF frameworks were considered.

Ref Code	Formula	Net type	reference
DIBJEF	$[Eu_6(\mu_3\text{-}OH)_8(H_2O)_2](H_2TPPS)_3\cdot 2H_3O^+$	3D	[92]
DIBJIJ	$[Eu_6(\mu_6\text{-}O)(\mu_3\text{-}OH)_8(H_2O)_{14}](H_2TPPS)_2$	3D	[92]
PUFNUB	$[Sm(H_2TPPS)](H_3O)]\cdot H_2O$	3D	[93]
SUBGIH	$[Tb(CoTPPS)(H_3O)]\cdot 2H_2O$	3D	[94]
UQUCUG	$[Gd(H_2TPPS)(]H_3O)]\cdot nH_2O$	3D	[95]
WADHUH	$[Eu(VTPPS)H_2O]$	3D	[96]
WADJAP	$[Tb(VTPPS)H_2O]$	3D	[96]
WADJET	$[Dy(VTPPS)H_2O]$	3D	[96]
XUGWAZ	$[Dy(H_2TPPS)(H_3O)]\cdot 2H_2O$	3D	[97]
YIVWIL	$[Eu(ZnTPPS)H_3O]$	3D	[98]
ABEFUL	$[Tb(H_2TPPS)H_3O]$	3D	[99]
RALZAH	$[Sm(VOTPPS)\ H_3O]$	3D	[100]
RALZEL	$[Sm(VOTPPS)\ H_3O]\cdot 2N_2$	3D	[100]
HIYBEY	$[Tb(ZnTPPS)H_3O]$	3D	[101]
FASGIS	$[Tb(H_2O)_3](CoTPPS)H_3O]$	3D	[102]
FARXUU	$[Sm(His)(H_2O)][Sm(H_3O)_3](H_2TPPS)_2]\cdot 5H_2O$	3D	[103]

There are three different structure types reported for porphyrinic MOFs built up with this functionality. Demel et al reported a europium-based MOF built with 5,10,15,20-tetrakis(4-sulfonatophenyl) porphyrin (H_2TPPS, Figure 1-10g) which underwent a structural transformation when dehydrated during the thermal activation process. The SBU was transformed from 6-connected $[Eu_6(\mu_6\text{-}O)(\mu_3\text{-}OH)_8(H_2O)_{14}]^{8+}$ to 12-connected $[Eu_6(\mu_3\text{-}OH)_8(H_2O)_2]^{10+}$.[92] However, it was not reported if this change was reversible.

Chen et al has reported a series of lanthanide based 3D MOFs using the H_2TPPS ligand with similar structures and a general formula of $[Ln(H_2TPPS)(H_3O)]$.[93-103] Frameworks with Zn, Co and V metalated porphyrin cores were obtained directly via a one pot synthesis by using suitable metal salts.[96, 98, 102] The framework was made up from a chain like inorganic SBU with Ln ions linked by four sulfonate groups from four different porphyrin units (Figure 1-13). The porphyrin units were connected to four different Ln ions and stack on top of each other along the c-axis. The framework had well defined 1D channels running along the c-axis.

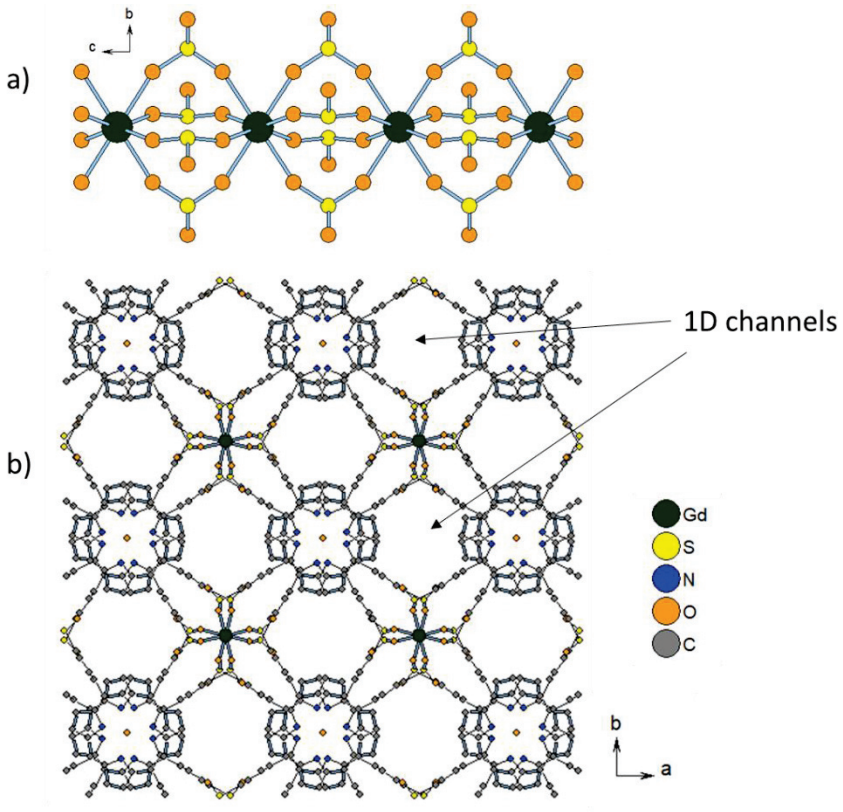

Figure 1-13 Structure of $[Ln(H_2TPPS)(H_3O)]$ reported by Chen et al. a) Chain like inorganic SBU in $[Gd(H_2TPPS)(]H_3O)]$ viewed along the a-axis. b) Framework viewed along the c-axis showing 1D channels in $[Gd(H_2TPPS)(H_3O)]$. [95] *Solvent molecules and hydrogen atoms are omitted for clarity.*

Catecholate

Table 1-9 Reported porphyrinic MOFs using ligands with catecholate functionality in literature. Only 2D and 3D MOF frameworks were considered.

Ref Code	Formula	Net type	reference
N/A	Not reported	Not reported	[104]

Jin et al reported several crystalline solids based on meso-tetrakis(3,4-dihydroxyphenyl)porphyrin (H_{10}-PorphCat, Figure 1-10h) and Cu, Co and Ni. The actual structures of these solids were not determined as the authors were interested in synthesizing hybrid composites via thermolysis. The BET surface areas reported by the authors were, 354 m^2g^{-1}, 135 m^2g^{-1}, 221 m^2g^{-1} respectively for the Ni, Co and Cu variants before thermolysis.

Trimethoxy

Table 1-10 Reported porphyrinic MOFs using ligands with trimethoxy functionality in literature.

Ref Code	Formula	Net type	reference
REZXAX	MgTMPP·CH2Cl2	1D	[105]
REZXEB	ZnTMPP·CH_2Cl_2	1D	[105]

There have been no 2D or 3D MOFs reported with trimethoxy functionalized porphyrins. However, Bhuyan et al reported two 1D coordination polymers, MgTMPP and ZnTMPP with a similar structure using the ligand 5,10,15,20-tetrakis(3,4,5-trimethoxyphenyl)porphyrin (H_2TMPP, Figure 1-10i). The two solids were synthesized by metalating the H_2TMPP with Mg and Zn. The metalated porphyrinic units self-assembled via axial coordination of the central metal ion with two different methoxy group oxygens from two adjacent units resulting in the 1D coordination polymer (Figure 1-14). This ligand was mentioned due to its similarity with one of the ligands investigated in this work, 5,10,15,20-tetrakis(3,4,5-trihydroxyphenyl)porphyrin (H_{14}-PorphGal), which has hydroxyl groups instead of the methoxy groups.

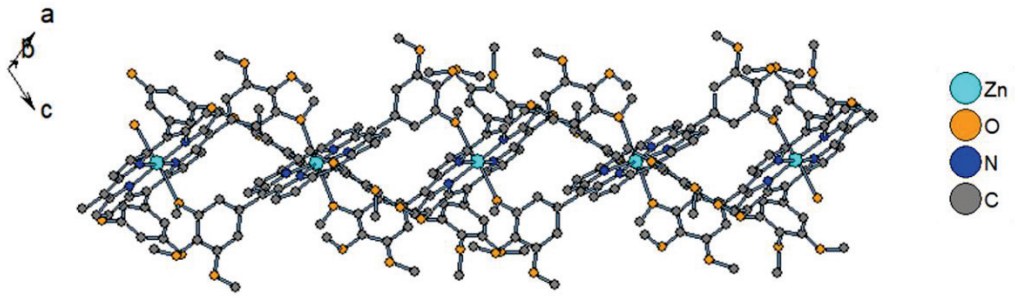

Figure 1-14 1D coordination network of ZnTMPP. Hydrogen atoms are omitted for clarity.

1.7. Limitations of current Porphyrinic MOFs

The poor chemical stability of carboxylate MOFs based on divalent metal ions such as Zn^{2+}, Cu^{2+} particularly in regards to water exposure is well known. MOF-5 [$Zn_4O(BDC)_3$ BDC^{2-}=1,4-benzodicarboxylate] which is based on Zn^{2+} is known to rapidly degrade on exposure to humidity even at room temperature.[106] Some MOFs such as HKUST-1 [$Cu_3(BTC)_2$ BTC^{3-}=1,3,5-benzenetricarboxylate] show moderate steam stability[107] but degrades over time in water at room temperature.[108] Two mechanisms have been proposed for the degradation of carboxylate based MOFs with exposure to water due to the breaking of the M-O linkage (Figure 1-15). Ligand displacement is where a water molecule is inserted in to M-O bond which leads to the formation of a hydrated metal ion and a free ligand (Figure 1-15a) while hydrolysis involves the cleavage of the M-O bond and the dissociation of water into a hydroxide ion and a proton (Figure 1-15b).[107] As mentioned earlier, most porphyrinic MOFs are built up using the carboxylate functionality and divalent metal ions. Thus, they share the same limitations regarding chemical stability as general carboxylate MOFs. This is a major issue as stability in water is essential for any wide-scale use of MOFs as most applications such as separation processes or catalysis will involve exposure to humidity at some level.

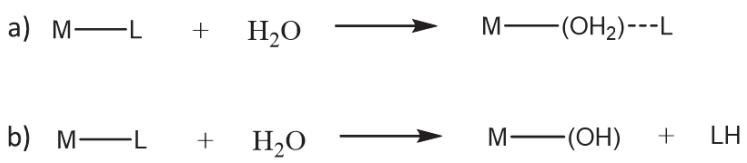

Figure 1-15 Proposed mechanisms for the breaking of the M-O linkage in carboxylate based MOFs in the presence of water. a) ligand displacement b) hydrolysis

The importance of the metal-ligand bond strength on the hydrothermal stability of MOFs was demonstrated in a study conducted by Low et al. The authors investigated the steam stability of various MOFs as a function of temperature and indicated that stronger metal-ligand bonds correlated with higher hydrothermal stability.[107] One way to increase the strength of the metal ligand bond is to increase the charge of the metal.[10] In the study mentioned, for carboxylate based MOFs, the ones built up with higher valence metals such as Cr^{3+} [Cr-MIL-101, $Cr_3F(H_2O)_2O(BDC)_3{\cdot}nH_2O$, BDC^{2-}= benzenedicarboxylate] and Al^{3+} [Al-MIL-53, Al(OH)[BDC]] showed higher hydrothermal stability than the MOFs with divalent Zn (MOF-5, MOF-69C) (Figure 1-16). The carboxylate anion can be considered as a hard base; thus, the increased charge density of higher valence metal ions can lead to stronger M-O bonds. The emergence of water stable carboxylate porphyrinic MOFs based on metal ions such as Zr^{4+}, Al^{3+} and Fe^{3+} has further demonstrated this increased chemical stability.

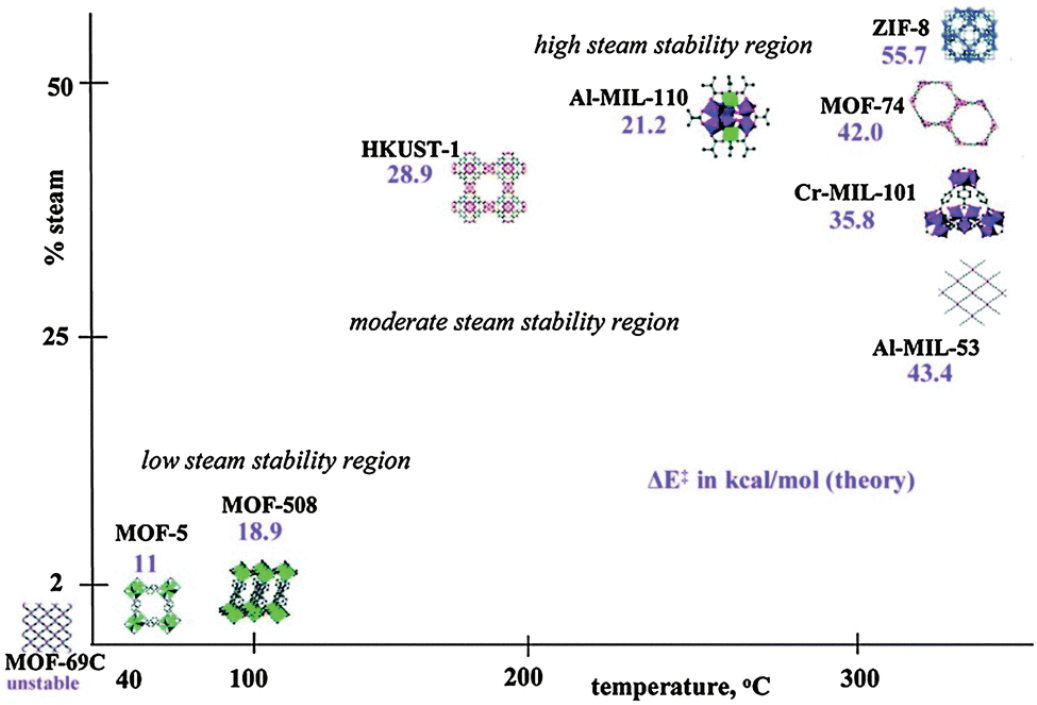

Figure 1-16 Steam stability map proposed by Low et al in their study.[107] Image reproduced from reference 107.

Zhou et al has reported several porphyrinic MOFs based on Zr clusters that have increased chemical stability.[42, 44-45] PCN-222 [chemical formula $Zr_6(\mu_3\text{-}OH)_8(OH)_8(H_2TCPP)_2$] is one such stable MOF with an 8 connected $Zr_6(\mu_3\text{-}OH)_8(OH)_8(COO)_8$ cluster and a 4-connected tetra(4-carboxyl-phenyl) porphyrin (TCPP) linker (Figure 1-17).[42] The authors reported that the framework can be obtained with the porphyrins in the free base form or metalated with Fe, Mn, Co, Ni, Cu and Zn by using metalloligands as the precursor. The 3D framework contains large hexagonal 1D open channels with a diameter of 3.7 nm along the c-axis. PCN-222(Fe) has a BET surface area of 2200 m^2g^{-1} and showed remarkable stability in boiling water and concentrated HCl solutions for 24 hours. Authors also demonstrated the ability of the PCN-222(Fe) to act as an oxidation catalyst towards different substrates such as pyrogallol with hydrogen peroxide as the oxidant.

Al-PMOF reported by Fateeva et al[109] and $[Fe^{II}pzTCPP(Fe^{III}OH)_2]^4$ MOF reported by our lab are two examples of water stable porphyrinic MOFs which are built up from Al^{3+} and Fe^{3+} respectively. Both the MOFs have a similar framework with an infinite $[M(OH)O_4]_n$ chain inorganic SBU. These two MOF systems will be further discussed in chapter 3 of this work. Recently, a water stable MOF based on In^{3+} has also been reported which has the same inorganic SBU as the two MOFs mentioned earlier.[110]

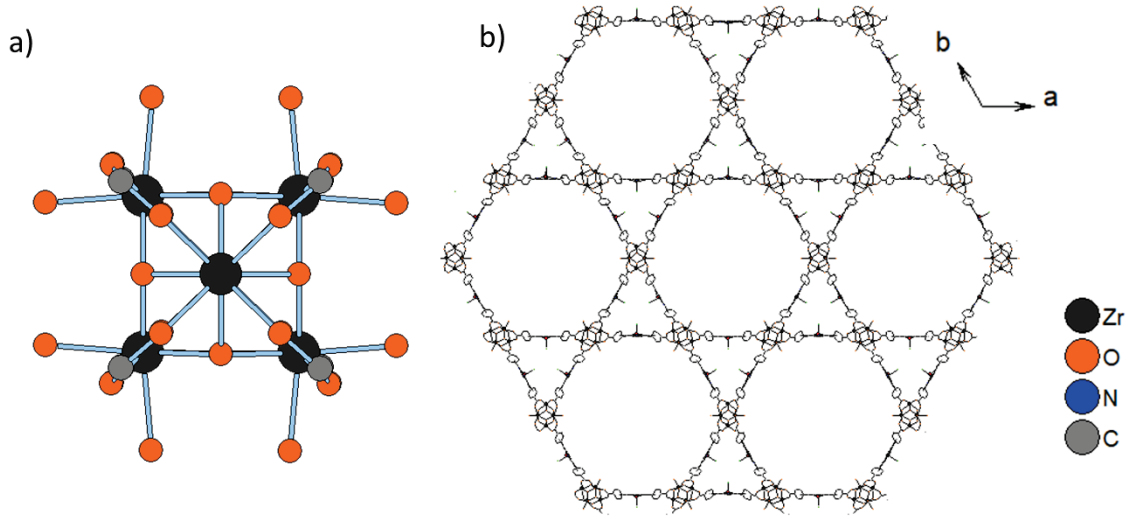

Figure 1-17 a) The 8-connected $Zr_6(\mu_3\text{-}OH)_8(OH)_8(COO)_8$ cluster of PCN-222 b) Framework of PCN-222 viewed along the c-axis. Hydrogens and solvent molecules are omitted for clarity.[42]

Another route to increasing the metal ligand bond strength in MOFs is the use of ligand functionalities which are more basic. Long et al suggested this with their work concerning MOFs which contained azolate based ligands where the strength of the M-L bond, hence the chemical stability correlated with the pK_a of the ligand used.[111] Thus, using functionalities with higher pK_a values than for the carboxylate group (pK_a ~4.76)[112] is a viable strategy to achieve stable structures.

Wang et al reported two porphyrinic MOFs based on the pyrazolate functionality (pK_a ~14)[112], PCN-601 and PCN-602, which displayed remarkable chemical stability in acidic and basic conditions as described earlier. [50]

Phenolates such as catecholates (pK_{a1} ~9.5; pK_{a2} ~14)[113] and gallates (pK_{a1} ~9.3; pK_{a2} ~11; pK_{a3}~14)[113-114] also have pK_a values higher than the carboxylate groups and can lead to more stable MOFs. A MOF built up using the gallate functionality and Zr^{4+} reported by Mouchaham et al, MIL-163 [chemical formula Zr(H_2-TzGal), H_6-TzGal=5,5'-(1,2,4,5-tetrazine-3,6-diyl)bis(benzene-1,2,3-triol)], has displayed stability in boiling water and in phosphate buffer solution (pH 7.4).[115] Nguyen et al reported a catecholate based MOF, Fe-CAT-5 [chemical formula Fe(THO)·Fe(SO_4) $(DMA)_3$, THO^{6-} = triphenylene-2,3,6,7,10,11-hexakis(olate), DMA = dimethylammonium] which was stable in water.[116] However, there have been no porphyrinic MOFs reported using the gallate functionality and there is only one report of a coordination polymer constructed from a catecholate porphyrinic ligand. Therefore, using gallate and catecholate functionalities to obtain MOFs with enhanced water and chemical stability in general remains a path little explored.

There have been over 300 porphyrinic MOF structures reported in the Cambridge structural database (estimated using the MOF subset in the CSD database). However, the number of porphyrinic MOFs which have been reported to be stable in water (immersed in water for at least 24 hours) is limited and are summarised in Table 1-11. This highlights the difficulty of obtaining these stable materials.

Table 1-11 Porphyrinic MOFs which have been reported in literature to be stable in water (reported as stable after at least 24 hours of exposure to water)

MOF	Formula	Metals in the porphyrin core	Reference
Al-PMOF	$(AlOH)_2$ M-TCPP	H_2, Co^{2+}, Cu^{2+}, Zn^{2+}	109
	$[Fe^{II}pzTCPP(Fe^{III}OH)_2]$	Fe^{2+}	4
JLU-Liu7	$(InOH)_2(H_2TCPP)$	H_2	110
NUPF-1	$Zr_6(\mu_3\text{-}O)_4(\mu_3\text{-}OH)_4(OH)_4(H_2O)_4(ML)_2$	H_2, $Ru(CO)^{2+}$	117
NUPF-3	$[NH_2(CH_3)_2][In\text{-}InL\cdot(HCOO)\cdot(H_2O)]$	In^{3+}	118
MOF-525	$Zr_6O_4(OH)_4$(M-TCPP)$_3$	H_2, Cu^{2+}, Fe^{3+}	119
MOF-545	$Zr_6O_8(H_2O)_8$(M-TCPP)$_2$	H_2, Cu^{2+}, Fe^{3+}	119
PCN-134	$Zr_6O_4[OH]_6[H_2O]_2[BTB]_2$[M-TCPP]	H_2, Ni^{2+}	40
PCN-222	$Zr_6(\mu_3\text{-}OH)_8(OH)_8$(M-TCPP)$_2$	H_2, Fe^{3+}, Mn^{3+}, Co^{2+}, Ni^{2+}, Cu^{2+}, Zn^{2+}	42
PCN-224	$[Zr_6(\mu_3\text{-}OH)_8(OH)_{10}]_2$(M-TCPP)$_3$	H_2, Fe^{3+}, Co^{2+}, Ni^{2+},	44
PCN-225	$Zr_6(\mu_3\text{-}O)_4(\mu_3\text{-}OH)_4(OH)_4(H_2O)_4$(M-TCPP)$_2$	H_2, Zn^{2+}	45
PCN-230	$Zr_6O_4(OH)_4$(TCP-3)$_3$	H_2	46
PCN-600	$[Fe_3O(OH)]_2$(M-TCPP)$_3$	H_2, Fe^{3+}, Mn^{3+}, Co^{2+}, Ni^{2+}	48
PCN-601	$[Ni_8(OH)_4(H_2O)_2]$(NiTPzP)$_3$	Ni^{2+}	50
PCN-602	$[Ni_8(OH)_4(H_2O)_2]$(NiTPPzP)$_3$	Ni^{2+}	51
CAU-18a	$[Ce_4(H_2TCPP)_3]\cdot 22H_2O$	H_2	120
CAU-19-H	$[Ce_3$(M-TCPP)$_2$(benzoate)$(H_2O)_2$	H_2, Co^{2+}, Zn^{2+}	120
Ir-PMOF-1(Hf)	$(Hf_6(\mu_3\text{-}O)_8(OH)_2(H_2O)_{10}]_2(Ir(TCPP)Cl)_3$	Ir^{3+}	121
FJI-H6	$Zr_6O_4(OH)_4(H_2TBPP)_3$	H_2, Cu^{2+}	122
FJI-H7	$Hf_6O_4(OH)_4(H_2TBPP)_3$	H_2, Cu^{2+}	122

BTB= benzene tribenzoate

Refer to Figure 1-18 for H_2TCPP, H_2TBPP, H_2TCP-3 and HL

Refer to Figure 1-10 for H_2TPzP and H_2TPPzP

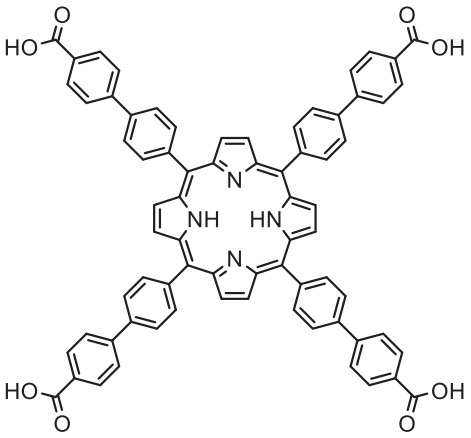

4',4''',4'''',4''''''-(porphyrin-5,10,15,20-tetrayl) tetrakis(([1,1'-biphenyl]-4-carboxylic acid)) (H_2TBPP)

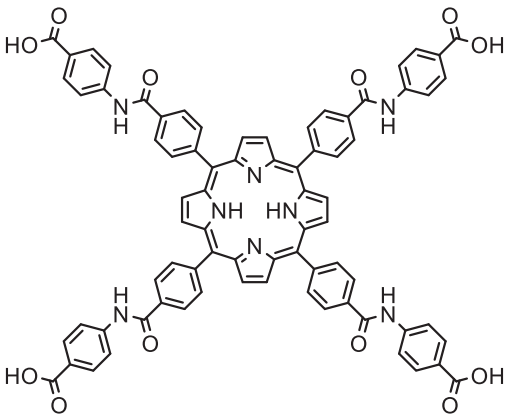

4,4',4'',4'''-((4,4',4'',4'''-(porphyrin-5,10,15,20-tetrayl)tetrakis(benzoyl)) tetrakis(azanediyl))tetrabenzoic acid (H_2L)

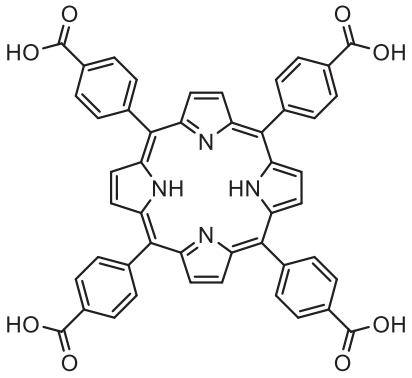

5,10,15,20-tetrakis(4-carboxyphenyl)porphyrin (H_2TCPP)

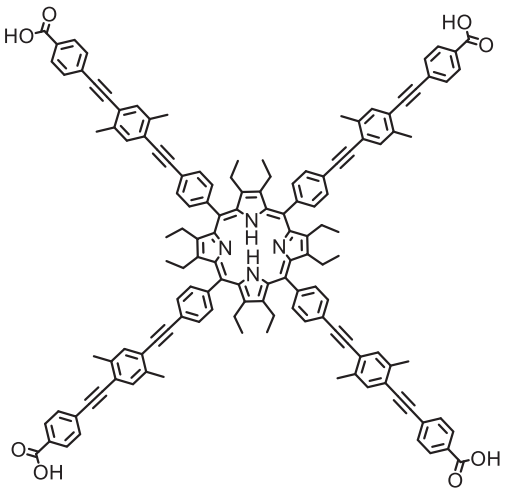

H_2TCP-3

Figure 1-18 Porphyrin ligands found in MOFs mentioned in Table 1-11

1.8. Objectives of this work

The main objective of this work was to design stable functional porous materials based on porphyrinic ligands and study their potential applications in catalysis. The ultimate goal was to understand the structure-activity relationship using these crystalline materials.

The strategy employed to achieve these materials was two-fold,

- Investigate existing stable carboxylate porphyrinic MOF platforms (Fe^{3+} and Al^{3+} based) and modify them to impart new functionalities.
- Explore the synthesis of novel MOFs by using porphyrinic ligands with functionalities which are less commonly seen in literature such as tetrazolate, catecholate and gallate with an aim of obtaining stable frameworks.

Therefore, four different types of porphyrin ligands were used for the work presented in this thesis (Figure 1-19). Chapter 2 will briefly discuss the properties of porphyrins in general and detail the synthesis and characterisation of these ligands.

Chapter 3 details the investigation in to two different MOF systems with TCPP based ligands and Fe^{3+} and Al^{3+} metal ions. Goal was to modify these systems to obtain new material with new potential functionalities. First system was based on Fe^{3+} which was published by our lab and attempts made to modify the framework of this MOF is presented in the first part of the chapter. Following this, the study of the reactivity of Fe^{3+} with a cobalt metalated TCPP is presented. The next part of the chapter details the efforts made to synthesise new variations of an Al^{3+} based MOF and present the preliminary catalysis work performed with these materials.

Chapter 4 discusses the article published by our group on a novel MOF based on the H_2TTPP ligand and Fe^{3+}. The chapter will briefly introduce tetrazolate based MOFs and the potential for obtaining extended frameworks with spin crossover properties with this ligand.

Chapter 5 focusses on MOF systems based on two hydroxyphenyl containing porphyrinic ligands, H_{10}-PorphCat and H_{14}-PorphGal. The first part of the chapter will detail the work done with H_{10}-PorphCat as part of a long-term study with the Institut Lavoisier de Versailles. Second part will discuss the exploratory work done with high valent metal ions and H_{14}-PorphGal which led to the synthesis of MOF frameworks with high chemical stability. The published article based on this stable MOF framework is also provided.

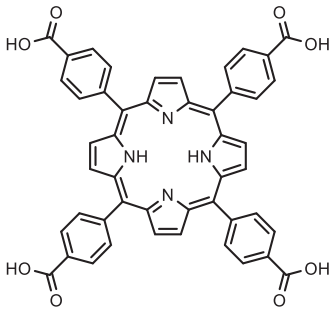

5,10,15,20-Tetrakis(4-carboxyphenyl) porphyrin
(H_2TCPP)

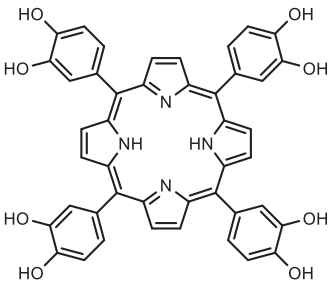

5,10,15,20-Tetrakis(3,4-dihydroxyphenyl)porphyrin
(H_{10}-PorphCat)

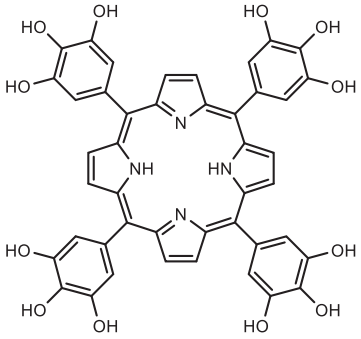

5,10,15,20-tetrakis(3,4,5-trihydroxyphenyl)porphyrin
(H_{14}-PorphGal)

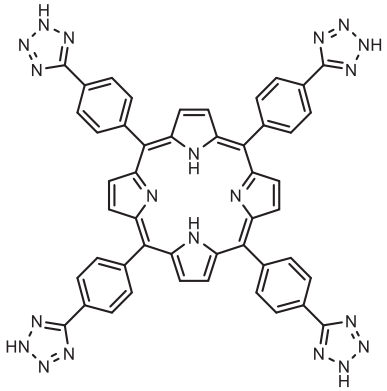

5,10,15,20-tetrakis(4-(2*H*-tetrazol-5-yl)phenyl)
porphyrin
(H_2TTPP)

Figure 1-19 Porphyrinic ligands investigated for MOF synthesis in this work.

1.9. References

1. Yilmaz, B.; Müller, U., Catalytic Applications of Zeolites in Chemical Industry. *Topics in Catalysis* **2009,** *52* (6), 888-895.
2. Hoskins, B. F.; Robson, R., Design and construction of a new class of scaffolding-like materials comprising infinite polymeric frameworks of 3D-linked molecular rods. A reappraisal of the zinc cyanide and cadmium cyanide structures and the synthesis and structure of the diamond-related frameworks [N(CH3)4][CuIZnII(CN)4] and CuI[4,4',4'',4'''-tetracyanotetraphenylmethane]BF4.xC6H5NO2. *Journal of the American Chemical Society* **1990,** *112* (4), 1546-1554.
3. Yaghi, O. M.; Li, G.; Li, H., Selective binding and removal of guests in a microporous metal-organic framework. *Nature* **1995,** *378* (6558), 703-706.
4. Fateeva, A.; Clarisse, J.; Pilet, G.; Grenèche, J.-M.; Nouar, F.; Abeykoon, B. K.; Guegan, F.; Goutaudier, C.; Luneau, D.; Warren, J. E.; Rosseinsky, M. J.; Devic, T., Iron and Porphyrin Metal–Organic Frameworks: Insight into Structural Diversity, Stability, and Porosity. *Crystal Growth & Design* **2015,** *15* (4), 1819-1826.
5. Taylor, J. M.; Mah, R. K.; Moudrakovski, I. L.; Ratcliffe, C. I.; Vaidhyanathan, R.; Shimizu, G. K. H., Facile Proton Conduction via Ordered Water Molecules in a Phosphonate Metal–Organic Framework. *Journal of the American Chemical Society* **2010,** *132* (40), 14055-14057.
6. Li, M.-X.; Miao, Z.-X.; Shao, M.; Liang, S.-W.; Zhu, S.-R., Metal-Organic Frameworks Constructed from 2,4,6-Tris(4-pyridyl)-1,3,5-triazine. *Inorganic Chemistry* **2008,** *47* (11), 4481-4489.
7. Choi, H. J.; Dinca, M.; Dailly, A.; Long, J. R., Hydrogen storage in water-stable metal-organic frameworks incorporating 1,3- and 1,4-benzenedipyrazolate. *Energy & Environmental Science* **2010,** *3* (1), 117-123.
8. Nordin, N. A. H. M.; Ismail, A. F.; Mustafa, A.; Goh, P. S.; Rana, D.; Matsuura, T., Aqueous room temperature synthesis of zeolitic imidazole framework 8 (ZIF-8) with various concentrations of triethylamine. *RSC Advances* **2014,** *4* (63), 33292-33300.
9. Eddaoudi, M.; Kim, J.; Rosi, N.; Vodak, D.; Wachter, J.; O'Keeffe, M.; Yaghi, O. M., Systematic Design of Pore Size and Functionality in Isoreticular MOFs and Their Application in Methane Storage. *Science* **2002,** *295* (5554), 469-472.
10. Devic, T.; Serre, C., High valence 3p and transition metal based MOFs. *Chemical Society reviews* **2014,** *43* (16), 6097-6115.
11. Zhang, M.; Bosch, M.; Gentle Iii, T.; Zhou, H.-C., Rational design of metal-organic frameworks with anticipated porosities and functionalities. *CrystEngComm* **2014,** *16* (20), 4069-4083.
12. Yaghi, O. M.; O'Keeffe, M.; Ockwig, N. W.; Chae, H. K.; Eddaoudi, M.; Kim, J., Reticular synthesis and the design of new materials. *Nature* **2003,** *423* (6941), 705-714.
13. Ferey, G., Hybrid porous solids: past, present, future. *Chemical Society reviews* **2008,** *37* (1), 191-214.
14. O'Keeffe, M.; Yaghi, O. M., Deconstructing the Crystal Structures of Metal–Organic Frameworks and Related Materials into Their Underlying Nets. *Chemical reviews* **2012,** *112* (2), 675-702.
15. Shen, J.-Q.; Wei, Y.-S.; Liao, P.-Q.; Lin, R.-B.; Zhou, D.-D.; Zhang, J.-P.; Chen, X.-M., Unique (3,9)-connected porous coordination polymers constructed by tripodal ligands with bent arms. *CrystEngComm* **2016,** *18* (22), 4115-4120.
16. Tonigold, M.; Lu, Y.; Bredenkötter, B.; Rieger, B.; Bahnmüller, S.; Hitzbleck, J.; Langstein, G.; Volkmer, D., Heterogeneous Catalytic Oxidation by MFU-1: A Cobalt(II)-Containing Metal–Organic Framework. *Angewandte Chemie International Edition* **2009,** *48* (41), 7546-7550.
17. Cavka, J. H.; Jakobsen, S.; Olsbye, U.; Guillou, N.; Lamberti, C.; Bordiga, S.; Lillerud, K. P., A New Zirconium Inorganic Building Brick Forming Metal Organic Frameworks with Exceptional Stability. *Journal of the American Chemical Society* **2008,** *130* (42), 13850-13851.

18. Devic, T.; David, O.; Valls, M.; Marrot, J.; Couty, F.; Férey, G., An Illustration of the Limit of the Metal Organic Framework's Isoreticular Principle Using a Semirigid Tritopic Linker Obtained by “Click” Chemistry. *Journal of the American Chemical Society* **2007,** *129* (42), 12614-12615.
19. Devic, T.; Serre, C.; Audebrand, N.; Marrot, J.; Férey, G., MIL-103, A 3-D Lanthanide-Based Metal Organic Framework with Large One-Dimensional Tunnels and A High Surface Area. *Journal of the American Chemical Society* **2005,** *127* (37), 12788-12789.
20. Zhuang, J.-L.; Ceglarek, D.; Pethuraj, S.; Terfort, A., Rapid Room-Temperature Synthesis of Metal–Organic Framework HKUST-1 Crystals in Bulk and as Oriented and Patterned Thin Films. *Advanced Functional Materials* **2011,** *21* (8), 1442-1447.
21. Stock, N.; Biswas, S., Synthesis of Metal-Organic Frameworks (MOFs): Routes to Various MOF Topologies, Morphologies, and Composites. *Chemical reviews* **2012,** *112* (2), 933-969.
22. Hu, Z.; Castano, I.; Wang, S.; Wang, Y.; Peng, Y.; Qian, Y.; Chi, C.; Wang, X.; Zhao, D., Modulator Effects on the Water-Based Synthesis of Zr/Hf Metal–Organic Frameworks: Quantitative Relationship Studies between Modulator, Synthetic Condition, and Performance. *Crystal Growth & Design* **2016,** *16* (4), 2295-2301.
23. Schaate, A.; Roy, P.; Godt, A.; Lippke, J.; Waltz, F.; Wiebcke, M.; Behrens, P., Modulated Synthesis of Zr-Based Metal–Organic Frameworks: From Nano to Single Crystals. *Chemistry – A European Journal* **2011,** *17* (24), 6643-6651.
24. Stock, N., High-throughput investigations employing solvothermal syntheses. *Microporous and Mesoporous Materials* **2010,** *129* (3), 287-295.
25. Sumida, K.; Horike, S.; Kaye, S. S.; Herm, Z. R.; Queen, W. L.; Brown, C. M.; Grandjean, F.; Long, G. J.; Dailly, A.; Long, J. R., Hydrogen storage and carbon dioxide capture in an iron-based sodalite-type metal-organic framework (Fe-BTT) discovered via high-throughput methods. *Chemical Science* **2010,** *1* (2), 184-191.
26. Bauer, S.; Serre, C.; Devic, T.; Horcajada, P.; Marrot, J.; Ferey, G.; Stock, N., High-throughput assisted rationalization of the formation of metal organic frameworks in the iron (III) aminoterephthalate solvothermal system. *Inorganic chemistry* **2008,** *47* (17), 7568-7576.
27. Banerjee, R.; Phan, A.; Wang, B.; Knobler, C.; Furukawa, H.; O'Keeffe, M.; Yaghi, O. M., High-Throughput Synthesis of Zeolitic Imidazolate Frameworks and Application to CO₂ Capture. *Science* **2008,** *319* (5865), 939-943.
28. Mansuy, D., A brief history of the contribution of metalloporphyrin models to cytochrome P450 chemistry and oxidation catalysis. *Comptes Rendus Chimie* **2007,** *10* (4–5), 392-413.
29. Chin, D.-H.; La Mar, G. N.; Balch, A. L., Mechanism of autoxidation of iron(II) porphyrins. Detection of a peroxo-bridged iron(III) porphyrin dimer and the mechanism of its thermal decomposition to the oxo-bridged iron(III) porphyrin dimer. *Journal of the American Chemical Society* **1980,** *102* (13), 4344-4350.
30. Abrahams, B. F.; Hoskins, B. F.; Robson, R., A new type of infinite 3D polymeric network containing 4-connected, peripherally-linked metalloporphyrin building blocks. *Journal of the American Chemical Society* **1991,** *113* (9), 3606-3607.
31. Gao, W.-Y.; Chrzanowski, M.; Ma, S., Metal-metalloporphyrin frameworks: a resurging class of functional materials. *Chemical Society reviews* **2014,** *43* (16), 5841-5866.
32. Huh, S.; Kim, S.-J.; Kim, Y., Porphyrinic metal-organic frameworks from custom-designed porphyrins. *CrystEngComm* **2016,** *18* (3), 345-368.
33. Shultz, A. M.; Farha, O. K.; Hupp, J. T.; Nguyen, S. T., A Catalytically Active, Permanently Microporous MOF with Metalloporphyrin Struts. *Journal of the American Chemical Society* **2009,** *131* (12), 4204-4205.
34. Farha, O. K.; Shultz, A. M.; Sarjeant, A. A.; Nguyen, S. T.; Hupp, J. T., Active-Site-Accessible, Porphyrinic Metal−Organic Framework Materials. *Journal of the American Chemical Society* **2011,** *133* (15), 5652-5655.

35. Lee, C. Y.; Farha, O. K.; Hong, B. J.; Sarjeant, A. A.; Nguyen, S. T.; Hupp, J. T., Light-Harvesting Metal–Organic Frameworks (MOFs): Efficient Strut-to-Strut Energy Transfer in Bodipy and Porphyrin-Based MOFs. *Journal of the American Chemical Society* **2011,** *133* (40), 15858-15861.
36. Son, H.-J.; Jin, S.; Patwardhan, S.; Wezenberg, S. J.; Jeong, N. C.; So, M.; Wilmer, C. E.; Sarjeant, A. A.; Schatz, G. C.; Snurr, R. Q.; Farha, O. K.; Wiederrecht, G. P.; Hupp, J. T., Light-Harvesting and Ultrafast Energy Migration in Porphyrin-Based Metal–Organic Frameworks. *Journal of the American Chemical Society* **2013,** *135* (2), 862-869.
37. Beyzavi, M. H.; Vermeulen, N. A.; Howarth, A. J.; Tussupbayev, S.; League, A. B.; Schweitzer, N. M.; Gallagher, J. R.; Platero-Prats, A. E.; Hafezi, N.; Sarjeant, A. A.; Miller, J. T.; Chapman, K. W.; Stoddart, J. F.; Cramer, C. J.; Hupp, J. T.; Farha, O. K., A Hafnium-Based Metal–Organic Framework as a Nature-Inspired Tandem Reaction Catalyst. *Journal of the American Chemical Society* **2015,** *137* (42), 13624-13631.
38. Deria, P.; Gómez-Gualdrón, D. A.; Hod, I.; Snurr, R. Q.; Hupp, J. T.; Farha, O. K., Framework-Topology-Dependent Catalytic Activity of Zirconium-Based (Porphinato)zinc(II) MOFs. *Journal of the American Chemical Society* **2016,** *138* (43), 14449-14457.
39. Wang, T. C.; Bury, W.; Gómez-Gualdrón, D. A.; Vermeulen, N. A.; Mondloch, J. E.; Deria, P.; Zhang, K.; Moghadam, P. Z.; Sarjeant, A. A.; Snurr, R. Q.; Stoddart, J. F.; Hupp, J. T.; Farha, O. K., Ultrahigh Surface Area Zirconium MOFs and Insights into the Applicability of the BET Theory. *Journal of the American Chemical Society* **2015,** *137* (10), 3585-3591.
40. Yuan, S.; Qin, J.-S.; Zou, L.; Chen, Y.-P.; Wang, X.; Zhang, Q.; Zhou, H.-C., Thermodynamically Guided Synthesis of Mixed-Linker Zr-MOFs with Enhanced Tunability. *Journal of the American Chemical Society* **2016,** *138* (20), 6636-6642.
41. Feng, D.; Jiang, H.-L.; Chen, Y.-P.; Gu, Z.-Y.; Wei, Z.; Zhou, H.-C., Metal–Organic Frameworks Based on Previously Unknown Zr8/Hf8 Cubic Clusters. *Inorganic Chemistry* **2013,** *52* (21), 12661-12667.
42. Feng, D.; Gu, Z.-Y.; Li, J.-R.; Jiang, H.-L.; Wei, Z.; Zhou, H.-C., Zirconium-Metalloporphyrin PCN-222: Mesoporous Metal–Organic Frameworks with Ultrahigh Stability as Biomimetic Catalysts. *Angewandte Chemie International Edition* **2012,** *51* (41), 10307-10310.
43. Feng, D.; Gu, Z.-Y.; Chen, Y.-P.; Park, J.; Wei, Z.; Sun, Y.; Bosch, M.; Yuan, S.; Zhou, H.-C., A Highly Stable Porphyrinic Zirconium Metal–Organic Framework with shp-a Topology. *Journal of the American Chemical Society* **2014,** *136* (51), 17714-17717.
44. Feng, D. W.; Chung, W. C.; Wei, Z. W.; Gu, Z. Y.; Jiang, H. L.; Chen, Y. P.; Darensbourg, D. J.; Zhou, H. C., Construction of Ultrastable Porphyrin Zr Metal-Organic Frameworks through Linker Elimination. *Journal of the American Chemical Society* **2013,** *135* (45), 17105-17110.
45. Jiang, H.-L.; Feng, D.; Wang, K.; Gu, Z.-Y.; Wei, Z.; Chen, Y.-P.; Zhou, H.-C., An Exceptionally Stable, Porphyrinic Zr Metal–Organic Framework Exhibiting pH-Dependent Fluorescence. *Journal of the American Chemical Society* **2013,** *135* (37), 13934-13938.
46. Liu, T.-F.; Feng, D.; Chen, Y.-P.; Zou, L.; Bosch, M.; Yuan, S.; Wei, Z.; Fordham, S.; Wang, K.; Zhou, H.-C., Topology-Guided Design and Syntheses of Highly Stable Mesoporous Porphyrinic Zirconium Metal–Organic Frameworks with High Surface Area. *Journal of the American Chemical Society* **2015,** *137* (1), 413-419.
47. Liu, D.; Liu, T.-F.; Chen, Y.-P.; Zou, L.; Feng, D.; Wang, K.; Zhang, Q.; Yuan, S.; Zhong, C.; Zhou, H.-C., A Reversible Crystallinity-Preserving Phase Transition in Metal–Organic Frameworks: Discovery, Mechanistic Studies, and Potential Applications. *Journal of the American Chemical Society* **2015,** *137* (24), 7740-7746.
48. Wang, K.; Feng, D.; Liu, T.-F.; Su, J.; Yuan, S.; Chen, Y.-P.; Bosch, M.; Zou, X.; Zhou, H.-C., A Series of Highly Stable Mesoporous Metalloporphyrin Fe-MOFs. *Journal of the American Chemical Society* **2014,** *136* (40), 13983-13986.
49. Yuan, S.; Liu, T.-F.; Feng, D.; Tian, J.; Wang, K.; Qin, J.; Zhang, Q.; Chen, Y.-P.; Bosch, M.; Zou, L.; Teat, S. J.; Dalgarno, S. J.; Zhou, H.-C., A single crystalline porphyrinic titanium metal-organic framework. *Chemical Science* **2015,** *6* (7), 3926-3930.

50. Wang, K.; Lv, X.-L.; Feng, D.; Li, J.; Chen, S.; Sun, J.; Song, L.; Xie, Y.; Li, J.-R.; Zhou, H.-C., Pyrazolate-Based Porphyrinic Metal–Organic Framework with Extraordinary Base-Resistance. *Journal of the American Chemical Society* **2016,** *138* (3), 914-919.
51. Lv, X.-L.; Wang, K.; Wang, B.; Su, J.; Zou, X.; Xie, Y.; Li, J.-R.; Zhou, H.-C., A Base-Resistant Metalloporphyrin Metal–Organic Framework for C–H Bond Halogenation. *Journal of the American Chemical Society* **2017,** *139* (1), 211-217.
52. Qin, J.-S.; Du, D.-Y.; Li, M.; Lian, X.-Z.; Dong, L.-Z.; Bosch, M.; Su, Z.-M.; Zhang, Q.; Li, S.-L.; Lan, Y.-Q.; Yuan, S.; Zhou, H.-C., Derivation and Decoration of Nets with Trigonal-Prismatic Nodes: A Unique Route to Reticular Synthesis of Metal–Organic Frameworks. *Journal of the American Chemical Society* **2016,** *138* (16), 5299-5307.
53. Park, J.; Feng, D.; Yuan, S.; Zhou, H.-C., Photochromic Metal–Organic Frameworks: Reversible Control of Singlet Oxygen Generation. *Angewandte Chemie International Edition* **2015,** *54* (2), 430-435.
54. Wang, X.-S.; Meng, L.; Cheng, Q.; Kim, C.; Wojtas, L.; Chrzanowski, M.; Chen, Y.-S.; Zhang, X. P.; Ma, S., Three-Dimensional Porous Metal–Metalloporphyrin Framework Consisting of Nanoscopic Polyhedral Cages. *Journal of the American Chemical Society* **2011,** *133* (41), 16322-16325.
55. Wang, X.-S.; Chrzanowski, M.; Kim, C.; Gao, W.-Y.; Wojtas, L.; Chen, Y.-S.; Peter Zhang, X.; Ma, S., Quest for highly porous metal-metalloporphyrin framework based upon a custom-designed octatopic porphyrin ligand. *Chemical communications* **2012,** *48* (57), 7173-7175.
56. Wang, X.-S.; Chrzanowski, M.; Gao, W.-Y.; Wojtas, L.; Chen, Y.-S.; Zaworotko, M. J.; Ma, S., Vertex-directed self-assembly of a high symmetry supermolecular building block using a custom-designed porphyrin. *Chemical Science* **2012,** *3* (9), 2823-2827.
57. Chen, Y.; Hoang, T.; Ma, S., Biomimetic Catalysis of a Porous Iron-Based Metal–Metalloporphyrin Framework. *Inorganic Chemistry* **2012,** *51* (23), 12600-12602.
58. Gao, W.-Y.; Zhang, Z.; Cash, L.; Wojtas, L.; Chen, Y.-S.; Ma, S., Two rare indium-based porous metal-metalloporphyrin frameworks exhibiting interesting CO2 uptake. *CrystEngComm* **2013,** *15* (45), 9320-9323.
59. Gao, W.-Y.; Wojtas, L.; Ma, S., A porous metal-metalloporphyrin framework featuring high-density active sites for chemical fixation of CO2 under ambient conditions. *Chemical communications* **2014,** *50* (40), 5316-5318.
60. Zhang, W.; Wojtas, L.; Aguila, B.; Jiang, P.; Ma, S., Metal–Metalloporphyrin Framework Modified with Flexible tert-Butyl Groups for Selective Gas Adsorption. *ChemPlusChem* **2016,** *81* (8), 714-717.
61. Gao, W.-Y.; Tsai, C.-Y.; Wojtas, L.; Thiounn, T.; Lin, C.-C.; Ma, S., Interpenetrating Metal–Metalloporphyrin Framework for Selective CO2 Uptake and Chemical Transformation of CO2. *Inorganic Chemistry* **2016,** *55* (15), 7291-7294.
62. Johnson, J. A.; Chen, S.; Reeson, T. C.; Chen, Y. S.; Zeng, X. C.; Zhang, J., Direct X-ray Observation of Trapped CO2 in a Predesigned Porphyrinic Metal–Organic Framework. *Chemistry-A European Journal* **2014,** *20* (25), 7632-7637.
63. Johnson, J. A.; Zhang, X.; Reeson, T. C.; Chen, Y.-S.; Zhang, J., Facile Control of the Charge Density and Photocatalytic Activity of an Anionic Indium Porphyrin Framework via in Situ Metalation. *Journal of the American Chemical Society* **2014,** *136* (45), 15881-15884.
64. Johnson, J. A.; Luo, J.; Zhang, X.; Chen, Y.-S.; Morton, M. D.; Echeverría, E.; Torres, F. E.; Zhang, J., Porphyrin-Metalation-Mediated Tuning of Photoredox Catalytic Properties in Metal–Organic Frameworks. *ACS Catalysis* **2015,** *5* (9), 5283-5291.
65. Johnson, J. A.; Petersen, B. M.; Kormos, A.; Echeverría, E.; Chen, Y.-S.; Zhang, J., A New Approach to Non-Coordinating Anions: Lewis Acid Enhancement of Porphyrin Metal Centers in a Zwitterionic Metal–Organic Framework. *Journal of the American Chemical Society* **2016,** *138* (32), 10293-10298.
66. Kosal, M. E.; Chou, J.-H.; Wilson, S. R.; Suslick, K. S., A functional zeolite analogue assembled from metalloporphyrins. *Nat Mater* **2002,** *1* (2), 118-121.

67. Burnett, B. J.; Barron, P. M.; Choe, W., Recent advances in porphyrinic metal-organic frameworks: materials design, synthetic strategies, and emerging applications. *CrystEngComm* **2012,** *14* (11), 3839-3846.
68. Sharma, C. V. K.; Broker, G. A.; Huddleston, J. G.; Baldwin, J. W.; Metzger, R. M.; Rogers, R. D., Design Strategies for Solid-State Supramolecular Arrays Containing Both Mixed-Metalated and Freebase Porphyrins. *Journal of the American Chemical Society* **1999,** *121* (6), 1137-1144.
69. Seidel, R. W.; Oppel, I. M., Assembly of a rhomboidally distorted (4,4)-net based polymeric sheet structure bearing copper(ii) 5,10,15,20-tetra(4-pyridyl)porphyrin. *CrystEngComm* **2010,** *12* (4), 1051-1053.
70. Zou, C.; Zhang, Z.; Xu, X.; Gong, Q.; Li, J.; Wu, C.-D., A Multifunctional Organic–Inorganic Hybrid Structure Based on MnIII–Porphyrin and Polyoxometalate as a Highly Effective Dye Scavenger and Heterogenous Catalyst. *Journal of the American Chemical Society* **2012,** *134* (1), 87-90.
71. Seidel, R. W.; Oppel, I. M., 1D and 2D solid-state metallosupramolecular arrays of freebase 5,10,15,20-tetra(4-pyridyl)porphyrin, peripherally linked by zinc and manganese ions. *Structural Chemistry* **2009,** *20* (1), 121-128.
72. Carlucci, L.; Ciani, G.; Proserpio, D. M.; Porta, F., Four new 2D porous polymeric frames from the self-assembly of silver triflate and silver tosylate with free-base and Zn-metallated 5,10,15,20-tetra(4-pyridyl)porphyrin. *CrystEngComm* **2005,** *7* (11), 78-86.
73. Ohmura, T.; Usuki, A.; Mukae, Y.; Motegi, H.; Kajiya, S.; Yamamoto, M.; Senda, S.; Matsumoto, T.; Tatsumi, K., Supramolecular Porphyrin-Based Metal–Organic Frameworks with Fullerenes: Crystal Structures and Preferential Intercalation of C70. *Chemistry – An Asian Journal* **2016,** *11* (5), 700-704.
74. Carlucci, L.; Ciani, G.; Proserpio, D. M.; Porta, F., Open Network Architectures from the Self-Assembly of AgNO3 and 5,10,15,20-Tetra(4-pyridyl)porphyrin (H2tpyp) Building Blocks: The Exceptional Self-Penetrating Topology of the 3D Network of [Ag8(ZnIItpyp)7(H2O)2](NO3)8. *Angewandte Chemie International Edition* **2003,** *42* (3), 317-322.
75. Sun, D.; Tham, F. S.; Reed, C. A.; Boyd, P. D. W., Extending supramolecular fullerene-porphyrin chemistry to pillared metal-organic frameworks. *Proceedings of the National Academy of Sciences* **2002,** *99* (8), 5088-5092.
76. Schmittel, M.; He, B.; Fan, J.; Bats, J. W.; Engeser, M.; Schlosser, M.; Deiseroth, H.-J., Cap for Copper(I) Ions! Metallosupramolecular Solid and Solution State Structures on the Basis of the Dynamic Tetrahedral [Cu(phenAr2)(py)2]+ Motif. *Inorganic Chemistry* **2009,** *48* (17), 8192-8200.
77. Ohmura, T.; Usuki, A.; Fukumori, K.; Ohta, T.; Ito, M.; Tatsumi, K., New Porphyrin-Based Metal−Organic Framework with High Porosity: 2-D Infinite 22.2-Å Square-Grid Coordination Network. *Inorganic Chemistry* **2006,** *45* (20), 7988-7990.
78. Taylor, S. K.; Jameson, G. B.; Boyd, P. D. W., A New Polymeric Framework Formed by the Self Assembly of 5,10,15,20-tetra(3-pyridyl)porphyrin, HgI2 And C60. *Supramolecular Chemistry* **2005,** *17* (7), 543-546.
79. Zha, Q.; Ding, C.; Rui, X.; Xie, Y., A Novel Porphyrin-Based Ligand Containing Four 4,4′-Dipyridylamine Moieties: Syntheses, Structures, and Luminescent Properties of Mn(II), Cu(II), Zn(II), and Cd(II) Coordination Polymers. *Crystal Growth & Design* **2013,** *13* (10), 4583-4590.
80. DeVries, L. D.; Barron, P. M.; Hurley, E. P.; Hu, C.; Choe, W., "Nanoscale Lattice Fence" in a Metal–Organic Framework: Interplay between Hinged Topology and Highly Anisotropic Thermal Response. *Journal of the American Chemical Society* **2011,** *133* (38), 14848-14851.
81. Hagrman, D.; Hagrman, P. J.; Zubieta, J., Solid-State Coordination Chemistry: The Self-Assembly of Microporous Organic–Inorganic Hybrid Frameworks Constructed from Tetrapyridylporphyrin and Bimetallic Oxide Chains or Oxide Clusters. *Angewandte Chemie International Edition* **1999,** *38* (21), 3165-3168.
82. Xie, M.-H.; Yang, X.-L.; Zou, C.; Wu, C.-D., A SnIV–Porphyrin-Based Metal–Organic Framework for the Selective Photo-Oxygenation of Phenol and Sulfides. *Inorganic Chemistry* **2011,** *50* (12), 5318-5320.

83. Abrahams, B. F.; Hoskins, B. F.; Michail, D. M.; Robson, R., Assembly of porphyrin building blocks into network structures with large channels. *Nature* **1994,** *369* (6483), 727-729.
84. Lipstman, S.; Goldberg, I., Porphyrin Framework Solids. Hybrid Supramolecular Assembly Modes of Tetrapyridylporphyrin and Aqua Nitrates of Lanthanoid Ions. *Crystal Growth & Design* **2010,** *10* (4), 1823-1832.
85. Yucesan, G.; Golub, V.; O'Connor, C. J.; Zubieta, J., Solid state coordination chemistry: organic/inorganic hybrid frameworks constructed from tetrapyridylporphyrin and vanadium oxide chains. *CrystEngComm* **2004,** *6* (57), 323-325.
86. Sengupta, A.; Datta, S.; Su, C.; Herng, T. S.; Ding, J.; Vittal, J. J.; Loh, K. P., Tunable Electrical Conductivity and Magnetic Property of the Two Dimensional Metal Organic Framework [Cu(TPyP)Cu2(O2CCH3)4]. *ACS Applied Materials & Interfaces* **2016,** *8* (25), 16154-16159.
87. Lipstman, S.; Goldberg, I., Supramolecular Crystal Chemistry of Tetra(3-pyridyl)porphyrin. 2. Two- and Three-Dimensional Coordination Networks with Cobalt and Cadmium Ions. *Crystal Growth & Design* **2010,** *10* (11), 5001-5006.
88. Deiters, E.; Bulach, V.; Hosseini, M. W., Heterobimetallic coordination networks based on metallaporphyrins bearing four pyridine N-oxide groups as coordinating sites. *Dalton Trans.* **2007,** (37), 4126-4131.
89. Jiang, W.; Yang, J.; Liu, Y.-Y.; Song, S.-Y.; Ma, J.-F., A Stable Porphyrin-Based Porous mog Metal–Organic Framework as an Efficient Solvent-Free Catalyst for C–C Bond Formation. *Inorganic Chemistry* **2017,** *56* (5), 3036-3043.
90. Guo, Z.; Yan, D.; Wang, H.; Tesfagaber, D.; Li, X.; Chen, Y.; Huang, W.; Chen, B., A Three-Dimensional Microporous Metal–Metalloporphyrin Framework. *Inorganic Chemistry* **2015,** *54* (1), 200-204.
91. Abeykoon, B.; Greneche, J.-M.; Jeanneau, E.; Chernyshov, D.; Goutaudier, C.; Demessence, A.; Devic, T.; Fateeva, A., Tuning the iron redox state inside a microporous porphyrinic metal organic framework. *Dalton Trans.* **2017,** *46* (2), 517-523.
92. Demel, J.; Kubát, P.; Millange, F.; Marrot, J.; Císařová, I.; Lang, K., Lanthanide-Porphyrin Hybrids: from Layered Structures to Metal–Organic Frameworks with Photophysical Properties. *Inorganic Chemistry* **2013,** *52* (5), 2779-2786.
93. Tong, C.; Ronghua, H.; Zhigang, L.; Hualong, C.; Juan, L., A New 3− D Lanthanide Porphyrin: Synthesis, Structure and Photophysical Properties. *结构化学* **2015,** *34* (2), 279-284.
94. Chen, W.-T.; Xu, Y.-P.; Luo, Q.-Y.; Dai, Y.-K.; Huang, S.-L.; Guo, P.-Y., Photophysical and electrochemical properties of a novel 4f–3d heterometallic porphyrin. *Journal of Porphyrins and Phthalocyanines* **2014,** *18* (07), 600-603.
95. Chen, W.-T.; Hu, R.-H.; Chen, H.-L.; Zhang, X.; Fu, H.-R., Synthesis, characterization and properties of a gadolinium tetra(4-sulfonatophenyl)porphyrin. *Journal of the Iranian Chemical Society* **2015,** *12* (2), 277-282.
96. Pei, Y.-P.; Huang, J.-G.; Hu, R.-H.; Yang, Y.-X.; Zhou, J.; Chen, W.-T., Metal-induced property variation for a series of lanthanide-vanadium porphyrins. *Journal of Porphyrins and Phthalocyanines* **2015,** *19* (06), 811-818.
97. Chen, W.-T.; Luo, Q.-Y.; Xu, Y.-P.; Dai, Y.-K.; Huang, S.-L.; Guo, P.-Y., Hydrothermal synthesis, crystal structure and properties of a thermally stable dysprosium porphyrin with a three-dimensional porous open framework. *Inorg. Chem. Commun.* **2014,** *49*, 16-18.
98. Chen, W.-T.; Luo, Z.-G.; Wang, Y.-F.; Zhang, X.; Fu, H.-R., Synthesis, structure, photophysical and electrochemical properties of a novel metalloporphyrin with a condensed three-dimensional porous open framework. *Inorganica Chimica Acta* **2014,** *414*, 1-7.
99. Chen, W.-T.; Hu, R.-H.; Xu, Y.-P.; Luo, Q.-Y.; Dai, Y.-K.; Huang, S.-L.; Guo, P.-Y., Photophysical and electrochemical properties of a novel lanthanide tetra(4-sulfonatophenyl)porphyrin. *Journal of the Iranian Chemical Society* **2015,** *12* (6), 937-942.

100. Chen, W.-T.; Yamada, Y.; Liu, G.-N.; Kubota, A.; Ichikawa, T.; Kojima, Y.; Guo, G.-C.; Fukuzumi, S., X-Ray crystal structure of [HSm{VIVO(TPPS)}]n and encapsulation of nitrogen molecules in 1-D channels. *Dalton Trans.* **2011,** *40* (48), 12826-12831.
101. Chen, W.-T.; Hu, R.-H.; Wang, Y.-F.; Zhang, X.; Liu, J., A Tb–Zn tetra(4-sulfonatophenyl)porphyrin hybrid: Preparation, structure, photophysical and electrochemical properties. *Journal of Solid State Chemistry* **2014,** *213*, 218-223.
102. Chen, W.-T.; Huang, J.-G.; Luo, Q.-Y.; Xu, Y.-P.; Fu, H.-R., A novel terbium-cobalt tetra(4-sulfonatophenyl)porphyrin: Synthesis, structure and photophysical and electrochemical properties. *Journal of Porphyrins and Phthalocyanines* **2015,** *19* (01-03), 154-159.
103. Pei, Y.-P.; Huang, J.-G.; Chen, H.-L.; Kuang, H.-M.; Zhou, J.; Yang, Y.-X.; Chen, W.-T., A samarium hybrid with porphyrin and amino acid as mixed ligands: Electrochemical and photophysical properties. *Journal of Porphyrins and Phthalocyanines* **2015,** *19* (10), 1140-1146.
104. Jin, S.; Hill, J. P.; Ji, Q.; Shrestha, L. K.; Ariga, K., Supercapacitive hybrid materials from the thermolysis of porous coordination nanorods based on a catechol porphyrin. *Journal of Materials Chemistry A* **2016,** *4* (15), 5737-5744.
105. Bhuyan, J.; Sarkar, S., Self-Assembly of Magnesium and Zinc Trimethoxyphenylporphyrin Polymer as Nanospheres and Nanorods. *Crystal Growth & Design* **2011,** *11* (12), 5410-5414.
106. Ming, Y.; Purewal, J.; Yang, J.; Xu, C.; Soltis, R.; Warner, J.; Veenstra, M.; Gaab, M.; Müller, U.; Siegel, D. J., Kinetic Stability of MOF-5 in Humid Environments: Impact of Powder Densification, Humidity Level, and Exposure Time. *Langmuir* **2015,** *31* (17), 4988-4995.
107. Low, J. J.; Benin, A. I.; Jakubczak, P.; Abrahamian, J. F.; Faheem, S. A.; Willis, R. R., Virtual High Throughput Screening Confirmed Experimentally: Porous Coordination Polymer Hydration. *Journal of the American Chemical Society* **2009,** *131* (43), 15834-15842.
108. DeCoste, J. B.; Peterson, G. W.; Schindler, B. J.; Killops, K. L.; Browe, M. A.; Mahle, J. J., The effect of water adsorption on the structure of the carboxylate containing metal-organic frameworks Cu-BTC, Mg-MOF-74, and UiO-66. *Journal of Materials Chemistry A* **2013,** *1* (38), 11922-11932.
109. Fateeva, A.; Chater, P. A.; Ireland, C. P.; Tahir, A. A.; Khimyak, Y. Z.; Wiper, P. V.; Darwent, J. R.; Rosseinsky, M. J., A water-stable porphyrin-based metal-organic framework active for visible-light photocatalysis. *Angewandte Chemie* **2012,** *51* (30), 7440-4.
110. Luo, J.; Wang, J.; Cao, Y.; Yao, S.; Zhang, L.; Huo, Q.; Liu, Y., Assembly of an indium-porphyrin framework JLU-Liu7: a mesoporous metal-organic framework with high gas adsorption and separation of light hydrocarbons. *Inorganic Chemistry Frontiers* **2017,** *4* (1), 139-143.
111. Colombo, V.; Galli, S.; Choi, H. J.; Han, G. D.; Maspero, A.; Palmisano, G.; Masciocchi, N.; Long, J. R., High thermal and chemical stability in pyrazolate-bridged metal-organic frameworks with exposed metal sites. *Chemical Science* **2011,** *2* (7), 1311-1319.
112. Satchell, J. F.; Smith, B. J., Calculation of aqueous dissociation constants of 1,2,4-triazole and tetrazole: A comparison of solvation models. *Physical Chemistry Chemical Physics* **2002,** *4* (18), 4314-4318.
113. Krogsgaard, M.; Nue, V.; Birkedal, H., Mussel-Inspired Materials: Self-Healing through Coordination Chemistry. *Chemistry – A European Journal* **2016,** *22* (3), 844-857.
114. Tytko, K.-H.; Gras, D., *Mo Molybdenum: Oxomolybdenum Species in Aqueous Solutions (Continued) Oxomolybdenum Species in Nonaqueous Solvents Oxomolybdenum Species in Melts Peroxomolybdenum Species*. Springer Science & Business Media: 2013.
115. Mouchaham, G.; Cooper, L.; Guillou, N.; Martineau, C.; Elkaïm, E.; Bourrelly, S.; Llewellyn, P. L.; Allain, C.; Clavier, G.; Serre, C.; Devic, T., A Robust Infinite Zirconium Phenolate Building Unit to Enhance the Chemical Stability of Zr MOFs. *Angewandte Chemie International Edition* **2015,** *54* (45), 13297-13301.
116. Nguyen, N. T. T.; Furukawa, H.; Gándara, F.; Trickett, C. A.; Jeong, H. M.; Cordova, K. E.; Yaghi, O. M., Three-Dimensional Metal-Catecholate Frameworks and Their Ultrahigh Proton Conductivity. *Journal of the American Chemical Society* **2015,** *137* (49), 15394-15397.

117. Xu, L.; Luo, Y.-P.; Sun, L.; Xu, Y.; Cai, Z.-S.; Fang, M.; Yuan, R.-X.; Du, H.-B., Highly Stable Mesoporous Zirconium Porphyrinic Frameworks with Distinct Flexibility. *Chemistry – A European Journal* **2016,** *22* (18), 6268-6276.
118. Xu, L.; Zhai, M.-K.; Lu, X.-C.; Du, H.-B., A robust indium-porphyrin framework for CO2 capture and chemical transformation. *Dalton Trans.* **2016,** *45* (46), 18730-18736.
119. Morris, W.; Volosskiy, B.; Demir, S.; Gándara, F.; McGrier, P. L.; Furukawa, H.; Cascio, D.; Stoddart, J. F.; Yaghi, O. M., Synthesis, Structure, and Metalation of Two New Highly Porous Zirconium Metal–Organic Frameworks. *Inorganic Chemistry* **2012,** *51* (12), 6443-6445.
120. Rhauderwiek, T.; Heidenreich, N.; Reinsch, H.; Øien-Ødegaard, S.; Lomachenko, K. A.; Rütt, U.; Soldatov, A. V.; Lillerud, K. P.; Stock, N., Co-Ligand Dependent Formation and Phase Transformation of Four Porphyrin-Based Cerium Metal–Organic Frameworks. *Crystal Growth & Design* **2017,** *17* (6), 3462-3474.
121. Wang, Y.; Cui, H.; Wei, Z.-W.; Wang, H.-P.; Zhang, L.; Su, C.-Y., Engineering catalytic coordination space in a chemically stable Ir-porphyrin MOF with a confinement effect inverting conventional Si-H insertion chemoselectivity. *Chemical Science* **2017,** *8* (1), 775-780.
122. Zheng, J.; Wu, M.; Jiang, F.; Su, W.; Hong, M., Stable porphyrin Zr and Hf metal-organic frameworks featuring 2.5 nm cages: high surface areas, SCSC transformations and catalyses. *Chemical Science* **2015,** *6* (6), 3466-3470.

Chapter 2:
Synthesis of Porphyrin Ligands

Table of Contents

2. Synthesis of porphyrin ligands

2.1. Introduction to porphyrins

Porphyrins are biologically important naturally occurring macrocyclic compounds. They have a basic structure as shown in Figure 2-1a and are ubiquitously found in natural systems. One of the most well-known porphyrins is heme (Figure 2-1b). It plays a vital role in O_2 storage and transport (myoglobin and haemoglobin), electron transport (cytochrome b and c) and O_2 activation and utilization (cytochrome P450).

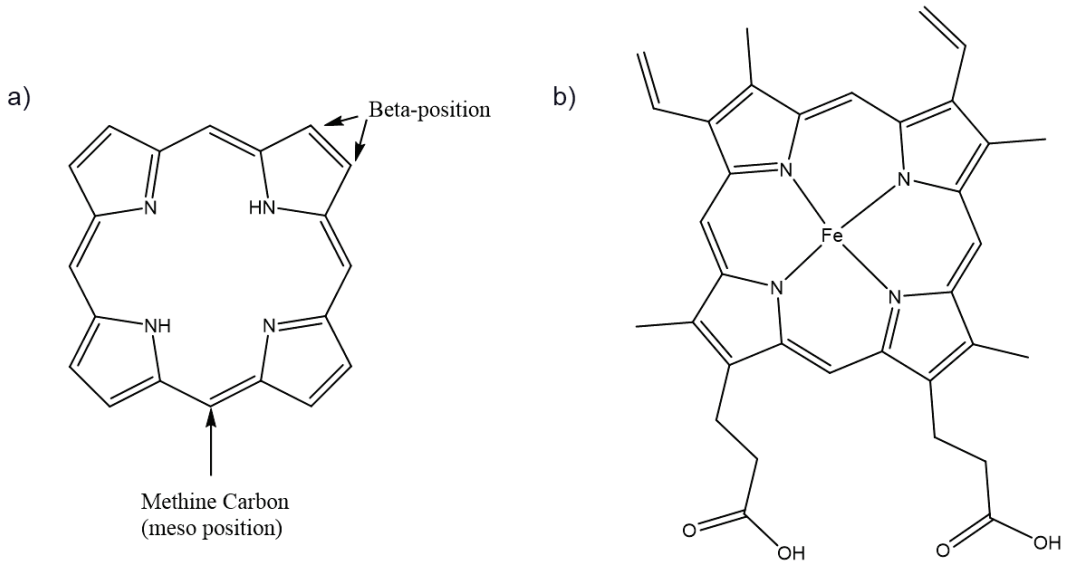

Figure 2-1 a) The basic structure of a porphyrin b) heme group which contains a Fe(II) in the porphyrin core

2.1.1. Roles of porphyrins in natural systems:

Oxygen transport - Haemoglobin and myoglobin are high molecular weight protein systems containing iron(II) porphyrin units which are responsible for oxygen transport in animals.[1] Dioxygen is bound to the Fe(II) in the porphyrin core at its vacant coordination site, which is then transported to their destinations in the body.

Electron transfer- The cytochromes are iron porphyrin containing electron transferring proteins which are found in aerobic cells and undergo reversible Fe(III)-Fe(II) redox changes during their catalytic cycles.[1] They are part of the electron transport chain where electrons are transported from a donor (such as NADH in eukaryotes) to O_2 at the end which is reduced to water.

Hydrogen peroxide utilization and destruction - Catalase is a heme enzyme which catalyses the decomposition of hydrogen peroxide generated during various life processes to produce oxygen and water thus protecting the cell from oxidative damage by reactive oxygen species.[2] Heme

peroxidases are enzymes catalysing the oxidation of a variety of organic and inorganic compounds using hydrogen peroxide.[2]

Hydrocarbon oxidation-This process first involves the cytochrome P-450 in the ferric state [Fe(III)] combining with a hydrocarbon followed by a one electron reduction to form a ferrous [Fe(II)] P-450-substrate complex.[3] This reduced form of P-450 reacts with molecular oxygen in manner where one of the O-atoms is reduced to water and the other is introduced into the organic substrate. Cytochrome P-450 works on many types of substrates such as steroids, fatty acids, certain amino acids etc.

Light harvesting- Chlorophylls, which are closely related magnesium containing derivatives of porphyrins (chlorophylls are usually based on chlorins which are more reduced, i.e. contain more hydrogens, compared to porphyrins) are a class of molecules vital for photosynthesis, which allows plants to absorb energy from light.[4]

Due to this ubiquitous nature and immense biological importance and fascinating properties (which will be discussed later), porphyrins and related compounds have attracted a large interest by scientists in the fields of chemistry, biology and medicine.[5-6]

2.1.2. Synthesis of porphyrins

The synthesis of porphyrins have been greatly developed during the past 100 years.[7-9] Porphyrins can be substituted at both the meso and the beta positions (Figure 2-1a) to obtain either symmetrical or asymmetrical molecules. Presently, there are many synthetic methodologies known, among which, the tetramerization of pyrroles.[8, 10] The optimum strategy for the synthesis depends on the nature of the desired porphyrin; meso-substituted, beta-substituted, symmetrical or asymmetrical.

This work focuses on symmetrical tetraphenyl porphyrins with the same functionalised phenyl group at each *meso* position, which can be synthesised by the acid catalysed condensation reaction of pyrrole with specific aldehydes, followed by oxidation of the resulting colourless porphyrinogen. Rothemund et al originally developed this procedure back in 1941 where a benzaldehyde and pyrrole in pyridine were reacted at 220 °C in a sealed glass tube under nitrogen for 48h, which resulted in the corresponding tetraphenyl porphyrin in 10% yield.[11] Adler and Longo subsequently refined this procedure in 1967 to give an improved yield of around 20% (Figure 2-2a).[12] In the Adler-Longo method, the benzaldehyde and pyrrole are refluxed in propionic acid in air where the porphyrinogen intermediate is oxidized by oxygen *in situ* to produce the porphyrin (general mechanism given on Figure 2-3). The product usually can be recovered via filtration. The increasing electron-withdrawing

nature of the p-substituted aryl aldehyde have shown to have a positive effect on the rate of the porphyrin formation as demonstrated by Kim et al.[13] This is attributed to electron-withdrawing substituents making the carbonyl carbon more susceptible for the nucleophilic attack step (Figure 2-3). However, the final yield of the product also depends on the facility of the purification. This method is well suited for large scale syntheses (> 1g) despite the modest yield (around 20%) due to its relative simplicity.

In the late 1980's, Lindsey et al developed a one-pot two-step room temperature synthetic method using trifluoroacetic acid (TFA) or boron trifluoride (BF_3) as the catalyst.[14] This method involves a condensation step at room temperature where equilibrium is achieved followed by an oxidation step (Figure 2-2b). The Lindsey method gives a higher yield (up to 50%) and milder reaction conditions utilised enables the use of aldehydes which are not stable under the required conditions for the Adler-Longo method. However, Lindsey's method requires the use of low reactant concentrations (between 0.01M-0.1M) in order to minimize side reactions that lead to the formation of pyrrole oligomers. This requires the removal of large amounts of solvents and makes it impractical for larger scale synthesis. Furthermore, the end product usually needs to be purified by column chromatography whereas with the Adler method the products usually can be purified via filtration and recrystallization.

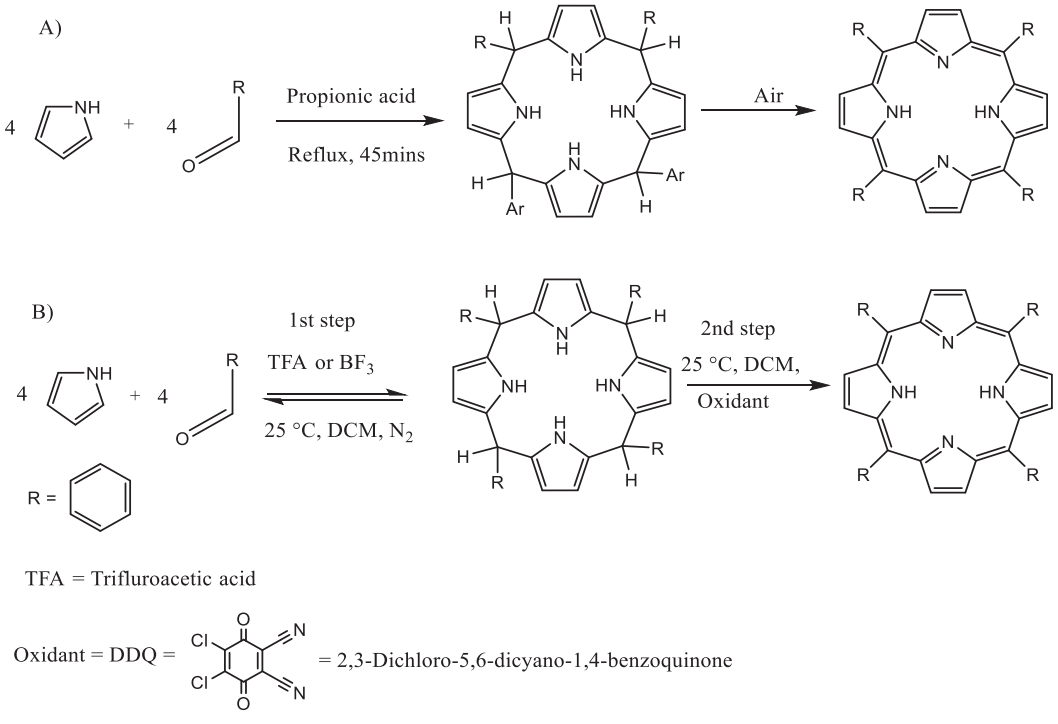

Figure 2-2 a) one step Adler-Longo synthesis b) two step Lindsey synthesis.

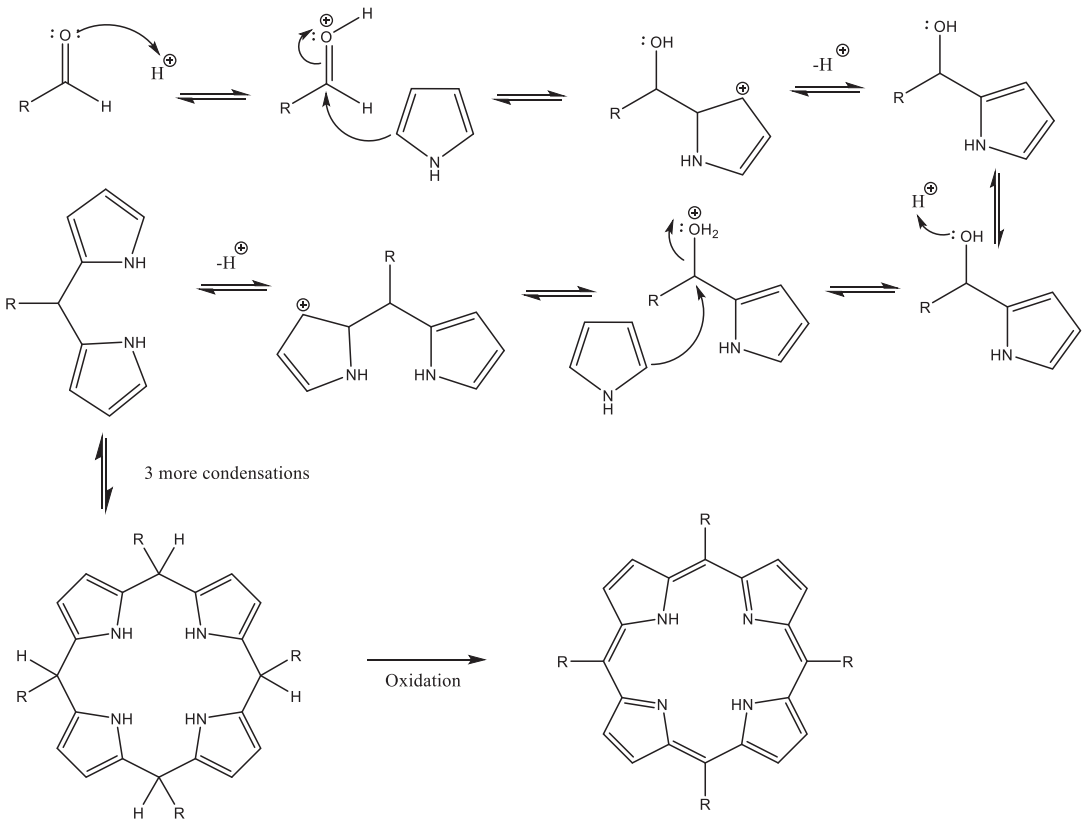

Figure 2-3 General mechanism for acid catalysed porphyrin synthesis.

In this work, Adler-Longo method is used for the porphyrin synthesis as the starting aldehydes are stable under the reaction conditions required and the resultant porphyrins can be purified relatively easily by filtration followed by recrystallization.

2.1.3. Properties of porphyrins

Chemical properties

The porphyrin macrocycle is an aromatic system consisting of four "pyrrole type" rings joined by four methine (meso) carbon bridges (Figure 2-1). A porphyrin ring has a total of 22-π electrons, but only 18 of them are delocalized according to the Hückel's rule of aromaticity (4n+2 where n=4).

Various metal ions (e.g. Zn^{2+}, Cu^{2+}, Ni^{2+}, Sn^{4+}, Mn^{3+}, Fe^{3+}) can be inserted into the porphyrin cavity.[5] Inversely, demetalation of metalloporphyrins can usually be achieved by the treatment with acids.

Chemical and thermal stability

The porphyrin ring shows general stability under strongly acidic and basic conditions. The two NH protons (pK_a ~16) can be removed by strong bases forming a dianion and a dication can be formed with the protonation of the two free nitrogen atoms (pK_a~5-6).[5-6] Porphyrins also show high thermal stability up to around 400 °C in air.[5-6, 15]

NMR spectroscopy

The ^{1}H-NMR spectrum of typical free base porphyrins displays N-H protons at very high field (~ -3 ppm) while the β–pyrrolic protons show up at low field (8-10 ppm). This is due to the anisotropic effect arising from the aromatic ring current. N-H protons are endocyclic with respect to the aromatic ring current thus experience a shielding effect, while the peripheral β–pyrrolic protons are exocyclic with respect to the porphyrin ring current thus experience a deshielding environment.[5, 16]

Photochemistry

Porphyrins exhibit characteristic absorption and fluorescence properties in the visible region which make them useful as photosensitizers. In a typical UV-visible spectrum of a porphyrin, there are two different types of bands due to the delocalized highly conjugated π system. The very intense band around 380-430 nm region is called the Soret band or B-band (molar extinction coefficients of around 10^{5} $M^{-1}cm^{-1}$). The weaker bands appearing in the 500-750 nm region are called Q bands (molar extinction coefficients of around 10^{4} $M^{-1}cm^{-1}$). These absorption bands can be explained using the Gouterman's four orbital model based on π to π* transitions between the two highest occupied molecular orbitals (HOMO) and the two lowest unoccupied molecular orbitals (LUMO).[17] The excitation of the porphyrin from its ground state to its second excited state gives rise to the Soret band while Q bands correspond to excitation from the ground state to two vibrational states of the first excited state. In free base porphyrins, the two vibrational excited states are non-degenerate due to the x and y polarization caused by the D_{2h} symmetry further splitting the Q band to four bands (Figure 2-4). [17]

The metalation of the porphyrin core leads to a change in the symmetry of the porphyrin from D_{2h} to D_{4h} (4-fold symmetry) as the two protons on the inner nitrogens are lost (Figure 2-4). Thus, as a result of higher symmetry the two vibrational excited states become degenerate reducing the number of Q bands in the UV spectra of metalloporphyrins in the visible region (Figure 2-5).[17]

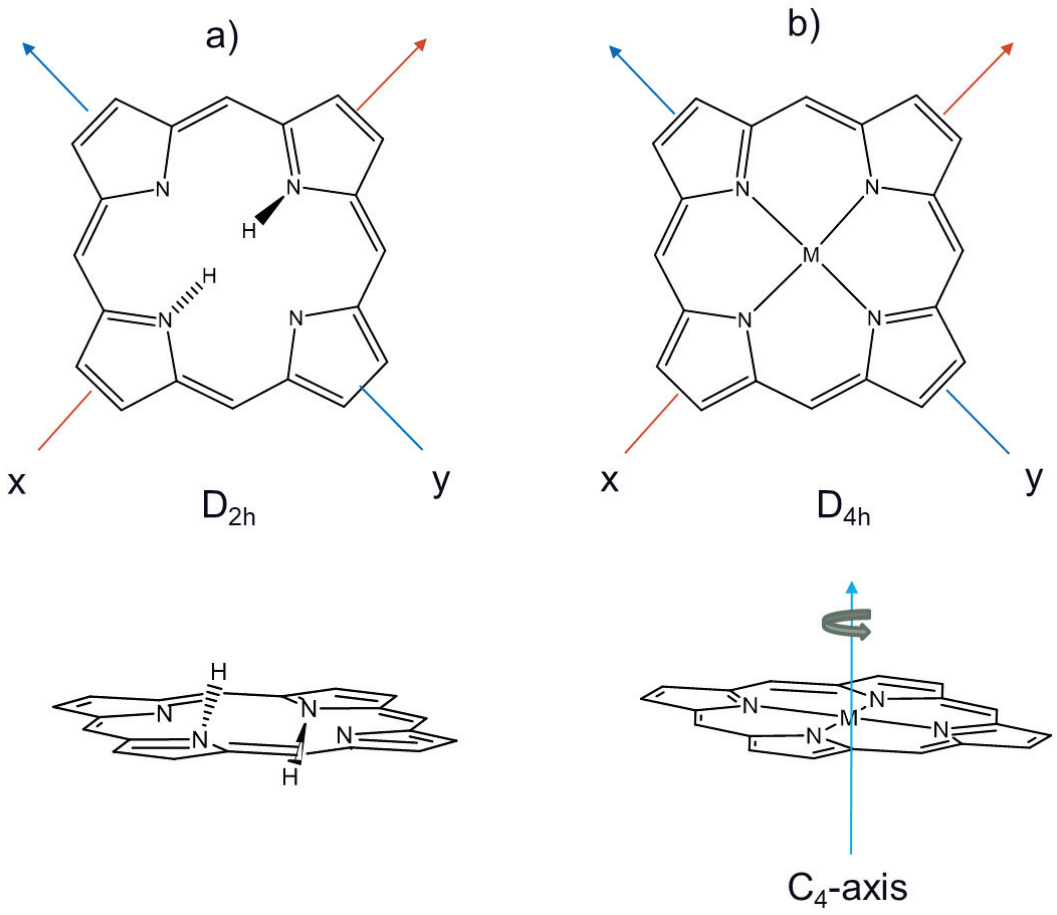

Figure 2-4. a) Free base porphyrin with D_{2h} symmetry which lacks a C_4-axis due to the NH hydrogens which sit above and below the plane. B) Metalated porphyrin with D_{4h} symmetry with a C_4-axis. The plane perpendicular to the C_4 axis is indicated with the X and Y arrows.

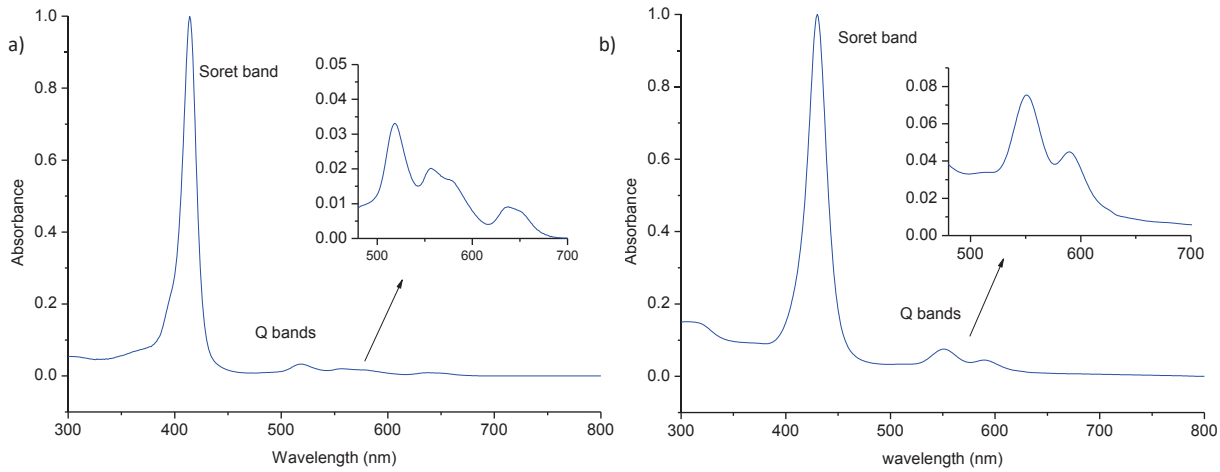

Figure 2-5 UV–vis spectra for (a) a free-base porphyrin and (b) metalated porphyrin.

Free base porphyrins are usually fluorescent in the red region (600-800 nm) of the spectrum. Metalated paramagnetic porphyrins usually do not show fluorescence but fluorescence from porphyrins metalated with closed-shell diamagnetic metals such as Mg(II) and Zn(II) has been observed.[18]

Redox properties

Porphyrins and metalloporphyrins can undergo redox reactions at the metal centre and or in the ligand itself.[19-20] Furthermore, the redox potentials can be tuned with the choice of the metals and the substituents on the porphyrin rings.[21-23]

2.1.4. Porphyrin applications

One of the most studied applications of porphyrins has been as oxidation catalysts. Particularly, iron and manganese porphyrins have been studied extensively as enzyme mimics for oxidation reactions.[24-27] Iron(III) porphyrins have been used as models to mimic cytochrome P-450 in the catalytic oxidation of organic substrates.[24-27] However, in these systems the metalloporphyrins need to be kept apart as they can easily undergo catalytic deactivation via Iron-oxo bridge formation.[28]

Metalloporphyrins with metals such as iron and cobalt have also been demonstrated as good electrocatalysts for reduction of CO_2 to CO[29-30] and the oxygen reduction reaction.[31-33]

2.1.5. Porphyrins as functional building blocks for MOFs

Structurally, porphyrins offer an ideal ligand which is robust with a relatively rigid square planar geometry, large geometrical dimensions and a high thermal stability to form extended architectures. As molecules, they have interesting applications such as catalysis which can lead to these architectures having the same properties. As mentioned in chapter 1, MOF structures enable the control of porphyrin arrangement and to keep these species apart, preventing the self-deactivation.

In this work, four different porphyrins were synthesized as ligands/metalloligands for MOF synthesis (Figure 2-6). This chapter will discuss the synthetic procedures employed and the characterisation of these four porphyrins.

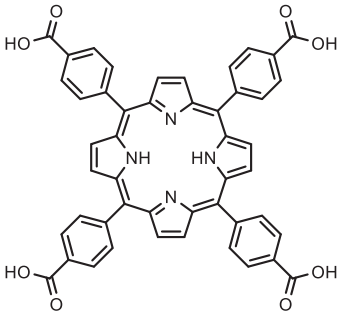

5,10,15,20-Tetrakis(4-carboxyphenyl)porphyrin
(H_2TCPP)

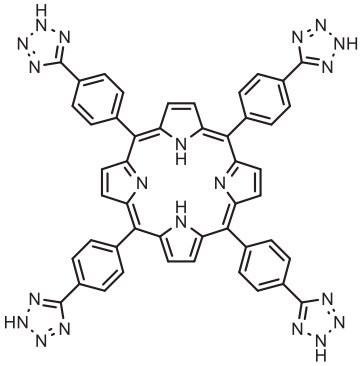

5,10,15,20-tetrakis(4-(2*H*-tetrazol-5-yl)phenyl)
porphyrin
(H_2TTPP)

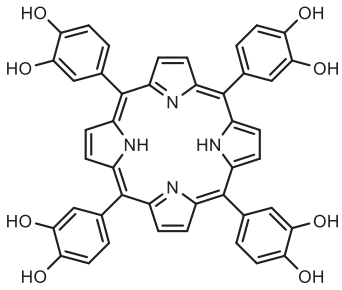

5,10,15,20-Tetrakis(3,4-dihydroxyphenyl)porphyrin
(H_{10}-PorphCat)

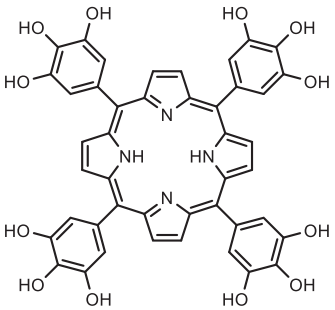

5,10,15,20-tetrakis(3,4,5-trihydroxyphenyl)porphyrin
(H_{14}-PorphGal)

Figure 2-6 The four porphyrin ligands investigated within the scope of this study.

2.2. Synthesis of porphyrin ligands used in this work

2.2.1. Carboxylic acid based porphyrin ligands

Synthesis

The general synthetic route employed to obtain the carboxylic acid based porphyrin ligands are shown on Figure 2-7 and has already been reported in literature.[34] The first step involved the synthesis of the 5,10,15,20-tetrakis(4-methoxycarbonylphenyl)porphyrin (H_2TEsterP), using the Adler method[12] with a yield of 17%, in a gram scale.

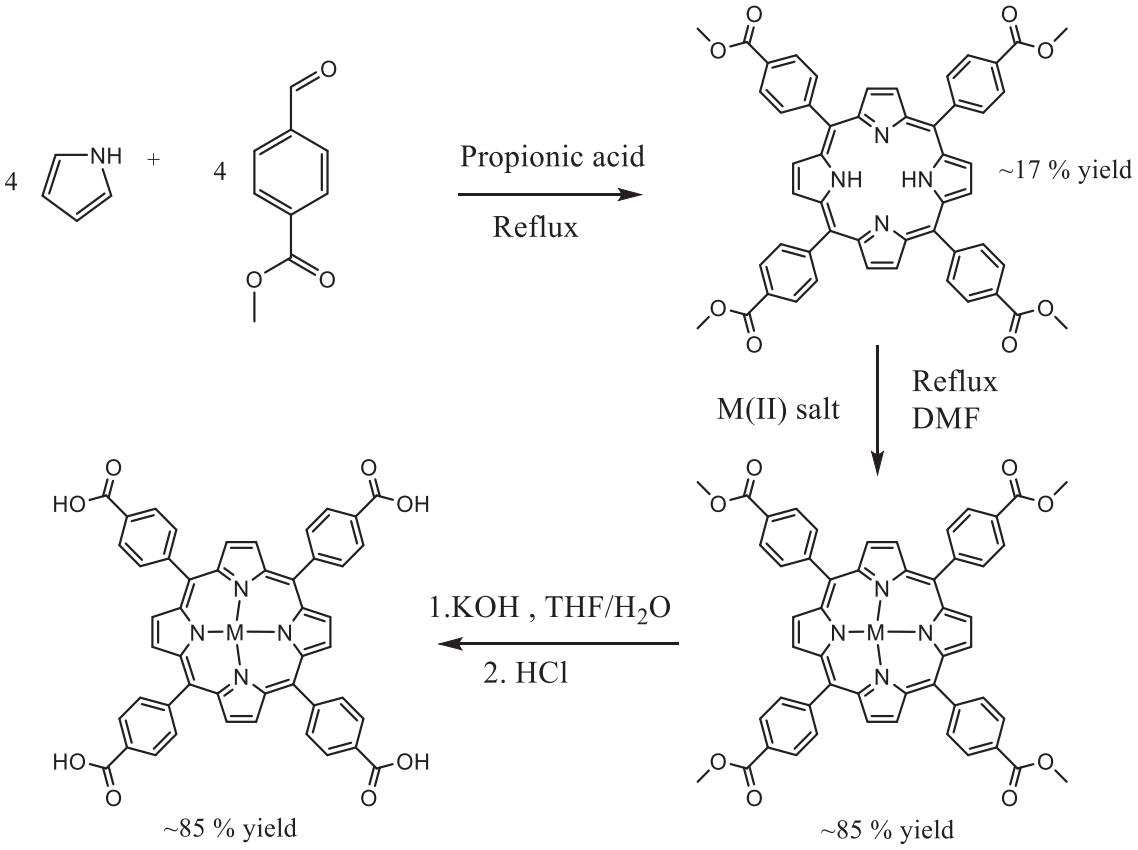

Figure 2-7 General synthetic route followed to obtain the carboxylic acid containing porphyrin ligands.[34]

Metal insertion

Metal ion insertion was carried out for the H_2TEsterP with iron, manganese and cobalt following classical procedures.

Iron metalation was attempted via refluxing in DMF with five-time excess of anhydrous iron(II) chloride under atmospheric conditions. However, this lead to the formation of iron oxide impurities simultaneously to the metalation. Thus, the synthesis was modified where only a 1.5 times excess anhydrous iron(II) chloride was used in an inert atmosphere.

Cobalt was inserted using a mixed solvent system (chloroform/ anhydrous ethanol) and cobalt(II) acetate tetra hydrate as the metal source at a lower refluxing temperature.

The counter ion present for the Fe(III) metalated ester porphyrin was determined to be a chloride ion as indicated by the mass spectrometry data shown on Figure 2-8 [i.e. FeTEsterP(Cl)]. The counter ions for the Mn(III) and Co(III) metalated ester porphyrins are likely to be hydroxide ions or acetate ions which are present in the reaction mixture [MnTEsterP(X), CoTEsterP(X), X= OH^-, CH_3COO^-] (the synthetic details are provided in the experimental section).

All three metalation reactions can be performed in a gram scale and with a yield approaching 85%.

Hydrolysis of ester

The cleavage of ester groups of the metalated TEsterP was achieved via classical base hydrolysis using excess KOH followed by addition of HCl. HCl addition is needed to protonate the carboxylate groups which render the porphyrin species soluble in basic media. The resulting metalated porphyrin containing the carboxylic acid groups (metalated 5,10,15,20-tetrakis(4-carboxyphenyl) porphyrin, MTCPP), on the other hand is insoluble in water and precipitates out of solution. The syntheses were performed in a gram scale and a yield of around 85% was observed for the products.

Similar to the ester porphyrin the counter ions present for the Fe(III) metalated TCPP was determined to be a chloride ion as indicated by the mass spectrometry data (Figure 2-9). The counter ions for the Mn(III) and Co(III) metalated TCPP were not determined precisely. However, these are likely to be chloride or hydroxide ions which are present under synthesis conditions (X= Cl^-, OH^-).

Characterisation

NMR spectroscopy and Mass spectrometry

NMR spectrum for H_2TesterP is shown on appendix section A.1.1. The NMR spectra for paramagnetic samples were not measured.

Mass spectrometry was a valuable technique to probe whether the complete metalation of all the free base porphyrins was achieved. The absence of the peak corresponding to the molecular ion for H_2TEster at 846 m/z along with the presence of the molecular ion for the metalated complex confirmed complete metalation. Mass spectra for all the syntheses is shown in the appendix section A.1.2.

The ester hydrolysis step was also confirmed with the use of mass spectrometry. The absence of the peaks corresponding to any ester protected species along with the presence of the peak

corresponding to the metalated TCPP confirmed the complete hydrolysis reaction of the ester groups. Mass spectra for the metalated TCPP are given in the appendix section A.1.2.

The mass spectrometry data of Fe(III) metalated TEsterP and TCPP are shown in Figure 2-8 and Figure 2-9. The peaks at 935 m/z and 879 m/z can be assigned to the chloride containing complexes $[FeTEsterP\text{-}Cl]^+$ and $[FeTCPP\text{-}Cl]^+$ respectively which indicates the presence of the chloride ion for charge balance.

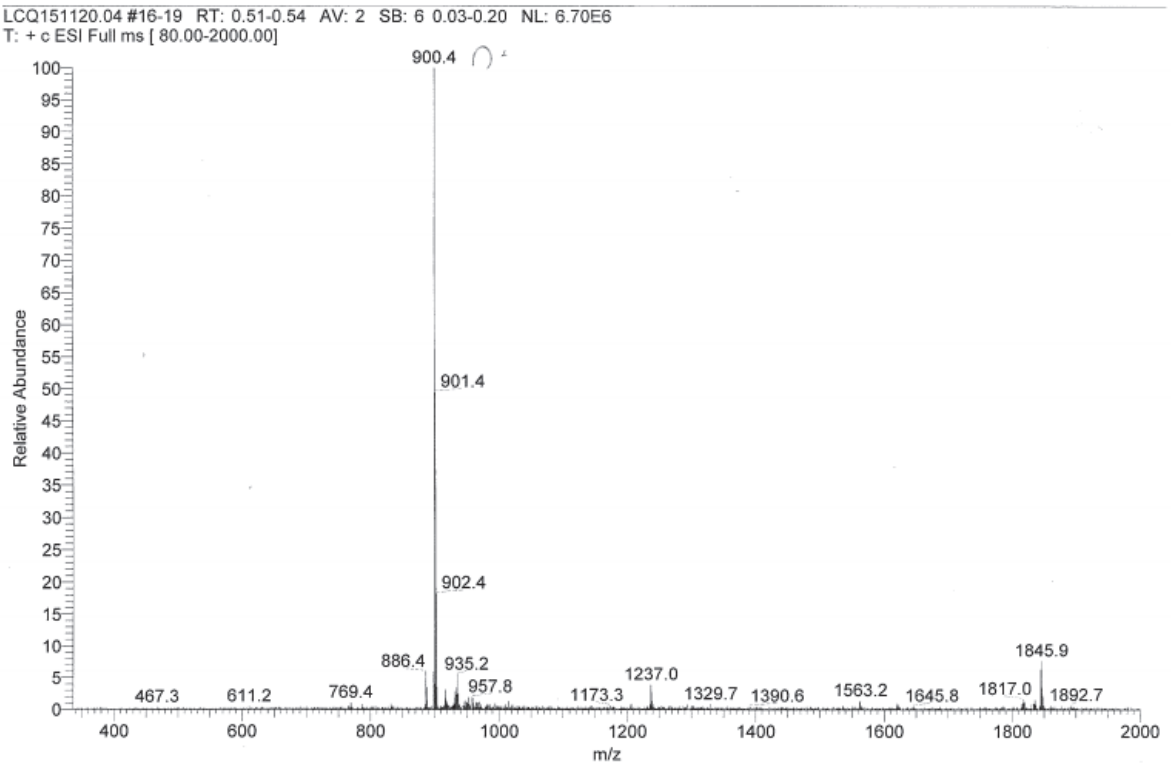

Figure 2-8 Mass spectrometry data for FeTEsterP(Cl). The molecular ion [$(FeTEsterP)^+$] peak is at 900 m/z. The peak at 935 m/z is assigned to the complex [$FeTesterP\text{-}Cl]^+$ which indicates the presence of a chloride counter ion.

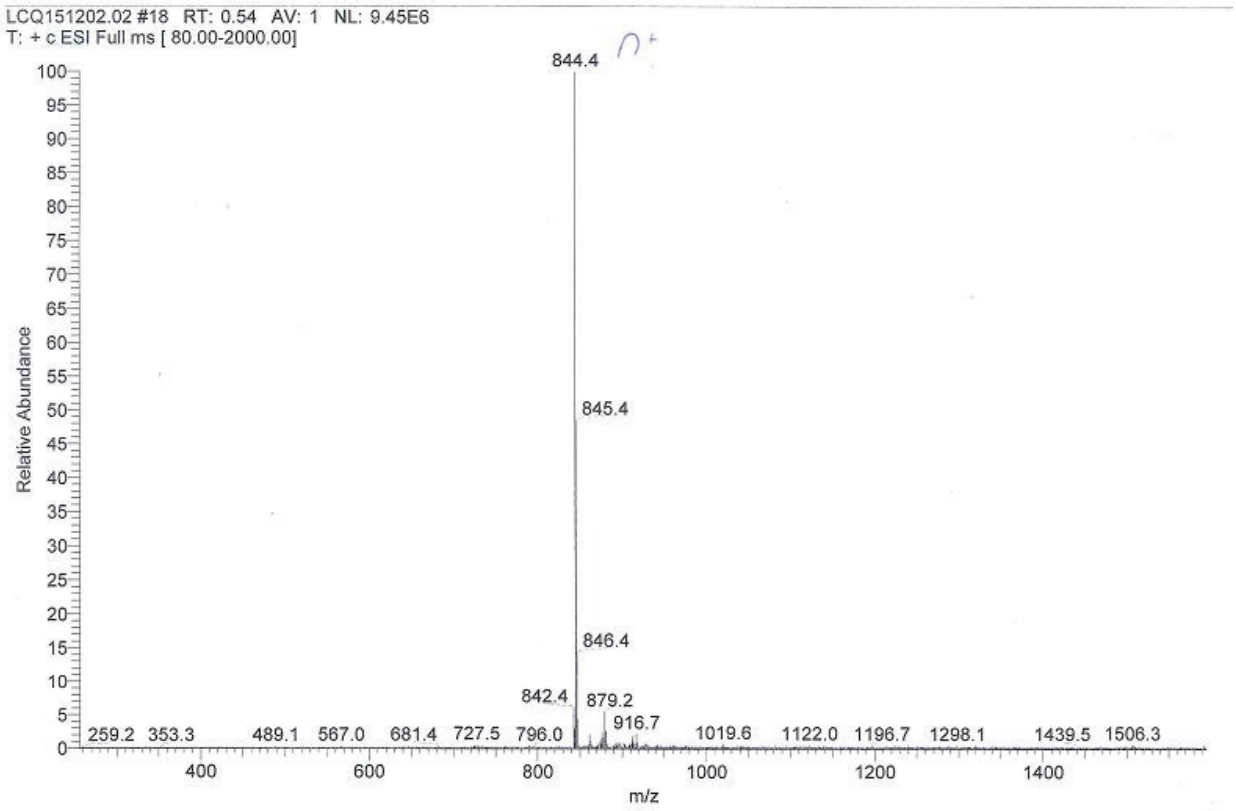

Figure 2-9 Mass spectrometry data for FeTCPP(Cl). Peak corresponding to the molecular ion, $(FeTCPP)^+$, is at 844 m/z. The peak at 879 m/z is assigned to the complex $[FeTCPP\text{-}Cl]^+$ which indicates the presence of a chloride counter ion.

UV-vis spectroscopy

UV-Vis spectroscopy is a useful technique for the study of porphyrin metalation. As mentioned earlier (Figure 2.4 and 2.5) the metalation increases the symmetry of the free base porphyrin from D_{2h} to D_{4h}, which in turn reduces the number of bands. Furthermore, the UV spectra also depend on the charge and the coordination number of the central metal ion. UV spectra for the different metalated porphyrins are shown in Figure 2-10 (Individual UV spectra for each product is given in the appendix section A.1.3).

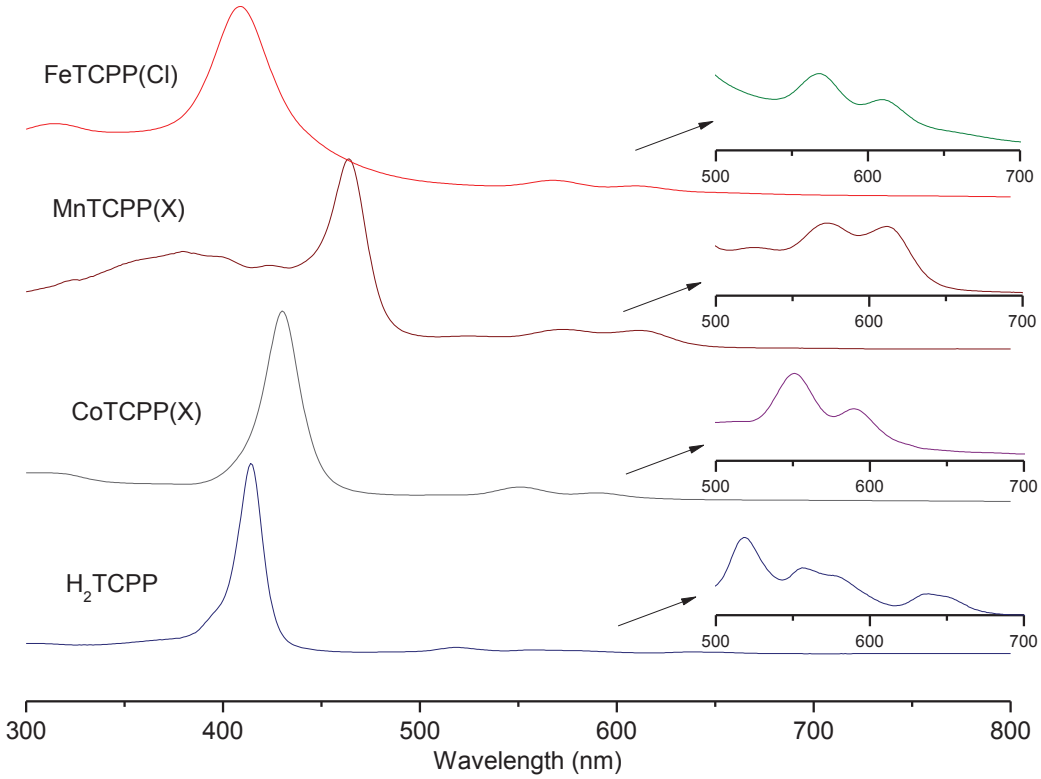

Figure 2-10 UV spectra of H_2TCPP compared to the metalated variations. (UV spectra were measured in 0.1M NaOH aqueous solution). Inserts provided a zoomed in view of the Q bands. Soret band and the Q bands change as a function of the metal coordinated in the porphyrin core.

Table 2-1 Soret Band and Q bands of metalated TCPP compared to H_2TCPP measured in 0.1 M NaOH.

	Soret Band (nm)	**Q bands (nm)**
H_2TCPP	415	518, 556, 586, 642
CoTCPP(X)	430	551, 590
MnTCPP(X)	380,401, 464	525, 573, 611
FeTCPP(Cl)	409	568, 609

The UV-vis spectrum of MnTCPP(X) is a special case as there are three Soret bands. This can be attributed to the eg orbitals of manganese ion strongly perturbing the π-electron system of the porphyrin.[35-36]

IR-spectroscopy

IR spectra of CoTEsterP(X), MnTEsterP(X) and FeTEsterP(Cl) compared to the free base porphyrin, H_2TEsterP are shown on Figure 2-11 . All the porphyrins gave similar IR spectra where the peaks at 1714 cm^{-1} and 1270 cm^{-1}can be assigned to the ester C=O and C-O stretches, while the peak at 1604 cm^{-1} can be assigned to the C=C stretch of the porphyrin ring.

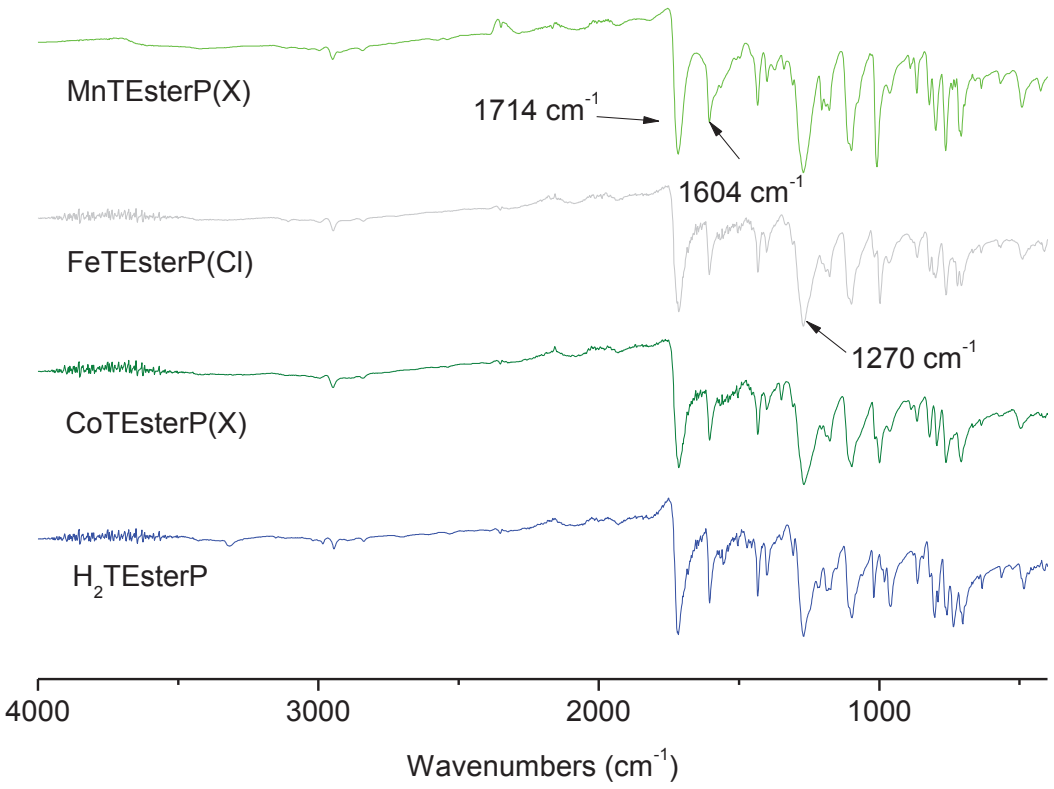

Figure 2-11 IR spectra of metalated TEsterP compared to free base H_2TesterP

IR spectra of CoTCPP(X), MnTCPP(X) and FeTCPP(Cl) compared to the free base porphyrin, H_2TCPP is shown on Figure 2-12. The IR spectra of FeTCPP(Cl), CoTCPP(X) are similar to that of H_2TCPP where the peaks around 1690 cm^{-1} and 1390 cm^{-1} can be assigned to the C=O and the C-O stretches of the carboxylic acid group. The peak at 1604 cm^{-1} can be assigned to the C=C stretch of the porphyrin ring. The broad peak around 2950 cm^{-1} is attributed to the OH stretch of the carboxylic acid group. IR-spectrum for MnTCPP(X) appeared different to the others and in addition to the above-mentioned peaks, there was a peak present at 1733 cm^{-1} whose orgin was not determined.

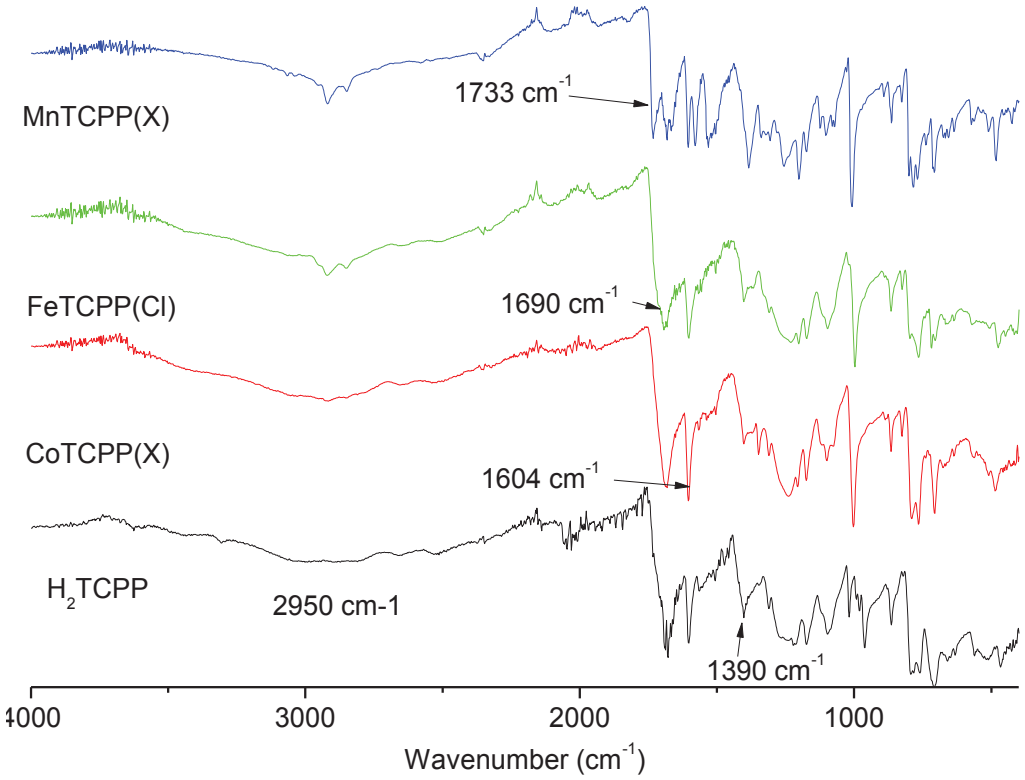

Figure 2-12 IR spectra of metalated TCPP compared to free base H_2TCPP.

2.2.2. Catechol based porphyrin ligands

Synthesis

The synthesis of dimethoxyphenyl porphyrin, 5,10,15,20-tetrakis(3,4-dimethoxyphenyl)porphyrin [$H_2T(OMe)_2PP$] has been reported using the Lindsey method in literature.[37] In this work it was synthesized via the Adler method in a gram scale with a 15% yield.[12] The product obtained via filtration requires further purification via a silica gel column (CH_2Cl_2:CH_3OH:Et_3N,100:2:1) where triethylamine (Et_3N) prevents the protonation of the porphyrin during the column.

The metalation of $H_2T(OMe)_2PP$ with $NiCl_2$ was achieved by using a mixed solvent system of chloroform/ethanol with excess metal salt and triethylamine as a base (the reaction was followed by UV-vis spectroscopy, refer to the experimental section) and was performed in a gram scale with a yield of 80 % within 72 hours.

To go from methoxy to hydroxy function, ether cleavage was performed by the use of BBr_3 reagent[38] but led to the demetalation in the course of this reaction. Therefore, a different ether cleavage method was attempted for $NiT(OMe)_2PP$ which involved refluxing in excess pyridinium chloride at 224 °C (Figure 2-13a).[39] The resultant solid was purified by first washing with water to get

rid of the unreacted pyridinium chloride via centrifugation. The solid was then dissolved in THF and filtered. Any unreacted $NiT(OMe)_2PP$ was removed by washing with chloroform to obtain the product in 77% yield. This method prevents total demetalation, however, 7% of the free base porphyrin was present in the final product.

The ether cleavage of the methoxy groups of $H_2T(OMe)_2PP$ to yield H_{10}-PorphCat was successfully achieved using BBr_3 via two slightly different strategies (Figure 2-13b, see experimental section for details) which were adopted from a synthesis of trihydroxyphenyl containing porphyrin reported in literature.[38] The purification methods were developed in this work.

The reaction was performed in a gram scale and 65% yield was obtained using method 1 which resulted in a violet coloured solid as the final product. However, this yield was not reproducible as subsequent attempts gave much lower yields around 25%.

In order to improve the yield, pure BBr_3 was used in method 2. The purification step employed was also changed. Methanol was used to quench the reaction mixture and almost all of the solvent was evaporated. Afterwards, water was added which resulted in a precipitate which was filtered and washed with acidic water (pH ~3-4) to obtain a green coloured solid as the product in a gram scale with an estimated yield of around 85%. However, the exact yield of the product could not be determined due to the presence of a mixture of species as described below.

NMR analysis showed that this product is a mixture of protonated and unprotonated freebase H_{10}-PorphCat. The major product was the diprotonated porphyrin, H_{12}-$PorphCat^{2+}$, while the unprotonated H_{10}-PorphCat was present at around 25%. Most likely, Br^- or Cl^- are present to account for the charge balance in the product (i.e. H_{12}-PorphCat-2X, X= Br^- or Cl^-). The method 2 was decided as the preferred method going forward due to the higher amount of product obtained compared to method 1.

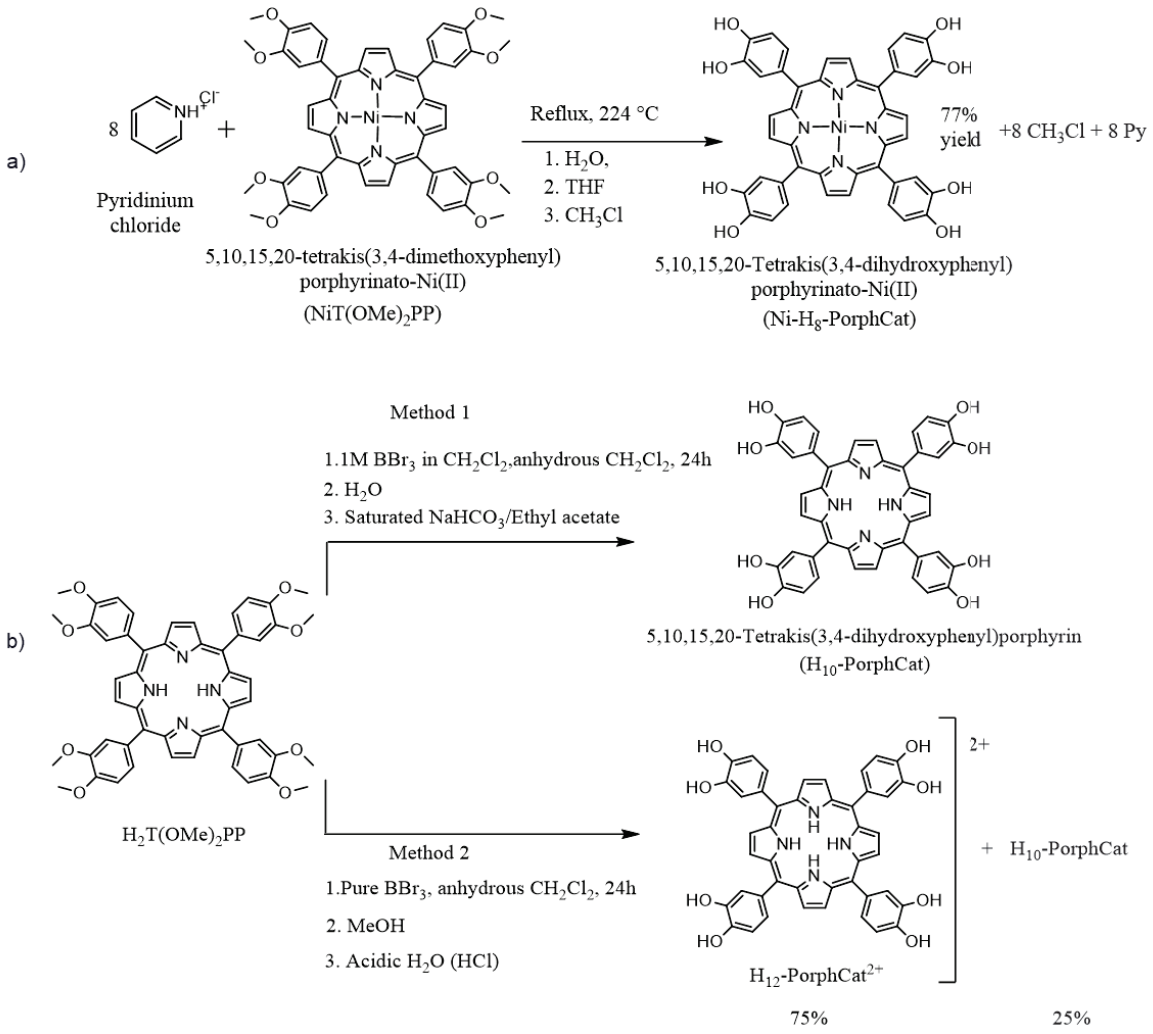

Figure 2-13 a) Ether cleavage of $NiT(OMe)_2PP$ with pyridinium chloride to yield Ni-H_8-PorphCat b) Two different synthesis procedures/purification methods used for the ether cleavage of the methoxy groups of $H_2T(OMe)_2PP$ using BBr_3 as mentioned in the text. Method 2 results in a mixture of protonated and unprotonated species.

Characterisation

NMR spectroscopy

NMR spectrum for the product obtained for the metalation of $H_2T(OMe)_2PP$ with Ni is given in Figure 2-14. One clear change that is observed in $NiT(OMe)_2PP$ compared to the free base porphyrin is the complete disappearance of the NH peak at around -2.9ppm.

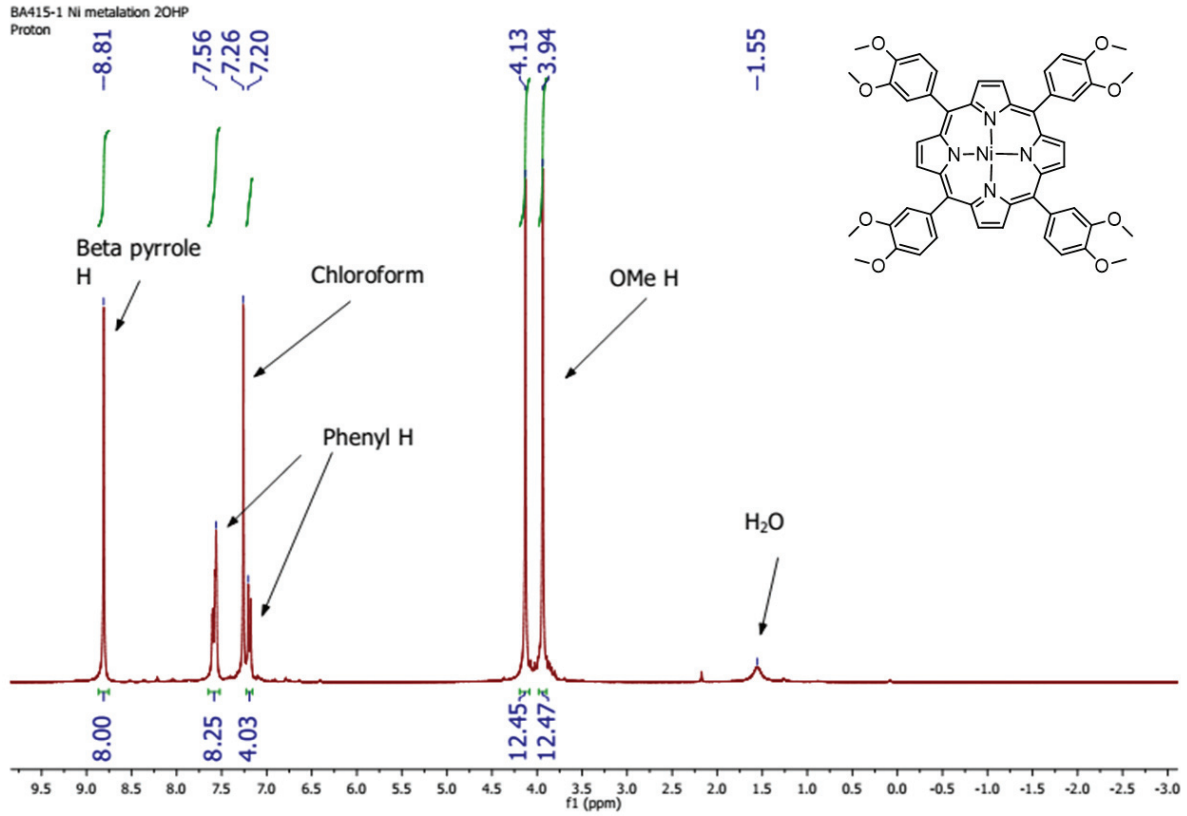

Figure 2-14 NMR spectrum of $NiT(OMe)_2PP$ in chloroform.

Ether cleavage of the methoxy groups of $NiT(OMe)_2PP$ was achieved via refluxing in pyridinium chloride. However, as shown in Figure 2-15 the total product obtained contained 7% free base porphyrin, H_{10}-PorphCat. This indicates that there was a small degree of demetalation during the reaction.

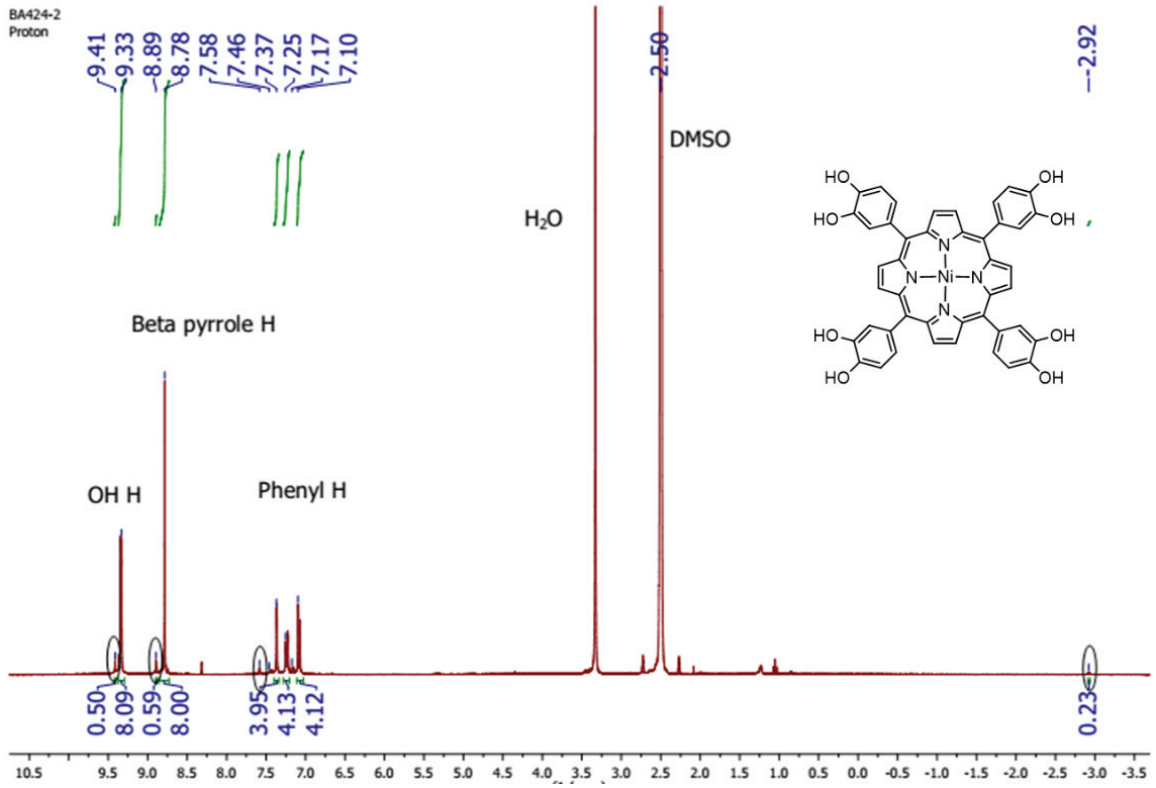

Figure 2-15 NMR spectrum (DMSO) of product obtained from the ether cleavage of the methoxy groups of NiT(OMe)$_2$PP with pyridinium chloride. The circled peaks represent the free base porphyrin, H_{10}-PorphCat, which is present at 7% compared to Ni-H_8-PorphCat. This indicates a degree of demetalation during the reaction.

For the ether cleavage of the methoxy groups of $H_2T(OMe)_2PP$ with BBr_3, the two different methods yielded differently coloured solids (purple and green). When analysing the NMR spectra, it can be seen that the method 2 yields the diprotonated form, H_{12}-PorphCat^{2+}, compared to the method 1 (Figure 2-16 and Figure 2-17). The pyrrolic NH peak corresponds to four protons and is shifted downfield compared to the freebase form (-0.29 ppm compared to ~-3 ppm for free base porphyrins) which is normally observed for protonated porphyrins.[40-41] The major product is the diprotonated H_{10}-PorphCat (H_{12}-PorphCat^{2+}) while the unprotonated species is present at 25%.

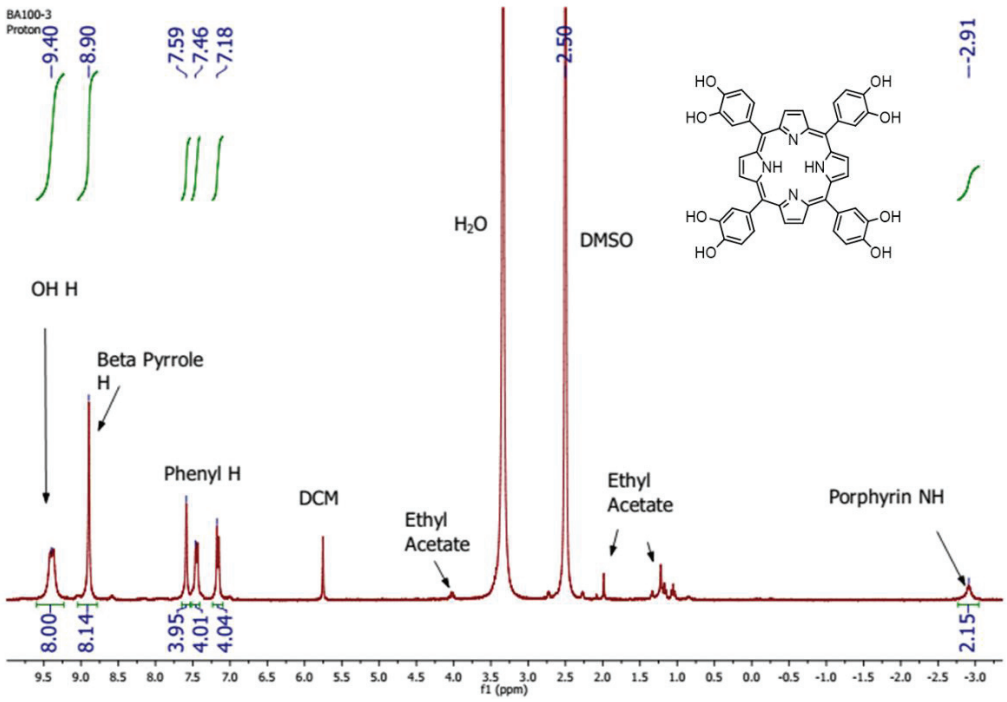

Figure 2-16 NMR spectrum (DMSO) for the products of the purification method 1 for the ether cleavage of the methoxy groups of $H_2T(OMe)_2PP$.

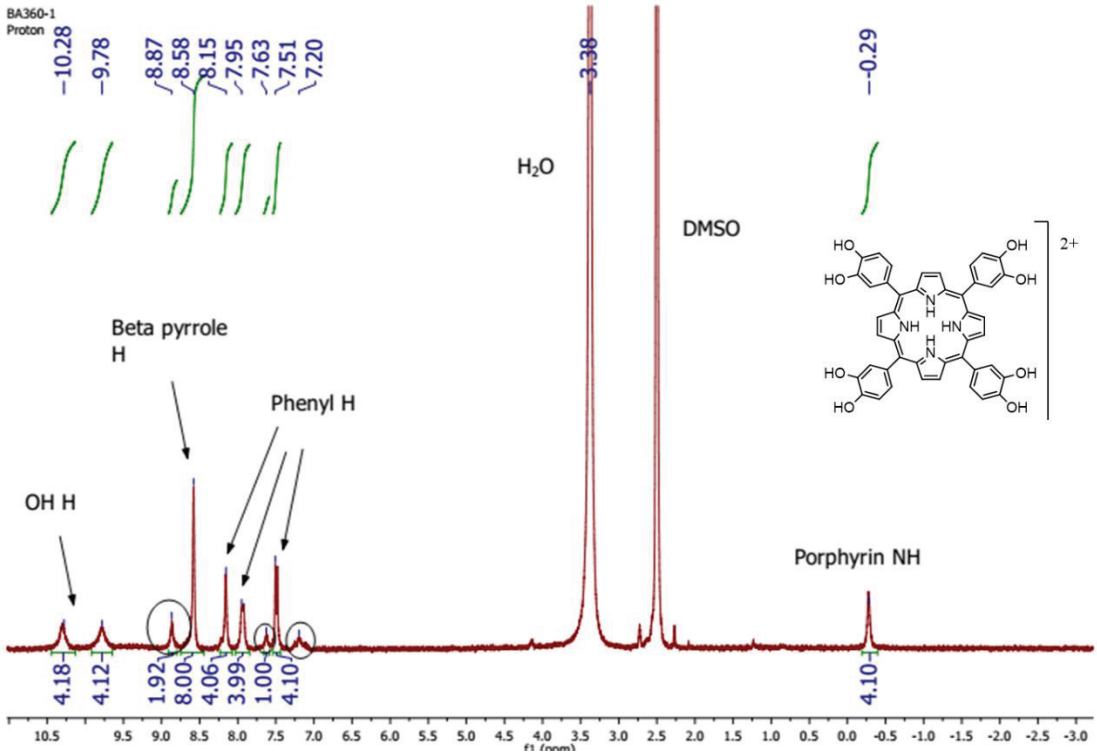

Figure 2-17 NMR spectrum (DMSO)of the product obtained from the method 2 of the BBr_3 ether cleavage. The major product obtained is the diprotonated species of H_{10}-PorphCat (H_{12}-PorphCat $^{2+}$). The circled peaks represent the unprotonated H_{10}-PorphCat which is present at 25% compared to the major product

Mass spectrometry

Mass spectrometry data for both methods used with BBr_3 ether cleavage of $H_2T(OMe)_2PP$ indicated the presence of the mono protonated molecular ion, $[(H_{10}\text{-PorphCat})+H]^+$ at 743 m/z and did not have any peaks corresponding to any methoxy containing species. Mass spectrometry data is given the section A.2.2 of the appendix.

UV-Vis spectroscopy

Figure 2-18 showed the progress of the nickel metalation of $H_2T(OMe)_2PP$ followed via UV-vis spectroscopy. As shown, the reaction was continued until the peaks due to the protonated $H_2T(OMe)_2PP$ were not visible upon the addition of HCl to the aliquots. Table 2-2 shows the peaks observed for the UV-vis spectra of the final product, $NiT(OMe)_2PP$ compared to the starting material, $H_2T(OMe)_2PP$. The Soret band was at 422nm and only one Q band was visible at 531 nm.

The products from both methods of the BBr_3 ether cleavage gave similar UV-vis spectra in DMF (Figure 2-19). This indicated that in DMF the porphyrin is in its free base form. The product of the $NiT(OMe)_2PP$ ether cleavage with pyridinium chloride gave a UV-vis spectrum with only one Q band visible as shown in Figure 2-19C.

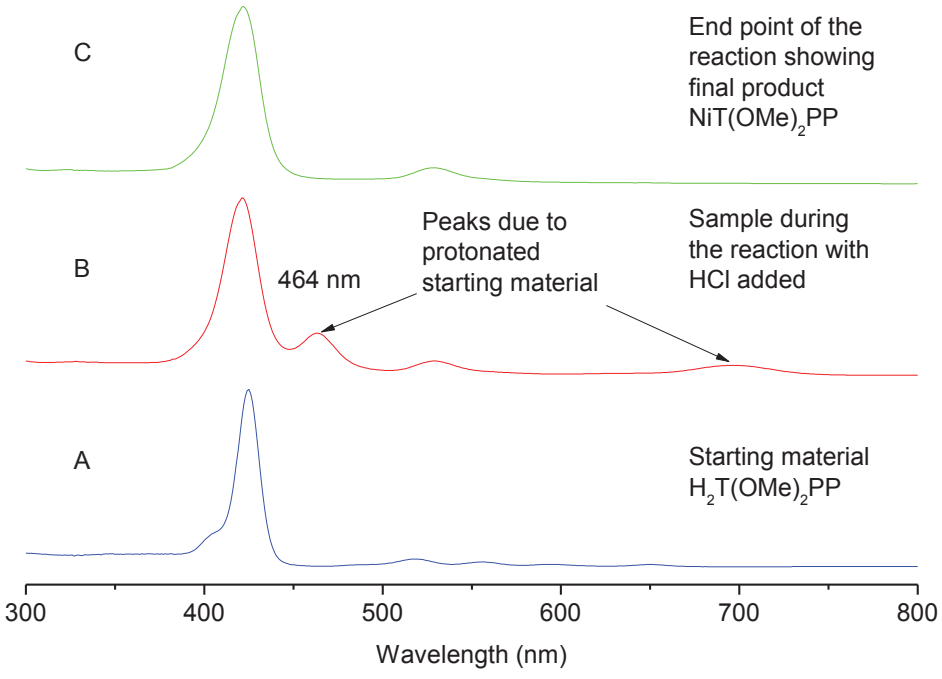

Figure 2-18 Reaction progress followed via UV-Vis spectroscopy for the Ni metalation of $H_2T(OMe)_2PP$. A) Starting material, B) spectrum of the sample during the reaction after HCl was added to the aliquot. Shoulder peak is due to the protonated free base porphyrin, C) UV-vis spectrum at the end point of the reaction with the final product, $NiT(OMe)_2PP$ where there is no appearance of the shoulder peak at 464nm after HCl is added to the aliquot.

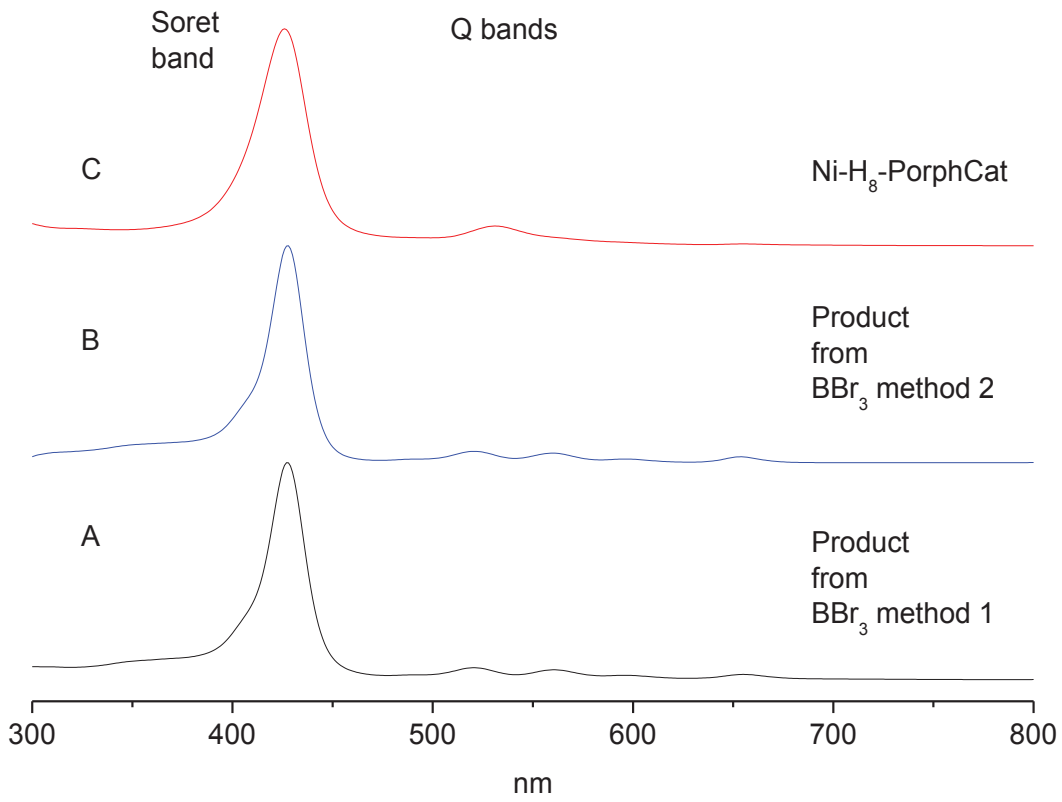

Figure 2-19 UV-vis spectra of catechol porphyrins in DMF. A) H_{10}-PorphCat obtained from the BBr_3 ether cleavage method 1 B) H_{12}-PorphCat-2X obtained from BBr_3 ether cleavage method 2 C) Ni-H_8-PorphCat obtained from the ether cleavage of $NiT(OMe)_2PP$ with pyridinium chloride.

Table 2-2 The peaks observed in UV-vis spectra for the methoxy and catechol porphyrins. $H_2T(OMe)_2PP$ and $NiT(OMe)_2PP$ were measured in chloroform while the rest where measured in DMF.

	Soret band (nm)	**Q bands (nm)**
$H_2T(OMe)_2PP$	425	518, 558, 595, 652
$NiT(OMe)_2PP$	422	530
H_{10}-PorphCat	427	520,561,596,654
Ni-H_8-PorphCat	425	531

IR spectroscopy

IR spectra for $H_2T(OMe)_2PP$, H_{12}-PorphCat-2X (X= Br^- or Cl^-) from method 2 and Ni-H_8-PorphCat are shown on Figure 2-20. The broad peak at 3100 cm^{-1} in the spectra for hydroxy group containing porphyrins (Ni-H_8-PorphCat, H_{12}-PorphCat-2X) represents the OH stretch which is not present in the methoxy group containing porphyrin, $H_2T(OMe)_2PP$. The peak at around 2830 cm^{-1} in the $H_2T(OMe)_2PP$ spectrum can be assigned to the CH stretch of the methoxy group.

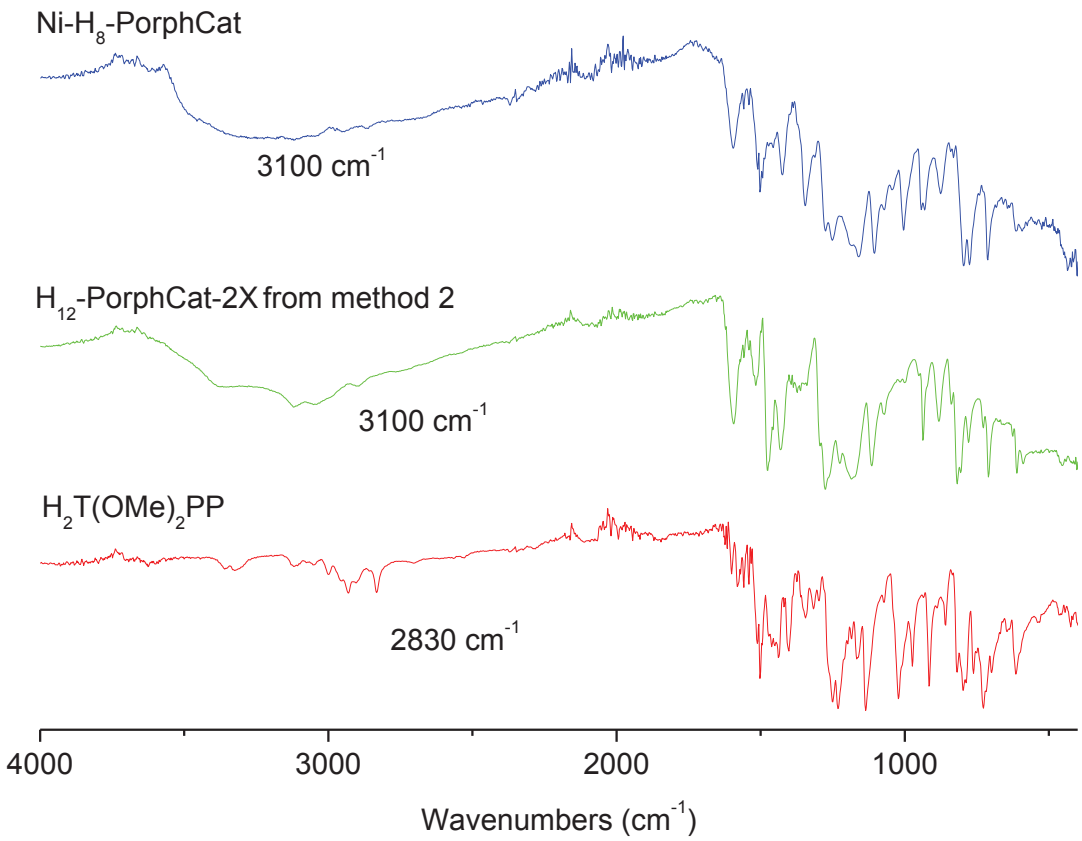

Figure 2-20 IR spectra for Ni-H_8-PorphCat, H_{12}-PorphCat-2X from method 2 and $H_2T(OMe)_2PP$.

2.2.3. Gallol based porphyrin ligands

Synthesis

The synthesis of the trimethoxy protected porphyrin, 5,10,15,20-tetrakis(3,4,5-trimethoxyphenyl) porphyrin (H_2TtrimPP) has been previously reported in literature via the Lindsey method.[38] In this work, Adler method was used as shown in Figure 2-21 in a gram scale with a yield of 15%. The product was purified by washing with methanol.

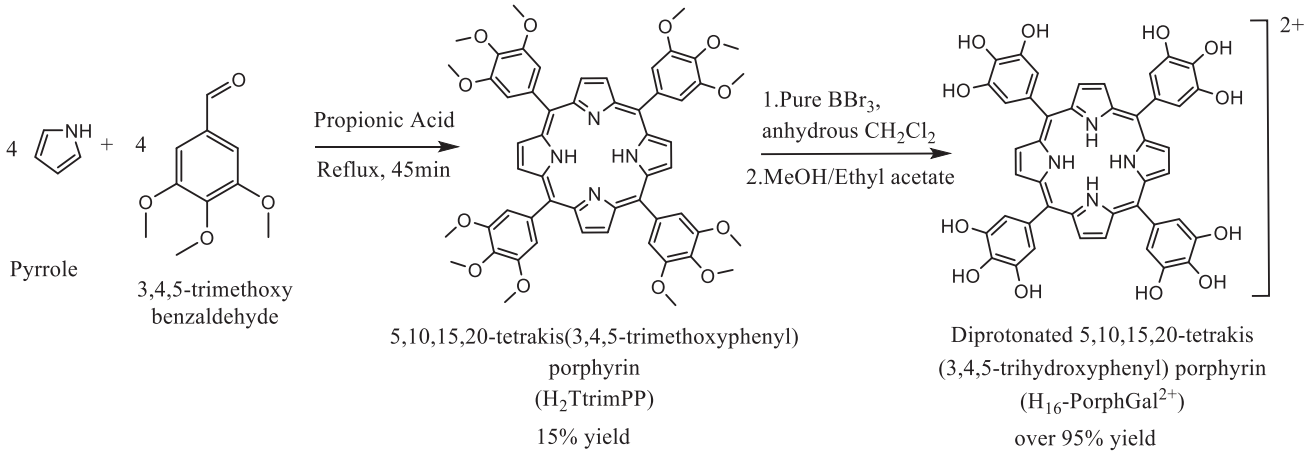

Figure 2-21 Synthesis procedure used to obtain 5,10,15,20-tetrakis(3,4,5-trihydroxyphenyl)porphyrin.

The ether cleavage of the methoxy groups of H_2TtrimPP was achieved using pure BBr_3 similar to what has been reported before.[38] However, the purification method using successive washing with methanol and ethyl acetate to obtain the final product was developed in this work. Similar to what was seen with catechol porphyrin, the resultant product, H_{16}-PorphGal^{2+}, was in the diprotonated form. Br^- ions are present as counter ions as indicated in the mass spectrometry data. The product, H_{16}-PorphGal-2Br was obtained at over 95% yield.

Characterisation

NMR spectroscopy and Mass spectrometry

NMR spectroscopy and mass spectrometry confirmed the successful synthesis of H_2TtrimPP. All the spectra are given in section A.3.1 and A.3.2 of the appendix.

The NMR spectrum after BBr_3 ether cleavage indicated that the product obtained was in the diprotonated form, H_{16}-PorphGal^{2+}, as there are four pyrrolic NH protons present and the peak is shifted downfield compared to the free base form(-0.11 ppm compared to ~-3 ppm for free base porphyrins) (Figure 2-22).[40-41] The mass spectrometry data confirmed that the ether cleavage of the methoxy groups was complete as no peaks correlating to methoxy species were present. Furthermore, the mass spectrometry data (Figure 2-23) indicated a peak present at 887.1 m/z which was assigned to a bromine ion associated with diprotonated H_{14}-PorphGal(H_{16}-PorphGal^{2+}).

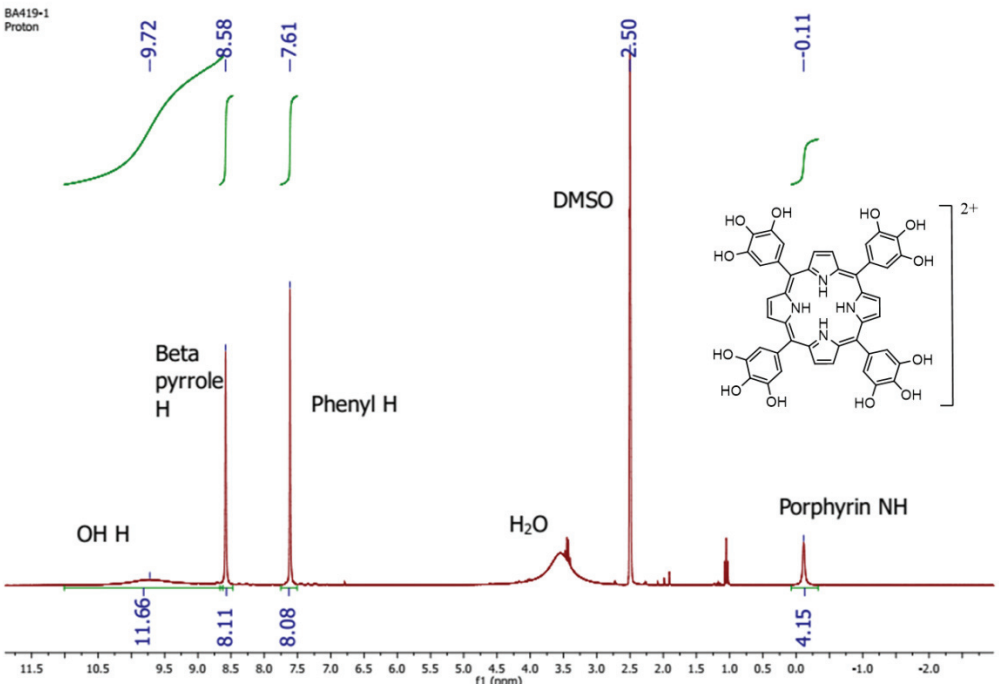

Figure 2-22 NMR spectrum in DMSO for H_{14}-PorphGal which is present in the diprotonated form (H_{16}-PorphGal^{2+}) as indicated by the presence of two extra porphyrin NH protons.

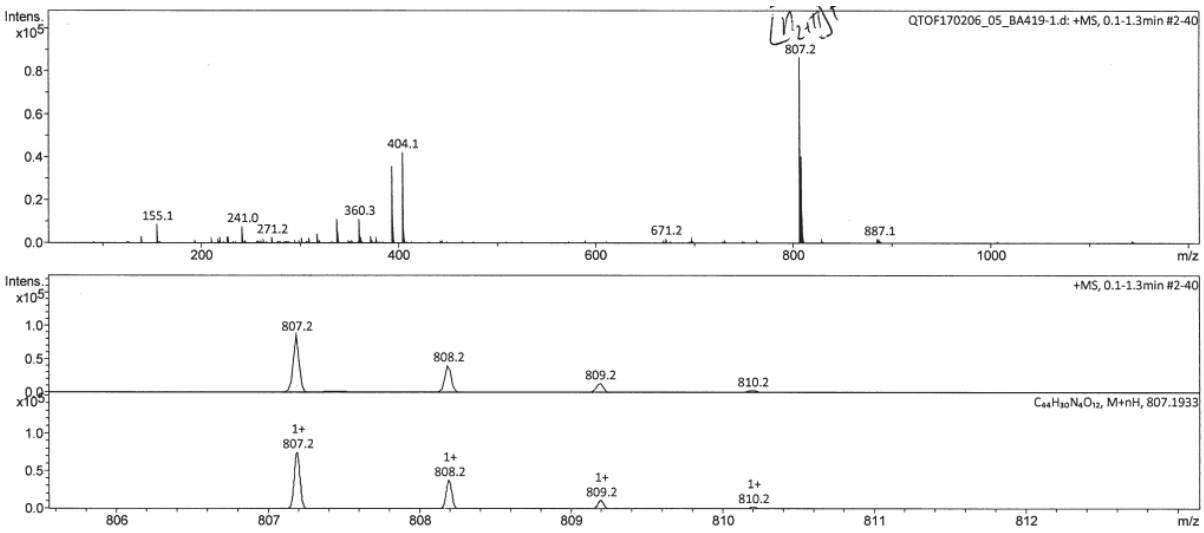

Figure 2-23 Mass spectrometry data for H_{16}-PorphGal-2Br in THF. The monoprotonated molecular ion (H_{14}-PorphGal+H^+)$^+$ at 807.2 m/z along with the absence of any methoxy species confirm the complete ether cleavage of the methoxy groups of H_2TtrimPP. The peak at 887.1 m/z can be attributed to the (H_{14}-PorphGal+2H^++Br^-)$^+$ complex which indicate that Br^- is present as a counter ion.

UV-vis spectroscopy

Solution phase UV-vis spectra for H_{16}-PorphGal-2Br and H_2TtrimPP in DMF are shown on Figure 2-24 and Table 2-3 summarises the peaks observed. In this solution phase, H_{16}-PorphGal-2Br is present in the unprotonated free base form (H_{14}-PorphGal) as it has a UV spectra of a normal free base porphyrin as opposed to one for a protonated porphyrin.[42]

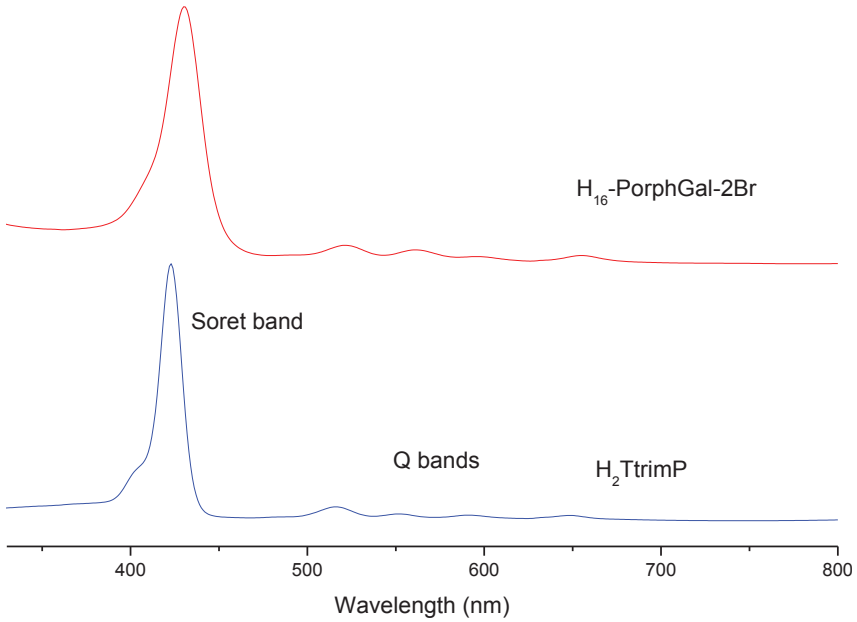

Figure 2-24 UV spectra of H_2TtrimPP and H_{16}-PorphGal-2Br porphyrins in DMF.

Table 2-3 Table showing the peaks observed with UV-vis spectrometry for H_2TtrimPP and H_{16}-PorphGal-2Br in DMF.

	Soret band(nm)	**Q bands (nm)**
H_2TtrimPP	423	516, 552, 592, 648
H_{16}-PorphGal-2Br	430	522, 560,598,655

IR spectroscopy

The IR spectra for H_{16}-PorphGal-2Br and H_2TtrimPP are shown on Figure 2-25. The methoxy CH stretch of the H_2TtrimPP is present at 2820 cm^{-1} while the OH stretch of the hydroxy groups of H_{16}-PorphGal-2Br is present at around 3100 cm^{-1}. This indicates the successful cleavage of the methoxy groups of H_2TtrimPP to yield the hydroxyl group of H_{16}-PorphGal-2Br.

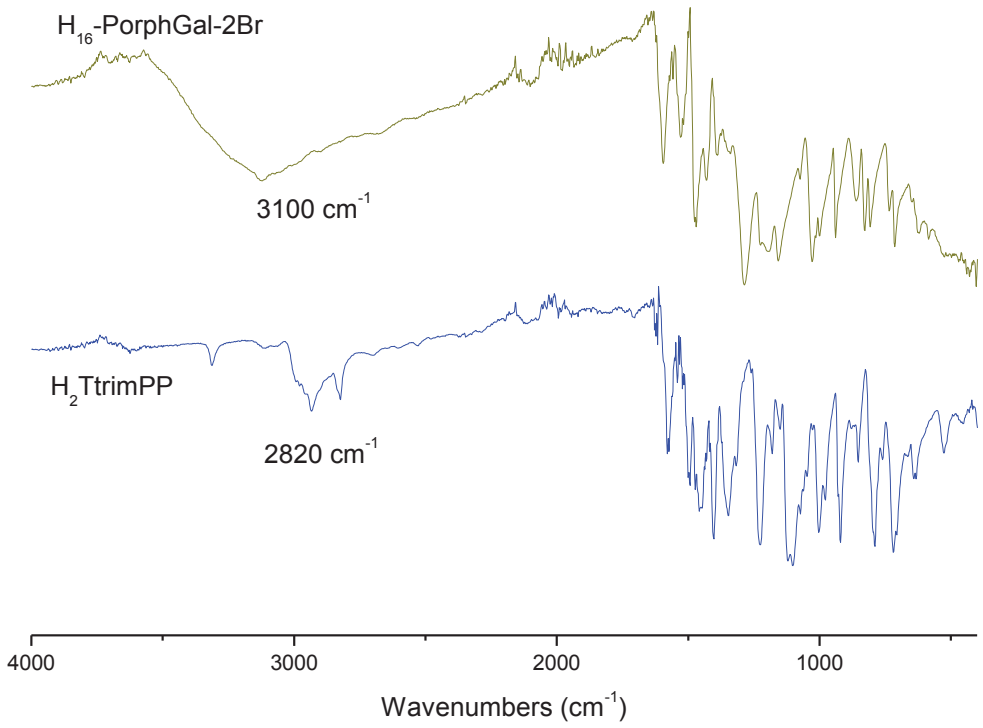

Figure 2-25 IR spectra for H_{16}-PorphGal-2Br and H_2TtrimPP.

2.2.4. Tetrazole based porphyrin ligands

Synthesis

Synthesis of 5,10,15,20-tetrakis(4-(2H-tetrazol-5-yl)phenyl)porphyrin (H_2TTPP) has been reported before by Gauuan et al.[43] In this work, the nitrile functionalised porphyrin synthesis (H_2TCyanoP) was achieved via the Adler synthesis instead of using the Lindsey method employed by the authors. The 1,3-dipolar cycloaddition of sodium azide to the nitrile group to synthesize the tetrazole functionalised porphyrin (H_2TTPP) was achieved following a reported method.[43] The reaction was performed in a gram scale and the limiting step, yield wise was the synthesis of the cyano porphyrin (H_2TCyanoP) (Figure 2-26). It must be noted that care must be taken when handling sodium azide as it can be explosive.

The metalation of the two porphyrins were not attempted as it would likely lead to the formation of polymers as the nitrile group and the tetrazolate group can coordinate to metal ions.

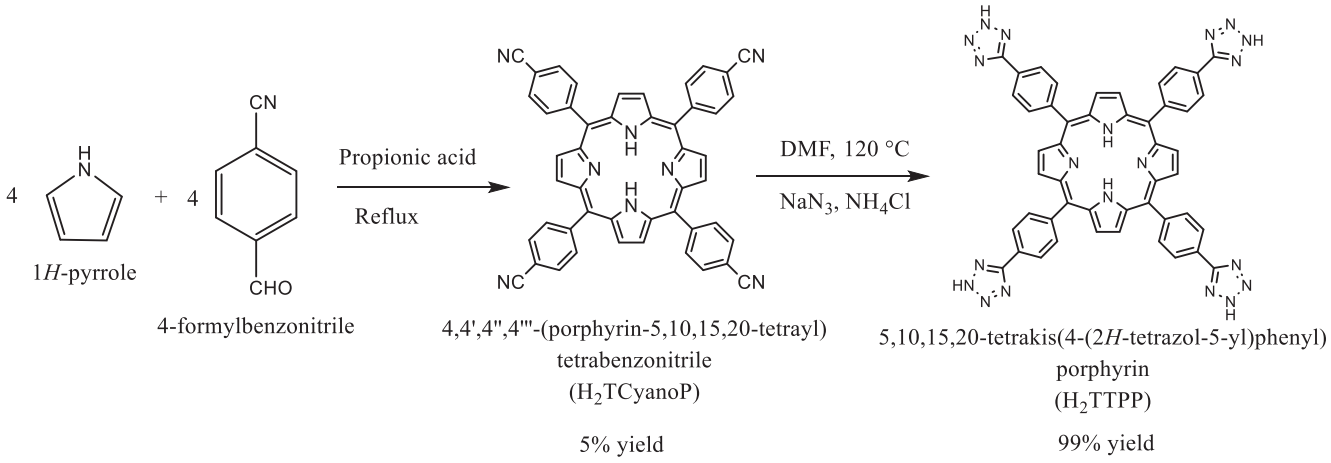

Figure 2-26 Synthesis of 5,10,15,20-tetrakis(4-(2H-tetrazol-5-yl)phenyl)porphyrin (H_2TTPP).

Characterisation

NMR and Mass spectrometry

NMR spectroscopy and mass spectrometry confirmed the synthesis of the products and are shown in the appendix section A.4.1 and A.4.2).

UV-vis spectroscopy

The UV-vis spectra for H_2TCyanoP and H_2TTPP are shown on Figure 2-27 and are typical of free base porphyrins with a Soret band and four Q bands (Table 2-4).

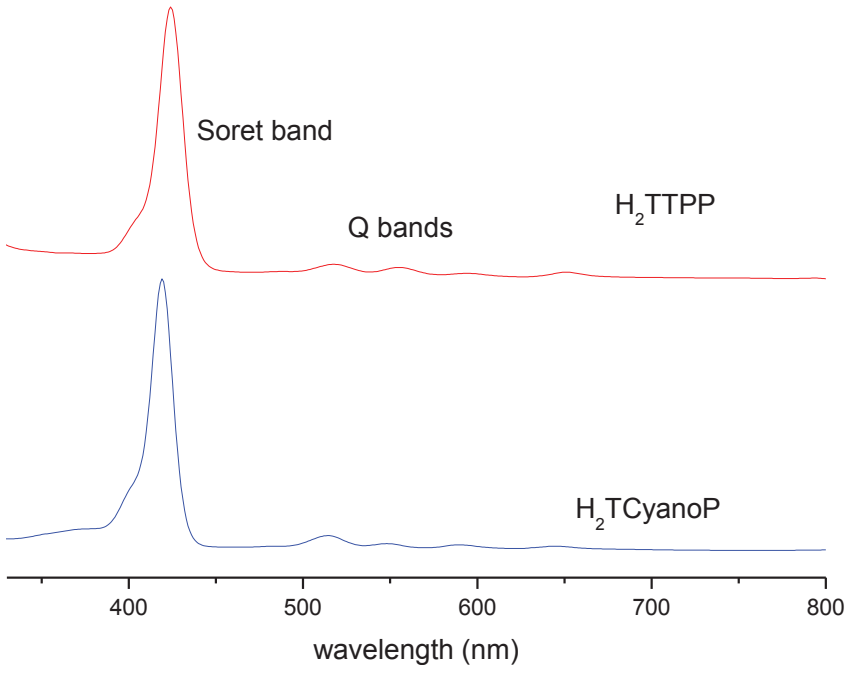

Figure 2-27 UV spectra of H_2TCyanoP and H_2TTPP in DMF.

Table 2-4 Table showing the peaks observed with UV-vis spectrometry for H_2TcyanoP and H_2TTPP.

	Soret band (nm)	Q bands (nm)
H_2TCyanoP	419	513,549, 589,645
H_2TTPP	424	518, 555,595,651

IR spectroscopy

IR spectroscopy is a useful technique to follow the second step of the H_2TTPP synthesis. The CN stretch present at 2220 cm^{-1} for the H_2TCyanoP disappears upon the conversion of the CN group to the tetrazole group as shown in Figure 2-28.

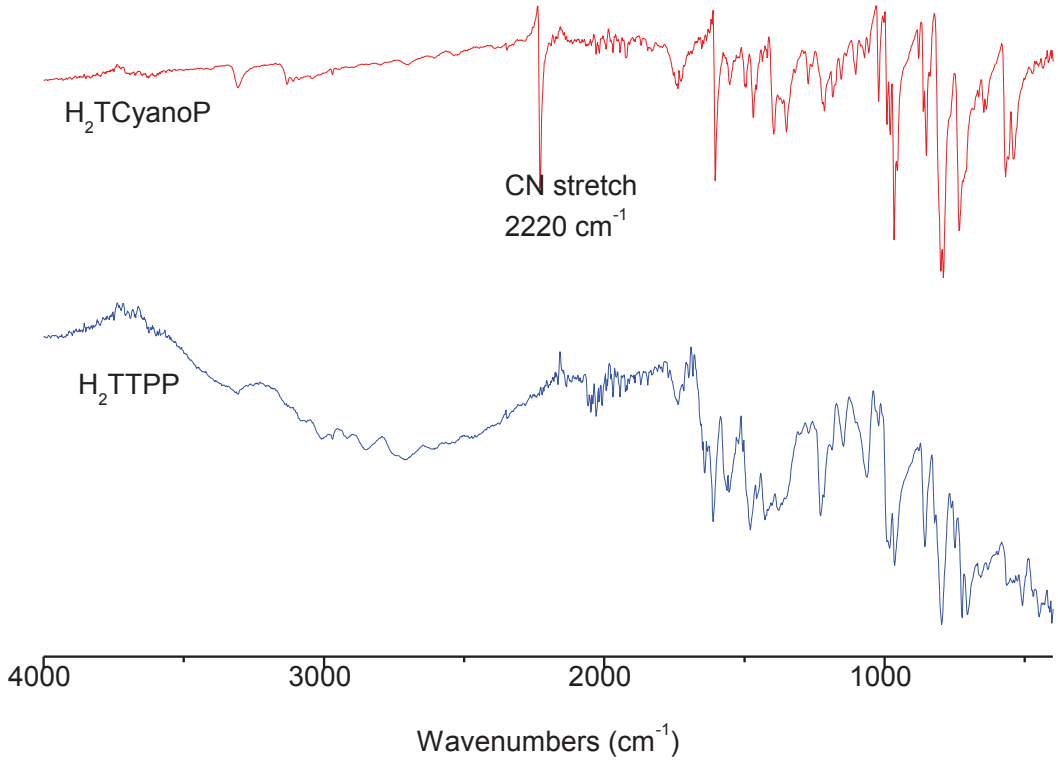

Figure 2-28 IR spectra of H_2TayanoP (top) and H_2TTPP (bottom).

2.2.5. Conclusions

Iron, manganese and cobalt metalated porphyrin ligands with the carboxylic acid functional group (TCPP) were successfully synthesized in a gram scale (3 synthesis steps, ~12% total yield).

The catechol functional group based H_{10}-PorphCat was synthesized in a gram scale (2 synthesis steps, ~13% yield). Nickel was successfully inserted in to the methoxy protected $H_2T(OMe)_2PP$, and the methoxy groups were successfully hydrolysed using pyridinium chloride to yield Ni-H_8-PorphCat with a small extent of demetalation (3 synthesis steps, 9% total yield).

Gallol functionalised H_{14}-PorphGal porphyrin was synthesized in a gram scale via the intermediate porphyrin H_2TtrimPP. The ether cleavage of the H_2TtrimPP using BBr_3 yielded the diprotonated form of the porphyrin ligand, H_{16}-PorphGal-2Br (2 synthesis steps, ~14% total yield).

H_2TTPP with the tetrazole functional group was successfully synthesized in a gram scale via the intermediate product, H_2TCyanoP (2 synthesis steps, ~5% yield).

2.3. Experimental section

General methods

All reagents were of commercial origin and used as received from different providers as shown in the table below.

Table showing the providers for different reagents used in syntheses.

Reagent	**Provider**
Pyrrole	ACROS organics
methyl 4-formylbenzoate	Sigma-Aldrich
3,4-dimethoxybenzaldehyde	Sigma-Aldrich
3,4,5-trimethoxybenzaldehyde	Sigma-Aldrich
4-formylbenzonitrile	TCI chemicals
$Mn(CH_3COO)_2{\cdot}4H_2O$	Alfa Aesar
$Co(CH_3COO)_2{\cdot}4H_2O$	Alfa Aesar
Anhydrous $FeCl_2$	ACROS organics
Anhydrous $NiCl_2$	Sigma-Aldrich
BBr_3 pure	Sigma-Aldrich
BBr_3 1M in dichloromethane	Sigma-Aldrich
Pyridinium chloride	Sigma-Aldrich

^{1}H NMR spectroscopy was performed on a AVS 300 Bruker spectrometer at the Centre Commun de RMN at the University of Claude Bernard Lyon 1.

Infrared spectroscopy was performed with a Nicolet 380 FT-IR spectrometer coupled with the attenuated total reflectance (ATR) accessory.

UV-vis spectroscopy was performed with a SAFAS Monaco UV-mc^2 spectrophotometer.

Mass spectrometry was performed at the Centre Commun de Spectrométrie de Mass at the University of Claude Bernard Lyon 1 on a MicrOTOFQ II – Bruker in electrospray ionisation mode (ESI).

Carboxylic acid based porphyrin ligands

Synthesis of 5,10,15,20-tetrakis(4-methoxycarbonylphenyl)porphyrin (H_2TEsterP, $C_{52}H_{38}N_4O_8$)

Methyl 4-formylbenzoate (10.0 g, 60.9 mmol) and propionic acid (70 mL) were combined in a round bottom flask to which pyrrole (4.2 mL, 60.5 mmol) was added (pyrrole was purified with a silica micro column before the usage). The mixture was refluxed for 45 minutes and left to return to room temperature. The mixture was then filtered and the solid obtained was washed with ~50 mL warm deionised water five times and with pentane three times to yield the purple product (2.16 g, 2.55 mmol, yield 17%). NMR ^{1}H ($CDCl_3$, 300 MHz) δ/ppm: -2.81 (s, 2H, NH), 4.11 (s, 12H, $COOCH_3$), 8.31 (d, 8H, phenyl H, J = 8.2 Hz), 8.44 (d, 8H, phenyl H, J = 8.2 Hz), 8.82 (s, 8H, porphyrin H); FTIR cm^{-1}**:** 1714 (m, TCPP ester C=O stretch), 1604 (m, aromatic C=C stretch of TCPP); UV-vis ($CHCl_3$) λ_{max}/nm: 421 (Soret), 517, 550, 591, 646 (Q bands).

Synthesis of 5,10,15,20-tetrakis(4-methoxycarbonylphenyl)porphyrinato-Mn(III)-X [MnTEsterP(X), $C_{52}H_{36}N_4O_8MnX$, X= OH^-, CH_3COO^-]

A solution of H_2TEsterP (2.00 g, 2.36 mmol) and $Mn(CH_3COO)_2{\cdot}4H_2O$ (2.93 g, 11.9 mmol) in 200 mL of DMF was refluxed for 12 hours. After, the mixture was left to cool down to room temperature and DMF was evaporated using a rotary evaporator. The obtained solid was completely dissolved in chloroform and washed with deionised water. The organic layer was dried over anhydrous magnesium sulfate and evaporated to afford dark green solid which was recrystallized with dichloromethane/pentane to obtain dark green product (1.52 g, 1.59 mmol, yield 70% for X=OH^-). ESI-MS (m/z): 899.4 [$(MnTEsterP)^+$]; FTIR cm^{-1}**:** 1714 (m, TCPP ester C=O stretch), 1604 (m, aromatic C=C stretch of TCPP); UV-vis ($CHCl_3$) λ_{max}/nm: 377, 400, 472 (Soret) 524, 576, 613 (Q bands).

Synthesis of 5,10,15,20-tetrakis(4-methoxycarbonylphenyl)porphyrinato-Co(III)-X [CoTEsterP(X), $C_{52}H_{36}N_4O_8CoX$, X= OH^-, CH_3COO^-]

A solution of H_2TEsterP (1.00 g, 1.17 mmol) in chloroform and $Co(CH_3COO)_2{\cdot}4H_2O$ (1.50 g, 6.02 mmol) in anhydrous ethanol (150 mL) was refluxed for 3 days. Reaction was followed via TLC and UV-vis spectroscopy and after each day additional 300 mg of $Co(CH_3COO)_2{\cdot}4H_2O$ was added. Once the reaction was complete mixture was cooled to room temperature and the solvent was evaporated. The resultant solid was dissolved in dichloromethane and the solution was filtered using celite. The filtrate was washed with deionised water and the organic layer was extracted and dried with anhydrous sodium sulfate. The red product was obtained by evaporation of the solvent followed by a recrystallization using dichloromethane/pentane and drying at 70 °C for 12hours (0.883 g, 0.978

mmol, yield 82 % for X=OH^-). ESI-MS (m/z): 903.4 [$(CoTEsterP)^+$]; FTIR cm^{-1}**:** 1714 (m, TCPP ester C=O stretch), 1604 (m, aromatic C=C stretch of TCPP); UV-vis ($CHCl_3$) λ_{max}/nm: 430 (Soret), 543, 588 (Q bands).

Synthesis of 5,10,15,20-tetrakis(4-methoxycarbonylphenyl)porphyrinato-Fe(III)-chloride [FeTEsterP(Cl), $C_{52}H_{36}N_4O_8FeCl$]

A solution of H_2TEsterP (1.50 g, 1.77 mmol) and anhydrous $FeCl_2$ (0.290 g, 2.31 mmol) in 250 mL of DMF was refluxed for 12 hours under an argon atmosphere. After, the mixture was left to cool down to room temperature and ¾ of the DMF was evaporated using a rotary evaporator. Then 200mL of deionised water and 40mL of 1M HCl is added and left for 1 hour so the precipitate would form. The solid was filtered to obtain a brownish solid which was dissolved in THF and centrifuged to remove any insoluble impurities if present. The solid obtained by evaporation was recrystallized with dichloromethane/pentane to obtain the brownish product (1.4 g, 1.50 mmol, yield 85%). ESI-MS (m/z): 900.4 [$(FeTEsterP)^+$]; FTIR cm^{-1}**:** 1714 (m, TCPP ester C=O stretch), 1604 (m, aromatic C=C stretch of TCPP); UV-vis ($CHCl_3$) λ_{max}/nm: λ 416 (Soret), 507, 571, 610 (Q bands).

Synthesis of 5,10,15,20-tetrakis(4-carboxyphenyl)porphyrinato-Mn(III)-X [MnTCPP(X), $C_{48}H_{28}N_4O_8MnX$, X= Cl^-, OH^-]

MnTEsterP(X) (1.46 g, 1.52 mmol) was stirred in THF (100 mL), to which a solution of KOH (1.03 g, 18.2 mmol) in deionised water (50 mL) was introduced. This mixture was refluxed for 12 hours. After cooling down to room temperature, THF was evaporated. Additional deionised water was added to the resulting water phase and the solid was fully dissolved (60 mL), then the homogeneous solution was acidified with 1M HCl until no further precipitate was detected. A dark green solid was collected by filtration, which was added to 300mL of deionised water and left stirring overnight. The dark green solid was collected by filtration, washed with water and dried under vacuum to obtain the dark green product (1.13 g, 1.25 mmol, 82 % yield for X=OH^-). ESI-MS (m/z)**:** 843.12 [$(MnTCPP)^+$]; FTIR cm^{-1}**:** 2950 (w broad, carboxylic acid OH stretch), 1733 (m), 1688 (m, TCPP carboxylic acid C=O), 1605 (m, aromatic C=C stretch of TCPP); UV-vis (0.1M NaOH) λ_{max}/nm: 380, 401, 464 (Soret), 525, 573,611 (Q bands).

Synthesis of 5,10,15,20-tetrakis(4-carboxyphenyl)porphyrinato-Co(III)-X

[CoTCPP(X), $C_{48}H_{28}N_4O_8CoX$, X= Cl^-, OH^{-1}]

CoTEsterP(X) (1.65 g, 1.83 mmol) was stirred in THF (150 mL), to which a solution of KOH (1.23 g, 21.9 mmol) in deionised water (75 mL) was introduced. This mixture was refluxed for 12 hours. After cooling down to room temperature, THF was evaporated. Additional deionised water was added to the resulting water phase and the solid was fully dissolved (heat if needed) (50mL), then the homogeneous solution was acidified by slowly adding 1M HCl until no further precipitate was detected. A red solid was collected by filtration, which was added to 300 mL of deionised water and left stirring overnight. The solid collected by filtration and washed with deionised water and dried under vacuum to obtain the red product (1.47 g, 1.83 mmol, yield 86% for X=OH^-). ESI-MS (m/z): 847.12 [$(CoTCPP)^+$]; FTIR cm^{-1}: 2950 (w broad, carboxylic acid OH stretch), 1690 (m, TCPP C=O stretch), 1604 (m, aromatic C=C stretch) cm^{-1}; UV-vis (0.1M NaOH) λ_{max}/nm: 430 (Soret), 551, 590 (Q bands).

Synthesis of 5,10,15,20-tetrakis(4-carboxyphenyl)porphyrinato-Fe(III)-chloride

[FeTCPP(Cl), $C_{48}H_{28}N_4O_8FeCl$]

FeTEsterP(Cl) (1.40 g, 1.55 mmol) was stirred in THF (100 mL), to which a solution of KOH (1.00 g, 18.2 mmol) in deionised water (50 mL) was introduced. This mixture was refluxed for 12 hours. After cooling down to room temperature, THF was evaporated. Additional deionised water was added to the resulting water phase and the solid was fully dissolved (heat if needed) (60 mL), then the homogeneous solution was acidified with 30mL of 1M HCl until no further precipitate was detected. A reddish violet solid was collected by filtration, which was added to 300mL of deionised water and left stirring overnight. The reddish violet solid was collected by filtration, washed with deionised water and dried under vacuum to obtain the reddish violet product (1.30 g, 1.47 mmol, 99% yield). ESI-MS (m/z): 844.12 [$(FeTCPP)^+$]; FTIR cm^{-1}: 2950 (w broad, carboxylic acid OH stretch), 1690 (m, TCPP C=O stretch), 1604 (m, aromatic C=C stretch); UV-vis (0.1M NaOH) λ_{max}/nm: 409 (Soret), 568, 609 (Q bands).

Catechol based porphyrin ligands

Synthesis of 5,10,15,20-tetrakis(3,4-dimethoxyphenyl)porphyrin [$H_2T(OMe)_2PP$, $C_{52}H_{46}N_4O_8$]

3,4-dimethoxybenzaldehyde (10.8 g, 65 mmol) and propionic acid (70 ml) were combined in a round bottom flask to which pyrrole (5 ml, 71.5 mmol) was added (pyrrole was purified with a silica micro column before the usage). The resultant mixture was refluxed for 45 minutes. After the reaction mixture had cooled down, 600 mL of deionised water was added. To the resultant brown solution, 2M NaOH was added until the mixture was neutralised (500 ml) which resulted in a precipitate. A brown

solid was obtained by filtrations followed by washing three times with deionised water and three times with pentane and drying overnight at 65 °C. The violet product (1.84 g, 2.15 mmol, yield 15%) was obtained by purification via a silica gel column (dichloromethane: triethylamine, 100:1 → dichloromethane: methanol: triethylamine, 100:1:1 → dichloromethane: methanol: triethylamine, 100:2:1) where the first two fractions were concentrated followed by recrystallization with dichloromethane/methanol. NMR ^{1}H (DMSO, 300 MHz):δ -2.89 (s, 2H, NH), 3.87 (s, 12H, $COCH_3$), 4.05 (s, 12H, $COCH_3$) 7.37 (d, 4H, phenyl H, J = 8.3 Hz), 7.69 (d, 4H, phenyl H, J = 7.2 Hz), 7.81 (s, 4H, aromatic) 8.90 (s, 8H, porphyrin H); ESI-MS (m/z): 855.5 [($H_2T(OMe)2PP+H)^+$]; FTIR cm^{-1}; 2830(w, methoxy CH_3 stretch), 1500(m, aromatic C=C stretch), 1435 (s, aromatic C=C stretch); UV-vis ($CHCl_3$) λ_{max}/nm : 425 (Soret), 518, 558, 595, 652 (Q bands).

Synthesis of 5,10,15,20-tetrakis(3,4-dimethoxyphenyl)porphyrinato-Ni(II)

[NiT(OMe)$_2$PP, $C_{52}H_{44}N_4O_8Ni$]

Dry $H_2T(OMe)_2PP$ (1.40 g, 1.63 mmol) was dissolved in 125 mL of chloroform and anhydrous $NiCl_2$ (0.850 g, 6.56 mmol) in 125 mL of anhydrous ethanol. The resultant solutions were combined and triethylamine was added to the mixture (2.28 mL, 16.4 mmol) and refluxed. The reaction was followed using TLC and UV-vis (when UV-vis spectra was measured, a few drops of 1M HCl was added to the aliquot to protonate any free base porphyrin present). Additional $NiCl_2$(60 hrs 0.850 g, 6.56 mmol/ 66 hrs 1.70 g, 13.1 mmol) was periodically added. Once the UV spectrum showed the disappearance of the shoulder peak at 460 nm (which indicates the presence of the protonated free base porphyrin) the reaction was stopped (72 hours). Afterwards, most of the solvent of the resultant mixture was evaporated and deionised water (100 mL) was added. Filtration of the resultant precipitate yields a reddish solid which was redissolved in chloroform and further washed with deionised water. The organic layer was dried with anhydrous sodium sulfate and the solvent was evaporated followed by drying the solid under vacuum to obtain the reddish violet product (1.18 g, 1.30 mmol, 80% yield). NMR ^{1}H ($CDCl_3$, 300 MHz) δ/ppm: 3.94 (s, 12H, OCH_3), 4.13 (s, 12H, OCH_3) 7.20 (d, 4H, phenyl H, J = 8.1 Hz), 7.56 (d, 8H, phenyl H, J = 11.2 Hz), 8.81 (8H, s, porphyrin H); UV-vis ($CHCl_3$) λ_{max}/nm: 422 (Soret), 530 (Q bands).

Synthesis of 5,10,15,20-tetrakis(3,4-dihydroxyphenyl)porphyrin)- Method -1

[H$_{10}$-PorphCat, $C_{44}H_{30}N_4O_8$]

$H_2T(OMe)_2PP$ (1.00 g, 1.16 mmol) was dissolved in anhydrous dichloromethane (100 mL) in a round bottom flask and an inert atmosphere was established. Then BBr_3 (20.0 ml of 1M solution, 20.0 mmol) was added at -70 °C (acetone/water bath) and the reaction mixture was maintained at this

temperature for 1 hour. After, the reaction was left to cool down to room temperature and allowed to proceed. After 24 hours, the reaction was quenched by adding glacial water. Saturated $NaHCO_3$ was added to the greenish reaction mixture followed by ethyl acetate and the organic layer was separated and dried with anhydrous sodium sulfate. The solid obtained from evaporating the organic layer was washed with dichloromethane. The violet colored product was obtained via filtration (560 mg, 0.755 mmol, 65% yield). NMR ^1H (DMSO, 300 MHz) δ/ppm: -2.91 (s, 2H, porphyrin NH), 7.18 (d, 4H, phenyl H, J = 7.9 Hz), 7.46 (d, 4H, phenyl H, J = 8.5 Hz), 7.59 (s, 4H, phenyl H), 8.90 (s, 8H, porphyrin H), 9.40 (d, 8H, OH H, J = 10.4 Hz); FTIR cm^{-1}; 3100 (broad, OH stretch), 1595 (m, aromatic C=C stretch), 1475 (s, aromatic C=C stretch); UV-vis (DMF); λ_{max}/nm: 427 (Soret), 520 561, 596, 654 (Q bands).

Synthesis of diprotonated 5,10,15,20-tetrakis(3,4-dihydroxyphenyl)porphyrin – Method 2 – [H_{12}-PorphCat-2X, $C_{44}H_{32}N_4O_8X_2$, X= Br^- or Cl^-]

Dry $H_2T(OMe)_2PP$ (1.07 g, 1.25 mmol) was dissolved in anhydrous dichloromethane (120 mL) in a round bottom flask and an inert atmosphere was established. Then pure BBr_3 (4.0 ml, 41.2 mmol) was carefully added in a dropwise manner at -70 °C (acetone/water bath) and the reaction mixture was left to return to room temperature slowly. After 24 hours, the reaction was quenched by adding cold methanol (90 mL) dropwise in an ice bath. Then most of the solvent was removed and deionised water was added (100 mL). The green precipitate was filtered and washed with acidic water (pH ~3-4) and dried at 100 °C overnight to yield the green product (0.920 g, ~85% yield). NMR ^1H (DMSO, 300 MHz) δ/ppm: H_{12}-PorphCat-2X -0.29 (s, 4H, NH), 7.51 (d, 4H, phenyl H, J= 8.1 Hz), 7.95 (d, 4H, phenyl H, J= 7.2 Hz), 8.15 (s, 4H, phenyl H), 8.58 (s, 8H, porphyrin H), 9.78 (s, 4H, OH H), 10.28 (s, 4H, OH H) H_{10}-PorphCat present at 25% 7.20 (phenyl H) 7.63 (phenyl H), 8.87 (porphyrin H); ESI-MS (m/z): 743.5 [(H_{10}-PorphCat)+H]$^+$); FTIR cm^{-1}; 3100 (broad, OH stretch), 1596 (m, aromatic C=C stretch), 1479 (s, aromatic C=C stretch); UV-vis (DMF) λ_{max}/nm: 427 (Soret), 520 561, 596, 654 (Q bands).

Synthesis of 5,10,15,20-tetrakis(3,4-dihydroxyphenyl)porphyrinato-Ni(II) [Ni-H_8-PorphCat, $C_{44}H_{28}N_4O_8Ni$]

Dry $NiT(OMe)_2PP$ (1.17 g, 1.28 mmol) and pyridinium chloride (30 g, 379 mmol) were combined in a 100mL round bottom flask and the solids were mixed well (the pyridinium chloride should be filled up to about half way mark of the round bottom flask in order to facilitate the reflux). The mixture was refluxed for 2.5 hours using a metallic bath and left to cool down to room temperature. Afterwards 75 mL of deionised water was added to the reddish solid and sonicated for 15 minutes. The resultant suspension was centrifuged and further washed with deionised water three more times. After drying, the reddish solid was redissolved in THF and was filtered with a fritted glass filter loaded with silica.

The reddish product was obtained by evaporating the filtrate and washing with chloroform (0.790 g, 0.988 mmol, 77% yield). NMR ^{1}H (DMSO, 300 MHz) δ/ppm; Ni-H_8-PorphCat 7.10 (d, 4H, phenyl H, J = 8.0 Hz), 7.25 (dd, 4H, phenyl H, J = 8.0, 2.1 Hz), 7.37 (d, 4H, phenyl H, J = 2.1 Hz), 8.78 (s, 8H, porphyrin H), 9.33 (d, 8H, OH H, J = 5.2 Hz) H_{10}-PorphCat present at 7% : -2.92 (porphyrin NH), 7.17 (phenyl H), 7.46 (phenyl H), 7.58 (phenyl H), 8.89 (porphyrin H), 9.41 (OH H); FTIR cm^{-1}; 3100 (broad, OH stretch), 1600 (m, aromatic C=C stretch), 1426 (s, aromatic C=C stretch); UV-vis (DMF) λ_{max}/nm: λ 425 (Soret), 531 (Q bands).

Gallol based porphyrin ligand

Synthesis of 5,10,15,20-tetrakis(3,4,5-trimethoxyphenyl)porphyrin [H_2TtrimPP, $C_{56}H_{54}N_4O_{12}$]

3,4,5-trimethoxybenzaldehyde (10.1 g, 51.5 mmol) and propionic acid (100 ml) were combined in a round bottom flask to which pyrrole (3.6 ml, 51.9 mmol) was added (pyrrole was purified with a silica micro column before the usage). The resultant mixture was refluxed for 45 minutes and left to cool down to room temperature. Afterwards, the reaction mixture was filtered and washed with methanol. A violet solid was obtained by drying in the oven at 70 °C (1.92 g, 1.97 mmol, yield 15 %). NMR ^{1}H (DMSO, 300 MHz) δ/ppm: -2.94 (s, 2H, NH), 3.89 (s, 24H, OCH_3), 3.99 (s, 12H, OCH_3) 7.51 (s, 8H, phenyl H), 8.94 (s, 8H, porphyrin H); ESI-MS (m/z): 975.4 [(H_2TtrimPP)+H]$^+$; FTIR cm^{-1}; 2820(w, methoxy CH_3 stretch), 1575(m, aromatic C=C stretch), 1456 (s, aromatic C=C stretch); UV-vis(DMF) λ_{max}/nm: 423 (Soret), 516, 552, 592, 648 (Q bands)

Synthesis of diprotonated 5,10,15,20-tetrakis(3,4,5-trihydroxyphenyl)porphyrin [H_{16}-PorphGal-2Br, $C_{44}H_{32}N_4O_{12}Br_2$]

Dry H_2TtrimPP (1.38 g, 1.42 mmol) was dissolved in anhydrous dichloromethane (120 mL) in a round bottom flask and an inert atmosphere was established. Then pure BBr_3 (7.0 mL, 72.6 mmol) was carefully added in a dropwise manner at -70 °C (acetone/water bath) and the reaction mixture was left to return to room temperature slowly. After 24 hours, the reaction was quenched by adding methanol (100 mL) dropwise in an ice bath and the mixture was left stirring for 15 minutes. Afterwards, the solvent was removed under reduced pressure. Once all the solvent was removed, the solid was redissolved in methanol and the methanol was evaporated again and this process was repeated for 4 cycles. During the 4th cycle, only ¾ of the methanol was removed. Ethyl acetate was added to the mixture which resulted in a green precipitate which was washed further with ethyl acetate and recovered by centrifugation. The green product was obtained by drying under vacuum for 12 hours (1.386 g, 99% yield). NMR ^{1}H (DMSO, 300 MHz) δ/ppm: -0.11 (s, 4H, NH), 7.61 (s, 8H, phenyl H), 8.58 (s, 8H, porphyrin H), 9.72 (broad s, 12H, OH H); ESI-MS (m/z): 807.2 [(H_{14}-PorphGal)+H]$^+$; FTIR

cm^{-1}; 3100 (broad, OH stretch), 1604 (m, aromatic C=C stretch), 1463 (s, aromatic C=C stretch); UV-vis(DMF) λ_{max}/nm: 430 (Soret), 522, 560, 598, 655 (Q bands).

Tetrazole based porphyrin ligand

Synthesis of 4,4',4'',4'''-(porphyrin-5,10,15,20-tetrayl)tetrabenzonitrile [H_2TCyanoP, $C_{48}H_{26}N_8$]

4-formylbenzonitrile (9.40 g, 72 mmol) and propionic acid (100 ml) were combined in a round bottom flask to which pyrrole (5.0 ml, 72 mmol) was added (pyrrole was purified with a silica micro column before the usage). The resultant mixture was refluxed for 45 minutes and left to cool down to room temperature. Afterwards, the mixture was filtered with deionised water. The resultant solid was triturated with methanol and sonicated in acetonitrile. The solid is then filtered with as little acetone as possible and dried at 80 °C to obtained the purple coloured product (0.650 g, 0.91 mmol, 5.1% yield). NMR ^{1}H (DMSO, 300 MHz) δ/ppm: -3.00 (s, 2H, NH), 8.33 (d, 8H, phenyl H, J = 7.9 Hz), 8.42 (d, 8H, phenyl H, J = 7.8 Hz), 8.88 (s, 8H, porphyrin H); ESI-MS (m/z): 715.5[(H_2TCyanoP+H)$^+$]; FTIR cm^{-1}: 2220 (m, CN stretch), 1604 (m, aromatic C=C stretch); UV-vis(DMF) λ_{max}/nm: 419 (Soret), 513, 549, 589, 645 (Q bands).

Synthesis of 5,10,15,20-tetrakis(4-(2H-tetrazol-5-yl)phenyl)porphyrin [H_2TTPP, $C_{48}H_{30}N_{20}$]

A solution of H_2TCyanoP (0.30 g, 0.42 mmol), NaN_3 (0.24 g, 3.67 mmol), NH_4Cl (0.18 g, 3.37 mmol), and DMF (25 mL) was heated at 120 °C for 3 days. Additional NaN_3 (0.17 g, 2.59 mmol) and NH_4Cl (0.11 g, 2.05 mmol) were added to push the reaction to completion. The DMF was evaporated under reduced pressure followed by the addition of cold deionised water (10 mL). The resulting solution was acidified with 6 M HCl then dichloromethane (10 mL) was added. The resulting precipitate was collected and dried under vacuum to provide a violet solid (0.37 g, 0.41 mmol, 99% yield). NMR ^{1}H (DMSO, 300 MHz) δ/ppm: -2.89 (s, 2H, NH), 8.50 (s, 16H, phenyl H), 8.95 (s, 8H, porphyrin H); ESI-MS (m/z): 887.2[(H_2TTPP+H)$^+$]; FTIR cm^{-1}: 1604 (m, aromatic C=C stretch), 1564 (tetrazole ring stretch); UV-vis(DMF) λ_{max}/nm: 424 (Soret), 518, 555, 595,651 (Q bands).

2.4. References

1. Scott Mathews, F., The structure, function and evolution of cytochromes. *Progress in Biophysics and Molecular Biology* **1985,** *45* (1), 1-56.
2. Frew, J.; Jones, P., Structure and functional properties of peroxidases and catalases. *Advances in inorganic and bioinorganic mechanisms* **1984,** *3*, 175-212.
3. Guengerich, F. P., Human Cytochrome P450 Enzymes. In *Cytochrome P450: Structure, Mechanism, and Biochemistry*, de Montellano, P. R. O., Ed. Springer US: Boston, MA, 1995; pp 473-535.
4. Katz, J. J.; Norris, J. R.; Shipman, L. L.; Thurnauer, M. C.; Wasielewski, M. R., Chlorophyll function in the photosynthetic reaction center. *Annual review of biophysics and bioengineering* **1978,** *7* (1), 393-434.
5. Smith, K. M., *Porphyrins and metalloporphyrins*. Elsevier Amsterdam: 1975; Vol. 9.
6. Kadish, K. M.; Smith, K. M.; Guilard, R., *The Porphyrin Handbook: Inorganic, organometallic and coordination chemistry*. Elsevier: 2000; Vol. 3.
7. Fischer, H., Über Porphyrine und ihre Synthesen. *Berichte der deutschen chemischen Gesellschaft (A and B Series)* **1927,** *60* (12), 2611-2651.
8. Rothemund, P., FORMATION OF PORPHYRINS FROM PYRROLE AND ALDEHYDES. *Journal of the American Chemical Society* **1935,** *57* (10), 2010-2011.
9. Vicente, M. G. H.; Kevin, M. S., Porphyrins and Derivatives Synthetic Strategies and Reactivity Profiles. *Current Organic Chemistry* **2000,** *4* (2), 139-174.
10. Nguyen, L. T.; Senge, M. O.; Smith, K. M., Simple Methodology for Syntheses of Porphyrins Possessing Multiple Peripheral Substituents with an Element of Symmetry. *The Journal of Organic Chemistry* **1996,** *61* (3), 998-1003.
11. Rothemund, P.; Menotti, A. R., Porphyrin Studies. IV.1 The Synthesis of α,β,γ,δ-Tetraphenylporphine. *Journal of the American Chemical Society* **1941,** *63* (1), 267-270.
12. Adler, A. D.; Longo, F. R.; Finarelli, J. D.; Goldmacher, J.; Assour, J.; Korsakoff, L., A simplified synthesis for meso-tetraphenylporphine. *The Journal of Organic Chemistry* **1967,** *32* (2), 476-476.
13. Kim, J. B.; Leonard, J. J.; Longo, F. R., Mechanistic study of the synthesis and spectral properties of meso-tetraarylporphyrins. *Journal of the American Chemical Society* **1972,** *94* (11), 3986-3992.
14. Lindsey, J. S.; Schreiman, I. C.; Hsu, H. C.; Kearney, P. C.; Marguerettaz, A. M., Rothemund and Adler-Longo reactions revisited: synthesis of tetraphenylporphyrins under equilibrium conditions. *The Journal of Organic Chemistry* **1987,** *52* (5), 827-836.
15. Chen, C.-T.; Cha, I.; Hsieh, S. J., Thermal Stability of Robust Unsymmetrical Copperporphyrins with Multiple Diphenylamino and Nitro Substituents. *Journal of the Chinese Chemical Society* **1998,** *45* (6), 741-748.
16. Becker, E. D.; Bradley, R. B.; Watson, C. J., Proton Magnetic Resonance Studies of Porphyrins. *Journal of the American Chemical Society* **1961,** *83* (18), 3743-3748.
17. Gouterman, M., Spectra of porphyrins. *Journal of Molecular Spectroscopy* **1961,** *6*, 138-163.
18. Becker, R. S.; Allison, J. B., METALLOPORPHYRINS. ELECTRONIC SPECTRA AND NATURE OF PERTURBATIONS. I. TRANSITION METAL ION DERIVATIVES1a. *The Journal of Physical Chemistry* **1963,** *67* (12), 2662-2669.
19. Worthington, P.; Hambright, P.; Williams, R. F. X.; Reid, J.; Burnham, C.; Shamim, A.; Turay, J.; Bell, D. M.; Kirkland, R.; Little, R. G.; Datta-Gupta, N.; Eisner, U., Reduction potentials of seventy-five free base porphyrin molecules: Reactivity correlations and the prediction of potentials. *Journal of Inorganic Biochemistry* **1980,** *12* (4), 281-291.
20. Tsutsui, M.; Srivastava, T. S., INDUCED REDOX REACTIONS OF METALLOPORPHYRINS AND THEIR IMPLICATIONS IN BIOLOGICAL SYSTEMS*. *Annals of the New York Academy of Sciences* **1973,** *206* (1), 404-408.
21. Bottomley, L. A.; Olson, L.; Kadish, K. M., Redox Tuning of Iron Porphyrins. In *Electrochemical and Spectrochemical Studies of Biological Redox Components*, AMERICAN CHEMICAL SOCIETY: 1982; Vol. 201, pp 279-311.

22. Santosh, G.; Ravikanth, M., Tuning of redox and photophysical properties of porphyrins by successive introduction of one, two, three and four meso-furyl groups. *Chemical Physics Letters* **2007,** *448* (4–6), 248-252.
23. Wolberg, A., Redox Properties of Tetraphenylporphyrin Complexes. *Israel Journal of Chemistry* **1974,** *12* (6), 1031-1035.
24. Mansuy, D., Cytochromes P-450 and model systems: great diversity of catalyzed reactions. In *Pure and Applied Chemistry*, 1994; Vol. 66, p 737.
25. Groves, J. T., The bioinorganic chemistry of iron in oxygenases and supramolecular assemblies. *Proceedings of the National Academy of Sciences of the United States of America* **2003,** *100* (7), 3569-3574.
26. Mansuy, D., A brief history of the contribution of metalloporphyrin models to cytochrome P450 chemistry and oxidation catalysis. *Comptes Rendus Chimie* **2007,** *10* (4–5), 392-413.
27. Fukushima, M.; Mizutani, Y.; Maeno, S.; Zhu, Q.; Kuramitz, H.; Nagao, S., Influence of Halogen Substituents on the Catalytic Oxidation of 2,4,6-Halogenated Phenols by Fe(III)-Tetrakis(p-hydroxyphenyl) porphyrins and Potassium Monopersulfate. *Molecules* **2012,** *17* (1), 48.
28. Sheldon, R. A., *Metalloporphyrins in Catalytic Oxidation*. Marcel Dekker: New York, USA, 1994
29. Manbeck, G. F.; Fujita, E., A review of iron and cobalt porphyrins, phthalocyanines and related complexes for electrochemical and photochemical reduction of carbon dioxide. *Journal of Porphyrins and Phthalocyanines* **2015,** *19* (01-03), 45-64.
30. Zahran, Z. N.; Mohamed, E. A.; Naruta, Y., Bio-inspired cofacial Fe porphyrin dimers for efficient electrocatalytic CO2 to CO conversion: Overpotential tuning by substituents at the porphyrin rings. **2016,** *6*, 24533.
31. Wang, B., Recent development of non-platinum catalysts for oxygen reduction reaction. *Journal of Power Sources* **2005,** *152*, 1-15.
32. Wasylenko, D. J.; Rodríguez, C.; Pegis, M. L.; Mayer, J. M., Direct Comparison of Electrochemical and Spectrochemical Kinetics for Catalytic Oxygen Reduction. *Journal of the American Chemical Society* **2014,** *136* (36), 12544-12547.
33. Pegis, M. L.; McKeown, B. A.; Kumar, N.; Lang, K.; Wasylenko, D. J.; Zhang, X. P.; Raugei, S.; Mayer, J. M., Homogenous Electrocatalytic Oxygen Reduction Rates Correlate with Reaction Overpotential in Acidic Organic Solutions. *ACS Central Science* **2016,** *2* (11), 850-856.
34. Feng, D.; Gu, Z.-Y.; Li, J.-R.; Jiang, H.-L.; Wei, Z.; Zhou, H.-C., Zirconium-Metalloporphyrin PCN-222: Mesoporous Metal–Organic Frameworks with Ultrahigh Stability as Biomimetic Catalysts. *Angewandte Chemie International Edition* **2012,** *51* (41), 10307-10310.
35. Boucher, L. J., Manganese porphyrin complexes. *Coordination Chemistry Reviews* **1972,** *7* (3), 289-329.
36. Fagadar-Cosma, E.; Mirica, M. C.; Balcu, I.; Bucovicean, C.; Cretu, C.; Armeanu, I.; Fagadar-Cosma, G., Syntheses, Spectroscopic and AFM Characterization of Some Manganese Porphyrins and Their Hybrid Silica Nanomaterials. *Molecules* **2009,** *14* (4), 1370.
37. Aghabali, A.; Safari, N., Effects of methoxy-substituted metalloporphyrins in catalytic alkene epoxidation by n-Bu4NHSO5. *Journal of Porphyrins and Phthalocyanines* **2010,** *14* (04), 335-342.
38. Jiang, L.; Lu, F.; Li, H.; Chang, Q.; Li, Y.; Liu, H.; Wang, S.; Song, Y.; Cui, G.; Wang, N.; He, X.; Zhu, D., Third-Order Nonlinear Optical Properties of an Ultrathin Film Containing a Porphyrin Derivative. *The Journal of Physical Chemistry B* **2005,** *109* (13), 6311-6315.
39. Schmid, C. R.; Beck, C. A.; Cronin, J. S.; Staszak, M. A., Demethylation of 4-Methoxyphenylbutyric Acid Using Molten Pyridinium Hydrochloride on Multikilogram Scale. *Organic Process Research & Development* **2004,** *8* (4), 670-673.
40. Walter, R. I.; Ojadi, E. C. A.; Linschitz, H., A proton NMR study of the reactions with acid of meso-tetraphenylporphyrins with various numbers of 4-(dimethylamino) groups. *The Journal of Physical Chemistry* **1993,** *97* (50), 13308-13312.

41. Zakavi, S.; Omidyan, R.; Talebzadeh, S., The influence of protonation on the structure and spectral properties of porphine: UV-vis, 1H NMR and ab initio studies. *RSC Advances* **2016,** *6* (85), 82219-82226.
42. Rudine, A. B.; DelFatti, B. D.; Wamser, C. C., Spectroscopy of Protonated Tetraphenylporphyrins with Amino/Carbomethoxy Substituents: Hyperporphyrin Effects and Evidence for a Monoprotonated Porphyrin. *The Journal of Organic Chemistry* **2013,** *78* (12), 6040-6049.
43. Gauuan, P. J. F.; Trova, M. P.; Gregor-Boros, L.; Bocckino, S. B.; Crapo, J. D.; Day, B. J., Superoxide dismutase mimetics: synthesis and structure–activity relationship study of MnTBAP analogues. *Bioorganic & Medicinal Chemistry* **2002,** *10* (9), 3013-3021.

Chapter 3:

Carboxylate Based Porphyrinic MOFs

Table of Contents

3. Carboxylate based porphyrinic MOFs

3.1. Introduction

Ligands with carboxylate functionality have been the most investigated with regards to porphyrinic MOFs, where majority of the work has been done with the tetrakis(4-carboxyphenyl) porphyrin linker, mainly due to its commercial availability and/or facile synthesis.[1-3] Carboxylate based MOFs often present limitations regarding aqueous stability as discussed in chapter 1. Studies have shown that increasing the charge of the metal usually leads to an enhancement of the hydrothermal stability of the carboxylate based MOFs.[4] The carboxylate anion can be considered as a hard base; thus, the increased charge density of higher valence metal ions can lead to stronger M-O bonds. Therefore, using higher valance metal ions such as Fe^{3+} and Al^{3+} in the inorganic SBU can result in more stable carboxylate MOFs.

Fe porphyrin based MOF with a chain like inorganic SBU published by our lab, [Fe^{II}pzTCPP($Fe^{III}OH)_2$], and Al-PMOF {chemical formula [H_2TCPP($Al^{III}OH)_2$]} published by Fateeva et al are two such stable carboxylate porphyrin MOFs.[5-6] The work presented in this chapter will focus on two main topics. One involves the investigation of the reactivity of Fe with tetrakis(4-carboxyphenyl) porphyrin based ligands and the other entails the exploration of the synthesis of Mn^{3+} and Fe^{3+} metalated Al-PMOF material.

- *Reactivity of Fe with tetrakis(4-carboxyphenyl) porphyrin*

[Fe^{II}pzTCPP($Fe^{III}OH)_2$] was synthesised via the solvothermal reaction of hydrated iron chloride and free base tetrakis(4-carboxyphenyl) porphyrin (H_2TCPP) in the presence of pyrazine as described in the presented article.[5] When the three compounds were reacted in solvothermal conditions in DMF, a mixture of two phases was obtained, [Fe^{II}pzTCPP($Fe^{III}OH)_2$] and [Fe^{II}TCPP($Fe^{II}pz)_2$] (Figure 3-1). To obtain the phase pure [Fe^{II}pzTCPP($Fe^{III}OH)_2$], a two-step synthetic procedure was adapted. First $FeCl_3.6H_2O$ and H_2TCPP were reacted and an intermediate solid was isolated (Figure 3-1). Then this solid was allowed to react with pyrazine to obtain the pure [Fe^{II}pzTCPP($Fe^{III}OH)_2$] phase. In this work, we tried to investigate the nature of this intermediate phase as it could lead to information about the mechanism of the MOF formation. Furthermore, the possibility of replacing the pyrazine ligand with other N-donors was also investigated. N-donors such as imidazole are less likely to act as bridging ligands thus have the potential to yield an extended structure with coordinatively unsaturated Fe sites (Figure 3-2b), resembling Fe-heme systems.[7] This work is presented in detail in section 3.3 of the chapter.

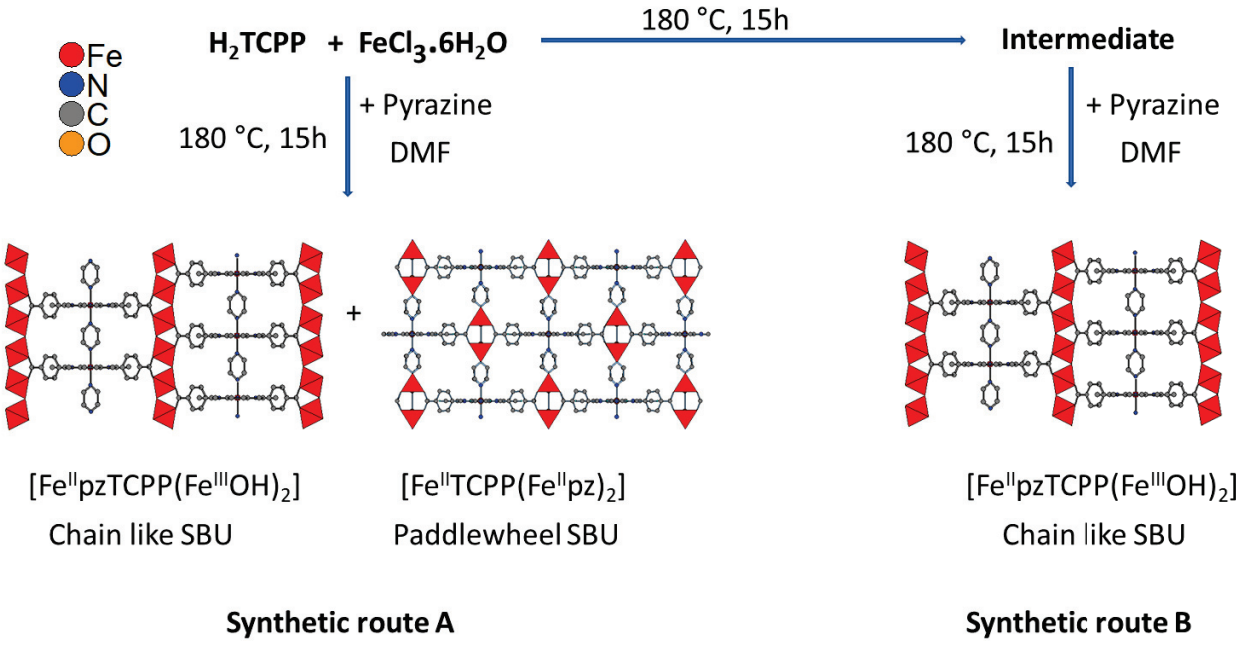

Figure 3-1 Different synthetic routes employed to obtain [Fe^{II}pzTCPP(Fe^{III}OH)$_2$].[5] Hydrogens are omitted for clarity.

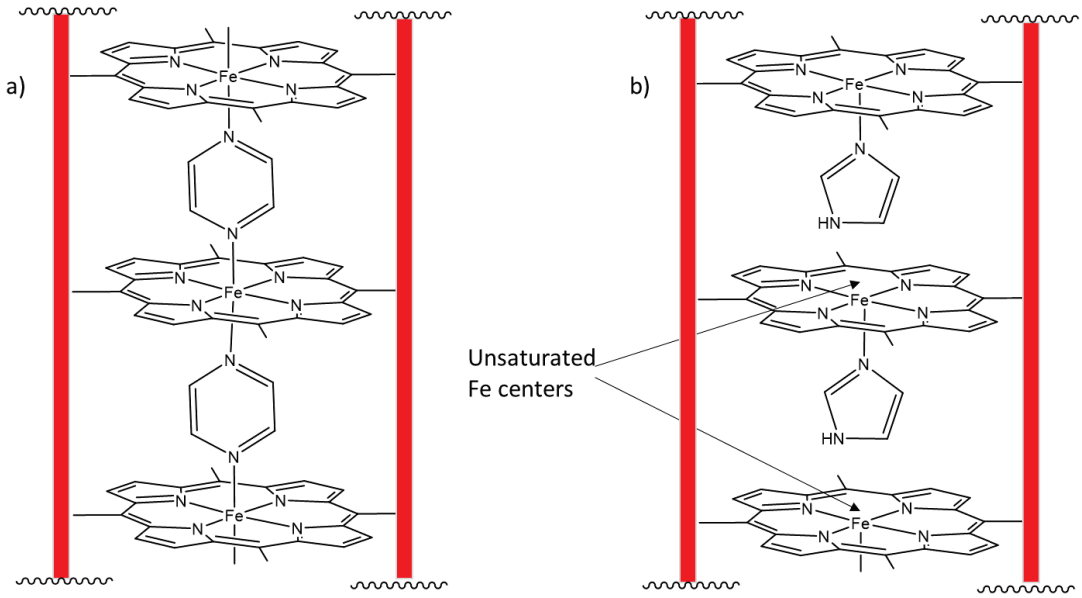

Figure 3-2 a) A schematic representation of the porphyrin Fe centres in [Fe^{II}pzTCPP(Fe^{III}OH)$_2$] where Fe is coordinated to pyrazine bridging ligands. b) Conceptual drawing of a possible framework obtained by replacing pyrazine with imidazole resulting in unsaturated Fe centres.

The reactivity of $FeCl_3.6H_2O$ and Co metalated TCPP ligand was also investigated with the goal of obtaining a stable Fe based porphyrinic MOF with cobalt in the porphyrin cores. Co metalated porphyrins have shown promising results as catalysts for CO_2 reduction and being incorporated into a

stable Fe based framework have the potential to yield material which can be used as heterogeneous catalysts. This is presented in section 3.4 of the chapter.

- *Exploration of the synthesis of Mn^{3+} and Fe^{3+} metalated Al-PMOF material*

Al-PMOF, [H_2TCPP($Al^{III}OH)_2$], is a water stable MOF published by Fateeva et al. It was synthesised with a non-metalated porphyrinic core and post-synthetically metalated Al-PMOF variations with divalent zinc,[6] cobalt,[8] and copper[9] have been reported. Zn-Al-PMOF has shown photocatalytic activity towards H_2 generation, Co-Al-PMOF has shown electrocatalytic activity for CO_2 reduction and Cu-Al-PMOF was proven to be active in CO_2 photoreduction. Thus, having different metals in the porphyrin core enables one to tune the functionality of the material. The most studied metalloporphyrins are the Fe and Mn metalated porphyrins which have been used as models to mimic cytochrome P-450 in the catalytic oxidation of organic substrates and as catalysts for various other oxidation reactions.[10-11] However, Mn and Fe metalated Al-PMOFs have not been reported before. Thus, obtaining Mn and Fe metalated Al-PMOF is investigated in section 3.5 of the chapter.

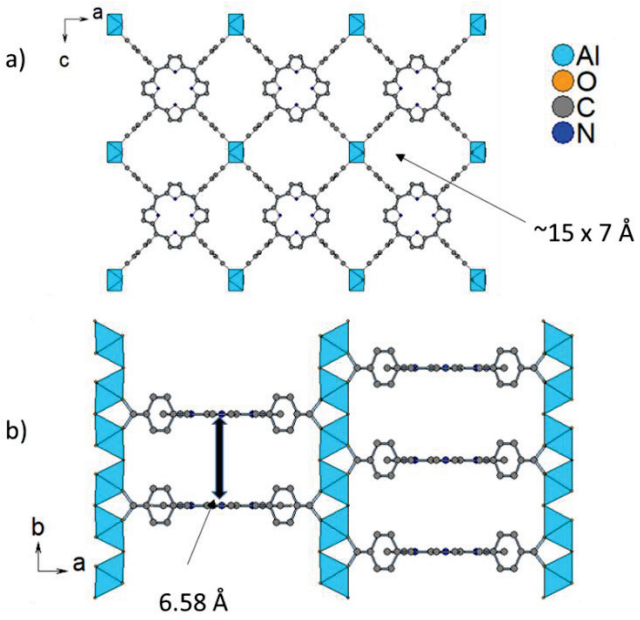

Figure 3-3 Framework of Al-PMOF a) view along the b-axis showing pores of ~15 x 7 Å b) view along the c-axis. The distance between 2 porphyrins is ~6.58 Å.[6] Hydrogens are omitted for clarity.

3.2. Article

CRYSTAL GROWTH & DESIGN

Article

pubs.acs.org/crystal

Iron and Porphyrin Metal–Organic Frameworks: Insight into Structural Diversity, Stability, and Porosity

Alexandra Fateeva,*[,†,⊥] Jade Clarisse,[†] Guillaume Pilet,[†] Jean-Marc Grenèche,[‡] Farid Nouar,[§] Brian K. Abeykoon,[†] Frédéric Guegan,[†] Christelle Goutaudier,[†] Dominique Luneau,[†] John E. Warren,[∥,⊥] Matthew J. Rosseinsky,[⊥] and Thomas Devic[§]

[†]Université de Lyon, Université Claude Bernard Lyon 1, Laboratoire des Multimatériaux et Interfaces, UMR CNRS 5615, 43 Bd du 11 Nov 1918, 69622 Villeurbanne, France

[‡]Institut des Molécules et des Matériaux du Mans, UMR CNRS 6283, Université du Maine, Avenue Olivier Messiaen, 72085 Le Mans, France

[§]Institut Lavoisier, UMR CNRS 8180, Université de Versailles Saint-Quentin-en-Yvelines, 45 avenue des Etats-Unis, 78035 Versailles cedex, France

[∥]School of Materials, The University of Manchester, Manchester M13 9PL, U.K.

[⊥]Department of Chemistry, University of Liverpool, Liverpool, L69 7ZD, U.K.

Supporting Information

ABSTRACT: Reaction of iron(IIII)chloride with the free base tetrakis(4-carboxyphenyl)porphyrin (H_2TCPP) in the presence of different bases leads to the formation of a series of iron/porphyrin metal–organic frameworks. Such a crystal engineering approach led to the obtaining of four structures presenting three different topologies and inorganic secondary building units. Depending on the synthesis conditions, isolated Fe^{III} octahedra, diiron(II) paddle wheel dimers, or extended $[Fe^{III}(OH)O_4]_n$ chains could be obtained in a controlled manner. The influence of the synthetic conditions on the final structure and the oxidation state of iron is discussed. Stability of the porous solids towards air and water is studied, and their intrinsic porosity is assessed.

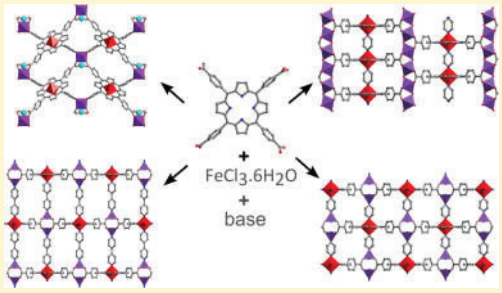

INTRODUCTION

Porphyrins are valuable building blocks in metal–organic framework (MOF) synthesis. From a structural aspect, such an extended square planar ligand favors the formation of ordered frameworks with potentially significant porosity.[1,2] Considering the chemical properties, porphyrins are stable, hydrophobic molecules allowing the creation of some chemically stable frameworks when used with a high valence metal.[3−8] As porphyrins can be metalated in their center, heterometallic frameworks with open metal sites other than the ones belonging to the inorganic building block are accessible for applications such as catalysis.[9−12] The optical and redox properties of porphyrins have also led to light harvesting frameworks.[13−15]

Since the first examples of a metalloporphyrin frameworks were described by Robson[16] and Goldberg,[17−19] remarkable progress has been made in this field, details of which can be found in valuable review articles.[1,2,10,11,20,21] So far, the majority of structures reported are based on divalent cations (e.g., Zn^{II}, Co^{II}) in the inorganic building units,[22,23] such as, for instance, the noticeable case of pillared paddle wheel frameworks.[24−26] However, most stable porous materials reported are based on higher valence metals like the aluminum Al-PMOF or the zirconium-porphyrin materials.[3−6] Because of the iron redox related properties, both Fe^{II} and Fe^{III} states can be accessed in MOF architectures[27−29] leading to a great structural diversity and versatility of synthesis. Moreover, the redox activity of iron can also be exploited in the frameworks themselves, Fe-based MOFs being indeed considered in relation to applications such as gas separation,[30−32] catalysis,[33,34] and lithium-ion battery electrodes.[35−38] Furthermore, iron-based coordination polymers are of low toxicity and thus have been studied for biomedical applications.[39,40] Yet, porphyrinic iron-based porous coordination polymers are still relatively scarce, and since the report on the MIL-141 system[38] (MIL: Material from Institute Lavoisier, a series of porous MOFs based on Fe^{III} and Ni^{II}-TCPP linker) only one more example has very recently been described to the best of the authors' knowledge.[41] In the present work the reactivity of the tetrakis(4-carboxyphenyl)-porphyrin H_2TCPP with iron was investigated; the impact of synthetic conditions on the obtained MOF architectures was studied, and four new porphyrinic MOFs structures are described. These syntheses led to the metalation of porphyrins by iron concurrently to the MOF formation, giving heme-based

Received: December 22, 2014
Revised: February 6, 2015
Published: February 27, 2015

ACS Publications © 2015 American Chemical Society

DOI: 10.1021/cg501855k
Cryst. Growth Des. 2015, 15, 1819−1826

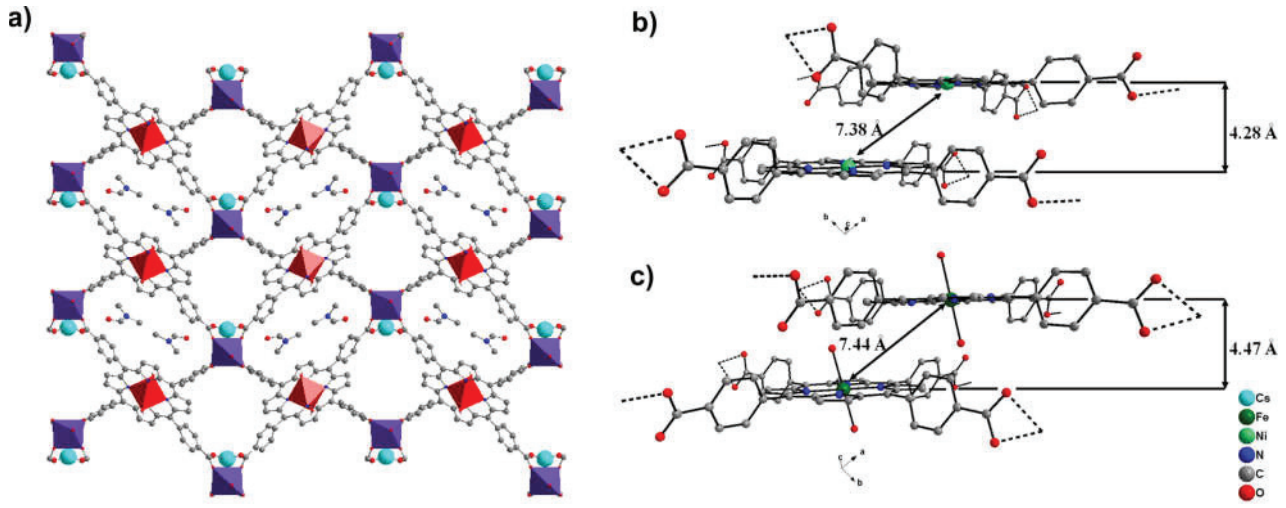

Figure 1. (a) Crystal structure of **1** along the [100] direction (b) distances between adjacent porphyrin planes for MIL-141 (Ni) (c) for compound **1**.

porous structures that might be of interest for fundamental studies of Fe-porphyrins.[42] The effect of an inorganic or organic base used during the synthesis course on the topology of the final material is highlighted in this study. This latter can not only direct the three-dimensional (3D) architecture formation but also impact the final redox state of iron and hence the nature of the secondary metallic building unit. The thermal and chemical stability as well as accessible porosity of all the obtained materials were characterized and are described below.

EXPERIMENTAL SECTION

Synthesis. All chemicals were obtained from commercial sources and used without further purification.

*Synthesis of MIL-141(Fe) **1**.* In a typical synthesis, tetrakis(4-carboxyphenyl)porphyrin H_2TCPP (45 mg, 0.057 mmol) and $FeCl_3 \cdot 6H_2O$ (25 mg, 0.093 mmol) were dissolved in 5 mL of dimethylformamide (DMF) in 25 mL Teflon-lined autoclave and 0.05 mL of 2 M CsOH solution (0.1 mmol) was added. The mixture was stirred for 5 min at room temperature and then placed in a programmable oven at 160 °C for 12 h (heating rate 1 °C/min, cooling rate 0.2 °C/min). The crystalline solid was obtained by filtration and washed with DMF and acetone until the filtrate solution became clear 50 mg of material was obtained.

*Synthesis of FeTCPP(Febpy)$_2$ **2**.* H_2TCPP (75 mg, 0.095 mmol) and $FeCl_3 \cdot 6H_2O$ (75 mg, 0.28 mmol) were dissolved in 15 mL of DMF in a 45 mL Teflon-lined reactor. 4,4′-Bipyridine was added to the reaction mixture (30 mg, 0.19 mmol), and the solution was stirred for 5 min at room temperature. The reactor was then transferred to a programmable oven at 180 °C for 15 h (heating rate 0.2 °C/min, cooling rate 0.2 °C/min). The crystalline solid was filtered under a vacuum and washed with DMF and acetone until the filtrate solution became clear; 80 mg of material was obtained.

*Synthesis of FeTCPPFe **3**.* H_2TCPP (90 mg, 0.11 mmol) and $FeCl_3 \cdot 6H_2O$ (90 mg, 0.33 mmol) were dissolved in 10 mL of DMF in a 45 mL Teflon-lined reactor; no base was added for this synthesis. After stirring 5 min at room temperature, the solution was allowed to react at 180 °C for 15 h (heating rate 0.5 °C/min, cooling rate 0.8 °C/min). The solid obtained was filtered under a vacuum and washed with DMF and acetone until the filtrate solution became clear; 120 mg of material was obtained.

*Synthesis of FeTCPP(Fepz)$_2$ and FepzTCPP(FeOH)$_2$ Mixed Phase Compound **4**$_A$ and **4**$_B$.* H_2TCPP (90 mg, 0.11 mmol) and $FeCl_3 \cdot 6H_2O$ (90 mg, 0.33 mmol) were dissolved in 10 mL of DMF in a 45 mL Teflon-lined reactor. Pyrazine was added to the reaction mixture (20 mg, 0.25 mmol), and the solution was stirred for 5 min at room temperature. The reactor was then transferred in a programmable oven at 180 °C for 15 h (heating rate 0.5 °C/min, cooling rate 0.8 °C/min). The crystalline solid obtained was filtered under a vacuum and washed with DMF and acetone until the filtrate solution became clear; 110 mg of material was obtained.

*Synthesis of FepzTCPP(FeOH)$_2$ **4**$_B$.* A total of 100 mg of compound **3** was placed in 10 mL of DMF in a 45 mL Teflon-lined autoclave, and pyrazine was added to the suspension (20 mg, 0.25 mmol). The mixture was placed in a programmable oven at 180 °C for 15 h (heating rate 0.5 °C/ min, cooling rate 0.8 °C/min). The crystalline solid obtained was filtered under a vacuum and washed with DMF and acetone until the filtrate solution became clear; 85 mg of material was obtained.

Characterizations. Supporting Information contains details of the different techniques used in this study (single crystal and powder X-ray diffraction, infrared spectroscopy, scanning electron microscopy, thermal analyses, gas sorption measurements, and ^{57}Fe Mössbauer spectrometry).

RESULTS AND DISCUSSION

Synthesis. All solids were prepared under similar solvothermal conditions. Syntheses were carried out from a free base tetracarboxyphenyl porphyrin and iron(III) chloride hexahydrate in dimethylformamide between 160 and 180 °C, use of lower temperatures typically leading to a lower crystallographic quality. Without the use of any base, a poorly crystalline compound (**3**) was obtained for which the structure remains so far unclear. Therefore, a base generally had to be added to achieve a crystalline material. For this purpose, different agents were tested: an inorganic alkaline hydroxide CsOH and two organic bases: 4,4′-bipyridine (bpy) and pyrazine (pz). Four different frameworks could be obtained; their structures and properties are described hereafter.

Inorganic Base Case: Compound 1. In the presence of an alkaline hydroxide (CsOH in this case but an isomorphic compound could also be obtained with KOH), unsurprisingly, a MIL-141 type structure was obtained[7] with the composition $[Fe^{III}TCPPFe^{III}Cs^{I}]_n \cdot x$DMF (Figure 1a). The main difference with the first MIL-141 reported synthesis is that a free base was used in this work instead of a nickel porphyrin. Therefore, the porphyrin became metalated by iron in the course of the solvothermal reaction. As in the MIL-141 structure, iron(III)

DOI: 10.1021/cg501855k
Cryst. Growth Des. 2015, 15, 1819−1826

building ions were in a distorted octahedral $\{O_6\}$ environment with oxygen atoms belonging to carboxylate groups from four different porphyrins in order to define a *pts*-type framework (with S = Fe, Pt = porphyrin). Fe^{III}–O bond lengths range from 1.921(4) Å to 2.184(4) Å, as summarized in Table 1, and

Table 1. Important Fe–N/O Bond Lengths (in Å) in Structures 1, 2, 4_A, and 4_B and Bond Valence Sum Calculation for SBU Iron in Each Phase

	porphyrin core		SBU		SBU BVS	
	Fe–N	Fe–O	Fe–N	Fe–O	Fe^{II}	Fe^{III}
1	1.986(4)	2.05(1)		1.982(4)	2.69	2.88
				2.184(4)		
2	1.982(5)		2.080(9)	2.048(4)	2.15	2.32
	2.003(4)					
$\mathbf{4_A}$	1.982(8)		2.09(1)	2.034(1)	2.19	2.37
	1.93(1)					
$\mathbf{4_B}$	1.999(2)			2.012(1)	3.08	3.29
	1.978(2)			1.918(1)		

are in agreement for Fe^{III} from the bond valence calculation. O–Fe^{III}–O angles that range from 61.4(1)°/145.6(2) to 109.9(2)°/152.3(2)° are far from the ideal values but in agreement with those observed in structures previously reported.[7] Iron(III) porphyrin was obtained during the course of the reaction, and the central iron (located on an inversion center) is in an octahedral $\{N_4O_2\}$ geometry, bearing disordered H_2O/OH^- as axial ligands. In this case, Fe^{III}–N and Fe^{III}–O bond lengths are equal to 1.986(4) Å and 2.05(1) Å, respectively. N–Fe^{III}–N/O bond angles range from 83.0(3)° to 97.0(3)° and O–Fe^{III}–O are assumed to be equal to 180°, due to symmetry. Each metalloporphyrin is connected to four iron(III), forming a triply interpenetrated framework with two types of channels. The overall framework being anionic, charge neutrality is ensured by an extra-framework alkaline ion Cs^I located in one type of channels. The main structural difference with the nickel(II) porphyirn based MIL-141 compound is the coordination of the central metal ion. The coordination of nickel(II) in the porphyrin core leads to a square planar metalloligand, whereas in the case of iron(III) a slightly distorted octahedral geometry is obtained. The coordination of axial ligands to iron(III) induces a slight distance lengthening between two adjacent porphyrin planes (4.47(1) vs 4.26(1) Å) (see Figures 1b and 1c).

Organic Base: 4,4′-Bipyridine Leading to Iron(II) Pillared Paddle Wheel Framework 2. In the case where the alkaline hydroxide was replaced by the 4,4′-bipyridine, and the starting metal source being still $FeCl_3{\cdot}6H_2O$, an iron(II) coordination polymer was obtained. This time, bipyridine acted not only as a base but also as a coligand in the MOF architecture. The introduction of a soft bipyridine base along with the reducing DMF media at high temperature contributed to the stabilization of the low iron oxidation state. Besides, nitrogen-containing aromatic bases are well established to promote autoreduction of iron(III) porphyrins to iron(II) compounds upon axial coordination.[43,44] Single crystal data showed that the compound **2** crystallized in a tetragonal space group, and its composition was $[Fe^{II}TCPP(Fe^{II}bpy)_2]_n{\cdot}x$DMF (Figure 2). This structure is isotopic to several pcu-b topology porphyrin pillared paddle wheel frameworks reported in the literature with other divalent ions.[24,25] Iron(II) in the porphyrin core is located in mostly perfect octahedral $\{N_6\}$ geometry, coordinated to six nitrogen atoms (four porphyrinic nitrogens and the two bpy axial ligands). The Fe–N bond lengths are equal to 1.982(5) Å (plane) and 2.003(4) Å (axial), while N–Fe–N bond angles adopt ideal values for this type of environment (90° and 180°). The inorganic building unit is composed of iron paddle wheel Fe^{II} dimers linked by carboxylate oxygens in equatorial positions and by two bipyridyls axially. Such an SBU is quite common for MOFs based on divalent metals even if more rarely reported in the case of iron(II) due to the high reactivity of diiron paddlewheels with oxygen.[45−47] Bond valence calculations confirmed the Fe^{II} oxidation state (Table 1). Each iron cation is then located in a $\{O_4N_1\}$ square-base pyramidal environment with the oxygen atoms forming the base of the pyramid. Fe–O and Fe–N bond lengths are equal to 2.048(4) Å and 2.080(9) Å, respectively. The sixth position of the iron environment is occupied by the neighbored iron ion and the Fe···Fe distance is equal to 2.821(3) Å, which is in good agreement with structures previously reported in the literature for other diiron(II) paddle wheel dimers.[46−48] According to the classification defined by Choe et al.,[24] this structure exhibits an heterogeneous pillared connectivity as the bpy pillars link the FeTCPP macrocycles to $\{Fe_2(COO)_4\}$ dimers giving a porphyrin to paddle wheel

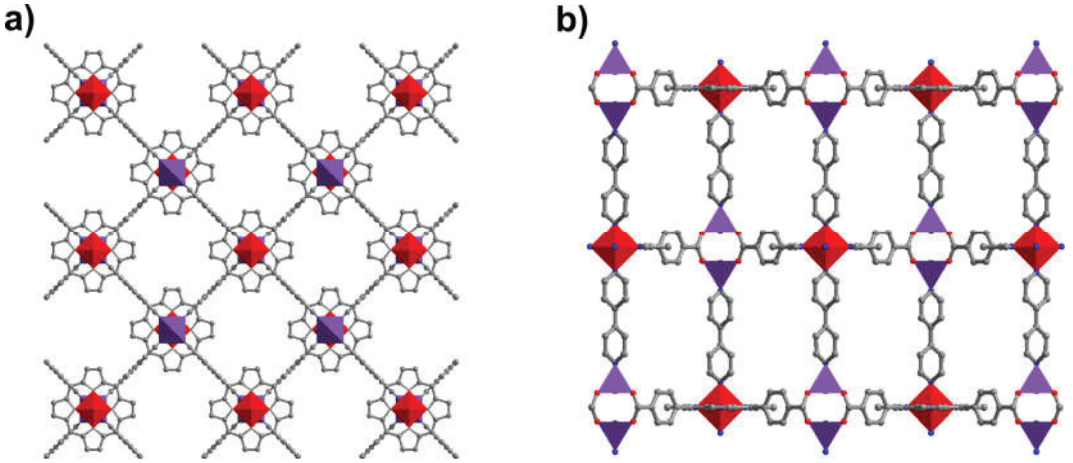

Figure 2. (a) Crystal structure of **2** viewed along the [001] direction (b) along [010].

DOI: 10.1021/cg501855k
Cryst. Growth Des. 2015, 15, 1819−1826

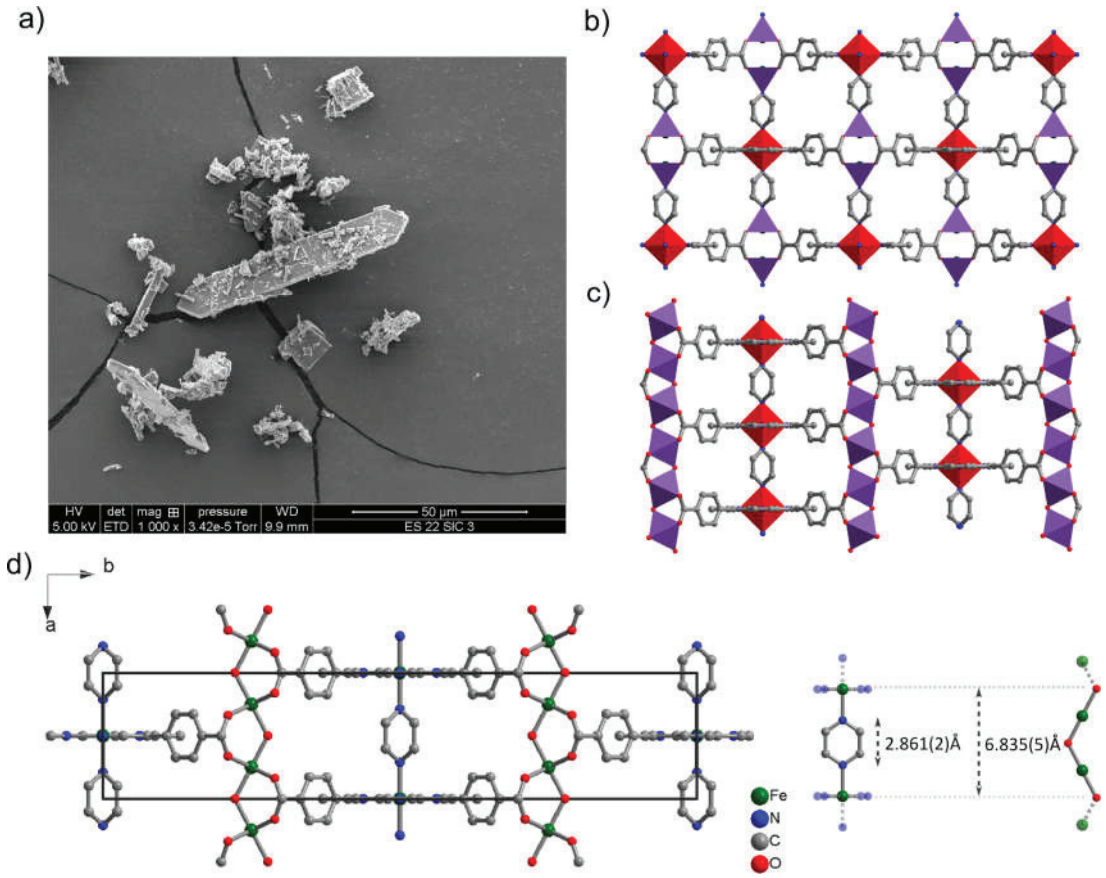

Figure 3. (a) SEM picture of the one step reaction products $\mathbf{4}_A$ and $\mathbf{4}_B$ showing prismatic and square plate crystals (b) $\mathbf{4}_A$ structure down the [010] direction (c) $\mathbf{4}_B$ structure along the [001] direction, and (d) size matching of the pyrazine and the $[Fe(OH)O_4]_n$ chain.

stacking sequence. The crystallinity of the solid was degraded when exposed to air, which could have been due to the loss of the solvent or a hydrolysis and a partial oxidation of Fe^{II} dimers[46] leading to a change in the coordination sphere. This observation is in line with the generally moderate chemical stability observed for M^{II} carboxylate MOFs when compared to the M^{III} ones.[49]

Pyrazine: Two Polymorphic Frameworks $\mathbf{4}_A$ and $\mathbf{4}_B$. When the bipyridine was replaced by its shorter and weaker base analogue pyrazine in the synthesis procedure, a mixture of two different crystalline compounds was obtained. First, isoreticular to compound **2**, a tetragonal phase $\mathbf{4}_A$ with pcu-b topology, exhibiting the pillared paddle wheel framework where pyrazine replaced the bipyridyl linkers from the previously described compound **2**. This phase was obtained as prismatic crystals and was, again, formed of iron(II) paddle wheel dimers giving the formulation: $[Fe^{II}TCPP(Fe^{II}pz)_2]_n{\cdot}x$DMF (Figure 3a,b). The porphyrinic core was again metalated by an iron(II), as determined by single-crystal X-ray diffraction. The iron atoms are located exactly in the same environment as those in the structure **2**: (a) iron cation within the porphyrin core is located in a $\{N_6\}$ octahedral geometry where four nitrogen atoms belong to the porphyrin and the two others to two pyrazine molecules. Fe—N bond lengths are equal to 1.992(6) Å (plane of the octahedron) and 1.961(1) Å (tops of the octahedron). These bond lengths are comparable with those observed in the case of **2**. The N—Fe—N bond angles then adopt ideal values due to symmetry; (b) irons forming dimers connecting metalated porphyrins together are in a $\{O_4N_1\}$ square-base pyramidal environment. The nitrogen atoms belong to the pyrazine molecule, whereas the oxygen atoms come from the carboxylate functions of the porphyrin. Fe—N and Fe—O bonds lengths are found to be equal to 2.09(1) Å and 2.034(1) Å, respectively. The second iron atom of the dimer occupies the sixth position in this open environment. In that case, the Fe···Fe distance is equal to 2.767(4) Å.

Interestingly, a second phase was simultaneously formed during the synthesis. This time square planar crystals were observed (Figure 3a), and single-crystal X-ray diffraction analysis revealed the formation of an orthorhombic phase with both Fe^{II} and Fe^{III} metallic centers. In this later compound of formulation $[Fe^{II}pzTCPP(Fe^{III}OH)_2]_n{\cdot}x$DMF the coordination environment of the iron(II) inside the porphyrin core remained unchanged with a perfect octahedral environment (Fe—N equal to 1.978(2) Å and 1.999(2) Å; N—Fe—N bond angles are equal to the theoretical values of 90° and 180°) as illustrated in Figure 3c. However, the inorganic building unit of the framework was very different compared to those observed for the previous structures. With a fry-topology structure[50] similar to that of Al-PMOF,[3] the coordination of the Fe^{III} ion consisted of four carboxylate-derived oxygen atoms in the equatorial plane and two μ_2 axial OH bridging the adjacent Fe^{III} centers to form an infinite $[Fe(OH)O_4]_n$ chain, similar to those found in numerous M^{III} based MOFs such as MIL-53, MIL-60, or MIL-68.[51−53] Fe—O bond lengths of oxygen atoms belonging to carboxylate groups are equal to 2.012(2) Å,

DOI: 10.1021/cg501855k
Cryst. Growth Des. 2015, 15, 1819−1826

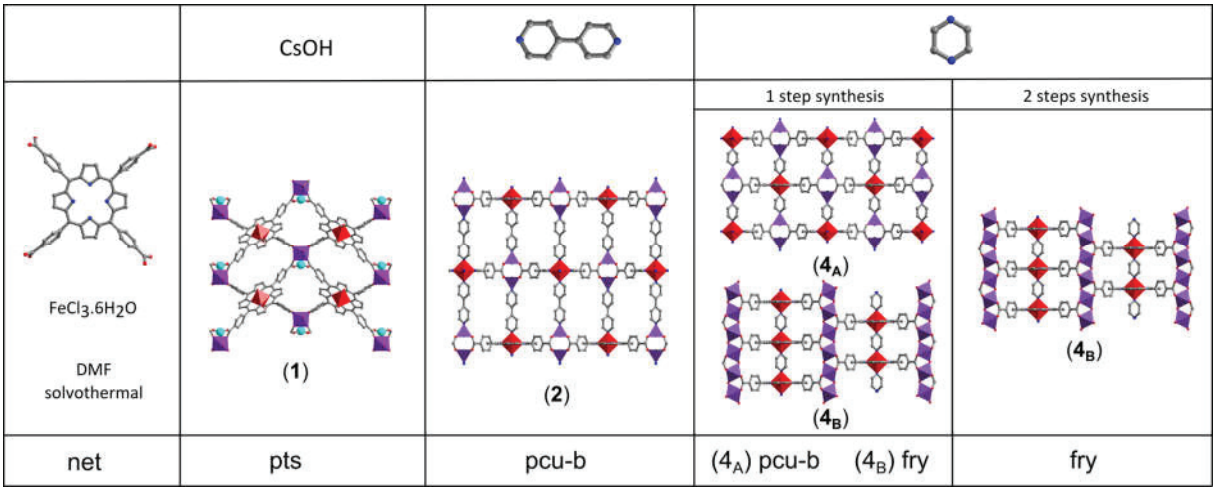

Figure 4. Porous porphyrinic frameworks obtained from the reaction of the H_2TCPP with $FeCl_3{\cdot}6H_2O$ and varying the base used in the solvothermal synthesis.

while those involving μ_2-OH are shorter and equal to 1.918(1) Å. O–Fe–O bond angles range from 88.33(7)° to 91.67(7)° (cis) and equal to 180° (trans). Here, the perfect match between the iron-pyrazine-iron distance and the size of the repeating dimeric unit (Figure 3d) found in $[Fe(OH)O_4]_n$ chains (about 6.8 Å, as found here (6.835 Å) and in other Fe^{III}-based MOFs such as MIL-53[36] and MIL-68[38]) probably explains the concomitant formation of this phase. A noteworthy point is that when the composition of the starting mixture was changed, varying the pyrazine/$FeCl_3$ ratio, both phases were still formed concurrently. $FeCl_2$ as the iron source resulted in formation of amorphous material. To achieve the formation of a phase pure compound, another synthetic method had to be used. As the pyrazine was thought to be promoting the stabilization of the iron(II) oxidation state in the final compound,[43,44] first the porphyrin was allowed to react with iron(III) chloride alone under solvothermal conditions in DMF, and the solid product (**3**) was collected and dried. The structure of this compound remains unclear for now as the quality of the crystals obtained allowed only a unit cell determination from single crystal diffraction analysis. This solid was insoluble in most organic solvents including DMF, suggesting the formation of a polymeric compound. Nitrogen sorption isotherm measured at 77 K gave a BET surface area of 440 $m^2\ g^{-1}$ (Figure S10) further supporting the formation of an extended open framework. In a second step compound (**3**) was allowed to react with pyrazine in DMF under solvothermal conditions. After this second synthesis step only square plate crystals were observed by SEM (Figure S14) suggesting a phase pure $\mathbf{4_B}$ formation. This last compound showed no degradation under air; therefore Mössbauer spectrometry could be performed and confirmed the iron spin state and valence in the bulk solid (see below).

From the structural considerations above, it appears that very different architectures are accessible from the porphyrin/iron/base system, as summarized in Figure 4. In terms of inorganic SBU, paddle wheel dimers were observed for Fe^{II} in compounds **2** and $\mathbf{4_A}$, when for Fe^{III} isolated ions and a $[Fe(OH)O_4]_n$ chain were obtained in compounds **1** and $\mathbf{4_B}$ respectively. To the best of our knowledge only μ_3-oxo centered $\{Fe_3O(CO_2)_6\}$ trimers[8] and isolated $\{FeO_6\}$ octahedra[7] were known as building units in Fe/porphyrin MOFs until now. Topological analysis of these four structures reveals a pts and fry nets for Fe^{III}-based compounds **1** and $\mathbf{4_B}$ respectively, which are relatively rare in porphyrinic MOFs materials,[3,7,16,54] whereas compounds **2** and $\mathbf{4_A}$ exhibit pcu-b topology widely encountered.[20,24,25,55] In terms of stability, it was clearly observed by powder X-ray diffraction that Fe^{II}-based compound **2** was air unstable (Figure S2). The isoreticular compound $\mathbf{4_A}$ was not isolated as a pure phase material, but it can be assumed that it would have a similar sensitivity to air. Because of the low redox potential of Fe^{II}, the corresponding coordination polymers are very sensitive to air and therefore scarcely encountered in SBU of porous MOF structures. Both Fe^{III}-based compounds **1** and $\mathbf{4_B}$ were air stable, and this observation led us to test their chemical stability toward hydrolysis. To do so both materials were immersed in water and allowed to stand for 24 h; after that time the solids were filtered and dried. As shown in Figure S19 the supernatant was colored in the case of **1** attesting of a leaching of porphyrinic linkers into the aqueous media when for $\mathbf{4_B}$ water remained colorless. The recovered solids were analyzed by PXRD (Figures S20 and S22) that showed no significant change in crystallinity for both phases. This attests to a certain water stability toward hydrolysis for the two Fe^{III}-based MOFs, which is in good agreement with the general trend of an enhanced stability for trivalent frameworks.[49,53] The resistance to hydrolysis is clearly superior here for the compound presenting an extended SBU $[Fe(OH)O_4]_n$ chain when compared to the one built up from isolated $\{FeO_6\}$ octahedra.

^{57}Fe Mössbauer Spectrometry on Compound $\mathbf{4_B}$. The ^{57}Fe Mössbauer spectrum of $\mathbf{4_B}$ was recorded at 300 K and 77 K. At both temperatures, the hyperfine structure which consists of a quadrupolar doublet with well resolved lines should be described by means of two quadrupolar components. As observed in Figure 5 which illustrates the 77 K Mössbauer spectrum, one can clearly note an asymmetry which is not due to some preferential texture, as checked after rotating the sample with respect to the γ-beam. It is clear that the lack of resolution prevents *a priori* from a single fitting model leading to solutions that are strongly fitting conditions dependent. Nevertheless, the values of isomer shift are *a priori* consistent with the presence of high spin (HS) ferric species, but it has to be emphasized that those observed for low spin (LS) ferrous

DOI: 10.1021/cg501855k
Cryst. Growth Des. 2015, 15, 1819–1826

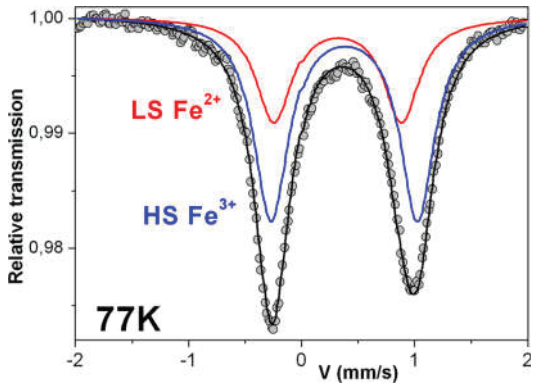

Figure 5. Mössbauer spectrum recorded at 77 K illustrating the decomposition into two quadrupolar components attributed to HS Fe^{III} and LS Fe^{II} species, as discussed in the text.

species are not so different. However, one can distinguish the main component (isomer shift δ = 0.50(2) mm/s; quadrupolar splitting Δ = 1.29 (2) mm/s at 77 K) and the minor one (δ = 0.42(2) mm/s; Δ = 1.12(2) mm/s at 77 K). By comparing these hyperfine values to those of MIL-53(Fe)[56] and those of iron-tetraphenyl porphyrin complex bearing two axially coordinated pyridine ligands $Fe^{II}(TPP)(py)_2$,[57,58] it should be concluded that HS Fe^{III} and LS Fe^{II} are present with respective proportions of 2/3 and 1/3 approximately, assuming the same Lamb recoilless factor values for both components: such a description does support the structural model established from X-ray diffraction.

Accessible Surface Area. Achievement of permanently porous porphyrin based frameworks is sometimes delicate as the porosity preservation upon solvent removal can be challenging.[10] For this reason different activation procedures were used in order to characterize the accessible surface area of these solids. Solids with Fe^{III} based inorganic building unit could be activated with classical methods (vacuum heating overnight), whereas Fe^{II} based solids had to be activated by the supercritical CO_2 drying method[59,60] to reduce the surface tension during solvent removal and prevent the collapse of the pores.

Nitrogen sorption isotherm was measured after activating compound **1** under a vacuum at 180 °C overnight (Figure 6a); a BET surface area of 420(10) $m^2\ g^{-1}$ was obtained (pore volume 0.19 $cm^3\ g^{-1}$), a value in good agreement with the one calculated from the crystal structure using the nonorthoSA program[61] (calc. 468 $m^2\ g^{-1}$). Thermal stability and structural flexibility were checked by variable temperature diffraction (Figure S5). The compound retained its crystallinity up to 200 °C in air; decomposition of the framework occurred at higher temperatures. No noticeable structural flexibility for **1** upon desolvation at high temperatures was observed, in good agreement with what was previously reported for MIL-141 (Ni), where a bulky Cs^+ ion resulted in a rather rigid structure when compared to smaller cations (K^+, Na^+, Li^+).[7]

The intrinsic porosity of the second Fe^{III}-based framework (compound $\mathbf{4_B}$) could also be assessed by N_2 adsorption at 77 K after classical activation procedure (Figure 6a). For this compound, a reversible type I isotherm was measured, a BET surface area of 760(20) $m^2\ g^{-1}$ and a pore volume of 0.33 $cm^3\ g^{-1}$ were extracted. This value was lower than the theoretically expected one (1460 $m^2\ g^{-1}$), yet structural preservation upon solvent departure and reexposure to air is evidenced by post-BET PXRD (Figure S4).

For the Fe^{II}-based compound **2** a loss of porosity occurred concurrently to the loss in crystallinity if the solids were activated by traditional methods. Therefore, supercritical carbon dioxide (SCD)[60] was used to perform the activation. This activation method preserved, at least partially, the intrinsic porosity of solid (**2**) upon solvent removal, as shown by nitrogen sorption isotherms (77 K); a BET surface area of 900 $m^2\ g^{-1}$ was obtained (Figure 6b). This value was again lower than the theoretical one (2900 $m^2\ g^{-1}$), which could be due to an unavoidable partial collapse of the structure during the activation process as well as an overestimate in the theoretical surface area. Yet it was clearly demonstrated that the intrinsic porosity is accessible in this pillared porphyrin structure. The lack of BET surface area data for other pillared porphyrin frameworks in the literature, possibly because of similar stability issues, does not allow us to draw comparisons with other isotopic compounds.

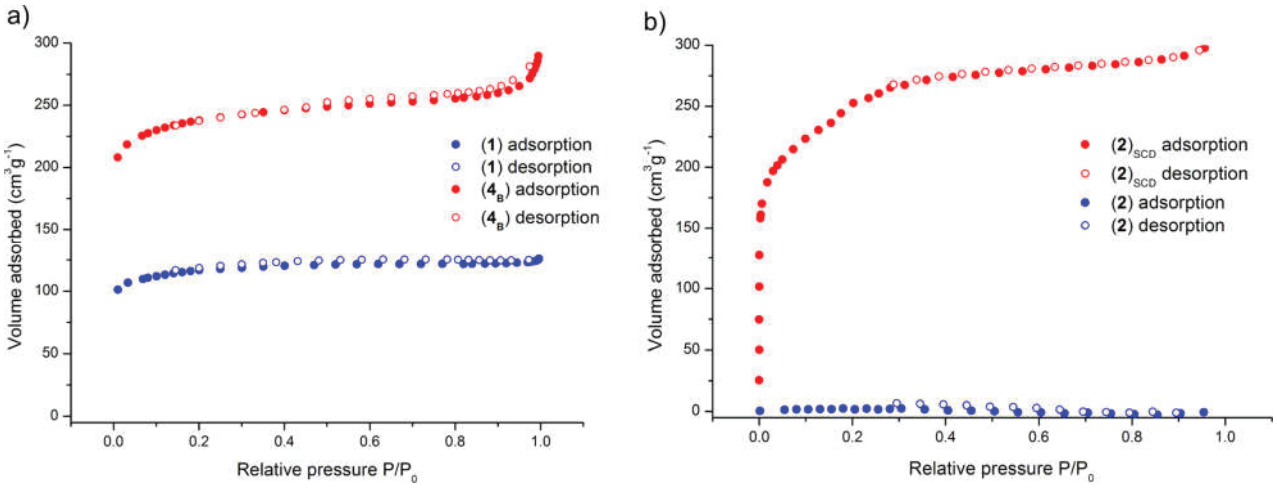

Figure 6. (a) N_2 sorption isotherms for compounds **1** and $\mathbf{4_B}$ after thermal activation under a vacuum (b) N_2 sorption isotherms for compound **2** with (red) and without (blue) supercritical drying procedure.

DOI: 10.1021/cg501855k
Cryst. Growth Des. 2015, 15, 1819−1826

CONCLUSION

In summary, the reactivity of iron(III) with the H_2TCPP porphyrinic linker in the presence of different bases toward formation of porous networks was studied. The metallic cation used here presents two easily accessible redox states: Fe^{II} and Fe^{III}; therefore compounds with either redox state in the inorganic building unit could be obtained. For Fe^{II} MOFs, formation of two paddle wheel networks was evidenced, and compound **2** was a second reported example demonstrating the accessible porosity for a MOF based on diiron paddle wheel SBU. In the case of Fe^{III}-based MOFs, a MIL-141 type compound was obtained in the presence of the cesium hydroxide when the use of pyrazine led to the formation of a porous polymer with a $[Fe(OH)O_4]_n$ chain of corner sharing μ_2-OH SBU. This work illustrates the synthesis versatility for iron-based extended porphyrinic materials.

ASSOCIATED CONTENT

Supporting Information

Details of characterization results and crystallographic cif files. This material is available free of charge via the Internet at http://pubs.acs.org.

AUTHOR INFORMATION

Corresponding Author

*E-mail: alexandra.fateeva@univ-lyon1.fr.

Notes

The authors declare no competing financial interest.

ACKNOWLEDGMENTS

The authors acknowledge the French Ministry of National Education, Research and Technology, the University of Lyon 1, and CNRS for financial support and the CTμ (Centre Technologique des Microstructures) of the University of Lyon 1 for providing the scanning electron microscopy facility.

REFERENCES

(1) Burnett, B. J.; Barron, P. M.; Choe, W. *CrystEngComm* **2012**, *14*, 3839.
(2) Gao, W.-Y.; Chrzanowski, M.; Ma, S. *Chem. Soc. Rev.* **2014**, *43*, 5841.
(3) Fateeva, A.; Chater, P. A.; Ireland, C. P.; Tahir, A. A.; Khimyak, Y. Z.; Wiper, P. V.; Darwent, J. R.; Rosseinsky, M. J. *Angew. Chem., Int. Ed.* **2012**, *51*, 7440.
(4) Feng, D.; Chung, W.-C.; Wei, Z.; Gu, Z.-Y.; Jiang, H.-L.; Chen, Y.-P.; Darensbourg, D. J.; Zhou, H.-C. *J. Am. Chem. Soc.* **2013**, *135*, 17105.
(5) Jiang, H.-L.; Feng, D.; Wang, K.; Gu, Z.-Y.; Wei, Z.; Chen, Y.-P.; Zhou, H.-C. *J. Am. Chem. Soc.* **2013**, *135*, 13934.
(6) Feng, D.; Gu, Z. Y.; Li, J. R.; Jiang, H. L.; Wei, Z.; Zhou, H. C. *Angew. Chem., Int. Ed. Engl.* **2012**, *51*, 10307.
(7) Fateeva, A.; Devautour-Vinot, S.; Heymans, N.; Devic, T.; Grenèche, J.-M.; Wuttke, S.; Miller, S.; Lago, A.; Serre, C.; De Weireld, G.; Maurin, G.; Vimont, A.; Férey, G. *Chem. Mater.* **2011**, *23*, 4641.
(8) Wang, K.; Feng, D.; Liu, T.-F.; Su, J.; Yuan, S.; Chen, Y.-P.; Bosch, M.; Zou, X.; Zhou, H.-C. *J. Am. Chem. Soc.* **2014**, *136*, 13983.
(9) Shultz, A. M.; Farha, O. K.; Hupp, J. T.; Nguyen, S. T. *J. Am. Chem. Soc.* **2009**, *131*, 4204.
(10) Suslick, K. S.; Bhyrappa, P.; Chou, J. H.; Kosal, M. E.; Nakagaki, S.; Smithenry, D. W.; Wilson, S. R. *Acc. Chem. Res.* **2005**, *38*, 283.
(11) Nakagaki, S.; Ferreira, G.; Ucoski, G.; Dias de Freitas Castro, K. *Molecules* **2013**, *18*, 7279.
(12) Zhao, M.; Ou, S.; Wu, C.-D. *Acc. Chem. Res.* **2014**, *47*, 1199.
(13) Xie, M.-H.; Yang, X.-L.; Zou, C.; Wu, C.-D. *Inorg. Chem.* **2011**, *50*, 5318.
(14) Son, H.-J.; Jin, S.; Patwardhan, S.; Wezenberg, S. J.; Jeong, N. C.; So, M.; Wilmer, C. E.; Sarjeant, A. A.; Schatz, G. C.; Snurr, R. Q.; Farha, O. K.; Wiederrecht, G. P.; Hupp, J. T. *J. Am. Chem. Soc.* **2012**, *135*, 862.
(15) Lee, C. Y.; Farha, O. K.; Hong, B. J.; Sarjeant, A. A.; Nguyen, S. T.; Hupp, J. T. *J. Am. Chem. Soc.* **2011**, *133*, 15858.
(16) Abrahams, B. F.; Hoskins, B. F.; Michail, D. M.; Robson, R. *Nature* **1994**, *369*, 727.
(17) Krupitsky, H.; Stein, Z.; Goldberg, I.; Strouse, C. *J. Inclusion Phenom. Mol. Recognit. Chem.* **1994**, *18*, 177.
(18) Diskin-Posner, Y.; Dahal, S.; Goldberg, I. *Chem. Commun.* **2000**, 585.
(19) Diskin-Posner, Y.; Dahal, S.; Goldberg, I. *Angew. Chem., Int. Ed.* **2000**, *39*, 1288.
(20) DeVries, L.; Choe, W. *J. Chem. Crystallogr.* **2009**, *39*, 229.
(21) Zou, C.; Wu, C.-D. *Dalton Trans.* **2012**, *41*, 3879.
(22) Deiters, E.; Bulach, V.; Hosseini, M. W. *Chem. Commun.* **2005**, 3906.
(23) Lin, K.-J. *Angew. Chem., Int. Ed.* **1999**, *38*, 2730.
(24) Choi, E.-Y.; Barron, P. M.; Novotny, R. W.; Son, H.-T.; Hu, C.; Choe, W. *Inorg. Chem.* **2008**, *48*, 426.
(25) Chung, H.; Barron, P. M.; Novotny, R. W.; Son, H.-T.; Hu, C.; Choe, W. *Cryst. Growth Des.* **2009**, *9*, 3327.
(26) Farha, O. K.; Shultz, A. M.; Sarjeant, A. A.; Nguyen, S. T.; Hupp, J. T. *J. Am. Chem. Soc.* **2011**, *133*, 5652.
(27) Xu, Z.; Meng, W.; Li, H.; Hou, H.; Fan, Y. *Inorg. Chem.* **2014**, *53*, 3260.
(28) Dhakshinamoorthy, A.; Alvaro, M.; Chevreau, H.; Horcajada, P.; Devic, T.; Serre, C.; Garcia, H. *Catal. Sci. Technol.* **2012**, *2*, 324.
(29) Breeze, M. I.; Clet, G.; Campo, B. C.; Vimont, A.; Daturi, M.; Grenèche, J.-M.; Dent, A. J.; Millange, F.; Walton, R. I. *Inorg. Chem.* **2013**, *52*, 8171.
(30) Bloch, E. D.; Queen, W. L.; Krishna, R.; Zadrozny, J. M.; Brown, C. M.; Long, J. R. *Science* **2012**, *335*, 1606.
(31) Bloch, E. D.; Murray, L. J.; Queen, W. L.; Chavan, S.; Maximoff, S. N.; Bigi, J. P.; Krishna, R.; Peterson, V. K.; Grandjean, F.; Long, G. J.; Smit, B.; Bordiga, S.; Brown, C. M.; Long, J. R. *J. Am. Chem. Soc.* **2011**, *133*, 14814.
(32) Yoon, J. W.; Seo, Y.-K.; Hwang, Y. K.; Chang, J.-S.; Leclerc, H.; Wuttke, S.; Bazin, P.; Vimont, A.; Daturi, M.; Bloch, E.; Llewellyn, P. L.; Serre, C.; Horcajada, P.; Grenèche, J.-M.; Rodrigues, A. E.; Férey, G. *Angew. Chem., Int. Ed.* **2010**, *49*, 5949.
(33) Xiao, D. J.; Bloch, E. D.; Mason, J. A.; Queen, W. L.; Hudson, M. R.; Planas, N.; Borycz, J.; Dzubak, A. L.; Verma, P.; Lee, K.; Bonino, F.; Crocellà, V.; Yano, J.; Bordiga, S.; Truhlar, D. G.; Gagliardi, L.; Brown, C. M.; Long, J. R. *Nat. Chem.* **2014**, *6*, 590.
(34) Dhakshinamoorthy, A.; Alvaro, M.; Garcia, H. *Chem. Commun.* **2010**, *46*, 6476.
(35) Wiers, B. M.; Foo, M.-L.; Balsara, N. P.; Long, J. R. *J. Am. Chem. Soc.* **2011**, *133*, 14522.
(36) Férey, G.; Millange, F.; Morcrette, M.; Serre, C.; Doublet, M.-L.; Grenèche, J.-M.; Tarascon, J.-M. *Angew. Chem., Int. Ed.* **2007**, *46*, 3259.
(37) Combelles, C.; Yahia, M. B.; Pedesseau, L.; Doublet, M. L. *J. Phys. Chem. C* **2010**, *114*, 9518.
(38) Fateeva, A.; Horcajada, P.; Devic, T.; Serre, C.; Marrot, J.; Grenèche, J.-M.; Morcrette, M.; Tarascon, J.-M.; Maurin, G.; Férey, G. *Eur. J. Inorg. Chem.* **2010**, *2010*, 3789.
(39) Horcajada, P.; Chalati, T.; Serre, C.; Gillet, B.; Sebrie, C.; Baati, T.; Eubank, J. F.; Heurtaux, D.; Clayette, P.; Kreuz, C.; Chang, J.-S.; Hwang, Y. K.; Marsaud, V.; Bories, P.-N.; Cynober, L.; Gil, S.; Ferey, G.; Couvreur, P.; Gref, R. *Nat. Mater.* **2010**, *9*, 172.
(40) Baati, T.; Njim, L.; Neffati, F.; Kerkeni, A.; Bouttemi, M.; Gref, R.; Najjar, M. F.; Zakhama, A.; Couvreur, P.; Serre, C.; Horcajada, P. *Chem. Sci.* **2013**, *4*, 1597.
(41) Wang, K.; Feng, D.; Liu, T.-F.; Su, J.; Yuan, S.; Chen, Y.-P.; Bosch, M.; Zou, X.; Zhou, H.-C. *J. Am. Chem. Soc.* **2014**, *136*, 13983–13986.

DOI: 10.1021/cg501855k
Cryst. Growth Des. 2015, 15, 1819–1826

(42) Anderson, J. S.; Gallagher, A. T.; Mason, J. A.; Harris, T. D. *J. Am. Chem. Soc.* **2014**, *136*, 16489−16492.
(43) Del Gaudio, J.; La Mar, G. N. *J. Am. Chem. Soc.* **1978**, *100*, 1112.
(44) Shin, K.; Kramer, S. K.; Goff, H. M. *Inorg. Chem.* **1987**, *26*, 4103.
(45) Zhao, M.; Song, D.; Lippard, S. J. *Inorg. Chem.* **2006**, *45*, 6323.
(46) Friedle, S.; Kodanko, J. J.; Fornace, K. L.; Lippard, S. J. *J. Mol. Struct.* **2008**, *890*, 317.
(47) Kongpatpanich, K.; Horike, S.; Sugimoto, M.; Kitao, S.; Seto, M.; Kitagawa, S. *Chem. Commun.* **2014**, *50*, 2292.
(48) Zheng, Y.-Z.; Xue, W.; Tong, M.-L.; Chen, X.-M.; Zheng, S.-L. *Inorg. Chem.* **2008**, *47*, 11202.
(49) Low, J. J.; Benin, A. I.; Jakubczak, P.; Abrahamian, J. F.; Faheem, S. A.; Willis, R. R. *J. Am. Chem. Soc.* **2009**, *131*, 15834.
(50) Rosi, N. L.; Kim, J.; Eddaoudi, M.; Chen, B.; O'Keeffe, M.; Yaghi, O. M. *J. Am. Chem. Soc.* **2005**, *127*, 1504.
(51) Serre, C.; Millange, F.; Thouvenot, C.; Noguès, M.; Marsolier, G.; Louër, D.; Férey, G. *J. Am. Chem. Soc.* **2002**, *124*, 13519.
(52) Barthelet, K.; Riou, D.; Nogues, M.; Férey, G. *Inorg. Chem.* **2003**, *42*, 1739.
(53) Devic, T.; Serre, C. *Chem. Soc. Rev.* **2014**, *43*, 6097.
(54) Gao, W.-Y.; Zhang, Z.; Cash, L.; Wojtas, L.; Chen, Y.-S.; Ma, S. *CrystEngComm* **2013**, *15*, 9320.
(55) Zou, C.; Zhang, T.; Xie, M.-H.; Yan, L.; Kong, G.-Q.; Yang, X.-L.; Ma, A.; Wu, C.-D. *Inorg. Chem.* **2013**, *52*, 3620.
(56) Devic, T.; Horcajada, P.; Serre, C.; Salles, F.; Maurin, G.; Moulin, B.; Heurtaux, D.; Clet, G.; Vimont, A.; Grenèche, J.-M.; Ouay, B. L.; Moreau, F.; Magnier, E.; Filinchuk, Y.; Marrot, J.; Lavalley, J.-C.; Daturi, M.; Férey, G. *J. Am. Chem. Soc.* **2009**, *132*, 1127.
(57) Kobayashi, H.; Maeda, Y.; Yanagawa, Y. *Bull. Chem. Soc. Jpn.* **1970**, *43*, 2342.
(58) Li, J.; Nair, S. M.; Noll, B. C.; Schulz, C. E.; Scheidt, W. R. *Inorg. Chem.* **2008**, *47*, 3841.
(59) Nelson, A. P.; Farha, O. K.; Mulfort, K. L.; Hupp, J. T. *J. Am. Chem. Soc.* **2008**, *131*, 458.
(60) Farha, O. K.; Hupp, J. T. *Acc. Chem. Res.* **2010**, *43*, 1166.
(61) Düren, T. http://www.see.ed.ac.uk/~tduren/research/surface_area/; Web site for obtaining the source code of the program to calculatethe accessible surface area.

DOI: 10.1021/cg501855k
Cryst. Growth Des. 2015, 15, 1819−1826

3.3. Investigating the reactivity of the free base tetrakis(4-carboxyphenyl) porphyrin with iron(III)

3.3.1. Investigating the nature of the intermediate product in the synthesis of [Fe^{II}pzTCPP($Fe^{III}OH)_2$]

In the two-step synthesis procedure for obtaining [Fe^{II}pzTCPP($Fe^{III}OH)_2$], a poorly crystallised intermediate product is resulted from the solvothermal reaction between $FeCl_3.6H_2O$ and H_2TCPP at 180 °C. When this intermediate product was further reacted with pyrazine, the final framework, [Fe^{II}pzTCPP($Fe^{III}OH)_2$], was obtained (Figure 3-1 Synthetic route B). The structure of this intermediate product remains unknown as crystals of sufficient quality were not obtained for single crystal X-ray diffraction studies. However, the solid appeared to be polymeric as seen by its insolubility in organic solvents such as DMF and presence of coordinated carboxylate groups in the IR spectrum. Furthermore, the product also showed intrinsic porosity indicating an open framework. It would be interesting to gain a better picture of this intermediate product as it would offer an insight in to what changes are brought about by the addition of pyrazine and how it affects the nature of the SBU and the overall framework. This would lead to a fundamental understanding of the formation of this MOF. Thus, the possibility of obtaining better quality single crystals in order to solve the structure of the intermediate phase was explored by varying reaction parameters as summarised in Table 3-1 (All the reactions attempted are given in appendix section B.1). A total of 11 reactions were attempted for this purpose.

Table 3-1 Summary of synthesis parameters investigated for the reaction between H_2TCPP and $FeCl_3.6H_2O$.

Parameter	
Isotherm temperature	120-150-180 °C
Solvent (at 180 °C)	DMF, DEF
Additives (DMF as solvent and at 180 °C)	HCl (15 eq compared to H_2TCPP) H_2O (10% of total solvent)

For the range considered in this study, the isotherm temperature showed no effect on the crystal morphology or size as similar square shaped crystals of around 100 µm were obtained for the synthesis at 120 °C and at 180 °C with DMF as the solvent. However, fewer crystals were present in the resultant mother liquor from the synthesis at 120 °C. For the syntheses at 180 °C, the additives and the solvent change from DMF to DEF had an effect on the crystal morphology. DMF as solvent resulted in square shaped crystals of around 100 µm, with or without HCl as an additive. However,

when H_2O was added fine needle shaped crystals were obtained which were smaller than the square shaped crystals observed before. When DEF was used as the solvent, resultant crystals were again, needle shaped and were similar to those observed with H_2O as an additive. However, crystals of sufficient quality for single crystal x-ray diffraction could not be obtained from the syntheses.

The use of DEF as solvent and lower isotherm temperature of 120 °C resulted in amorphous solids as shown by the pxrd patterns (Figure 3-4a). The samples obtained from syntheses with HCl and H_2O as additives in DMF at 180 °C were less crystalline compared to the sample from the synthesis without any additives (Figure 3-4a). The IR spectra of these samples show that the products obtained had coordinated carboxylate groups by the presence of the asymmetric and symmetric C=O stretches at 1596 $cm^{-1}$and 1398 cm^{-1}(Figure 3-4b).

The formation of a gel product was observed during some of the syntheses which was a major obstacle in obtaining reliable data. Attempts were made to investigate this phenomenon by changing various reaction conditions. The synthesis temperature was lowered from 180 °C to 150 °C, the $FeCl_3.6H_2O$ was pre-dissolved in DMF or in DEF and the oven was preheated at 180 °C before the introduction of the reactants, but a trend could not be established for the formation of the gel. Gel formation has been reported before for iron porphyrin systems where it was attributed to the polymerization of acetaldehyde that results from the oxidative decomposition of DEF and DMF, which could be the cause of this phenomenon observed in this work.[12]

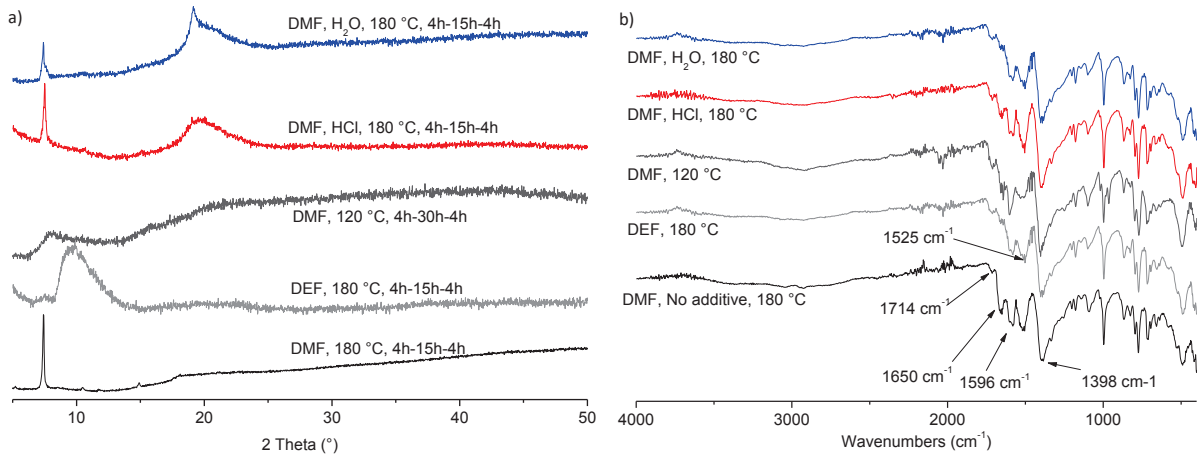

Figure 3-4 a) Effect of changing the temperature, the solvent, and different additives on the pxrd patterns. b) IR spectra of the samples (1714 cm^{-1}= uncoordinated COOH C=O stretch, 1650 cm^{-1} = DMF C=O stretch, 1596 $cm^{-1}$and 1398 cm^{-1}= asymmetric and symmetric of coordinated carboxylate C=O stretches, 1525 cm^{-1} = porphyrin aromatic C=C stretch.)

3.3.2. Investigating the possibility of replacing the pyrazine axial ligand with a different N-donor in [Fe^{II}pzTCPP($Fe^{III}OH)_2$]

The study of iron porphyrin systems which resemble heme prosthetic groups found in nature is of great interest as it can lead to a fundamental understanding of biological processes. The reactive nature of iron porphyrin complexes makes studying these systems difficult as in absence of a protein superstructure, they tend to undergo irreversible bimolecular condensation reactions, forming Fe-oxo dimers.[13] Thus, much effort has been made to construct systems such as picket-fence porphyrins which can prevent the self-deactivation of reactive porphyrin motifs, and enable their study.[14] Recently, MOFs with Fe-porphyrin motifs, which can also prevent self-deactivation reactions have received attention as platforms for studying the reactivity of Fe-porphyrins.[7]

Most iron porphyrin systems studied employ a N-donor axial ligand such as imidazole coordinated to the Fe^{2+} centre which aids in binding O_2 to the vacant sixth coordination site. In [Fe^{II}pzTCPP($Fe^{III}OH)_2$], pyrazine coordinates to two Fe^{2+} centres in two co-facial porphyrin cores with its two nitrogens acting as a bridging ligand (Figure 3-2a). If pyrazine could be replaced with a N-donor such as imidazole it would be possible to obtain a system with coordinatively unsaturated Fe centres (Figure 3-2b).

Thus, possibility of replacing pyrazine with different N-donor ligands such as imidazole, 4-methyl-imidazole, pyrrolidine, and pyridine (Figure 3-5b) was investigated.

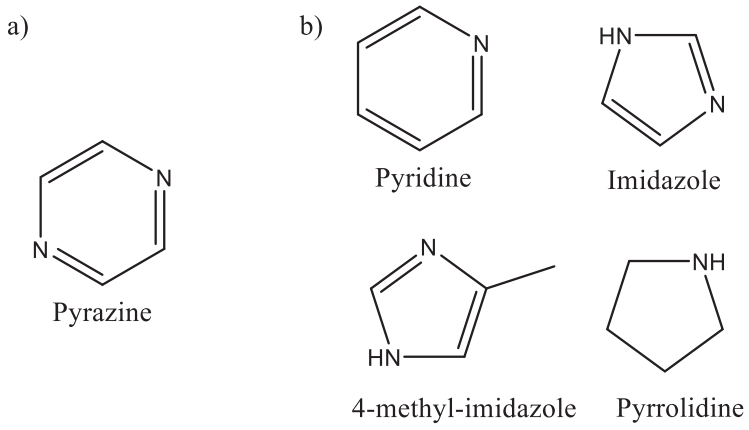

Figure 3-5 a) N-donor present in the published framework b) Different N-donors used for the exploratory syntheses.

To introduce these heterocycles into the above-mentioned porphyrinic MOFs, both the synthetic routes A and B (Figure 3-1) were investigated.

One step synthesis was attempted replacing the pyrazine with imidazole, 4-methyl imidazole or pyrrolidine and keeping the other synthesis parameters unchanged. Syntheses with pyrrolidine and imidazole resulted in solids with poor crystallinity while 4-methyl imidazole resulted in an amorphous

solid (Figure 3-6a). The IR spectra of the samples showed the characteristic bands which indicate the presence of coordinated carboxylate groups (1589 cm^{-1}, asymmetric C=O stretch; 1400 cm^{-1}, symmetric C=O stretch) (Figure 3-6b). Furthermore, N_2 adsorption measurements conducted for the products indicated that the solids have permanent porosity with the one with pyrrolidine the most porous with a BET surface area of 357 m^2g^{-1} (Figure 3-7).

When looking at single crystals, syntheses with imidazole and pyrrolidine both resulted in small square shaped crystals of around 100 µm while 4-methyl imidazole resulted in mainly irregular shaped grains. Thus, it seems the size of the N-donor molecules is affecting the difference in crystallinity and the crystal morphology as similar sized imidazole and pyrrolidine results in similar pxrd patterns and similar shaped crystals compared to what is observed for the relatively bigger 4-methyl imidazole. However, crystals of sufficient quality for single x-ray diffraction could not be obtained thus further structural studies were not possible.

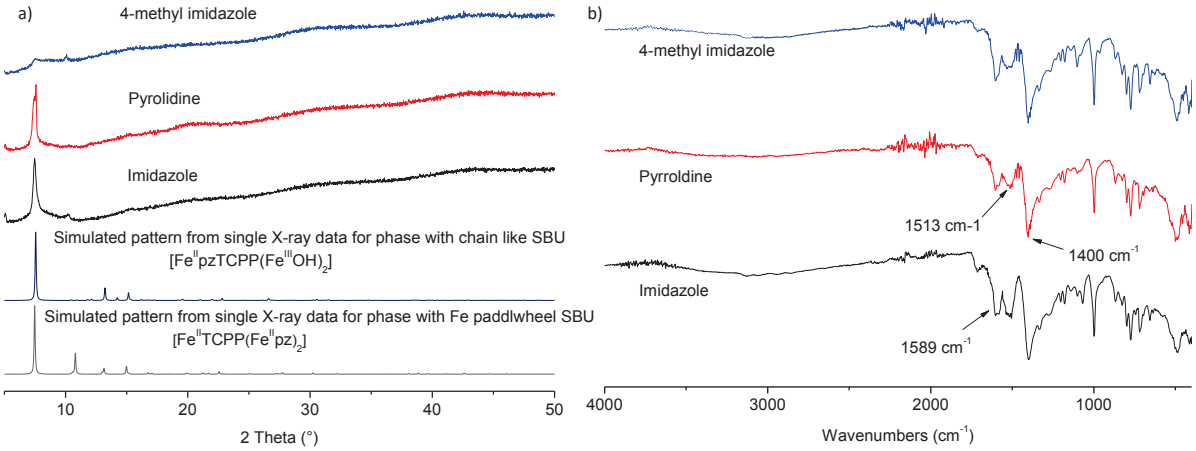

Figure 3-6 a) PXRD data for single-step syntheses with various N-donors. b) IR spectra for products from the single-step syntheses with different N-donors.

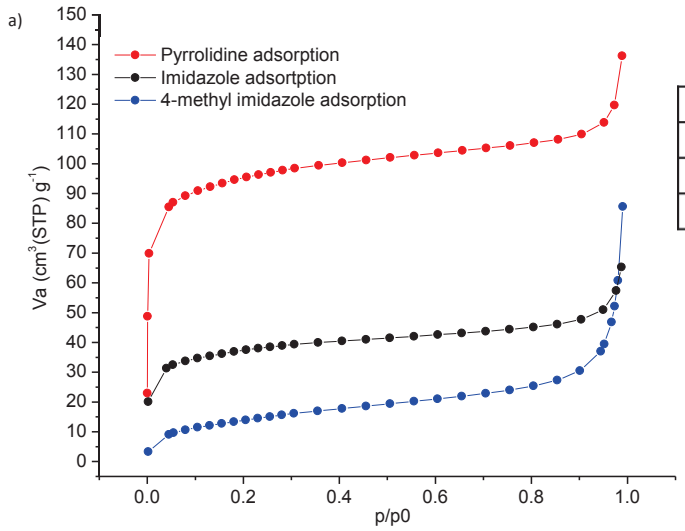

b)

N-donor	BET surface area (m^2g^{-1})
Imidazole	135
Pyrrolidine	357
4-methyl-imidazole	52

Figure 3-7 a) N_2 adsorption isotherms at 77K for the products from the single step syntheses with different N-donors b) BET surface areas.

The synthesis route B was attempted with imidazole, 4-methyl imidazole, pyrrolidine addition in the second step of the synthesis and was compared to the use of pyrazine. Syntheses with N-donors other than pyrazine resulted in poorly crystalized solids with a similar PXRD pattern to each other and to the starting intermediate (Figure 3-8a). This possibly indicates that, these N-donors have little effect on the structure of the intermediate product. This could be due to the ability of pyrazine to fit between 2 co-facial porphyrin molecules and coordinate to them, giving rise to a templating effect in determining the final structure of [Fe^{II}pzTCPP($Fe^{III}OH)_2$]. The IR spectra of the products with the N-donors from the 2-step synthesis all showed the characteristic bands of coordinated carboxylate groups (Figure 3-8b) suggesting that polymeric phases are formed. All the syntheses resulted in small square shaped single crystals similar to what was observed for the one step synthesis, but the quality of the crystals was not sufficient for single crystal x-ray diffraction studies. Thus, further structural studies were not possible.

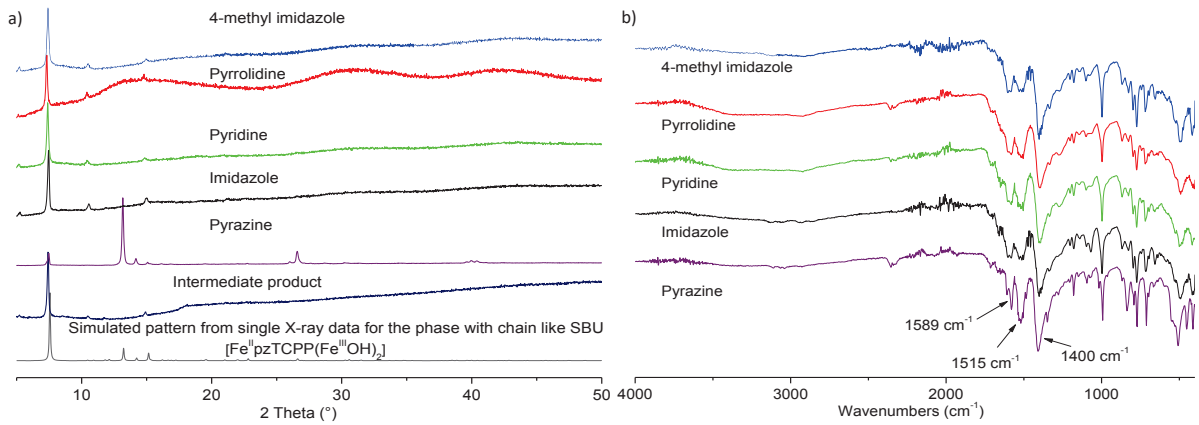

Figure 3-8 a) PXRD data for 2-step syntheses with N-donors. PXRD measurements performed with instrument 2. b) IR spectra for the 2-step syntheses with different N-donors.

Attempts were also made to replace the pyrazine in the [Fe^{II}pzTCPP($Fe^{III}OH)_2$] structure with imidazole using solvent assisted ligand exchange (SALE) methods reported by Hupp et al.[15] [Fe^{II}pzTCPP($Fe^{III}OH)_2$] and 20 times excess imidazole were combined in DMF and heated at 100 °C for 72 hours. The reaction solution was analysed with mass-spectrometry for the presence of pyrazine (Figure 3-9). No peaks corresponding to pyrazine were detected indicating that no pyrazine was liberated. Furthermore, there was no qualitative change in the morphology of the single crystals. The reaction was repeated with HCl with a pH of 0.5 as the solvent. This acidic condition digested the MOF.

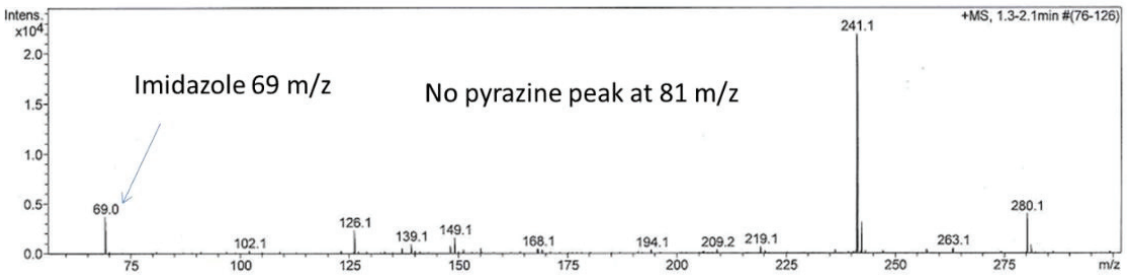

Figure 3-9 Mass spectrometry data for the attempted solvent assisted ligand exchange of pyrazine with imidazole in [Fe^{II}pzTCPP($Fe^{III}OH)_2$],

3.3.3. Conclusion and perspectives for the investigation in to the reactivity of free base tetrakis(4-carboxyphenyl) porphyrin with iron(III)

A total of 11 reactions were attempted in investigating the nature of the intermediate product. The formation of a gel was observed in 6 reactions which made analysis difficult. To prevent gel formation in the future, this system could be investigated using dry solvents under anaerobic conditions. The goal of obtaining single crystals of sufficient quality for single crystal diffraction studies was not achieved. This was possibly due to the poor quality of the crystals and their small size as they did not show diffraction using the laboratory diffractometer.

For the investigation of the possibility to replace pyrazine with a different N-donor, 3 attempts were made with the single step approach while 4 attempts were made with the two-step approach. Both approaches yielded solids which were coordination polymers but single crystals of sufficient quality were not obtained. Furthermore, 2 attempts were made to replace the pyrazine in the structure using solvent assisted ligand exchange technique, but were not successful. Additional analyses would have been beneficial to give insight into sample composition but were not performed due to time constraints and the unavailability of equipment. Mass spectrometry could have been used to analyse washed samples after digesting in 0.1M NaOH to assess if the desired N-donor was part of the polymeric structure. In addition, TGA analysis could also have given information about possible MOF formulae as well as details about thermal stability. Solid state UV-vis spectra of the products

could have provided details about the oxidation state of iron in the porphyrin cores as Fe^{3+} would show a blue shifted Soret band compared to Fe^{2+}.[16]

Considering the fact that frameworks with microporosity were obtained for the one step synthesis process, it is worth further investigating different temperatures and solvent systems to see if products with better crystallinity could be obtained.

It appears that pyrazine has a templating effect in constructing the final framework of $[Fe^{II}pzTCPP(Fe^{III}OH)_2]$ from the intermediate product. Indeed, the use of other N-donor ligands did not result in a similar framework. This could be due to its perfect fit size wise in the framework along with the ability to act as a bridge between two Fe^{2+} centres. An interesting N-donor to investigate would be piperazine. Even though this molecule is not aromatic, it could potentially act as a bridging ligand with its two N atoms.

3.4. Investigating the reactivity of cobalt metalated tetrakis(4-carboxyphenyl) porphyrin with iron(III)

The photocatalytic and electrocatalytic activity of cobalt porphyrins for CO_2 reduction have been well studied.[17-18] Incorporation of such metalloporphyrins in stable MOF structures can lead to stable heterogeneous catalysts. Kornienko et al demonstrated the catalytic CO_2 reduction properties of a MOF system based on cobalt metalated Al-PMOF.[19] However, very few stable porphyrinic MOFs have been based on iron containing inorganic SBUs.[20] Inorganic SBUs based on trivalent iron can result in stable frameworks as shown in the previous section. Besides, the presence of iron in the inorganic building block can be possibly exploited to enhance the redox activity of the MOFs.[21]

We therefore attempted to obtain a stable porous MOF based on CoTCPP(X) and iron. The summary of synthesis parameters investigated are given in Table 3-2 (details for all the attempted reactions are given in appendix section B.2). The synthesis details for the Co metalated TCPP [CoTCPP(X) X= OH^- or Cl^-] ligand are given in chapter 2. For calculating the ratios of reactants, the molar mass of CoTCPP(OH) was used.

Table 3-2 Different parameters investigated for studying the reactivity of Fe^{3+} with CoTCPP(OH).

Parameter	
Metal precursor	$FeCl_3.6H_2O$
Solvent	DMF
Isotherm temperature	120 -150 -190 °C
Heating program (heating time, isotherm, cooling time)	12h-60h-4h, 4h-72h-4h at 150 °C 4h-72h-4h at 190 °C
Metal/ligand ratio	1 at 120 °C 0.6, 1, 1.5, 3 at 150 °C 0.8, 1, 2 at 190 °C
Concentration (porphyrin ligand)	10mM, 2.5mM at 150 °C 10mM, 17mM at 190 °C
Additives	HCl (3 eq compared to the porphyrin ligand) @ 150 °C

For this system, a total of 14 different reactions were attempted. Synthesis at 120 °C produced a gel while syntheses at 150 °C and 190 °C resulted in solids. The most of the focus of the study was directed towards the syntheses at 150 °C (9 attempted syntheses) due to the promising results obtained initially.

The products obtained from the syntheses at 150 °C with a heating program of 4h-72h-4h, DMF as the solvent, 1:1 metal to porphyrin ratio and 10 mM porphyrin concentration showed low crystallinity as shown by the pxrd data (Figure 3-11). However, the square shaped single crystals were analysed using single crystal X-ray diffraction. The structure corresponded to a 3-D polymeric phase with a tentatively assigned formula, $[CoTCPP(H_2O)_2(Fe^{III}OH)_2]$ (Figure 3-10).

Structure of $[CoTCPP(H_2O)_2(Fe^{III}(OH)_2]$

From single crystal diffraction data, the formula $[CoTCPP(H_2O)_2(Fe^{III}OH)_2]$ was tentatively assigned to this new phase considering the similarities to the published structure, $[Fe^{II}pzTCPP(Fe^{III}OH)_2]$. Figure 3-10 shows the structure of $[CoTCPP(H_2O)_2(Fe^{III}OH)_2]$ along the a, b and c axes, Table 3-3 gives the lattice parameters of the $[CoTCPP(H_2O)_2(Fe^{III}(OH)_2]$ phase compared to that of $[Fe^{II}pzTCPP(Fe^{III}OH)_2]$ and Table 3-4 gives bond lengths and angles of the inorganic SBU and the porphyrin core for the two structures.

In the inorganic SBU of $[CoTCPP(H_2O)_2(Fe^{III}OH)_2]$, Fe^{3+} is equatorially coordinated to 4 carboxylate oxygen atoms and axially to two μ_2-OH, which bridge the adjacent Fe^{3+} centres. This gives rise to an infinite $[Fe(OH)O_4]_n$ chain similar to what is observed for $[Fe^{II}pzTCPP(Fe^{III}OH)_2]$ structure (shown previously in Figure 3-1). There are two different Fe-O bond lengths for the bonds involving the 4 oxygen atoms belonging to acid groups. One set of Fe-O bond lengths equal to 1.9940(2) Å while the other is 1.9315(2). The Fe-O bond lengths involving the μ_2-OH are shorter and equal to 1.8838(4) Å. O-Fe-O bond angles range from 88.278(16)° to 93.477(16)° (cis) and from 177.171(22)° to 171.225(16)° (trans) indicating that the Fe^{3+} is in a distorted octahedral arrangement in the inorganic SBU.

When looking at the porphyrin linker, the cobalt inside the porphyrin core has water molecules bound at the axial positions and is in an octahedral environment (Co-N bong lengths equal to 1.9504(2) Å and 1.9729(2) Å; Co-O bond lengths equal 2.0661(6) Å; N-Co-N and O-Co-O bond angles are equal to the theoretical values of 180° while N-Co-O bond angles are equal to the theoretical values of 90°). Both Co^{2+} and Co^{3+} have been reported with similar bond lengths in porphyrinic structures. When considering other MOF structures with the same Co-TCPP linker, majority have been reported as Co^{2+}. Lions et al reported a Co^{2+} metalated Al-PMOF which had a reported average Co-N bond length of 1.9744(1) Å.[8] Another Co(II)-TCPP linker based MOF reported by Barron et al had a Co-N bond length of 1.9852(71) Å.[22] Therefore, an oxidation state of +2 was tentatively assigned to the cobalt in the porphyrin.

In this structure, each porphyrin unit is connected to 8 different Fe atoms while each Fe is connected to 4 different porphyrin linkers. The $[Fe(OH)O_4]_n$ chains run parallel to each other and are interconnected by the porphyrins giving rise to channels of ~13 Å x 8.7 Å along the c-axis (Figure 3-10c). The porphyrins are arranged co-facially along the c-axis with a distance of 6.505(2) Å between 2 parallel cobalt centres. The connecting porphyrins between $[Fe(OH)O_4]_n$ chains do not link at the same level with the chains and thus are not perpendicular to the c-axis and tilt above or below the plane of the b-axis in an alternating fashion when viewed along the a-axis (Figure 3-10a and b).

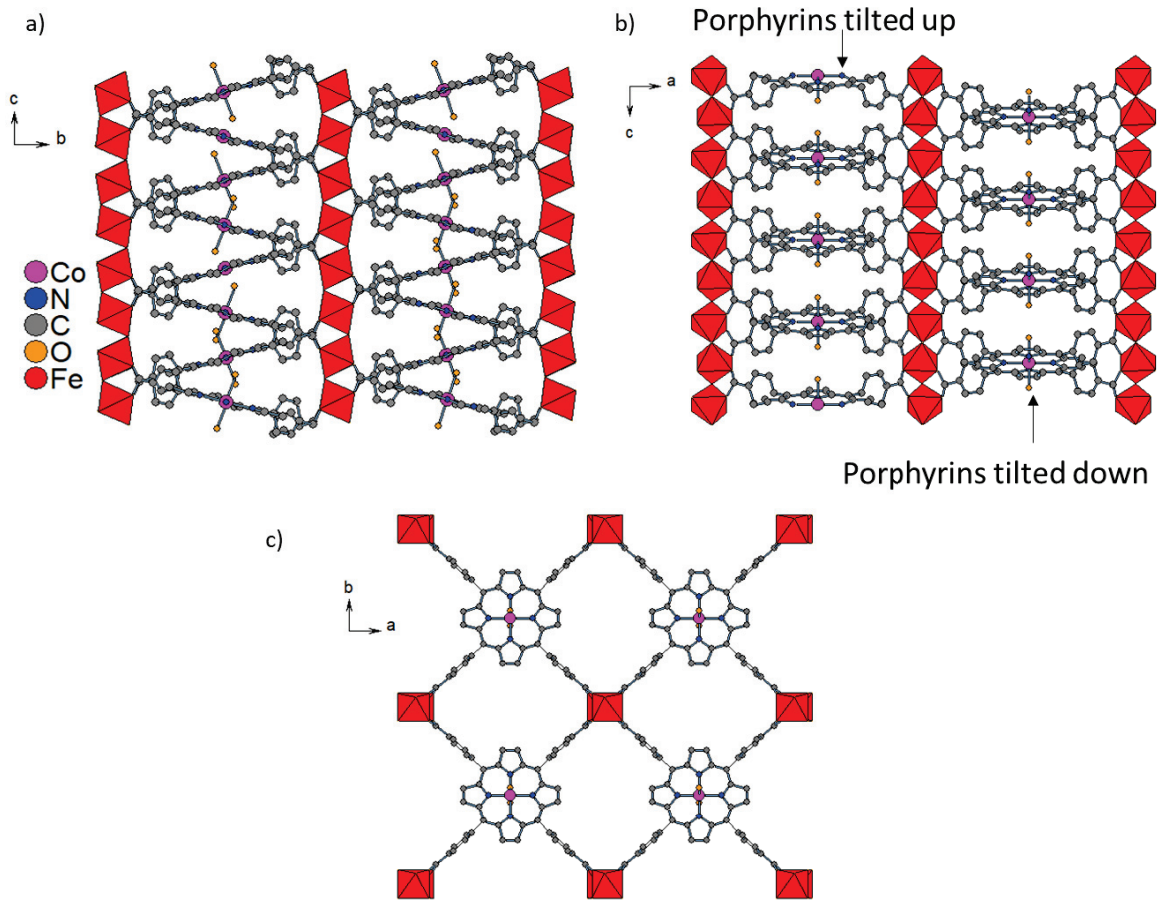

Figure 3-10 Structure of $[CoTCPP(H_2O)_2(Fe^{III}OH)_2]$. a) along the a-axis b) along the b-axis c) along the c-axis. Hydrogen atoms are omitted for clarity.

Table 3-3 Lattice parameters for $[CoTCPP(H_2O)_2(Fe^{III}OH)_2]$ compared to that of the published $[Fe^{II}pzTCPP(Fe^{III}OH)_2]$ structure.

Ref	Crystal system	a (Å)	b (Å)	c (Å)	α (°)	β (°)	λ (°)	V (Å^3)
$[CoTCPP(H_2O)_2(Fe^{III}OH)_2$	oP	33.512(4)	15.7671(19)	6.505(2)	90	90	90	3437(16)
$[Fe^{II}pzTCPP(Fe^{III}OH)_2]$	oP	6.835(2)	32.355(4)	16.896(2)	90	90	90	3737(1)

Table 3-4 Bond lengths and bond angles of the porphyrin core and the chain like SBU in $[CoTCPP(H_2O)_2(Fe^{III}OH)_2]$ compared to those of the published $[Fe^{II}pzTCPP(Fe^{III}OH)_2]$.

	Porphyrin Core (Å)	SBU (Å)	O-Fe-O SBU Bond angles in SBU (°)
$[CoTCPP(H_2O)_2(Fe^{III}OH)_2]$	Co-N(porphyrin) 1.9504(2), 1.9729(2) Co-O(water) 2.0661(6)	Fe-O(carboxylate) 1.9940(2), 1.9315(2) Fe-O (μ_2-OH) 1.8838(4)	Cis 88.278(16) - 93.477(16) Trans 177.171(22)-171.225(16)
$[Fe^{II}pzTCPP(Fe^{III}OH)_2]$	Fe-N(porphyrin) 1.999(2) Fe-N(pyrazine) 1.978(2)	Fe-O(carboxylate) 2.012(1) Fe-O(μ_2-OH) 1.918(1)	Cis 88.33(7) - 91.67(7) Trans 180

Further attempts were made to improve the quality of the single crystals and the crystallinity. Keeping all other conditions unchanged, metal to ligand ratio was screened and 1:1 stoichiometry was found to be optimal when compared with other attempted ratios as indicated by pxrd patterns (Figure 3-11). Lowering the concentration (2.5 mM) or adding HCl (3 equivalents compared to the porphyrin ligand) both had a detrimental effect on the crystallinity. Decreasing the heating rate from 0.52 °C/min to 0.17 °C/min and decreasing the isotherm time from 72 to 60 hours (i.e. 12h-60h-4h instead of 4h-72h-4h for the heating program), also resulted in material with very low crystallinity. When observing single crystals, the syntheses at 150 °C with a heating program of 4h-72h-4h generally resulted in a mixture of square shape and needle shape single crystals along with irregular shaped grains. The synthesis with an oven program of 12h-60h-4h produced only irregular shaped grains. However, the quality of the single crystals obtained from these syntheses were not sufficient for single crystal X-ray diffraction studies.

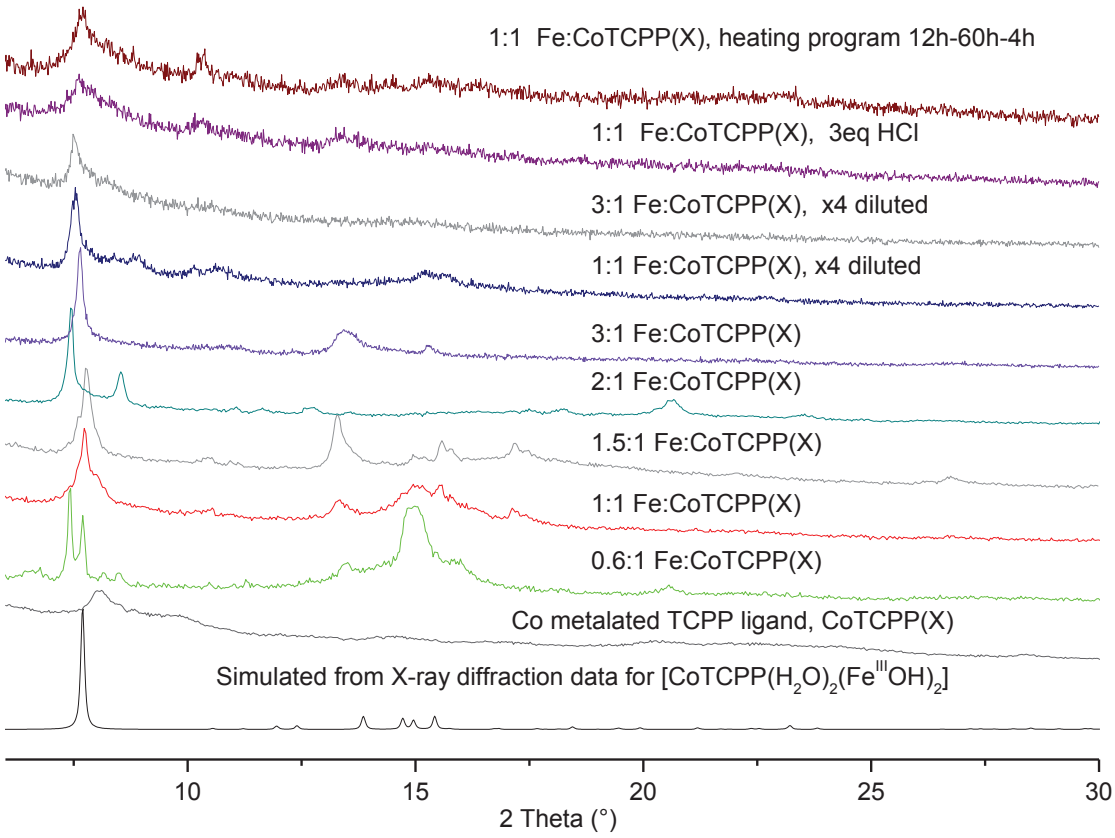

Figure 3-11 PXRD data of samples synthesised at 150 °C. All reactions were performed with a heating program of 4h-72h-4h unless noted otherwise.

Increasing the isotherm temperature to 190 °C while maintaining the heating program as 4h-72h-4h and the reactant concentration as 10 mM (for the porphyrin ligand) led to better crystallized solids but with different pxrd patterns to what was observed at 150 °C (Figure 3-12a). The PXRD patterns of these samples do not match the calculated pattern for $[CoTCPP(H_2O)_2(Fe^{III}OH)_2]$ or the framework described earlier $[Fe^{II}pzTCPP(Fe^{III}OH)_2]$. Furthermore, only fine dark needle shaped crystals of around 50 µm were obtained at 190 °C. The metal to ligand ratios tested at these conditions, 1:1 and 0.8:1, had no effect on the crystallinity or the crystal morphology.

A 1.7-times higher concentration (17 mM for the porphyrin ligand) while maintaining the other conditions unchanged (temperature: 190 °C, heating program: 4h-72h-4h, metal to ligand ratio of 1:1, solvent: DMF) resulted in a slightly better crystallized sample (Figure 3-12a), but had no effect on the single crystal morphology. However, a metal to ligand ratio of 2:1 at this reactant concentration had a detrimental effect on the crystallinity (Figure 3-12a). Single crystals of sufficient quality could not be obtained for this phase.

The IR spectra of the sample synthesised at 150 °C and at 190 °C are similar (Figure 3-12b). Both spectra show the characteristic asymmetric and symmetric stretches at 1600 cm^{-1} and 1400 cm^{-1} of coordinated carboxylate groups.

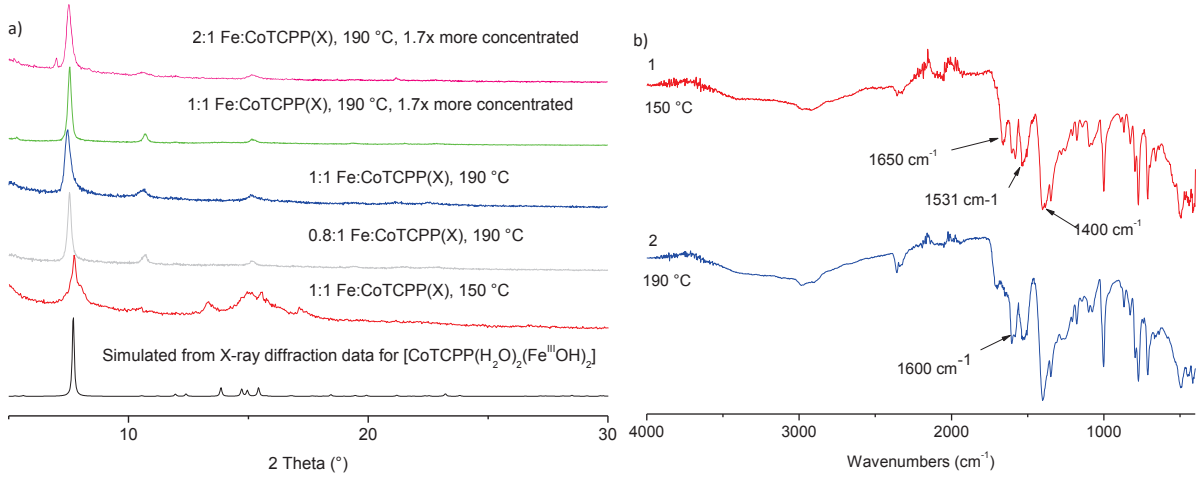

Figure 3-12 a) PXRD data. b) IR spectra for 1) Sample prepared at 150 °C and 2) Sample prepared at 190 °C with 1:1 metal to ligand ratio and a heating program of 4h-72h-4h.

Changing the solvent towards a DMF/water mixture at 150 °C resulted in the formation of a different crystalline phase (Figure 3-13). Seven reactions were performed with this solvent system where stoichiometry, temperature and solvent composition were varied with the goal to obtain a single crystalline sample (the reaction details are given in appendix section B.2).

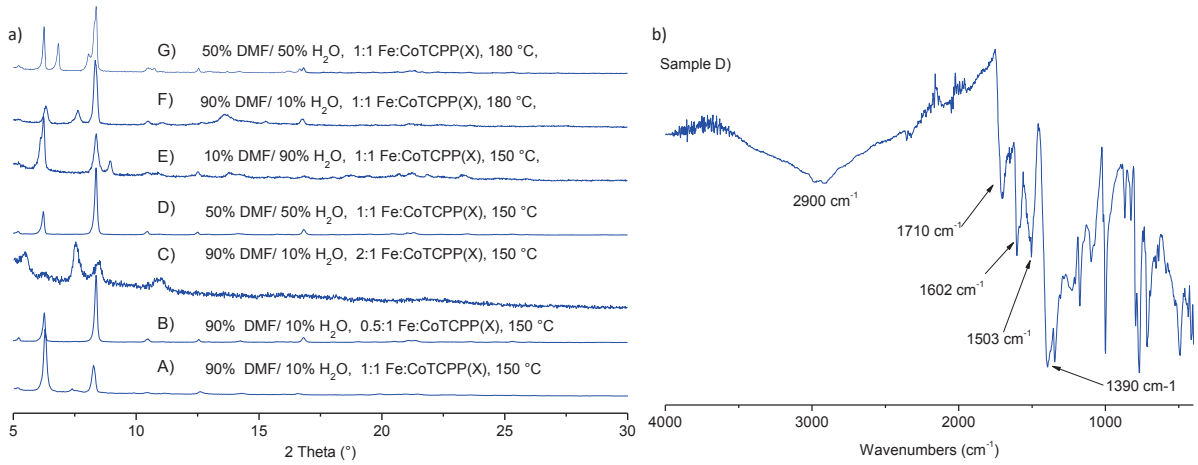

Figure 3-13 a) PXRD data for products of syntheses with a mixed solvent system of DMF/water b) IR spectrum of sample D, which was used for lattice parameter determination. Sample was dried at 150 °C before the IR spectrum was measured. Peak assignment: 2900 cm^{-1} = OH stretch of uncoordinated COOH, 1710 cm^{-1} = CO stretch of uncoordinated COOH, 1602 cm^{-1} and 1390 cm^{-1} = asymmetric and symmetric stretch of coordinated carboxylate groups, 1504 cm^{-1} = aromatic C=C stretch.

For syntheses at 150 °C using 90% DMF in the solvent, the effect of the metal to ligand ratio was investigated. Increasing this ratio from 0.5:1 to 1:1 did not produce noticeable changes in the PXRD pattern while increasing it further to 2:1 had a detrimental effect on the crystallinity and resulted in a different PXRD pattern (Figure 3-13a-C). Using the 1:1 ratio, the DMF content was decreased from 90 to 50% which led to better crystallinity and the lattice parameters were assigned from single crystal diffraction, but structural elucidation was not achieved (Figure 3-13a-D, Table 3-5). Decreasing the DMF content further (10%) resulted in a lower crystallinity and a mixture of phases (Figure 3-13a-E).

Table 3-5 Lattice parameters obtained for the single crystal from the synthesis D (Figure 3-13a-D).

	Crystal system	a (Å)	b (Å)	c (Å)	α (°)	β (°)	λ (°)	V ($Å^3$)	Reflections	Collection time per image (s)
1	mP	17.94(7)	9.46 (3)	33.89 (12)	90.2 (3)	100.7 (3)	89.9 (11)	5650 (20)	26/36 72%	400

The effect of the temperature was then considered: increasing the temperature from 150°C to 180°C resulted in a lower crystallinity and in the formation of additional phases along with the phase observed at 150 °C using 90% and 50% DMF in the solvent (Figure 3-13a-F and G).

The exact nature of the products obtained remains unknown due to the lack of structural data. However, the solids were insoluble in DMF and the IR spectra showed characteristic bands observed for coordinated carboxylate groups (Figure 3-13b) suggesting the formation of a polymeric compound. Furthermore, the presence of prominent bands at 2900 cm^{-1} (uncoordinated COOH OH stretch) and 1710 cm^{-1} (uncoordinated COOH C=O stretch) indicate that both coordinated and uncoordinated

carboxylate groups are present in the product obtained at 150 °C with a DMF/water content of 50%/50% (Figure 3-13b).

3.4.1. Conclusions and perspectives

A new phase was obtained from the reaction between $FeCl_3.6H_2O$ and Co metalated TCPP ligand and structural resolution revealed a new MOF with the chemical formula $[CoTCPP(H_2O)_2(Fe^{III}OH)_2]$. However, the bulk phase crystallinity was poor and repeated attempts made to improve crystallinity and to obtain better quality crystals were not successful.

Two other different coordination polymer products were also obtained, one at an isotherm temperature of 190 °C with DMF as the solvent and the other by using a water/DMF solvent mixture at 150 °C. However, lack of single crystals of sufficient quality for X-ray diffraction hindered further structural analysis. Only 4 reactions were attempted for the synthesis of solids obtained at a temperature of 190 °C. The effect of solvent and the heating program were not investigated. Thus, there is room for further synthesis optimisation for this product and further analysis.

A technique which could have provide insight in to the composition of these materials is energy-dispersive X-ray spectroscopy (EDX). This analysis could indicate the ratio between Co and Fe present in the samples which in turn could give the ratio between the ligand and the metal in the framework. Furthermore, UV-vis spectroscopy could have been used to probe if there is any demetalation of Co from the porphyrin cores. In addition, TGA analysis could also give information about possible MOF formulae as well as details about thermal stability and purity, particularly for the phase $[CoTCPP(H_2O)_2(Fe^{III}OH)_2]$.

3.5. Synthesis of Fe and Mn metalated Al-PMOF

As stated before, Fe^{3+} and Mn^{3+} metalated porphyrins have been used as models to mimic cytochrome P-450 in the catalytic oxidation of organic substrates and other oxidation reactions.[10-11] Thus, obtaining stable MOFs with these units can lead to heterogeneous catalysts with properties similar to what has been observed with homogeneous systems. Iron and manganese porphyrin based MOF systems have been previously reported in literature.[23] However, there have only been a few reports concerning water stable MOFs, among which are Zr (Figure 1-17 in chapter 1) and Fe based MOFs as described in chapter 1.[20, 24] Al-PMOF, $[H_2TCPP(Al^{III}OH)_2]$, is a water stable Al^{3+} based MOF published by Fateeva et al, with an $[Al(OH)O_4]$ chain like SBU.[6] The MOF is synthesised with a non-metalated porphyrinic core (i.e. H_2-Al-PMOF) and Al-PMOF variations post-synthetically metalated with divalent zinc,[6] cobalt[8] and copper[9] are known. However, Mn^{3+} and Fe^{3+} metalated Al-PMOF

phases have not been reported. Thus, the goal was to explore the possibility to achieve these two materials.

3.5.1. Synthesis of Mn^{3+} metalated Al-PMOF

Synthesis optimisation

Synthesis of the Mn^{3+} metalated Al-PMOF was attempted by directly reacting Mn^{3+} metalated TCPP ligand (MnTCPP(X), X= Cl^- or OH^-, for calculations molar mass of MnTCPP(OH) was used) with $AlCl_3.6H_2O$ to form the corresponding framework. In total, 15 reactions were performed for the synthesis optimisation and the parameters screened are summarised in Table 3-6. Details of the attempted syntheses are given in appendix section B.4).

The post-synthetic Mn^{3+} metalation of porphyrinic MOFs had not been reported before in literature to the best of the authors knowledge. Due to time constraints, this synthetic route was not explored but remains a possible method to explore in future syntheses.

Table 3-6 Summary of parameters used for synthesis optimisation of Mn^{3+} metalated Al-PMOF.

Parameter	
Ratio of M/L	2
Solvent system (DMF, water) (%vol)	(100%, 0 %), (90%,10%), (50%, 50%), (0%, 100%)
Isotherm temperature	120 -140-150-160-180-190 °C
Isotherm time	15h
Heating rate	9h (0.31 °C/min), 18h (0.15 °C/h) @190 °C
Cooling rate	Over 4h
Additives, equivalents relative to MnTCPP(OH)	Benzoic acid (2 equivalents, 10 equivalents) Potassium hydroxide (4 equivalents)

The reported synthesis for the free base Al-PMOF (H_2-Al-PMOF) was performed in water, and the same conditions were used in an initial attempt for the synthesis of Mn metalated Al-PMOF (180 °C for 16 hours, heating rate: 0.86 °C/min cooling rate: 1.7 °C/min, metal to ligand ratio of 2:1). However, this resulted in very small quantity of product, insufficient to be analysed.

In a subsequent exploratory synthesis at a different temperature (160 °C, heating program 3h-16h-4h) several different solvent compositions were tested. The synthesis with pure DMF resulted in a solid product with a higher yield. This is possibly due to the increased solubility of the Mn metalated TCPP in DMF relative to that in water, even at a lower temperature. However, a solvent system

composed of 50%/50% DMF/water resulted in the most crystalline Al-PMOF phase (Figure 3-14). A higher proportion of water (90% vs 50% water) resulted in obtaining a mixture of phases.

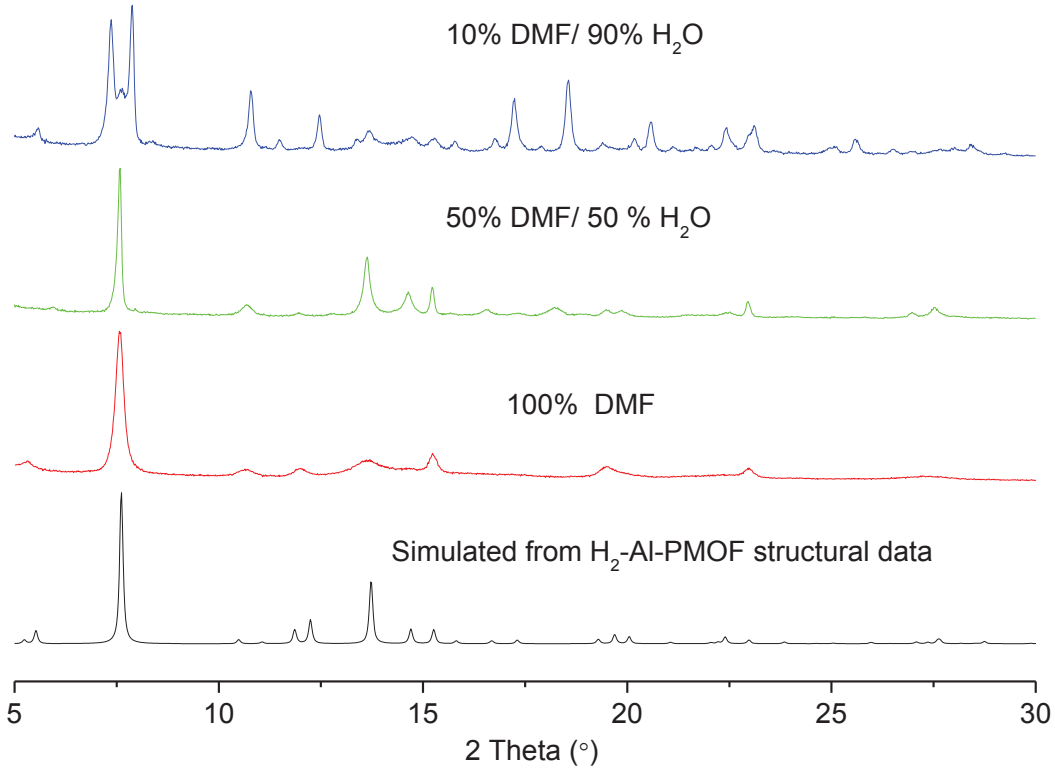

Figure 3-14 PXRD patterns for Mn-Al-PMOF samples investigating the solvent composition. Syntheses performed at 160 °C with a heating program of 3h-16h-4h.

TGA analysis of the sample synthesised at 160 °C with a 50%/50% DMF/water composition showed that the experimental remaining mass % at high temperature was lower than theoretical remaining mass %, which can be due to possible demetalation of the Mn from the porphyrin cores during the synthesis. In order to investigate this, solution phase UV-vis spectroscopy on the digested MOF sample in 0.1M aqueous NaOH solution was used. The relative content of the Mn metalated TCPP and H_2TCPP were determined via analysing standard curves from which the Mn occupancy was calculated with a rough error of around 2% (error was estimated by using samples of known concentrations, details of the procedure for calculating the Mn occupancy are given in appendix section B.4). The analysis of the UV-vis data indicated that this sample had 84% Mn occupancy. The demetalation of samples from other two solvent compositions was not assessed due to the poor crystallinity of these solids. Therefore, other parameters were investigated keeping the 50%/50% DMF/water composition for the solvent in order to minimize the demetalation.

Once the solvent composition was set to 50%/50% DMF/water, the effect of the temperature on the crystallinity and demetallation was investigated. The syntheses performed at 190 °C and 160 °C resulted in products isostructural to H_2-Al-PMOF, while synthesis at 120 °C produced a different phase (Figure 3-15a). The rate of demetalation was probed with UV-vis spectroscopy and indicated that the synthesis at 160 °C led to a higher Mn demetalation (84% Mn occupancy) compared to the synthesis at 190 °C (Mn occupancy 96%) as shown in Figure 3-15b. This is possibly due the higher temperature favouring the formation of the MOF product and thus the precipitation of the MOF crystallites. This would decrease the interaction of the Mn metalated porphyrins with the reaction mixture in a homogeneous state compared to the synthesis at the lower temperature. Therefore, the optimum temperature was set at 190 °C for this solvent system.

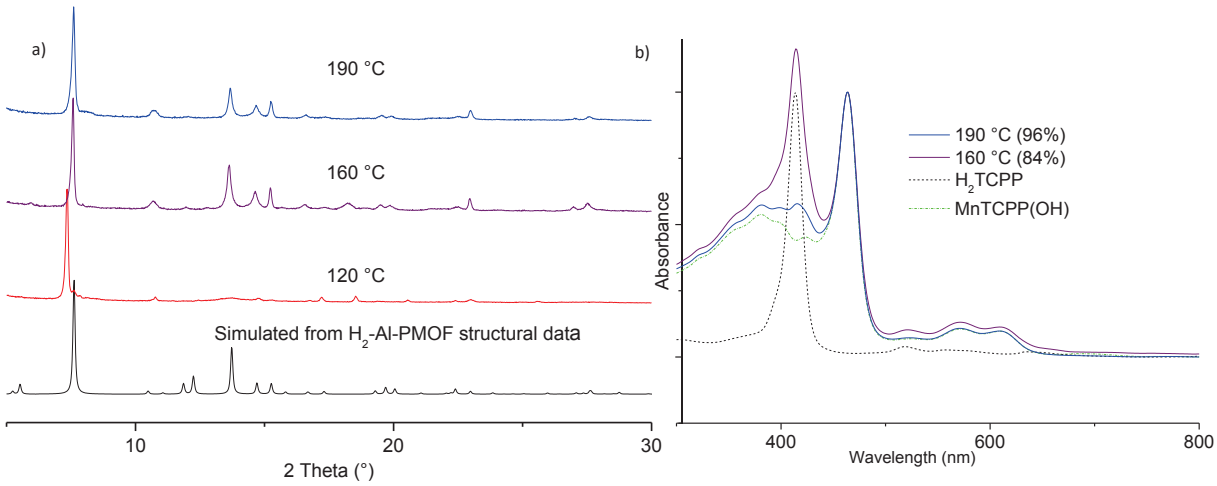

Figure 3-15 a) PXRD data comparing samples from Mn-Al-PMOF syntheses performed at different isotherm temperatures with 50%/50% DMF/water as solvent. b) solution phase (0.1 NaOH) UV-vis spectra for samples synthesised at 160 °C and 190 °C. Peak at 414 nm represents the Soret band of the free base porphyrin, H_2TCPP. Mn occupancy in the porphyrin is shown in parenthesis.

Benzoic acid was investigated as a modulator for the Mn-Al-PMOF synthesis at 190 °C (heating rate 0.31 °C/min, isotherm time 15h); modulators can coordinate to metal ions in solution and slow down the crystallisation process which can lead to better crystallinity. The PXRD patterns obtained for the products with different amounts of benzoic acid as additive were similar (Figure 3-17a), but the presence of benzoic acid had a positive effect on the accessible surface area as shown by the BET surface area calculations performed (10 equivalents 1324 $m^2 g^{-1}$ > 2 equivalents 1231 $m^2 g^{-1}$ > no added benzoic acid 1070 $m^2 g^{-1}$, equivalents are given referring to the porphyrin ligand, Figure 3-18). This could be due to the increasing number of defects in the framework due the presence of benzoic acid as observed for the UiO-66 series of MOFs.[25] The morphology of the crystallites was also different for the solid obtained with 10 equivalents of benzoic acid compared to the other two (Figure 3-16c).

However, UV-vis data indicated that benzoic acid also favours the demetalation of Mn from the porphyrin core (Figure 3-17b).

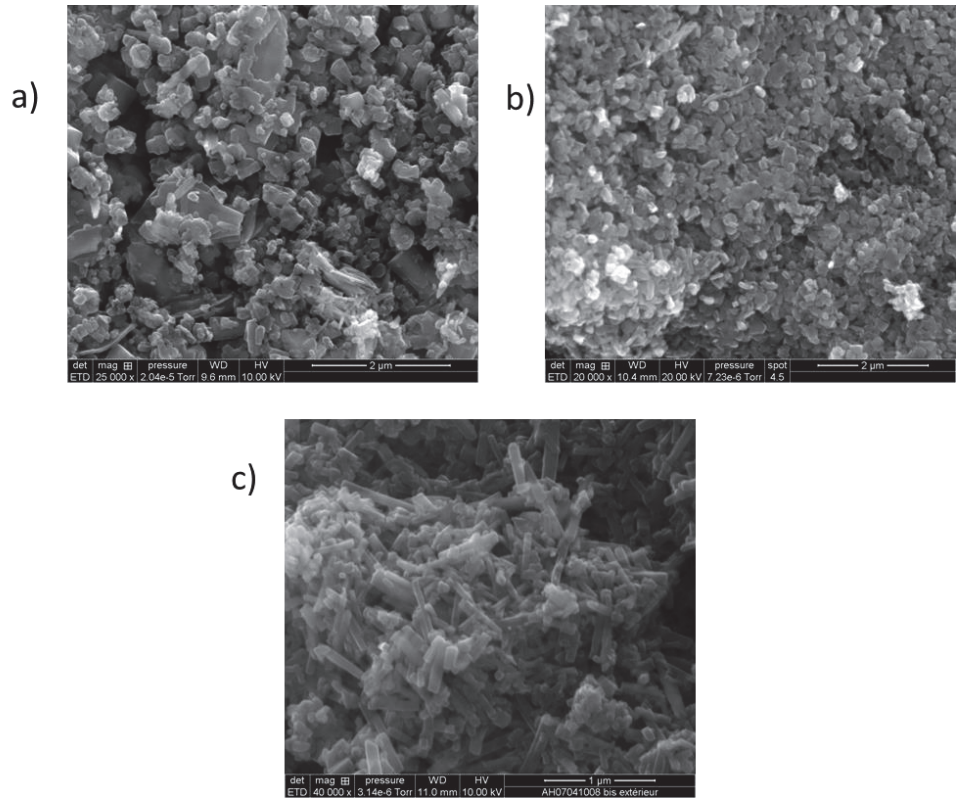

Figure 3-16 SEM images for syntheses performed at 190 °C (heating rate 0.31 °C/min, 15h isotherm) investigating the effect of adding benzoic acid. a) no benzoic acid b) two equivalents of benzoic acid c) ten equivalents of benzoic acid.

The effect of the heating rate for a synthesis temperature of 190 ° (isotherm time: 15h) was also investigated (Figure 3-17a). Both heating rates resulted in material with similar crystallinity and porosity (BET surface area of 1300 m^2 g^{-1} for 0.15 °C/min compared to 1231 m^2 g^{-1} for 0.31 °C/min which lies within a 5% error which can be expected for BET surface area measurements, Figure 3-18). Furthermore, the effect of heating rate on the demetalation was negligible when comparing the samples synthesised with 2 equivalents of benzoic acid (0.31 °C/min: 94% Mn occupancy, 0.15 °C/min: 95% Mn occupancy).

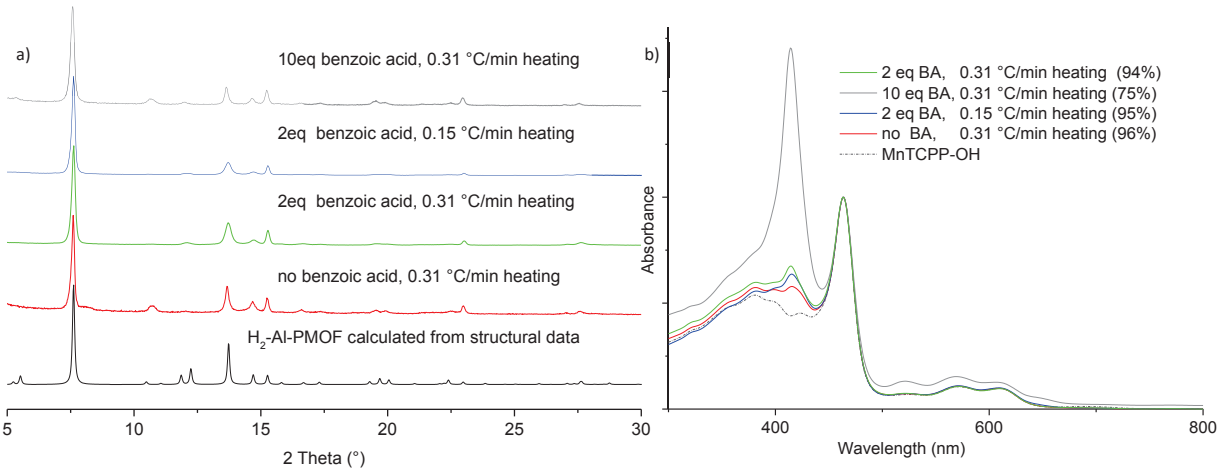

Figure 3-17 a) PXRD data for samples of Mn-Al-PMOF syntheses investigating the effect of adding benzoic acid at variable heating rates at 190 °C (isotherm time 15h). b) Solution phase (0.1 NaOH) UV-vis spectra of the samples. Mn occupancy in the porphyrin is given in parenthesis

.

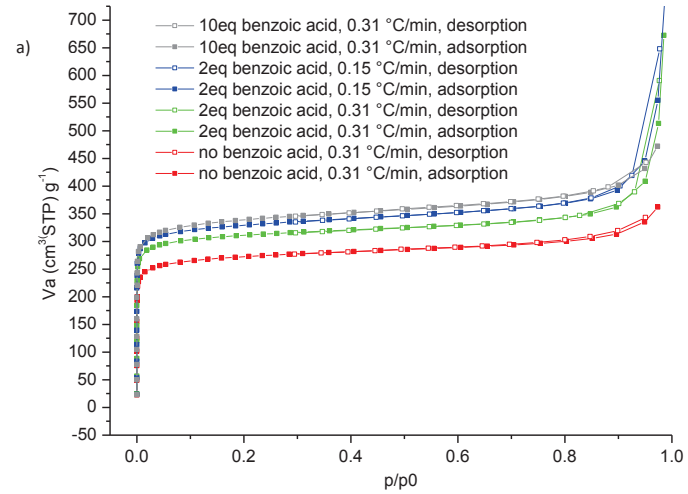

b)

Sample	BET surface area (m^2g^{-1})
No benzoic acid, 0.31 °C/min	1070
2 eq benzoic acid , 0.31 °C/min	1231
2 eq benzoic acid, 0.15 °C/min	1300
10 eq benzoic acid, 0.31 °C/min	1324

Figure 3-18 a) N_2 adsorption/desorption isotherms at 77K for the samples from the syntheses performed at 190 °C for investigating the effect of benzoic acid addition and the heating rate. b) BET surface areas calculated for the samples.

Thermogravimetric analysis (TGA) was used to determine the relative purity of the samples. In most TGA curves, an excess of remaining mass was observed compared to the theoretical value for the [MnTCPP-OH($Al^{III}OH)_2$] MOF formula (after the level of Mn demetalation was accounted for). The inorganic residue at the end of the TGA analysis was determined to be a mixture of Mn_2AlO_4 and Al_2O_3 via PXRD analysis of the residual solid (PXRD analysis is given in appendix section B.4). The excess remaining mass was attributed to inorganic impurities formed during the synthesis, most likely to be aluminium oxide species. The weight% of the impurities was estimated using this difference between the experimental and the theoretical remaining mass % after the framework degradation in air. Our aim was to maximize the Mn occupancy in the porphyrin cores (i.e. above 90%) and minimize the impurity formation. Table 3-7 gives a summary of the TGA analyses of the remaining mass % of

samples which had more than 90% Mn occupancy as calculated from UV-vis spectroscopy. According to this table, the best synthesis conditions were a temperature of 190 °C with 2 equivalents benzoic acid and a heating rate of 0.15 °C/min (1 weight% of impurity).

The syntheses were also performed at lower temperatures (120 °C, 140 °C, 150 °C) in attempt to minimize the formation of aluminium oxide impurities. Four equivalents of potassium hydroxide were used in order to promote deprotonation of the four carboxylic acids to help solubilise the porphyrin ligand in the solvent (50%/50% water/DMF) at a lower temperature. Figure 3-19 shows the pxrd data obtained for products at lower temperatures in basic conditions (120 °C, 140 °C and 150 °C). Below 140 °C only amorphous material is formed, whereas at higher temperatures, the Al-PMOF phase is obtained. However, porosity of the solids obtained with KOH as an additive at 140 °C and 150 °C (calculated BET surface areas of 1112 $m^2 g^{-1}$ and 1138 $m^2 g^{-1}$ respectively) were lower than with the previous method. This is possibly due to the presence of more inorganic/organic impurities in the samples prepared in basic conditions. The synthesis at 140 °C resulted in a sample with around 3 weight% of inorganic impurities. The synthesis at 150 °C resulted in a sample with a lower experimental remaining mass % compared to the theoretical remaining mass % from the TGA data. This can imply that the sample had organic impurities. When looking at the IR spectra of the two samples, sample from the synthesis at 150 °C has a stronger peak at 1714 cm^{-1} which represents the C=O stretch of the uncoordinated carboxylic acid group which can indicate that more unreacted ligand is present compared to the sample synthesised at 140 °C, possibly due to insufficient washing.

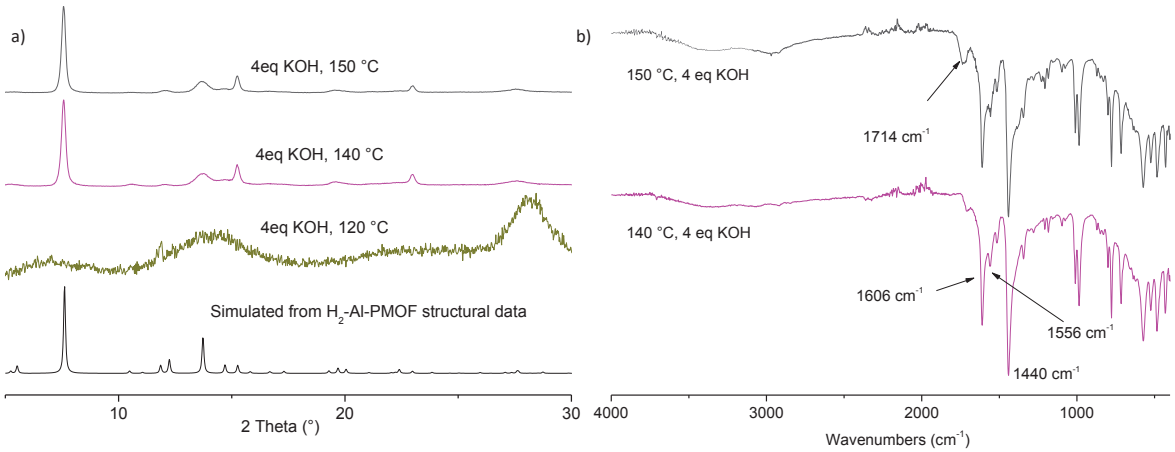

Figure 3-19 a) PXRD data for Mn-Al-PMOF samples synthesised at lower temperatures in basic conditions (isotherm time of 16h). The pxrd analysis was performed with instrument 2. b) IR spectra for the samples synthesised at 140 °C and 150 °C in basic conditions.

Table 3-7 TGA analysis for the products from syntheses presenting ≥ 90% Mn occupancy. Theoretical remaining mass % is calculated for the MOF formula [MnTCPP-OH($Al^{III}OH)_2$] and was attributed to metal oxides, [(2/4)Mn_2AlO_4 + (3/4)Al_2O_3]. TGA graphs are given in appendix section B.4).

Sample	Mn occupancy from UV-vis spectroscopy data	Experimental remaining mass %	Theoretical remaining mass % (for (2/4)Mn_2AlO_4+ (3/4) Al_2O_3)	Difference in experimental and theoretical remaining mass%	Estimated weight% of inorganic impurity
140 °C, KOH	96%	19.7	17.3	2.4	3
150 °C, KOH	94%	15.9	17.3	-1.4	-
190 °C, No additive	96%	20.9	18.1	2.8	4
190 °C, 2eq benzoic acid, 0.31 °C/min heating	94%	18.2	15.9	2.3	3
190 °C, 2eq benzoic acid, 0.15 °C/min heating	95%	19.1	18.1	1.0	1

Optimum synthesis conditions

In total, 15 different reactions were performed and the optimum conditions determined are as follows (all the reactions are given in the appendix section B.4):

- Solvent: DMF/water 50%/50% mixture
- Isotherm temperature: 190 °C
- Heating program (heating time, isotherm time, cooling time): 18h - 15h - 4h
- Additive: 2 equivalents of benzoic acid

The Mn-Al-PMOF {chemical formula [MnTCPP-OH($Al^{III}OH)_2$]} synthesised had 95% Mn occupancy in the porphyrin cores in the framework and was obtained in over 90% yield (with regards to the porphyrin ligand). This compound is slightly less crystalline than the synthesised free base Al-PMOF (H_2-Al-PMOF) (Figure 3-20). The formation of aluminium oxide impurities was minimised to have only 1 weight% of impurities in the final product. The synthesis was repeated three times and results were reproducible for all the three batches. Thus, it can be concluded that the synthesis optimisation for Mn-Al-PMOF was successful.

Other water stable Mn porphyrin containing MOF systems such as PCN-600 have shown higher porosity compared to the Mn-Al-PMOF system (2200 m^2g^{-1} compared with 1300 m^2g^{-1} for Mn-Al-PMOF). However, supercritical CO_2 activation methods were required in the case of PCN-600[20] while Mn-Al-PMOF can be activated using traditional vacuum heating methods.

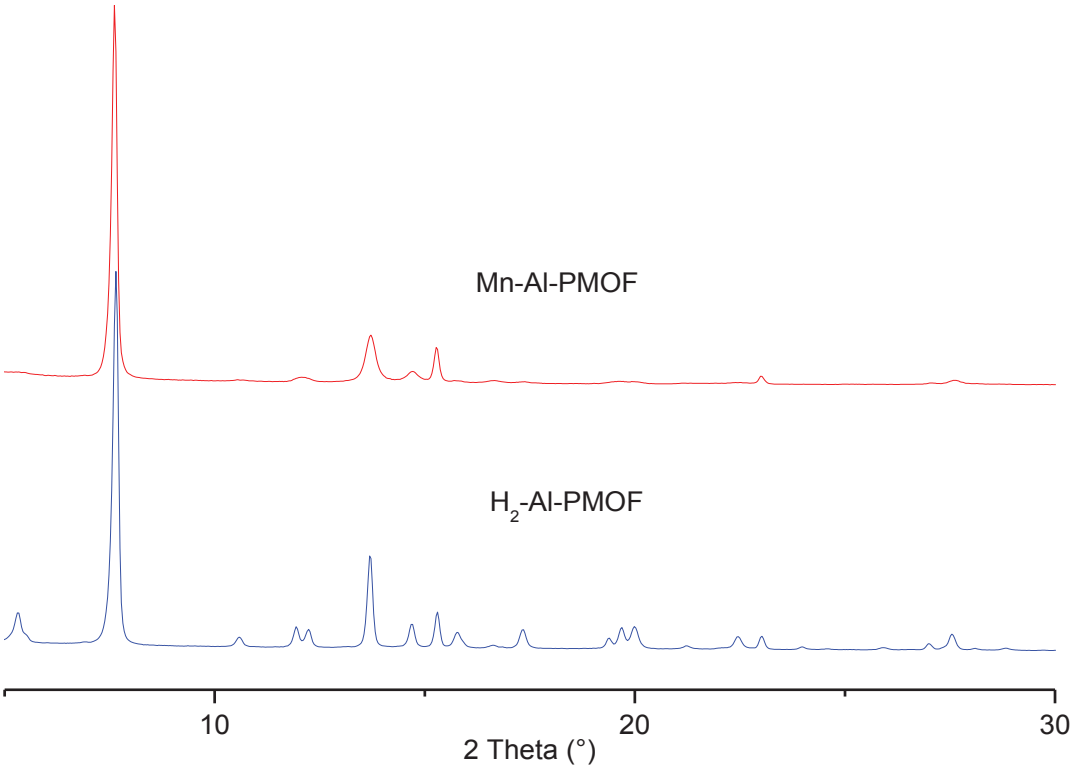

Figure 3-20 PXRD patterns for the Mn-Al-PMOF synthesised with optimum conditions and synthesised free base Al-PMOF.

Characterisation

IR spectroscopy

The IR spectra obtained for the activated Mn-Al-PMOF and H_2-Al-PMOF are similar and are shown on Figure 3-21. The peaks at 1606 cm^{-1} and 1440 cm^{-1} represent the asymmetric and symmetric C=O stretch of coordinated carboxylate groups while the peak at 1556 cm^{-1} arises from the aromatic C=C stretch. The IR spectrum of the as synthesised Mn-Al-PMOF sample has peaks that can be assigned to DMF (C=O stretch at 1660 cm-1) and acetone (C=O stretch at 1725 cm^{-1}, CH_3 symmetric deformation at 1360 cm^{-1}) which disappear upon activation under vacuum at 160 °C.

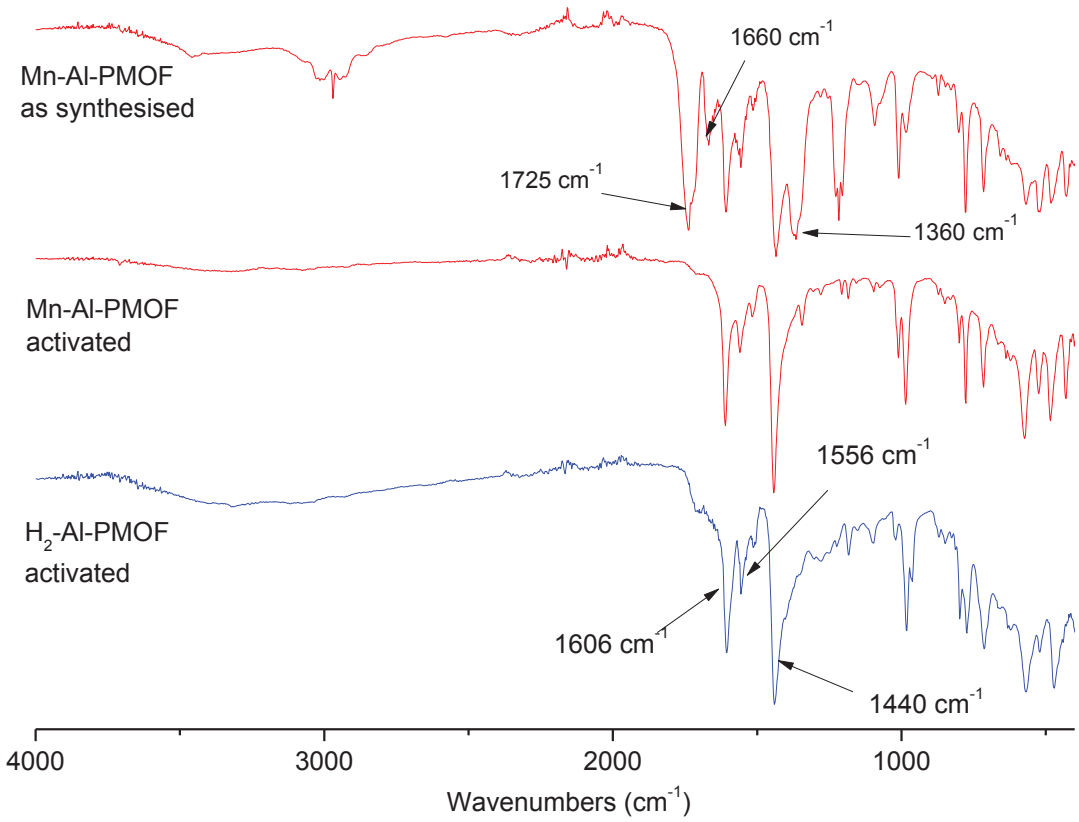

Figure 3-21 IR spectra for Mn-Al-PMOF and H_2-Al-PMOF samples.

TGA analysis

In the Mn-Al-PMOF sample before activation, around 5% of mass is lost between 30 °C and 150 °C which can be attributed to the loss of adsorbed and coordinated water, DMF or acetone (Figure 3-22) as seen with the IR spectra (Figure 3-21). Further 5% is lost up to 240 °C which can be attributed to any coordinated DMF molecules. The decomposition of the MOF starts around 270 °C. With the activated sample, around 5% of mass is lost between 30 °C and 240 °C which can be attributed to the loss of water adsorbed from air. The remaining mass at 800 °C is 19.1 % (theoretical 18.1 %, difference 1.0%). This corresponds to roughly 1 weight% of aluminium oxide impurity species in the starting Mn-Al-PMOF material (Table 3-8). This is comparable to what is observed for the synthesised H_2-Al-PMOF which has a difference between the theoretical and experimental remaining mass % of 0.7 and a corresponding aluminium oxide impurity presence of 1 weight%.

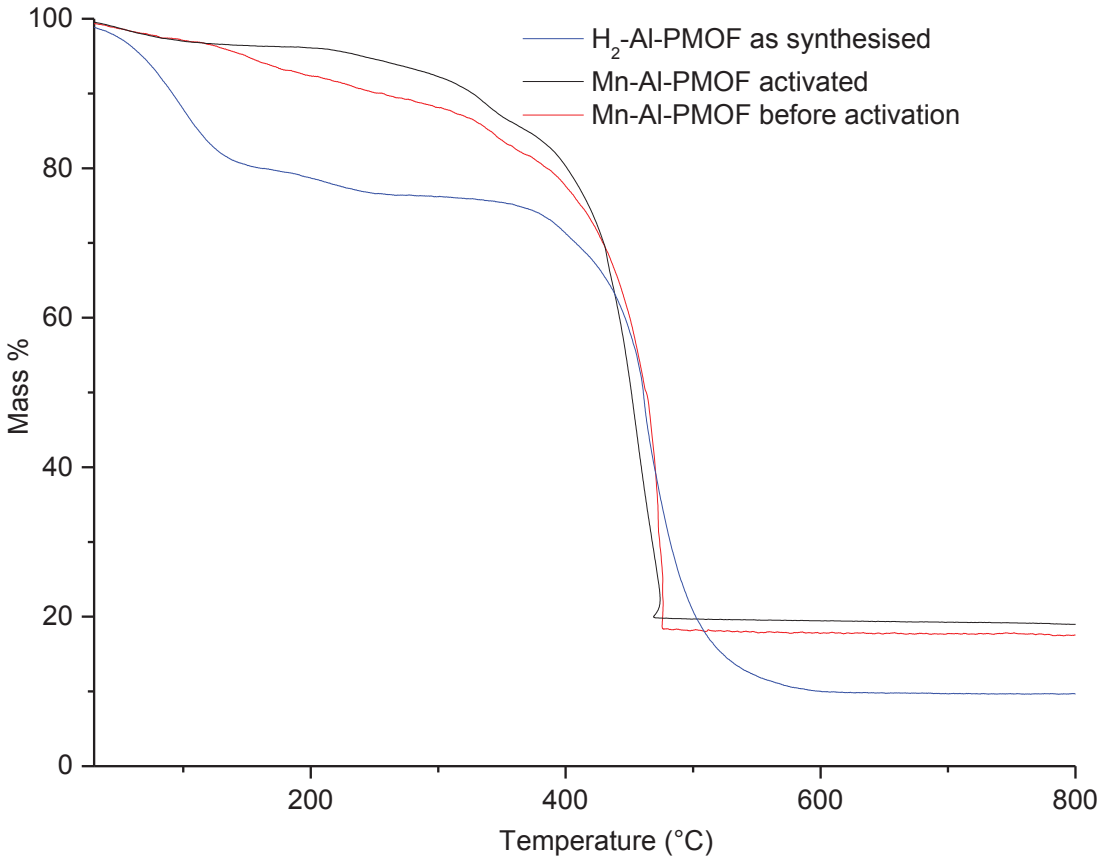

Figure 3-22 a) TGA data for Mn-Al-PMOF before and after activation at 160 °C under vacuum for 12 hours. The TGA data for as synthesised H_2-Al-PMOF is also shown.

Table 3-8 TGA analysis of the remaining mass % for Mn-Al-PMOF and H_2-Al-PMOF.

	Temperature (°C)	Proposed formula	Experimental remaining mass %	Theoretical remaining mass %	Difference between experimental and theoretical mass%	Estimated impurity weight%
Activated Mn-Al-PMOF	240 800	MnTCPP-OH($Al^{III}OH)_2$ (2/4) Mn_2AlO_4 + (3/4) Al_2O_3	96.2 19.1	- 18.1	- 1.0	1
As synthesised H_2-Al-PMOF	245 800	H_2TCPP($Al^{III}OH)_2$ Al_2O_3	76.8 9.7	- 9.0	- 0.7	1

BET measurements

Mn-Al-PMOF was activated at 160 °C for 12 hours under vacuum before the N_2 adsorption/desorption measurements were carried out at 77K and the isotherms obtained are shown on Figure 3-23a. There was no change in the pxrd pattern after activation indicating the structure remains intact (Figure 3-23b) upon the removal of solvent molecules such as DMF and acetone as seen with the IR spectra (Figure 3-21). The BET surface area calculated for the Mn-Al-PMOF was 1300 m^2g^{-1} which is slightly lower than what has been reported for H_2- Al-PMOF (1400 m^2g^{-1}).

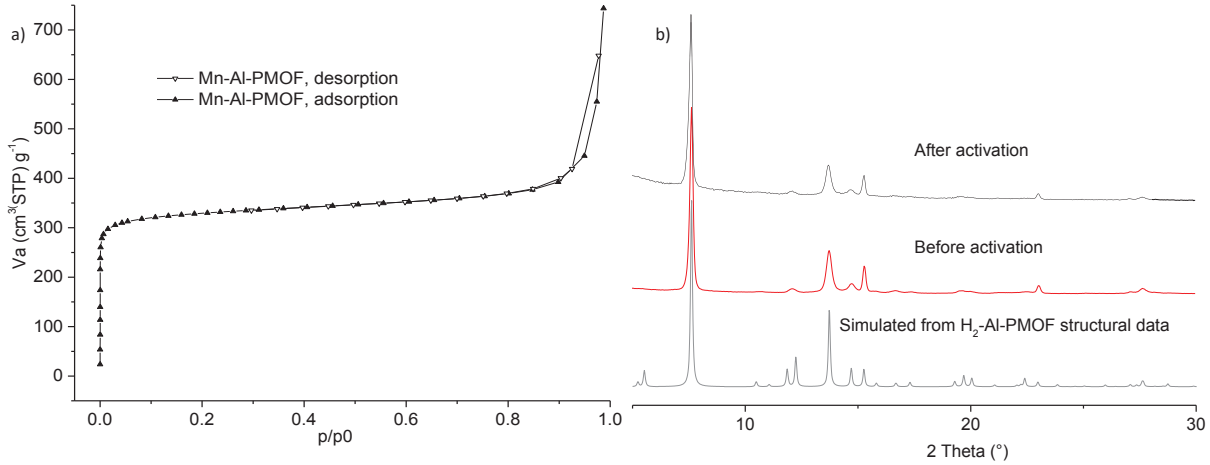

Figure 3-23 a) N_2 Adsorption/desorption isotherms at 77K for Mn-Al-PMOF. b) PXRD data for before and after activation of the Mn-Al-PMOF at 160 °C under vacuum for 12 hours compared to the simulated pattern of H_2-Al-PMOF from structural data.

3.5.2. Synthesis of Fe^{3+} metalated Al-PMOF

Synthesis

Method 1

Post-synthetic metalation was explored as a strategy to obtain the Fe metalated Al-PMOF. It was first attempted by reacting a solution of anhydrous $FeCl_2$ in DMF with a suspension of the H_2-Al-PMOF at 120 °C for 48 hours under anaerobic conditions. However, the metalation was not successful as the resultant product obtained had little or no Fe occupancy in the porphyrin cores as evidenced from the solution phase (0.1M NaOH) UV-vis analysis performed on the sample (Figure 3-24).

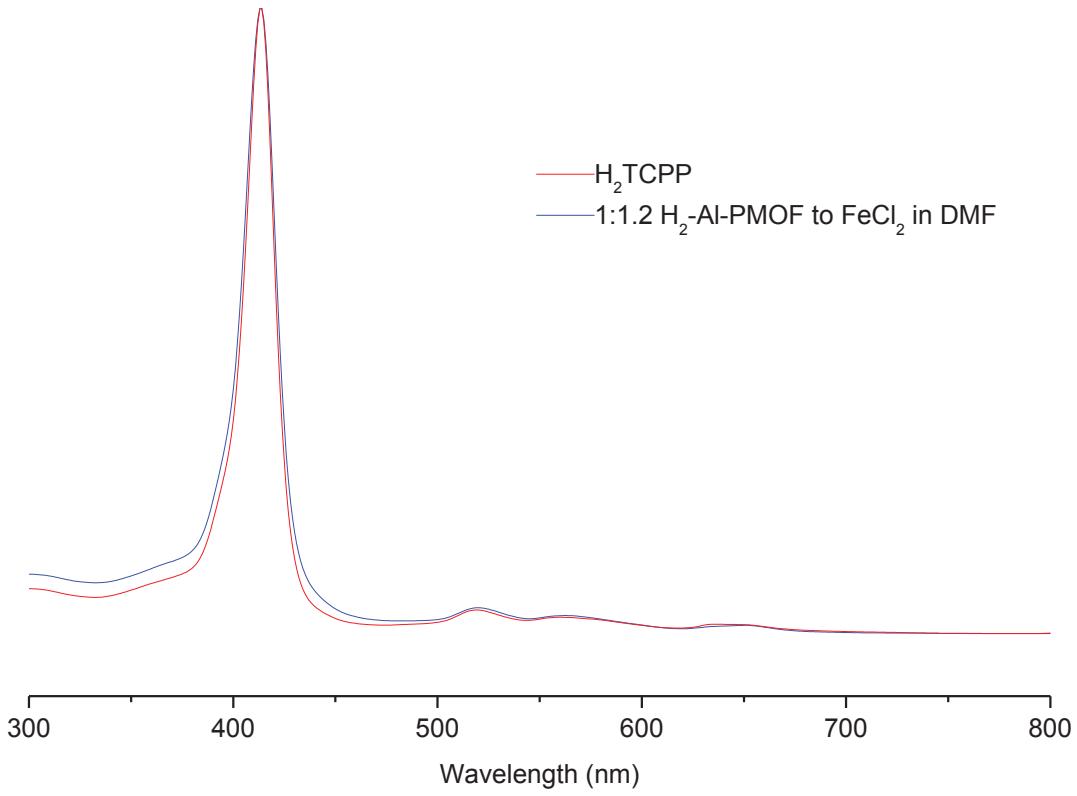

Figure 3-24 Solution phase (0.1m NaOH) UV-vis spectrum of the product from the attempted metalation of the H_2-Al-PMOF with anhydrous $FeCl_2$ in DMF compared to the spectrum of H_2TCPP.

Subsequently, another route was explored using a method adopted from literature where N-(6-(6-(pyridin-2-ylamino)pyridin-2-yl)pyridin-2-yl)pyridin-2-amine was metalated with Fe^{2+}.[26] In this synthesis, a solution of $Fe(SCN)_2$ in methanol was freshly prepared and ascorbic acid was used to prevent the oxidation of Fe^{2+}. For the H_2-Al-PMOF metalation, this solution was heated at 100 °C for 48 hours and unlike the previous method, anaerobic conditions were not required. Various ratios of H_2-Al-PMOF to $Fe(SCN)_2$ [H_2-Al-PMOF: $Fe(SCN)_2$ 1:1.2, 1:2.0, 1:6.0] were investigated to achieve the maximum Fe insertion. Yield of around 65% (35 mg) was obtained starting from 50 mg of H_2-Al-PMOF for reactions with all three ratios.

The resultant solids all preserved crystallinity (Figure 3-25a) but the solution phase UV-vis spectra on digested samples showed the presence of a mixture of FeTCPP and H_2TCPP indicating incomplete metalation (Figure 3-25b). Syntheses with 1:2 and 1:6 H_2-Al-PMOF to $Fe(SCN)_2$ ratios resulted in similar metalation levels while the synthesis with 1:1.2 ratio showed lower Fe occupancy.

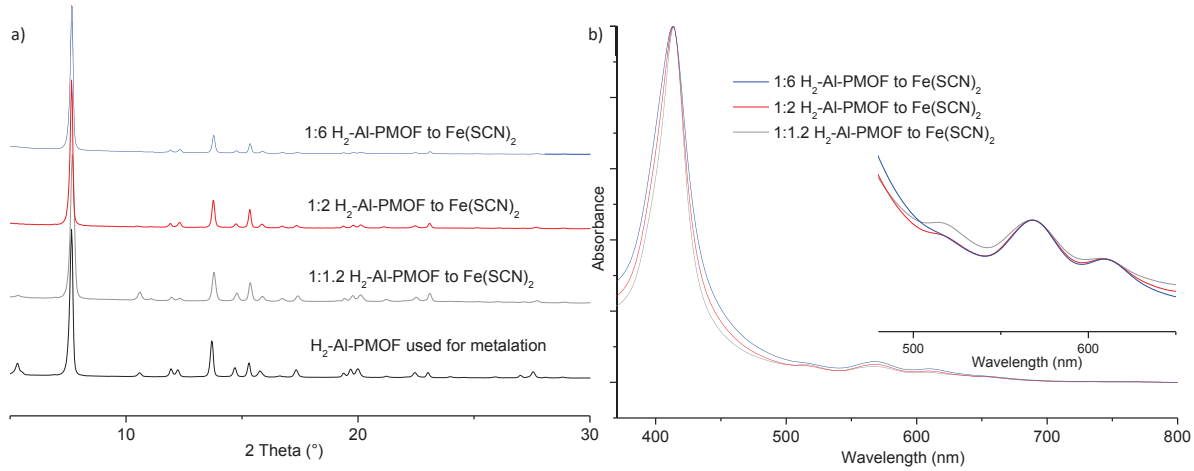

Figure 3-25 a) PXRD data for the samples from H_2-Al-PMOF metalation with $Fe(SCN)_2$ b) Solution phase (0.1 M NaOH) UV-vis spectra for the samples from the Fe metalation of H_2-Al-PMOF. The insert displays a zoom in region of the spectrum of the Q bands of Fe metalated TCPP at 569 nm and 610 nm. The peak at 518 nm represents one of the Q bands of H_2TCPP.

TGA analysis was used to further probe the Fe occupancy using the MOF formula [FeTCPP-OH($Al^{III}OH)_2$]. A Fe occupancy lower than 100% will result in an experimental remaining mass % which is less than the theoretical remaining mass %. This is due to the formation of less Fe_2O_3 in the residue due to the lower presence of Fe in the starting sample. Therefore, the Fe occupancy can be estimated from this difference. TGA analysis indicated that the synthesis with H_2-Al-PMOF to $Fe(SCN)_2$ ratio of 1:6 resulted in around 80% Fe occupancy compared to 60% for the synthesis with 1:2 H_2-Al-PMOF to $Fe(SCN)_2$ ratio. UV-vis studies using standard curve analysis, could give more precise occupancy values, however, this was not performed in this study due to time constraints. Thus, according to the estimated results from the TGA analysis, using 6 equivalents of iron thiocyanate was proposed as the best conditions for method 1.

The N_2 adsorption/desorption studies performed on the sample prepared using 6 equivalents of iron thiocyanate indicated a BET surface area of 988 m^2g^{-1} (Figure 3-35a).

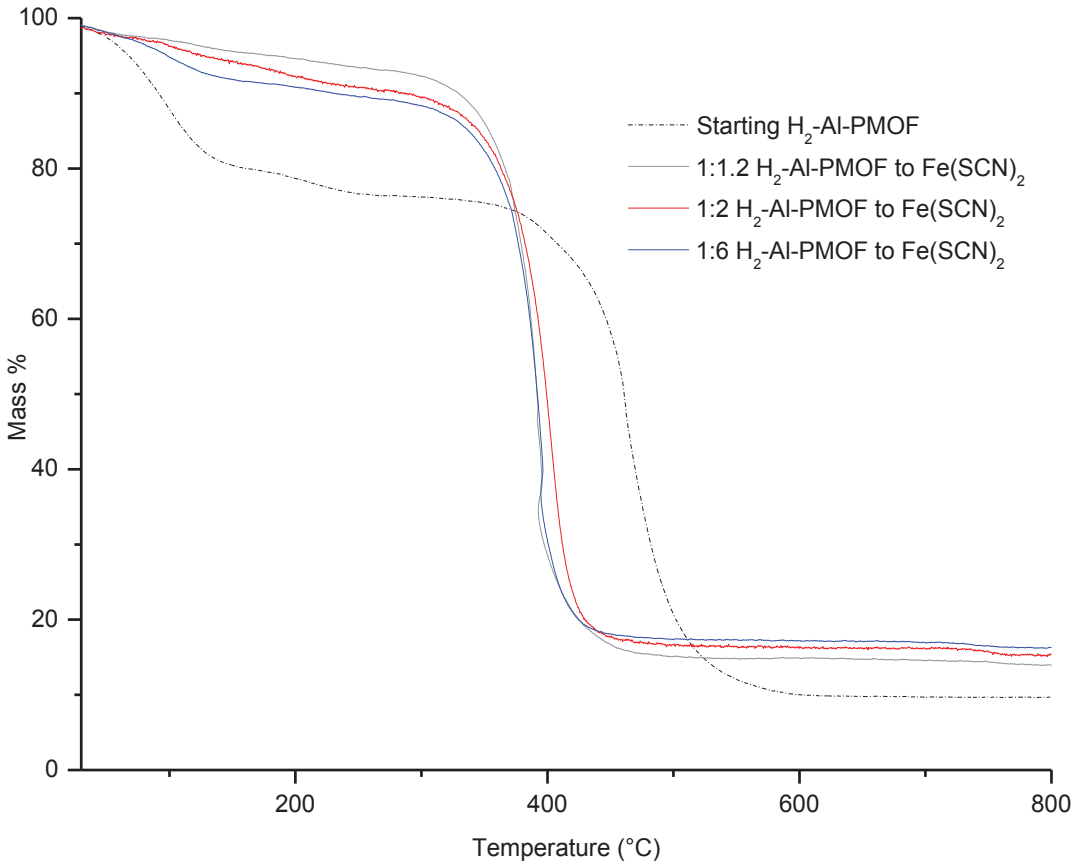

Figure 3-26 a) TGA data for the Fe-Al-PMOF samples obtained for the H_2-Al-PMOF metalation with $Fe(SCN)_2$.

Table 3-9 TGA analysis for the products from method 1 with the estimated Fe occupancy levels. Theoretical remaining mass % is calculated for the MOF formula [FeTCPP-OH($Al^{III}OH)_2$] and was attributed to metal oxides (0.5Fe_2O_3 + Al_2O_3).

Sample	Experimental remaining mass %	Theoretical remaining mass % (for 0.5 Fe_2O_3 + Al_2O_3)	Difference between experimental and theoretical remaining mass %	Fe occupancy estimated from the difference
1:1.2 H_2-Al-PMOF to $Fe(SCN)_2$ ratio	13.9	18.0	-4.1	40%
1:2 H_2-Al-PMOF to $Fe(SCN)_2$ ratio	15.3	17.5	-2.2	60%
1:6 H_2-Al-PMOF to $Fe(SCN)_2$ ratio	16.3	17.3	-1.0	80%
Starting H_2-Al-PMOF	9.7	9.0	0.7	-

Method 2

The synthesis of the Fe-Al-PMOF was also attempted by directly reacting Fe^{3+} metalated TCPP ligand with $AlCl_3.6H_2O$. In total 14 different reactions were performed for synthesis optimisation and the summary of parameters investigated are shown in Table 3-10. Details of all the attempted syntheses are given in appendix section B.5.

Table 3-10 Summery of parameters used in method 2 for the synthesis optimisation of Fe metalated Al-PMOF.

Parameter	
Solvent system (DMF, Water) (%vol)	(90%, 10 %), (50%, 50%), (10%,90%)
Metal to ligand ratio	2:1, 1.3:1 at 190 °C
Isotherm temperature	120 -140-150-160-190 °C
Isotherm time	16h, 24h
Heating rate	9h (0.31 °C/min), 3h (0.92°C/h) at 190 °C
Cooling rate	Over 4h
Additives	Benzoic acid, (at 160 °C and 190 °C) Potassium hydroxide (at 120-140-150 °C)

The effect of the solvent content was first probed for synthesis at 190 °C using a heating program of 9h-24h-4h. From the conditions attempted, only 50%/50% DMF/water mixture allowed to obtain the desired phase with decent crystallinity (Figure 3-27). Therefore, 50%/50% DMF/water mixture was used for further trials.

The heating rate (0.92°C/min versus 0.31 °C/min) and the isotherm length (16 hours versus 24 hours), when probed at 190 °C, did not have an effect on the pxrd pattern or the yield (Figure 3-28a). Therefore, influence of the synthesis temperature was investigated using an isotherm time of 16 hours (heating program 3h-16h-4h). Increasing the temperature led to increased crystallinity (Figure 3-28b). Furthermore, unlike with Mn-Al-PMOF, there were no demetalation issues in the case with Fe-Al-PMOF synthesis. Thus, the shortest program and a temperature of 190 °C was chosen for further studies.

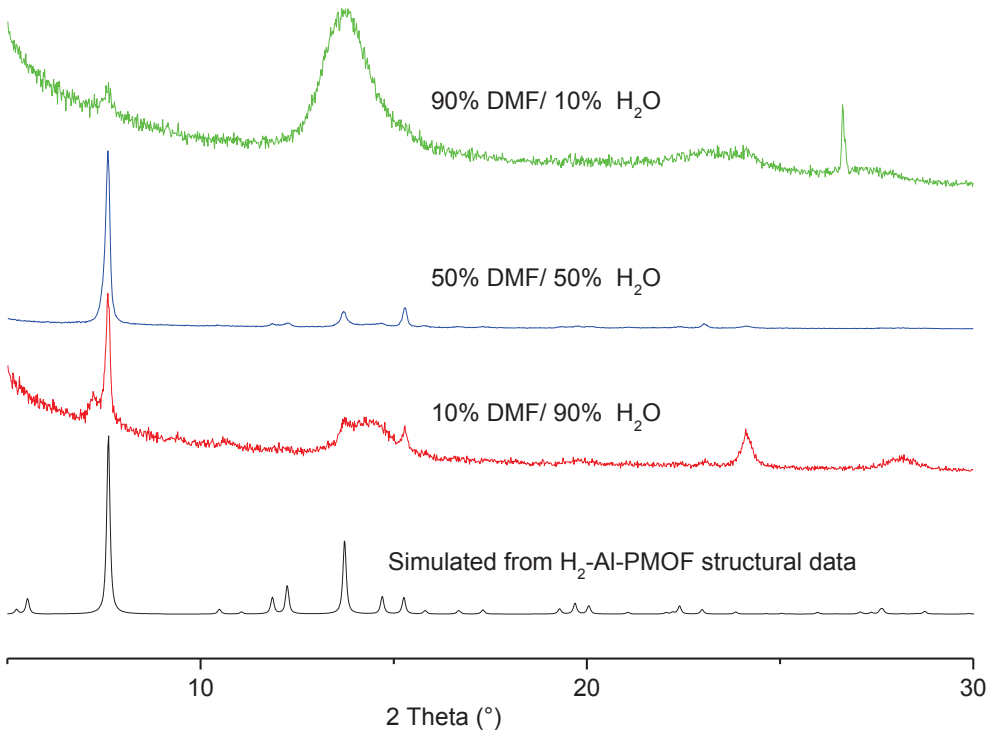

Figure 3-27 PXRD data for the products from syntheses investigating the effect of the solvent content for obtaining Fe-Al-PMOF at 190 °C with an isotherm time of 24h (heating program 9h-24h-4h).

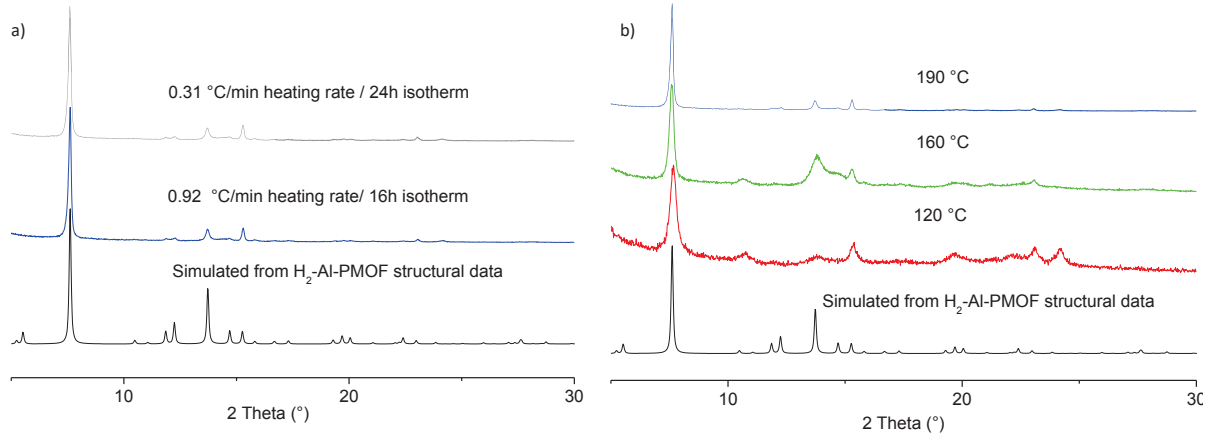

Figure 3-28 a) PXRD patterns for samples from syntheses performed at 190 °C with different heating rates and isotherm times with 50%/50% DMF/water as solvent b) PXRD patterns for products from syntheses performed at different temperatures with a heating program of 3h-16h-4h with the same solvent.

These last synthetic conditions (190 °C, heating program: 3h-16h-4h) were repeated three times and the samples obtained indicated the presence of an impurity which was identified as boehmite, [AlO(OH)] via pxrd analysis (Figure 3-29). Attempts were made to dissolve the impurity using an acidic solution of HCl at pH 2.5. However, as seen in the figure there was no change observed after the acidic treatment. Therefore, this synthesis at 190 °C did not yield reproducible results in terms of phase purity and other parameters were investigated further in order to improve reproducibility.

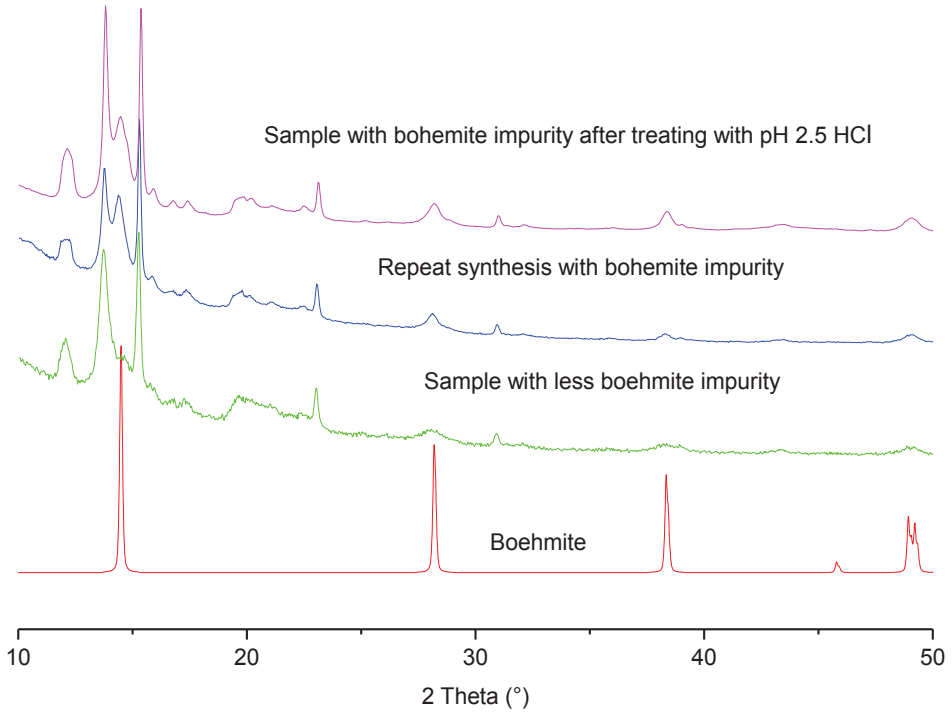

Figure 3-29 PXRD of Fe-Al-PMOF samples synthesised with the same conditions at 190 °C with a heating program of 3h-16h-4h with no additives. One sample has a significant presence of boehmite which is indicated by the peaks at 2 theta angles of 15 °, 28 °, 38 °, 48 ° while the other has less boehmite present. Also shown is the pxrd of the sample after leaving in pH 2.5 HCl for 24h. There is no change in the pxrd pattern indicating the boehmite impurity is still present after acid treatment.

Since the formation of boehmite, [AlO(OH)], as an inorganic impurity was confirmed, TGA analysis was used as a tool to probe the relative purity of the samples synthesised, in a similar manner to the process followed with the Mn-Al-PMOF synthesis optimisation. The remaining mass % was calculated using the [FeTCPP-OH($Al^{III}OH)_2$] MOF formula with Fe_2O_3 and Al_2O_3 as the remaining inorganic residue. The weight% of these impurities was estimated using the excess remaining mass % of the TGA curves (summary of samples analysed is provided in Table 3-11). The goal of following work was to minimize this impurity formation during the synthesis.

The use of benzoic acid as an additive was investigated at a synthesis temperature of 190 °C (2 equivalents relative to the porphyrin ligand, heating program 3h-16h-4h, solvent 50%/50% DMF/water) and did not have an effect on the crystallinity but the TGA analysis showed that more impurities were formed (10 weight% impurities with benzoic acid compared to 4 weight% without benzoic acid, Table 3-11). Therefore, benzoic acid had a detrimental effect on the sample quality.

To minimize the formation of the aluminium oxide impurities, synthesis at lower temperatures (120 °C, 140 °C and 150 °C) were explored with the presence of four equivalents of potassium hydroxide as an additive to facilitate the solubility of the Fe^{3+} metalated TCPP in the solvent used (50%/50% DMF/water). The synthesis at 120 °C resulted in amorphous material while the reactions at 140 °C and 150 °C resulted in the Al-PMOF phase (Figure 3-30). At 140 °C, a relatively pure product

was obtained according to the TGA data (1 weight% impurities). However, very little solid was recovered from this synthesis (~20% yield compared to 63% yield for synthesis at 190 °C with no additives and a heating program of 3h-16h-4h) which made it difficult to obtain the product in large enough quantities for further studies. The synthesis at 150 °C under basic conditions resulted in more impurities in the product obtained (8 weight%).

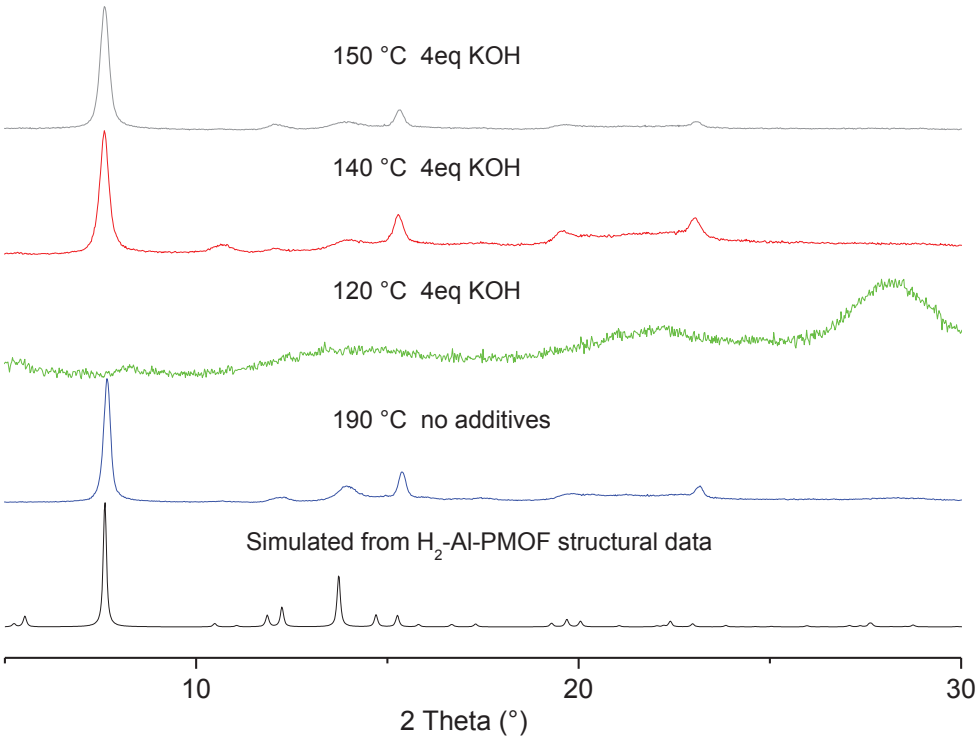

Figure 3-30 PXRD data for the samples synthesised at lower temperatures (120 °C, 140 °C, 150 °C) with 4 eq of KOH as an additive and a heating program of 3h-16h-4h for Fe-Al-PMOF synthesis optimisation. The synthesis performed at 190 °C without base is shown as a comparison. These pxrd patterns were measured using a different diffractometer (Instrument 2)

It was hypothesised that a lower presence of aluminium ions in solution might lead to the formation of less oxide species such as boehmite at 190 °C (heating program 3h-16h-4h, solvent 50%/50% DMF/water). Thus, a metal to ligand ratio was lowered from 2:1 to of 1.3:1. Additionally, the reaction mixture was degassed with argon before heating to minimize the dissolved oxygen present to further impede the formation of aluminium oxide species. The synthesis resulted in a product with the Al-PMOF phase (Figure 3-31a). Analysis of the PXRD patterns indicated that this sample qualitatively contained less boehmite impurity compared to a sample synthesised with a 2:1 metal to ligand ratio without the Ar degassing step (Figure 3-31b). This was confirmed with the TGA analysis (2 weight% impurities compared to 4 weight% impurities). Furthermore, the synthesis was reproducible and the product was obtained in 47% yield (with regards to the FeTCPP(Cl) ligand used), which is lower than what was observed for the synthesis with 2:1 metal to ligand ratio without the Ar

degassing step (63%). However, the reproducibility and the improved purity compensate for this decrease in yield.

The synthesis using 2:1 metal to ligand ratio with Ar degassing at 190 °C resulted in a relatively impure product (11 weight% of impurities) with lower crystallinity compared to the samples obtained with a metal to ligand ratio of 1.3:1 (Figure 3-31a). Therefore, the lower metal to ligand ratio was selected as best at the conditions tested.

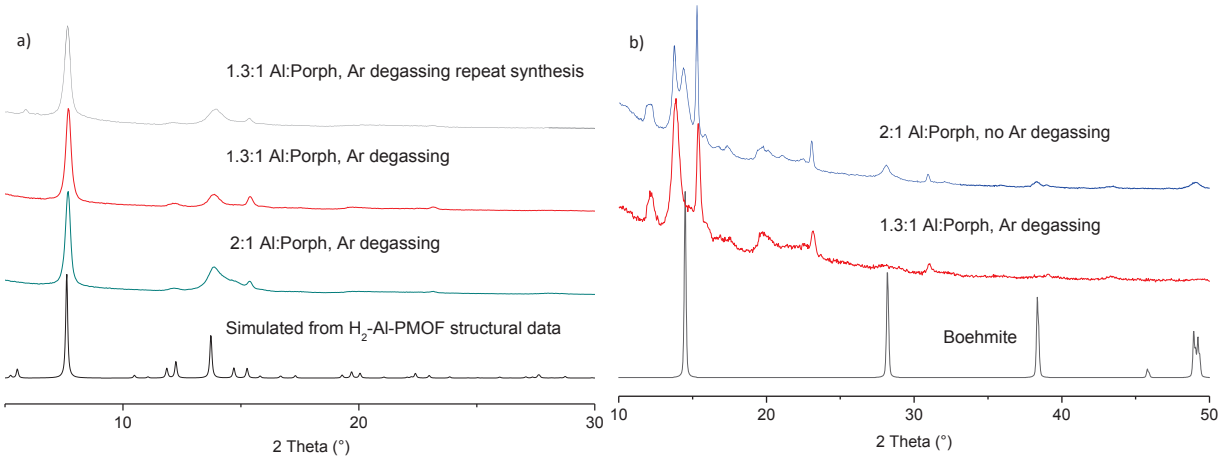

Figure 3-31 a) PXRD data of the samples of the Fe-Al-PMOF syntheses where the reaction mixture was degassed with Ar before heating at 190° C (heating program 3h-16h-4h) b) PXRD data for the samples of the Fe-Al-PMOF syntheses where the reaction mixture was degassed with Ar before heating (1.3:1 Al:porphyrin ratio, 190 °C, 3h-16h-4h) and where there was no Ar degassing (2:1 Al:porphyrin ratio, 190° C, 3h-16h-4h). Ar degassing and using an Al:porphyrin ratio of 1.3:1 results in qualitatively less boehmite impurity as indicated by reduced intensity of the peaks at 2 theta angles of 15 °, 28 °, 38 °, 48 °.

Table 3-11 Theoretical and experimental remaining mass % for selected Fe-Al-PMOF samples from TGA analysis and the estimated weight% of the inorganic impurities. Theoretical remaining mass % is calculated for the MOF formula [FeTCPP-OH($Al^{III}OH)_2$] and attributed to 0.5Fe_2O_3 + Al_2O_3. Syntheses are performed with the oven program 3h-16h-4h. TGA graphs are given in appendix section B.5.

Sample	Experimental remaining mass %	Theoretical remaining mass % (for 0.5Fe_2O_3 + Al_2O_3)	Difference between theoretical and experimental remaining mass %	Estimated weight% of the inorganic impurities
2:1 Al:FeTCPP(Cl), 4eq KOH, 140 °C	18.7	18	0.7	1
2:1 Al:FeTCPP(Cl), 4eq KOH, 150 °C	26.3	19.2	7.1	8
2:1 Al:FeTCPP(Cl), 190 °C, 2eq benzoic acid	24.9	16.8	8.1	10
2:1 Al:FeTCPP(Cl), 190 °C	20.7	18.3	2.4	4
2:1 Al:FeTCPP(Cl), 190 °C, repeat of above where more boehmite present	31.1	18.7	12.4	16
2:1 Al:FeTCPP(Cl), 190 °C, Ar degassing	26.4	17.8	8.6	11
1.3:1 Al:FeTCPP(Cl), 190 °C, Ar degassing	19.8	18.3	1.5	2
1.3:1 Al:FeTCPP(Cl), 190 °C, Ar degassing, repeat synthesis of above	20.3	18.6	1.7	2

Optimum synthesis conditions for Fe Al-PMOF

Fe-Al-PMOF {chemical formula [FeTCPP-OH($Al^{III}OH)_2$]} was synthesised by using two different methods. For method 1, which involved post synthetic Fe metalation of H_2-Al-PMOF, 6 equivalents of $Fe(SCN)_2$ for every equivalent of H_2-Al-PMOF results in the highest Fe occupancy in the porphyrin cores with around 80%.

For method 2, a total of 14 reactions were performed with various parameters and the optimum conditions determined are as follows:

- Solvent- 50% DMF/ 50% H_2O
- Metal to ligand ratio- 1.3:1
- Temperature/heating program-190 °C/3h-16h-4h
- The reaction mixture is degassed with Ar prior to heating

Method 2 results in a product with 100% Fe occupancy in the porphyrin cores (solution phase UV-vis spectrum is provided in the appendix section B.5). However, this sample is less crystalline compared to the sample obtained from method 1 (Figure 3-32). Thus, the choice between the two methods involves a compromise in crystallinity or the Fe occupancy in the porphyrin cores. However, lower relative crystallinity is not necessarily disadvantageous for potential catalytic applications if the active sites are accessible. Thus, method 2 is better due to it resulting in a product with 100% Fe occupancy in the porphyrin cores which provides more catalytic centres.

Similar to Mn-Al-PMOF, Fe-Al-PMOF can be activated via classical methods (under vacuum for 12 hours at 160 °C) which eliminates the need for supercritical activation methods required in some other reported water stable porphyrinic MOFs, which display higher BET surface areas.[20]

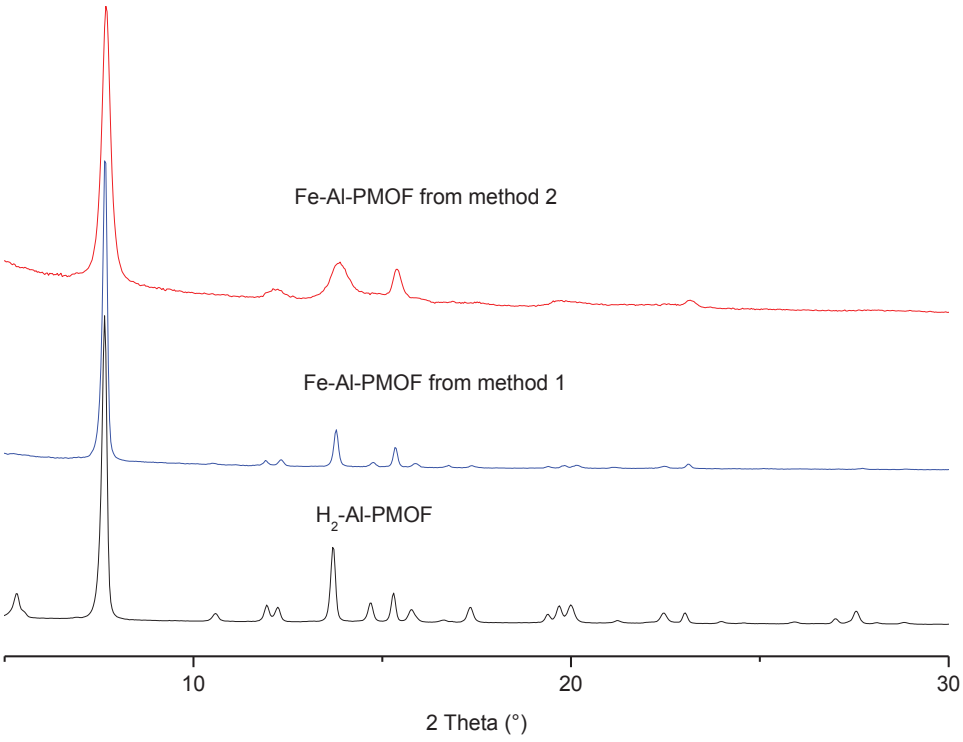

Figure 3-32 PXRD data comparing the samples prepared from the optimised synthetic conditions from method 1 and method 2 and the synthesised free base Al-PMOF.

Characterisation

IR spectroscopy

IR spectra of the activated Fe-Al-PMOF samples obtained from the two methods are similar to that of the freebase Al-PMOF (Figure 3-33). The peaks at 1606 cm^{-1} and 1440 cm^{-1} represents the asymmetric and symmetric C=O stretch of coordinated carboxylate groups while 1556 cm^{-1} represents the aromatic C=C stretch of the porphyrin ligand. The peak around 1714 cm^{-1} indicates the presence

of an uncoordinated COOH groups (C=O stretch). This can be from any unreacted FeTCPP(Cl) ligand left or any defects in structure which results in uncoordinated COOH groups. Furthermore, the IR spectrum of Fe-Al-PMOF obtained from method 1 does not have a strong band around 2150 cm^{-1} which represents the SCN stretch indicating there is no thiocyanate coordinated to Fe porphyrin centres in the product.

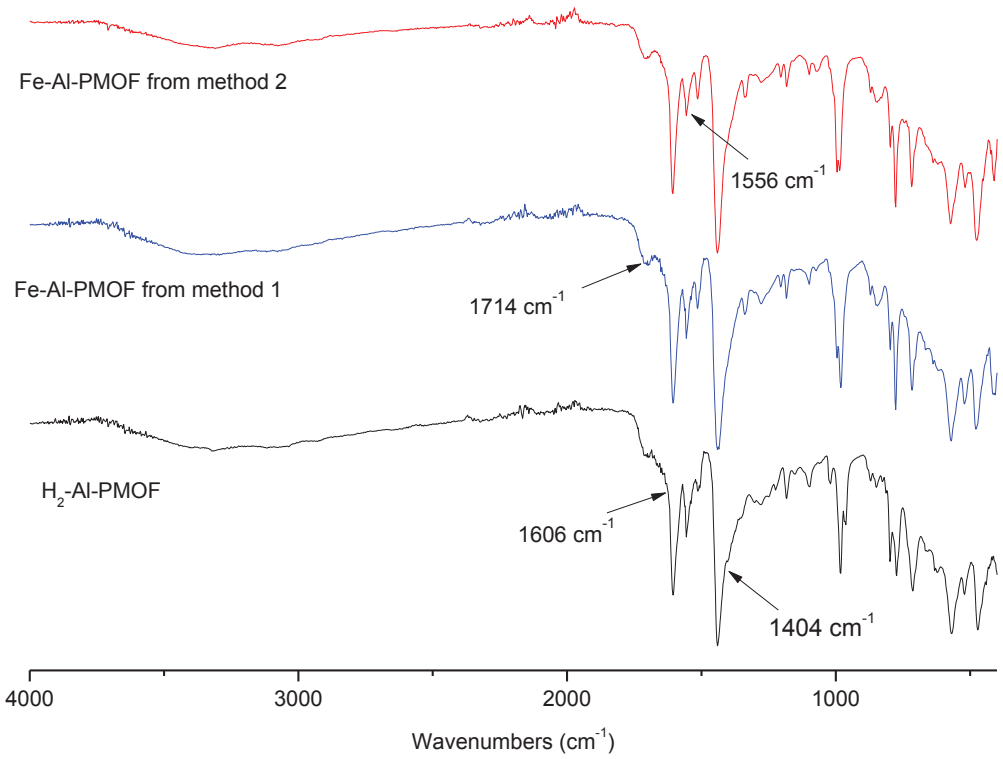

Figure 3-33 IR spectra of the activated Fe-Al-PMOF samples prepared with the final optimised synthesis conditions and free base Al-PMOF.

TGA analysis

Activated samples from both methods show a mass loss of 5% between 30 °C and 240 °C which can be attributed to the loss of water adsorbed from air (Figure 3-34). The decomposition of the samples starts around 275 °C. The remaining mass % at 800 °C for the sample from method 1 is 16.3 % (theoretical 17.3 %). This difference between the theoretical value and the experimental value corresponds to around 80% Fe occupancy of porphyrin cores in the framework. The remaining mass % at 800 °C for the sample from method 2 is 19.8 % (theoretical 18.3 %). This extra mass % can be attributed to aluminium oxide species which is formed during the synthesis and represent 2 weight%.

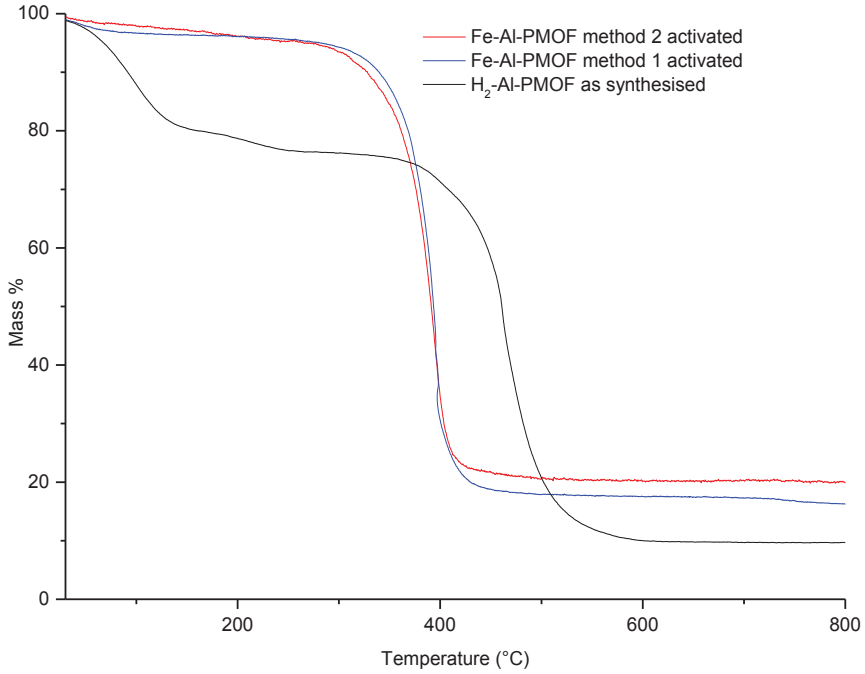

Figure 3-34 TGA data for the Fe-Al-PMOF samples prepared with the two different methods compared to freebase Al-PMOF.

Table 3-12 Analysis of experimental and theoretical mass % from the TGA data for Fe-Al-PMOF from the two methods.

Sample	Temperature (°C)	Proposed formula	Experimental remaining mass %	Theoretical remaining mass %	Difference between experimental and theoretical mass%	
Activated Fe-Al-PMOF Method 1	240 800	FeTCPP-OH($Al^{III}OH$)$_2$ (1/2) Fe_2O_3 + Al_2O_3	95.7 16.3	- 17.3	- -1.0	80% Fe occupancy
Activated Fe-Al-PMOF Method 2	240 800	FeTCPP-OH($Al^{III}OH$)$_2$ (1/2) Fe_2O_3 + Al_2O_3	95.4 19.8	- 18.3	- 1.5	2 weight% of impurity
As synthesised H_2-Al-PMOF	245 800	H_2TCPP($Al^{III}OH$)$_2$ Al_2O_3	76.8 9.7	- 9.0	- 0.7	-

BET surface area analysis

The samples were activated at 160 °C for 12 hours under vacuum before the N_2 sorption measurements at 77K were carried out and the isotherms observed are given in Figure 3-35a. There was no change in the pxrd pattern before and after activation indicating the structure remains intact after the procedure (Figure 3-35b). The BET surface areas calculated for the Fe-Al-PMOF from method 1 and method 2 were 988 m^2g^{-1} and 1033 m^2g^{-1} respectively. These values fall within the 5% error which is usually found in BET measurements thus indicate similar accessible surface areas. However, they are lower than what has been reported for the free base Al-PMOF (1400 m^2g^{-1}).

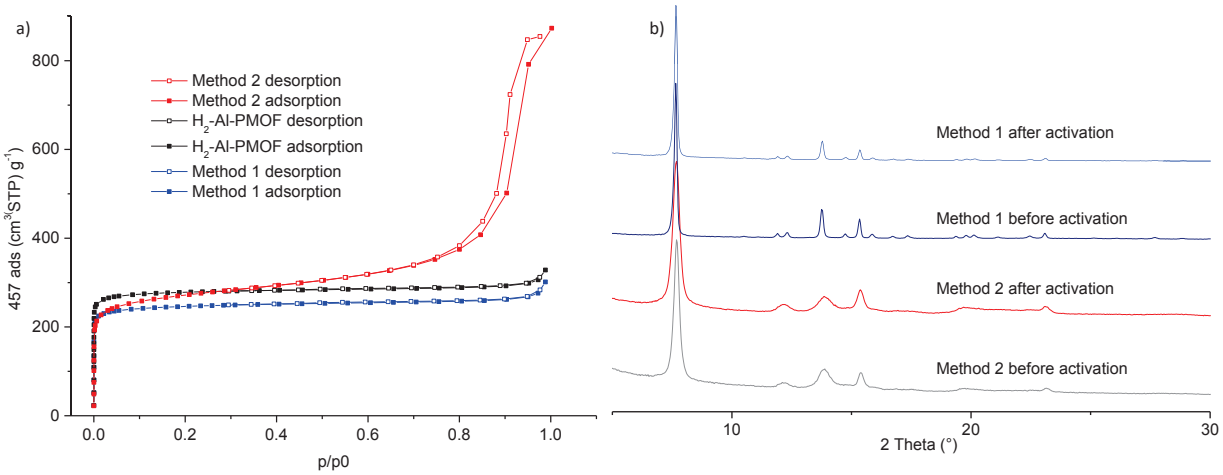

Figure 3-35 a) N_2 adsorption/desorption isotherms at 77K for the Fe-Al-PMOF samples obtained with the two methods compared to free base Al-PMOF used for method 1. b) PXRD data for the Fe-Al-PMOF samples obtained from the two methods before and after activation at 160 °C under vacuum for 12 hours.

3.5.3. Conclusions and perspectives of the synthetic studies of Mn and Fe metalated Al-PMOF

Mn-Al-PMOF was successfully obtained via the optimisation of synthetic parameters for the solvothermal reaction between $AlCl_3.6H_2O$ and MnTCPP(OH). Fe-Al-PMOF was obtained via optimisation of two different synthetic routes. Method 1 explored the post synthetic metalation of H_2-Al-PMOF by iron thiocyanate and Fe-Al-PMOF material was obtained with around 80% Fe occupancy in the porphyrin cores. Method 2 involved the use of FeTCPP(Cl) as the starting ligand and the MOF was obtained with 100% Fe occupancy in the porphyrin cores but with lower crystallinity compared to method 1.

H_2-Al-PMOF obtained starting from the free base porphyrin shows higher crystallinity compared to the metalated Al-PMOF obtained starting from metalloporphyrin ligands. Thus, a possible method to increase the crystallinity might be to attempt to obtain the Fe and Mn metalated material in a one-step synthesis starting with the free base TCPP ligand. The fact that the porphyrin cores in the H_2TCPP ligand is not metalated with Al^{3+} during the reaction can be used as an advantage in a one pot synthesis to obtain differently metalated porphyrin cores. This type of porphyrinic MOF synthesis has already been reported by Smythe et al where porphyrin core was metalated with different first row transition metals while having Cd^{2+}, which has a larger ionic radius, in the inorganic SBU and thus worthwhile exploring in the case with Al-PMOF.[12]

3.6. Evaluation of M-Al-PMOF material as heterogeneous catalysts

The potential of Fe^{3+} and Mn^{3+} metalated Al-PMOF materials as heterogeneous catalysts was explored with different types of reactions. Initially, the oxidation of hexane, toluene and cyclohexene was attempted but more promising results were obtained in the cyclopropanation of styrene with ethyl diazoacetate (EDA).[27] Therefore, this reaction was further investigated in more details (Figure 3-36).

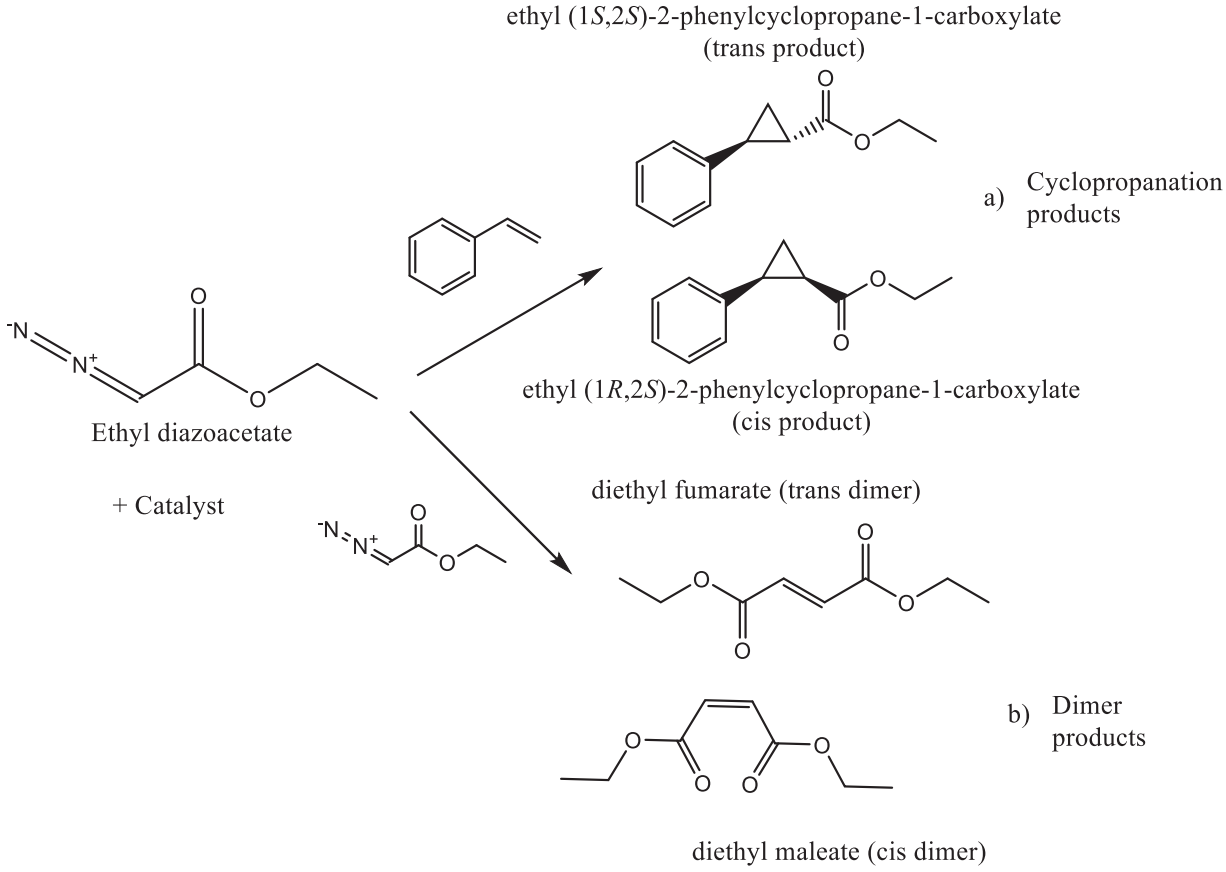

Figure 3-36 Reaction of ethyl diazoacetate with styrene in the presence of the catalyst. a) The cyclopropanation products formed b) dimerization products formed due to the self-reaction of EDA.

The reaction was performed at 60 °C in toluene with a catalyst: styrene: EDA ratio of 1:1000:1200 (details provided in the experimental section). Mn-Al-PMOF showed increased selectivity towards the cyclopropanation products compared to Fe-Al-PMOF (Figure 3-37). However, with Fe-Al-PMOF, the reaction rate was much higher compared to the Mn-Al-PMOF. The reaction in the presence of Fe-Al-PMOF was completed in 2 hours, while with Mn-Al-PMOF the completion was not achieved even after 42 hours (EDA is still present as shown in Figure 3-37b). Therefore, the different metals in the porphyrin core have a different effect on the catalytic activity towards this reaction.

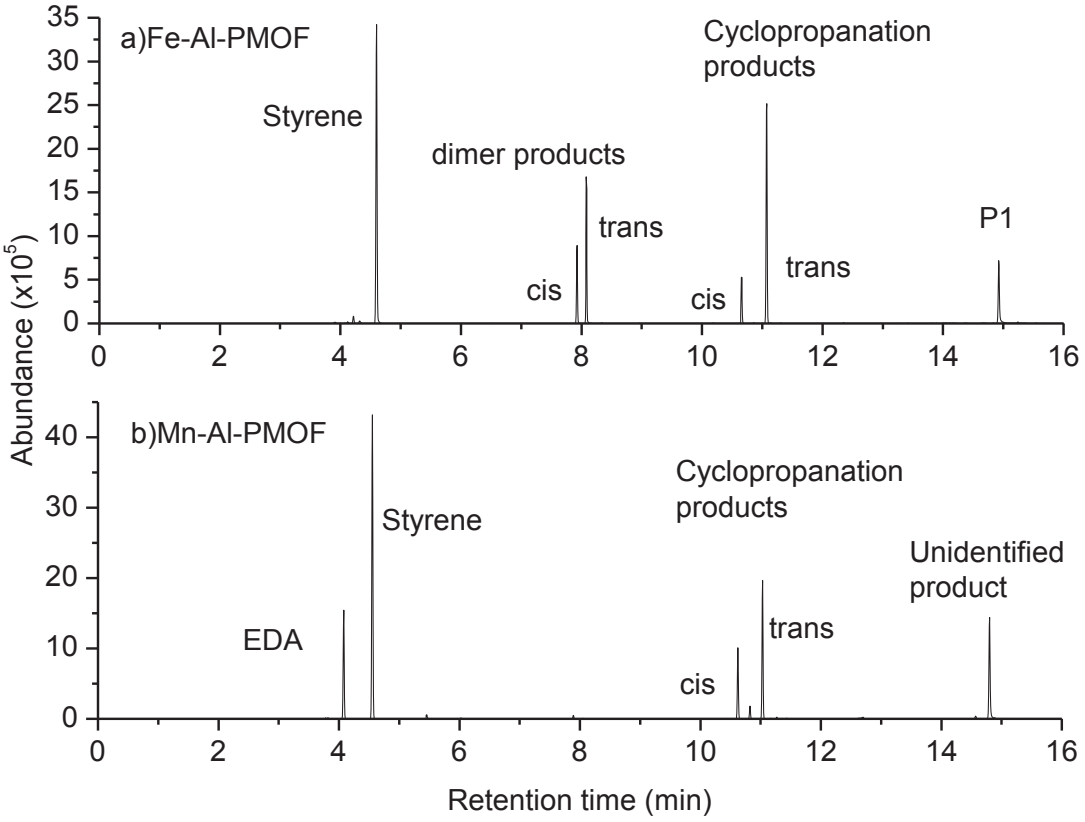

Figure 3-37. The GC-MS data obtained for the cyclopropanation of styrene with EDA using a) Fe-Al-PMOF and b) Mn-Al-PMOF.

The reaction with both the catalysts led to the formation of unexpected products. The product obtained with Mn-Al-PMOF was not determined[1] but the one obtained with Fe-Al-PMOF was identified as 3,4,5-triethyl-4,5-dihydro-1*H*-pyrazole-3,4,5-tricarboxylate (P1) (^{1}H NMR provided in the appendix section B.6). The formation of this product can be explained by a 1,3-dipolar cycloaddition of EDA to diethyl maleate or fumarate (Figure 3-38 step4) as previously reported by Basato et al using a ruthenium catalyst with EDA. [28]

[1] In fact, this product was identified by GC-MS as pyrazoline:

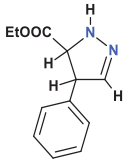

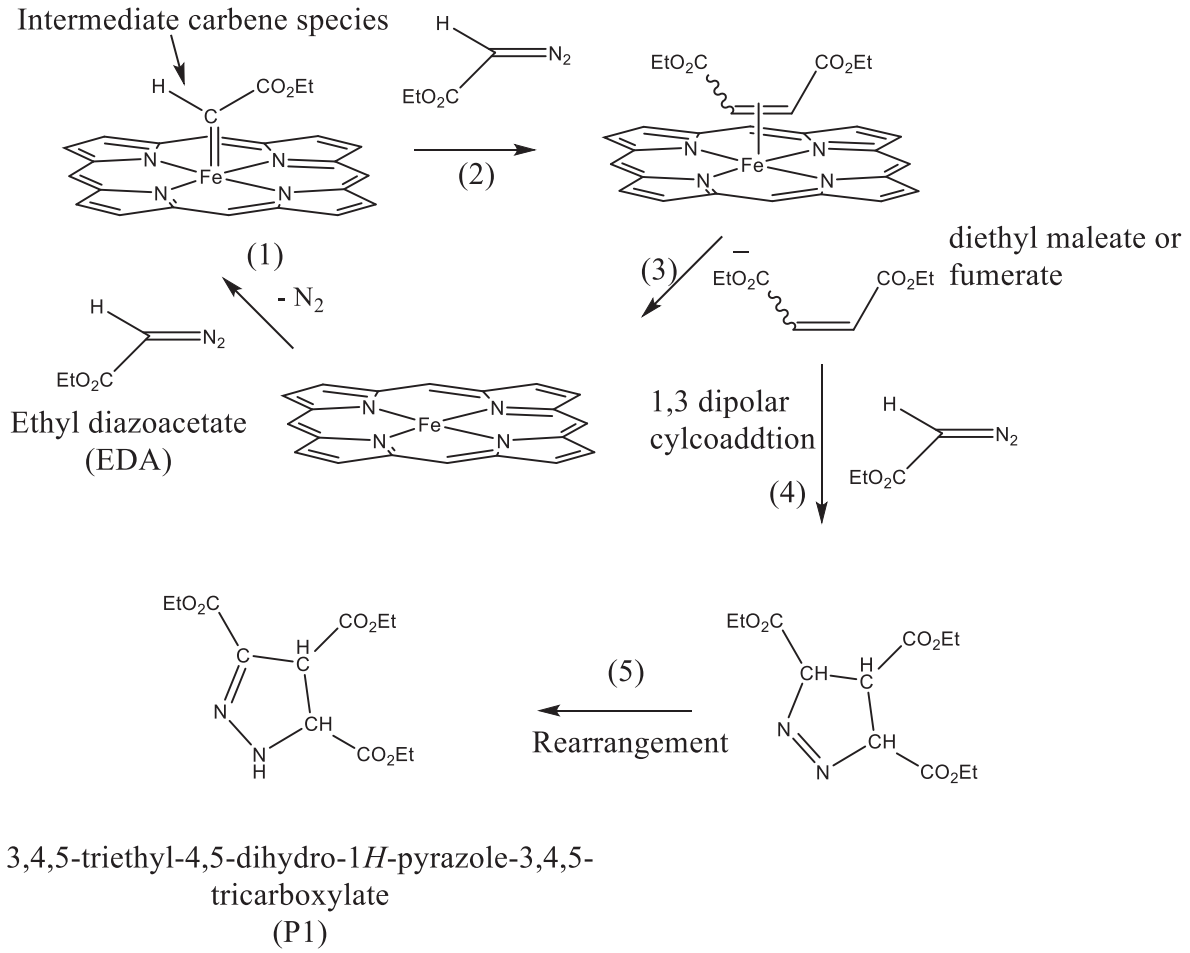

Figure 3-38 Schematic representation of the possible mechanism for the formation of the dimer products and 3,4,5-triethyl-4,5-dihydro-1H-pyrazole-3,4,5-tricarboxylate (P1). P1 is formed via a 1,3-dipolar addition of EDA to either diethyl maleate or fumarate (step 4).

The formation of the product P1 with Fe-Al-PMOF was further investigated. The reaction was attempted with just EDA without styrene to favour the P1 formation. This product was obtained with a selectivity of 41% compared to the dimer products, ethyl fumarate and ethyl maleate (toluene, catalyst: EDA ratio = 1:1200, T = 60 °C) (Figure 3-39a). To compare the heterogeneous catalytic activity of Fe-Al-PMOF with that of a homogeneous catalyst, the iron metalated ester porphyrin [5,10,15,20-tetrakis(4-methoxycarbonylphenyl)porphyrinato]-Fe(III) chloride, (FeTEsterP(Cl), synthesis described in chapter 2] was used in the same reaction conditions. Importantly, very different product distributions were obtained with heterogeneous and homogeneous systems. First, only traces of P1 product were obtained with homogeneous FeTEsterP(Cl). Secondly, homogeneous FeTEsterP(Cl) was very selective to the formation of the cis-dimer (diethyl maleate) while Fe-Al-PMOF catalysed the formation of trans-dimer as the principal product (Figure 3-39). This finding indicates that the framework structure of the Fe-Al-PMOF plays an essential role for the formation of P1. This can be explained by the fact that the 1,3-dipolar cycloaddition reaction (Figure 3-38 step4) occurs in the pores of the MOF which renders the dimer products (diethyl maleate or fumarate) in close proximity with a

free EDA molecule in a confined space. In the homogeneous system, this arrangement favourable for the P1 formation is not achieved.

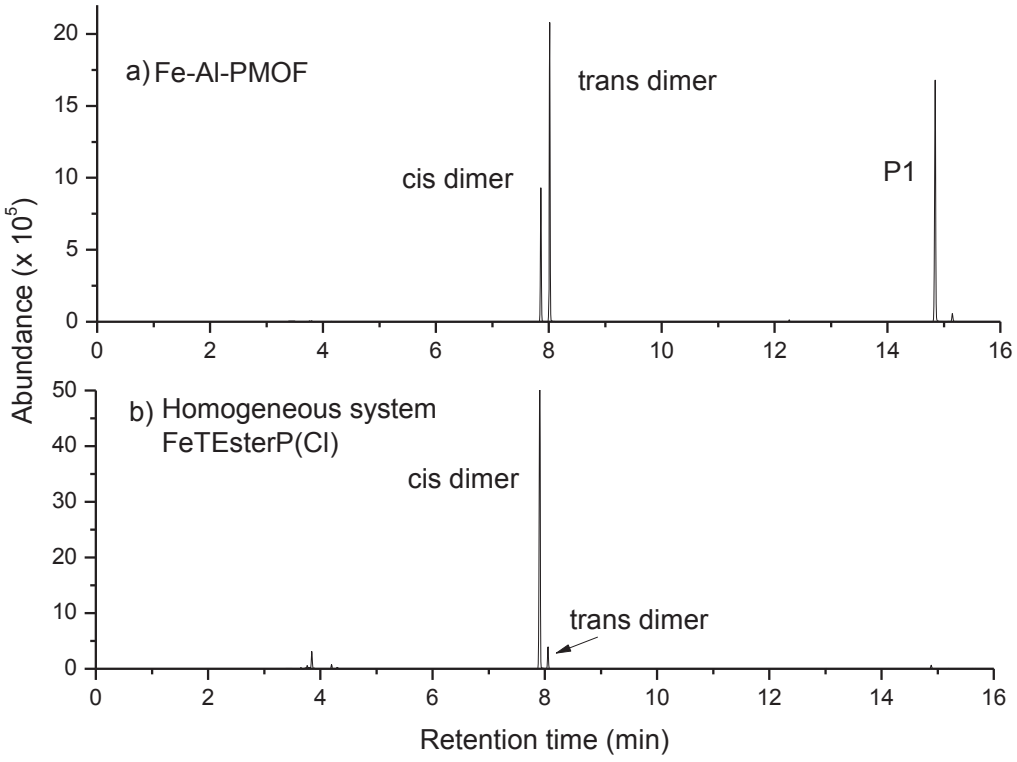

Figure 3-39. Selectivity of the reaction of the Fe-Al-PMOF with EDA compared to the homogeneous system with FeTesterP(Cl). Reaction followed using GC-MS.

The recyclability of the Fe-Al-PMOF catalyst was then investigated. The solid was recovered by centrifugation and washed with toluene 5 times before each run (details in the experimental section). Quite unexpectedly, the selectivity of Fe-Al-PMOF to P1 formation increased in each successive run. Furthermore, the rate of the reaction also slowed down and the reaction time was increased to achieve a complete EDA conversion. In the 4th run, EDA was still left in the reaction mixture after 1 hour and complete consumption was achieved after 2 hours. In the 5th run, EDA was not completely consumed even after 3 hours. Remarkably, the selectivity to P1 progressively increased to reach 89 % in the 5th run (Table 3-13, Figure 3-40). The possibility of any contamination with the adsorbed reaction products from the previous runs was eliminated via running a blank run without the addition of EDA which resulted in no products. Furthermore, the structure of the Fe-Al-PMOF framework was intact which was evidenced by the PXRD data (Figure 3-41).

Table 3-13 Investigating the recyclability of the Fe-Al-PMOF. Selectivity is calculated via GC-MS analysis.

Run	Time	Diethyl maleate (cis dimer) %	Diethyl fumarate (trans dimer) %	P1 %
1	1h	18	41	41
2	1h	12	46	42
3	1h	11	41	48
4	1h* 2h	10 9	28 24	62 67
5	1h* 2h* 3h*	10 8 6	20 10 5	70 82 89

* EDA is not completely consumed.

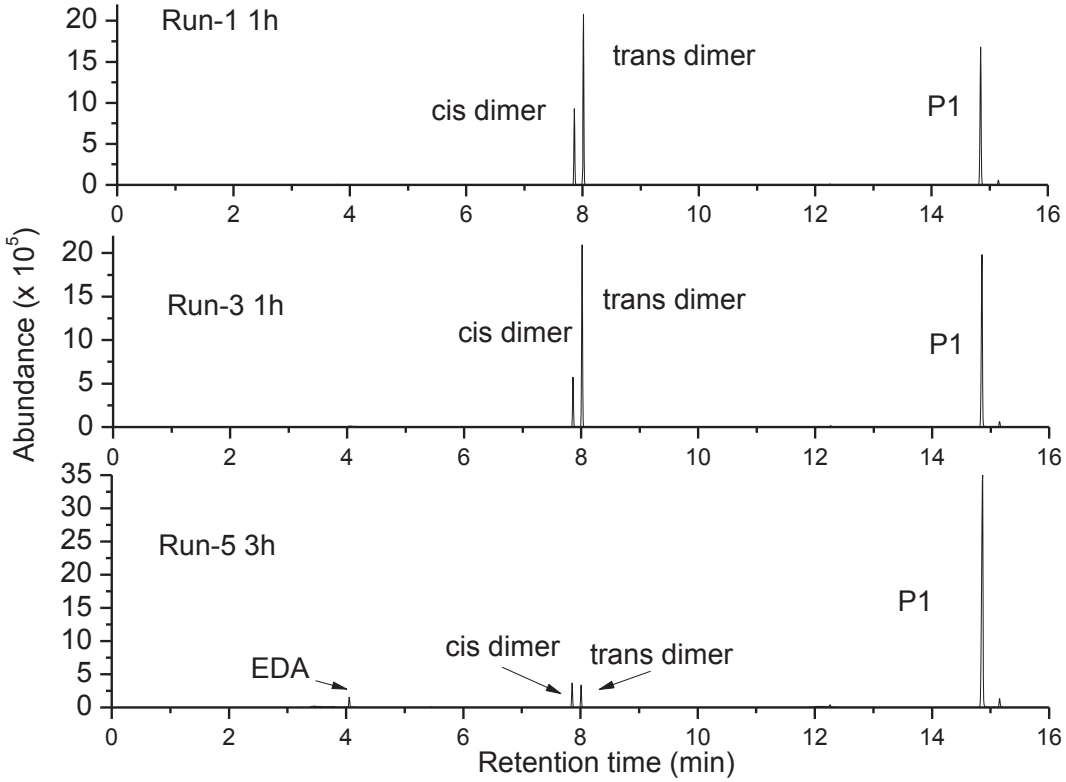

Figure 3-40 GC-MS data for investigating the recyclability of the catalyst.

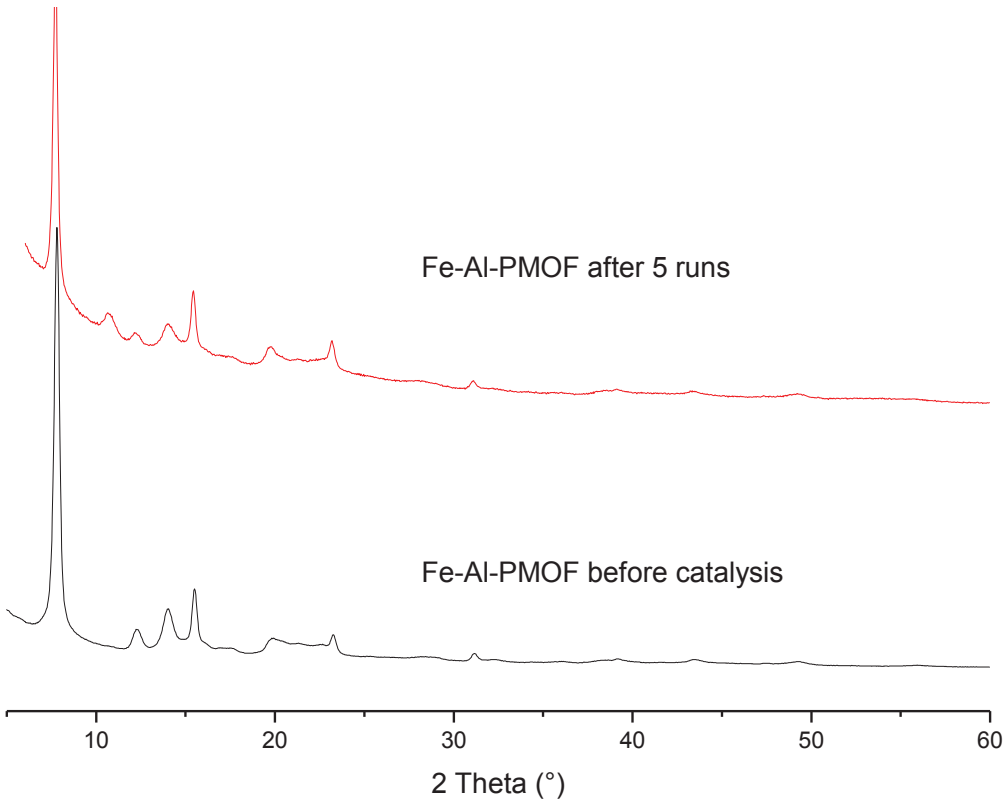

Figure 3-41 PXRD patterns of Fe-Al-PMOF before and after catalysis.

The formation of P1 depends on the presence of both the dimer product and EDA. If the dimer product is formed very rapidly, a major proportion of EDA present will be used for the formation of EDA dimers, thus leading to a decrease of the available EDA amount for the formation of P1. In the presence of smaller number of catalytic sites, the rate of the formation of the dimers should be diminished and the formation of P1 might be favoured. To check this hypothesis, the reaction was performed using less catalyst, 10% of the previous amount (catalyst: EDA ratio = 0.1:1200). Indeed, in this case, the reaction selectivity to P1 was very high (96 % after 3 h) (Table 3-14), very close to 89 % observed in the 5th run of the recyclability study (Table 3-13 run 5). However, a smaller catalyst loading resulted in a slower rate of reaction. Even after 6 hours, EDA was still present in the reaction mixture (Figure 3-42). Therefore, it can be concluded, that the most likely reason for the higher P1 selectivity and for the slower reaction rate observed in the successive runs of the reaction is the gradual deactivation of catalytic sites.

Table 3-14 Investigation of the reaction with a lower amount of the catalyst. Selectivity is calculated via GC-MS analysis.

Time	Diethyl maleate (cis dimer) %	Diethyl fumarate (trans dimer) %	P1 %
1h	10	21	69
2h	6	5	89
3h	2	2	96

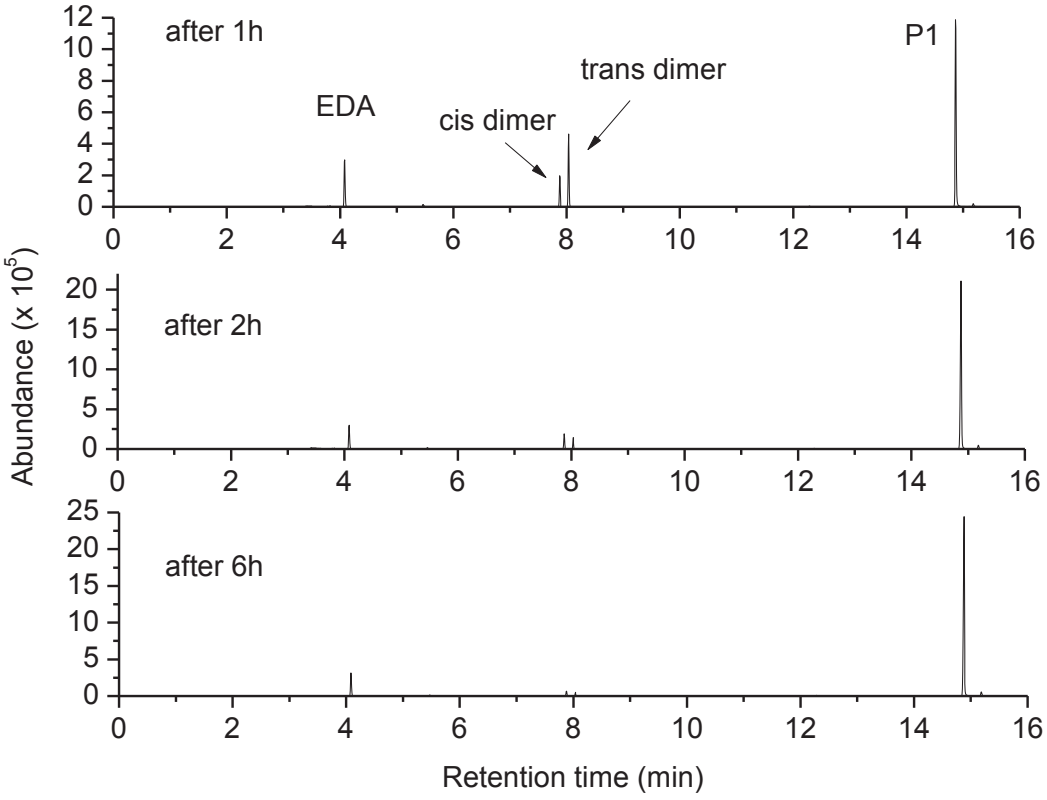

Figure 3-42 GC-MS data for the investigation of P1 with EDA using less Fe-Al-PMOF (catalyst: EDA = 0.1:1200).

Importantly, even with this deactivation of the catalyst, a selectivity of close to 90% for P1 can be achieved for the reaction with EDA. This is higher than what was reported by Basato et al with their ruthenium based catalyst (maximum yield of 17% after 96 hours). Furthermore, this activity is due to the porous nature of the framework of Fe-Al-PMOF as a similar homogeneous system did not provide the P1 product. Thus, this work demonstrates very promising catalytic properties of Fe-Al-PMOF for the formation of P1.

3.7. General conclusion of chapter 3

In this chapter the, reactivity of Fe^{3+} and Al^{3+} with tetrakis(4-carboxyphenyl) porphyrin based ligands was investigated. Coordination polymer materials were obtained for the reactions between Fe^{3+} and free base tetrakis(4-carboxyphenyl) porphyrin. However, further investigations in to the exact nature of solids were hampered by the lack of single crystals of sufficient quality for X-ray diffraction studies. The reaction between Fe^{3+} and cobalt metalated tetrakis(4-carboxyphenyl) porphyrin ligand led to the identification of a new MOF phase. However, the resultant product had low crystallinity and attempts made at amelioration were not successful.

The reactivity of Al^{3+} with MnTCPP(OH) and FeTCPP(Cl) led to the successful syntheses of Mn and Fe metalated Al-PMOF material. Furthermore, Fe metalated Al-PMOF was also obtained from the post synthetic metalation of the free base Al-PMOF. The catalytic properties of Fe-Al-PMOF for the formation of a cyclic pyrazoline product from ethyl diazoacetate was also demonstrated. A more in-depth look in to other types of reactions initially studied (such as oxidation of hexane/cyclohexane) remains as a potential avenue for further investigating the catalytic activity of these material.

3.8. Experimental section

General methods

All reagents were of commercial origin and used as received from different providers as shown in the table below.

Table showing the providers for different reagents used in syntheses.

Reagent	**Provider**
Anhydrous $FeCl_2$	ACROS organics
$AlCl_3.6H_2O$	Fluka analytical
$FeCl_3.6H_2O$	Sigma-Aldrich
$FeSO_4 \cdot 7H_2O$	Sigma-Aldrich
H_2TCPP	TCI chemicals
Pyrazine	Sigma-Aldrich
Imidazole	Fluorochem
4-methyl-imidazole	Sigma-Aldrich
Pyrrolidine	Sigma-Aldrich
pyridine	Sigma-Aldrich
Benzoic acid	Sigma-Aldrich
KSCN	Fluka analytical

The cobalt, manganese and iron metalated TCPP ligands were synthesised as per chapter 2.

Infrared spectroscopy was performed with a Nicolet 380 FT-IR spectrometer coupled with the attenuated total reflectance (ATR) accessory.

UV-vis spectroscopy was performed with a SAFAS Monaco UV-mc^2 spectrophotometer.

Mass spectrometry was performed at the Centre Commun de Spectrométrie de Mass at the University of Claude Bernard Lyon 1 on a MicrOTOFQ II – Bruker in electrospray Ionisation mode (ESI).

Powder X Ray diffraction was performed with two different instruments:

1) PANanlytical XpertPro MRD diffractometer with a Cu Kα1 radiation (λ = 1.540598 Å) used with 40 kV and 30mA settings in θ/θ reflection geometry. This is the default instrument used unless stated otherwise.

2) Bruker D8 Advance diffractometer with Cu Kα1 radiation (λ = 1.540598 Å) used with 50 kV and 50 mA settings in θ/θ reflection geometry with a variable divergence slit for axial exposure of 4mm of sample. The measurements were performed by Ruben Vera at the Centre for Diffractometry at Lyon 1.

Scanning electron microscopy (SEM) were performed on FEI Quanta 250 FEG and Zeiss Merlin Compact microscopes in the microscopy centre of Lyon1 University. Samples were mounted on stainless pads and sputtered with ~2 nm of carbon to prevent charging during observation.

TGA measurements were performed with 2 different instruments:

1) Mettler-Toledo TGA / DSC STARe system. Approximately 3 mg of sample was introduced into an alumina crucible of 70 µl and heated from 25 °C to 800 °C at a rate of 10 °C min $^{-1}$ under air flow (20 mL.min^{-1} + 10 mL.min^{-1} balance). The analyses were performed by Oleksandra Veselska at Institut de Recherche sur la Catalyse et l'Environnement de Lyon (IRCELYON).

2) Mettler-Toledo GA / DSC 2 system with a DSC rod with 6 thermocouples. Approximately 3mg of sample was introduced in to an alumina crucible with a volume of 150 µL and heated from 30 °C to 1000 °C at a rate of 10 °C min $^{-1}$ under air flow (50 mL.min^{-1}). The analyses were performed by Dr. Rodica Chiriac and François Toche at Laboratory of Multimaterial and Interfaces (LMI) of Lyon 1.

Surface areas were measured by N_2 adsorption and desorption at 77.3 K using a BEL Japan Belsorp Mini apparatus volumetric adsorption analyser. The BET surface calculations were performed using points at the pressure range $0 < P/P_0 < 0.10$

Investigating the reactivity of free base tetrakis(4-carboxyphenyl) porphyrin with iron(III)

Investigating the nature of the intermediate product in the synthesis of [Fe^{II}pzTCPP(Fe^{III}OH)$_2$]

Typical synthesis involved combining the H_2TCPP ligand (3 equivalents), $FeCl_3.6H_2O$ (1 equivalent) and the solvent in a Teflon reactor and stirring at room temperature for 10 minutes. Afterwards, the reaction mixture was sealed in a stainless-steel autoclave and heated at the desired temperature with the desired heating program. The product was recuperated via filtration followed by first washing with DMF until there was no color in the filtrate, and then with acetone three more times. The details of the exact reaction conditions investigated are given in appendix section B.1, Table B-1.

Investigating the possibility of replacing the pyrazine axial ligand with a different N-donor in [Fe^{II}pzTCPP(Fe^{III}OH)$_2$]

For the single step approach, H_2TCPP (45 mg, 0.057 mmol), $FeCl_3.6H_2O$ (45 mg, 0.171 mmol), N-donor ligand (3 equivalents compared to H_2TCPP) and 5 mL of DMF were combined in a Teflon reactor and stirred at room temperature for 10 minutes. Afterwards, the reaction mixture was sealed in a stainless-steel autoclave and heated at 180 °C for 15 hours. Heating step was done at 0.65 °C/min (4 hours) while the reaction mixture was cooled to room temperature over 4 hours. The product was

recuperated via filtration followed by first washing with DMF until there was no color in the filtrate and then washing with acetone three more times. The details of the exact reaction conditions utilised are given in the appendix section B.1, Table B-2.

For the 2-step route, the intermediate product was prepared first following the reported procedure. H_2TCPP (90 mg, 0.114 mmol), $FeCl_3.6H_2O$ (90 mg, 0.333 mmol) and 10 mL DMF were combined in a Teflon reactor. After stirring for 10 minutes at room temperature, the reaction mixture was sealed in a stainless-steel autoclave and heated at 180 °C for 15 hours. Heating step was done at 0.65 °C/min (4 hours) while the reaction mixture was cooled to room temperature over 4 hours. The product was recuperated via filtration followed by first washing with DMF until there was no color in the filtrate and then washing with acetone three more times, which resulted in a dark crystalline solid (absolute yield 0.103 mg).

Afterwards, the prepared intermediate product (30 mg, 0.038 mmol), the N-donor ligand (3 equivalents compared to the intermediate product) and 5 mL of DMF were combined in a Teflon reactor and stirred at room temperature for 10 minutes. The reaction mixture was then sealed in a stainless-steel autoclave and was heated at 180 °C for 15 hours. Heating step was done at 0.65 °C/min (4 hours) while the reaction mixture was cooled to room temperature over 4 hours. The product was recuperated via filtration followed by washing with DMF until there was no color in the filtrate and then washing with acetone three more times. The details of the exact reaction conditions studied are given in the appendix section B.1 Table B-3.

Investigating the reactivity of cobalt metalated tetrakis(4-carboxyphenyl) porphyrin with iron(III)

Typical synthesis involved combining Co metalated TCPP ligand, $FeCl_3.6H_2O$, additives (if used) and the solvent in a teflon reactor and stirring at room temperature for 10 minutes. Then the reaction mixture was sealed in a stainless-steel autoclave and heated at the desired temperature with the desired heating program. The product was recuperated via filtration followed by washing with DMF until there was no color in the filtrate and then three more times with acetone. The details of the exact reaction conditions investigated are given in the appendix section B.2 Table B-4.

Single crystals which allowed the structural elucidation via single crystal X-ray diffraction for the $[CoTCPP(H_2O)_2(Fe^{III}OH)_2]$ phase, were obtained as follows:

Cobalt metalated TCPP ligand (45 mg, 0.052 mmol), $FeCl_3.6H_2O$ (15 mg, 0.056 mmol) and 5 mL of DMF were combined in a teflon reactor and stirred for 10 minutes at room temperature. The resultant mixture was then sealed in a stainless-steel autoclave and heated at 150 °C for 72 hours where the

temperature was increased over 4 hours (0.52 °C/min) to reach the isotherm and then cooled downed to room temperature over 4 hours. The structural elucidation was done analysing the square shaped single crystals observed in the mother liquor.

Synthesis of Mn^{3+} metalated Al-PMOF

Synthesis of Mn-Al-PMOF using the final optimised conditions is as follows:

Mn^{3+} metalated TCPP (53 mg, 0.062 mmol) and $AlCl_3.6H_2O$ (30 mg, 0.125 mmol) were combined with 2.5 mL of DMF and 2.5 mL of deionised water in a Teflon reactor and stirred at room temperature for 10 minutes. The resultant mixture was then sealed in a stainless-steel autoclave and heated at 190 °C for 15 hours where the temperature was increased over 18 hours (0.15 °C/min) to reach the isotherm and then cooled downed to room temperature over 4 hours. The solid was recovered by centrifugation, washed five times with DMF and three times with acetone. After drying in air, the MOF was obtained as a dark greenish solid (57 mg, 97% yield). FTIR cm^{-1}**:** 1606 (s, coordinated asymmetric C=O stretch), 1556 (m, aromatic C=C stretch of TCPP), 1440 (s, coordinated symmetric C=O stretch); UV-vis (0.1M NaOH) λ_{max}/nm: 464 [Soret MnTCPP(OH)], 415 (Soret H_2TCPP) 525, 573,611 [Q bands MnTCPP(OH)].

Synthesis of Fe^{3+} metalated Al-PMOF

Method 1

Synthesis of H_2-Al-PMOF was adopted from the literature and slightly modified where a 1.5:1 aluminium chloride to H_2TCPP ratio was used and is as follows:

H_2TCPP (65 mg, 0.082 mmol), $AlCl_3 \cdot 6H_2O$ (30 mg, 0.125 mmol) and deionised water (5 mL) were combined in a Teflon reactor and stirred for 10 minutes at room temperature. The resultant mixture was then sealed in a stainless-steel autoclave and heated at 180 °C for 16 hours where the temperature was increased over 3 hours (0.86 °C/min) to reach the isotherm and then cooled downed to room temperature over 1.5 hours. The solid was recovered by centrifugation, washed three times with DMF and put in 25 mL DMF where it was heated for 12 hours at 80 °C. Afterwards, the solid was washed three more times each with DMF and acetone. After drying in air, the MOF was obtained as a maroonish solid in a 78% yield (56 mg).

Preparation of 0.1 M $Fe(SCN)_2$ methanolic solution used for the Fe metalation of H_2-Al-PMOF was adopted from the procedure reported in literature[26] and is as follows:

$FeSO_4 \cdot 7H_2O$ (277 mg, 1.00 mmol) and KSCN (194 mg, 2.00 mmol) were mixed in 10 mL of methanol and stirred for 30 minutes. 5 mg of ascorbic acid was added to afford a colourless suspension (ascorbic acid prevents the oxidation of Fe^{2+} to Fe^{3+}). The resultant precipitate was separated via centrifugation and removed to obtain a clear, colourless solution which must be used immediately.

Optimised synthesis for Fe-Al-PMOF by metalation of H_2-Al-PMOF using $Fe(SCN)_2$ in method 1:

A suspension of H_2-Al-PMOF (50 mg, 0.057 mmol) in 0.3 mL of methanol was prepared in a vial. To this, 3.4 mL of a 0.1 M methanolic solution of $Fe(SCN)_2$ (0.34 mmol) and 5.4 mg of ascorbic acid were added. The vial was closed and the reddish suspension was heated at 100 °C for 48 hours. The solid was then recovered via centrifugation, washed three times with DMF followed by washing three more times with methanol. After drying in air, the MOF was obtained as a dark solid (35 mg, 65% yield). FTIR cm^{-1}**:** 1714 (uncoordinated COOH stretch), 1606 (s, coordinated asymmetric C=O stretch), 1556 (m, aromatic C=C stretch of TCPP), 1440 (s, coordinated symmetric C=O stretch); UV-vis (0.1M NaOH) λ_{max}/nm: 409 [Soret FeTCPP(OH)], 518 (Q band H_2TCPP), 568, 609 [Q bands FeTCPP(OH)].

Method 2

Synthesis of Fe metalated Al-PMOF using the final optimised conditions for method 2 is as follows:

Fe^{3+} metalated TCPP (82.5 mg, 0.094 mmol) and $AlCl_3.6H_2O$ (30 mg, 0.125 mmol) were combined with 2.5 mL of DMF and 2.5 mL of deionised water in a Teflon reactor and stirred and degassed with argon at room temperature for 10 minutes. The resultant mixture was then sealed in a stainless-steel autoclave and heated at 190 °C for 16 hours where the temperature was increased over 3 hours (0.92 °C/min) to reach the isotherm and then cooled downed to room temperature over 4 hours. The solid was recovered by centrifugation, washed three times with DMF and heated in 10 mL DMF at 80 °C for 12 hours. Afterwards the solid was washed again with DMF three more times followed by washing with acetone for three times. After drying in air, the MOF was obtained as a dark solid (42 mg, 48 % yield). FTIR cm^{-1}**:** 1714 (uncoordinated COOH stretch), 1606 (s, coordinated asymmetric C=O stretch), 1556 (m, aromatic C=C stretch of TCPP), 1440 (s, coordinated symmetric C=O stretch); UV-vis (0.1M NaOH) λ_{max}/nm: 409 [Soret FeTCPP(OH)], 568, 609 [Q bands FeTCPP(OH)].

Catalysis studies of M-Al-PMOF

Investigation of the cyclopropanation of styrene with EDA using the M-Al-PMOF catalysts

For the catalysis studies, Fe-Al-PMOF obtained from method 2 was used due to the higher occupancy of Fe in the porphyrin cores.

Catalyst was weighed directly in a 3mL vial (1.2 mg, 0.001 mmol for Fe-Al-PMOF) and was combined with styrene (0.115 mL, 1.0 mmol) and 0.735 mL of toluene. The mixture was degassed with argon for 5 minutes and maintained in an inert atmosphere. Following, ethyl diazoacetate (0.150 mL, 1.2 mmol) was added to the reaction mixture with a syringe and heated at 60 °C with stirring. The reaction was followed via GC-MS method. At appropriate times, 10 µL of the reaction mixture was withdrawn and diluted with 400 µL of acetonitrile prior to GC-MS analysis.

GC-MS analysis was performed on a Hewlett Packard GC system 6890 with a Carl Roth Roticap-5 column coupled with a Hewlett Packard MS selective detector 5973.

Investigation of the formation of 3,4,5-triethyl-4,5-dihydro-1H-pyrazole-3,4,5-tricarboxylate from ethyl diazoacetate with Fe-Al-PMOF as the catalyst

Fe-Al-PMOF was weighed directly in a 3mL vial (1.2 mg, 0.001 mmol) and 0.850 mL of toluene was added. The mixture was degassed with argon for 5 minutes and maintained in an inert atmosphere. Following, ethyl diazoacetate (0.150 mL, 1.2 mmol) was added to the reaction mixture and heated at 60 °C with stirring.

For studying the recyclability of the MOF, the solid was recovered by centrifugation after the reaction and washed with toluene for 5 times. Afterwards, the toluene was removed with a pipette, and the recovered solid was directly used for the following run.

3.9. References

1. Gao, W.-Y.; Chrzanowski, M.; Ma, S., Metal-metalloporphyrin frameworks: a resurging class of functional materials. *Chemical Society reviews* **2014,** *43* (16), 5841-5866.
2. Guo, Z.; Chen, B., Recent developments in metal-metalloporphyrin frameworks. *Dalton Trans.* **2015,** *44* (33), 14574-14583.
3. Huh, S.; Kim, S.-J.; Kim, Y., Porphyrinic metal-organic frameworks from custom-designed porphyrins. *CrystEngComm* **2016,** *18* (3), 345-368.
4. Devic, T.; Serre, C., High valence 3p and transition metal based MOFs. *Chemical Society reviews* **2014,** *43* (16), 6097-6115.
5. Fateeva, A.; Clarisse, J.; Pilet, G.; Grenèche, J.-M.; Nouar, F.; Abeykoon, B. K.; Guegan, F.; Goutaudier, C.; Luneau, D.; Warren, J. E.; Rosseinsky, M. J.; Devic, T., Iron and Porphyrin Metal–Organic Frameworks: Insight into Structural Diversity, Stability, and Porosity. *Crystal Growth & Design* **2015,** *15* (4), 1819-1826.
6. Fateeva, A.; Chater, P. A.; Ireland, C. P.; Tahir, A. A.; Khimyak, Y. Z.; Wiper, P. V.; Darwent, J. R.; Rosseinsky, M. J., A water-stable porphyrin-based metal-organic framework active for visible-light photocatalysis. *Angewandte Chemie* **2012,** *51* (30), 7440-4.
7. Anderson, J. S.; Gallagher, A. T.; Mason, J. A.; Harris, T. D., A Five-Coordinate Heme Dioxygen Adduct Isolated within a Metal–Organic Framework. *Journal of the American Chemical Society* **2014,** *136* (47), 16489-16492.
8. Lions, M.; Tommasino, J. B.; Chattot, R.; Abeykoon, B.; Guillou, N.; Devic, T.; Demessence, A.; Cardenas, L.; Maillard, F.; Fateeva, A., Insights into the mechanism of electrocatalysis of the oxygen reduction reaction by a porphyrinic metal organic framework. *Chemical communications* **2017,** *53* (48), 6496-6499.
9. Liu, Y.; Yang, Y.; Sun, Q.; Wang, Z.; Huang, B.; Dai, Y.; Qin, X.; Zhang, X., Chemical Adsorption Enhanced CO2 Capture and Photoreduction over a Copper Porphyrin Based Metal Organic Framework. *ACS Applied Materials & Interfaces* **2013,** *5* (15), 7654-7658.
10. Mansuy, D., Cytochromes P-450 and model systems: great diversity of catalyzed reactions. In *Pure and Applied Chemistry*, 1994; Vol. 66, p 737.
11. Groves, J. T., The bioinorganic chemistry of iron in oxygenases and supramolecular assemblies. *Proceedings of the National Academy of Sciences of the United States of America* **2003,** *100* (7), 3569-3574.
12. Smythe, N. C.; Butler, D. P.; Moore, C. E.; McGowan, W. R.; Rheingold, A. L.; Beauvais, L. G., A heterobimetallic metal-organic framework with tunable reactive metal sites: synthesis, characterization, and reactivity. *Dalton Trans.* **2012,** *41* (26), 7855-7858.
13. Chin, D.-H.; La Mar, G. N.; Balch, A. L., Mechanism of autoxidation of iron(II) porphyrins. Detection of a peroxo-bridged iron(III) porphyrin dimer and the mechanism of its thermal decomposition to the oxo-bridged iron(III) porphyrin dimer. *Journal of the American Chemical Society* **1980,** *102* (13), 4344-4350.
14. Collman, J. P.; Fu, L., Synthetic Models for Hemoglobin and Myoglobin. *Accounts of chemical research* **1999,** *32* (6), 455-463.
15. Karagiaridi, O.; Bury, W.; Mondloch, J. E.; Hupp, J. T.; Farha, O. K., Solvent-Assisted Linker Exchange: An Alternative to the De Novo Synthesis of Unattainable Metal–Organic Frameworks. *Angewandte Chemie International Edition* **2014,** *53* (18), 4530-4540.
16. Twyman, L. J.; Ge, Y., Porphyrin cored hyperbranched polymers as heme protein models. *Chemical communications* **2006,** (15), 1658-1660.
17. Grodkowski, J.; Behar, D.; Neta, P.; Hambright, P., Iron Porphyrin-Catalyzed Reduction of CO2. Photochemical and Radiation Chemical Studies. *The Journal of Physical Chemistry A* **1997,** *101* (3), 248-254.
18. Behar, D.; Dhanasekaran, T.; Neta, P.; Hosten, C. M.; Ejeh, D.; Hambright, P.; Fujita, E., Cobalt Porphyrin Catalyzed Reduction of CO2. Radiation Chemical, Photochemical, and Electrochemical Studies. *The Journal of Physical Chemistry A* **1998,** *102* (17), 2870-2877.

19. Kornienko, N.; Zhao, Y.; Kley, C. S.; Zhu, C.; Kim, D.; Lin, S.; Chang, C. J.; Yaghi, O. M.; Yang, P., Metal–organic frameworks for electrocatalytic reduction of carbon dioxide. *J. Am. Chem. Soc* **2015,** *137* (44), 14129-14135.
20. Wang, K.; Feng, D.; Liu, T. F.; Su, J.; Yuan, S.; Chen, Y. P.; Bosch, M.; Zou, X.; Zhou, H. C., A series of highly stable mesoporous metalloporphyrin Fe-MOFs. *Journal of the American Chemical Society* **2014,** *136* (40), 13983-6.
21. Dhakshinamoorthy, A.; Alvaro, M.; Garcia, H., Aerobic oxidation of thiols to disulfides using iron metal-organic frameworks as solid redox catalysts. *Chemical communications* **2010,** *46* (35), 6476-6478.
22. Barron, P. M.; Wray, C. A.; Hu, C.; Guo, Z.; Choe, W., A Bioinspired Synthetic Approach for Building Metal−Organic Frameworks with Accessible Metal Centers. *Inorganic Chemistry* **2010,** *49* (22), 10217-10219.
23. Farha, O. K.; Shultz, A. M.; Sarjeant, A. A.; Nguyen, S. T.; Hupp, J. T., Active-Site-Accessible, Porphyrinic Metal-Organic Framework Materials. *Journal of the American Chemical Society* **2011,** *133* (15), 5652-5655.
24. Feng, D.; Gu, Z.-Y.; Li, J.-R.; Jiang, H.-L.; Wei, Z.; Zhou, H.-C., Zirconium-Metalloporphyrin PCN-222: Mesoporous Metal–Organic Frameworks with Ultrahigh Stability as Biomimetic Catalysts. *Angewandte Chemie International Edition* **2012,** *51* (41), 10307-10310.
25. Atzori, C.; Shearer, G. C.; Maschio, L.; Civalleri, B.; Bonino, F.; Lamberti, C.; Svelle, S.; Lillerud, K. P.; Bordiga, S., Effect of Benzoic Acid as a Modulator in the Structure of UiO-66: An Experimental and Computational Study. *The Journal of Physical Chemistry C* **2017,** *121* (17), 9312-9324.
26. Bonnet, S.; Siegler, M. A.; Costa, J. S.; Molnar, G.; Bousseksou, A.; Spek, A. L.; Gamez, P.; Reedijk, J., A two-step spin crossover mononuclear iron(ii) complex with a [HS-LS-LS] intermediate phase. *Chemical communications* **2008,** (43), 5619-5621.
27. Zhu, S.-F.; Zhou, Q.-L., Iron-catalyzed transformations of diazo compounds. *National Science Review* **2014,** *1* (4), 580-603.
28. Basato, M.; Tubaro, C.; Biffis, A.; Bonato, M.; Buscemi, G.; Lighezzolo, F.; Lunardi, P.; Vianini, C.; Benetollo, F.; Del Zotto, A., Reactions of Diazo Compounds with Alkenes Catalysed by [RuCl(cod)(Cp)]: Effect of the Substituents in the Formation of Cyclopropanation or Metathesis Products. *Chemistry – A European Journal* **2009,** *15* (6), 1516-1526.

Chapter 4:
Tetrazolate Based Porphyrinic MOFs

Table of Contents

4. Tetrazolate based porphyrinic MOFs

4.1. Azolate based ligands

Tetrazoles are part of the azole family, which are five-membered aromatic nitrogen heterocycles. They are sp^2 hybridized N-donors and have the same coordination behaviour as pyridines. Even though azoles are generally known as bases (azolium is the protonated form) they can also be deprotonated to yield the corresponding azolate ion (Figure 4-1).

The acidity and the basicity of azole/azolate rings are directly related to the number of N-atoms in the ring due to their electron-withdrawing nature. The more N-atoms in the rings lead to a higher acidity (Figure 4-1). Due to this reason, tetrazole has a similar acidity to that of a carboxylic acid (4.90 pKa compared to 4.76 pKa for acetic acid) whereas, the other azoles are basic (pKa> 10).[1] In addition, tetrazolates are considered to be slightly softer than carboxylates, according to the hard-soft acid base (HSAB) theory.

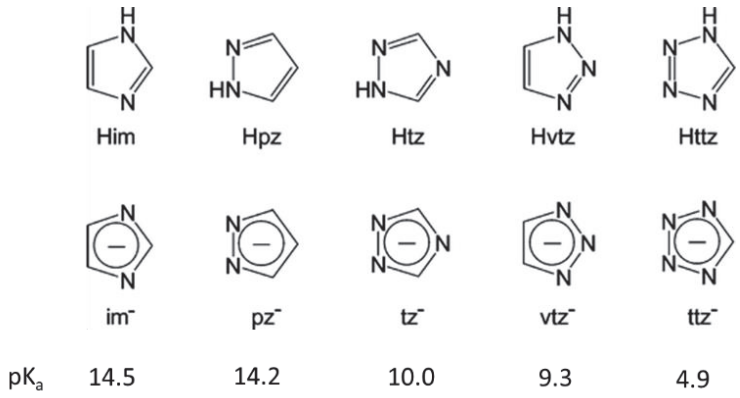

Figure 4-1 Different azoles and their corresponding azolate ion, imidazole (Him), pyrazole (Hpz), 1,2,4-triazole (Htz), 1,2,3-triazole (Hvtz), and tetrazole (Httz). pKa values are given on the bottom.[1]

There are many examples of MOF structures with azolate based ligands.[2] Imidazole has been used to synthesise number of frameworks, aptly named as zeolitic imidazolate frameworks (ZIFs), with zeolite-type topologies and tetrahedral metal ions (e.g. Zn^{2+}, Co^{2+}). ZIFs exhibit permanent porosity and high thermal and chemical stability, which have made them potential candidates for applications such as separation and storage of gases.[3] Likewise, there are reported examples for pyrazolate, triazolate and tetrazolate based frameworks. [2, 4]

Pyrazolates, triazolates and tetrazolates can have similar binding modes to the *syn*,*syn*-μ-η^1,η^1- bidentate bridging mode of carboxylates, which is the basis of well-known SBUs such as the octahedral $M_4O(RCOO)_6$ (Figure 4-2). Thus, analogues for some carboxylate SBUs have been observed with pyrazolates, triazolate and tetrazolates. Tonigold et al reported a pyrazolate analogue,

$Co(II)_4O(pz)_6$, of the well-known MOF-5 SBU, $M_4O(RCOO)_6$, with the MOF, $[Co(II)_4O(bdpb)_3]$ (H_2bdpb= 1,4-bis[(3,5-dimethyl)- pyrazol-4-yl]benzene).[5]

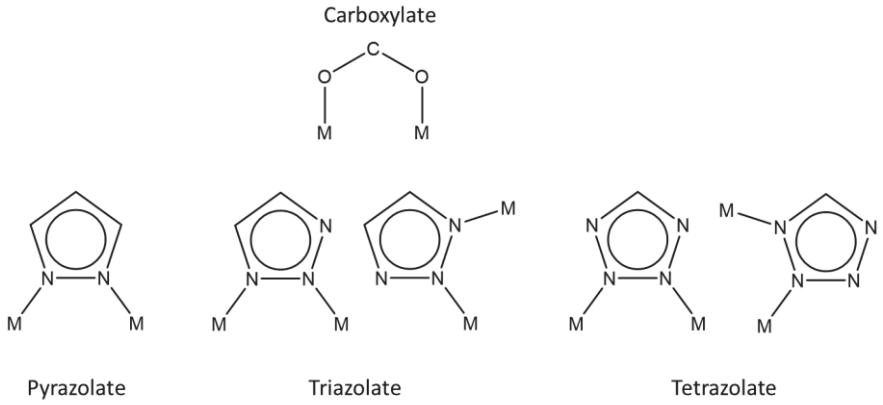

Figure 4-2 Syn,syn-μ-η^1,η^1-bidentate bridging mode of carboxylates, and similar bridging modes possible for pyrazolates, triazolates and tetrazolates.

Azole based isomorphous analogues for the 8-connected $M_4Cl(RCOO)_8$ cluster[6] and $M_4O(RCOO)_8$ cluster[7] seen for carboxylates have been observed for both pyrazolates[8] and triazolates[9] and this trend continues with tetrazolates[10] as described in the published article (Figure 4-3). The SBU obtained with pyrazolate ligand is isomorphous, but not isostructural to the tetrazolate and triazolate ones as the bridging Cl^- is missing. This is due to the acetate salts being required to form the framework with the pyrazolate ligand as opposed to the chloride salts used in other two cases (use of acetate salts in DMF was necessary for the authors to promote the deprotonation of the pyrazole group due to its higher pK_a). The pyrazolate framework is neutral while the triazolate and the tetrazolate frameworks have an anionic charge which is balanced by $Cu(DMF)_6^{2+}$ cations present in the pores. The chemical stability of the overall framework was found to positively correlate with the pK_a of the azoles, where the tetrazolate ligand [H_3BTT = 1,3,5-tri(1H-tetrazol-5-yl)benzene] pK_a < triazolate ligand [H_3BTTri = 1,3,5-tri(1*H*-1,2,3-triazol-5-yl)benzene] pK_a < pyrazolate ligand [H_3BTP = 1,3,5-tri(1*H*-pyrazol-4-yl)benzene] pK_a.[11]

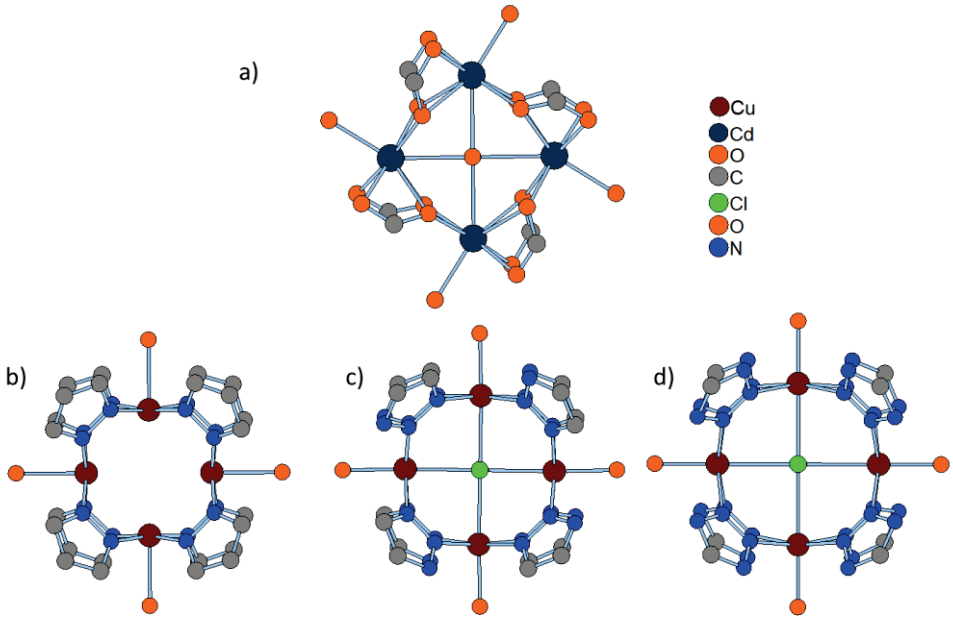

Figure 4-3 Isomorphous 8-connected $M_4Cl/O(L)_8$ SBUs reported for carboxylates and certain azolates. a) carboxylate (hexaethayltruxene-2,7,12-tricarboxylic acid) [7] b) pyrazolate (1,3,5-tri(1H-pyrazol-4-yl)benzene) [8] c) triazolate (1,3,5-tri(1H-1,2,3-triazol-5-yl)benzene) [9] d) tetrazolate (1,3,5-tri(1H-tetrazol-5-yl)benzene) [10] based ligands. Hydrogens are omitted for clarity.

4.2. MOFs with tetrazolate ligands

Tetrazoles, which have four nitrogen atoms that can coordinate, are able to act as either a multidentate ligand or a bridging building block in supramolecular assemblies. They can act as monodentate,[12] bidentate,[13-14] tridentate[15-16] and tetradentate[17-18] ligands in up to nine different metal-binding modes which yield various metal clusters that could be used as SBUs (Figure 4-4a). Most of the metal clusters reported are based on divalent metals, their diversity leads to structures with diverse net topologies. Such clusters include trinuclear μ^3-oxo-bridged 3-connected cluster with a $M_3O(ttz)_3$ unit (Figure 4-4b1),[19] trinuclear 6-connected linear cluster with a $M_3(ttz)_6$ unit (Figure 4-4b2),[13-14] 8-connected μ^4-chloro-bridged tetranuclear cluster with a $M_4Cl(ttz)_8$ unit (Figure 4-4b3),[14, 17] and pentanuclear oxo-bridged 8-connected cluster with a $M_5O_2(TTZ)_8$ unit (Figure 4-4b4).[20]

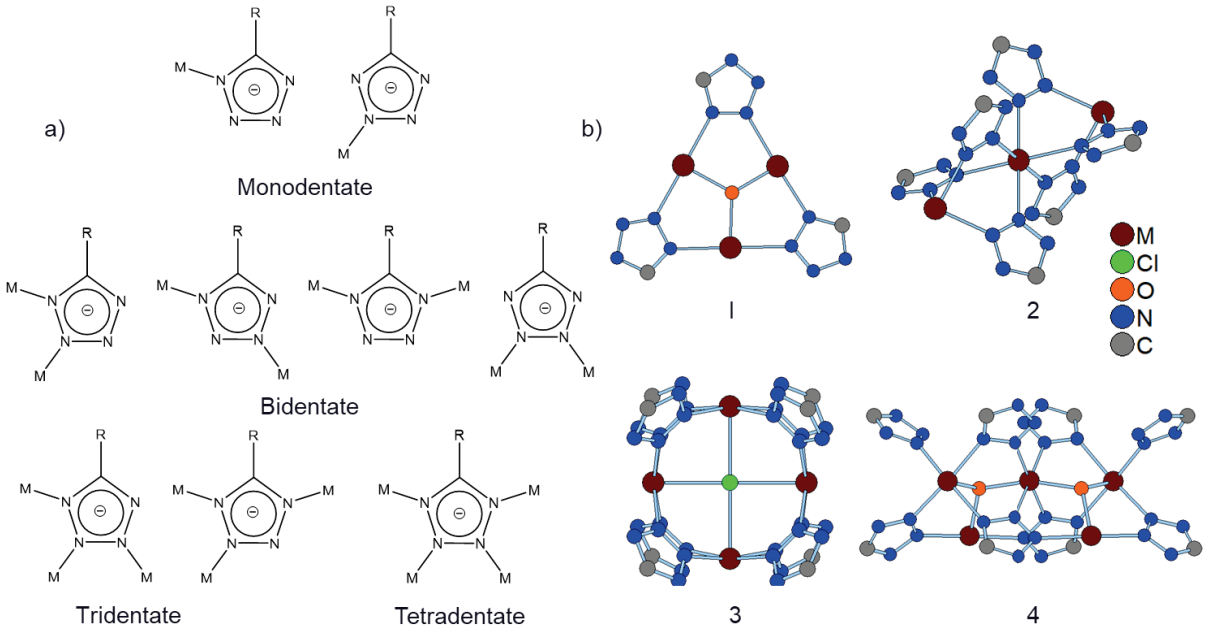

Figure 4-4 (a) Possible binding modes for the tetrazolate functional group. (b) Some reported tetrazolate based SBUs in literature. Hydrogens are omitted for clarity.

Most SBUs based on the tetrazolate ligands have been metal cluster based but a few extended chain like SBUs have also been reported (Table 4-1). However, these chain type SBUs are not common. CSD database reports 1380 total hits on coordination compound structures based on tetrazolate ligands of which 1050 are polymeric. Of these, structures with extended chain like SBUs, where the tetrazolate ligand is acting as a bridging ligand between each metal ion, have only been reported 10 times with 6 different types of SBUs. (Figure 4-5 shows the different types of chain like SBUs seen with the tetrazolate ligand acting as a bridging ligand). This is possibly due to the ability of tetrazolates to coordinate to multiple metal ions at the same time in a variety of binding modes with its 4 different N atoms, which can favour the formation of distinct metal clusters.

Chain SBU type 1 (Figure 4-5a) and 2 (Figure 4-5b) both consist of metal ions that are bridged by three tetrazolate ligands. In type 1, only N2 and N3 atoms of the tetrazolate are involved in the coordination, while in type 2, N2, N3 atoms and N1, N2 atoms are both involved in coordination in an alternating fashion. The other chain types involve additional species as bridging ligands (type 3 oxygen from DMF, type 4 F^-, type 5 N_3^-, type 6 Cl^-).

Table 4-1 Reported extended frameworks in literature with chain like SBUs where tetrazole ligand is acting as a bridging ligand. Only 2D and 3D structures were considered.

Ref Code	Formula	Net type	Chain SBU type	reference
ZARTAP	$[Fe_2(H_{0.67}bdt)_3]\cdot 4H_2O$	3D	1	[21]
DAXJET	$[Fe_2(H_{0.67}bdt)_3]\cdot 13H_2O$	3D	1	[22]
XOXCAP	$[Co_2(H_{0.67}bdt)_3]\cdot 20\ H_2O$	3D	1	[23]
REQUCN	$[Cu_3(cttz)_6(CH_3CN)_2(H_2O)_2]\cdot 2CH_3CN$	2D	2	[24]
REQCOH	$[Cu_3(cttz)_6(H_2O)_3\{(CH_3)_2CO\}]\cdot 3(CH_3)_2CO$	2D	2	[24]
VEMMUW	$[Cu(bdt)(DMF)\cdot 0.25DMF\cdot CH_3OH]$	3D	3	[13]
ZUDWUS	$[Fe_5F_7(H_2O)(HCOO)(amtetraz)_4]\cdot 1.5(Hdma)$	3D	4	[25]
ZUDXAS	$[Fe_5F_8(H_2O)_2(amtetraz)_4]\cdot (Hdma)$	3D	4	[25]
TORXAB	$[Cu(N_3)(ttz)]$	3D	5	[26]
VEMMIK	$[Mn_2(bdt)Cl_2(DMF)_2]\cdot 1.5CH_3OH\cdot H_2O$	3D	6	[13]

H_2bdt = 5,5'-(1,4-phenylene)bis(1*H*-tetrazole)
Hcttz = 5-cyanotetrazole
$[Hdma]^+$ = dimethylammonium cation
Hamtetraz-5 = aminotetrazole
Httz = 1-*H*-tetrazole

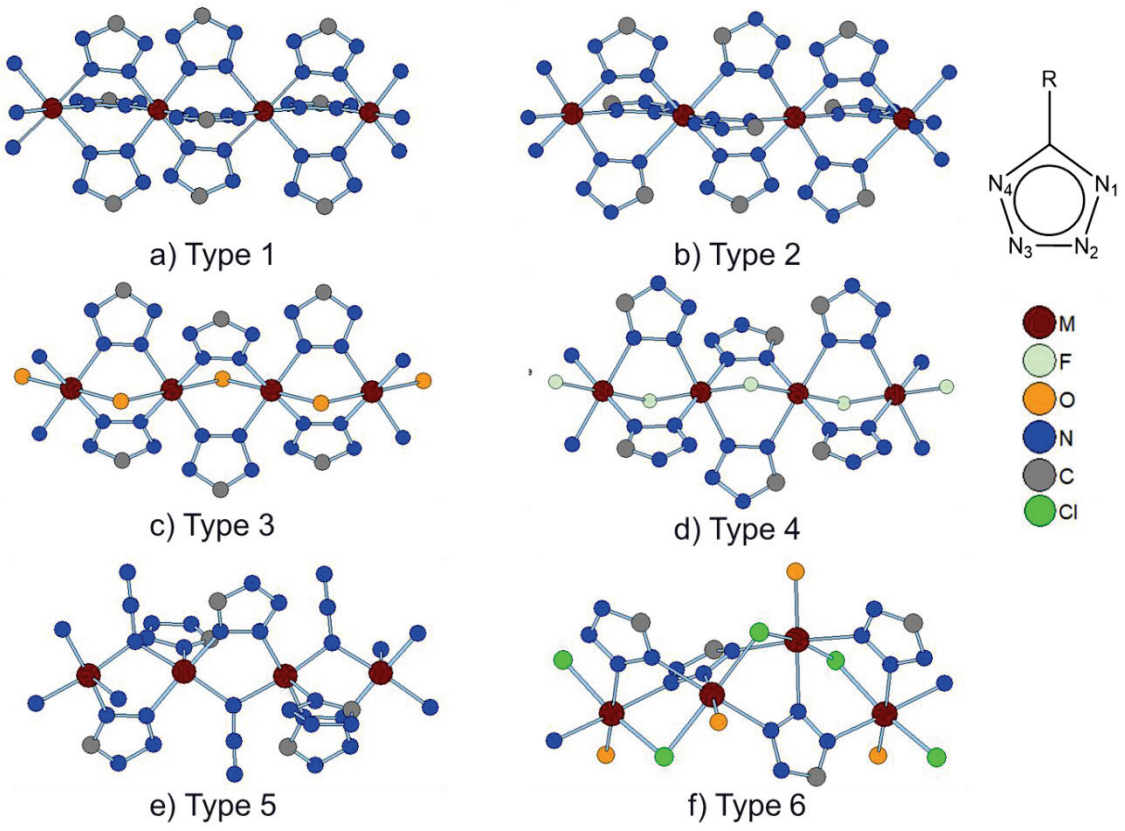

Figure 4-5 Different types of chain like SBUs reported in literature where tetrazole ligand is acting as a bridging ligand. Hydrogens are omitted for clarity.

4.3. Porphyrinic tetrazolate frameworks

Tetrazole functionalised porphyrin, 5,10,15,20-tetrakis(4-(2*H*-tetrazol-5-yl)phenyl)porphyrin (H_2TTPP) can be synthesised from a well-known [3 + 2] cycloaddition reaction starting with a nitrile-bearing porphyrin and sodium azide (synthetic details are provided in chapter 2).[27] However, MOF architectures using H_2TTPP as a building block have only been reported twice, UTSA-57 {chemical formula $[Mn(II)_{4.5}Cl(Mn(III)Cl\text{-}TTPP)_2(H_2O)_4]$} by Chen et al and PCN-526 {chemical formula $[Cd_{4.5}Cl(CdTTPP)_2]$} by Zhou et al (Figure 4-6). Both MOFs had the *scu* framework topology where the inorganic building block was based on divalent ions, Cd or Mn, arranged in square planar $[M_4Cl]^{7+}$ clusters with an overall SBU of $M_4Cl(ttz)_8$(solvent) as shown in Figure 4-6, which is a commonly observed SBU for tetrazolate based ligands as mentioned earlier.[28-29] There were Mn^{2+} and Cd^{2+} ions (represented by $M_{0.5}$ in the formula) present in the respective frameworks to balance their ionic charges.

UTSA-57, composed of $Mn_4Cl(ttz)_8(H_2O)_4$ moieties linked by Mn metalated TTPP as the 4-connected organic linker, exhibited permanent porosity with a BET surface area of 206.5 m^2g^{-1} and displayed moderately high performance for C_2H_2/CH_4 separation at room temperature.[28] PCN-526 is composed of $Cd_4Cl(ttz)_8$ inorganic blocks linked by Cd metalated TTPP ligand.[29] The authors demonstrated that PCN-526 can undergo a crystallinity preserving reversible phase transition triggered by an abrupt change in temperature from 298 K to 110 K where the $Cd_4Cl(ttz)_8$ clusters experience a rotation.

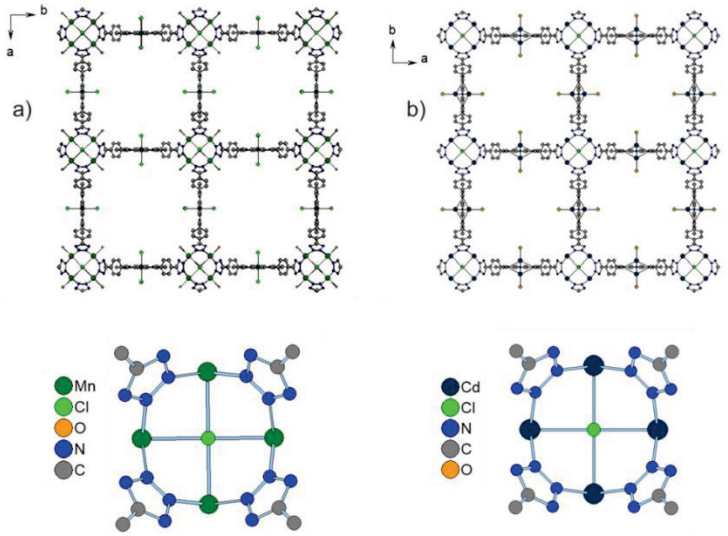

Figure 4-6 a) UTSA-57 MOF b) PCN-526 MOF (Cd located in the porphyrin core was modelled as two disordered parts by the authors). The corresponding $M_4Cl(ttz)_8$ SBU is shown below each framework. Hydrogens and solvent molecules are omitted for clarity.

These examples indicate that tetrazolate porphyrinic ligands have the potential to yield extended MOF architectures with permanent porosity. However, it remains an area under-explored, especially considering that tetrazolate based compounds have been studied as potential spin crossover (SCO) material. MOFs are known for having extended frameworks and high porosity. If SCO behaviour can be incorporated in to MOFs, they can be an ideal platform for obtaining functional material with potential applications such as in sensors.[30-31] However, in order to achieve this, ligands such as tetrazolates must be employed as common carboxylate ligands results in only high spin systems which do not show any spin crossover behaviour.

4.4. Spin cross over material

Spin Crossover (SCO) phenomenon is observed when some variation in external stimuli such as in temperature, pressure or light irradiation induces a change in the spin state of a metal complex. In SCO material, the metal d orbitals are not degenerate due to the crystal field generated by the ligands. For SCO to be possible, multiple spin states should be available to the metal ion. The ground spin state depends on the paring energy and the energy gap (ΔE) between the nonbonding and antibonding sets of d-based orbitals. ΔE larger than the paring energy results in a low-spin (LS) state while the inverse results in a high-spin (HS) state (Figure 4-7). For example, in the case of iron(II) ion in an octahedral geometry, $t_{2g}^4e_g^2$ ($^5T_{2g}$) (S=2) and $t_{2g}^6e_g^0$($^1A_{1g}$) (S=0) configurations correspond to the HS and LS states, respectively. A spin crossover can be caused by external perturbations such as temperature, pressure, light, or interaction with a guest molecule.[32]

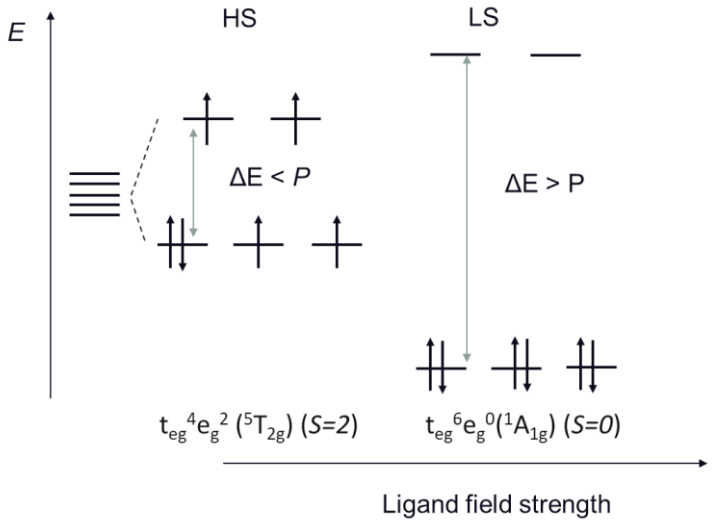

Figure 4-7 Electronic configuration for a d^6 iron(II) ion, in the HS state and in the LS state in an octahedral geometry. ΔE stands for energy splitting in an octahedral ligand field and P for the mean spin-pairing energy.

For a thermally induced SCO to occur, the energy difference between the first vibrionic levels of the LS and HS states, must be in the order of thermal energy, k_BT.[33] This condition leads to a very narrow range possible for ΔE_{HS} (11500-12500 cm^{-1} for Fe(II) systems) and ΔE_{LS} (19000-21000 cm^{-1} for Fe(II)systems) for a thermal spin transition to occur as reported by Gutlich et al.[33] Thermal SCO behaviour has been observed almost exclusively with 3d metal ions of d^4-d^7 electron configurations. The strength of the ligand field is increased with 4d and 5d metals which results in virtually all 4d and 5d transition metal complexes showing LS behaviour.[34]

The ligand plays a critical role in SCO material as it affects the ΔE of the system. A weak field ligand i.e. a ligand which has a relatively smaller ΔE in the spectrochemical series renders only the high spin state accessible. Most SCO systems are based on Fe(II) with N-donor ligands such as azolates which are strong field ligands that results in a sufficiently large ΔE to render the LS state accessible. Oxygen containing ligands such as carboxylates are medium field ligands which generally results in HS complexes and spin-crossover is not observed with them. Most of the SCO studies have been performed on iron, where Fe(II) is in a FeN_6 coordination environment.[35] This is not surprising as Fe(II) displays the largest possible spin state change where it goes from a diamagnetic LS to a HS state with four unpaired electrons as shown in Figure 4-7. Fe(III) based materials have also shown SCO behaviour but has been less studied.[36]

The change in spin state originates from a change in the number of unpaired electrons. This results in a change in the magnetic susceptibility which indicates the degree of magnetisation under an applied magnetic field. Thus, to characterise SCO compounds, usually magnetic susceptibility is measured as a function of temperature using a magnetometer such as a SQUID (superconducting quantum interference device) instrument.[34] X-ray crystallography is also very useful to assess the SCO behaviour as the change in spin state will lead to a change in bond lengths and cell volume. For example, when transitioning from HS to LS the bond lengths and the cell volume decrease. Another major technique used, particularly for Fe containing systems is Mössbauer spectroscopy, as Fe(II) and Fe(III) HS and LS spin systems will result in different values for isomer shift and the quadrupole splitting.[34] Other techniques such as optical spectroscopy (colour change) and vibrational spectroscopy (change in bond strength) have also been employed in studying these systems.[34]

The spin transitions can be accompanied by distinct changes in the physical properties of the framework such as colour. Thus, a spin crossover can transform external stimuli into information signals. Extended porous frameworks which can lead to guest dependant SCO behaviour are particularly intriguing for applications in sensor and memory devices.[30-31] Hoffmann-type MOFs, $[Fe(L)M(CN)_4]$ MOFs (pz = pyrazine type ligand, and M = Ni^{2+}, Pd^{2+}, or Pt^{2+}) are examples of porous

frameworks with guest dependant SCO behaviour which have shown potential as molecular sensors (Figure 4-8).[37] In 2001, Niel et al first reported the cooperative SCO behaviour near room temperature for this family of MOFs[38] and they have received great attention since then.[39] For example, Ohba et al reported a porous framework, $[Fe(pz)Pt(CN)_4]$ which undergoes a colour change from yellow to red upon the adsorption of CS_2, which switches the system from HS to LS.[31] This stabilisation of the LS state was observed only with CS_2 as other guest molecules investigated, such as water, alcohols, toluene and THF, stabilised the HS state.

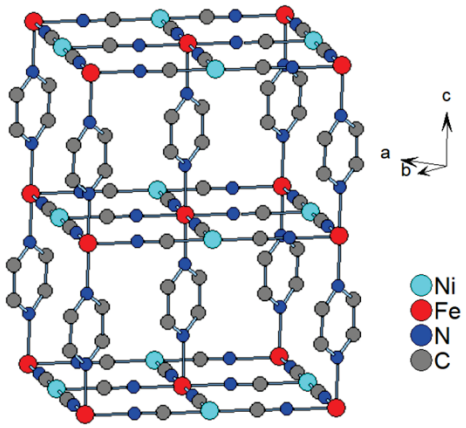

Figure 4-8 An example of a 3D Hofmann-type Iron(II) MOFs, $[Fe(pz)Ni(CN)_4]$ (pz = pyrazine).[30] Hydrogens are omitted for clarity.

4.5. Azole based SCO material

Azoles such as triazoles and tetrazoles have played a major role in the study of SCO materials. Fe(II) complexes with azole ligands can display a remarkable chromic effect with spin-crossover as a result of the change of electronic structure. Iron(II) triazole/tetrazole complexes, depending on the linker, can be violet in the LS state and colourless in the HS state making them potentially applicable in display devices.[40] For example a mononuclear complex, $[Fe(II)(ptz)_6](BF_4)_2$ (ptz = 1-propyltetrazole), was studied regarding chemical and physical influences on the SCO behaviour.[41] Dinuclear complexes such as $[Fe_2(Hsaltrz)_5(NCS)_4]\cdot 4MeOH$ (Hsaltrz = *N*-salicylidene-4-amino-1,2,4-triazole),[42] and trinuclear complexes such as $[Fe_3(npt)_6(C_2H_5OH)_4(H_2O)_2](ptol)_6$ (npt= 4-(4'-nitrophenyl)-1,2,4-triazole, ptol= *p*-tolylsulfonate)[43] showing SCO behaviour have also been reported (Figure 4-9).

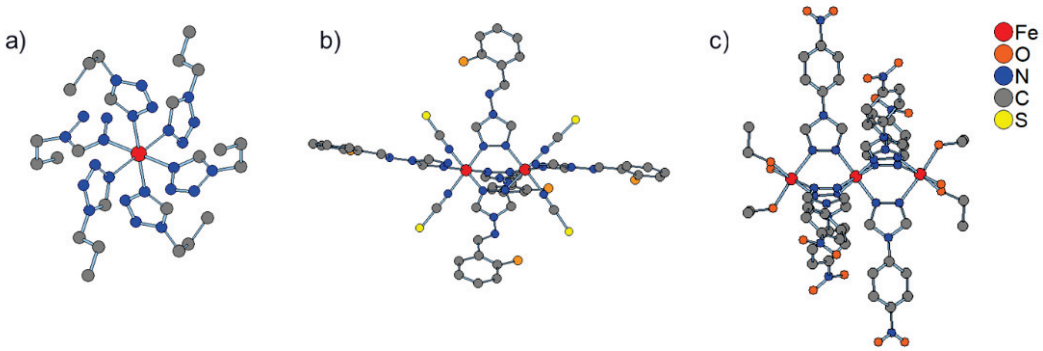

Figure 4-9 a) Mononuclear [Fe(II)(ptz)$_6$](BF$_4$)$_2$(ptz = 1-propyltetrazole) complex [41] b) Dinuclear [Fe$_2$(Hsaltrz)$_5$(NCS)$_4$]·4MeOH (Hsaltrz = N-salicylidene-4-amino-1,2,4-triazole) complex[42] c) Trinuclear [Fe$_3$(npt)$_6$(C$_2$H$_5$OH)$_4$(H$_2$O)$_2$](ptol)$_6$] (npt= 4-(4'-nitrophenyl)-1,2,4-triazole, ptol= p-tolylsulfonate) complex.[43] Hydrogens are omitted for clarity.

The first reported examples of coordination polymers displaying SCO behaviour were 1D triazole based compounds [Fe(Rtrz)$_2$](anion)$_2$(Rtrz = 4- substituted 1,2,4-triazole).[44] Since then, a number of SCO coordination polymers based on triazoles,[45] and tetrazoles,[46] with varying dimensionality have been reported. However, there have been only three reported examples of MOFs based on azole ligands with extended frameworks and permanent porosity which display reversible SCO behaviour, to the best of the authors knowledge.[47-49] Salles et al reported the framework Co(BDP) (BDP^{2-} = 1,4-benzene-dipyrazolate), which undergoes a HS to LS transition upon activation and a reversible transition to an intermediate spin state upon N_2 loading (Figure 4-10a).[47] Reed et al reported a metal–organic framework, Fe-BTTri {chemical formula Fe$_3$[(Fe$_4$Cl)$_3$(BTTri)$_8$]$_2$·18CH$_3$OH, H$_3$BTTri = 1,3,5-tris(1H-1,2,3-triazol-5-yl)benzene)}, that displays spin state change upon CO adsorption/ desorption (Figure 4-10b).[48] Sciortino et al reported a porous framework, [FePd(CN)$_4$(thiome)$_2$] (thiome = 4-[(E)-2-(5-methyl-2-thienyl)vinyl]-1,2,4-triazole), where the SCO behaviour can reversibly be turned off and on with the adsorption/desorption of water (Figure 4-10c).[49]

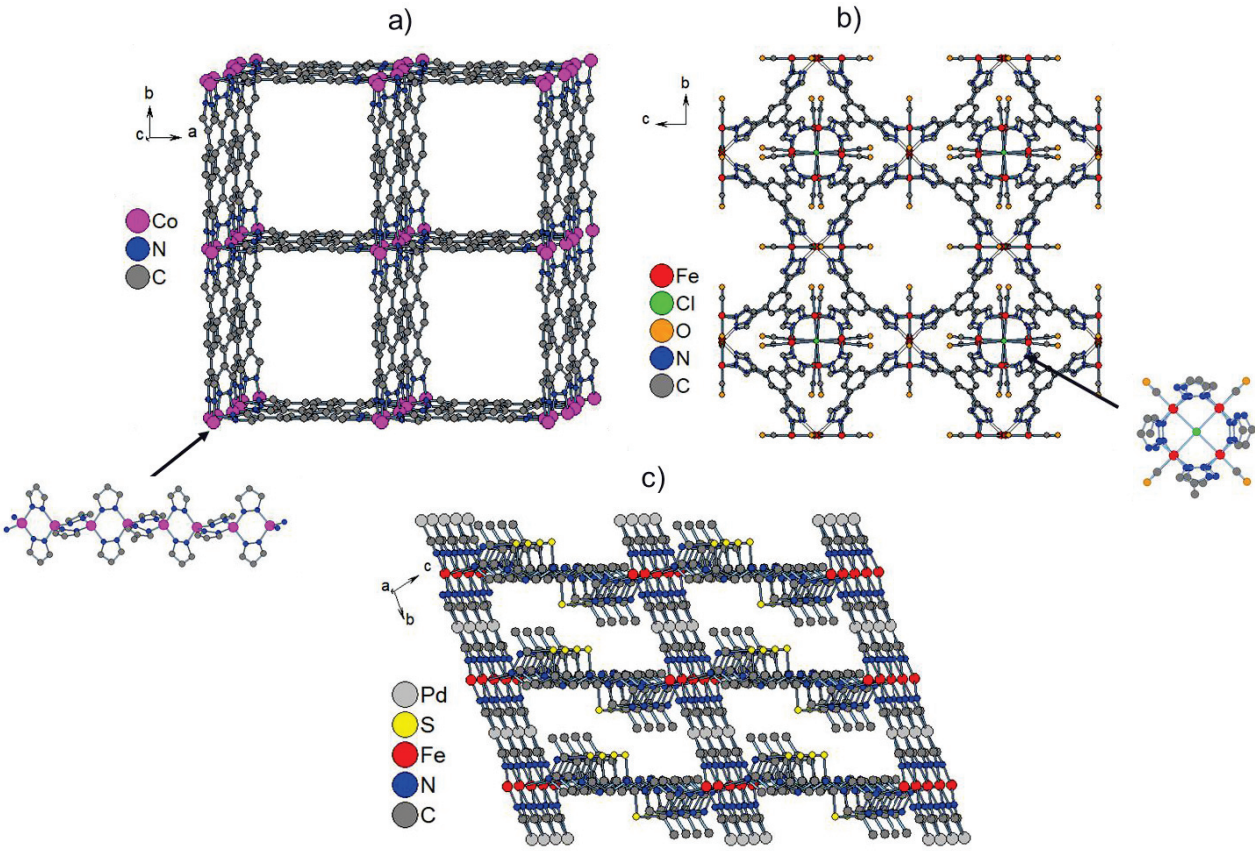

Figure 4-10 Reported azolate based porous extended frameworks a) Co(BDP) (BDP^{2-}= 1,4-benzene-dipyrazolate) [47] b) Fe-BTTri (H_3BTTri =1,3,5-tris(1H-1,2,3-triazol-5-yl)benzene) [48] c) [$FePd(CN)_4$(thiome)$_2$ (Hthiome = 4-[(E)-2-(5-methyl-2-thienyl)vinyl]-1,2,4-triazole).[49] Hydrogens are omitted for clarity.

As mentioned earlier, there are only two examples of porphyrinic tetrazolate MOFs reported and they offer great potential as ligands for porous functional material with SCO behaviour, if iron can be incorporated in to the framework. In addition, the tetrazolate functional group can potentially stabilize lower oxidation states of the iron due to its softer nature compared to the carboxylate functional group. Therefore, the goal of this work was to explore the synthesis of porous coordination polymers using a tetrazole functionalised porphyrin ligand.

4.6. Article

Dalton Transactions

PAPER

View Article Online
View Journal

Published on 07 December 2016. Downloaded by Université Claude Bernard Lyon on 15/12/2016 12:07:28.

Cite this: DOI: 10.1039/c6dt04208b

Tuning the iron redox state inside a microporous porphyrinic metal organic framework†

Brian Abeykoon,[a] Jean-Marc Grenèche,[b] Erwann Jeanneau,[a] Dmitry Chernyshov,[c] Christelle Goutaudier,[a] Aude Demessence,[d] Thomas Devic[e,f] and Alexandra Fateeva*[a]

Received 3rd November 2016,
Accepted 7th December 2016

DOI: 10.1039/c6dt04208b

www.rsc.org/dalton

Two new 3D porphyrin-based metal organic frameworks were obtained by solvothermally reacting iron(III) chloride, a free base (5,10,15,20-tetrakis[4-(2,3,4,5-tetrazolyl)phenyl]porphyrin) (H_2TTPP) and either pyrazine or 1,4-diazabicyclo[2.2.2]octane (DABCO). Both MOFs displayed a 3-D open framework of the **fry** topology, where the inorganic building unit is a chain of corner-sharing FeN_4O_2 octahedra and the porphyrinic linker is metallated with iron during the reaction course, with the N-donor base bridging the iron of the porphyrinic cores. Through thorough structural and spectroscopic analyses of the pyrazine containing material the chemical formula $[Fe^{II}pzTTP(Fe^{II}_{1-x}DMF_{1-x}Fe^{III}_{x}OH_x)]_n$ was inferred ($x \geq 0.25$). Whereas the already reported carboxylate analogue is built up from a pure iron(III) inorganic chain, here spectroscopic and structural studies evidenced a mixed valence iron(II/III) state, evidencing that, in agreement with the HSAB theory, the substitution of a carboxylate function by a tetrazolate one allows redox tuning. Finally, both materials feature one-dimensional channels of *ca.* 8 × 12 Å within the structures with permanent microporosity.

Introduction

Metal organic frameworks (MOFs) are sophisticated microporous crystalline solids composed of organic linkers and inorganic nodes. The versatility of their synthesis has allowed this class of coordination polymers to expand at an extraordinarily rapid pace over the past two decades. The main potential applications for these materials focus on gas storage and separation[1] and heterogeneous catalysis[2] and a considerable effort has been made to understand the structure/performance relationship in these fields. However, redox activity in this class of compounds remains underexplored considering their great potential use in applications such as electrochromic materials, battery materials, multiferroics, electrochemical sensors and electrocatalysts.[3]

We aimed to develop multifunctional redox active materials, using both a redox active ligand and a transition metal in an iron-based porphyrinic framework. Porphyrins have been indeed increasingly used since the 1990s as building units in MOFs to integrate their properties (such as oxidation catalysis, light harvesting) into porous materials.[4] More recently, the electrocatalytic properties of porphyrin-based MOFs have been investigated.[5] Their redox activity has led to the emergence of porphyrinic MOFs as potential candidates for applications such as photovoltaics[6] and electrocatalysts.[7] The manipulation of the redox state and electrochemical properties of an open framework has attracted tremendous interest very recently from a fundamental point of view for the study of the charge hopping mechanisms in ordered porous materials[8] but also regarding the great deal of potential applications these materials can offer as redox-active gas sensors,[9] electrochromic devices[10] and energy storage materials.[11] In this work, iron was utilized to construct open framework materials and promote redox activity. Fe II and Fe III are easily accessible redox states and can be used to create Fe-based mixed valence MOFs.[12]

A series of iron based MOFs were previously reported using carboxylate functionalized porphyrinic linkers (tetrakis(4-carboxyphenyl)porphyrin, TCPP), with either Fe II or Fe III metallic nodes.[13] Among these compounds one material exhibited an extended inorganic backbone: a chain of hydroxide bridged Fe III octahedra, $[Fe(OH)O_4]_n$. Such a motif is quite common in

[a]*Univ Lyon, Université Claude Bernard Lyon 1, Laboratoire des Multimatériaux et Interfaces, UMR CNRS 5615, F-69622 Villeurbanne, France. E-mail: alexandra.fateeva@univ-lyon1.fr*
[b]*Institut des Molécules et Matériaux du Mans, UMR CNRS 6283 Université du Maine – Avenue Olivier Messiaen, 72085 Le Mans, France*
[c]*Swiss-Norwegian Beamline, ESRF BP-220, 38043 Grenoble, France*
[d]*Institut de Recherches sur la Catalyse et l'Environnement de Lyon, Université Claude Bernard Lyon 1, CNRS UMR 5256, Villeurbanne, France*
[e]*Institut Lavoisier, UMR CNRS 8180, Université de Versailles Saint-Quentin-en-Yvelines, 45 avenue des Etats-Unis, 78035 Versailles cedex, France*
[f]*Institut des Matériaux de Nantes, 2 rue de la Houssinière, BP32229, 44322 Nantes cedex 3, France*

†Electronic supplementary information (ESI) available. CCDC 1514927 and 1514928. For ESI and crystallographic data in CIF or other electronic format see DOI: 10.1039/c6dt04208b

Published on 07 December 2016. Downloaded by Université Claude Bernard Lyon on 15/12/2016 12:07:28.

carboxylate-based MOFs, a well-known example being the MIL-53(Fe) phase with a terephthalate as the linker.[14] For the MIL-53(Fe) structure, several reports have shown the possibility to obtain the isostructural mixed valence Fe(II/III) compound where the charge balance is ensured either by an ammonium counter ion inside the pores, by post-synthesis lithium insertion[15] or by replacing the bridging anion by a neutral DMF ligand.[16] However, in porphyrin containing materials no such mixed valence was observed, all the Fe ions in the inorganic chain being in the ferric state. According to hard soft acid base (HSAB) theory, tetrazole functionalized porphyrin was considered to promote the stability of the Fe II redox state, as this N-donor ligand displays similar basicity but is slightly softer compared to the carboxylate one.

The structural diversity of tetrazolate-based MOFs is currently rather unexplored compared to the carboxylate-based ones. However, a number of tetrazole-based frameworks with a series of divalent ions arranged in chloride centred square $[M(II)_4Cl]^{7+}$ clusters[17] have been described by Long *et al.* The ability to obtain inorganic clusters that were isostructural to the ones observed with carboxylates was also demonstrated.[12b,18] Other reports have shown the potential to construct well-known carboxylate based SBU $M(II)_3(\mu_3\text{-}O/OH)(RCOO)_6L_3$ trimers[19] with tetrazolate linkers. However, only one example of a MOF architecture with the pure inorganic chain $[M(II)(F)N_4]_n$ (analogue to the largely encountered carboxylate-based motif) has been reported to the best of the authors' knowledge.[20]

Tetrazole (ttz) functionalized porphyrin (H_2TTPP) (5,10,15,20-tetrakis[4-(2,3,4,5-tetrazolyl)phenyl]porphyrin) can be easily synthesized on a gram-scale[21] from a well-known [3 + 2] cycloaddition reaction starting with nitrile-bearing porphyrin and sodium azide. Unlike TCPP it has been reported only twice as a building unit in MOF architectures.[22] In both reports the frameworks displayed a **scu**-topology and the inorganic SBU was based on divalent ions arranged in square planar $[M_4Cl]^{7+}$ clusters, the overall SBU being $M_4Cl(ttz)_8$–$(H_2O)_4$. Therefore only one framework topology was reported with TTPP, hence we targeted to further develop this structural diversity using coordination chemistry with the aim of producing new porous polymeric compounds. An iron and TTPP based framework with a new topology is described in this article, displaying mixed valence iron centres; structural studies, Mössbauer spectrometry and sorption analysis are presented.

Results and discussion

Synthesis

A solvothermal reaction in DMF between hydrated iron(III) chloride and H_2TTPP in the presence of a N-donor base (pyrazine or DABCO) achieved rod-shaped single crystals of compounds labelled **1** and **2** that were suitable for single crystal diffraction (see synthetic details in the ESI†). It is worth noting that no suitable crystalline material could be yielded by the use of iron(II) based salts during the synthesis although iron(II) is present in the resulting coordination polymer, see below. Therefore, iron(III) is partially reduced to the ferrous state during the reaction course, dimethylformamide that is used as a solvent is assumed to act here as a mild reducing agent, as metallic ion reduction has been observed before through DMF oxidation to carbamic acid.[23] A structural model could be refined from laboratory diffractometer measurements for both compounds; however a more accurate structural model obtained using synchrotron radiation diffraction was developed for pyrazine-containing compound **1**. Therefore, a detailed structural description is provided for **1** only. Compound **2** was observed to be isotopic to compound **1**.

Structural description

Compound **1** crystallizes in the orthorhombic *Cmmm* space group. It displays a three dimensional framework with two independent crystallographic positions occupied by iron atoms. The porphyrin entity is metallated by the iron atom Fe1 whose environment is completed by the nitrogen atoms from the pyrazine molecule leading to chains running along the *a* axis of the unit-cell. The three-dimensional framework is created by connection of the four tetrazolates of this building block to Fe2 through one-dimensional entities made of corner sharing FeN_4O_2 octahedra (Fig. 1). Similar unidimensional chains have only been previously reported once in the literature by Pimenta *et al.*, where the coordination proceeded by N1 and N2 tetrazolate nitrogen atoms whereas here, N2 and N3 are involved.[20] As shown in Fig. 1, this atomic arrangement leads to one-dimensional channels in the *a* direction that represent ~31.5% of the unit-cell volume. The observed electronic density within these voids could not be modelled from the X-ray data.

Iron atom Fe1, located in the center of the porphyrin, is in an almost perfect octahedral environment. It lies on the intersection of three mirror planes which creates ideal N–Fe–N bond angles of 90°. The Fe1–N distances lie in a narrow range between 1.964(5) Å and 1.991(5) Å and this is in good agreement with similar Fe II compounds reported in the literature.[24] The second iron atom, Fe2, lies in a slightly distorted octahedral environment with Fe–N distances of 2.147(3) Å and a shorter Fe–O distance of 2.018(3) Å. The N–Fe–N angles range from 86.11(18)° to 93.89(18)° and the N–Fe–O from 84.44(9)° to 95.56(9)°. Bond valence calculations[25] have been performed for Fe2 (Table S4†) and suggest a Fe II/Fe III mixed oxidation state for this atomic site.

Compared to the carboxylate-based compound reported before[13] this MOF adopts the same **fry** topology, with a slight increase in the distances between inorganic chains as the tetrazolate linker is slightly extended compared to the carboxylate one. The distance between the porphyrinic cores undergoes only a slight change as it is closely related to the nature of the bridging N-donor base. In the case of DABCO-containing compound **2**, this distance is increased (from 6.7530(2) to 7.160 (2)), this variation is mainly due to the corresponding nitrogen–iron bond length increase (from 1.964(1) to 2.267(1) for

 This journal is © The Royal Society of Chemistry 2016

Published on 07 December 2016. Downloaded by Université Claude Bernard Lyon on 15/12/2016 12:07:28.

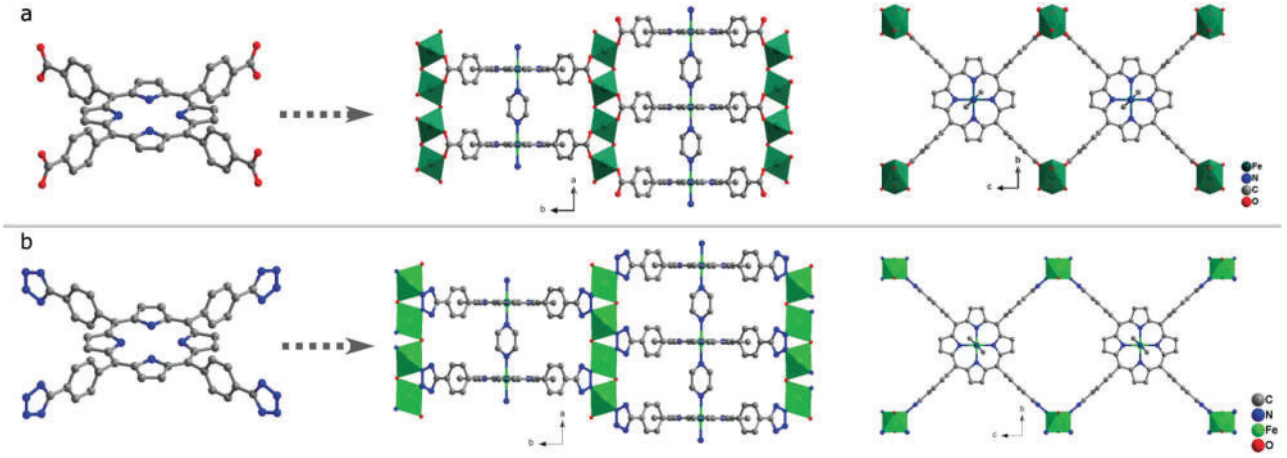

Fig. 1 a and b: Isotopic compounds obtained from the H_2TCPP and H_2TTPP porphyrins, structural view along the [001] and [100] directions.

1 and **2** respectively, see Fig. S1†) which is explained by a π-back bonding phenomenon, much stronger in the case of the conjugated pyrazine molecule.

The aforementioned mixed valence state would imply that a counter ion is present in the channels but this could not be located due to the high delocalization of the residual density within those voids. In similar carboxylate based 1-D motifs, the charge has previously been observed to be compensated by the replacement of some bridging hydroxyl groups by the neutral DMF molecule.[14]

To explore this possibility, temperature dependent IR spectroscopy was undertaken on compound **1** with heating from the initial room-temperature DMF-wet state under an inert atmosphere.

The spectra displayed in Fig. 2a show the presence of a broad band containing at least two peaks centered at 1665 cm^{-1} and 1645 cm^{-1} which are attributed to the ν(C═O) of free and bound DMF molecules respectively. Indeed, upon heating, the band at 1665 cm^{-1} strongly decreased and the lower wavenumber band became dominant at 1645 cm^{-1}. As this band was neither present in the parent porphyrinic linker nor in the bridging pyrazine (Fig. S4 and S5†), it was attributed to the iron-coordinated DMF molecules. The material integrity was mostly preserved over the temperature range in the timescale of the experiment as attested by the preservation of all other vibrational modes. At higher temperatures (above 250 °C) decomposition was noted from the broadening and loss of vibrational bands. To further confirm this assumption, a similar variable temperature experiment was performed with a sample that was first exchanged with ethanol four times, to remove all uncoordinated DMF. The spectra, seen in Fig. 2b, displayed an even clearer signal in this region, confirming the presence of a peak associated with the coordinated DMF molecule at 1645 cm^{-1}. The charge balance in this compound was thus accounted for by the replacement of an anionic bridging OH^- group by a neutral bridging DMF molecule and the chemical formula $[Fe^{II}pzTTP(Fe^{II}_{1-x}DMF_{1-x}Fe^{III}_xOH_x)]_n$ is intended, where as

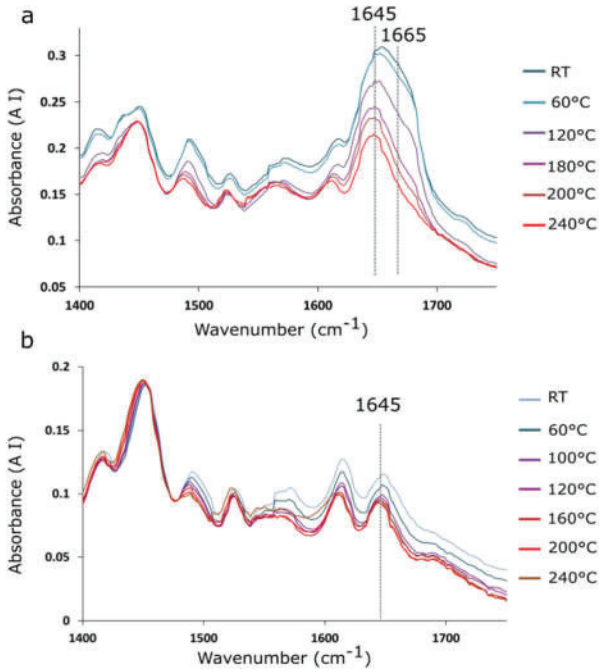

Fig. 2 a: Variable temperature IR spectra of **1** recorded in nitrogen starting from wet compound in DMF, b: variable temperature IR spectra of **1** recorded in nitrogen starting from wet compound exchanged with ethanol.

measured by Mössbauer spectrometry (see below) x is 0.25 for the fresh sample.

The phase purity of the bulk sample was confirmed from a Le Bail refinement of powder X-ray diffraction data (see ESI†). The cell parameters obtained from this refinement (a = 6.8420 (3) Å, b = 35.883(3) Å, c = 19.069(2) Å) show a slight expansion along the a and b axes and a reduction of the c parameter when compared to the single crystal data. These minor variations are attributed to a different solvation state of the powder sample, which was recorded in a DMF suspension

Published on 07 December 2016. Downloaded by Université Claude Bernard Lyon on 15/12/2016 12:07:28.

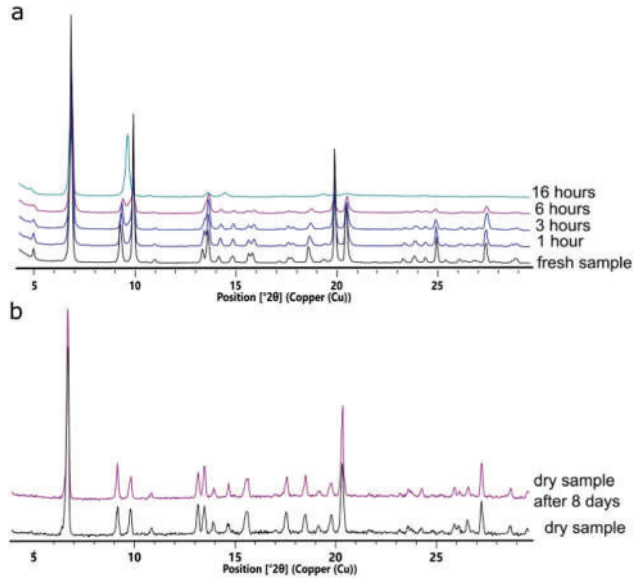

Fig. 3 a: Consecutive PXRD patterns for **1** under air during the course of 16 hours, b: PXRD of the dry sample kept under an inert atmosphere.

whereas the single crystal was not. The more highly solvated sample displayed a slightly larger cell.

Furthermore during PXRD experiments, certain changes in the pattern were observed as a function of measurement time. This was attributed to the structural changes occurring as the sample dried from the DMF-wet state. Re-immersion of the dry sample in DMF did not engender structural recovery, indicating that the structural change upon drying in air was irreversible. Single crystal diffraction of the dry sample yielded poor intensity and a low number of Bragg peaks were observed in powder diffraction, thus making the determination of the dry structure impossible. Fe II based materials are known to be often unstable when exposed to air. Therefore, an irreversible oxidation of the iron centers was suggested as a possible mechanism to explain the observed structural changes. To verify that an oxidation process was involved rather than the extra-framework DMF departure, the sample was filtered and dried at room temperature under an inert atmosphere inside a glove box. As illustrated in Fig. 3b, structural integrity is preserved for days for the dry sample in the absence of air.

To confirm and further explore the mixed valence state and the irreversible air oxidation of this material, Mössbauer studies were undertaken.

Mössbauer spectrometry

The ^{57}Fe Mössbauer spectrum of fresh compound **1** in DMF was recorded at 77 K after cooling down the powder sample suspended in DMF to yield a frozen state. It is compared with the spectrum obtained on the same sample after ageing for a few weeks and with that of a powdered sample after filtering the DMF and drying in air. The refined values of hyperfine data are listed in Table 1. As illustrated in Fig. 4, the hyperfine structure consists of a quadrupolar structure which can be decomposed into 3 different quadrupolar doublets with Lorentzian lines. One can unambiguously attribute the outer component to HS Fe II species corresponding to the Fe II in the inorganic building unit in good agreement with the values reported before for the HS Fe II tetrazolate chain.[20] The central part of the spectrum has to be decomposed into at least 2 quadrupolar components: one can be assigned to LS Fe II species of the porphyrin complex; indeed, it displays a similar signal to an analogous molecular motif bearing two N-coordinating pyridine ligands in axial positions[26] and matches well with the signal described before for a FeTCPP based MOF with a similar topology.[13] The other quadrupolar component is due to the HS Fe III located in the inorganic building unit, allowing one to conclude its mixed valence Fe state.

The inorganic SBU of the freshly prepared sample consists of approximately 75% of HS Fe II and 25% of HS Fe III. After the sample was kept in a closed vial in DMF under ambient conditions, considering the hyperfine structure, one observes a significant increase of the relative Fe III component in the inorganic SBU (from 25 to 40%), suggesting a slow oxidation phenomenon which is much stronger and faster for the air-dried sample (90% relative of HS Fe III).

Table 1 Refined values of hyperfine parameters derived from the Mössbauer spectra for compound **1** compared to literature data

Sample	δ (mm s^{-1}) (±0.01)	Δ (mm s^{-1}) (±0.02)	Attribution	% (±2)	Ref.
[Fe(TPP)(py)$_2$]	0.40	1.15	Fe(II)TPP (LS)		26
Fe(TCPP)(pz)$_2$	0.42	1.12	Fe(II)TCPP (LS)		13
Fe(II)Ttz HS	1.22	3.67	Fe(II)Ttz (HS)		20
1 in FMF (fresh sample)	0.42	1.09	Fe(II)TTPP (LS)	35	This work
	1.16	3.42	Fe(II)Ttz (HS)	50	
	0.52	1.40	Fe(III)Ttz (HS)	15	
1 in DMF (after ageing)	0.43	1.04	Fe(II)TTPP (LS)	37	This work
	1.17	3.44	Fe(II)Ttz (HS)	38	
	0.53	1.78	Fe(III)Ttz (HS)	25	
1 dried in air	0.39	0.83	Fe(II)TTPP (LS)	32	This work
	1.09	3.12	Fe(II)Ttz (HS)	7	
	0.44	1.42	Fe(III)Ttz (HS)	29	
	0.49	2.18	Fe(III)Ttz (HS)	33	

This journal is © The Royal Society of Chemistry 2016

Published on 07 December 2016. Downloaded by Université Claude Bernard Lyon on 15/12/2016 12:07:28.

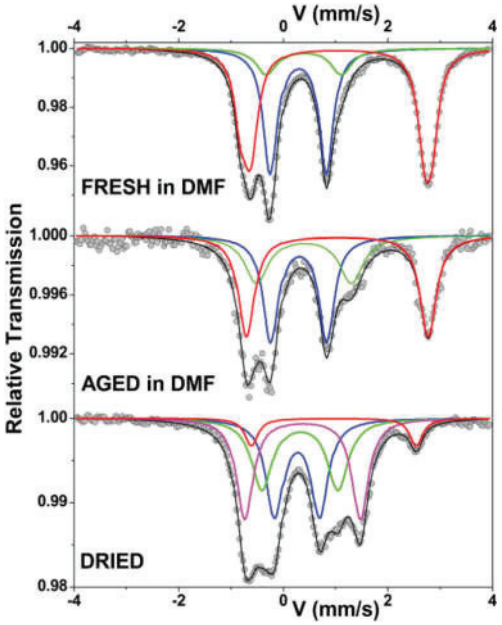

Fig. 4 Mössbauer spectra at different stages for compound **1**: red, blue, green and pink components are attributed to Fe(II)Ttz (HS), Fe(II)TTPP (LS), Fe(III)Ttz (HS) and Fe(III)Ttz (HS) species as listed in Table 1.

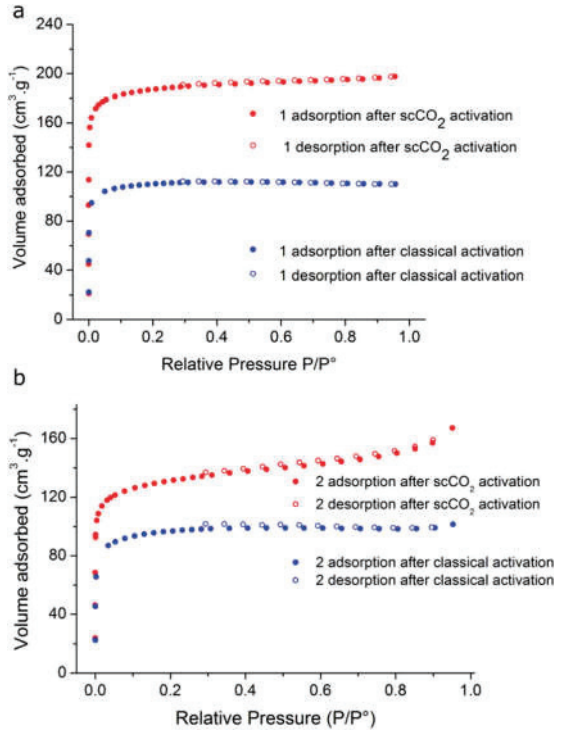

Fig. 5 Nitrogen sorption isotherms measured at 77 K for compound **1** (a) and **2** (b), comparison between classical and supercritical CO_2 activation.

Porosity

Nitrogen sorption isotherms were obtained for compounds **1** and **2** after a classical thermal activation under vacuum. Both samples displayed a permanent porosity with moderate BET surface areas of 430 $m^2\ g^{-1}$ and 370 $m^2\ g^{-1}$, respectively. As observed previously in several porphyrinic MOF systems, the accessible surface area could be increased by means of a supercritical CO_2 drying method. This process reduces the surface tension during solvent removal and to some extent prevents pore collapse. Applying supercritical activation allowed an improved BET surface area for compounds **1** and **2** of 750 $m^2\ g^{-1}$ and 510 $m^2\ g^{-1}$, respectively (Fig. 5). Here, comparison with the expected BET SA values is too complex to undertake due to the structural changes observed with PXRD during activation (Fig. S12†). The observed surface area for compound **1** is similar to the one obtained with the carboxylate phase displaying a similar morphology. The sorption studies outlined above provided evidence that the resulting dried material preserves a large intrinsic porosity even though precise quantitative conclusions are precluded due to the lack of structural data for the dry compounds.

This work evidences the first example of a mixed valence iron/tetrazole based open framework with intrinsic porosity.

Conclusions

In summary, by a reticular synthesis strategy mixed valence iron(II/III) MOFs with the **fry** topology were obtained based on tetrazolate linkers, with a similar topology to the carboxylate pure iron(III) material reported before. Structural data and Mössbauer spectrometry evidence unambiguously the mixed valence state for the iron inside the inorganic backbone. These materials display fair permanent porosity, but the lack of their chemical stability, due to iron(II) oxidation in air prevents the further exploration of their electrochemical properties. Nonetheless, for future work it is desirable to consider the construction of a framework of this topology with the replacement of the tetrazolate function by a pyrazolate one. This should enhance the chemical stability of the material and could be a useful strategy to allow further investigation of this type of mixed-valence MOF.

Acknowledgements

The authors kindly thank F. Bourdreux for the variable temperature IR analyses, Dr F. Nouar for supercritical CO_2 activation, A. Jouhara and P. Poizot for electrochemical measurements, the CTμ (Centre Technologique des Microstructures of University of Lyon) for providing the scanning electron microscopy facility and CRISTAL beamline at soleil synchrotron facility for powder diffraction data. The authors also acknowledge the French Ministry of National Education, Research and Technology, the University Lyon 1 and the CNRS for financial support; this work was supported by "cellule Energie du CNRS".

Published on 07 December 2016. Downloaded by Université Claude Bernard Lyon on 15/12/2016 12:07:28.

Notes and references

1 (*a*) J. R. Li, J. Sculley and H. C. Zhou, *Chem. Rev.*, 2012, **112**, 869–932; (*b*) D. Banerjee, A. J. Cairns, J. Liu, R. K. Motkuri, S. K. Nune, C. A. Fernandez, R. Krishna, D. M. Strachan and P. K. Thallapally, *Acc. Chem. Res.*, 2015, **48**, 211–219; (*c*) J. Liu, P. K. Thallapally, B. P. McGrail, D. R. Brown and J. Liu, *Chem. Soc. Rev.*, 2012, **41**, 2308–2322.

2 (*a*) M. Zhao, S. Ou and C. D. Wu, *Acc. Chem. Res.*, 2014, **47**, 1199–1207; (*b*) S. Ou and C. D. Wu, *Inorg. Chem. Front.*, 2014, **1**, 721–734; (*c*) D. Farrusseng, S. Aguado and C. Pinel, *Angew. Chem., Int. Ed.*, 2009, **48**, 7502–7513; (*d*) A. Corma, H. Garcia and F. Xamena, *Chem. Rev.*, 2010, **110**, 4606–4655; (*e*) A. H. Chughtai, N. Ahmad, H. A. Younus, A. Laypkov and F. Verpoort, *Chem. Soc. Rev.*, 2015, **44**, 6804–6849.

3 D. M. D'Alessandro, *Chem. Commun.*, 2016, **52**, 8957–8971.

4 B. F. Abrahams, B. F. Hoskins, D. M. Michail and R. Robson, *Nature*, 1994, **369**, 727–729.

5 (*a*) N. Kornienko, Y. Zhao, C. S. Kley, C. Zhu, D. Kim, S. Lin, C. J. Chang, O. M. Yaghi and P. Yang, *J. Am. Chem. Soc.*, 2015, **137**, 14129–14135; (*b*) I. Hod, M. D. Sampson, P. Deria, C. P. Kubiak, O. K. Farha and J. T. Hupp, *ACS Catal.*, 2015, **5**, 6302–6309.

6 J. Liu, W. Zhou, J. Liu, Y. Fujimori, T. Higashino, H. Imahori, X. Jiang, J. Zhao, T. Sakurai, Y. Hattori, W. Matsuda, S. Seki, S. K. Garlapati, S. Dasgupta, E. Redel, L. Sun and C. Woll, *J. Mater. Chem. A*, 2016, **4**, 12739–12747.

7 (*a*) S. R. Ahrenholtz, C. C. Epley and A. J. Morris, *J. Am. Chem. Soc.*, 2014, **136**, 2464–2472; (*b*) C.-W. Kung, T.-H. Chang, L.-Y. Chou, J. T. Hupp, O. K. Farha and K.-C. Ho, *Electrochem. Commun.*, 2015, **58**, 51–56.

8 (*a*) S. Patwardhan and G. C. Schatz, *J. Phys. Chem. C*, 2015, **119**, 24238–24247; (*b*) C. F. Leong, B. Chan, T. B. Faust and D. M. D'Alessandro, *Chem. Sci.*, 2014, **5**, 4724–4728; (*c*) L. E. Darago, M. L. Aubrey, C. J. Yu, M. I. Gonzalez and J. R. Long, *J. Am. Chem. Soc.*, 2015, **137**, 15703–15711.

9 (*a*) D. J. Zhang, J. C. Zhang, H. Z. Shi, X. L. Guo, Y. Y. Guo, R. C. Zhang and B. Q. Yuan, *Sens. Actuators, B*, 2015, **221**, 224–229; (*b*) F.-Y. Yi, D. Chen, M.-K. Wu, L. Han and H.-L. Jiang, *ChemPlusChem*, 2016, **81**, 675–690.

10 (*a*) C. R. Wade, M. Y. Li and M. Dinca, *Angew. Chem., Int. Ed.*, 2013, **52**, 13377–13381; (*b*) C. W. Kung, T. C. Wang, J. E. Mondloch, D. Fairen-Jimenez, D. M. Gardner, W. Bury, J. M. Klingsporn, J. C. Barnes, R. Van Duyne, J. F. Stoddart, M. R. Wasielewski, O. K. Farha and J. T. Hupp, *Chem. Mater.*, 2013, **25**, 5012–5017.

11 (*a*) Z. Y. Zhang, H. Yoshikawa and K. Awaga, *J. Am. Chem. Soc.*, 2014, **136**, 16112–16115; (*b*) G. Ferey, F. Millange, M. Morcrette, C. Serre, M. L. Doublet, J. M. Greneche and J. M. Tarascon, *Angew. Chem., Int. Ed.*, 2007, **46**, 3259–3263; (*c*) A. Fateeva, P. Horcajada, T. Devic, C. Serre, J. Marrot, J. M. Greneche, M. Morcrette, J. M. Tarascon, G. Maurin and G. Ferey, *Eur. J. Inorg. Chem.*, 2010, 3789–3794.

12 (*a*) L. E. Darago, M. L. Aubrey, C. J. Yu, M. I. Gonzalez and J. R. Long, *J. Am. Chem. Soc.*, 2015, **137**, 15703–15711; (*b*) L. Xie, S. Liu, C. Gao, R. Cao, J. Cao, C. Sun and Z. Su, *Inorg. Chem.*, 2007, **46**, 7782–7788; (*c*) L. Y. Feng, Y. H. Wang, C. W. Hu, Y. G. Li and E. B. Wang, *J. Mol. Struct.*, 2003, **650**, 115–122; (*d*) M. Maczka, A. Ciupa, A. Gagor, A. Sieradzki, A. Pikul and M. Ptak, *J. Mater. Chem. C*, 2016, **4**, 1186–1193; (*e*) Q. Sun, M. Liu, K. Li, Y. Han, Y. Zuo, J. Wang, C. Song, G. Zhang and X. Guo, *Dalton Trans.*, 2016, **45**, 7952–7959.

13 A. Fateeva, J. Clarisse, G. Pilet, J.-M. Grenèche, F. Nouar, B. K. Abeykoon, F. Guegan, C. Goutaudier, D. Luneau, J. E. Warren, M. J. Rosseinsky and T. Devic, *Cryst. Growth Des.*, 2015, **15**, 1819–1826.

14 T. R. Whitfield, X. Wang, L. Liu and A. J. Jacobson, *Solid State Sci.*, 2005, **7**, 1096–1103.

15 G. de Combarieu, M. Morcrette, F. Millange, N. Guillou, J. Cabana, C. P. Grey, I. Margiolaki, G. Ferey and J. M. Tarascon, *Chem. Mater.*, 2009, **21**, 1602–1611.

16 (*a*) M. I. Breeze, G. Clet, B. C. Campo, A. Vimont, M. Daturi, J.-M. Grenèche, A. J. Dent, F. Millange and R. I. Walton, *Inorg. Chem.*, 2013, **52**, 8171–8182; (*b*) M. E. Medina, Y. Dumont, J.-M. Greneche and F. Millange, *Chem. Commun.*, 2010, **46**, 7987–7989.

17 (*a*) M. Dincă, A. Dailly, Y. Liu, C. M. Brown, D. A. Neumann and J. R. Long, *J. Am. Chem. Soc.*, 2006, **128**, 16876–16883; (*b*) M. Dincă and J. R. Long, *J. Am. Chem. Soc.*, 2007, **129**, 11172–11176; (*c*) K. Sumida, S. Horike, S. S. Kaye, Z. R. Herm, W. L. Queen, C. M. Brown, F. Grandjean, G. J. Long, A. Dailly and J. R. Long, *Chem. Sci.*, 2010, **1**, 184–191; (*d*) M. Dincă, A. Dailly, C. Tsay and J. R. Long, *Inorg. Chem.*, 2008, **47**, 11–13.

18 S. Das, H. Kim and K. Kim, *J. Am. Chem. Soc.*, 2009, **131**, 3814–3815.

19 (*a*) J.-Q. Shen, Y.-S. Wei, P.-Q. Liao, R.-B. Lin, D.-D. Zhou, J.-P. Zhang and X.-M. Chen, *CrystEngComm*, 2016, **18**, 4115–4120; (*b*) S. Jeong, X. Song, S. Jeong, M. Oh, X. Liu, D. Kim, D. Moon and M. S. Lah, *Inorg. Chem.*, 2011, **50**, 12133–12140.

20 V. Pimenta, Q. H. H. Le, L. Clark, J. Lhoste, A. Hemon-Ribaud, M. Leblanc, J.-M. Greneche, G. Dujardin, P. Lightfoot and V. Maisonneuve, *Dalton Trans.*, 2015, **44**, 7951–7959.

21 P. J. F. Gauuan, M. P. Trova, L. Gregor-Boros, S. B. Bocckino, J. D. Crapo and B. J. Day, *Bioorg. Med. Chem.*, 2002, **10**, 3013–3021.

22 (*a*) Z. Guo, D. Yan, H. Wang, D. Tesfagaber, X. Li, Y. Chen, W. Huang and B. Chen, *Inorg. Chem.*, 2015, **54**, 200–204; (*b*) D. Liu, T.-F. Liu, Y.-P. Chen, L. Zou, D. Feng, K. Wang, Q. Zhang, S. Yuan, C. Zhong and H.-C. Zhou, *J. Am. Chem. Soc.*, 2015, **137**, 7740–7746.

23 I. Pastoriza-Santos and L. M. Liz-Marzan, *Adv. Funct. Mater.*, 2009, **19**, 679–688.

24 (*a*) W. Hiller, M. Hanack and M. G. Mezger, *Acta Crystallogr., Sect. C: Cryst. Struct. Commun.*, 1987, **43**,

 This journal is © The Royal Society of Chemistry 2016

1264–1267; (*b*) R. Patra, S. Bhowmik, S. K. Ghosh and S. P. Rath, *Dalton Trans.*, 2010, **39**, 5795–5806.
25 N. E. Brese and M. O'Keeffe, *Acta Crystallogr., Sect. B: Struct. Sci.*, 1991, **47**, 192–197.
26 (*a*) H. Kobayashi, Y. Maeda and Y. Yanagawa, *Bull. Chem. Soc. Jpn.*, 1970, **43**, 2342–2346; (*b*) J. Li, S. M. Nair, B. C. Noll, C. E. Schulz and W. R. Scheidt, *Inorg. Chem.*, 2008, **47**, 3841–3850.

Published on 07 December 2016. Downloaded by Université Claude Bernard Lyon on 15/12/2016 12:07:28.

4.7. Conclusion and perspectives

A tetrazolate based Fe(II)/(III) mixed valent MOF was obtained with a *fry* topology where the inorganic backbone consists of a [FeN_4O] chain which is similar to what has been observed with a carboxylate porphyrin based iron MOF reported before with a [$FeO_4(OH)$] inorganic chain.[50] The framework was not air stable due to the oxidation of the Fe(II) to Fe(III) in the backbone but the resultant solid after activation showed intrinsic microporosity. Due to this air instability, further investigation of electrochemical properties such as redox and spin crossover behaviour was not possible.

One way to possibly improve the stability of the framework could be by using a more basic N-donor ligand. As shown by Long et al, use of triazolates and pyrazolates can lead to frameworks with higher chemical stability.[11] Wand et al has reported a pyrazolate porphyrin based framework with a ftw-a topology, $[Ni_8(OH)_4(H_2O)_2](NiTPzP)_3$ (PCN-601) that had 12-connected $[Ni_8(OH)_4(H_2O)_2(pyrazolate)_{12}]$ nodes and a 4-connected Ni metalated 5,10,15,20-tetra(1*H*-pyrazol-4-yl)porphyrin (NiTPzP) linker. PCN-601 showed remarkable stability in acidic and basic conditions.[51] Thus, exploring Fe containing frameworks with pyrazolate based porphyrinic ligands is a possible strategy in order to obtain more stable material for investigation of their electrochemical and SCO properties. The pyrazolate equivalent of the [FeN_4O] chain like SBU has been reported by Spirkl et al.[52] The authors reported the MOF, [Fe^{III}(OH)bpz], synthesised using the 4,4'-bipyrazole linker (Figure 4-11). The structure of this MOF was stable heating up to 200 °C in air and up to 300 °C in nitrogen. This thermal stability in air represents a marked improvement in robustness compared to what was observed for the tetrazolate porphyrinic MOF. Considering the ability to obtain similar SBUs for pyrazolate and tetrazolate ligands, it seems plausible that an isotopic framework could be obtained with a pyrazolate porphyrinic ligand (Figure 4-12).

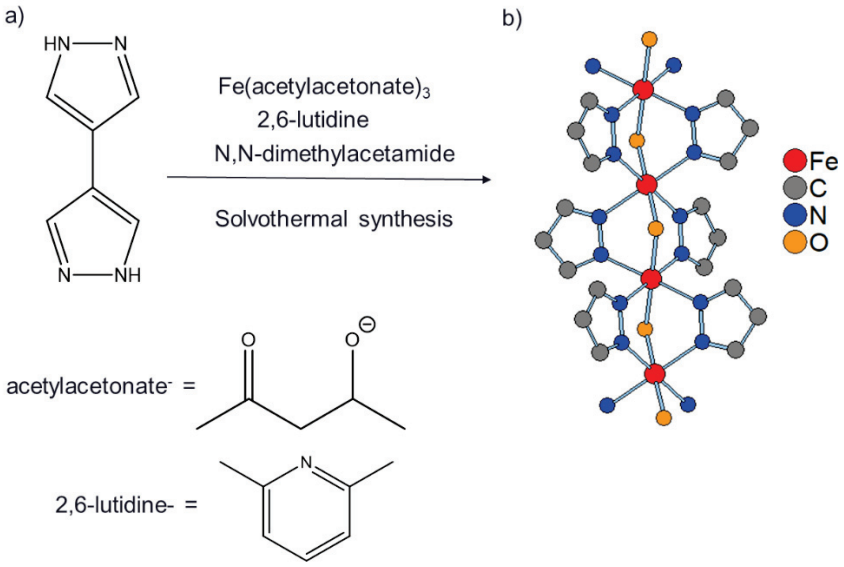

Figure 4-11 Synthesis of Fe-CFA-6. a) 4,4'-bipyrazole linker used for the syntheses of Fe-CFA-6. b) [FeN_4O)] chain like SBU [52]

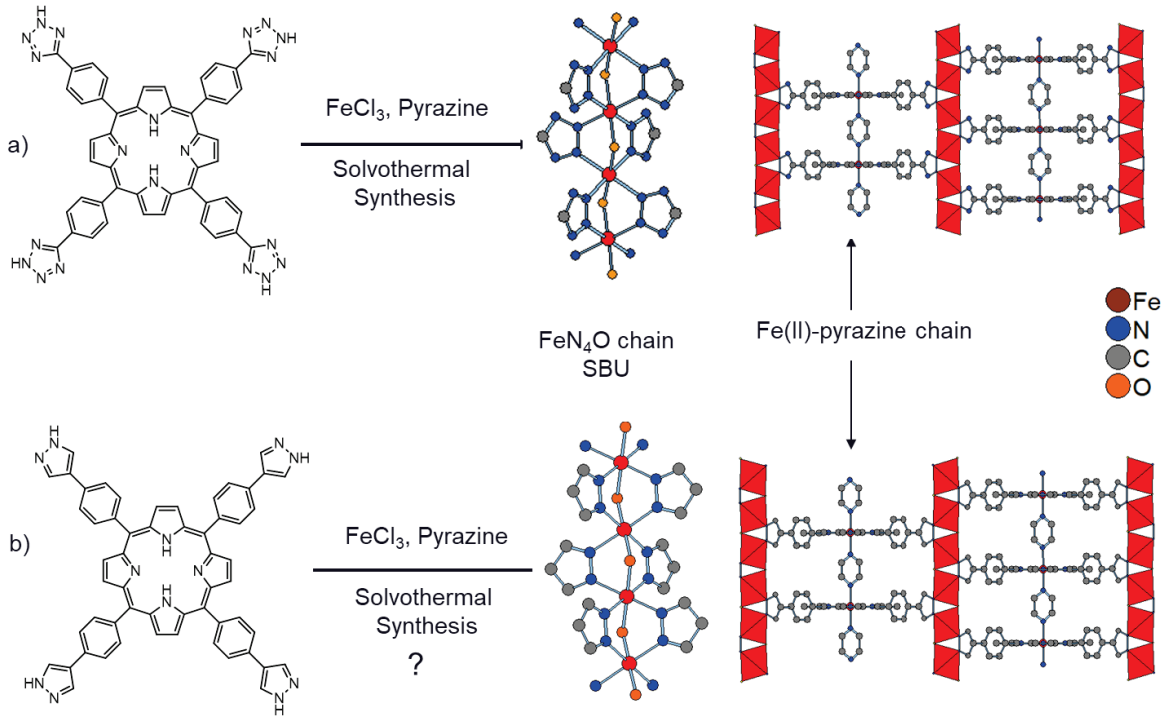

Figure 4-12 a) The structure and the SBU of the framework obtained with the tetrazolate porphyrinic ligand discussed in the published article b) The speculative structure and the SBU of a framework which is possible with a pyrazolate porphyrinic ligand.

MOFs with triply bridged Fe(III)-pyrazolate chain like SBUs have also been reported which have shown increased thermal and chemical stability. One such MOF is $Fe_2(bdp)_3$ (bdp = 1,4-benzenedipyrazole), reported by Herm et al (Figure 4-13).[53] This MOF was synthesised under anaerobic and dry conditions with $Fe(acetylacetonate)_3$ salt and DMF as solvent. Interestingly, once synthesised, the MOF was very stable and showed stability in solutions of pH=2 and heating up to 280

°C in air. Thus, it is worthwhile to investigate the reactivity of tetrazolate and pyrazolate porphyrinic MOFs under anaerobic and dry conditions to see if stable frameworks could be obtained.

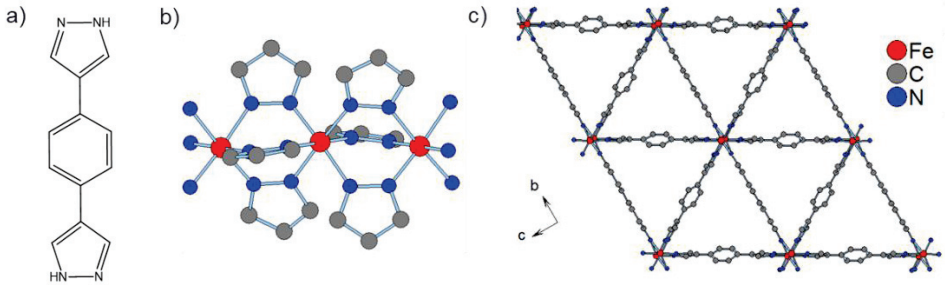

Figure 4-13 a) 1,4-benzenedipyrazole ligand used in the synthesis of $Fe_2(bdp)_3$. b) Triply bridged Fe(III)-pyrazolate chain like SBU c) Framework viewed along the b-axis. [53] Hydrogens are omitted for clarity.

4.8. References

1. Satchell, J. F.; Smith, B. J., Calculation of aqueous dissociation constants of 1,2,4-triazole and tetrazole: A comparison of solvation models. *Physical Chemistry Chemical Physics* **2002,** *4* (18), 4314-4318.
2. Zhang, J.-P.; Zhang, Y.-B.; Lin, J.-B.; Chen, X.-M., Metal Azolate Frameworks: From Crystal Engineering to Functional Materials. *Chemical reviews* **2012,** *112* (2), 1001-1033.
3. Phan, A.; Doonan, C. J.; Uribe-Romo, F. J.; Knobler, C. B.; O'Keeffe, M.; Yaghi, O. M., Synthesis, Structure, and Carbon Dioxide Capture Properties of Zeolitic Imidazolate Frameworks. *Accounts of chemical research* **2010,** *43* (1), 58-67.
4. Aromí, G.; Barrios, L. A.; Roubeau, O.; Gamez, P., Triazoles and tetrazoles: Prime ligands to generate remarkable coordination materials. *Coordination Chemistry Reviews* **2011,** *255* (5–6), 485-546.
5. Tonigold, M.; Lu, Y.; Bredenkötter, B.; Rieger, B.; Bahnmüller, S.; Hitzbleck, J.; Langstein, G.; Volkmer, D., Heterogeneous Catalytic Oxidation by MFU-1: A Cobalt(II)-Containing Metal–Organic Framework. *Angewandte Chemie International Edition* **2009,** *48* (41), 7546-7550.
6. Xie, L.; Liu, S.; Gao, C.; Cao, R.; Cao, J.; Sun, C.; Su, Z., Mixed-Valence Iron(II, III) Trimesates with Open Frameworks Modulated by Solvents. *Inorganic Chemistry* **2007,** *46* (19), 7782-7788.
7. Das, S.; Kim, H.; Kim, K., Metathesis in Single Crystal: Complete and Reversible Exchange of Metal Ions Constituting the Frameworks of Metal−Organic Frameworks. *Journal of the American Chemical Society* **2009,** *131* (11), 3814-3815.
8. Colombo, V.; Galli, S.; Choi, H. J.; Han, G. D.; Maspero, A.; Palmisano, G.; Masciocchi, N.; Long, J. R., High thermal and chemical stability in pyrazolate-bridged metal-organic frameworks with exposed metal sites. *Chemical Science* **2011,** *2* (7), 1311-1319.
9. Demessence, A.; D'Alessandro, D. M.; Foo, M. L.; Long, J. R., Strong CO2 Binding in a Water-Stable, Triazolate-Bridged Metal−Organic Framework Functionalized with Ethylenediamine. *Journal of the American Chemical Society* **2009,** *131* (25), 8784-8786.
10. Dincă, M.; Han, W. S.; Liu, Y.; Dailly, A.; Brown, C. M.; Long, J. R., Observation of Cu2+–H2 Interactions in a Fully Desolvated Sodalite-Type Metal–Organic Framework. *Angewandte Chemie International Edition* **2007,** *46* (9), 1419-1422.
11. Xiao, D. J.; Gonzalez, M. I.; Darago, L. E.; Vogiatzis, K. D.; Haldoupis, E.; Gagliardi, L.; Long, J. R., Selective, Tunable O2 Binding in Cobalt(II)–Triazolate/Pyrazolate Metal–Organic Frameworks. *Journal of the American Chemical Society* **2016,** *138* (22), 7161-7170.
12. Kostakis, G. E.; Abbas, G.; Anson, C. E.; Powell, A. K., Inclusion of a well resolved T4(2)6(2) water tape in a H-bonded, (4,7)-binodal 3D network. *CrystEngComm* **2009,** *11* (1), 82-86.
13. Dincă, M.; Yu, A. F.; Long, J. R., Microporous Metal−Organic Frameworks Incorporating 1,4-Benzeneditetrazolate: Syntheses, Structures, and Hydrogen Storage Properties. *Journal of the American Chemical Society* **2006,** *128* (27), 8904-8913.
14. Dincă, M.; Dailly, A.; Long, J. R., Structure and Charge Control in Metal–Organic Frameworks Based on the Tetrahedral Ligand Tetrakis(4-tetrazolylphenyl)methane. *Chemistry – A European Journal* **2008,** *14* (33), 10280-10285.
15. Wang, X.-S.; Tang, Y.-Z.; Huang, X.-F.; Qu, Z.-R.; Che, C.-M.; Chan, P. W. H.; Xiong, R.-G., Syntheses, Crystal Structures, and Luminescent Properties of Three Novel Zinc Coordination Polymers with Tetrazolyl Ligands. *Inorganic Chemistry* **2005,** *44* (15), 5278-5285.
16. Chen, Y.; Ren, Z.-G.; Li, H.-X.; Tang, X.-Y.; Zhang, W.-H.; Zhang, Y.; Lang, J.-P., Solvothermal syntheses, crystal structures, and luminescent properties of two novel silver(I) coordination polymers containing 5-aryl-substituted tetrazolate ligands. *Journal of Molecular Structure* **2008,** *875* (1–3), 339-345.

17. Dincă, M.; Dailly, A.; Tsay, C.; Long, J. R., Expanded Sodalite-Type Metal−Organic Frameworks: Increased Stability and H2 Adsorption through Ligand-Directed Catenation. *Inorganic Chemistry* **2008,** *47* (1), 11-13.
18. Wu, T.; Chen, M.; Li, D., A Coordination Polymer Containing Inorganic Buckybowl Analogues. *European Journal of Inorganic Chemistry* **2006,** *2006* (11), 2132-2135.
19. Deng, H.; Qiu, Y.-C.; Li, Y.-H.; Liu, Z.-H.; Zeng, R.-H.; Zeller, M.; Batten, S. R., Reversible shrinkage and expansion of a blue photofluorescent cadmium coordination polymer and in situtetrazole ligand synthesis. *Chemical communications* **2008,** (19), 2239-2241.
20. Jeong, S.; Song, X.; Jeong, S.; Oh, M.; Liu, X.; Kim, D.; Moon, D.; Lah, M. S., Metal–Organic Frameworks Based on Unprecedented Trinuclear and Pentanuclear Metal–Tetrazole Clusters as Secondary Building Units. *Inorganic Chemistry* **2011,** *50* (23), 12133-12140.
21. Yan, Z.; Li, M.; Gao, H.-L.; Huang, X.-C.; Li, D., High-spin versus spin-crossover versus low-spin: geometry intervention in cooperativity in a 3D polymorphic iron(ii)-tetrazole MOFs system. *Chemical communications* **2012,** *48* (33), 3960-3962.
22. Liu, W.-T.; Li, J.-Y.; Ni, Z.-P.; Bao, X.; Ou, Y.-C.; Leng, J.-D.; Liu, J.-L.; Tong, M.-L., Incomplete Spin Crossover versus Antiferromagnetic Behavior Exhibited in Three-Dimensional Porous Fe(II)-Bis(tetrazolate) Frameworks. *Crystal Growth & Design* **2012,** *12* (3), 1482-1488.
23. Ouellette, W.; Prosvirin, A. V.; Whitenack, K.; Dunbar, K. R.; Zubieta, J., A Thermally and Hydrolytically Stable Microporous Framework Exhibiting Single-Chain Magnetism: Structure and Properties of [Co2(H0.67bdt)3]·20 H2O. *Angewandte Chemie International Edition* **2009,** *48* (12), 2140-2143.
24. Szafranowska, B.; Beck, J., 5-Cyanotetrazolate as a Ligand and Linker in Copper(II) Complexes and Coordination Polymers. *European Journal of Inorganic Chemistry* **2013,** *2013* (18), 3167-3177.
25. Pimenta, V.; Le, Q. H. H.; Clark, L.; Lhoste, J.; Hemon-Ribaud, A.; Leblanc, M.; Greneche, J.-M.; Dujardin, G.; Lightfoot, P.; Maisonneuve, V., New iron tetrazolate frameworks: synthesis, temperature effect, thermal behaviour, Mossbauer and magnetic studies. *Dalton Trans.* **2015,** *44* (17), 7951-7959.
26. Hou, Z.-J.; Liu, Z.-Y.; Liu, N.; Yang, E.-C.; Zhao, X.-J., Four tetrazolate-based 3D frameworks with diverse subunits directed by inorganic anions and azido coligand: hydro/solvothermal syntheses, crystal structures, and magnetic properties. *Dalton Trans.* **2015,** *44* (5), 2223-2233.
27. Gauuan, P. J. F.; Trova, M. P.; Gregor-Boros, L.; Bocckino, S. B.; Crapo, J. D.; Day, B. J., Superoxide dismutase mimetics: synthesis and structure–activity relationship study of MnTBAP analogues. *Bioorganic & Medicinal Chemistry* **2002,** *10* (9), 3013-3021.
28. Guo, Z.; Yan, D.; Wang, H.; Tesfagaber, D.; Li, X.; Chen, Y.; Huang, W.; Chen, B., A Three-Dimensional Microporous Metal–Metalloporphyrin Framework. *Inorganic Chemistry* **2015,** *54* (1), 200-204.
29. Liu, D.; Liu, T.-F.; Chen, Y.-P.; Zou, L.; Feng, D.; Wang, K.; Zhang, Q.; Yuan, S.; Zhong, C.; Zhou, H.-C., A Reversible Crystallinity-Preserving Phase Transition in Metal–Organic Frameworks: Discovery, Mechanistic Studies, and Potential Applications. *Journal of the American Chemical Society* **2015,** *137* (24), 7740-7746.
30. Southon, P. D.; Liu, L.; Fellows, E. A.; Price, D. J.; Halder, G. J.; Chapman, K. W.; Moubaraki, B.; Murray, K. S.; Létard, J.-F.; Kepert, C. J., Dynamic Interplay between Spin-Crossover and Host−Guest Function in a Nanoporous Metal−Organic Framework Material. *Journal of the American Chemical Society* **2009,** *131* (31), 10998-11009.
31. Ohba, M.; Yoneda, K.; Agustí, G.; Muñoz, M. C.; Gaspar, A. B.; Real, J. A.; Yamasaki, M.; Ando, H.; Nakao, Y.; Sakaki, S.; Kitagawa, S., Bidirectional Chemo-Switching of Spin State in a Microporous Framework. *Angewandte Chemie International Edition* **2009,** *48* (26), 4767-4771.
32. Gutlich, P.; Garcia, Y.; Goodwin, H. A., Spin crossover phenomena in Fe() complexes. *Chemical Society reviews* **2000,** *29* (6), 419-427.
33. Gütlich, P.; Hauser, A.; Spiering, H., Thermal and Optical Switching of Iron(II) Complexes. *Angewandte Chemie International Edition in English* **1994,** *33* (20), 2024-2054.

34. Gütlich, P.; Gaspar, A. B.; Garcia, Y., Spin state switching in iron coordination compounds. *Beilstein Journal of Organic Chemistry* **2013,** *9*, 342-391.
35. Brooker, S., Spin crossover with thermal hysteresis: practicalities and lessons learnt. *Chemical Society reviews* **2015,** *44* (10), 2880-2892.
36. van Koningsbruggen, P. J.; Maeda, Y.; Oshio, H., Iron(III) Spin Crossover Compounds. In *Spin Crossover in Transition Metal Compounds I*, Gütlich, P.; Goodwin, H. A., Eds. Springer Berlin Heidelberg: Berlin, Heidelberg, 2004; pp 259-324.
37. Ni, Z.-P.; Liu, J.-L.; Hoque, M. N.; Liu, W.; Li, J.-Y.; Chen, Y.-C.; Tong, M.-L., Recent advances in guest effects on spin-crossover behavior in Hofmann-type metal-organic frameworks. *Coordination Chemistry Reviews* **2017,** *335*, 28-43.
38. Niel, V.; Martinez-Agudo, J. M.; Muñoz, M. C.; Gaspar, A. B.; Real, J. A., Cooperative Spin Crossover Behavior in Cyanide-Bridged Fe(II)−M(II) Bimetallic 3D Hofmann-like Networks (M = Ni, Pd, and Pt). *Inorganic Chemistry* **2001,** *40* (16), 3838-3839.
39. Ohtani, R.; Hayami, S., Guest-Dependent Spin-Transition Behavior of Porous Coordination Polymers. *Chemistry – A European Journal* **2017,** *23* (10), 2236-2248.
40. Kahn, O.; Martinez, C. J., Spin-transition polymers: from molecular materials toward memory devices. *Science* **1998,** *279* (5347), 44-48.
41. Chong, C.; Mishra, H.; Boukheddaden, K.; Denise, S.; Bouchez, G.; Collet, E.; Ameline, J.-C.; Naik, A. D.; Garcia, Y.; Varret, F., Electronic and Structural Aspects of Spin Transitions Observed by Optical Microscopy. The Case of [Fe(ptz)6](BF4)2. *The Journal of Physical Chemistry B* **2010,** *114* (5), 1975-1984.
42. Garcia, Y.; Robert, F.; Naik, A. D.; Zhou, G.; Tinant, B.; Robeyns, K.; Michotte, S.; Piraux, L., Spin Transition Charted in a Fluorophore-Tagged Thermochromic Dinuclear Iron(II) Complex. *Journal of the American Chemical Society* **2011,** *133* (40), 15850-15853.
43. Savard, D.; Cook, C.; Enright, G. D.; Korobkov, I.; Burchell, T. J.; Murugesu, M., Gradual spin crossover behaviour in a linear trinuclear FeII complex. *CrystEngComm* **2011,** *13* (16), 5190-5197.
44. Kroeber, J.; Audiere, J.-P.; Claude, R.; Codjovi, E.; Kahn, O.; Haasnoot, J. G.; Groliere, F.; Jay, C.; Bousseksou, A., Spin Transitions and Thermal Hysteresis in the Molecular-Based Materials [Fe(Htrz)2(trz)](BF4) and [Fe(Htrz)3](BF4)2.cntdot.H2O (Htrz = 1,2,4-4H-triazole; trz = 1,2,4-triazolato). *Chem. Mat.* **1994,** *6* (8), 1404-1412.
45. Bronisz, R., 1,4-Di(1,2,3-triazol-1-yl)butane as Building Block for the Preparation of the Iron(II) Spin-Crossover 2D Coordination Polymer. *Inorganic Chemistry* **2005,** *44* (13), 4463-4465.
46. Bronisz, R., Tetrazol-2-yl as a Donor Group for Incorporation of a Spin-Crossover Function Based on Fe(II) Ions into a Coordination Network. *Inorganic Chemistry* **2007,** *46* (16), 6733-6739.
47. Salles, F.; Maurin, G.; Serre, C.; Llewellyn, P. L.; Knöfel, C.; Choi, H. J.; Filinchuk, Y.; Oliviero, L.; Vimont, A.; Long, J. R.; Férey, G., Multistep N2 Breathing in the Metal−Organic Framework Co(1,4-benzenedipyrazolate). *Journal of the American Chemical Society* **2010,** *132* (39), 13782-13788.
48. Reed, D. A.; Xiao, D. J.; Gonzalez, M. I.; Darago, L. E.; Herm, Z. R.; Grandjean, F.; Long, J. R., Reversible CO Scavenging via Adsorbate-Dependent Spin State Transitions in an Iron(II)–Triazolate Metal–Organic Framework. *Journal of the American Chemical Society* **2016,** *138* (17), 5594-5602.
49. Sciortino, N. F.; Ragon, F.; Zenere, K. A.; Southon, P. D.; Halder, G. J.; Chapman, K. W.; Piñeiro-López, L.; Real, J. A.; Kepert, C. J.; Neville, S. M., Exploiting Pressure To Induce a "Guest-Blocked" Spin Transition in a Framework Material. *Inorganic Chemistry* **2016,** *55* (20), 10490-10498.
50. Fateeva, A.; Clarisse, J.; Pilet, G.; Grenèche, J.-M.; Nouar, F.; Abeykoon, B. K.; Guegan, F.; Goutaudier, C.; Luneau, D.; Warren, J. E.; Rosseinsky, M. J.; Devic, T., Iron and Porphyrin Metal–Organic Frameworks: Insight into Structural Diversity, Stability, and Porosity. *Crystal Growth & Design* **2015,** *15* (4), 1819-1826.
51. Wang, K.; Lv, X.-L.; Feng, D.; Li, J.; Chen, S.; Sun, J.; Song, L.; Xie, Y.; Li, J.-R.; Zhou, H.-C., Pyrazolate-Based Porphyrinic Metal–Organic Framework with Extraordinary Base-Resistance. *Journal of the American Chemical Society* **2016,** *138* (3), 914-919.

52. Spirkl, S.; Grzywa, M.; Zehe, C. S.; Senker, J.; Demeshko, S.; Meyer, F.; Riegg, S.; Volkmer, D., Fe/Ga-CFA-6 - metal organic frameworks featuring trivalent metal centers and the 4,4[prime or minute]-bipyrazolyl ligand. *CrystEngComm* **2015,** *17* (2), 313-322.
53. Herm, Z. R.; Wiers, B. M.; Mason, J. A.; van Baten, J. M.; Hudson, M. R.; Zajdel, P.; Brown, C. M.; Masciocchi, N.; Krishna, R.; Long, J. R., Separation of Hexane Isomers in a Metal-Organic Framework with Triangular Channels. *Science* **2013,** *340* (6135), 960-964.

Chapter 5:

Catecholate and Gallate Based Porphyrinic MOFs

Table of contents

5. Catecholate and gallate based porphyrinic MOFs

This chapter will present the work done on investigating the reactivity of two different hydroxyphenyl functionalised porphyrins: Catechol based 5,10,15,20-tetrakis(3,4-dihydroxyphenyl)porphyrin (H_{10}-PorphCat) and gallol based 5,10,15,20-tetrakis(3,4,5-trihydroxyphenyl)porphyrin (H_{14}-PorphGal) shown in Figure 5-1. The study concerning the catechol functionalised porphyrin was part of a long-term project in collaboration with the Institut Lavoisier de Versailles (ILV) and involved the synthesis optimisation of an iron MOF phase which led to obtaining single crystals for structural elucidation (Section 5.1).

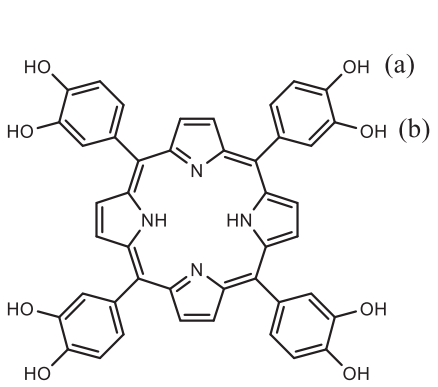

5,10,15,20-tetrakis(3,4-dihydroxyphenyl) porphyrin (H_{10}-PorphCat)

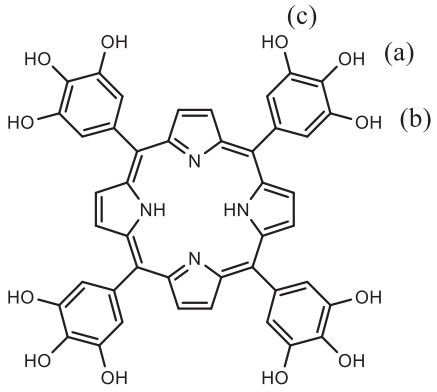

5,10,15,20-tetrakis(3,4,5-trihydroxyphenyl) porphyrin (H_{14}-PorphGal)

Figure 5-1 The two hydroxyphenyl functionalised porphyrin ligands studied in this chapter.

In section 5.2 of the chapter, the initial exploratory work performed using a gallol functionalised porphyrin and various trivalent metal ions is presented. The part of the study concerning the MOF phase obtained with trivalent rare earth metal ions was published in an article provided in the section 5.2.2.

5.1. Investigation of the reactivity of catechol porphyrin based ligands with Fe(III) for MOF synthesis

Metal-ligand bond strength is one of the main factors in determining the chemical stability of MOF frameworks as alluded to earlier. One approach to increasing this bond strength is by using functional groups which are more basic. 1,2-dihydroxyphenyl or catechol functionalities have a higher pK_a (pK_a a ~9.5; pK_a b ~14, a and b notation according to Figure 5-1)[1] compared to the carboxylic acid group (pK_a ~4.8).[2] There have been catecholate based MOFs reported in literature. Nguyen et al reported a series of 3D MOFs based on the linker triphenylene-2,3,6,7,10,11-hexakis(olate) (THO^{6-}).[3] One of the MOFs in this series, Fe-CAT-5 [chemical formula $Fe(THO)\cdot Fe(SO_4)(DMA)_3$, DMA=

dimethylammonium], showed stability in water and high proton conductivity. However, there is only one reported instance of a coordination polymer based on a catechol functionalised porphyrinic ligand. Jin et al reported several crystalline solids based on H_{10}-PorphCat and divalent Cu, Co and Ni.[4] The actual structures of these solids were not determined as the authors were interested in synthesising hybrid composites via thermolysis.

Reactivity of various trivalent metals (Fe^{3+}, Ga^{3+}, Al^{3+}, In^{3+}) with H_{10}-PorphCat based ligands have been investigated at ILV. These studies were performed using the nickel(II) metalated porphyrin (Ni-H_8-PorphCat) and have led to the identification of three different phases (Figure 5-2). Phases 1 and 3 had given microcrystalline powder and phase 2 resulted in single crystals. Gas adsorption measurements performed on phase 1 and phase 2 have indicated microporosity with BET surface areas of 475 and 760 m^2g^{-1} respectively (the adsorption studies for phase 3 were not completed). The unit cell parameters for the phases have been determined but attempts made to elucidate the structures have not been successful.

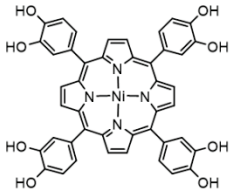

@ 150 °C for 48h

6 eq Metal salt,
30 eq additive
solvent

a) Phase 1

Metal salt	$AlCl_3$	$FeCl_3$	$InCl_3$
Solvent	DMF/H_2O	DMF	DEF
Additive	Pyrocatechol	Pyrocatechol	Pyrocatechol

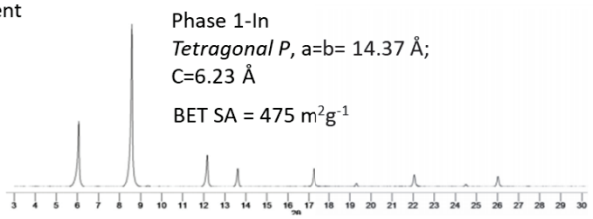

b) Phase 2

Metal salt	$AlCl_3$	$FeCl_3$	$Ga(NO_3).xH_2O$
Solvent	DEF	DEF	DEF
Additive	Pyrocatechol	Pyrocatechol	Pyrocatechol

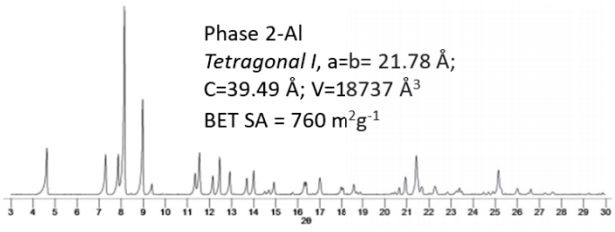

c) Phase 3

Metal salt	$InCl_3$	$In(NO_3)_3.xH_2O$
Solvent	DEF	DEF
Additive	Pyrocatechol	Pyrocatechol

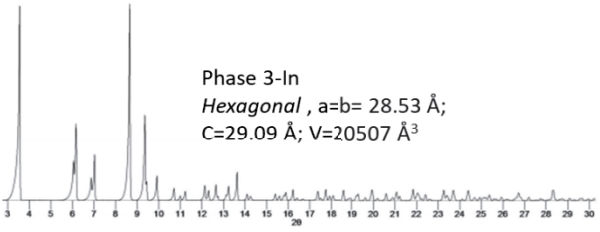

Figure 5-2 The different phases previously identified at ILV with Ni-H_8-PorphCat and various trivalent metal salts. The reaction conditions which have given each phase are indicated in the tables.

It was also demonstrated by Dr. A. Fateeva that when the nickel porphyrin is replaced by the free base (H_{10}-PorphCat), the phase 1 material could be obtained with low crystallinity. However, when pyrazine was added to the synthesis mixture, small single crystals of a material similar to phase 1 were obtained and the PXRD pattern evidenced a great increase of the crystallinity (Figure 5-4 a and b).

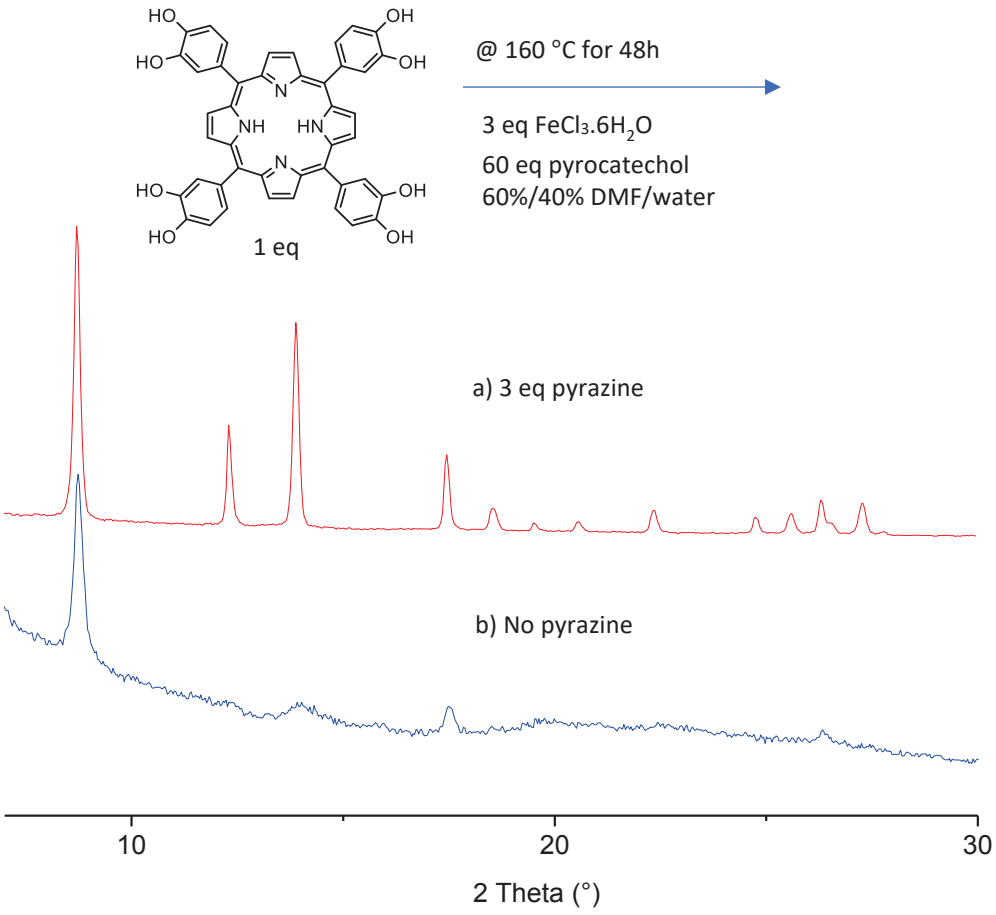

Figure 5-3 PXRD patterns observed for phase 1 obtained with H_{10}-PorphCat a) with and b) without pyrazine

In this section, the impact of the synthesis parameters on the crystal morphology was studied more in-depth with a goal of obtaining suitable single crystals for diffraction studies.

More precisely the parameters optimised were:

-pyrocatechol content

-pyrazine content

-temperature

-solvent composition

5.1.1. Synthesis optimisation

The synthetic parameters investigated are shown in Table 5-1. In total 18 reactions were attempted and the details are given in appendix section C.1.

The 1,2-dihydroxyphenyl (catechol) functionalised porphyrin was synthesised in a form with both the unprotonated and doubly protonated free base phases as described in chapter 2. For simplicity, the ligand used for the syntheses will be referred to as H_{10}-PorphCat (the molar mass of the pure freebase porphyrin ligand was used for calculating reactant ratios, 742.74 $gmol^{-1}$)

Table 5-1 Synthetic parameters investigated for the optimisation of the single crystals obtained.

Parameters investigated	
Additives	Pyrazine
Ratio of metal/ligand	3, 6
Isotherm temperature	140-150-160-180 °C
Heating rate and cooling rate	0.38 °C/min
Solvent mix (DMF/Water)	15%/85%, 20%/80%, 60%/40%, 80%/20%
Concentration of the porphyrin ligand	12.5 mM, 16.5 mM
Pyrocatechol amount	15 eq, 30 eq, 60 eq,

The starting point of the study was the conditions which gave the better crystallinity as shown in Figure 5-3a. The solvent composition was first investigated while keeping the other conditions the same (temperature 160 °C, metal: porphyrin: pyrazine: pyrocatechol = 3:1:3:60, porphyrin concentration = 12.5 mM). Increasing the DMF content from 60 to 80% had a detrimental effect on crystallinity as shown in Figure 5-4. Decreasing the DMF content to 20 % and 15% resulted in similar PXRD patterns. When the morphology of these later samples was examined by SEM (Figure 5-5), the largest single crystals (of around 25 µm for the largest observed) were found to arise from the synthesis using 20%/80% DMF/water mixture. This sample also had a large size distribution for the crystals (~2 µm - ~25 µm). However, due to the higher upper limit observed for the crystal size with this solvent composition, it was selected to investigate the remaining parameters.

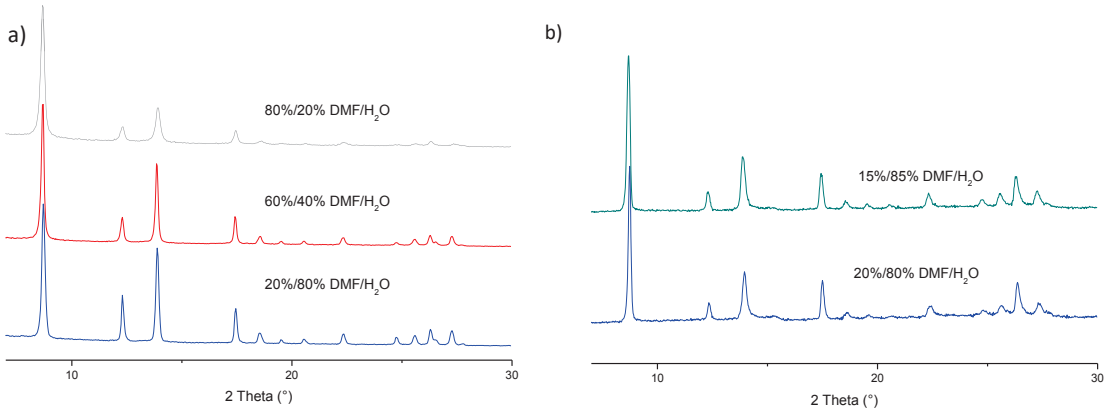

Figure 5-4 PXRD patterns for the solids obtained from the syntheses investigating the effect of the DMF and water content in the solvent. PXRD patterns in a) measured with instrument 1 and the patterns in b) measured with instrument 2.

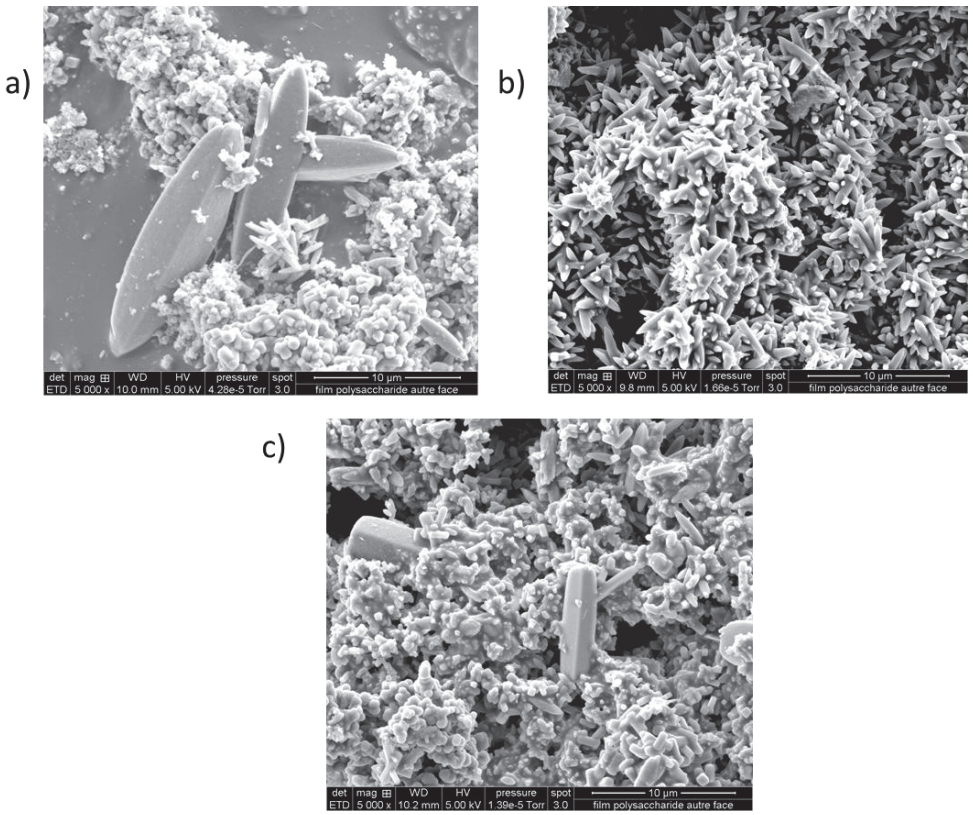

Figure 5-5 SEM images of the products obtained for the syntheses investigating DMF to water content in the solvent. a) 20%/80% DMF to water ratio b) 15%/85% DMF to water ratio c) 60%/40% DMF to water ratio.

The impact of the reactants concentration was next probed. Increasing the concentration by 1.3 times (16.5 mM vs 12.5 mM for the porphyrin ligand) had little effect on the PXRD pattern (Figure 5-6). However, this higher concentration produced qualitatively smaller single crystals when observed with SEM compared to the largest crystals observed with the lower concentration (Figure 5-6). Therefore, a concentration of 12.5 mM was kept as optimum for the subsequent reactions.

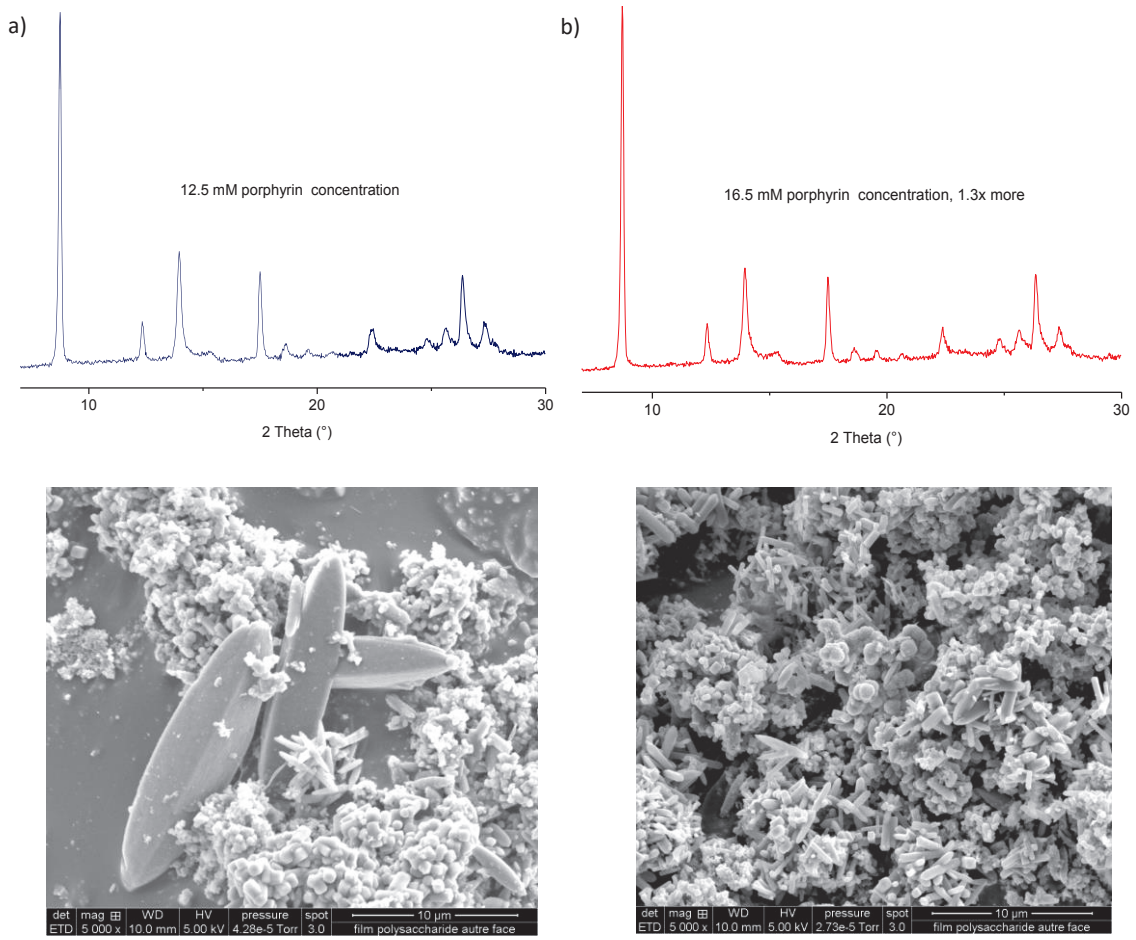

Figure 5-6 PXRD and SEM data comparing the effect of concentration on the samples obtained a) lower concentration (12.5 mM for the porphyrin) b)1.3 times higher concentration (16.5 mM for the porphyrin). solvent= 20%/80% DMF/water, metal: ligand: pyrazine: pyrocatechol = 3:1:3:60, temperature= 160 °C.

The metal to the porphyrin ligand ratio was then looked at while keeping the other reaction conditions unchanged (solvent 20%/80% DMF/water, porphyrin: pyrazine: pyrocatechol = 1:3:60, temperature= 160 °C, concentration = 12.5 mM for the porphyrin ligand). The analysis of the pxrd data indicated that a higher metal to ligand ratio of 6:1 leads to the formation of Fe_2O_3 impurities which is not seen with a metal to ligand ratio 3:1 (Figure 5-7). Therefore, the lower ratio was chosen as the metal to ligand ratio.

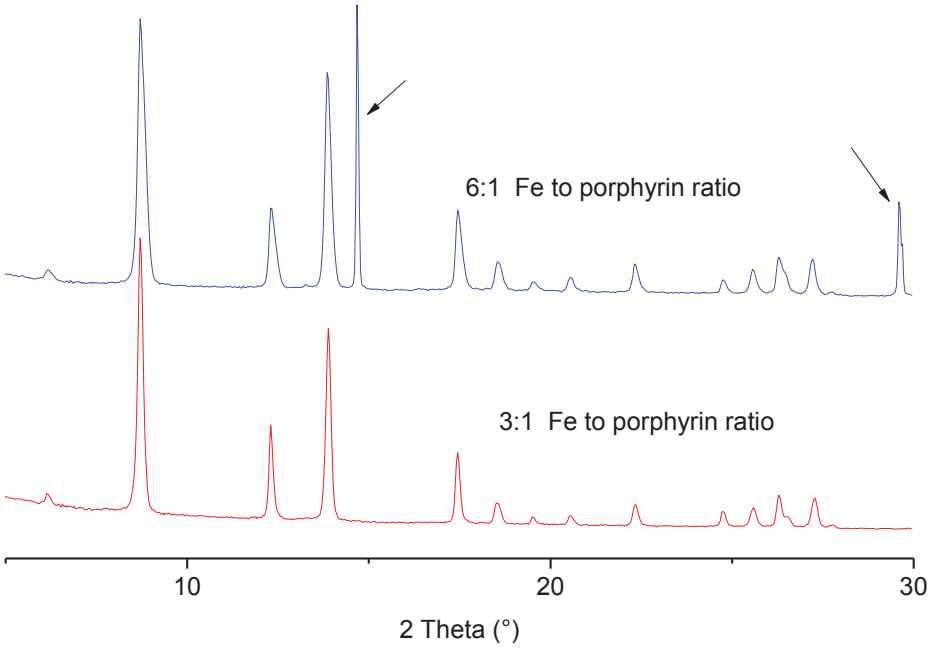

Figure 5-7 PXRD patterns for samples obtained from the syntheses investigating the metal to ligand ratio effect. The peaks with arrows pointed at them represent the Fe_2O_3 impurity.

The effect of temperature on the crystallinity and the crystal morphology was then investigated keeping the other parameters unchanged (solvent 20%/80% DMF/water, metal: porphyrin: pyrazine: pyrocatechol = 3:1:3:60 concentration = 12.5 mM for the porphyrin ligand). According to the pxrd data, the optimum synthesis temperature was assigned to be 150 and 160 °C as the solids obtained at 140 °C and 180 °C displayed lower crystallinity (Figure 5-8). SEM analysis showed that the samples obtained at 140 °C and 180 °C also had different morphologies to that observed for samples synthesised at 160 °C (Figure 5-9). Samples synthesised at 150 °C and 160 °C had the same morphologies and similar sizes (largest around 25 µm). Therefore, 160 °C was selected as the best temperature.

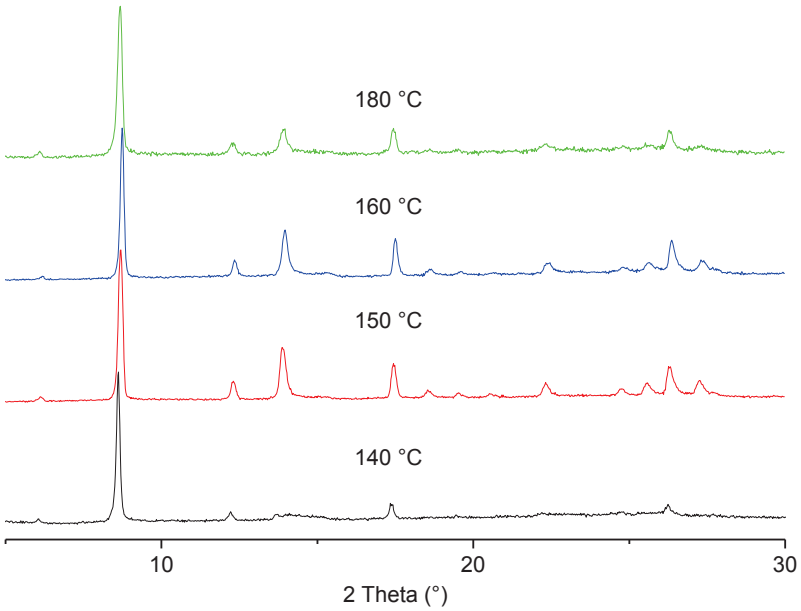

Figure 5-8 PXRD patterns of samples obtained for syntheses at different temperatures. The samples were analyzed using pxrd instrument 2.

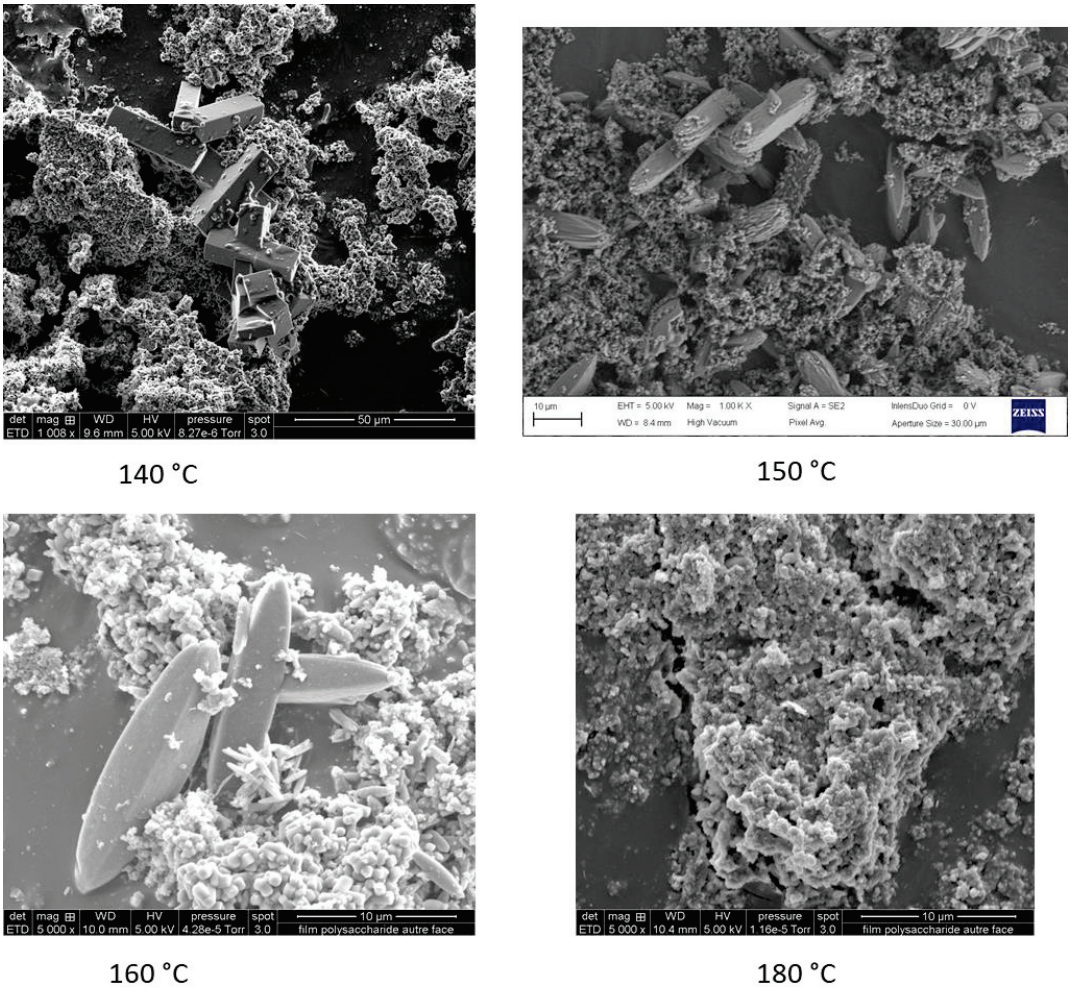

Figure 5-9 SEM images of samples synthesised at different temperatures (solvent 20%/80% DMF/water, metal: porphyrin: pyrazine: pyrocatechol = 3:1:3:60).

The amount of pyrocatechol was then investigated and was found to have a considerable influence on the size of the crystals. A lower pyrocatechol content increased the size of the crystals as shown on Figure 5-10. Thus, 15 equivalents of pyrocatechol were the optimum content tested as it led to the largest single crystals.

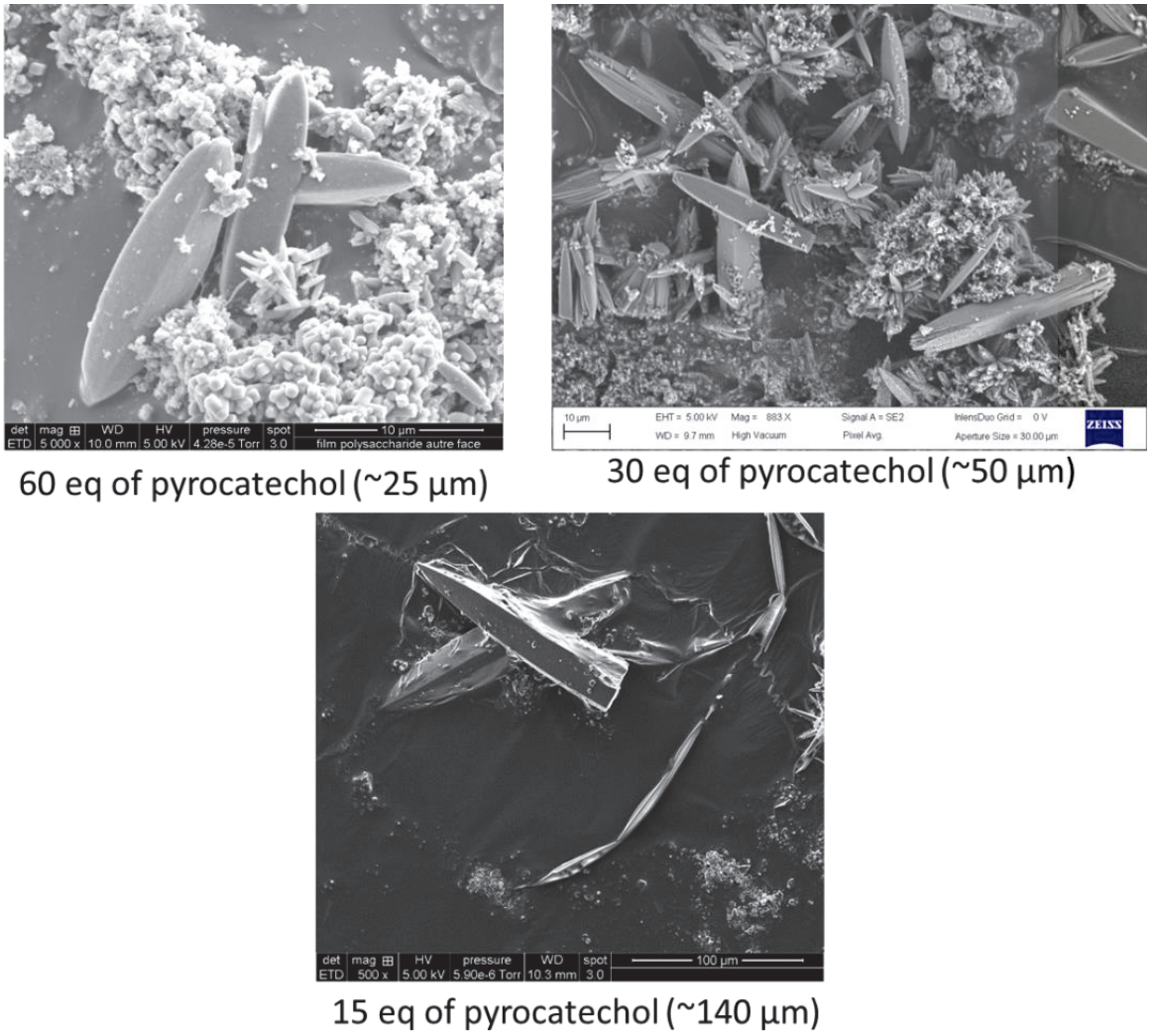

Figure 5-10 SEM images of syntheses performed with different pyrocatechol amounts. Number of equivalents (eq) are with respect the amount of porphyrinic ligand used. The size of the biggest crystals observed is shown in parentheses. These syntheses were performed at 160 °C.

In total 18, different reactions were performed for the synthesis optimisation and the size of the crystals were increased to 140 µm starting from under 20 µm. From all the parameters tested, the one which had the biggest effect on the crystal size was the amount of pyrocatechol present in the reaction mixture. The largest crystals were obtained from the synthesis at 160 °C, with a reactant ratio of 3:1:3:15 for metal: porphyrin: pyrazine: pyrocatechol and a DMF/water solvent mixture of 20%/80% and were analysed with synchrotron diffraction. The structural resolution is still ongoing.

5.1.2. Characterisation

TGA analysis

Analysis of the TGA data for the sample synthesised with the optimum conditions is shown on Figure 5-11.. There is around 5% mass loss between 30 °C and 100 °C which can be attributed to the loss of water or acetone. The framework degradation for the solids starts at around 170 °C.

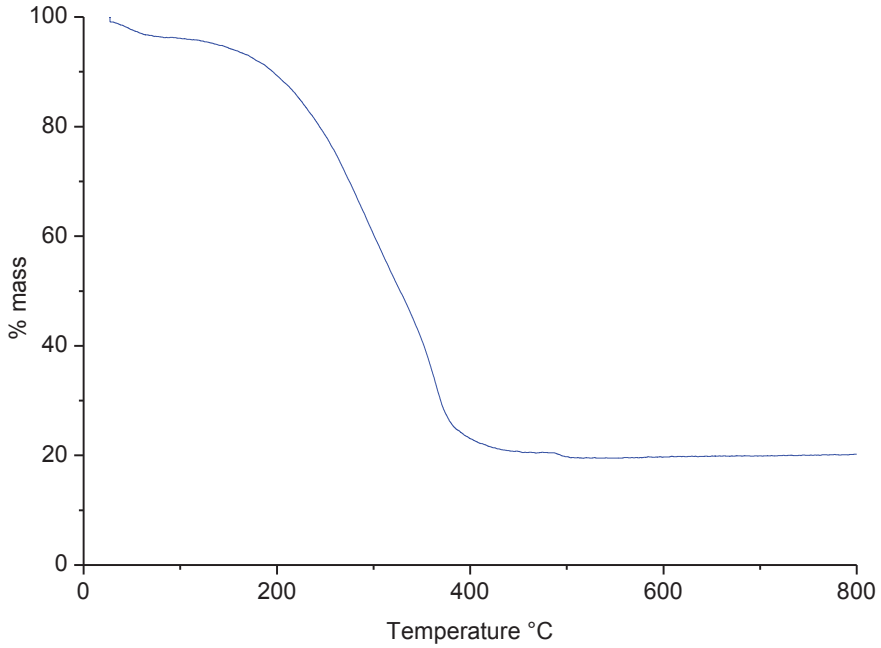

Figure 5-11 TGA analysis of the sample obtained with the optimized conditions.

IR spectroscopy

IR spectrum for the sample synthesised with the optimised conditions is shown in Figure 5-12; it is different to the spectrum of the starting porphyrin. The broad peak at around 3200 cm^{-1} corresponding to the OH stretch in the starting ligand is not present in the activated MOF sample. This indicates the loss of hydrogens and the coordination to the metal. However, the information that can be derived from the IR spectra is limited due to the lack of other defining features.

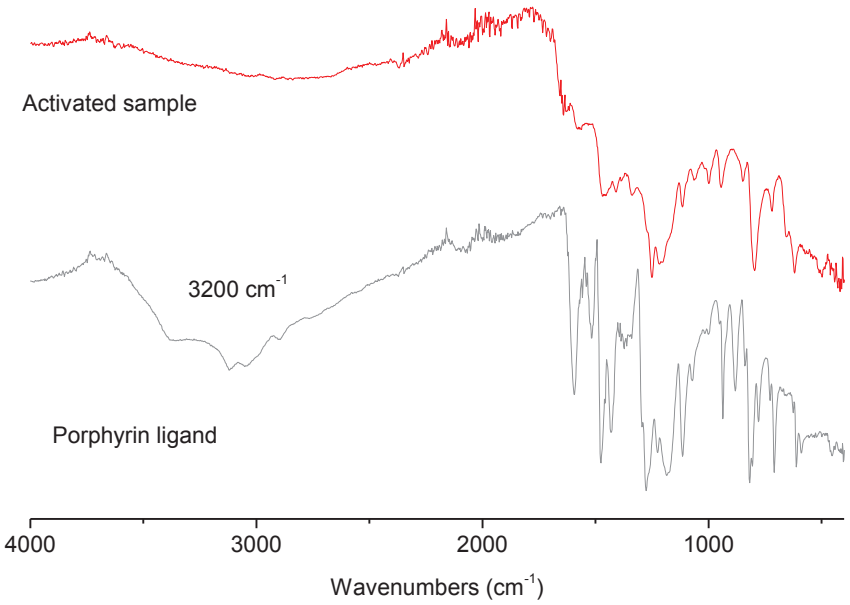

Figure 5-12 IR spectra for activated sample obtained with the optimised synthesis conditions and the starting ligand.

BET surface area analysis

The solid was activated at 120 °C under vacuum for 12 hours before the N_2 adsorption/desorption measurements. The pxrd patterns of the sample before and after the activation were similar with no shift in the peaks indicating that the framework does not change upon the activation (Figure 5-13). N_2 adsorption/desorption isotherms measured at 77 K are shown in Figure 5-14 and displayed a type 1 isotherm which indicates microporosity. The BET surface area calculated for the sample, 449 m^2g^{-1}, is similar to what was found out for the phase 1 synthesised at the Institut Lavoisier de Versailles with the Ni metalated H_8-PorphCat (475 m^2g^{-1}). However, the reproducibility of this data was not determined as only one batch was analysed.

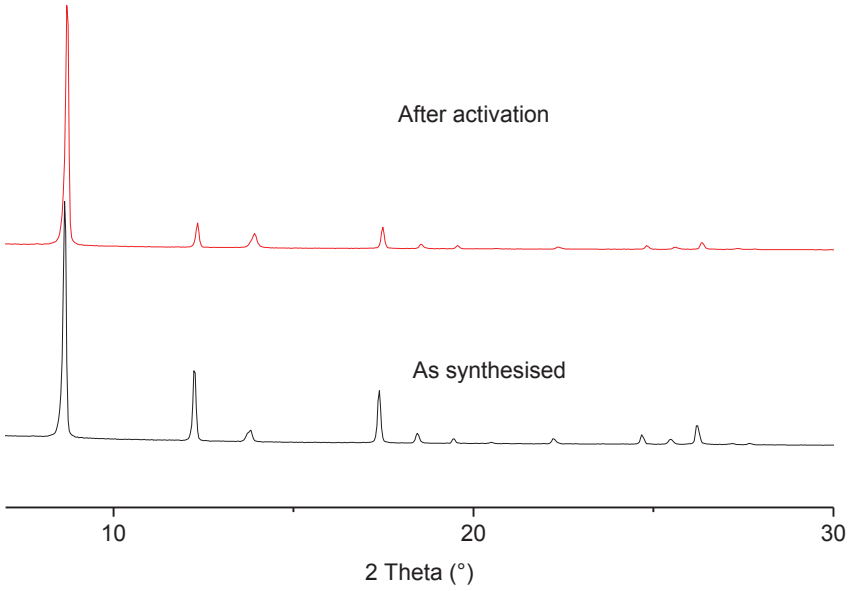

Figure 5-13 PXRD patterns for the sample before and after activation at 120 °C under vacuum for 12 hours.

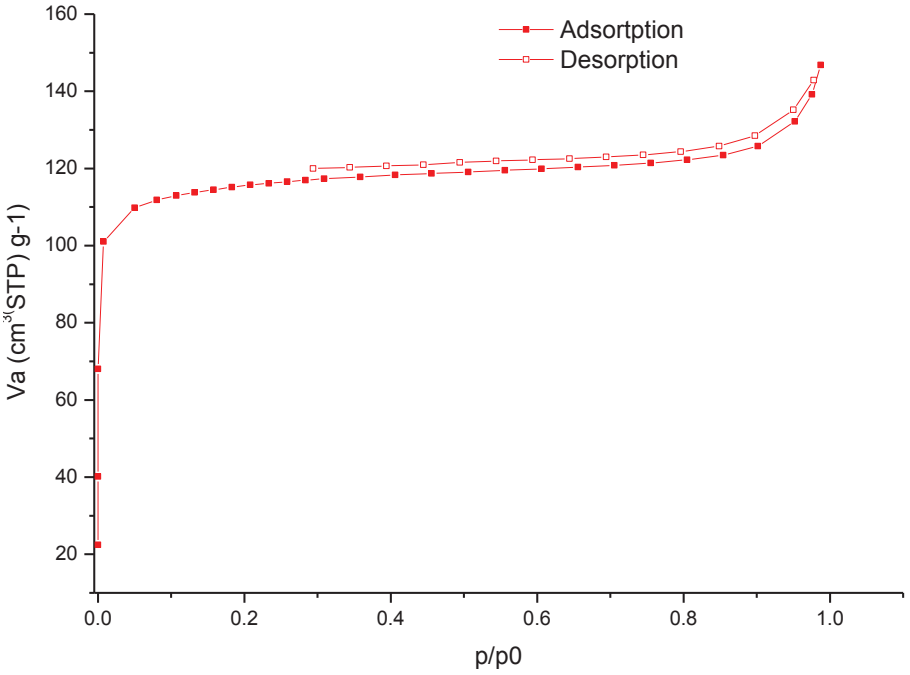

Figure 5-14 N_2 adsorption/desorption isotherms at 77 K for the sample from synthesised with the optimised conditions.

5.1.3. Conclusions and perspectives

This part of the study was a continuation of the investigation in to solids obtained at ILV with trivalent metal salts and H_{10}-PorphCat based ligands. The system with $FeCl_3.6H_2O$, H_{10}-PorphCat, pyrocatechol and pyrazine was optimised for obtaining better single crystals in terms of size via studying the effect of different parameters. The size of the single crystals was increased starting from under 20 µm up to increase to 140 µm. These crystals were analysed with synchrotron diffraction and the work relating to the structural resolution is still ongoing.

The characterisation of the bulk samples synthesised with the optimised conditions indicated that the framework possesses permanent porosity which is similar to what was obtained for a similar phase at ILV but the verification of its reproducibility is yet to be conducted. However, accurate analysis of the purity/composition of the sample is difficult without knowledge of the exact nature of the framework structure.

The effect of pyrazine as an additive on systems with other trivalent metal ions studied at ILV has not been determined. Therefore, investigating this remains an interesting possibility for these metal ions with both metalated and free base H_8-PorphCat ligands.

5.2. Investigating MOF synthesis with gallol porphyrin based ligands

Similar to earlier described catechol groups 1,2,3-trihydroxyphenol (gallol) functionality also has the potential to yield stable frameworks due to its high basicity (pK_aa ~9.3; pK_ab ~11 ; pK_ac ~14, a, b and c notation according to Figure 5-1).[5]

There are a few 3D MOF structures based on this functionality (Table 5-2) while there are no 2D frameworks reported to the best of the authors knowledge. All except one of these frameworks have been reported with gallic acid (3,4,5-trihydroxybenzoic acid) (Figure 5-15a) as the ligand with both gallol and carboxylate functionalities involved in metal coordination in the structure. The frameworks had chain like SBUs made up from MO_6 octahedra where four oxygen atoms come from the phenol groups and two from the carboxylate function (Figure 5-15b), with triangular channels along the c-axis (Figure 5-15c).

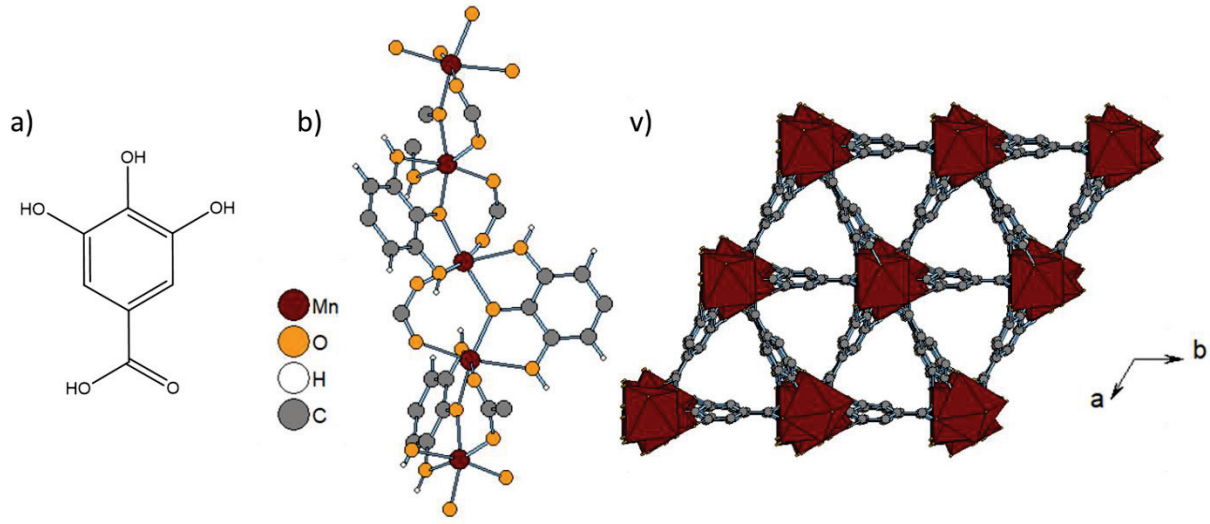

Figure 5-15 a) Ligand used, gallic acid (3,4,5-trihydroxybenzoic acid, H_4-GA) b) MO_6 chain like SBU seen in Mn(H_2-GA)·2H_2O c) View of the structure along the c-axis showing triangular channels.[6] Solvent molecules are omitted for clarity.

Table 5-2 Reported MOF structures based on the gallate functional group. Only 2D and 3D structures were considered.

Ref Code	Formula	Net type	reference
GELVEZ01	Mn(H_2-GA)·2H_2O	3D	[6]
GELVID01	Ni(H_2-GA)·2H_2O	3D	[6]
ITETEH	Fe(H_1-GA)·2H_2O	3D	[6]
N/A	Mg(H_2-GA)·2H2O	3D	[7]
TATYOF	[$Ca_3K_2(H_2O)_2(GA)_2$]·5H_2O	3D	[8]
N/A	[$Ca_2(H_2O)(H_2$-GA$)_2$]·2H_2O	3D	[8]
WUTBEU	Zr(H_2-TzGal)·x(H_2O)y(DMA)	3D	[9]

H_4-GA = 3,4,5-trihydroxybenzoic acid (gallic acid)
H_6-TzGal = 5,5'-(1,2,4,5-tetrazine-3,6-diyl)bis(benzene-1,2,3-triol)
DMA= Dimethylamine

One single MOF based solely on the gallate functionality, MIL-163 [chemical formula Zr(H_2-TzGal)·x(H_2O)y(DMA), H_6-TzGal = 5,5'-(1,2,4,5-tetrazine-3,6-diyl)bis(benzene-1,2,3-triol), DMA= Dimethylamine)], was reported in 2015 by the ILV.[9] In MIL-163, each Zr^{4+} is chelated by four TzGal linkers giving rise to an 8-fold coordination around the metal ion. Conversely each TzGal chelates four Zr^{4+} ions. This led to a porous framework comprised of ZrO_8 chains running along the c-axis (Figure 5-16b) interconnected by the TzGal linkers with square shaped channels of 12 Å×12 Å (Figure 5-16c). This material has shown remarkable chemical stability even in the presence of competitive coordinative species, such as phosphate ions.

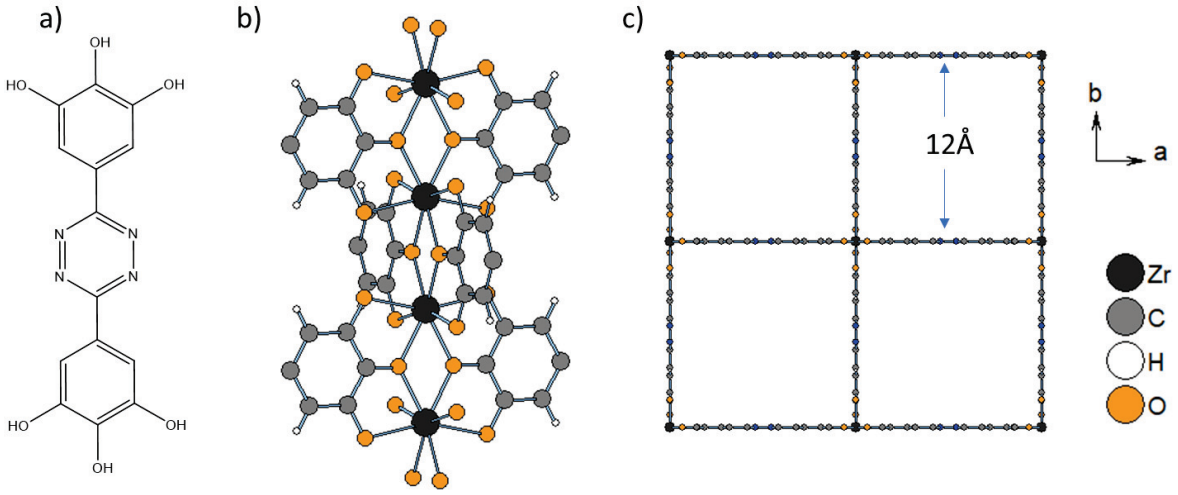

Figure 5-16 a) Ligand used, 5,5'-(1,2,4,5-tetrazine-3,6-diyl)bis(benzene-1,2,3-triol) (H_6-TzGal), b) ZrO_8 chain like SBU c) Structure of MIL-163 along the c-axis showing square shaped channels of 12 Å×12 Å (taking in to account van der Walls radii of atoms).[9] Solvent molecules are omitted for clarity.

Attempts were made to transpose MIL-163 topology into a framework starting with the porphyrinic ligand, 5,10,15,20-tetrakis(3,4,5-trihydroxyphenyl)porphyrin (H_{14}-PorphGal) and zirconium salts by Dr. Georges Mouchaham et al at the ILV. This led to the successful synthesis of the MIL-173(Zr) [Zr_2(H_6-PorphGal)(DMF,$H_2O)_n$] which is described in the article (section 5.2.2). Our contribution to this work involved synthesising the MIL-173-(Zr) for further analysis and carrying out the post-synthetic cobalt metalation. Furthermore, the reactivity of this porphyrin ligand with various RE metals was investigated using high throughput synthesis methods. The initial exploratory syntheses are described in section 5.2.1 and the characterisation of the solids obtained is discussed in the article.

The reactivity of this porphyrin ligand (H_{14}-PorphGal) with other trivalent metals was also investigated and the initial results obtained are described in section 5.2.3.

The ligand used for the study was synthesised according to the method described in chapter 2 and was obtained in the diprotonated form with two bromide counter ions for charge balance (H_{16}-PorphGal-2Br, $C_{44}H_{32}N_4O_{12}Br_2$, 968.55 $gmol^{-1}$)

5.2.1. Reactivity of RE metals with H_{14}-PorphGal

This work was performed at the ILV using their high-throughput synthesis facilities. These facilities are described in detail in the experimental section. For this study, the starting conditions were similar to those developed by G. Mouchaham for the MIL-173(Zr) phase synthesis: Metal to ligand ratio =3.6:1, isotherm temperature 120 °C, heating program 2h-12h-4h, solvent= 50%/50% DMF/water.

First, $Gd(NO_3)_3.6H_2O$ was used as the metal source due to gadolinium occupying the middle of lanthanide series. The high throughput set up was used to investigate the effect of different solvent composition and of the hydrochloric acid addition (the details of the reactions are given in appendix section C.2). The pxrd patterns of the products obtained are shown in Figure 5-17. A phase similar to MIL-173(Zr) was successfully obtained with Gd for all conditions except for 100% water (unknown phase) and with methanol (amorphous). Using pure DMF as a solvent provided lower crystallinity compared to the DMF/water mixtures. The effect of the addition of 2 equivalents of HCl is negligible in terms of the crystallinity of the product obtained. Therefore, the solvent system with 50%/50% DMF/water was further used without any additives.

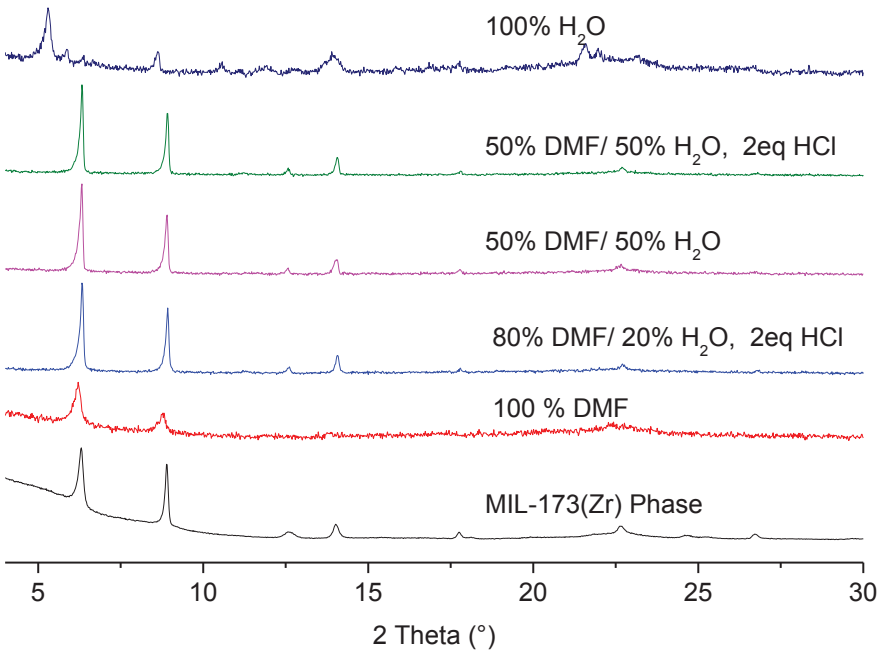

Figure 5-17 PXRD patterns for the samples from the initial syntheses investigating the solvent system for the MOF phase with $Gd(NO_3)_3.6H_2O$ using high throughput technique. PXRD measurements performed with instrument 3.

The synthesis was then reattempted in same conditions with $YCl_3.6H_2O$ and $LaCl_3.6H_2O$ as metal sources in order to obtain diamagnetic isostructural MOFs allowing solid state NMR studies (reaction details are given in appendix section C.2). All the syntheses resulted in a phase similar to that of MIL-173(Zr). In case of the La-based compound, single crystals were obtained and successfully used to solve the structure with single crystal X-ray diffraction.

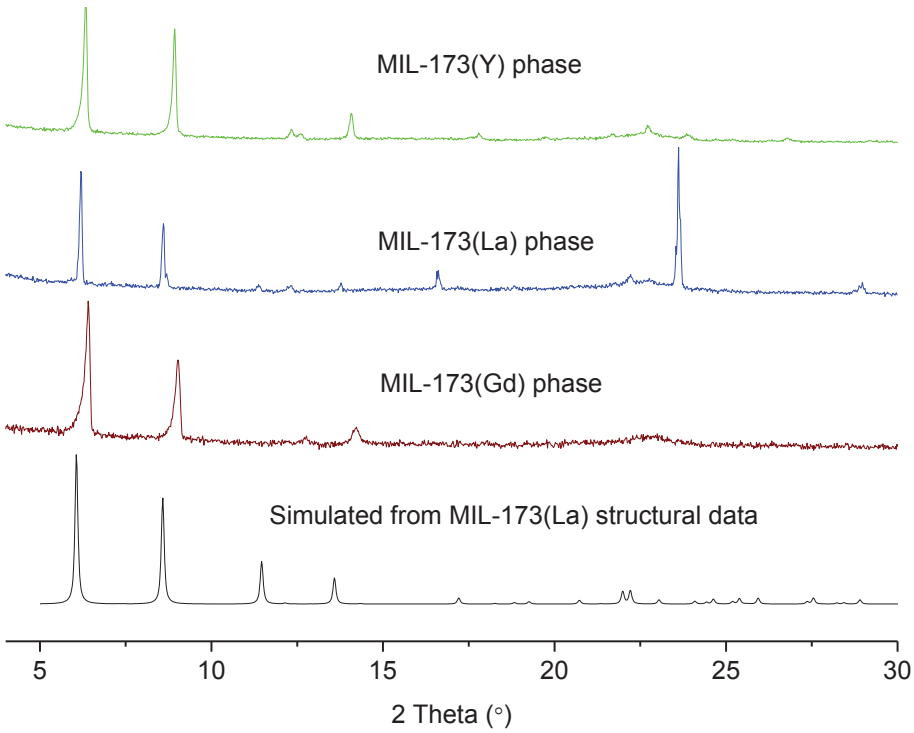

Figure 5-18 PXRD patterns for the samples obtained with various metal salts. Peaks at 16.5°, 23.7°, 28.8° for the La phase represents La-formate impurity. PXRD measurements performed with instrument 3.

The synthesis with La also resulted in the simultaneous formation of an impurity which was determined to be lanthanum formate. Thus, in order to minimize the formation of the impurity, syntheses were attempted using less La salt. These syntheses were carried out at Laboratoire des Multimatériaux et Interfaces (LMI) in a larger scale (i.e. reactant volume 2mL, reaction details are given in appendix section C.2). Synthesis using 1.8:1 ratio of La to porphyrin led to the phase pure material and was further used as stoichiometry conditions.

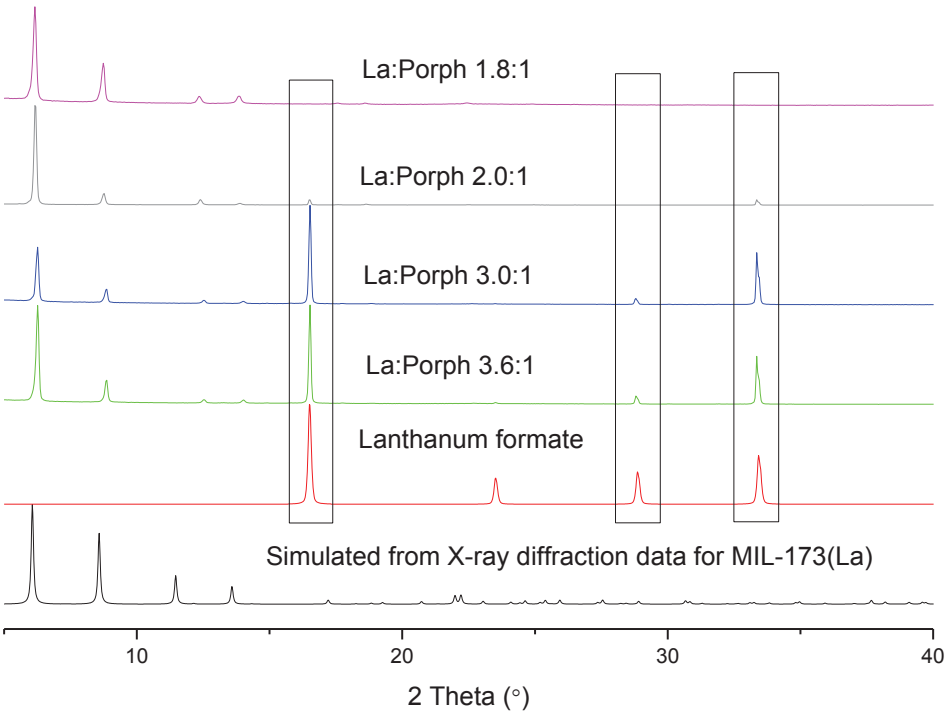

Figure 5-19 PXRD patterns for samples with various La/porphyrin stoichiometry used in the synthesis conditions. Peaks at 16.5°, 28.8° and 33.4° represent the lanthanum formate impurity.

The syntheses were repeated in an even larger scale (total reactant volume 4 mL) to obtain more material. In addition, the concentration of the reactants was doubled as it resulted in qualitatively bigger crystals of around 80 µm in length compared to 50 µm observed with the previous syntheses for the phase with lanthanum (the porphyrin concentration 20.6 mM vs 10.3 mM). Furthermore, the same framework was extended to Ce as well which was expected due to the similar chemistry of lanthanide metals (Figure 5-20). These were the final optimised conditions as described in the article.

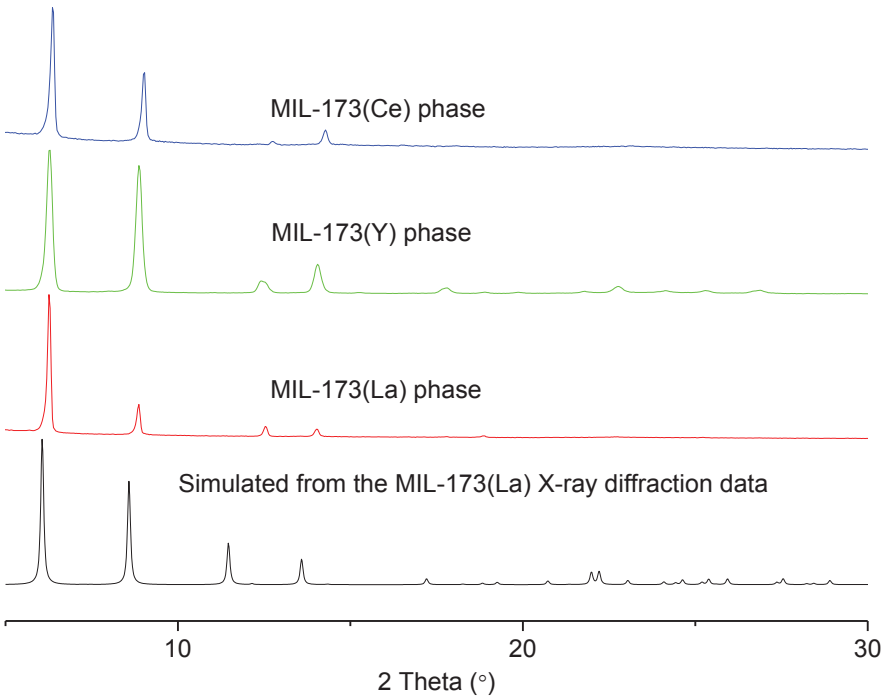

Figure 5-20 PXRD patterns for the samples performed in the final optimised conditions.

5.2.2. Article

The article provided in this section discusses the synthesis and the characterisation of a new MOF using the linker 5,10,15,20-tetrakis(3,4,5-trihydroxyphenyl)porphyrin, with Zr^{4+} and rare earth metals (Y^{3+}, La^{3+}, Ce^{3+}). As mentioned before, the post-synthetic metalation of MIL-173(Zr) with cobalt and the initial synthesis optimisation with rare earth metals were our contributions to this work.

ChemComm

COMMUNICATION

View Article Online
View Journal | View Issue

Published on 15 June 2017. Downloaded by Université Claude Bernard Lyon on 21/07/2017 09:35:18.

Check for updates

Cite this: *Chem. Commun.*, 2017, **53**, 7661

Received 16th April 2017,
Accepted 12th June 2017

DOI: 10.1039/c7cc04215a

rsc.li/chemcomm

Adaptability of the metal(III,IV) 1,2,3-trioxobenzene rod secondary building unit for the production of chemically stable and catalytically active MOFs†

Georges Mouchaham,[a] Brian Abeykoon,[b] Mónica Giménez-Marqués,[ac] Sergio Navalon,[c] Andrea Santiago-Portillo,[c] Maame Affram,[a] Nathalie Guillou,[a] Charlotte Martineau,[a] Hermenegildo Garcia,[c] Alexandra Fateeva[b] and Thomas Devic*[ad]

The use of a 5,10,15,20-tetrakis(3,4,5-trihydroxyphenyl)porphyrin has yielded a new MOF based on M-1,2,3-trioxobenzene chains that can be made of M = Zr(IV) or RE(III) (RE = rare earth), showing a very high and limited chemical stability, respectively. The robust metallated Zr-analogue, Co-MIL-173(Zr), has proven to be a heme-like heterogeneous catalyst suitable for aerobic oxidation of hydrocarbons.

Mastering the formation of metal-containing secondary building units (SBUs) to further produce Metal–Organic Frameworks (MOFs) of pre-established structures is one of the great achievements of MOF chemistry, paving the way to reticular chemistry and hence further the fine tuning of the sorption or physical properties. While discrete molecular SBUs have led to an archetypical series of carboxylate-based MOFs, rod SBUs[1] could also offer several advantages, such as an increased chemical stability[2,3] or long range charge transport.[4,5] Numerous isolated examples of rod-based MOFs have been reported, but carboxylate and hydroxycarboxylate ligands have also given rise to a prominent series of solids based on M(II) (MOF-74s/CPO-27s),[6] M(III) (MIL-53s)[7] (MIL stands for Materials Institute Lavoisier) and M(IV) (MIL-140s)[3] transition metals. Some of us recently identified in several 1-D coordination polymers a potential rod SBU built up solely from 1,2,3-trioxobenzene ("gallate") ligands and Zr ions.[8] The connection of these units through a linear bis-gallate ligand led to a flexible MOF (MIL-163) exhibiting an unprecedented chemical stability, especially towards complexing agents such as phosphate ions.[9] Here, we show that such a family can easily be extended to polytopic ligands of different symmetries (here a porphyrin of a square-like geometry), as well as cations of similar connectivity although different charge, namely rare-earths (RE), highlighting the robustness of such a SBU. We also demonstrate that the chemical stability can be tuned through the oxidation state of the cation and that such solids could be used after post-synthesis treatment as a platform for oxidation catalysis exclusively by molecular oxygen in the absence of any other oxidizing reagent.

MIL-173(Zr), formulated $\{Zr_2(H_6\text{-PorphGal})\}\cdot(DMA,H_2O)_n$ (DMA = *N*,*N*-dimethylamine), was obtained in a 74% yield by reacting $ZrCl_4$ and 5,10,15,20-tetrakis(3,4,5-trihydroxyphenyl)-porphyrin[10] (or H_{14}-PorphGal) in a mixture of *N*,*N*-dimethylformamide (DMF) and 1 M HCl aqueous solution at 130 °C (see the ESI† for details). The obtained dark violet microcrystalline powder composed of flattened octahedra (see Fig. S8, ESI,† for SEM pictures) was collected by centrifugation, abundantly washed with DMF and acetone and finally air dried. High-resolution X-ray powder diffraction (XRPD) data, suitable for structural determination, were collected on a conventional laboratory diffractometer.‡ XRPD diagram indexing and structure resolution revealed that MIL-173(Zr) crystallizes in a tetragonal setting consistent with the $I4_1/amd$ space group (a = 28.4436(6) Å, c = 14.9962(9) Å and V = 12132.5(9) Å^3). Its asymmetric unit consists of one Zr(IV) and one fraction of a metal-free PorphGal, all in special positions, together with disordered water and dimethylamine (DMA) molecules (see the ESI† for details and Fig. S1 for the final Rietveld plot). As expected,[8,9] MIL-173(Zr) is a 3-D rod-based MOF. Aligned along the [001] direction, these rods are built-up of edge-sharing ZrO_8 polyhedra where each Zr cation is chelated by four 1,2,3-trioxobenzene groups – two pairs laying along the [110] and [−110] directions, respectively – belonging to four different PorphGal linkers (Fig. 1a). The 1,2,3-trioxobenzene groups show a dihedral angle of 90° with their corresponding central porphyrin ring (Fig. 1b). Accordingly, each PorphGal

[a] *Institut Lavoisier, UMR 8180 CNRS Université de Versailles Saint-Quentin-en-Yvelines, Université Paris-Saclay, 45 avenue des Etats-Unis, 78035 Versailles cedex, France. E-mail: thomas.devic@cnrs-imn.fr*
[b] *Univ. Lyon, Université Claude Bernard Lyon 1, Laboratoire des Multimatériaux et Interfaces, UMR CNRS 5615, 69622 Villeurbanne, France*
[c] *Instituto Universitario de Tecnologia Quimica CSIC-UPV and Departamento de Quimica, Universidad Politecnica de Valencia, Av. De los Naranjos s/n, 46022 Valencia, Spain*
[d] *Institut des Matériaux Jean Rouxel (IMN), Université de Nantes, CNRS, 2 rue de la Houssinière, BP 32229, 44322 Nantes cedex 3, France*

† Electronic supplementary information (ESI) available: Synthetic procedures, powder XRD analysis, structure determination, solid state NMR, TGA, N_2 sorption measurements, UV-vis spectroscopy, Raman spectroscopy, SEM and EDX analysis, and details on the stability tests as well as catalytic studies. CCDC 1544198 and 1544211. For ESI and crystallographic data in CIF or other electronic format see DOI: 10.1039/c7cc04215a

Published on 15 June 2017. Downloaded by Université Claude Bernard Lyon on 21/07/2017 09:35:18.

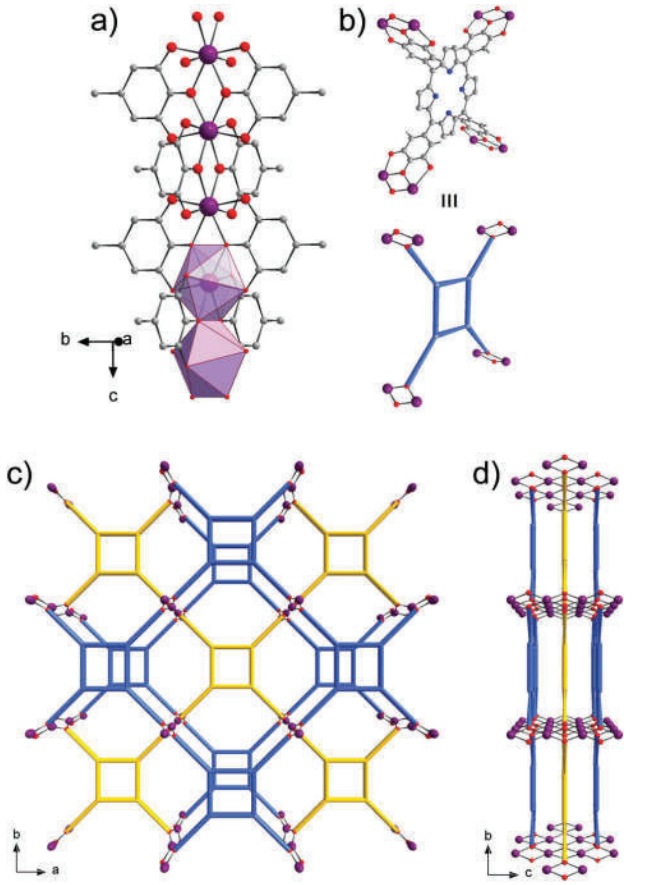

Fig. 1 Crystalline structure of MIL-173(M) (M = Zr, La, Ce, Y). (a) Chain of MO_8 polyhedra. (b) Connectivity between PorphGal and the M-cation. (c and d) Perspective views of the MOF along and orthogonally to M-chains, respectively.

bridges, orthogonally, four different Zr-chains (Fig. 1b) generating porphyrinic layers parallel to the (00l) plane with a square-shaped aperture, these PorphGal layers being finally packed in an AB fashion perpendicular to the Zr-chains (Fig. 1c) with a porphyrin–porphyrin distance of *ca.* 7.5 Å (Fig. 1d). The overall 3-D framework finally defines disc-shaped pores (free diameter ~16 Å, thickness ~4 Å) accessible through elliptic windows (aperture ~8 × 4 Å^2) as shown in Fig. S2 and S3 (ESI†). The ^{1}H and ^{13}C solid state NMR spectra (Fig. S9 and S10, ESI†) indicate the presence of entrapped water and DMA molecules, the latter arising from the degradation of DMF. Similarly to what was observed in related compounds,[8,9] very acidic protons (δ ~ 18.5 ppm) are also observed. The 2-D ^{1}H–^{13}C NMR spectrum (see Fig. S11, ESI†) suggests that this signal belongs to the remaining protons on the *meta* oxygen atoms of the gallol moieties, likely strongly hydrogen bonded to DMA, and ensuring the charge balance. Such a coordination of protonated phenol groups is very commonly observed in 1,2,3-trioxobenzene coordination solids, whatever the nature of the cation.[8,9,11–14] This leads ultimately to the formula $\{Zr_2(H_6\text{-PorphGal})\}\cdot(DMA,H_2O)_n$, which was also supported by thermogravimetric and elemental analysis (see the ESI† for details).

In light of similarities recently reported between the hexanuclear Zr- and RE-oxo-carboxylate clusters,[15–18] we further evaluated the reactivity of H_{14}-PorphGal with RE salts. Reproducing similar reaction conditions with $RECl_3$ (RE = Y, La, Ce) instead of $ZrCl_4$ (see the ESI† for details) allowed obtaining crystalline products in each case. XRD analysis indicates that these solids are isostructural with MIL-173(Zr) (Fig. S5, ESI†). In particular, crystals suitable for single crystal XRD analysis were obtained for RE = La, and unambiguously revealed that both solids present the same framework, although with a subtle modification of the unit cell parameters and symmetry (see Fig. S4 and Table S2, ESI†).

As noticed earlier[8,9] and in contrast to the case of carboxylate ligands, 1,2,3-trioxobenzene moieties prevent the formation of oxo and hydroxo bridges mainly due to their strong coordination ability, giving rise to Zr(IV) coordination compounds built up solely from organic ligands, even if the synthesis is carried out in the presence of a large excess of water. Moving from Zr(IV) to RE(III) only results in a slight variation of the interatomic distances. This reveals that such 1-D M(1,2,3-trioxobenzene)$_2$ motifs can easily adapt not only to cations of different charge, but also of variable size (ionic radii range here from 0.84 (Zr) to 1.160 (La) Å).[19] ^{13}C solid state NMR analysis carried out for RE = Y (see Fig. S13, ESI†) reveals again the presence of DMA. By analogy with the Zr material, the formula $\{RE_2(H_8\text{-PorphGal})\}\cdot(DMA,H_2O)_n$ is proposed, *i.e.* with a larger amount of phenolic protons to ensure the charge balance. Nevertheless, contrary to the case of MIL-173(Zr) and related solids, no peak is detected at a high chemical shift on the ^{1}H NMR spectrum (Fig. S12, ESI†), suggesting that the signal associated with the phenolic protons here overlaps with the ones associated with the aromatic protons. This fully agrees with the less marked acidic character of phenolic protons in MIL-173(RE), arising from a weaker electron withdrawing effect of the phenol-cation bond when moving from Zr(IV) to RE(III).

The impact of the metallic cation on both the porosity and the stability of MIL-173 was evaluated. Nitrogen sorption experiments carried out at −196 °C after evacuation under heating reveal that for both MIL-173(Zr) and MIL-173(Y) a type I isotherm (Fig. S14, ESI†) is present, associated with a BET surface area of *ca.* 780 and 515 m^2 g^{-1}, respectively. In contrast, no microporosity was detected for the larger RE (La, Ce). This phenomenon is attributed to partial collapse of the framework upon activation (see Fig. S7, ESI,† for XRPD after activation), the rather low coordination number (8) for such RE likely favoring such degradation.

The Zr(1,2,3-trioxobenzene)$_2$ motif was proven to induce a remarkable chemical stability for MIL-163, especially in the presence of complexing competitors such as phosphates.[9] Using highly diluted suspension of MOFs to maintain the buffer effect (1 mg mL^{-1}), the stability of MIL-173(Zr) and MIL-173(Y) was evaluated both in pure water and in a phosphate buffer saline solution (PBS, pH = 7.4), the latter being the simplest model of physiological media. No noticeable change was detected on the XRPD pattern after one week at 37 °C for MIL-173(Zr) neither in pure water nor in PBS (Fig. 2). In contrast, MIL-173(Y) was found to become completely amorphous in both media (Fig. 2). Hence, the behavior of MIL-173(Zr) is very similar to that of MIL-163 and strongly differs from that of archetypical Zr-carboxylates such as UiO-67 and MIL-140C which readily degrade in PBS,[9] confirming the robustness of the Zr(1,2,3-trioxobenzene)$_2$ motif. This increased

 This journal is © The Royal Society of Chemistry 2017

Published on 15 June 2017. Downloaded by Université Claude Bernard Lyon on 21/07/2017 09:35:18.

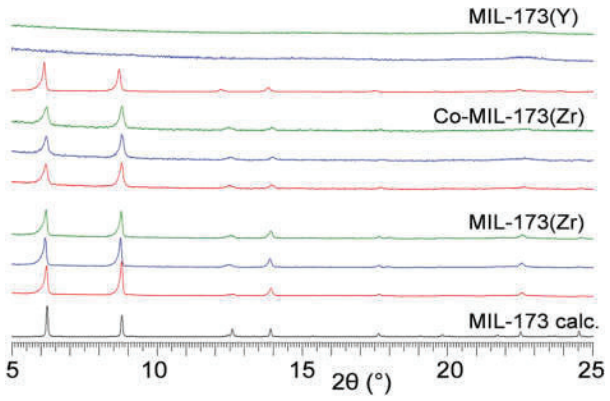

Fig. 2 From the bottom to the top: XRPD patterns (λ = 1.5406 Å) for MIL-173(Zr), Co-MIL-173(Zr), MIL-173(Y): calculated from the crystal structure (black), the as-synthesized (red); suspended in water for one week at 37 °C (blue); suspended in PBS for one week at 37 °C (green).

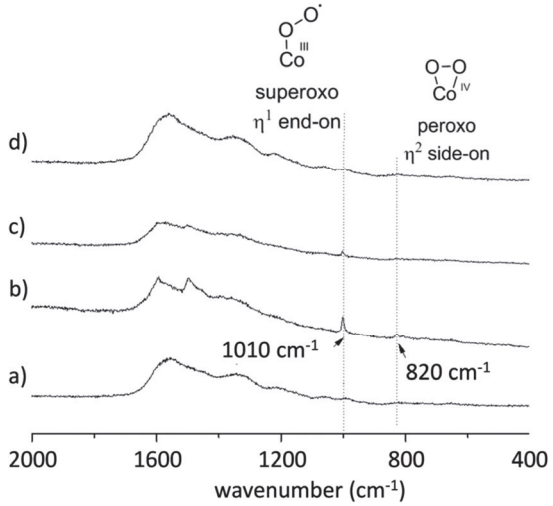

Fig. 3 Raman spectra of Co-MIL-173(Zr) exposed consecutively under different conditions: (a) N_2 flow at 120 °C for 3 h; (b) O_2 atmosphere at 120 °C; (c) N_2 atmosphere at 25 °C after cooling from 120 °C and O_2 atmosphere; (d) N_2 atmosphere after 24 h purge with N_2.

stability is clearly not achieved with RE, indicating that the nature of the complexing group, together with the related absence of an inorganic co-ligand (H_2O, OH^-, O^{2-}) seen as potential 'weak' points in MOF backbones are not the prime criteria driving the stability, but that the charge density of the cation here also strongly contributes to the stability.[20]

Structure determination together with solid state UV-vis spectroscopy showing the Q band multiplicity (see Fig. S16, ESI†) confirmed that the porphyrin cores are present in their free base form. In the most stable MIL-173(Zr) solid, this feature was used to introduce post-synthetically[21–24] catalytically active cations. Treatment of MIL-173(Zr) with Co(II) acetate in DMF at 120 °C afforded the corresponding Co-MIL-173(Zr) solid. While XRPD analysis (Fig. S6, ESI†) confirmed the retention of the framework, Energy Dispersive X-ray analysis (EDX) indicated a Zr : Co ratio equal to 2 : 1 (Table S3, ESI†), supporting the fact that the metalation was quantitative. This was further confirmed by solid state UV-vis spectroscopy: as shown in Fig. S16 (ESI†), the signal associated with the free porphyrin is not detected anymore after metalation. The metalation does not impact significantly the porosity, Co-MIL-173(Zr) presenting a type I nitrogen adsorption isotherm (see Fig. S14, ESI†) with a derived BET surface area of *ca.* 620 $m^2\ g^{-1}$, *i.e.* only slightly lower (−20%) than that of the free base form. As shown in Fig. 2, the metalation neither impacts on the chemical stability, Co-MIL-173(Zr) remaining as crystalline as MIL-173(Zr) after being suspended both in water and PBS. Therefore, the potential of Co-MIL-173(Zr) in oxidation catalysis[25,26] exclusively by molecular oxygen was then investigated.

During oxidation catalysis, the metal has to activate oxygen through coordination, and recent studies have shown that Co porphyrin–O_2 interactions can be probed in MOF materials.[27,28] EPR analysis performed at −173 °C first indicates that the Co adopts a +II oxidation state in Co-MIL-173(Zr) (Fig. S17, ESI†).[29] After exposure to O_2, a very broad EPR band appears, indicating that oxygen adsorption evolves towards the formation of radical oxygen species (Fig. S17, ESI†). Deeper insights were obtained from Raman spectroscopy (Fig. 3):[30,31] at 120 °C, exposure of Co-MIL-173(Zr) to O_2 leads to the appearance of additional peaks at 1010 and 820 cm^{-1} on the spectrum. These peaks are attributed to superoxo-Co(III) and peroxo-Co(IV) adducts, respectively,[30,31] indicating that an electron transfer occurs between the Co(II) centers and O_2 molecules. Once O_2 is removed and the solid cooled to room temperature, these signals vanish (Fig. 3c and d), indicating that the process is reversible and that the Co sites embedded in Co-MIL-173(Zr) can perform as active catalytic sites.[30]

With this in hand, the catalytic activity of Co-MIL-173(Zr) for the benzylic oxidation of hydrocarbons exclusively by molecular oxygen in the absence of any other oxidizing reagent or initiator was investigated. Indane was first taken as a case study. Preliminary controls showed a negligible (less than 5%) autooxidation of indane in the absence of MOFs. In contrast, in the presence of Co-MIL-173(Zr) (0.01 mol%), conversion of indane to a mixture of indanyl hydroperoxide, indanol and indanone as the three major products (see top of Fig. 4) was observed. Fig. 4a presents the time-conversion plot showing that at 120 °C the full conversion is reached after 18 h. In contrast, only 40% conversion is achieved with the non-metalated MIL-173(Zr), this activity being likely associated with defective Zr sites. While MIL-173(Zr) exhibits at this level of conversion a selectivity towards the three major products of 95%, this selectivity is achieved in the case of Co-MIL-173(Zr) at 100% indane conversion and the product distribution corresponds almost exclusively to the ol/one mixture. Hence, both in terms of conversion and selectivity, the presence of Co–porphyrin for oxygen activation is beneficial. Chemical analysis of the liquid phase after the removal of the solid reveals no Co or Zr, ruling out any contribution of leached metal to the observed catalytic performance. After completion of the reaction, Co-MIL-173(Zr) was recovered and reused in a consecutive run. The temporal profile (initial reaction rate, final indane conversion, selectivity, see Fig. 4) of the reused catalyst is coincident with that of fresh Co-MIL-173(Zr), indicating that the material is stable from the catalytic point of view. This is remarkable in view of the general behavior of metal porphyrins undergoing deactivation

Published on 15 June 2017. Downloaded by Université Claude Bernard Lyon on 21/07/2017 09:35:18.

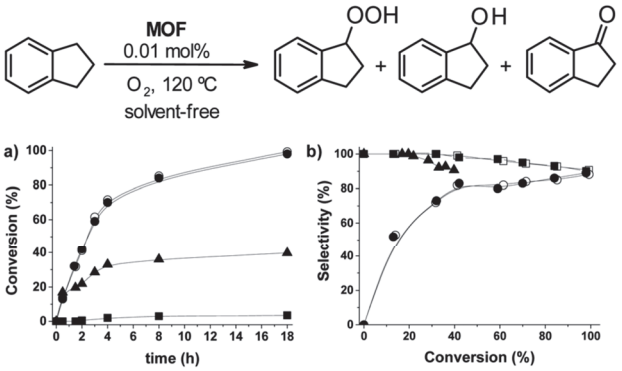

Fig. 4 Time-conversion plot (a) and conversion-selectivity plot (b) for the aerobic oxidation of indane using Co-MIL-173(Zr) (first use ○ and reused ●) and MIL-173(Zr) (▲). Blank control experiment in the absence of a solid catalyst (■). Selectivities towards indanyl hydroperoxide + indanol + indanone (first use ■ and reused □) or towards indanol + indanone (first use ● and reused ○). Selectivities towards indanyl hydroperoxide + indanol+indanone using MIL-173(Zr) (▲).

as homogeneous catalysts,[26,32–34] *e.g.* through the formation of oxo dimers. Besides indane, bulkier substrates (cumene, 1,3-diisopropylbenzene and 1,3,5-triisopropylenzene) were finally subjected to benzylic oxidation. The results are presented in Fig. S18–S20 (ESI†). In the case of cumene, a final conversion of about 80% with a selectivity towards alcohol and hydroperoxide of 100% was achieved, while in the case of the even bulkier 1,3-diisopropylbenzene and 1,3,5-triisopropylbenzene only the mono alcohol and hydroperoxide products were observed and the substrate reached a conversion of only 60 and 50% respectively. This trend is in agreement with the assumption that the reaction takes place mainly inside the pores of Co-MIL-173(Zr), the reaction rate being controlled by the diffusion of substrates and products within the pores.

To summarize, we showed here that the recently identified Zr(1,2,3-trioxobenzene)$_2$ rod-like motif is robust enough to be used for the preparation of the MOFs built up from ligands of various symmetries, and can even be extended to cations of lower charges (rare-earths). Such a charge has a profound impact on the chemical stability of this SBU, its resistance towards phosphates being limited to M(IV) (here Zr, but likely also Hf) cations. As the title solids incorporate free base porphyrins, they are prone for post-synthesis metalation leading to heterogeneous catalytic activity, not only expanding the scope of available heme-related MOFs,[21–24,35] but also offering new opportunities such as the combination of metallic sites together with very acidic protons to promote more complex reactions or specific adsorption features.

The authors declare no competing financial interests.

We acknowledge the labex CHARMMMAT (ANR-11-LABEX-0039) and the EU Marie Skłodowska-Curie (H2020-MSCA-IF-658224) actions for the postdoctoral fellowships of G. M. and M. G.-M., respectively. F. Nouar is acknowledged for SEM imaging and EDS analyses. This work was supported by the "cellule Energie" of the CNRS.

Notes and references

‡ Crystallographic data are available through the CCDC (1544198 and 1544211 for MIL-173(Zr) and MIL-173(La) respectively).†

1 A. Schoedel, M. Li, D. Li, M. O'Keeffe and O. M. Yaghi, *Chem. Rev.*, 2016, **116**, 12466–12535.
2 T. Devic and C. Serre, *Chem. Soc. Rev.*, 2014, **43**, 6097–6115.
3 V. Guillerm, F. Ragon, M. Dan-Hardi, T. Devic, M. Vishnuvarthan, B. Campo, A. Vimont, G. Clet, Q. Yang and G. Maurin, *et al.*, *Angew. Chem., Int. Ed.*, 2012, **51**, 9267–9271.
4 H. Leclerc, T. Devic, S. Devautour-Vinot, P. Bazin, N. Audebrand, G. Férey, M. Daturi, A. Vimont and G. Clet, *J. Phys. Chem. C*, 2011, **115**, 19828–19840.
5 L. Sun, T. Miyakai, S. Seki and M. Dincă, *J. Am. Chem. Soc.*, 2013, **135**, 8185–8188.
6 H. Deng, S. Grunder, K. E. Cordova, C. Valente, H. Furukawa, M. Hmadeh, F. Gandara, A. C. Whalley, Z. Liu and S. Asahina, *et al.*, *Science*, 2012, **336**, 1018–1023.
7 C. Serre, F. Millange, C. Thouvenot, M. Nogues, G. Marsolier, D. Louer and G. Férey, *J. Am. Chem. Soc.*, 2002, **124**, 13519–13526.
8 L. Cooper, N. Guillou, C. Martineau, E. Elkaim, F. Taulelle, C. Serre and T. Devic, *Eur. J. Inorg. Chem.*, 2014, 6281–6289.
9 G. Mouchaham, L. Cooper, N. Guillou, C. Martineau, E. Elkaïm, S. Bourrelly, P. L. Llewellyn, C. Allain, G. Clavier and C. Serre, *et al.*, *Angew. Chem., Int. Ed.*, 2015, **54**, 13297–13301.
10 L. Jiang, F. Lu, H. Li, Q. Chang, Y. Li, H. Liu, S. Wang, Y. Song, G. Cui and N. Wang, *et al.*, *J. Phys. Chem. B*, 2005, **109**, 6311–6315.
11 L. Cooper, T. Hidalgo, M. Gorman, T. Lozano-Fernandez, R. Simon-Vazquez, C. Olivier, N. Guillou, C. Serre, C. Martineau and F. Taulelle, *et al.*, *Chem. Commun.*, 2015, **51**, 5848–5851.
12 T. Hidalgo, L. Cooper, M. Gorman, T. Lozano-Fernández, R. Simón-Vázquez, G. Mouchaham, J. Marrot, N. Guillou, C. Serre and P. Fertey, *et al.*, *J. Mater. Chem. B*, 2017, **5**, 2813–2822.
13 P. J. Saines, H. H. M. Yeung, J. R. Hester, A. R. Lennie and A. K. Cheetham, *Dalton Trans.*, 2011, **40**, 6401–6410.
14 R. K. Feller and A. K. Cheetham, *Solid State Sci.*, 2006, **8**, 1121–1125.
15 D.-X. Xue, A. J. Cairns, Y. Belmabkhout, L. Wojtas, Y. Liu, M. H. Alkordi and M. Eddaoudi, *J. Am. Chem. Soc.*, 2013, **135**, 7660–7667.
16 D.-X. Xue, Y. Belmabkhout, O. Shekhah, H. Jiang, K. Adil, A. J. Cairns and M. Eddaoudi, *J. Am. Chem. Soc.*, 2015, **137**, 5034–5040.
17 P. Yi, H. Huang, Y. Peng, D. Liu and C. Zhong, *RSC Adv.*, 2016, **6**, 111934–111941.
18 M. Lammert, M. T. Wharmby, S. Smolders, B. Bueken, A. Lieb, K. A. Lomachenko, D. D. Vos and N. Stock, *Chem. Commun.*, 2015, **51**, 12578–12581.
19 R. D. Shannon, *Acta Crystallogr.*, 1976, **A32**, 751–767.
20 J. J. Low, A. I. Benin, P. Jakubczak, J. F. Abrahamian, S. A. Faheem and R. R. Willis, *J. Am. Chem. Soc.*, 2009, 15834–15842.
21 W. Morris, B. Volosskiy, S. Demir, F. Gandara, P. L. McGrier, H. Furukawa, D. Cascio, J. F. Stoddart and O. M. Yaghi, *Inorg. Chem.*, 2012, **51**, 6443–6445.
22 A. Fateeva, P. A. Chater, C. P. Ireland, A. A. Tahir, Y. Z. Khimyak, P. V. Wiper, J. R. Darwent and M. J. Rosseinsky, *Angew. Chem., Int. Ed.*, 2012, **51**, 7440–7444.
23 S. Takaishi, E. J. DeMarco, M. J. Pellin, O. K. Farha and J. T. Hupp, *Chem. Sci.*, 2013, **4**, 1509–1513.
24 D. Feng, Z.-Y. Gu, Y.-P. Chen, J. Park, Z. Wei, Y. Sun, M. Bosch, S. Yuan and H.-C. Zhou, *J. Am. Chem. Soc.*, 2014, **136**, 17714–17717.
25 C.-M. Che, V. K.-Y. Lo, C.-Y. Zhou and J.-S. Huang, *Chem. Soc. Rev.*, 2011, **40**, 1950–1975.
26 A. B. Sorokin, *Chem. Rev.*, 2013, **113**, 8152–8191.
27 A. T. Gallagher, M. L. Kelty, J. G. Park, J. S. Anderson, J. A. Mason, J. P. S. Walsh, S. L. Collins and T. D. Harris, *Inorg. Chem. Front.*, 2016, **3**, 536–540.
28 N. Lahanas, P. Kucheryavy and J. V. Lockard, *Inorg. Chem.*, 2016, **55**, 10110–10113.
29 I. M. Ruzic, T. D. Smith and J. R. Pilbrow, *J. Chem. Soc., Dalton Trans.*, 1982, 373–380.
30 J. Cho, R. Sarangi, H. Y. Kang, J. Y. Lee, M. Kubo, T. Ogura, E. I. Solomon and W. Nam, *J. Am. Chem. Soc.*, 2010, **132**, 16977–16986.
31 H. C. Mackin, M. Tsubaki and N.-T. Yu, *Biophys. J.*, 1983, **41**, 349–357.
32 J. A. S. J. Razenberg, A. W. Van Der Made, J. W. H. Smeets and R. J. M. Nolte, *J. Mol. Catal.*, 1985, **31**, 271–287.
33 R. J. M. Nolte, J. A. S. J. Razenberg and R. Schuurman, *J. Am. Chem. Soc.*, 1986, **108**, 2751–2752.
34 J. A. S. J. Razenberg, R. J. M. Nolte and W. Drenth, *J. Chem. Soc., Chem. Commun.*, 1986, 277–279.
35 M. Zhao, S. Ou and C.-D. Wu, *Acc. Chem. Res.*, 2014, **47**, 1199–1207.

 This journal is © The Royal Society of Chemistry 2017

5.2.3. Reactivity of other trivalent metal ions and H_{14}-PorphGal

A similar study was undertaken in the ILV using trivalent Fe, Al and In metal sources (reaction details are given in the appendix section C.2). The starting point for condition screening in this case was similar to the starting conditions used for the exploratory synthesis with the lanthanide ions (metal to ligand ratio =3.6:1, isotherm temperature 120 °C, solvent= 50%/50% DMF/water, porphyrin concentration= 10 mM)

The reactions with $FeCl_3.6H_2O$ did not lead to any crystalline solids. Reactions with $AlCl_3.6H_2O$ and $In(NO_3)_3.xH_2O$ resulted in solids displaying similar pxrd patterns. The In-based samples presented a slightly higher crystallinity (Figure 5-21a). When HCl was added to the reaction mixture, only amorphous solids were recovered. The In phase was further investigated by varying the indium source (conditions: 33%/67% DMF/water, 3.6:1 metal to ligand ratio, heating program 2h-48h-4h, temperature= 120 °C, porphyrin concentration= 10 mM) The most crystalline material was obtained when anhydrous indium chloride was used (Figure 5-21b).

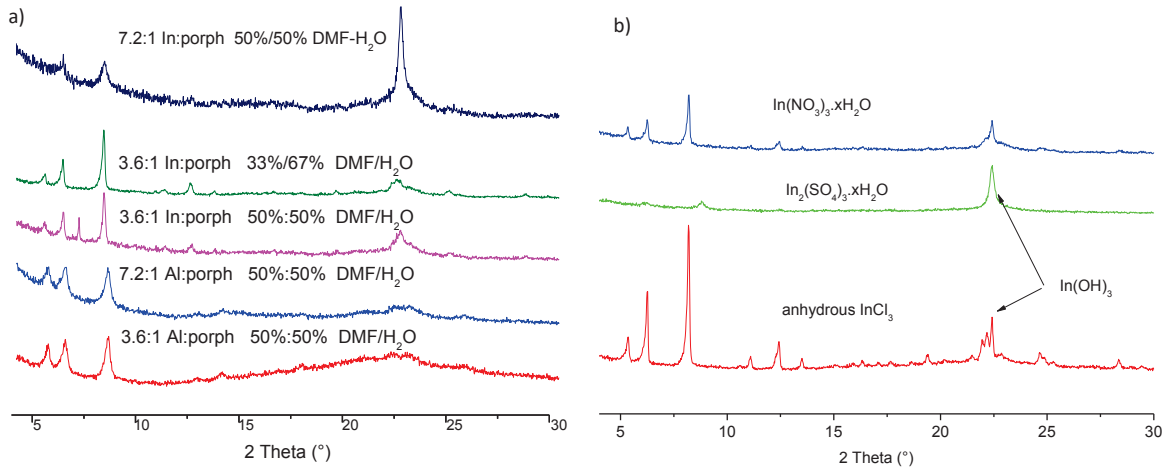

Figure 5-21 a) PXRD patterns of the crystalline samples obtained from the high throughput synthesis b) PXRD pattern for the samples obtained with different indium salts (33%/67% DMF/water, 3.6:1 metal to ligand ratio, heating program 2h-48h-4h). PXRD measurements performed with instrument 3.

The attempted syntheses did not yield single crystals under the conditions described above. Indium hydroxide was also simultaneously formed in these conditions as indicated by the PXRD pattern, and further washing the solid with water/DMF was not successful for the removal of the impurity. Thus, to promote the formation of single crystals, and also to possibly reduce the formation of $In(OH)_3$, pyrocatechol was used as a modulator (pyrocatechol can potentially coordinate to In^{3+} ions in solution and lower its effective concentration in the reaction mixture). However, pyrocatechol had a detrimental effect on the crystallinity and did not prevent the formation of $In(OH)_3$ (Figure 5-22).

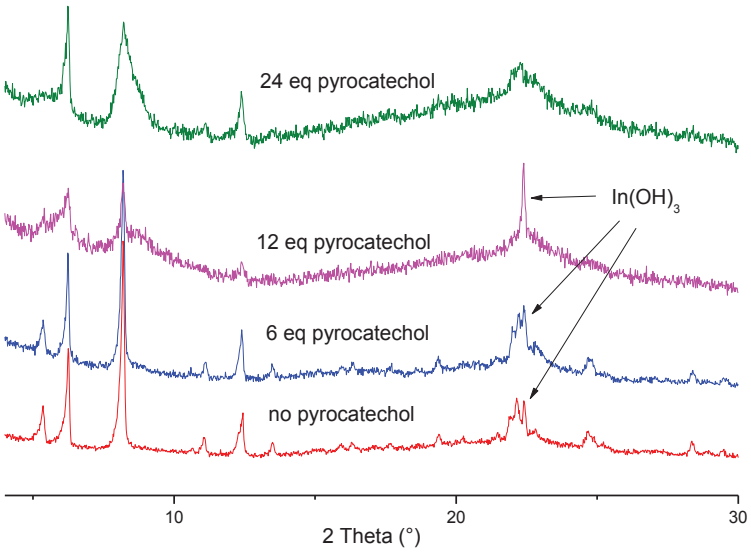

Figure 5-22 PXRD data for the samples from the syntheses with pyrocatechol as an additive in an attempt to obtain single crystals and to prevent the formation of $In(OH)_3$ (equivalents of pyrocatechol compared to the porphyrin ligand, 33%/67% DMF-water, 3.6:1 metal to ligand ratio, heating program 2h-48h-4h, temperature 120° C). PXRD measurements performed with instrument 3.

As mentioned before, previous synthetic conditions attempted for the reactions with Al^{3+}/In^{3+} did not yield single crystals. Therefore, further attempts were made to obtain single crystals for the reaction with In^{3+} by optimising the DMF to water composition while keeping the other reaction parameters unchanged (3.6:1 metal to ligand ratio, heating program 2h-48h-4h, temperature 120 °C, porphyrin concentration = 10mM). Rectangle shaped single crystals were obtained for a 5%/95% DMF/water composition and the structure of the phase was solved using single crystal X-ray diffraction.

This structure can be described as a 1-dimensional polymer where the indium metalated porphyrin is self-assembled via axial coordination with two different hydroxyl oxygens belonging two adjacent porphyrin units (Figure 5-23). This kind of structure has been seen for the Zn and Mg metalated methoxy functionalised porphyrin (5,10,15,20-tetrakis(3,4,5-trimethoxyphenyl)porphyrin) as described in chapter 1.[10] The formula, In-H_{12}-PorphGal -X can be tentatively assigned for this phase with X being a counter ion for charge balance. However, due to its one-dimensional nature, this phase was not further explored. In addition, this phase was different to what was observed at solvent conditions with lower amount of water (67% water content) as shown in Figure 5-24. Therefore, the structure of the material obtained at lower water compositions remains unknown.

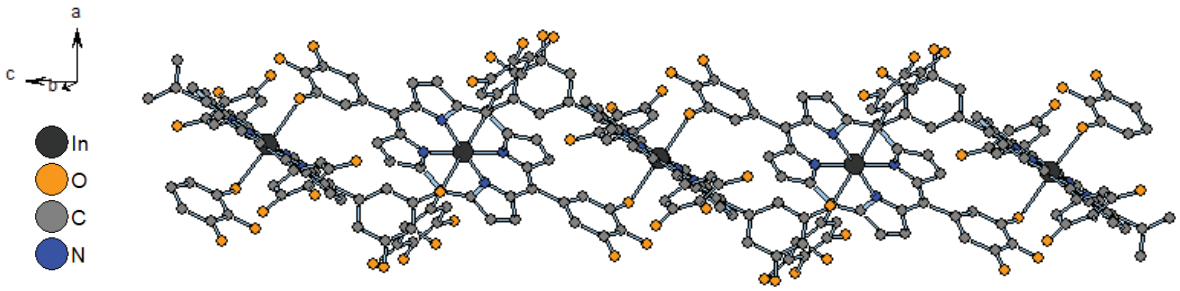

Figure 5-23 1-dimensional chain like structure of the product obtained with high water content in the solvent (5%/95% DMF-water). Hydrogens are omitted for clarity.

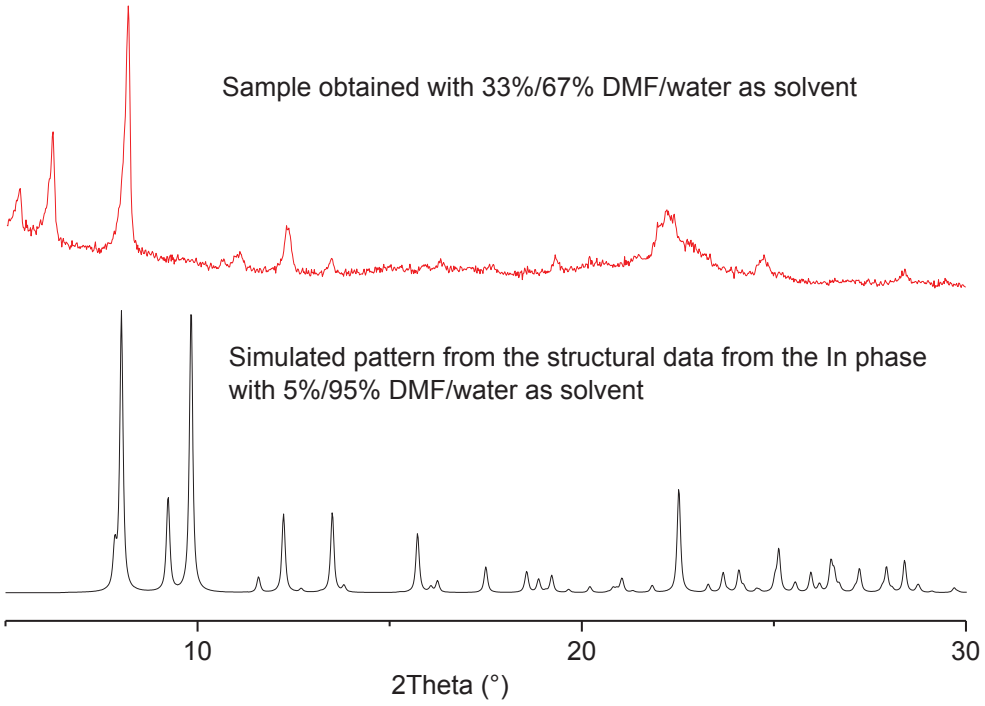

Figure 5-24 The PXRD data of the sample obtained with low water content in the solvent compared to the simulated pattern of the phase obtained with high water content in the solvent.

5.2.4. Conclusion and perspectives

The first porphyrinic MOF based on the gallate functionality, MIL-173(Zr), was successfully obtained at ILV and was demonstrated to possess enhanced chemical stability in various media. MIL-173(Zr) was successfully metalated post synthesis with Co and the resulting framework shows heme like heterogeneous catalytic activity with molecular oxygen as the oxidant. Therefore, it is worthwhile to pursue post-synthetic metalation with other metals such as iron in order to obtain differently metalated stable MOFs. This would potentially allow expanding the type of reactions that can be catalysed by this material.

A similar phase to the MIL-173(Zr) was also obtained with RE metal ions, Y^{3+}, Ce^{3+} and La^{3+} as mentioned in the article. These solids were less stable and partial collapse of the framework was observed upon solvent removal. However, a milder activation method such as supercritical CO_2 activation can be employed which could lead to the framework being intact upon solvent removal.

The investigation into other trivalent metals led to the synthesis of coordination polymers based on Al^{3+} and In^{3+}. Their structures remain unknown. Only one reaction temperature and isotherm time was investigated for the synthesis. Therefore, further investigation in to these parameters can potentially yield single crystals of this phase which can lead to resolving its structure. Another 1D-phase was obtained in the case of In^{3+} by using a higher water content in the solvent and the structure was elucidated via single crystal X-ray diffraction.

5.3. Chapter 5 conclusion

In this chapter, two different hydroxyphenyl functionalised ligands were investigated for MOF synthesis. The reactivity of free base 5,10,15,20-tetrakis(3,4-dihydroxyphenyl)porphyrin) (H_{10}-PorphCat), with hydrated $FeCl_3$, pyrocatechol and pyrazine was investigated as part of a long-term study with ILV. The synthesis optimisation led to better single crystals in terms of size. The bulk sample obtained also showed comparable permanent porosity to what had been observed with similar solids at ILV. Further analysis of the composition/purity of this material was difficult without the exact structure and the work relating to the structural resolution is still ongoing.

A new MOF was obtained at the ILV, MIL-173(Zr) with the ligand 5,10,15,20-tetrakis(3,4,5-trihydroxyphenyl)porphyrin, which was the first porphyrinic MOF built up with the gallate functionality. This material was successfully metalated with Co. Exploratory synthesis using this ligand along with rare earth metal ions (Y^{3+}, Ce^{3+}, La^{3+}) resulted in a series of MOFs which have an isotopic structure to MIL-173(Zr). The MIL-173(Zr) phase shows high chemical stability and remains a viable platform to obtain frameworks with differently metalated porphyrin cores with different potential applications as demonstrated by the heme like activity of Co-MIL-173(Zr) with molecular oxygen as the oxidant.

Exploratory work performed with other trivalent metal ions with the gallol functionalised porphyrinic ligand led to polymeric material with Al^{3+} and In^{3+}. One of the phases obtained with In^{3+} has a 1D structure as determined via single crystal X-ray diffraction. The structure of the other solids is unknown and remains an avenue for further investigation.

5.4. Experimental section

General methods

All reagents were of commercial origin and used as received.

Table showing the providers for different reagents used in syntheses.

Reagent	**Provider**
Pyrocatechol	Sigma-Aldrich
Anhydrous $ZrCl_4$	Sigma-Aldrich
$LaCl_3.6H_2O$	Prolabo
$CeCl_3.7H_2O$	Sigma-Aldrich
$YCl_3.6H_2O$	$YCl_3.6H_2O$
$GaCl_3.6H_2O$	Strem
$AlCl_3.6H_2O$	$YCl_3.6H_2O$
$In(NO_3)_3.xH_2O$	Sigma-Aldrich
$In_2(SO_4)_3.xH_2O$	Sigma-Aldrich
anhydrous $InCl_3$	Sigma-Aldrich

The synthesis of the porphyrin ligands is described in chapter 2.

Powder X Ray diffraction was performed with two different instruments:

1) PANanlytical XpertPro MRD diffractometer with Cu Kα1 radiation (λ = 1.540598 Å) used with 40 kV and 30mA settings in θ/θ reflection geometry. This is the default instrument used unless stated otherwise.

2) Bruker D8 Advance diffractometer with Cu Kα1 radiation (λ = 1.540598 Å) used with 50 kV and 50 mA settings in θ/θ reflection geometry with a variable divergence slit for axial exposure of 4mm of sample. The measurements were performed by Ruben Vera at the Centre for Diffractometry at Lyon 1.

Surface areas were measured by N_2 adsorption and desorption at 77.3 K using a BEL Japan Belsorp Mini apparatus volumetric adsorption analyser. The sample was re-activated under secondary vacuum at 60°C prior to sorption measurement. The BET surface calculations were performed using points at the pressure range $0 < P/P_0 < 0.10$

Thermogravimetric analysis (TGA) was performed with a Mettler-Toledo TGA / DSC STARe system. Approximately 3 mg of sample was introduced into an alumina crucible of 70 µl and heated from 25 ° C to 800 ° C at a rate of 10 °C min^{-1} under air flow (20 $mL.min^{-1}$ + 10 $mL.min^{-1}$ balance). The analyses were performed by Oleksandra Veselska at Institute of Research on Catalysis and Environment in Lyon (IRCELYON).

High throughput synthesis

High throughput studies were carried out at the Institut Lavoisier de Versailles with a setup which enabled synthesis, filtration and characterisation via powder X-ray diffraction for 24 reactions at a time. The reaction mixtures were prepared in mini-autoclaves which were then placed in a metallic block (Figure 5-25a). The autoclaves were then sealed and put in a temperature controlled oven and heated with a pre-determined heating program. Afterwards, the samples were transferred to a specially designed sample plate using a pipette (Figure 5-25b). Using the filtration block (Figure 5-25c), the samples were then washed with the solvent and left to dry.

PXRD analyses of the samples were performed in transmission geometry using a STOE HT powder diffractometer equipped with a xy-stage and a linear position sensitive detector (PSD) system using Cu-Kα1 radiation (PXRD instrument 3).

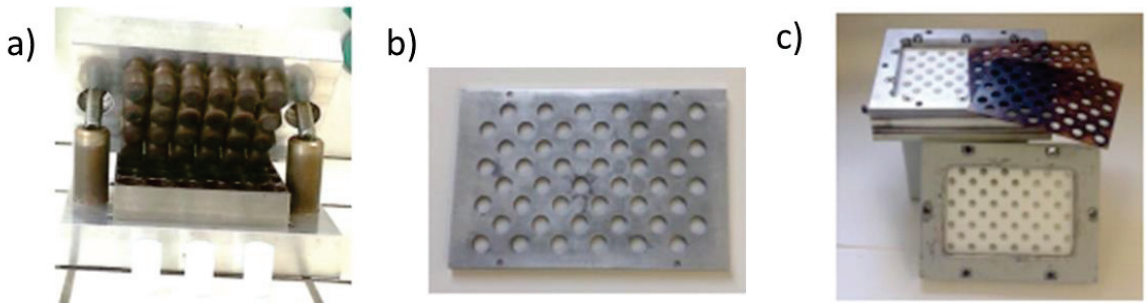

Figure 5-25 a) Metallic plate which can house 24 mini autoclaves. b) Filtration block c) Plate which the samples are transferred to for PXRD analysis. (Photo source -The Institut Lavoisier de Versailles)

Synthesis optimisation for the system with hydrated $FeCl_3$, H_{10}-PorphCat, pyrocatechol and pyrazine for obtaining better single crystals

Typical synthesis involved combining the free base meso-tetrakis(3,4-dihydroxyphenyl)porphyrin, $FeCl_3.6H_2O$, pyrocatechol and pyrazine with the solvent (mix of DMF-water) in a teflon lined autoclave for the reactions performed at 150 °C and 160 °C and in a glass vial for the syntheses performed at 140 °C. Then the reaction mixtures were heated at the desired temperature with the desired heating program. The solid was recovered by centrifugation, washed 3 times with DMF and 3 times with acetone and left to air-dry to obtain the solid products. The details of the exact reaction conditions investigated are given in the appendix section C.1.

The synthesis using the optimised conditions in a bigger scale is as follows:

The free base 5,10,15,20-Tetrakis(3,4-dihydroxyphenyl)porphyrin (46 mg, 0.062 mmol) $FeCl_3.6H_2O$ (46 mg, 0.170 mmol), pyrocatechol (100 mg, 0.900 mmol) and pyrazine (15 mg, 0.180 mmol) was combined with 1mL of DMF and 4 mL of deionised water in a teflon lined autoclave. The reaction mixture was then heated at an isotherm temperature of 160 °C for 48 hours. The temperature was increased at a of 0.38 °C/min (over 6 hours) to reach the isotherm and then cooled to room temperature over 6 hours. The solid was recovered by centrifugation, washed 3 times with DMF and 3 times with acetone and left to air-dry to obtain the dark violet solid products (53 mg)

5.5. References

1. Krogsgaard, M.; Nue, V.; Birkedal, H., Mussel-Inspired Materials: Self-Healing through Coordination Chemistry. *Chemistry – A European Journal* **2016,** *22* (3), 844-857.
2. Satchell, J. F.; Smith, B. J., Calculation of aqueous dissociation constants of 1,2,4-triazole and tetrazole: A comparison of solvation models. *Physical Chemistry Chemical Physics* **2002,** *4* (18), 4314-4318.
3. Nguyen, N. T. T.; Furukawa, H.; Gándara, F.; Trickett, C. A.; Jeong, H. M.; Cordova, K. E.; Yaghi, O. M., Three-Dimensional Metal-Catecholate Frameworks and Their Ultrahigh Proton Conductivity. *Journal of the American Chemical Society* **2015,** *137* (49), 15394-15397.
4. Jin, S.; Hill, J. P.; Ji, Q.; Shrestha, L. K.; Ariga, K., Supercapacitive hybrid materials from the thermolysis of porous coordination nanorods based on a catechol porphyrin. *Journal of Materials Chemistry A* **2016,** *4* (15), 5737-5744.
5. Tytko, K.-H.; Gras, D., *Mo Molybdenum: Oxomolybdenum Species in Aqueous Solutions (Continued) Oxomolybdenum Species in Nonaqueous Solvents Oxomolybdenum Species in Melts Peroxomolybdenum Species*. Springer Science & Business Media: 2013.
6. Saines, P. J.; Yeung, H. H. M.; Hester, J. R.; Lennie, A. R.; Cheetham, A. K., Detailed investigations of phase transitions and magnetic structure in Fe(iii), Mn(ii), Co(ii) and Ni(ii) 3,4,5-trihydroxybenzoate (gallate) dihydrates by neutron and X-ray diffraction. *Dalton Trans.* **2011,** *40* (24), 6401-6410.
7. Cooper, L.; Hidalgo, T.; Gorman, M.; Lozano-Fernandez, T.; Simon-Vazquez, R.; Olivier, C.; Guillou, N.; Serre, C.; Martineau, C.; Taulelle, F.; Damasceno-Borges, D.; Maurin, G.; Gonzalez-Fernandez, A.; Horcajada, P.; Devic, T., A biocompatible porous Mg-gallate metal-organic framework as an antioxidant carrier. *Chemical communications* **2015,** *51* (27), 5848-5851.
8. Hidalgo, T.; Cooper, L.; Gorman, M.; Lozano-Fernandez, T.; Simon-Vazquez, R.; Mouchaham, G.; Marrot, J.; Guillou, N.; Serre, C.; Fertey, P.; Gonzalez-Fernandez, A.; Devic, T.; Horcajada, P., Crystal structure dependent in vitro antioxidant activity of biocompatible calcium gallate MOFs. *Journal of Materials Chemistry B* **2017,** *5* (15), 2813-2822.
9. Mouchaham, G.; Cooper, L.; Guillou, N.; Martineau, C.; Elkaïm, E.; Bourrelly, S.; Llewellyn, P. L.; Allain, C.; Clavier, G.; Serre, C.; Devic, T., A Robust Infinite Zirconium Phenolate Building Unit to Enhance the Chemical Stability of Zr MOFs. *Angewandte Chemie International Edition* **2015,** *54* (45), 13297-13301.
10. Bhuyan, J.; Sarkar, S., Self-Assembly of Magnesium and Zinc Trimethoxyphenylporphyrin Polymer as Nanospheres and Nanorods. *Crystal Growth & Design* **2011,** *11* (12), 5410-5414.

Chapter 6:
General Conclusions and Perspectives

6. General conclusions and perspectives

The work presented in this thesis involved investigating the synthesis of stable MOFs via exploring the reactivity of various high valent metal ions with porphyrinic ligands carrying different coordinating functionalities.

The porphyrinic ligands used for the study was synthesised in the laboratory as detailed in chapter 2. Four types of porphyrinic ligands were obtained in a gram scale, which contained four different coordinating functionalities: carboxylic acid [5,10,15,20-tetrakis(4-carboxyphenyl) porphyrin, H_2TCPP], tetrazole [5,10,15,20-tetrakis(4-(2H-tetrazol-5-yl)phenyl)porphyrin, H_2TTPP], catechol [5,10,15,20-tetrakis(3,4-dihydroxyphenyl)porphyrin, H_{10}-PorphCat] and gallol [5,10,15,20-tetrakis(3,4,5-trihydroxyphenyl)porphyrin , H_{14}-PorphGal].

We first looked at two existing stable carboxylate based porphyrinic MOFs to explore the possibility of imparting new functionalities to them as discussed in chapter 3. The MOF published by our lab, [Fe^{II}pzTCPP($Fe^{III}OH)_2$] had shown stability in water but had saturated iron centres in the framework. Thus, we investigated the possibility of obtaining this framework with unsaturated metal centres via studying the reactivity of Fe^{3+} with the carboxylic acid functionalised porphyrin, H_2TCPP. This involved studying the nature of the intermediate formed during the synthesis procedure to gain an understanding of the overall MOF formation. However, this was not successful due to poor crystallinity of the crystals obtained and the formation of a gel product. Attempts were also made to replace the pyrazine in the framework with a different N-donor such as imidazole. While coordination polymer products were obtained, some of them showing microporosity, the nature of the structure of these materials remain unknown. However, further investigation of the effect of parameters such as temperature and solvent systems remains a possibility to advance the study of the porous material obtained.

Reactivity of Co metalated TCPP with Fe^{3+} was also investigated. The structure of a new phase, [CoTCPP($H_2O)_2$($Fe^{III}OH)_2$] was solved via single crystal X-ray diffraction. However, the crystallinity of the bulk phase was poor and the efforts made to improve it were not successful. Two other different coordination polymer products were also obtained which showed better bulk crystallinity but the lack of single crystals of sufficient quality for x-ray diffraction hindered further structural analysis. However, only a limited number of synthetic parameters were investigated due to time constraints. Therefore, there is room for further synthesis optimisation for these products and further analysis.

The other reported stable carboxylate MOF we studied, Al-PMOF, had also shown stability in water and in acidic media. Several variations of this MOF with differently metalated porphyrin cores

has been reported but frameworks with Mn^{3+} and Fe^{3+} had not been successfully synthesised. Our efforts led to the successful synthesis of the Mn-Al-PMOF and Fe-Al-PMOF via the optimisation of synthetic parameters for the solvothermal reaction between Al^{3+} and corresponding metalated TCPP ligand. Fe-Al-PMOF was also obtained from the post-synthetic metalation of the free base Al-PMOF but with lower Fe occupancy in the porphyrin cores.

The viability of the synthesised metalated Al-PMOF material as heterogeneous catalysts was investigated. Various reactions were screened and the most promising initial results were obtained for the formation of a cyclic pyrazoline product from ethyl diazoacetate catalysed by Fe-Al-PMOF, which showed good selectivity (up to 90%) and limited recyclability (up to 5 runs). Potential of these material to catalyse other reactions such as oxidations was not looked at in depth due to time constraints. Thus, the more in-depth investigation of other type of reactions for catalytic activity is a possibility moving forward.

Chapter 4 presented the article published entailing work performed with the tetrazole based porphyrinic ligand (H_2TTPP) with the initial goal of obtaining extended material with spin crossover properties. Here we demonstrated that the [FeN_4O] chain like SBU seen with carboxylate MOFs can be successfully extended to the tetrazolate functionality. The MOF, [Fe^{II}pzTTP(Fe^{II}_{1-x} DMF $_{1-x}$ Fe^{III}_x OH_x)] had a topology similar to the carboxylate based MOF investigated in chapter 2, [Fe^{II}pzTCPP($Fe^{III}OH)_2$], but with both $Fe^{2+}/^{3+}$present in the inorganic backbone. This led to its air instability and the degradation of the MOF which prevented the study of the spin crossover behaviour. A potential method to obtain a similar MOF with improved stability might be to use a pyrazole functionalised ligand instead. There have been pyrazolate based porphyrinic MOFs reported with exceptional stability. In addition, [FeN_4O] chain like SBU has also been observed with non-porphyrinic pyrazolate frameworks. Thus, further investigations along this path remains an intriguing possibility.

The work performed with the two hydroxyphenyl functionalised porphyrin ligands was discussed in chapter 5. The investigation of the reactivity of the catechol based porphyrin (H_{10}-PorphCat) with Fe^{3+} was part of a long-term study being conducted at ILV. The work done by us led to obtaining single crystals for one of the phases which was analysed with synchrotron radiation and the structural resolution of this phase is still ongoing. Initial characterisation of the bulk material was performed which indicated the presence of an air stable porous framework. The next step for this phase apart from completing the structural resolution is the verification of the reproductivity of the bulk sample, which is yet to be performed.

In chapter 5, we also presented the article published concerning the studies conducted with the gallol functionalised porphyrin (H_{14}-PorphGal) which led to the synthesis of the first porphyrinic

MOF phase based on this functionality, MIL-173(M). This MOF can be obtained with both Zr^{4+} and trivalent rare earth metal ions Y^{3+}, Ce^{3+} and La^{3+}. The MIL-173(Zr) phase showed high chemical stability and was obtained with the porphyrin linkers in the free base form. Co-MIL-173(Zr) was obtained via post synthetic metalation and was demonstrated to possess heme like catalytic properties with molecular oxygen as the oxidant. The scope of the possible reactions that can be catalysed with MIL-173(Zr) can be potentially expanded by the metalation of the porphyrin cores by different metals such as Fe.

Our investigation into the reactivity of H_{14}-PorphGal with other trivalent metals led to the synthesis of coordination polymers based on Al^{3+} and In^{3+}. However, their structure remains unknown. Only a limited number of parameters were probed during the exploratory research and further investigation in to these parameters can potentially yield single crystals of this phase which can lead to resolving their structures.

Appendix

A. Appendix Chapter 2

A.1. Carboxylic acid based porphyrin synthesis

A.1.1. NMR spectroscopy

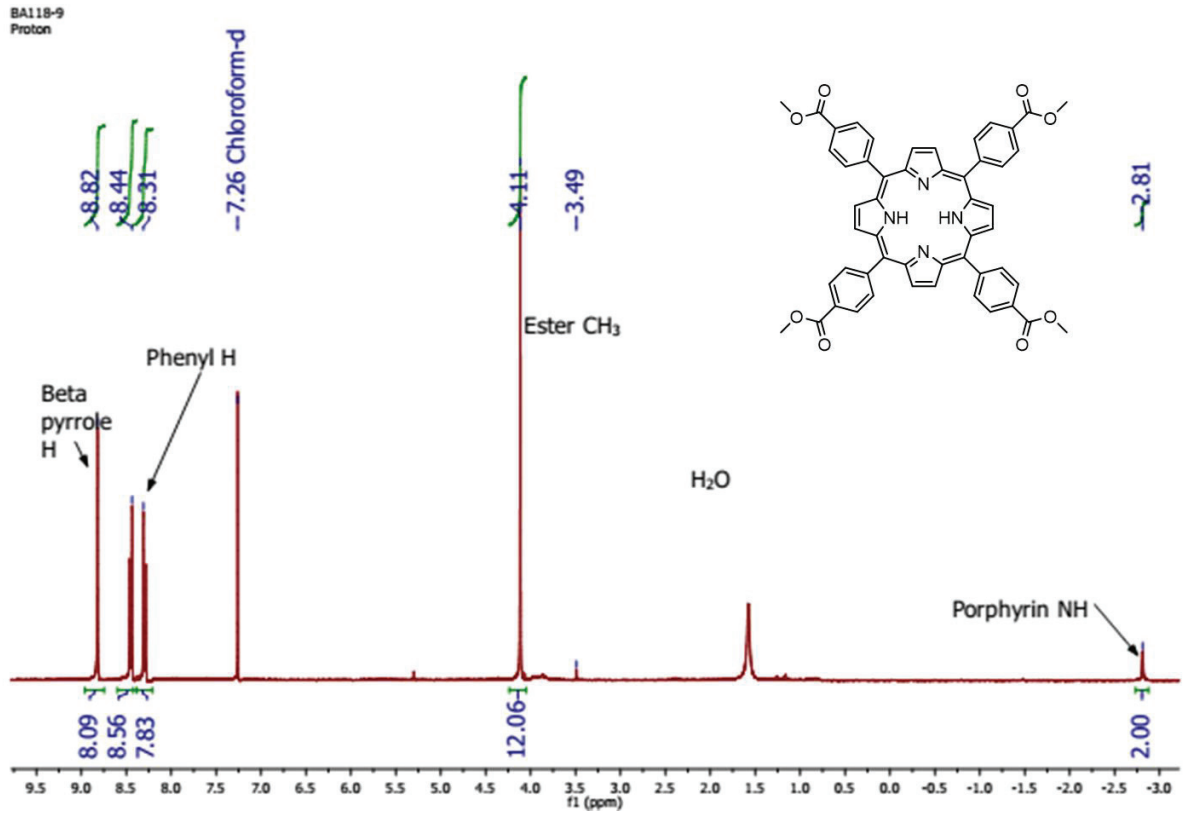

Figure A-1 NMR spectrum of H_2TEsterP in $CDCl_3$.

A.1.2. Mass spectrometry

ESI technique used for the mass spectrometry analysis. THF was used as solvent in this section unless stated otherwise.

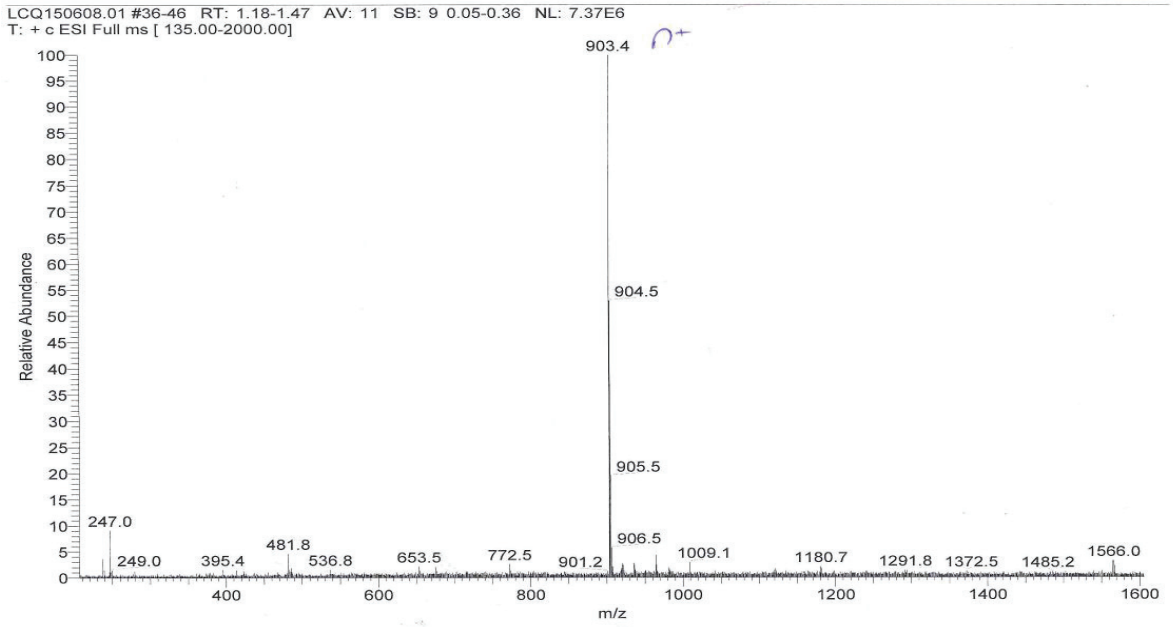

Figure A-2 Mass spectrometry data for CoTEsterP(X). The molecular ion [(CoTEsterP)$^+$] peak at 903 m/z along with the absence of a peak corresponding to the molecular ion for H_2TEsterP at 846 m/z confirms the complete metal insertion.

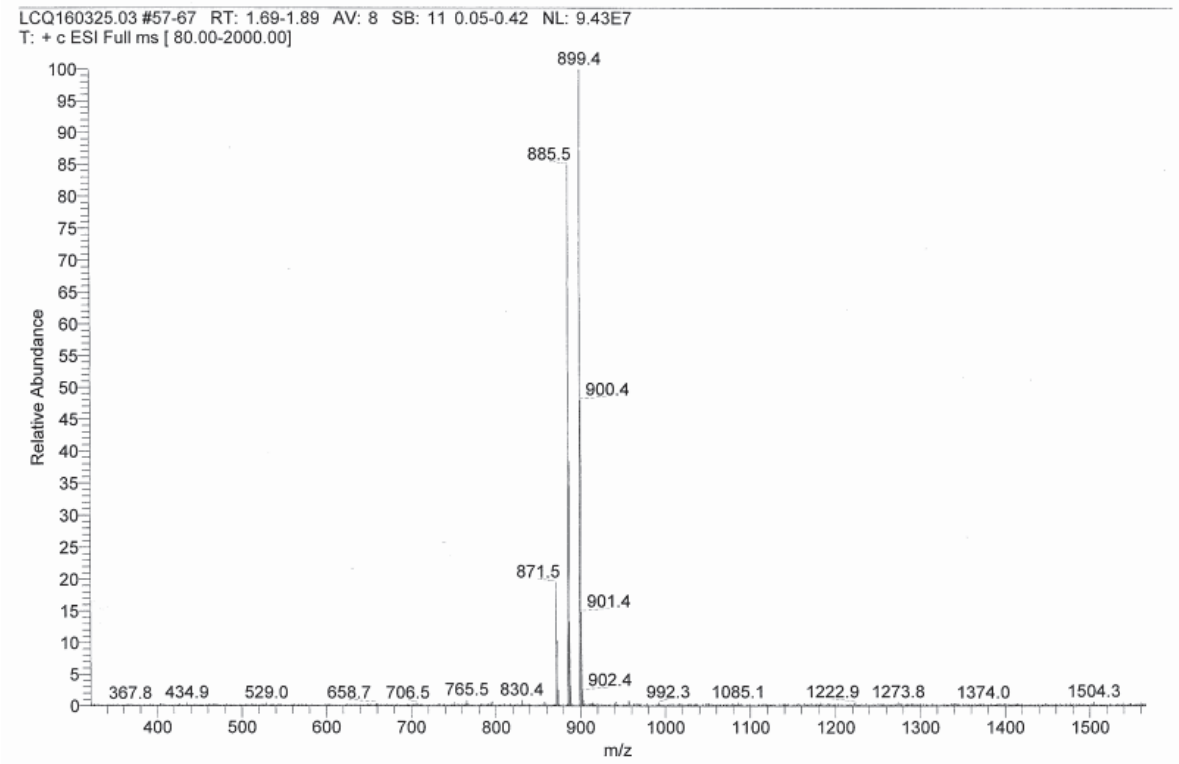

Figure A-3 Mass spectrometry data for MnTEsterP(X). The peak at 899.4 m/z corresponding to the molecular ion, (MnTEsterP)$^+$, along with the absence of a peak corresponding to the molecular ion for H_2TEsterP at 846 m/z confirms the complete metal insertion. The peaks at 885 m/z and 871 m/z can be explained by the loss of the ester CH_3 groups followed by the protonation of the oxygen during fragmentation.

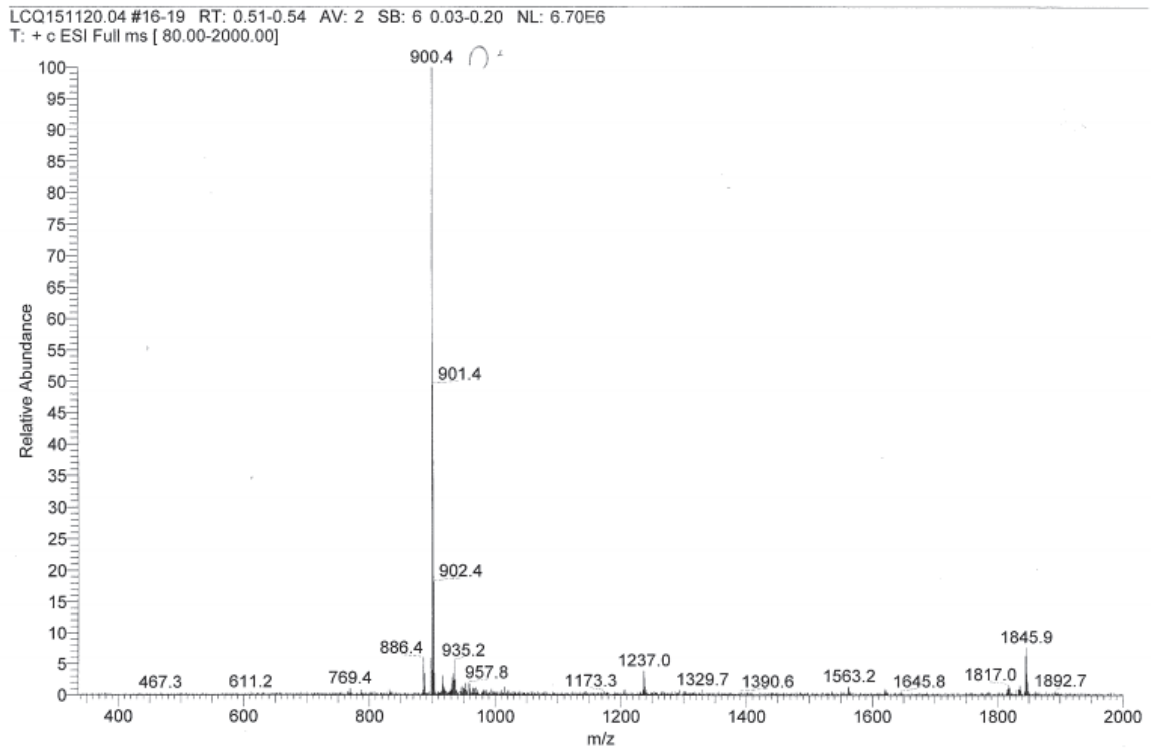

Figure A-4 Mass spectrometry data for FeTEsterP(Cl). The molecular ion [(FeTEsterP)$^+$] peak at 900 m/z along with the absence of a peak corresponding to the molecular ion for H_2TEsterP at 846 m/z confirm the complete metal insertion. The peak at 886 m/z can be explained by the loss of the ester CH_3 group followed by the protonation of the oxygen during fragmentation. The peak at 935 m/z is assigned to the complex [FeTesterP-Cl]$^+$ which indicates the presence of a chloride counter ion.

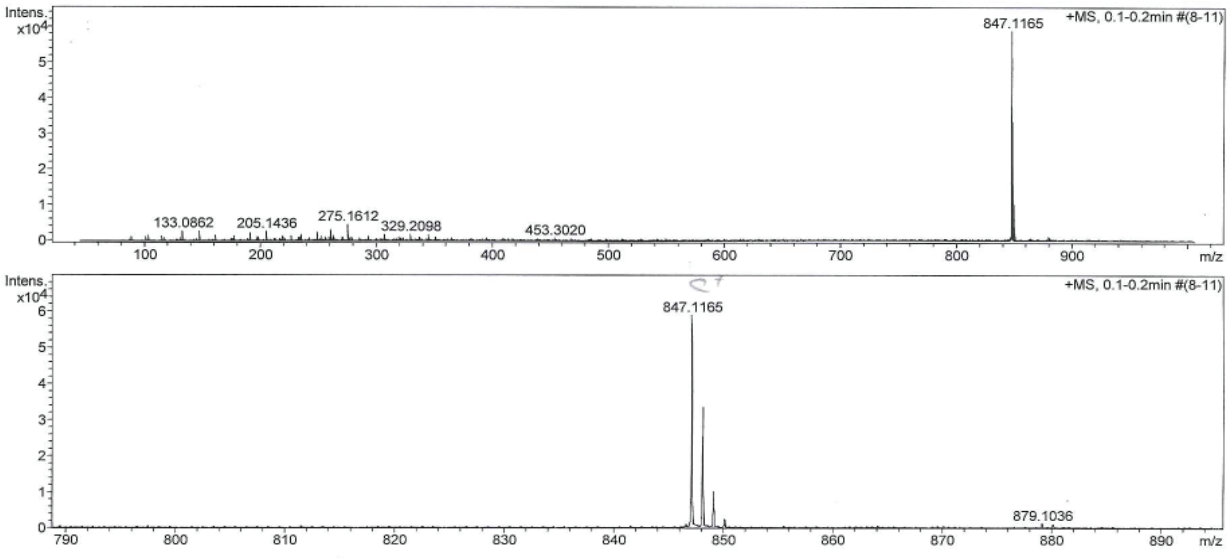

Figure A-5 Mass spectrometry data for CoTCPP(X). Peak corresponding to the molecular ion, (CoTCPP)$^+$, at 847.12 m/z and the absence of any peaks corresponding to the ester containing species confirm the complete hydrolysis of the ester groups.

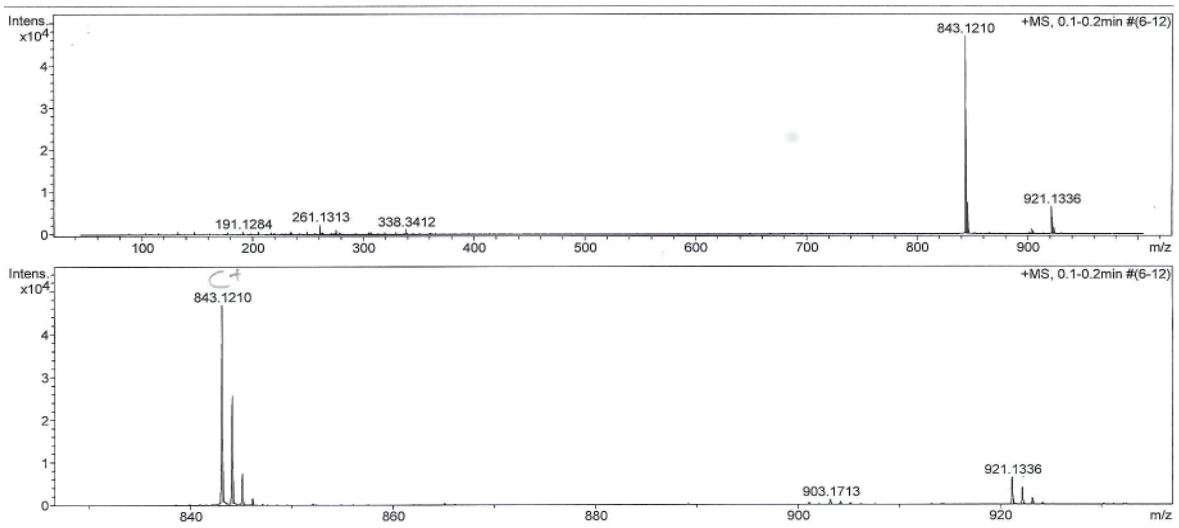

Figure A-6 Mass spectrometry data for MnTCPP(X). Peak corresponding to the molecular ion, $(MnTCPP)^+$, at 843.12 m/z and the absence of any peaks corresponding to the ester containing species confirm the complete hydrolysis of the ester groups.

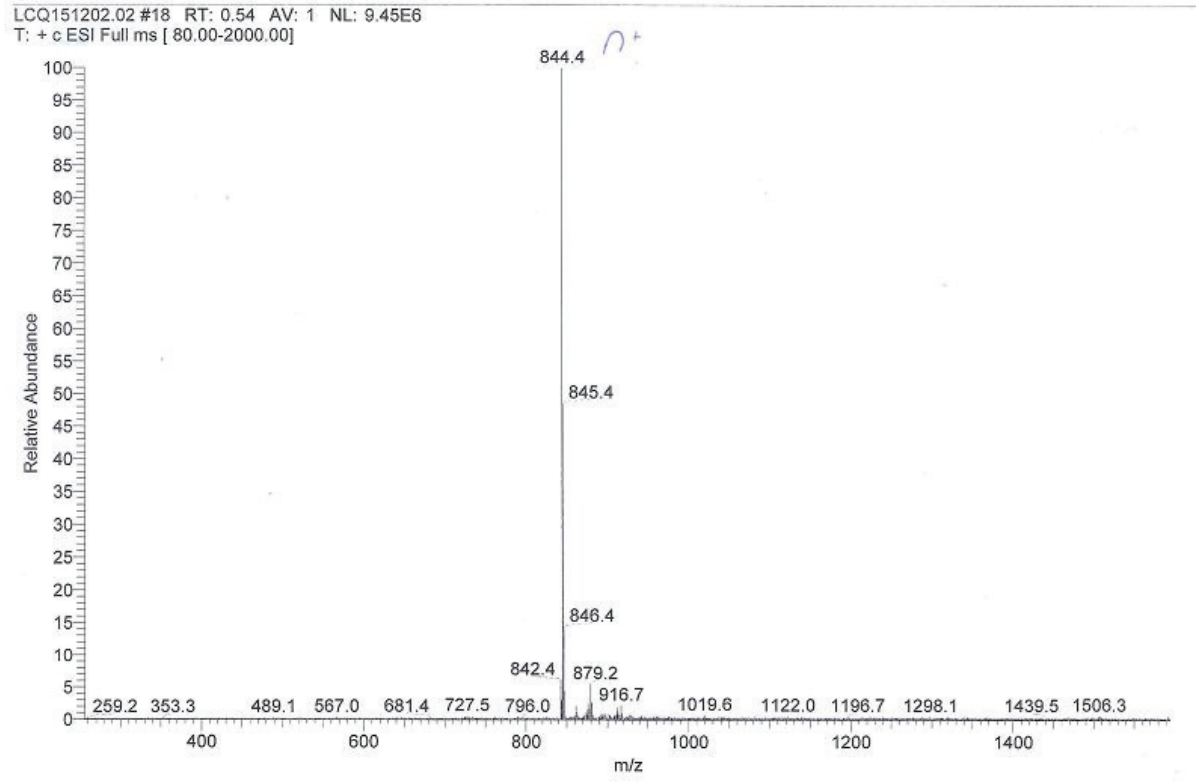

Figure A-7 Mass spectrometry data for FeTCPP(Cl). Peak corresponding to the molecular ion, $(FeTCPP)^+$, at 844.12 m/z and the absence of any peaks corresponding to the ester protected species confirm the complete hydrolysis of the ester groups. The peak at 879 m/z is assigned to the complex $[FeTCPP\text{-}Cl]^+$ which indicates the presence of a chloride counter ion.

A.1.3. UV-vis Spectroscopy

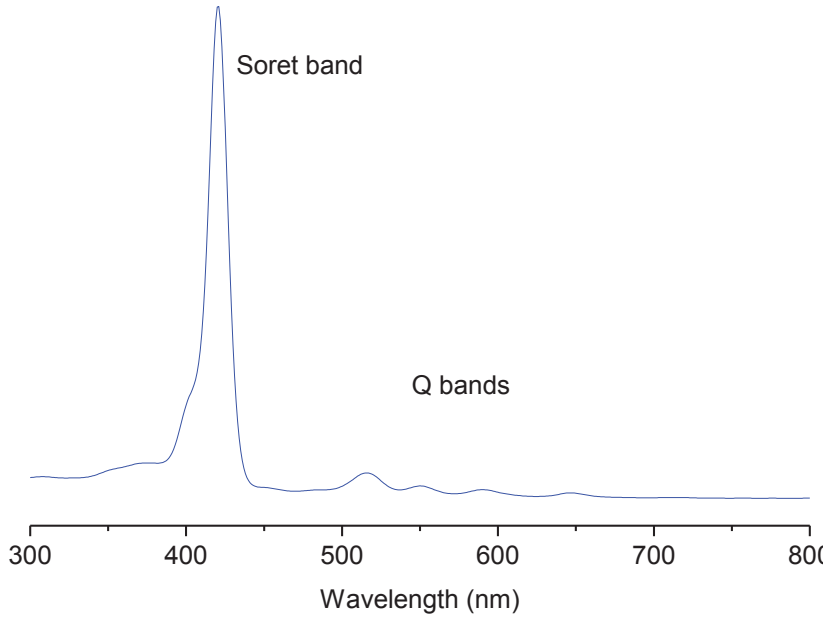

Figure A-8 UV-vis spectrum for H_2TEsterP in chloroform.

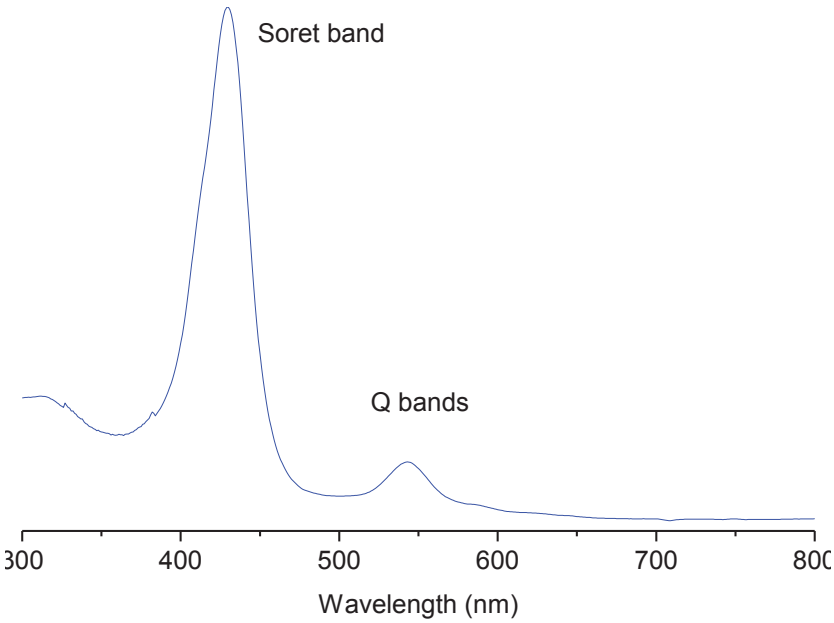

Figure A-9 UV-vis spectrum for the CoTEsterP(X) in chloroform.

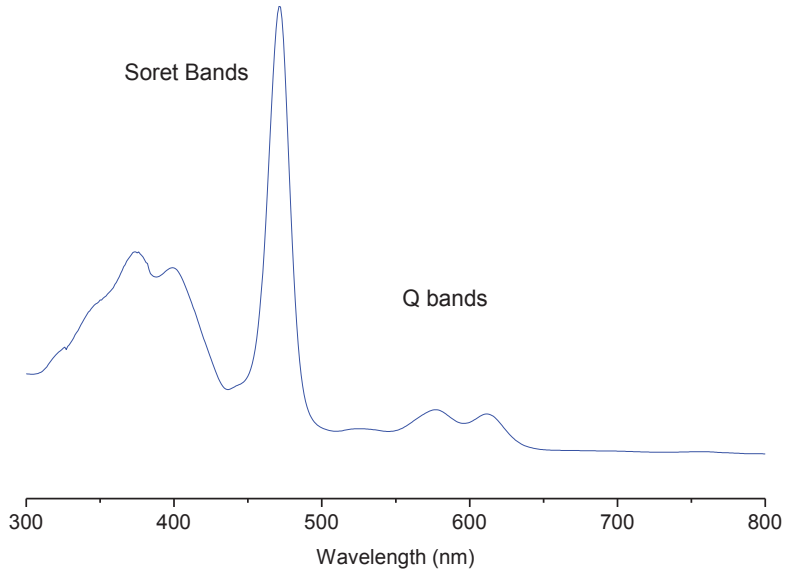

Figure A-10 UV-vis spectrum of the MnTEsterP(X) in chloroform.

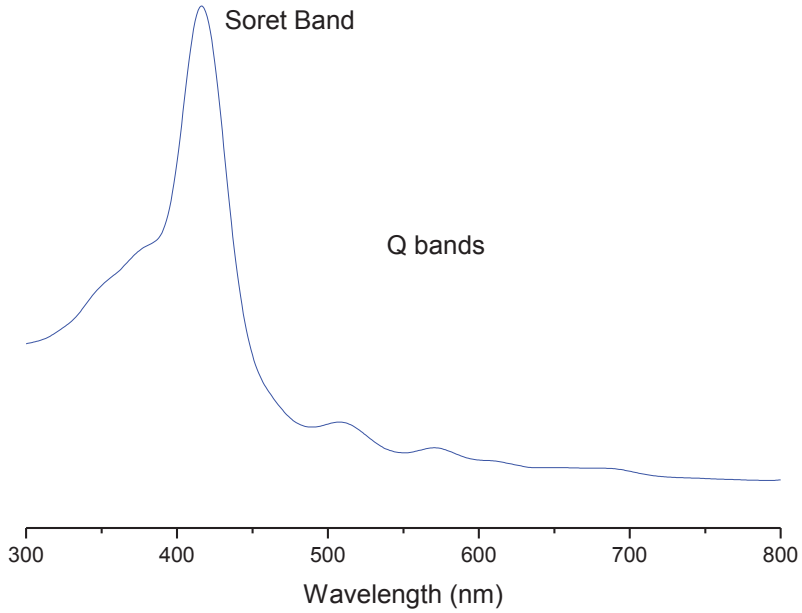

Figure A-11 UV-vis spectrum of the FeTEsterP(Cl) in chloroform.

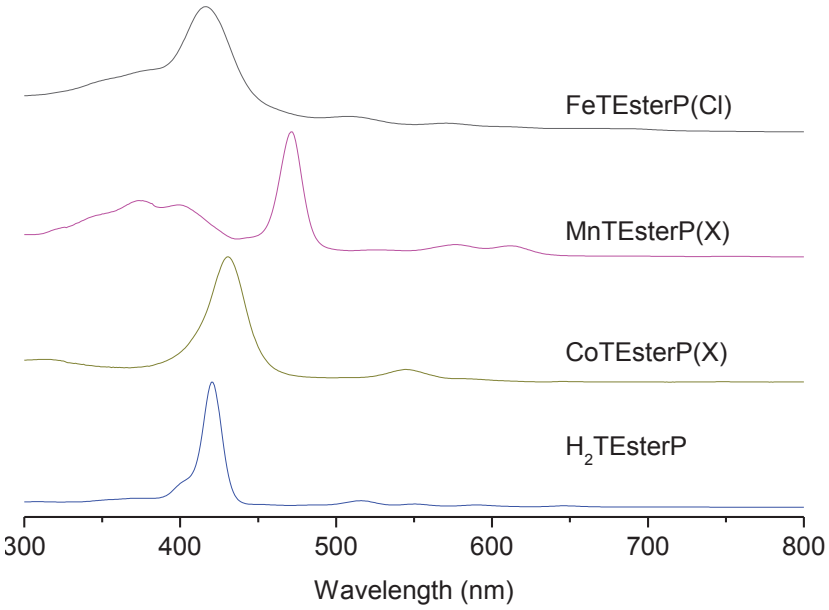

Figure A-12 UV-vis spectra of H_2TEsterP compared to the metalated variations. (UV spectra were measured in chloroform). Soret band and the Q bands change as a function of the metal coordinated in the porphyrin core.

Table A-1 Soret band and Q bands for the metalated TEsterP compared to the free base, H_2TEsterP (solvent is chloroform).

	Soret Band (nm)	**Q bands (nm)**
H_2TEsterP	421	517, 550, 591, 646
CoTEsterP(X)	430	543, 588
MnTEsterP(X)	377,400, 472	524,576,613
FeTesterP(Cl)	416	507, 571, 610

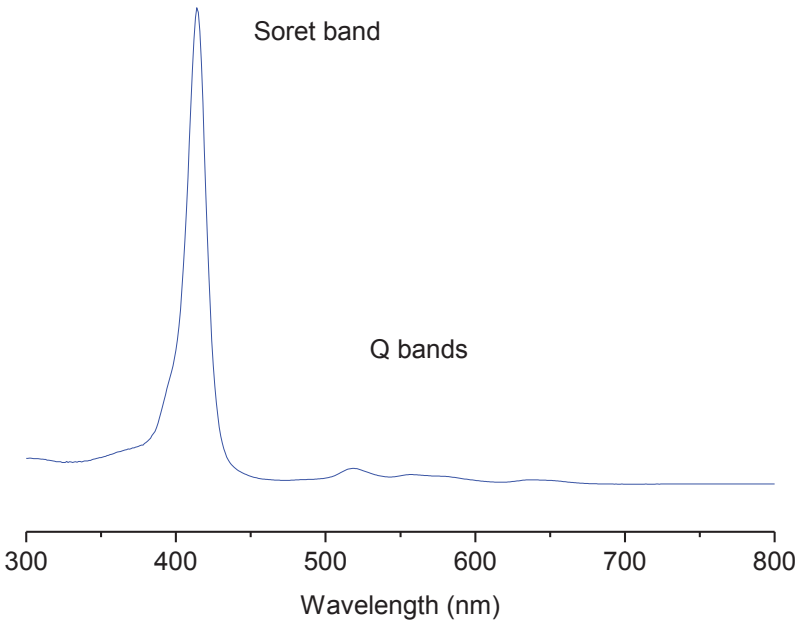

Figure A-13 UV-vis spectrum of H_2TCPP measured in 0.1M NaOH.

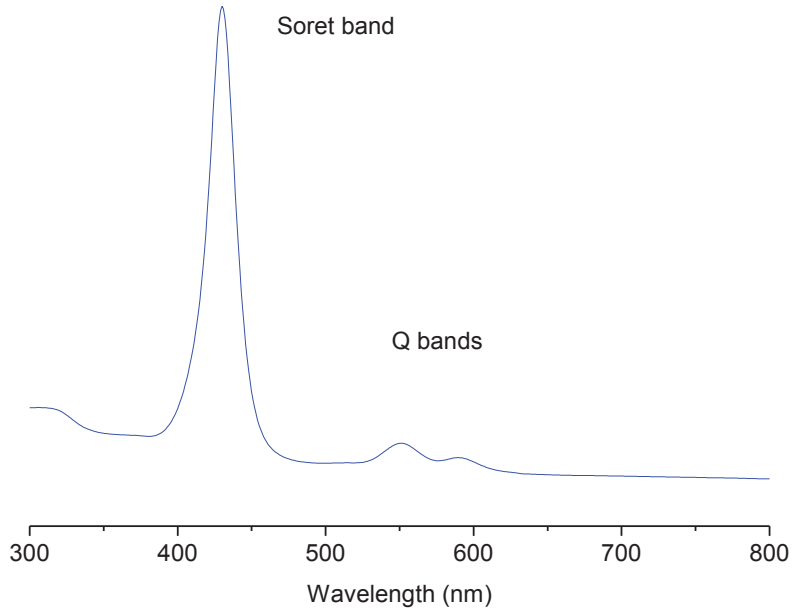

Figure A-14 UV-vis spectrum of CoTCPP(X) measured in 0.1M NaOH.

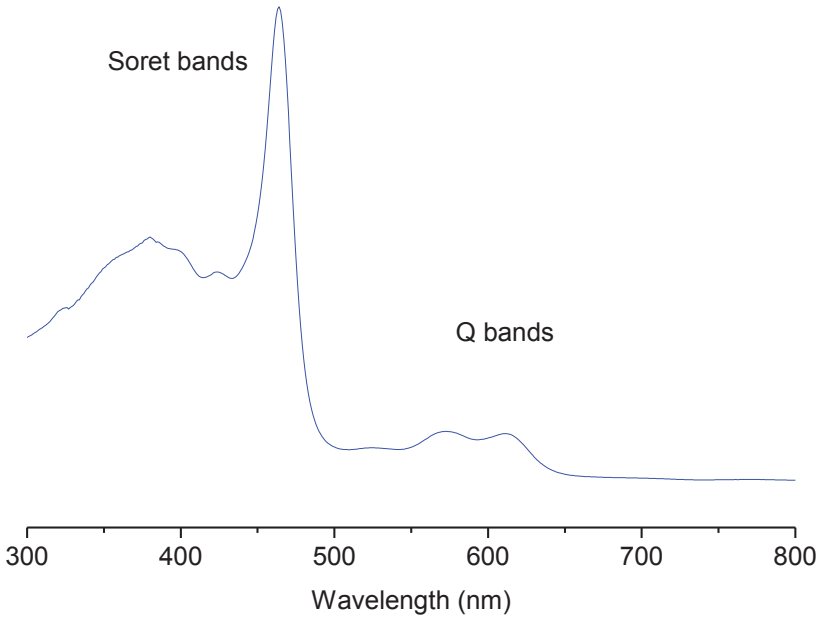

Figure A-15 UV-vis spectrum of MnTCPP(X) measured in 0.1M NaOH.

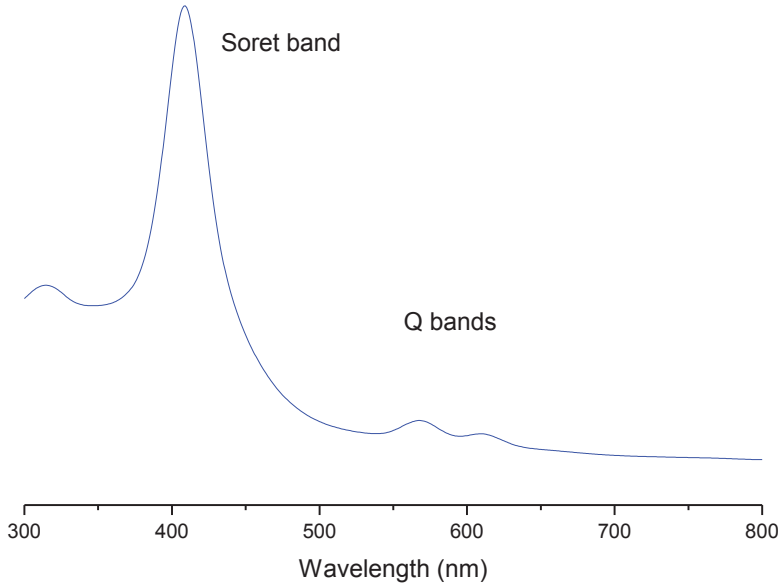

Figure A-16 UV-vis spectrum of FeTCPP(Cl) measured in 0.1M NaOH.

Table A-2 Soret Band and Q bands of metalated TCPP compared to H_2TCPP measured in 0.1 M NaOH.

	Soret Band (nm)	**Q bands (nm)**
H_2TCPP	415	518, 556, 586, 642
CoTCPP(X)	430	551, 590
MnTCPP(X)	380,401, 464	525, 573, 611
FeTCPP(Cl)	409	568, 609

A.1.4. IR spectroscopy

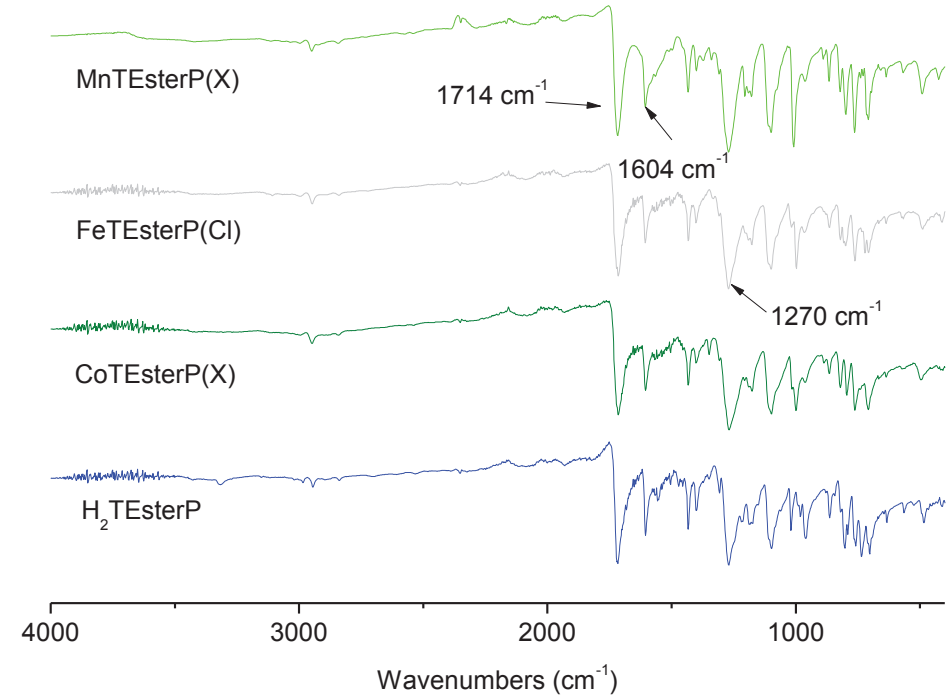

Figure A-17 IR spectra of metalated TEsterP compared to free base, H_2TEsterP.

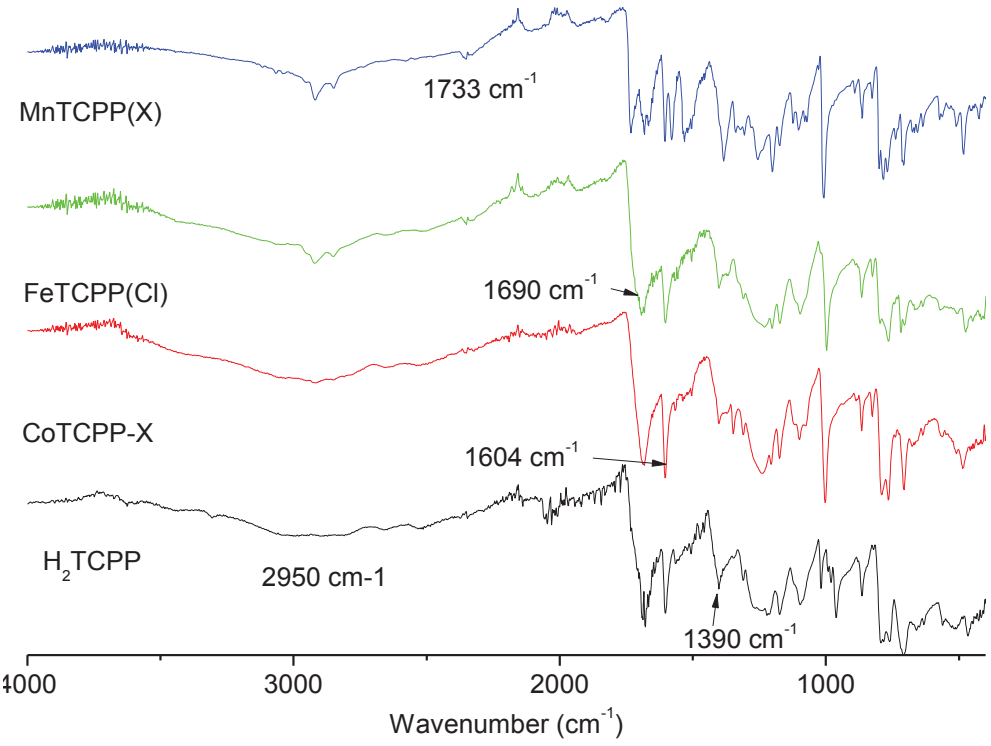

Figure A-18 IR spectra of metalated TCPP compared to free base, H_2TCPP.

A.2. Catechol based porphyrin synthesis

A.2.1. NMR spectroscopy

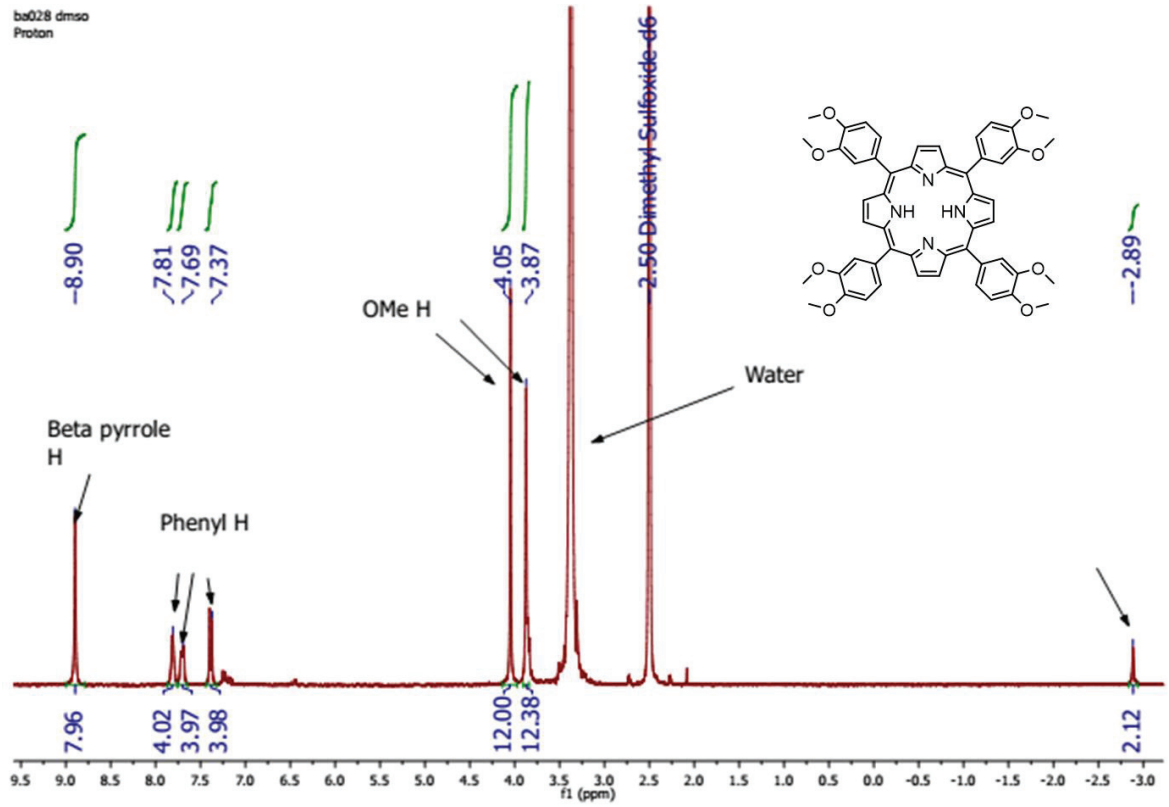

Figure A-19 NMR spectrum of $H_2T(OMe)_2PP$ in DMSO.

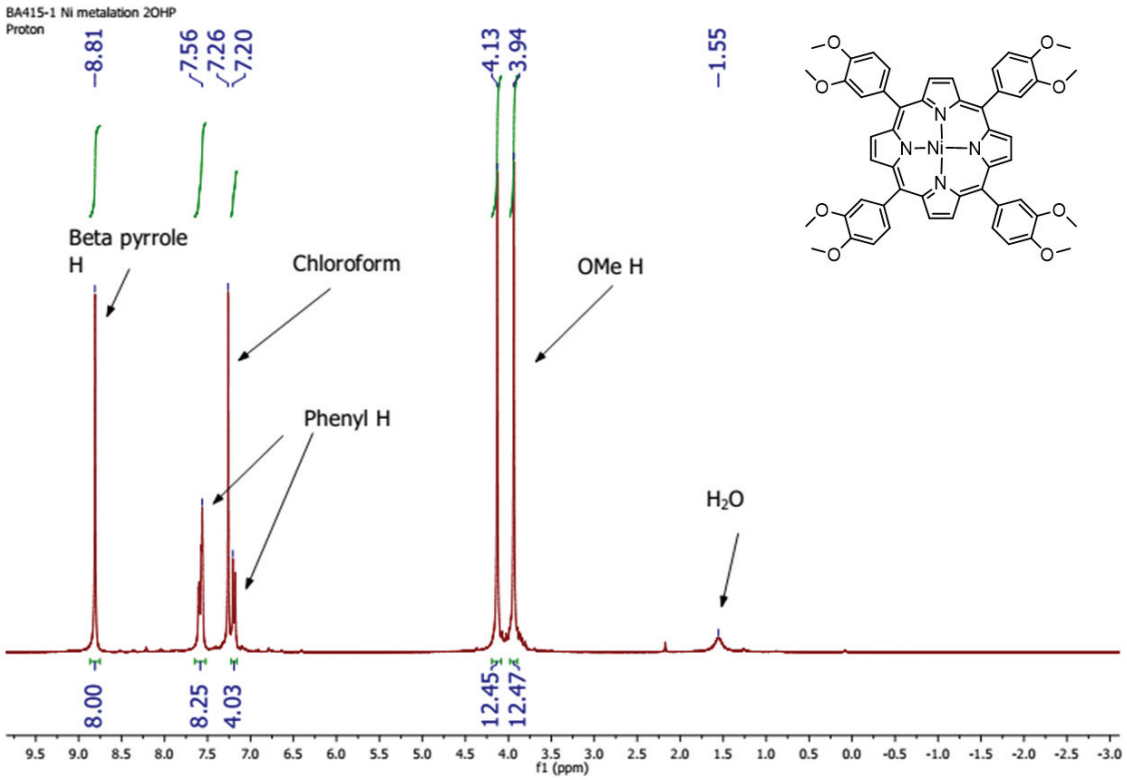

Figure A-20 NMR spectrum of NiT(OMe)$_2$PP in chloroform.

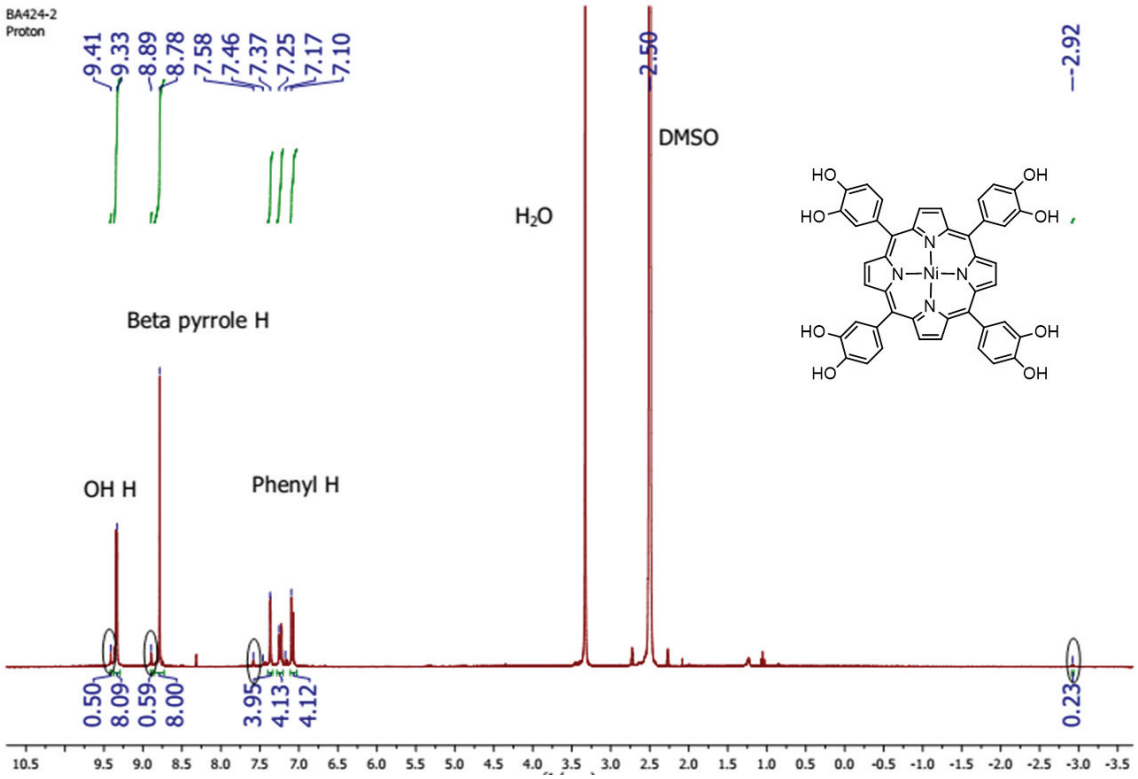

Figure A-21 NMR spectrum (DMSO) of product obtained from the ether cleavage of the methoxy groups of NiT(OMe)$_2$PP with pyridinium chloride. The circled peaks represent the free base porphyrin, H$_{10}$-PorphCat, which is present at 7% compared to Ni-H$_8$-PorphCat. This indicates a degree of demetalation during the reaction.

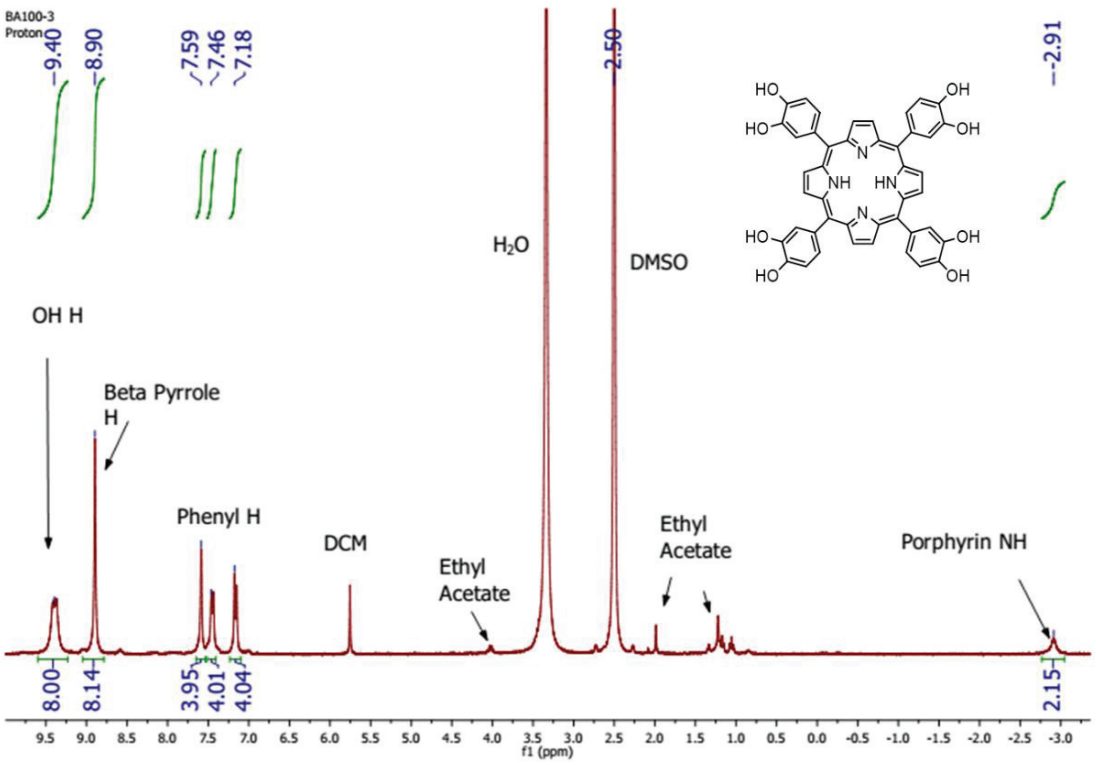

Figure A-22 NMR spectrum (DMSO) for the product of the synthesis method 1 for the ether cleavage of the methoxy groups of $H_2T(OMe)_2PP$.

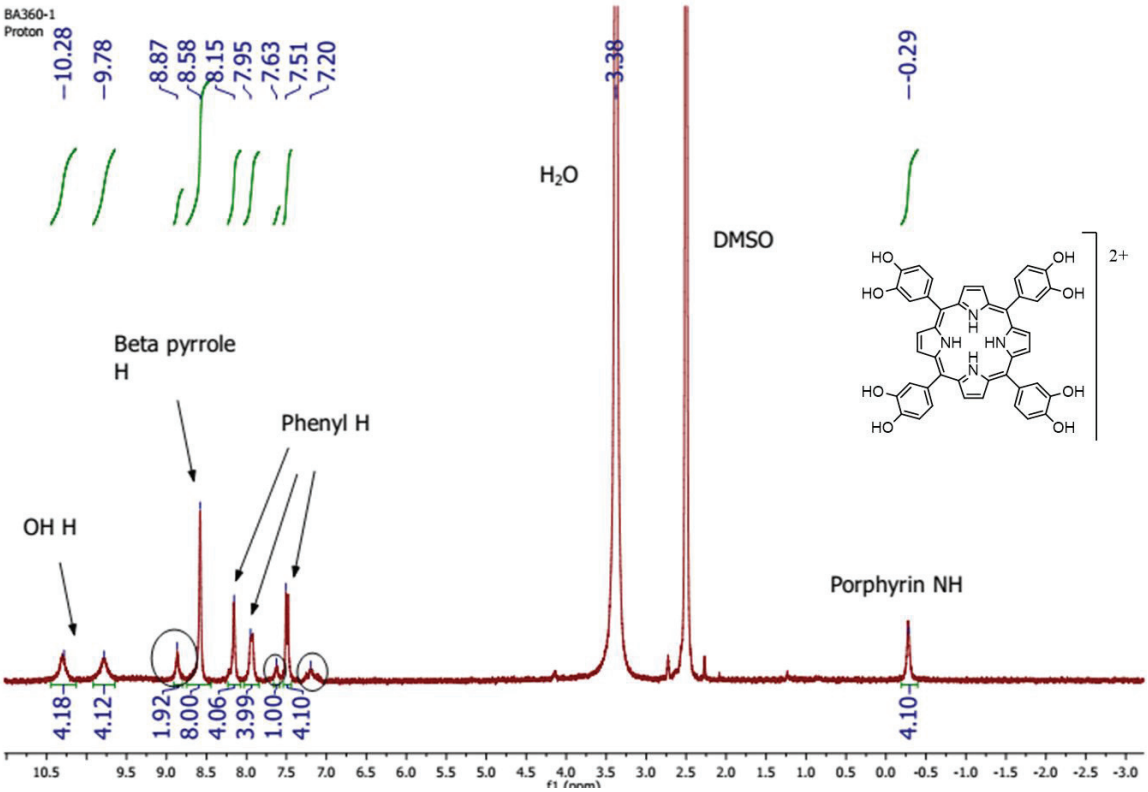

Figure A-23 NMR spectrum (DMSO) of the product obtained from the method 2 of the BBr3 ether cleavage. The major product obtained is the diprotonated species of H_{10}-PorphCat (H_{12}-PorphCat $^{2+}$). The circled peaks represent the unprotonated H_{10}-PorphCat which is present at 25% compared to the major product

A.2.2. Mass spectrometry

ESI technique used for the mass spectrometry analysis. CH_3OH was used as solvent unless stated otherwise.

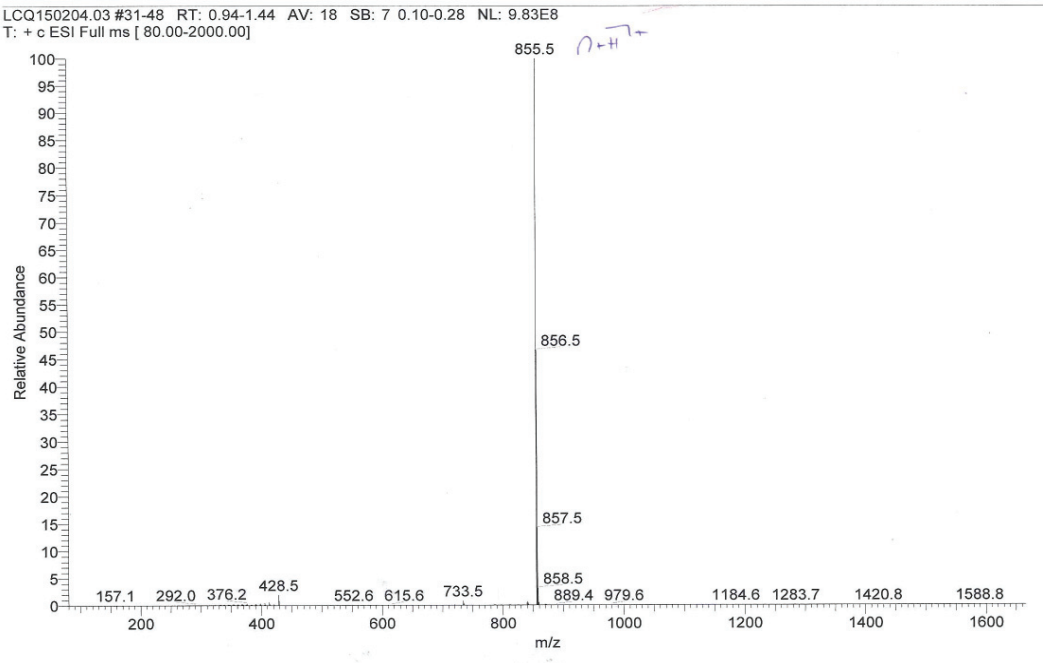

Figure A-24 Mass spectrometry data for $H_2T(OMe)_2PP$ (solvent is dichloromethane). The peak for the mono protonated molecular ion is at 855.5 m/z.

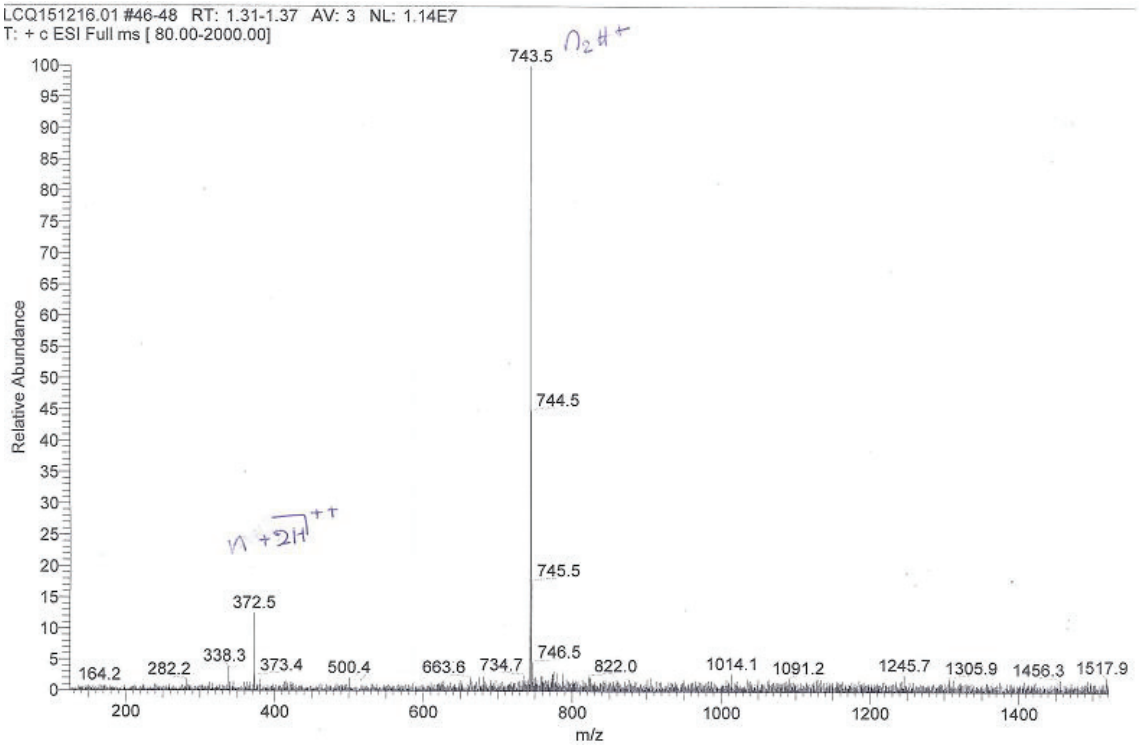

Figure A-25 Mass spectrometry data for the method 1 for the BBr_3 ether cleavage of $H_2T(OMe)_2PP$. The peak at 743.4 m/z corresponds to the mono protonated molecular ion and the peak at 372.4 m/z corresponds to the complex $(H_{10}$-PorphCat $+2H)^{2+}$.

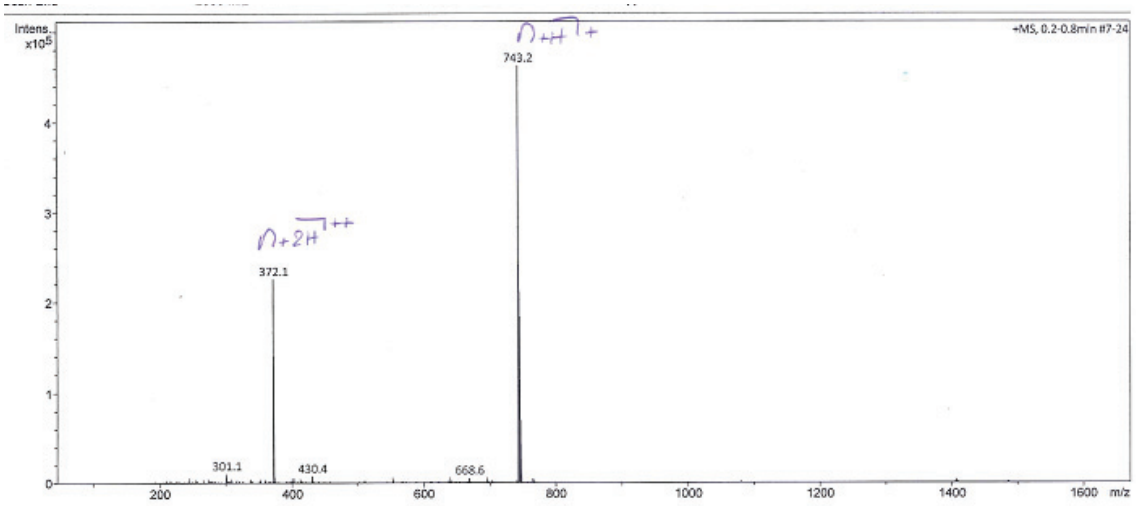

Figure A-26 Mass spectrometry data for the purification method 2 of the BBr_3 ether cleavage. The peak at 743.2 m/z corresponds to the mono protonated molecular ion and the peak at 372.1 m/z corresponds to the complex (H_{10}-PorphCat +2H)$^{2+}$.

A.2.3. UV-vis spectroscopy

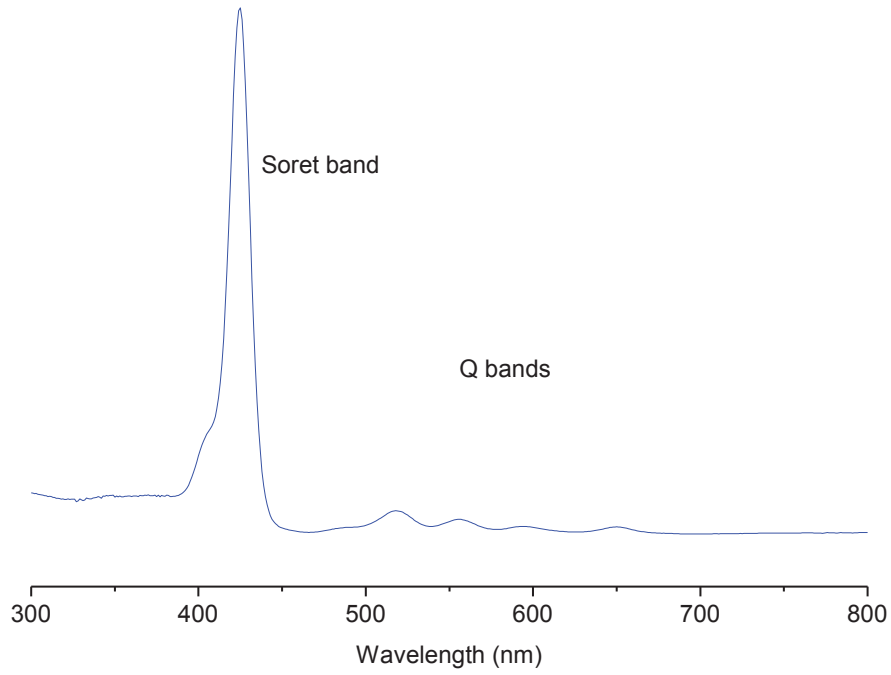

Figure A-27 The UV-vis spectrum of $H_2T(OMe)_2PP$ in chloroform.

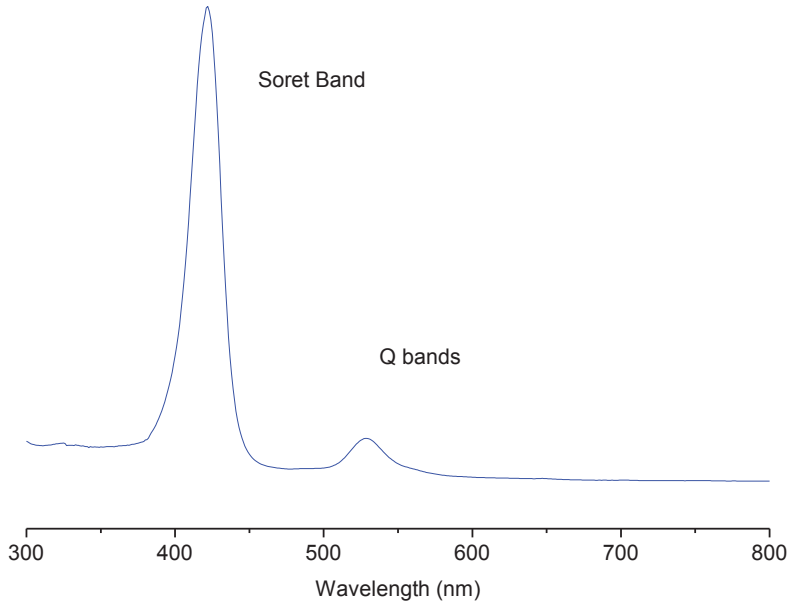

Figure A-28 The UV-vis spectrum of $NiT(OMe)_2PP$ in chloroform.

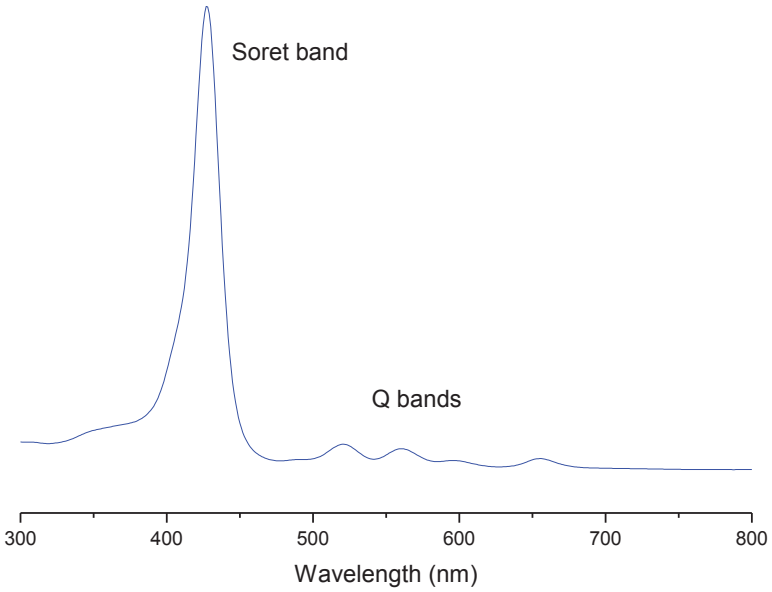

Figure A-29 The UV-vis spectrum of the product from the BBr_3 ether cleavage method 1, H_{10}-PorphCat, in DMF.

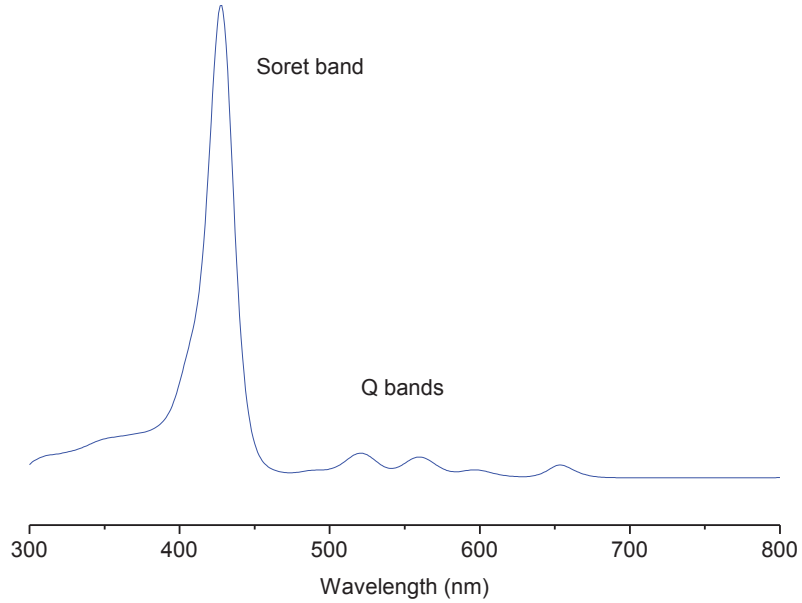

Figure A-30 The UV-vis spectrum of the product from the BBr_3 ether cleavage method 2, H_{12}-PorphCat-2X in DMF.

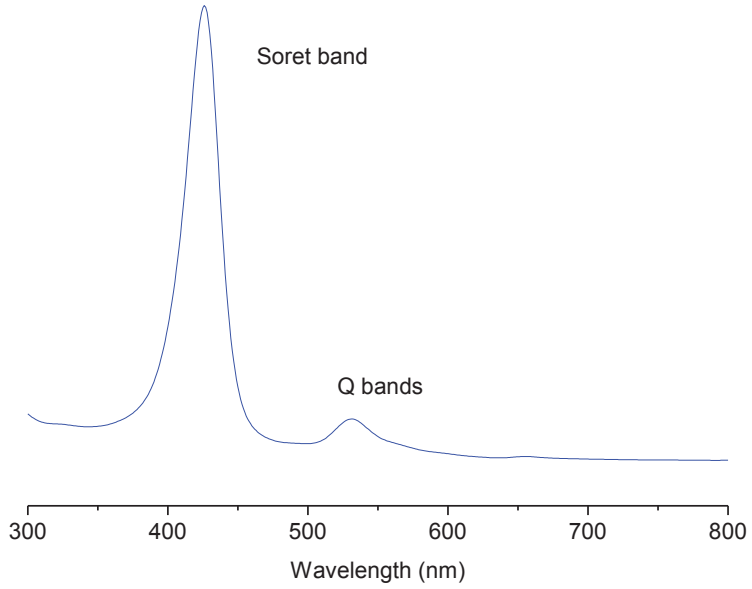

Figure A-31 The UV-vis spectrum of Ni-H_8-PorphCat in DMF.

Table A-3 The peaks observed in UV-vis spectra for the methoxy and catechol porphyrins. $H_2T(OMe)_2PP$ and $NiT(OMe)_2PP$ were measured in chloroform while the rest where measured in DMF

	Soret Band (nm)	**Q bands (nm)**
$H_2T(OMe)_2PP$	425	518, 558, 595, 652
$NiT(OMe)_2PP$	422	530
H_{10}-PorphCat	427	520,561,596,654
Ni-H_8-PorphCat	425	531

A.2.4. IR spectroscopy

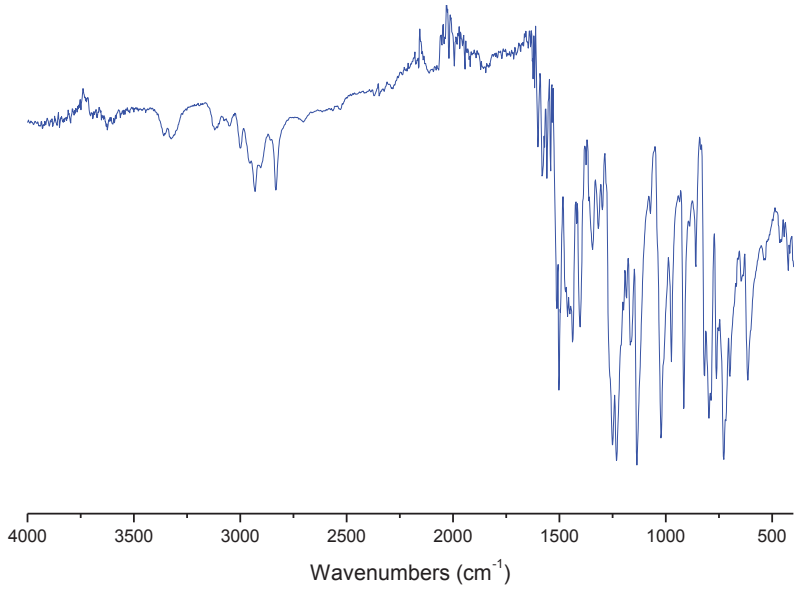

Figure A-32 IR spectrum for $H_2T(OMe)_2PP$. Peaks between 1600-1400 cm^{-1} is assigned to the aromatic C=C stretches of the porphyrin ring and the phenyl groups. The peak at 2830 cm^{-1} is assigned to the CH stretches of the methoxy groups.

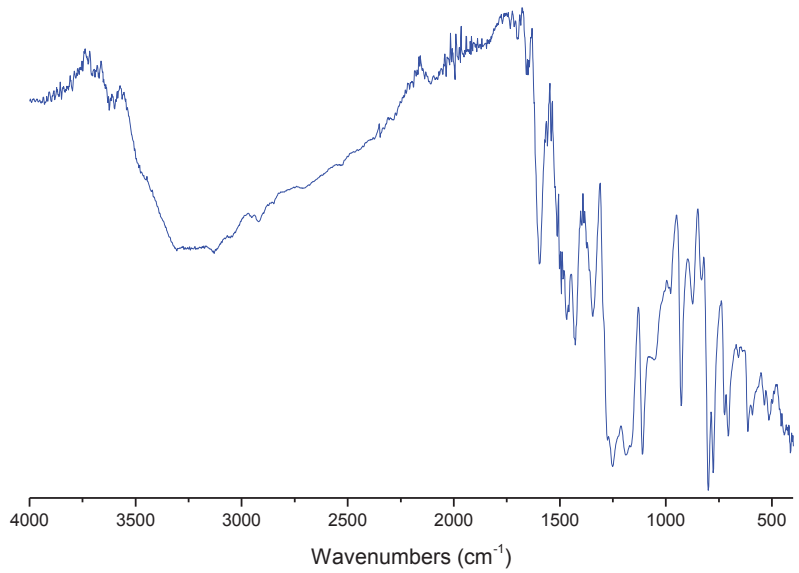

Figure A-33 IR spectrum for H_{10}-PorphCat from method 1. Peaks between 1600-1400 cm^{-1} is assigned to the aromatic C=C stretches of the porphyrin ring and the phenyl groups. The broad peak around 3100 cm^{-1} is assigned to the OH stretches of the hydroxy groups.

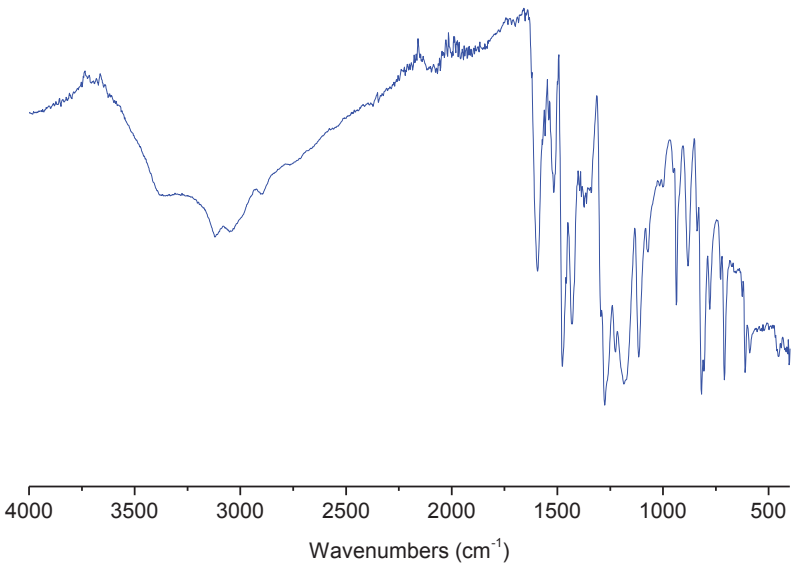

Figure A-34 IR spectrum for H_{12}-PorphCat $^{2+}$ from method 2. Peaks between 1600-1400 cm^{-1} is assigned to the aromatic C=C stretches of the porphyrin ring and the phenyl groups. The broad peak around 3100 cm^{-1} is assigned to the OH stretches of the hydroxy groups.

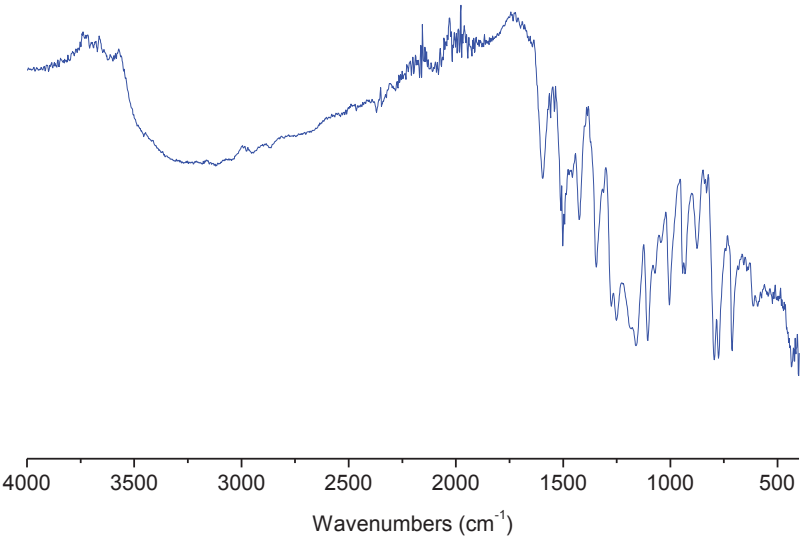

Figure A-35 IR spectrum for Ni-H_8-PorphCat. Peaks between 1600-1400 cm^{-1} is assigned to the aromatic C=C stretches of the porphyrin ring and the phenyl groups. The broad peak around 3100 cm^{-1} is assigned to the OH stretches of the hydroxy groups.

A.3. Gallol based porphyrin synthesis

A.3.1. NMR spectroscopy

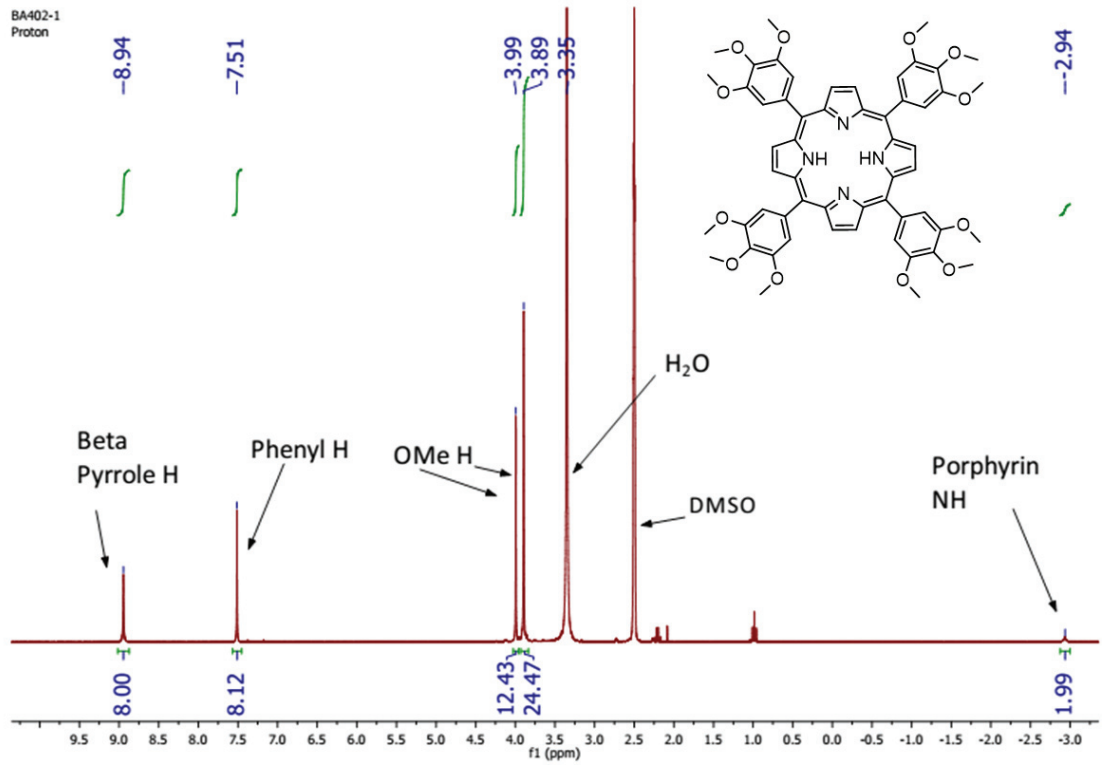

Figure A-36 NMR spectrum (DMSO) of H_2TtrimPP.

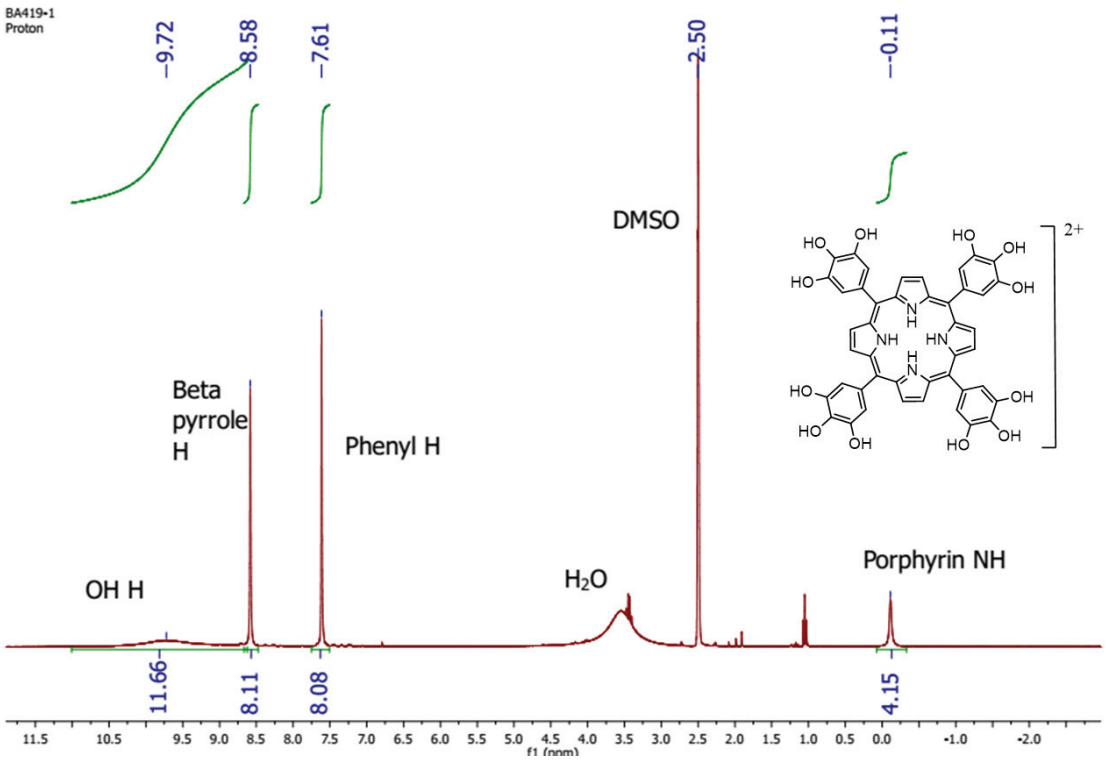

Figure A-37 NMR spectrum in DMSO for H_{14}-PorphGal in which is present in the diprotonated form (H_{16}-PorphGal^{2+}) as indicated by the presence of two extra porphyrin NH protons.

A.3.2. Mass spectrometry

ESI technique was used for the mass spectrometry analysis.

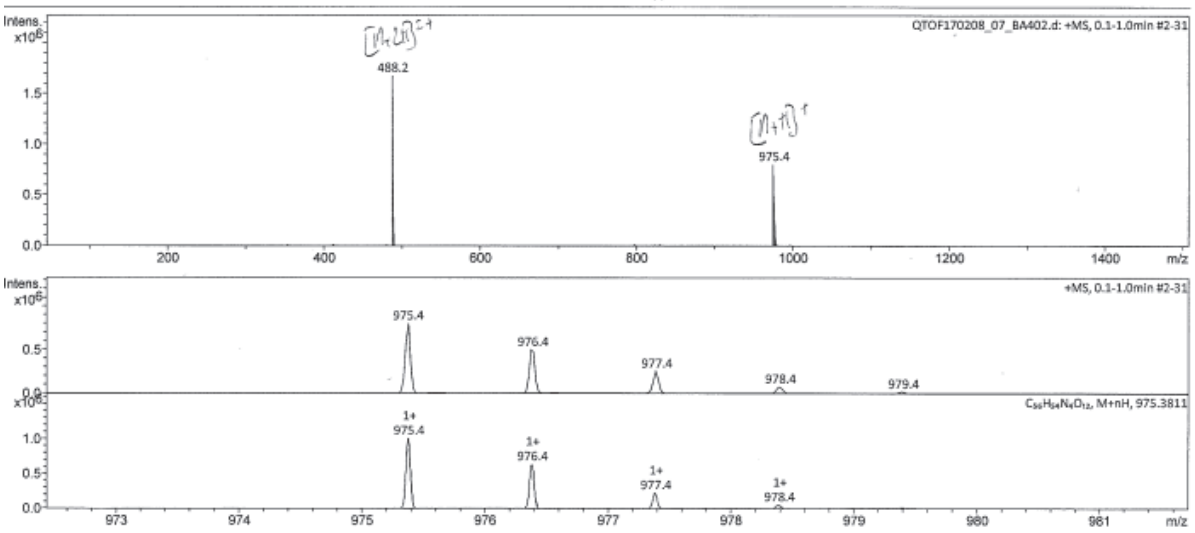

Figure A-38 Mass spectrometry data for H_2TtrimPP in THF. Monoprotonated molecular ion, $[(H_2TtrimPP)+H]^+$, is present at 975.4 m/z.

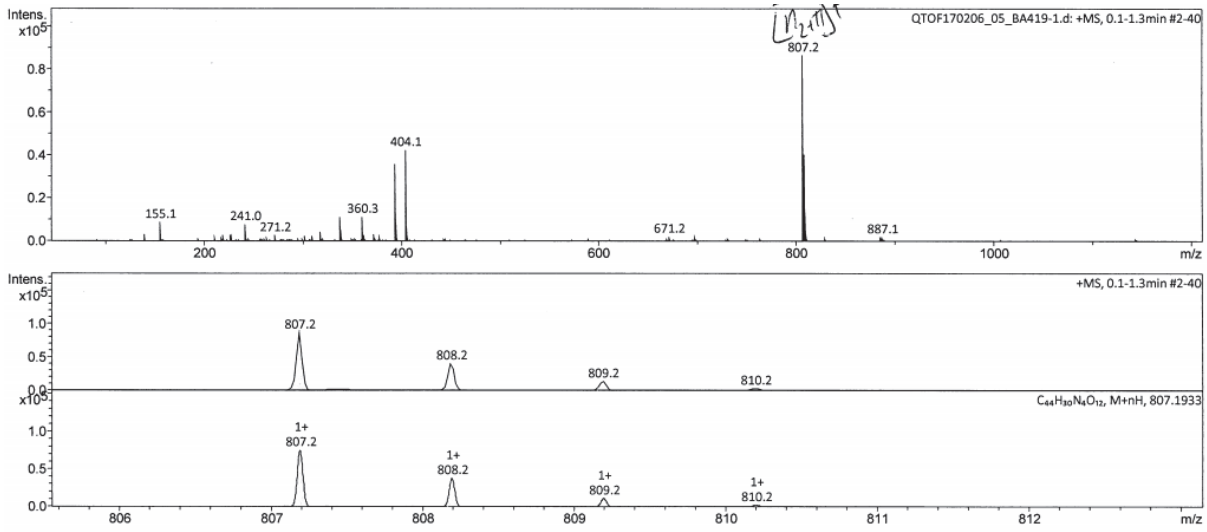

Figure A-39 Mass spectrometry data for H_{16}-PorphGal-2Br in THF. The monoprotonated molecular ion at 807.2 m/z along with the absence of any methoxy species confirm the complete ether cleavage of H_2TtrimPP methoxy groups. The peak at 887.1 m/z can be attributed to the $(H_{14}$-PorphGal +2H+Br$)^+$ complex which indicate that Br^- is present as a counter ion.

A.3.3. UV-vis spectroscopy

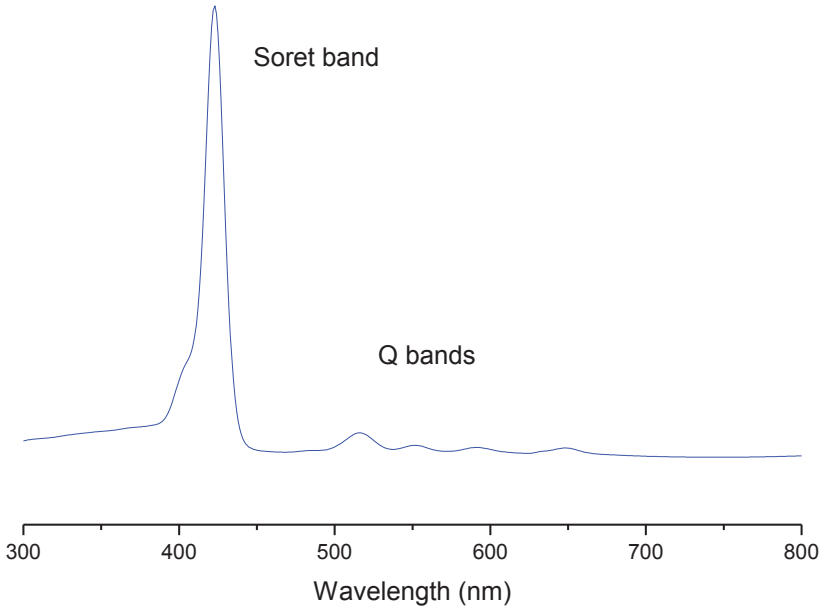

Figure A-40 UV-vis spectrum of H_2TtrimPP in DMF.

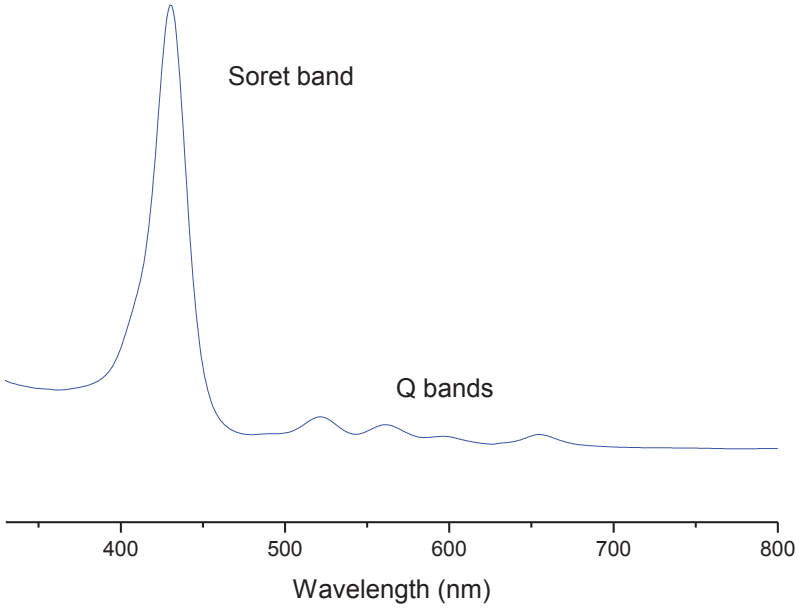

Figure A-41 UV-vis spectrum of H_{16}-PorphGal-2Br in DMF.

Table A-4 Table showing the peaks observed with UV-vis spectrometry for H_2TtrimP and H_{16}-PorphGal-2Br in DMF.

	Soret band(nm)	**Q bands (nm)**
H_2TtrimPP	423	516, 552, 592, 648
H_{16}-PorphGal-2Br	430	522, 560,598,655

A.3.4. IR spectroscopy

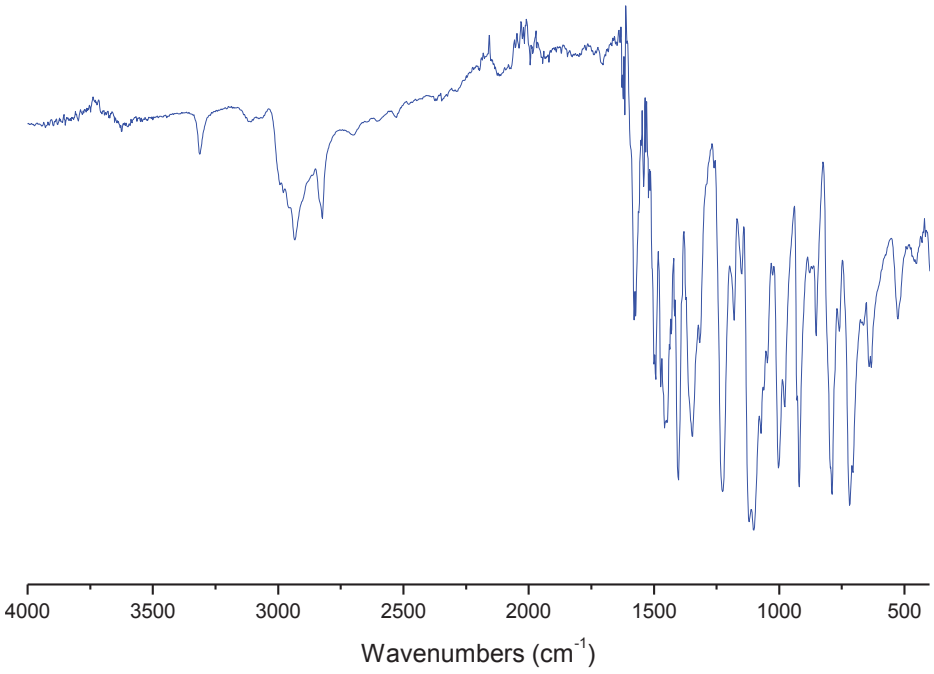

Figure A-42 IR spectrum for H_2TtrimPP. Peaks between 1600-1400 cm^{-1} is assigned to the aromatic C=C stretches of the porphyrin ring and the phenyl groups. The peak 2820 cm^{-1} is assigned to the CH stretch of the methoxy group.

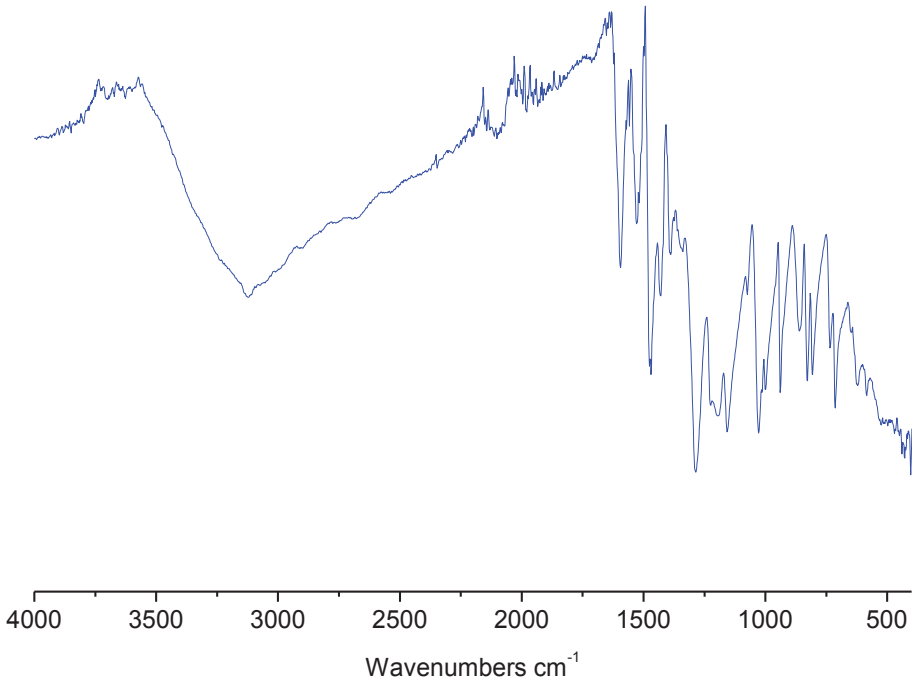

Figure A-43 IR spectrum for H_{16}-PorphGal-2Br. Peaks between 1600-1400 cm^{-1} is assigned to the aromatic C=C stretches of the porphyrin ring and the phenyl groups. The broad peak around 3100 cm^{-1} is assigned to the OH stretches of the hydroxy groups.

A.4. Tetrazole based porphyrin synthesis

A.4.1. NMR spectrometry

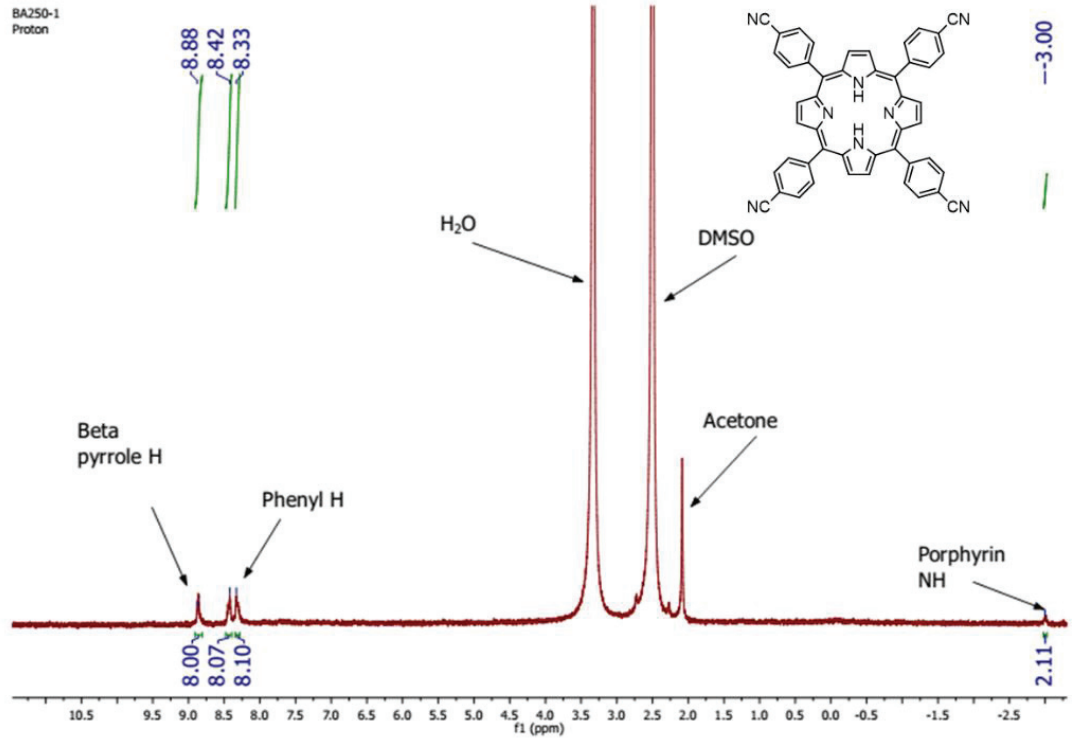

Figure A-44 *NMR spectrum of H_2TCyanoP in DMSO.*

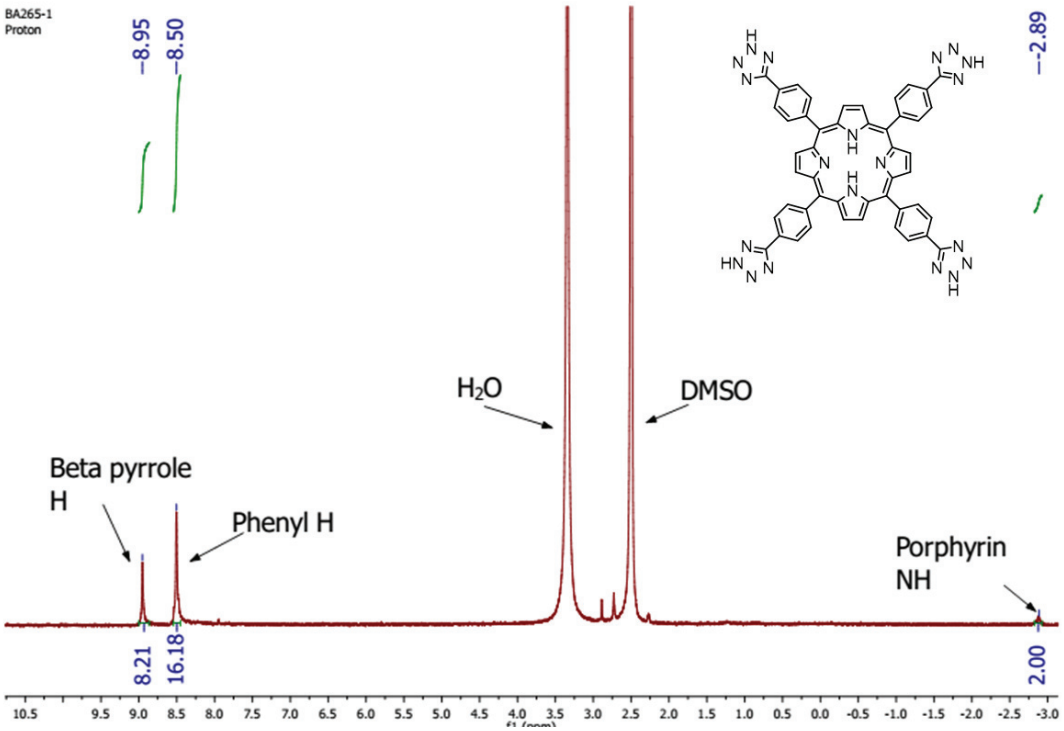

Figure A-45 NMR Spectrum of H_2TTPP in DMSO.

A.4.2. Mass spectrometry

ESI technique was used for the mass spectrometry analysis. DMF was used as solvent for the samples unless stated otherwise.

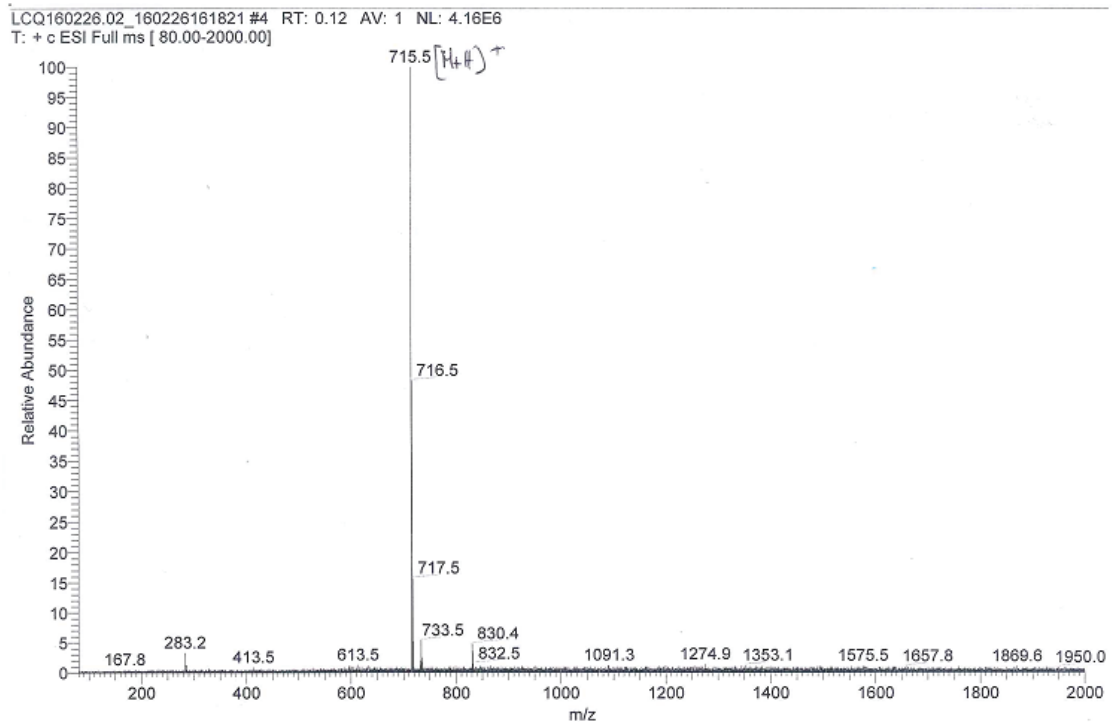

Figure A-46 Mass spectrometry data for H_2TcyanoP. Protonated molecular ion, $(H_2TCyanoP+H)^+$, present at 715.5 m/z confirm the expected product.

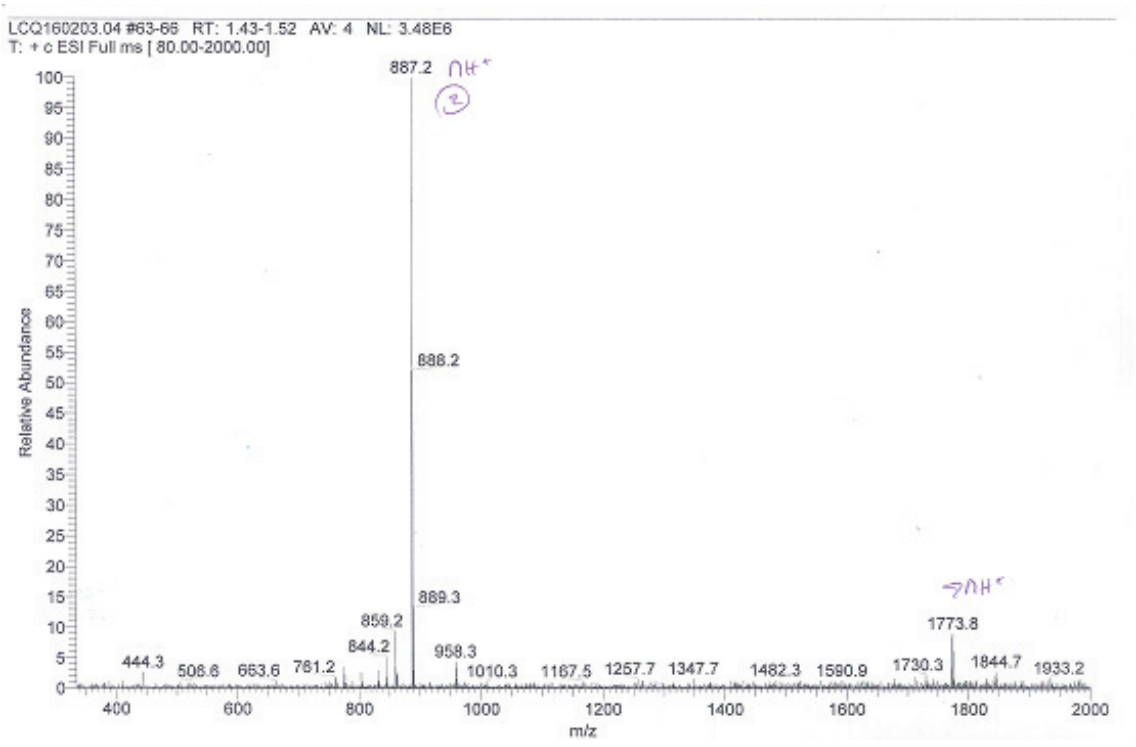

Figure A-47 Mass spectrometry data for H_2TTPP. Protonated molecular ion, $(H_2TTPP+H)^+$, present at 887.2 m/z confirm the expected product

A.4.3. UV-vis spectroscopy

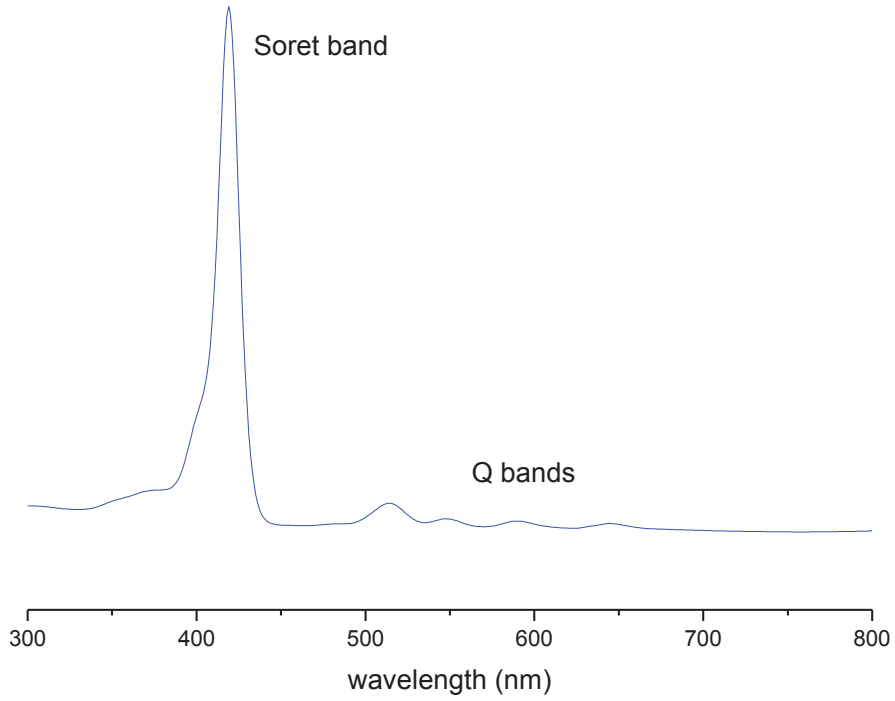

Figure A-48 UV-vis spectrum of H_2TCyanoP in DMF.

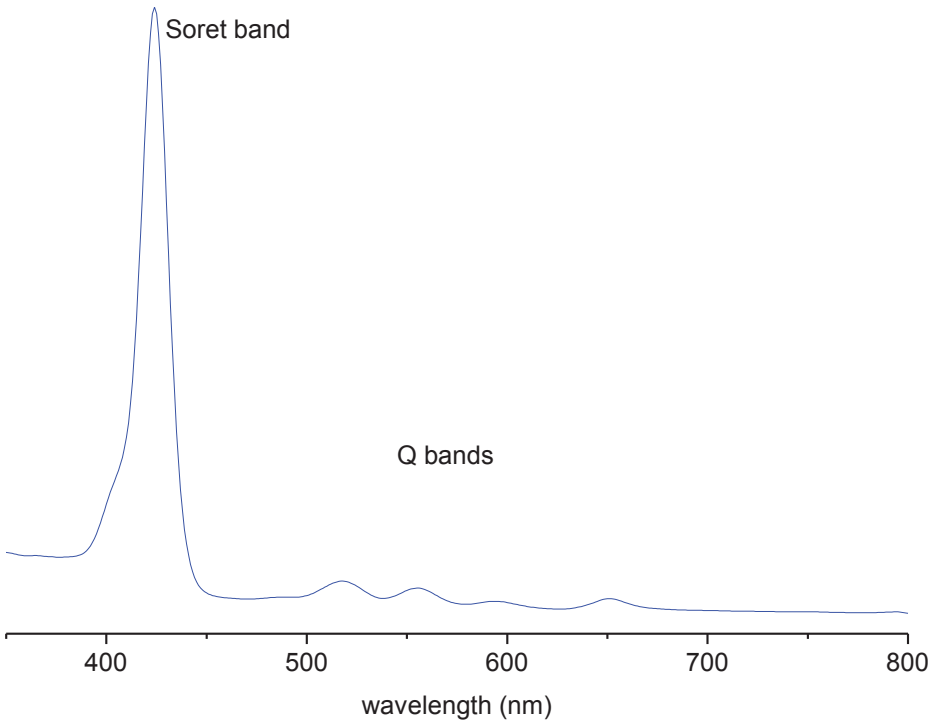

Figure A-49 UV-vis spectrum of H_2TTPP in DMF.

Table A-5 Table showing the peaks observed with UV-vis spectrometry for H_2TcyanoP and H_2TTPP.

	Soret band (nm)	**Q bands (nm)**
H_2TCyanoP	419	513,549, 589,645
H_2TTPP	424	518, 555,595,651

A.4.4. IR spectroscopy

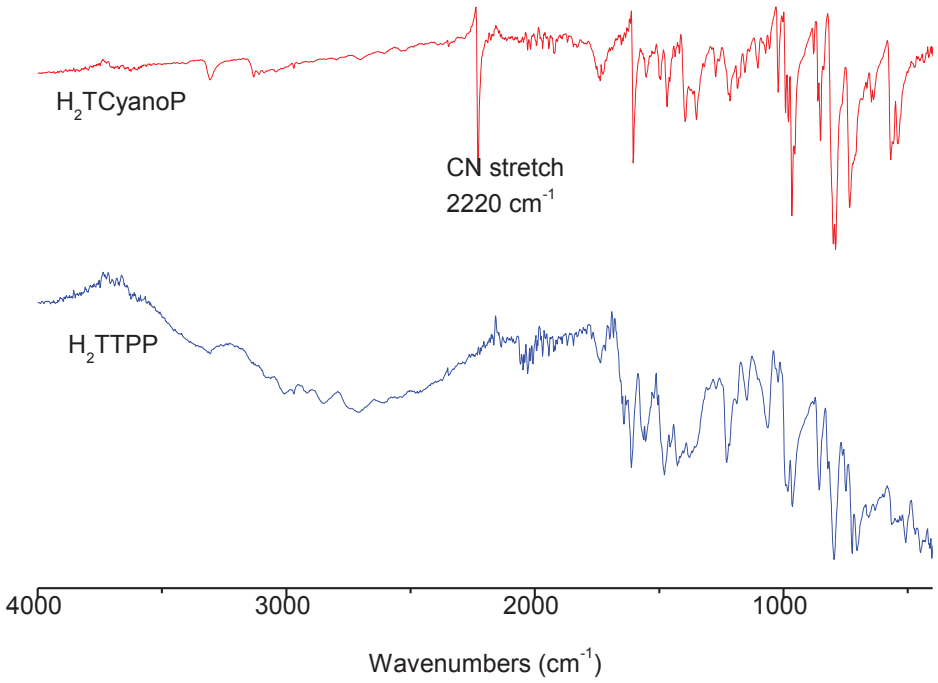

Figure A-50 IR spectra of H_2TCayanoP (top) and H_2TTPP (bottom). The CN stretch disappears when the cyano group is converted in to the tetrazole group.

A.5. Solubility of the porphyrins

All the porphyrins involved in this work are generally soluble in DMF.

Table A-6 Solubility of the porphyrins in various solvents.

Porphyrin	DCM	Toluene	Ethyl acetate	Water acidic	Water basic	Acetone	Methanol	THF
M-TEsterP	Yes	Yes	Yes	No under pH7	Causes hydrolysis	Slightly	NT	Yes
M-TCPP	No	No	No	No under pH 7	Yes	Sightly	NT	Yes but less than the ester
M-$T(OMe)_2PP$	Yes	NT	NT	No at pH 7	No at pH 7	NT	No	NT
M-H_8-PorphCat	No	NT	Soluble in reaction mixture under basic conditions, not after purification/drying	No under pH ~3-4	Yes	Yes	Yes	Yes
H_2TtrimPP	NT	NT	NT	NT	NT	NT	No	NT
H_{14}-PorphGal	No	NT	No	No under pH ~3-4	Yes	NT	Yes	Yes
H_2TCyanoP	NT	NT	NT	No at pH 7	No at pH 7	Slightly	No	NT
H_2TTPP	NT	NT	NT	No under pH 7	NT	NT	NT	NT

NT = Not tested

B. Appendix Chapter 3

B.1. Investigating the reactivity of the tetrakis(4-carboxyphenyl) porphyrin with iron(III)

Table B-1 Different syntheses attempted for investigating the nature of the intermediate product in the synthesis of [Fe^{II}pzTCPP($Fe^{III}OH)_2$] as discussed in chapter 3.3.1.

	H_2TCPP (mg)	H_2TCPP (mmol)	$FeCl_3.6H_2O$ (mg)	$FeCl_3.6H_2O$ (mmol)	Additive	Ratio (Fe:P)	Solvent (DMF) (mL)	Temp (°C)	Heating program (h)	Type	Amount of product (mg)	Crystal shape
1	30	0.038	30	0.114		3:1	5	120	4-30-4	solid	34	square
2	30	0.038	30	0.114		3:1	5	150	4-15-4	gel	-	-
3	90	0.114	90	0.341		3:1	10	180	4-15-4	solid	103	square
4	90	0.114	90	0.341		3:1	10	180	4-15-4	gel	-	-
5	30	0.038	30	0.114		3:1	5	180	4-15-4	gel	-	-
6	45	0.057	45	0.171		3:1	DEF 10	180	0-19-4	solid	45	needle
7	30	0.038	30	0.114		3:1	DEF 10	180	0-19-4	gel	-	-
8	45	0.057	45	0.171		3:1	DEF 10	180	0-19-4	gel	--	-
9	30	0.038	30	0.114	H_2O (0.5 mL)	3:1	5	180	4-15-4	solid	10	needle
10	30	0.038	30	0.114	H_2O (2.5 mL)	3:1	2.5	180	4-15-4	no solid	-	-
11	30	0.038	30	0.114	HCl (0.555 mmol)	3:1	5	180	4-15-4	solid	8	square

Fe:P = Ratio of $FeCl_3.6H_2O$: H_2TCPP

Legend = 120 °C | 150 °C | 180 °C

Table B-2 Different syntheses attempted for investigating the possibility of replacing the pyrazine axial ligand with a different N-donor in [Fe^{II}pzTCPP($Fe^{III}OH)_2$] in a single step reaction as discussed in chapter 3.3.2

	H_2TCPP (mg)	H_2TCPP (mmol)	$FeCl_3.6H_2O$ (mg)	$FeCl_3.6H_2O$ (mmol)	N-donor	N-donor (mg)	N-donor (mmol)	Ratio (Fe:P:N)	DMF (mL)	Amount of product (mg)	Crystal shape
1	45	0.057	45	0.171	Imidazole	11.6	0.171	3:1:3	5	52	square
2	45	0.057	45	0.171	pyrrolidine	12.1	0.171	3:1:3	5	46	square
3	45	0.057	45	0.171	4-methylimidazol	14.0	0.171	3:1:3	5	53	irregular shaped grains

The reactions were performed at 180 °C with a heating program of 4h-15h-4h

Fe:P:N = Ratio of $FeCl_3.6H_2O$: H_2TCPP:N-donor

Table B-3 Different syntheses attempted investigating the possibility of replacing the pyrazine axial ligand with a different N-donor in [Fe^{II}pzTCPP($Fe^{III}OH)_2$] in a two-step reaction as discussed in chapter 3.3.2. Molar mass of the intermediate product was approximated to be 800 g mol^{-1}.

	Intermediate (mg)	Intermediate (mmol)	N-donor	N-donor (mg)	N-donor (mmol)	Ratio (I:N)	DMF (mL)	Amount of product (mg)	Crystal shape
1	30	0.038	imidazole	7.7	0.113	1:3	5	15	square
2	30	0.038	pyridine	8.9	0.113	1:3	5	13	square
3	30	0.038	pyrrolidine	8.0	0.113	1:3	5	14	square
4	30	0.038	4-methyl-imidzaole	9.2	0.113	1:3	5	15	square
5	100	0.125	pyrazine	20	0.250	1:2	5	57	square

The reactions were performed at 180 °C with a heating program of 4h-15h-4h

I:N = Ratio of Intermediate: N-donor

B.2. Investigating the reactivity of cobalt metalated tetrakis(4-carboxyphenyl) porphyrin with iron(III)

Table B-4 Syntheses investigating the reactivity of Fe^{3+} with Co metalated TCPP as discussed in chapter 3.4

	CoTCPP(X) (mg)	CoTCPP(X) (mmol)	$FeCl_3.6H_2O$ (mg)	$FeCl_3.6H_2O$ (mmol)	Additive	Ratio (Fe:P)	DMF (mL)	Temp (°C)	Heating program (h)	Amount of product (mg)	Crystal shape
1	45	0.052	15	0.056		1:1	5	120	4-72-4	27	gel
2	45	0.052	9	0.033		0.6:1	5	150	4-72-4	14	needles + squares + irregular shaped grains
3	45	0.052	15	0.056		1:1	5	150	4-72-4	27	needles + squares + irregular shaped grains
4	45	0.052	15	0.056	HCl (0.150 mmol)	1:1	5	150	4-72-4	10	needles + squares + irregular shaped grains
5	45	0.052	15	0.056		1:1	20	150	4-72-4	22	needles + squares + irregular shaped grains
6	38	0.044	18	0.067		1.5:1	5	150	4-72-4	19	needles + squares + irregular shaped grains
7	45	0.052	30	0.111		2:1	5	150	4-72-4	23	needles + squares + irregular shaped grains
8	45	0.052	45	0.170		3:1	5	150	4-72-4	29	needles + squares + irregular shaped grains
9	45	0.052	45	0.170		3:1	20	150	4-72-4	16	needles + squares + irregular shaped grains
10	45	0.052	15	0.056		1:1	5	150	12-60-4	45	irregular shaped grains
11	45	0.052	11	0.042		0.8:1	5	190	4-72-4	7	fine needles
12	45	0.052	15	0.056		1:1	5	190	4-72-4	13	fine needles
13	45	0.052	15	0.056		1:1	3	190	4-72-4	12	fine needles
14	45	0.052	30	0.111		2:1	3	190	4-72-4	19	fine needles

For CoTCPP(X) X=OH^-
Fe:P= Ratio of $FeCl_3.6H_2O$: CoTCPP(X)

Legend = | 120 °C | 150 °C | 180 °C | 190 °C |

Table B-5 Syntheses investigating the reactivity of Fe^{3+} and Co metalated TCPP with a mixed solvent system with water and DMF as discussed in chapter 3.4

	CoTCPP(X) (mg)	CoTCPP(X) (mmol)	$FeCl_3.6H_2O$ (mg)	$FeCl_3.6H_2O$ (mmol)	Ratio (Fe:P)	H_2O (mL)	Solvent DMF (mL)	Temp (°C)	Heating program (h)	Amount of product (mg)	Crystal shape
1	90	0.104	15	0.056	1:2	0.5	4.5	150	4-72-4	48	needles
2	45	0.052	15	0.056	1:1	0.5	4.5	150	4-72-4	11	needles
3	45	0.052	30	0.111	2:1	0.5	4.5	150	4-72-4	40	irregular grains
4	45	0.052	15	0.056	1:1	2.5	2.5	150	4-72-4	26	needles
5	45	0.052	15	0.056	1:1	4.5	0.5	150	4-72-4	20	needles
6	45	0.052	15	0.056	1:1	0.5	4.5	180	4-72-4	25	needles
7	45	0.052	15	0.056	1:1	2.5	2.5	180	4-72-4	10	needles

For CoTCPP(X) X=OH^-
Fe:P= Ratio of $FeCl_3.6H_2O$: CoTCPP(X)

B.3. Investigating the reactivity between iron(III) and Fe^{3+} metalated TCPP

The possible synthesis of an iron metalated porphyrinic MOF with an iron based inorganic SBU was explored via the reactivity between Fe^{3+} and iron metalated TCPP [FeTCPP(Cl)]. Synthesis was attempted using the parameters shown on Table B-6 which resulted in a poorly crystallised solid. The solid was insoluble in DMF and the IR spectrum showed characteristic peaks for coordinated carboxylate groups indicating that the framework consists of a coordination polymer.

The mother liquor contained a mixture of fine needle shaped and square shaped crystals. However, crystals obtained were not of sufficient quality for structural determination via single crystal X-ray diffraction. Thus, the nature of the structure remains unclear for the product obtained from this synthesis.

Table B-6 Synthesis parameters attempted for investigating the reactivity of $FeCl_3.6H_2O$ with FeTCPP(Cl)

Parameter	
Metal source	$FeCl_3.6H_2O$
Metal to ligand ratio	2:1
Isotherm temperature	190 °C
Isotherm time/ Heating program	4h-72h-4h
Solvent	DMF

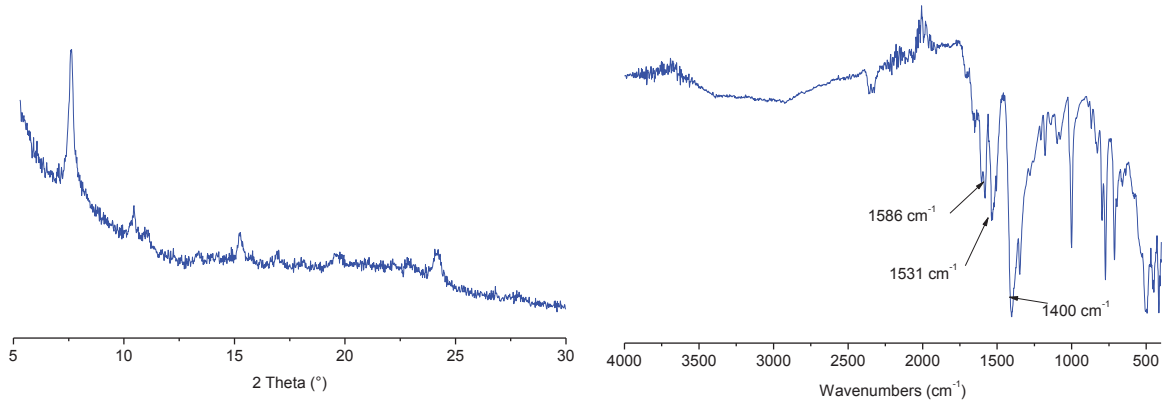

Figure B-1 a) PXRD pattern for the product from the reaction between $FeCl_3.6H_2O$ and FeTCPP(Cl). b) IR spectrum of the product. Peak assignment: 1586 cm^{-1} and 1400 cm^{-1} = asymmetric and symmetric stretch of coordinated carboxylate groups, 1531 cm^{-1} = aromatic C=C stretch.

B.4. Synthesis of Mn^{3+} metalated Al-PMOF

Synthesis

Table B-7 Reactions attempted for synthesis optimisation of Mn-Al-PMOF as discussed in chapter 3.5.1.

	MnTCPP(OH) (mg)	MnTCPP(OH) (mmol)	$AlCl_3.6H_2O$ (mg)	$AlCl_3.6H_2O$ (mmol)	Additive (mg)	Ratio (Al:P:A)	H_2O (mL)	DMF (mL)	Temp (°C)	Heating program (h)	Amount of product (mg)	Phase
1	53	0.062	30	0.125		2:1	2.5	2.5	120	3-16-4	165	other
2	53	0.062	30	0.125		2:1	4.5	0.5	120	3-16-4	56	other
3	53	0.062	30	0.125	KOH (13.5)	2:1:4	2.5	2.5	120	3-16-4	16	amorphous
4	53	0.062	30	0.125	KOH (13.5)	2:1:4	2.5	2.5	140	3-16-4	50	Al-PMOF
5	53	0.062	30	0.125	KOH (13.5)	2:1:4	2.5	2.5	150	3-16-4	36	Al-PMOF
6	53	0.062	30	0.125		2:1	0	5	160	3-16-4	27	Al-PMOF
7	53	0.062	30	0.125		2:1	4.5	0.5	160	3-16-4	82	other
8	53	0.062	30	0.125		2:1	2.5	2.5	160	3-16-4	50	Al-PMOF
9	53	0.062	30	0.125	Benzoic acid (75)	2:1:10	2.5	2.5	160	3-16-4	53	Al-PMOF
10	53	0.062	30	0.125	Benzoic acid (15)	2:1:2	2.5	2.5	160	15-15-4	57	Al-PMOF
11	53	0.062	30	0.125		2:1	2.5	2.5	190	9-15-4	36	Al-PMOF
12	53	0.062	30	0.125	Benzoic acid (75)	2:1:10	2.5	2.5	190	9-15-4	56	Al-PMOF
13	53	0.062	30	0.125	Benzoic acid (75)	2:1:10	0	5	190	9-15-4	102	Al-PMOF
14	53	0.062	30	0.125	Benzoic acid (15)	2:1:2	2.5	2.5	190	9-15-4	54	Al-PMOF
15	53	0.062	30	0.125	Benzoic acid (15)	2:1:2	2.5	2.5	190	18-15-4	57	Al-PMOF

Al:P:A= Ratio of $AlCl_3.6H_2O$: MnTCPP(OH): Additive

Legend = | 120 °C | 140° C | 150 °C | 160 °C | 190 °C |

PXRD

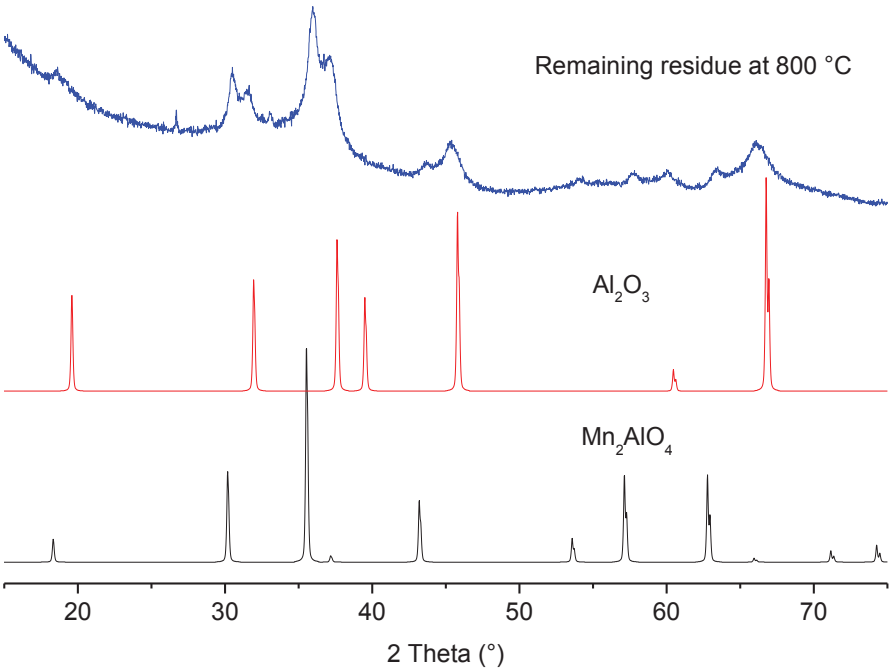

Figure B-2 PXRD pattern of the end residue after the TGA analysis for a Mn-Al-PMOF sample. The residue appears to be a mix of Mn_2AlO_4 and Al_2O_3.

UV-vis spectroscopy

Solution phase UV-vis spectroscopy was used to probe the Mn occupancy in the samples obtained. The measurements were carried out by first digesting the MOF (3 mg) in 0.1 NaOH (5 mL). The Mn occupancy was calculated using standard curves for the free base and Mn metalated TCPP.

Determination of the Mn occupancy of the Mn-Al-PMOF samples using standard curves

Frist step was to determine the extinction coefficients of H_2TCPP and MnTCPP(OH) at their absorption maximums using standard curves (Figure B-3).

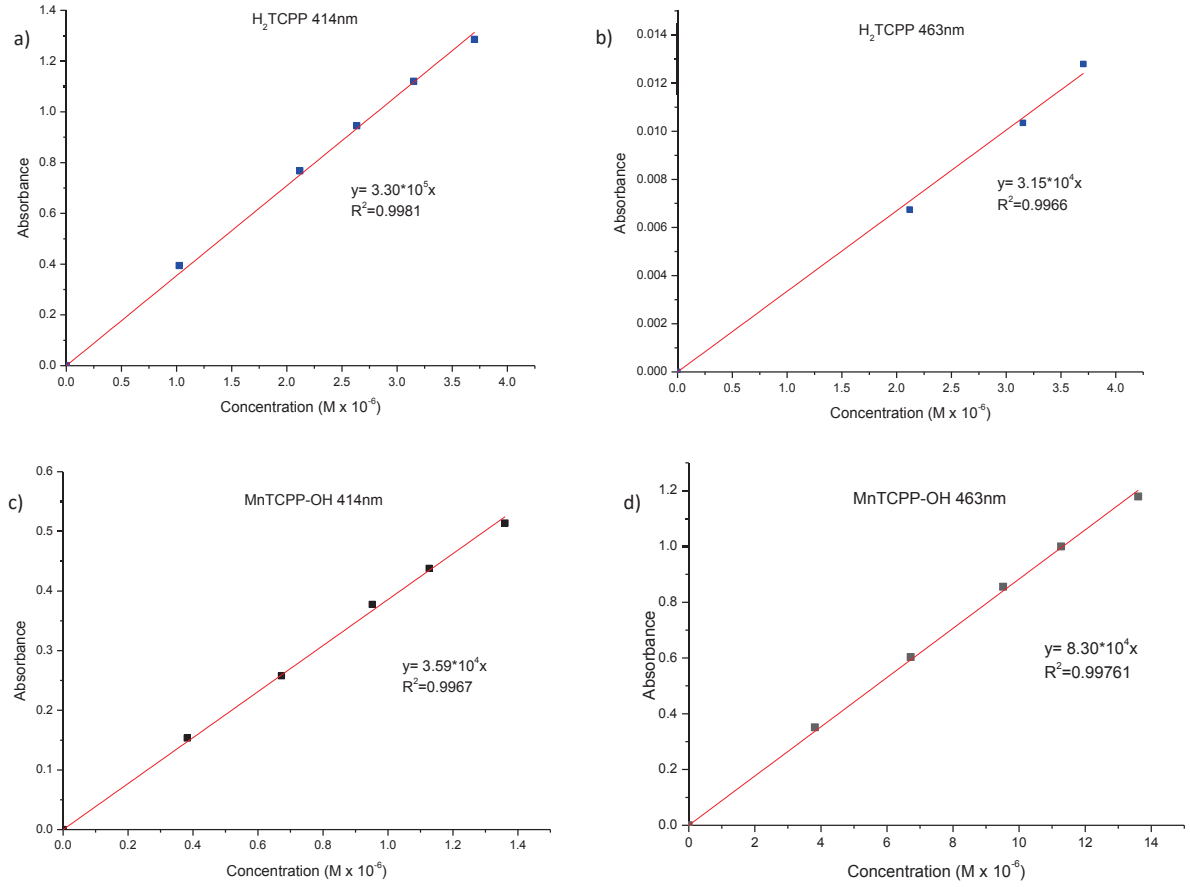

Figure B-3 a) Standard curve for H_2TCPP at 414 nm. b) Standard curve for H_2TCPP at 463 nm. c) Standard curve for MnTCPP(OH) at 414 nm d) Standard curve for MnTCPP(OH) at 463 nm.

The following equations derived from the Beer-Lambert law was used to determine the concentration of H_2TCPP and MnTCPP(OH) present in each Mn-Al-PMOF sample and the Mn occupancy.

$A_{(sample,463nm)} = A_{(MnTCPP\text{-}OH,\ 463\ nm)} + A_{(H2TCPP,\ 463\ nm)}$

$A_{(sample,414nm)} = A_{(MnTCPP\text{-}OH,\ 414\ nm)} + A_{(H2TCPP,\ 414\ nm)}$

$A_{(sample,463nm)} = [C_{(MnTCPP\text{-}OH)} .\varepsilon_{(MnTCPP\text{-}OH,\ 463\ nm)}. l] + [C_{(H2TCPP)} .\varepsilon_{(H2TCPP,\ 463\ nm)}. l]$

$A_{(sample,414nm)} = [C_{(MnTCPP\text{-}OH)} .\varepsilon_{(MnTCPP\text{-}OH,\ 414\ nm)}. l] + [C(_{H2TCPP)} .\varepsilon_{(H2TCPP,\ 414\ nm)}. l]$

$l = 1\ cm^{-1}$

$\varepsilon_{(MnTCPP\text{-}OH,\ 463\ nm)} = 8.30E{+}04\ L{\cdot}mol^{-1}{\cdot}cm^{-1}$

$\varepsilon_{(H2TCPP,\ 463\ nm)} = 3.15E{+}04\ L{\cdot}mol^{-1}{\cdot}cm^{-1}$

$\varepsilon_{(MnTCPP\text{-}OH,\ 414\ nm)} = 3.59E{+}04\ L{\cdot}mol^{-1}{\cdot}cm^{-1}$

$\varepsilon_{(H2TCPP,\ 414\ nm)} = 3.30E{+}05\ {\cdot}mol^{-1}{\cdot}cm^{-1}$

Thus $C_{(MnTCPPOH)}$ and $C_{(H2TCPP)}$ can be calculated allowing to determine the Mn occupancy

$$\text{Mn occupancy} = \frac{C_{(MnTCPPOH)}}{[C_{(MnTCPPOH)} + C_{(H2TCPP)}]} \times 100$$

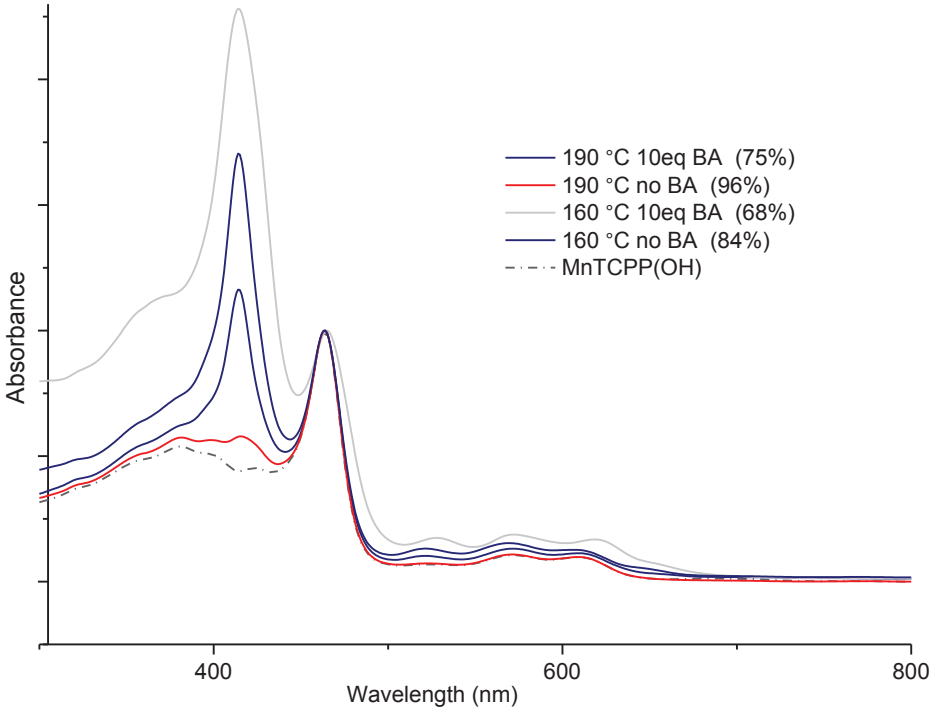

Figure B-4 UV-vis spectra of the products of the Mn-Al-PMOF syntheses at 160 °C (heating program 3h-16h-4h) and 190 °C (heating program, 9h-15h-4h) with and without benzoic acid (BA). Solvent used is a 50%/50% mix of DMF-water. Mn occupancy in the porphyrin is shown in parenthesis.

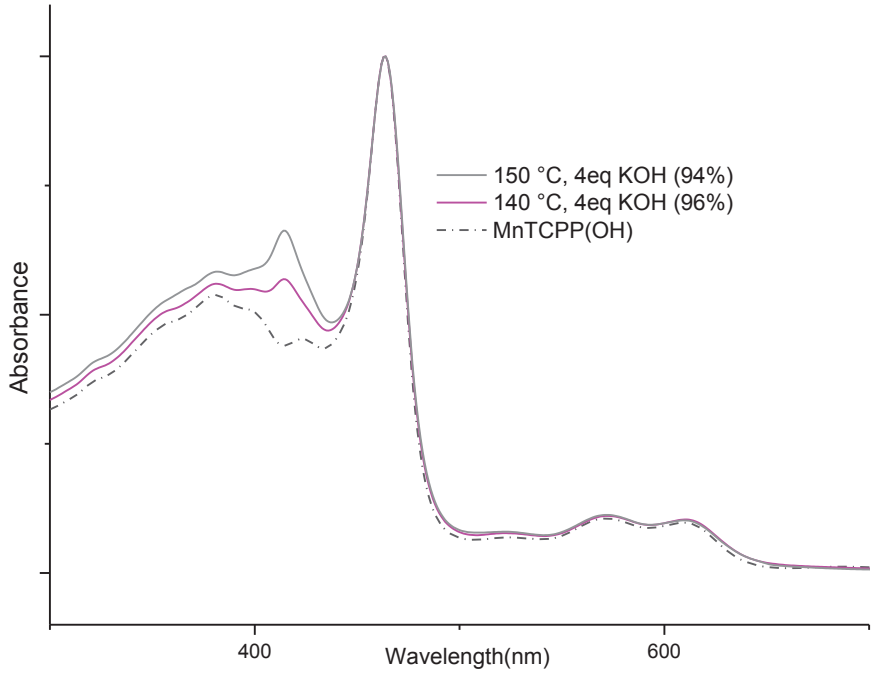

Figure B-5 UV-vis spectra of the products of the Mn-Al-PMOF syntheses at 150 °C and 140 °C with KOH (Solvent 50%-50% DMF-water, heating program 3h-16h-4h). Mn occupancy in the porphyrin calculated from a standard curve is shown in parenthesis.

TGA

TGA analysis was used as a measure to probe the relative purity of the samples as discussed in the main text in chapter 3.5.1.

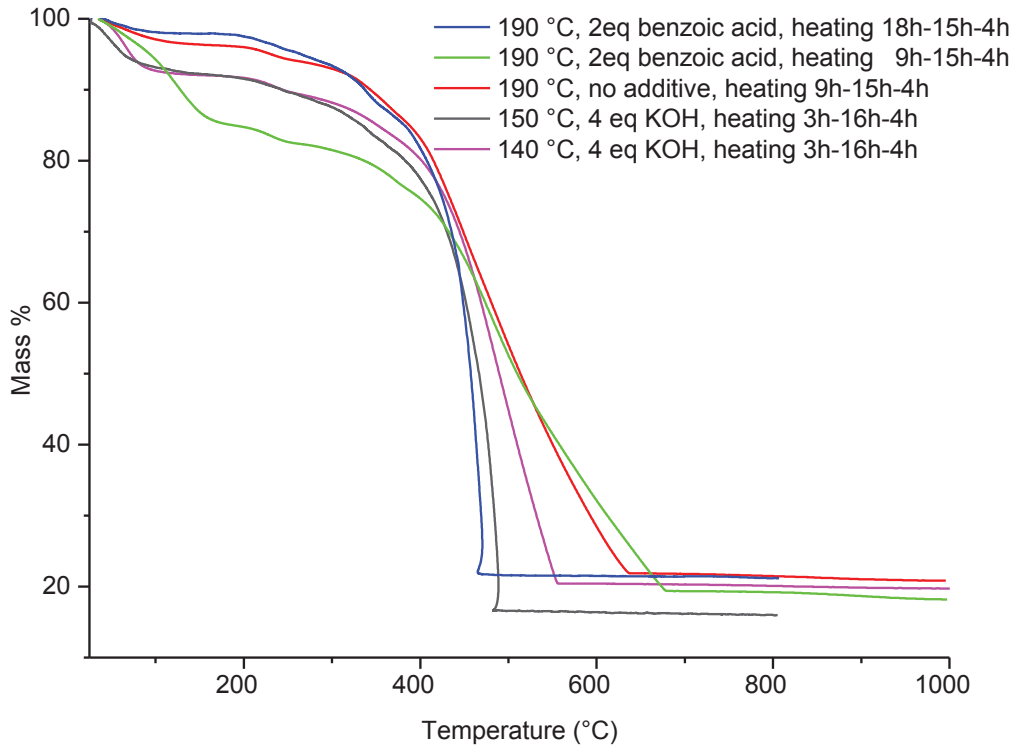

Figure B-6 TGA data for Mn-Al-PMOF syntheses which resulted in products with more than 90% Mn occupancy. Metal to ligand ratio is 2:1 and the solvent is a 50%/50% mix of DMF-water. The measurements up to 1000 °C were performed in a different TGA instrument (Instrument 2) to the measurement done up to 800° C (Instrument 1).

Calculation method of the aluminium oxide impurities from the TGA data

For simplicity, the Al_2O_3 was assigned to represent the aluminium oxide impurities present at the start.

Starting MOF → Inorganic residue

$[Mn(y)H_2(1\text{-}y)TCPP\text{-}OH(Al^{III}OH)_2] \longrightarrow (y).\ 2/4\ Mn_2AlO_4 + 3/4\ Al_2O_3 + (1\text{-}y).\ Al_2O_3$

For 1 mol of MOF

$$x(M\text{-}Al_2O_3) + M\text{-}MOF \longrightarrow Im$$

$$x(M\text{-}Al_2O_3) + (y).\ 2/4\ (M\text{-}Mn_2AlO_4) + 3/4(M\text{-}Al_2O_3) + (1\text{-}y).(M\text{-}Al_2O_3) \longrightarrow Rm$$

where

y = Mn occupancy in the porphyrin core
x = number of moles of the impurity Al_2O_3 for 1 mol of MOF
Im = Initial mass %
Rm = Remaining mass %
M-MOF = Molar mass of the MOF = $y(MnOH)\ (1\text{-}y)(H_2)\ C_{48}H_{24}N_4O_8(AlOH)_2$
$M\text{-}Al_2O_3$ = Molar mass of Al_2O_3 = 101.96 g/mol
$M\text{-}Mn_2AlO_4$ = Molar mass of Mn_2AlO_4 = 200.86 g/mol

Therefore by cross multiplying,

$$Rm\ [x(M\text{-}Al_2O_3) + M\text{-}MOF] = Im\ [x(M\text{-}Al_2O_3) + (y).\ 2/4\ (M\text{-}Mn_2AlO_4) + 3/4(M\text{-}Al_2O_3) + (1\text{-}y).\ (M\text{-}Al_2O_3)]$$

$$Rm.\ x(M\text{-}Al_2O_3) + Rm.\ M\text{-}MOF = Im.\ [x(M\text{-}Al_2O_3) + Im.\ (y).\ 2/4\ (M\text{-}Mn_2AlO_4) + Im.\ 3/4(M\text{-}Al_2O_3) + Im.\ (1\text{-}y).\ (M\text{-}Al_2O_3)$$

Therefore,

$$x = \frac{Rm.M\text{-}MOF - Im.\ (y).\ 2/4\ (M\text{-}Mn_2AlO_4) - Im.\ 3/4(M\text{-}Al_2O_3) - Im.\ (1\text{-}y)\ (M\text{-}Al_2O_3)}{(M\text{-}Al_2O_3)\ (Im - Rm)}$$

Amount of impurity in 1 mol of MOF = x(101.96)

$$\text{Therefore \%wt of impurity} = \frac{x(101.96)}{x(101.96) + M\text{-}MOF} \times 100$$

Example calculation for the sample prepared with 2:1 metal to ligand ratio, 2 eq of benzoic acid, 50%-50% DMF-water at 190 °C with a heating program of 18h-15h-4h

Im = 96.2%
Rm = 19.1%
y = 0.95 Mn occupancy
$M\text{-}MOF = (0.95)(MnOH)\ (1\text{-}0.95)(H_2)\ C_{48}H_{24}N_4O_8(AlOH)_2 = 941.15$ g/mol

$$x = \frac{Rm.M\text{-}MOF - Im.\ (y).\ 2/4\ (M\text{-}Mn_2AlO_2) - Im.\ 3/4(M\text{-}Al_2O_3) - Im.\ (1\text{-}y)\ (M\text{-}Al_2O_3)}{(M\text{-}Al_2O_3)\ (Im - Rm)}$$

x= 0.121 mol

$$\text{Therefore \%wt of impurity} = \frac{0.121 \times 101.96}{(0.121 \times 101.96) + 941.15} \times 100 = 1\%$$

N_2 adsorption/desorption studies and BET surface area analysis

The accessible surface areas of the samples were determined using N_2 adsorption/desorption at 77K.

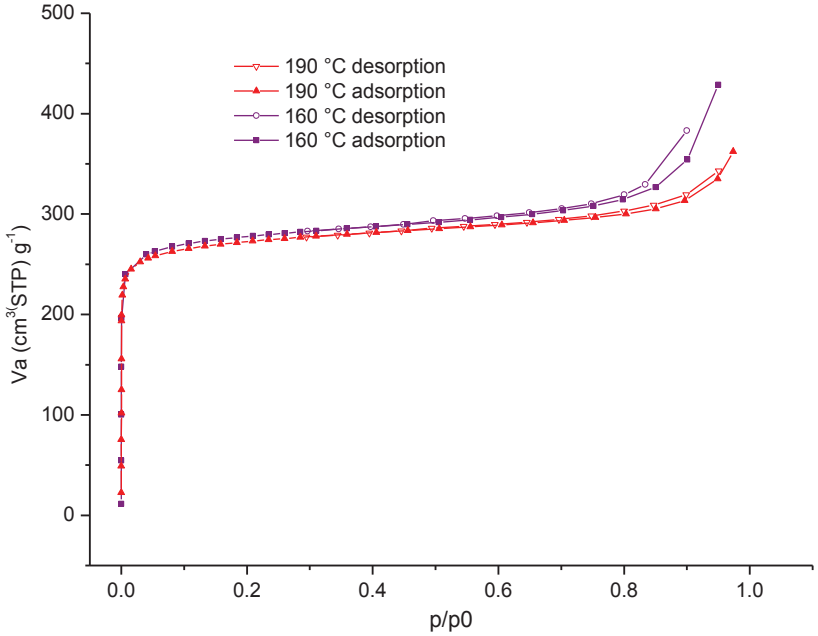

Figure B-7 N_2 adsorption/desorption isotherms at 77 K for products from Mn-Al-PMOF syntheses at 160 °C (3h-16h-4h) and 190 °C (9h-15h-4h) without any additives. Solvent used is a 50%/50% mix of DMF-water.

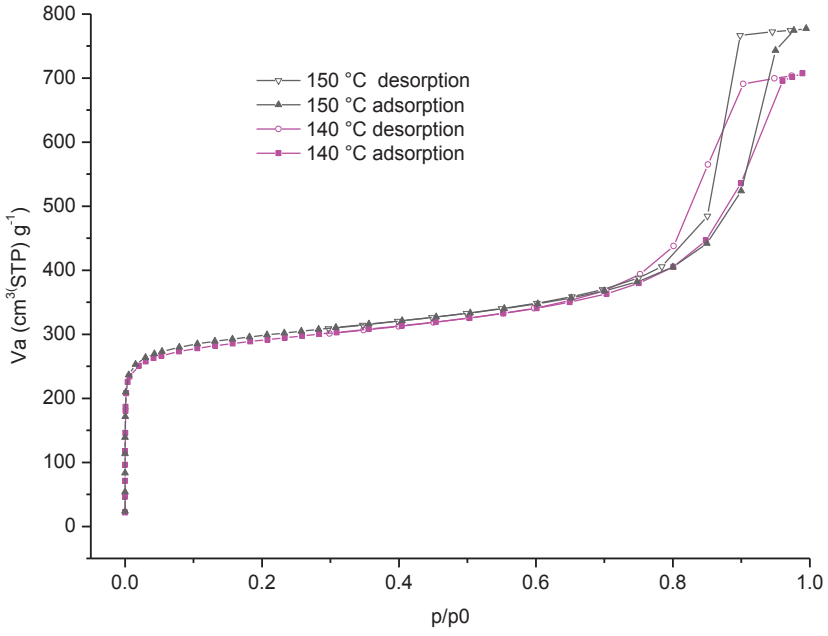

Figure B-8 N_2 adsorption/desorption isotherms at 77 K for products from Mn-Al-PMOF syntheses using 4 eq of KOH as an additive at 140 °C and 150 °C with a heating program of 3h-16h-4h. Solvent used is a 50%/50% mix of DMF-water.

Table B-8 Summary of BET surface areas calculated for the analysed products of chosen Mn-Al-PMOF syntheses (Solvent: 50%/50% DMF-water)

	Mn occupancy from UV	BET surface area ($m^2 g^{-1}$)
140 °C, 4 eq KOH, heating program 3h-16h-4h	96%	1112
150 °C, 4 eq KOH, heating program 3h-16h-4h	94%	1138
160 °C, no additives, heating program 3h-16h-4h	84%	1077
190 °C, no additive, heating program 9h-15h-4h	96%	1070
190 °C, 10 eq benzoic acid, heating program 9h-15h-4h	75%	1324
190 °C, 2 eq benzoic acid, heating program 9h-15h-4h	94%	1231
190 °C, 2 eq benzoic acid, heating program 18h-15h-4h	95%	1300

B.5. Synthesis of Fe^{3+} metalated Al-PMOF

Synthesis

Table B-9 Reactions attempted for the synthesis optimisation of Fe-Al-PMOF as discussed in chapter 3.5.2.

	FeTCPP(Cl) (mgl)	FeTCPP(Cl) (mmol)	$AlCl_3.6H_2O$ (mg)	$AlCl_3.6H_2O$ (mmol)	Additives (mg)	Ratio (Al:P:A)	H_2O (mL)	DMF (mL)	Temp (°C)	Heating program (h)	Amount of product (mg)	Phase
1	54	0.062	30	0.125		2:1	2.5	2.5	120	3-16-4	65	Al-PMOF
2	54	0.062	30	0.125	KOH (13.5)	2:1:4	2.5	2.5	120	3-16-4	16	amorphous
3	54	0.062	30	0.125	KOH (13.5)	2:1:4	2.5	2.5	140	3-16-4	12	Al-PMOF
4	54	0.062	30	0.125	KOH (13.5)	2:1:4	2.5	2.5	150	3-16-4	16	Al-PMOF
5	54	0.062	30	0.125		2:1	2.5	2.5	160	3-16-4	18	Al-PMOF
6	54	0.062	30	0.125	Benzoic acid (75)	2:1:10	2.5	2.5	160	3-16-4	50	Al-PMOF
7	54	0.062	30	0.125		2:1	0.5	4.5	190	9-24-4	54	Al-PMOF
8	54	0.062	30	0.125		2:1	2.5	2.5	190	9-24-4	36	Al-PMOF
9	54	0.062	30	0.125		2:1	4.5	0.5	190	9-24-4	16	Al-PMOF
10	54	0.062	30	0.125		2:1	2.5	2.5	190	3-16-4	36	Al-PMOF
11	54	0.062	30	0.125	Benzoic acid (75)	2:1:10	2.5	2.5	190	3-16-4	49	Al-PMOF
12	54	0.062	30	0.125	Benzoic acid (15)	2:1:2	2.5	2.5	190	3-16-4	33	Al-PMOF
13[a]	54	0.062	30	0.125		2:1	2.5	2.5	190	3-16-4	15	Al-PMOF
14[a]	82.5	0.094	30	0.125		1.3:1	2.5	2.5	190	3-16-4	42	Al-PMOF

Al:P:A= Ratio of $AlCl_3.6H_2O$: FeTCPP(Cl): Additive

[a] *The reaction mixture was degassed with Ar for 10 min before heating*

Legend = 120 °C | 140° C | 150 °C | 160 °C | 190 °C

UV-vis spectroscopy

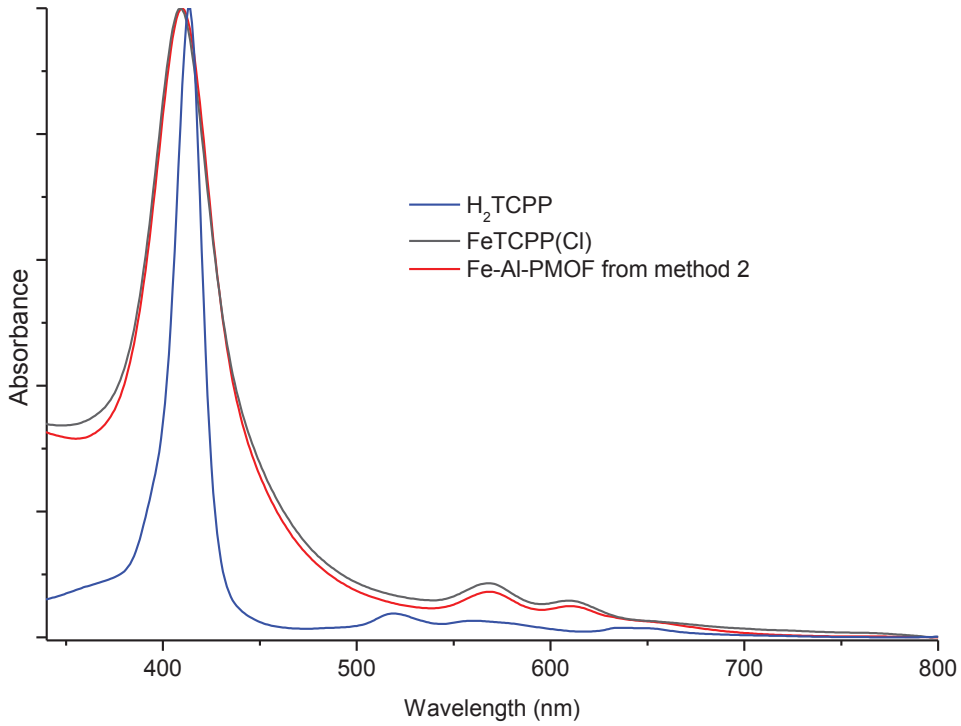

Figure B-9 Solution phase (0.1 M NaOH) UV-vis spectrum of the sample prepared with final optimised synthesis conditions for method 2 (synthetic conditions; Solvent 50%/50% DMF-water, 1.3:1 ratio of Al to FeTCPP(Cl), 190 °C, 3h-16h-4h, Ar degassing before heating). Also shown are the UV-vis spectra for FeTCPP(Cl) and H_2TCPP.

TGA analysis

As discussed in chapter 3.5.2, TGA analysis was used as a measure to probe the relative purity of the samples.

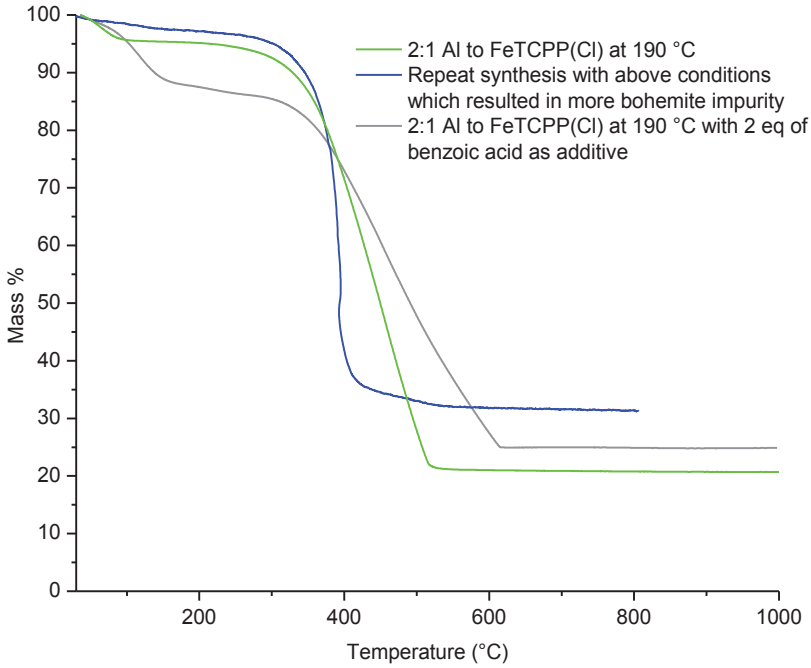

Figure B-10 TGA data of Fe-Al-PMOF samples synthesised at 190 °C with an Al to ligand ratio of 2:1 (Solvent: 50%/50% DMF-water, heating program: 3h-16h-4h)). A repeat of the same synthesis conditions results in products with different purity. Also shown is the TGA data for the sample prepared with 2 eq of benzoic acid with the same conditions. The TGA measurement where the end temperature is 800 °C was performed with TGA instrument 1 while measurements up to 1000 °C is performed with TGA instrument 2.

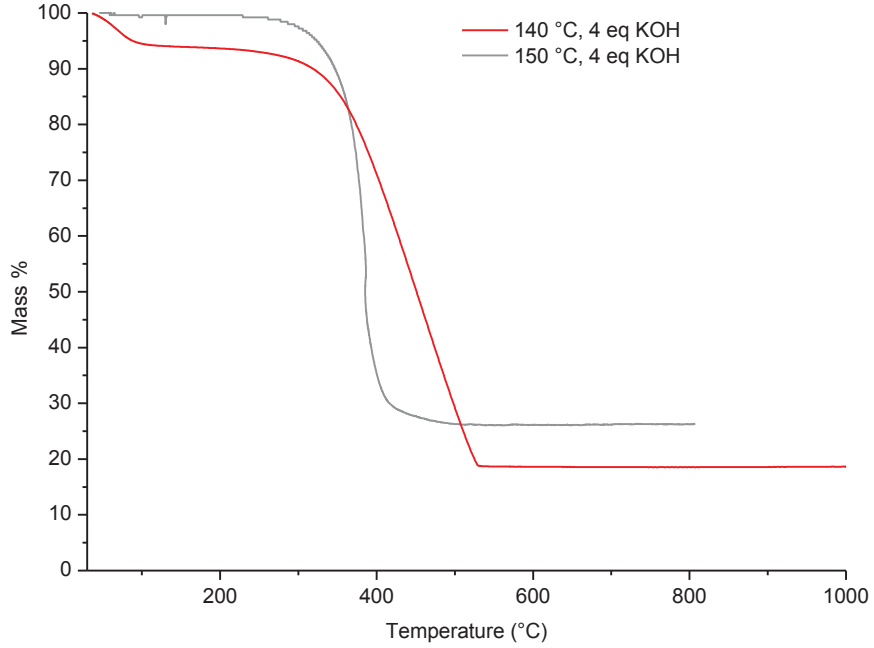

Figure B-11 TGA data for the products of the Fe-Al-PMOF syntheses with 4 equivalents of KOH at 140 °C and 150 °C (Solvent: 50%/50% DMF-water, heating program: 3h-16h-4h). The TGA measurement where the end temperature is 800 °C was performed with TGA instrument 1 while the measurement up to 1000 °C is performed with TGA instrument 2.

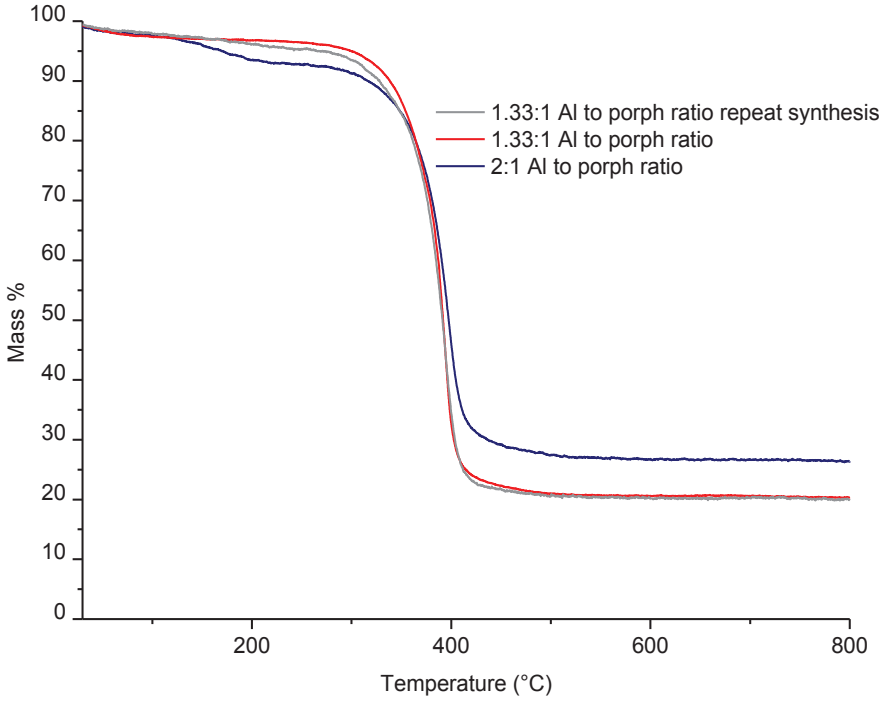

Figure B-12 TGA data for the products from the Fe-Al-PMOF syntheses with Ar degassing of the reaction mixture prior to heating (Solvent: 50%/50% DMF-water, heating program: 3h-16h-4h).

Calculation of weight% of the impurity from the TGA data

For simplicity, the Al_2O_3 was assigned to represent all the aluminium oxide impurities present at the start.

Starting MOF → Inorganic residue

$[FeTCPP\text{-}OH(Al^{III}OH)_2] \longrightarrow \frac{1}{2} Fe_2O_3 + Al_2O_3$

For 1 mol of MOF

$x(M\text{-}Al_2O_3) + M\text{-}MOF \longrightarrow Im$

$x(M\text{-}Al_2O_3) + \frac{1}{2}(M\text{-}Fe_2O_3) + (M\text{-}Al_2O_3) \longrightarrow Rm$

where

x = number of moles of the impurity Al_2O_3 for 1 mol of MOF
Rm = Remaining mass %
Im = Initial mass %
M-MOF = Molar mass of the MOF = 945.56 g/mol
$M\text{-}Al_2O_3$ = Molar mass of Al_2O_3 = 101.96 g/mol
$M\text{-}Fe_2O_3$ = Molar mass of $M\text{-}Fe_2O_3$ = 159.69 g/mol

Therefore by cross multiplying,

$Rm\,[x(M\text{-}Al_2O_3) + M\text{-}MOF] = Im\,[x(M\text{-}Al_2O_3) + \frac{1}{2}(M\text{-}Fe_2O_3) + (M\text{-}Al_2O_3)]$

$Rm.\,x(M\text{-}Al_2O_3) + Rm.\,M\text{-}MOF = Im.\,[x(M\text{-}Al_2O_3) + Im.\,\frac{1}{2}(M\text{-}Fe_2O_3) + Im.\,(M\text{-}Al_2O_3)$

Therefore,

$$x = \frac{Rm.M\text{-}MOF - Im.\,\frac{1}{2}(M\text{-}Fe_2O_3) - Im.\,(M\text{-}Al_2O_3)}{(M\text{-}Al_2O_3)\,(Im - Rm)}$$

Amount of impurity in 1 mol of MOF = x(101.96)

Therefore %wt of impurity = $\frac{x(101.96)}{x(101.96) + M\text{-}MOF} \times 100$

Example calculation for the sample synthesised with 1.33:1 Metal to ligand ratio, 3h-16h-4h heating program, Ar degassing.

Im = 95.40 %
Rm = 19.84 %

$$x = \frac{Rm.M\text{-}MOF - Im.\,\frac{1}{2}(M\text{-}Fe_2O_3) - Im.\,(M\text{-}Al_2O_3)}{(M\text{-}Al_2O_3)\,(Im - Rm)}$$

x= 0.184 mol in 1 mol of product

Therefore %wt of impurity = $\frac{0.184 \times 101.96}{0.184 \times 101.96 + 945.56} \times 100 = 2\%$

N_2 adsorption/desorption studies and BET surface area analysis

The accessible surface areas of the samples were determined using N_2 adsorption/desorption at 77K.

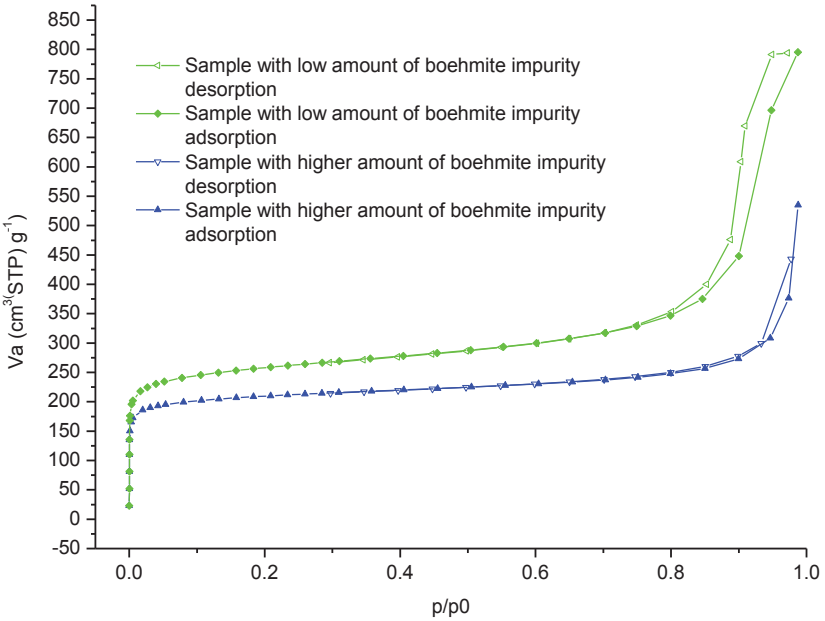

Figure B-13 N_2 adsorption/desorption isotherms at 77K for two different Fe-Al-PMOF samples synthesised with the same conditions at 190 °C (2:1 Al:Porph , 3h-16h-4h, 50%/50% DMF-water). One sample showed a large presence of the boehmite impurity while the other sample has less of the impurity.

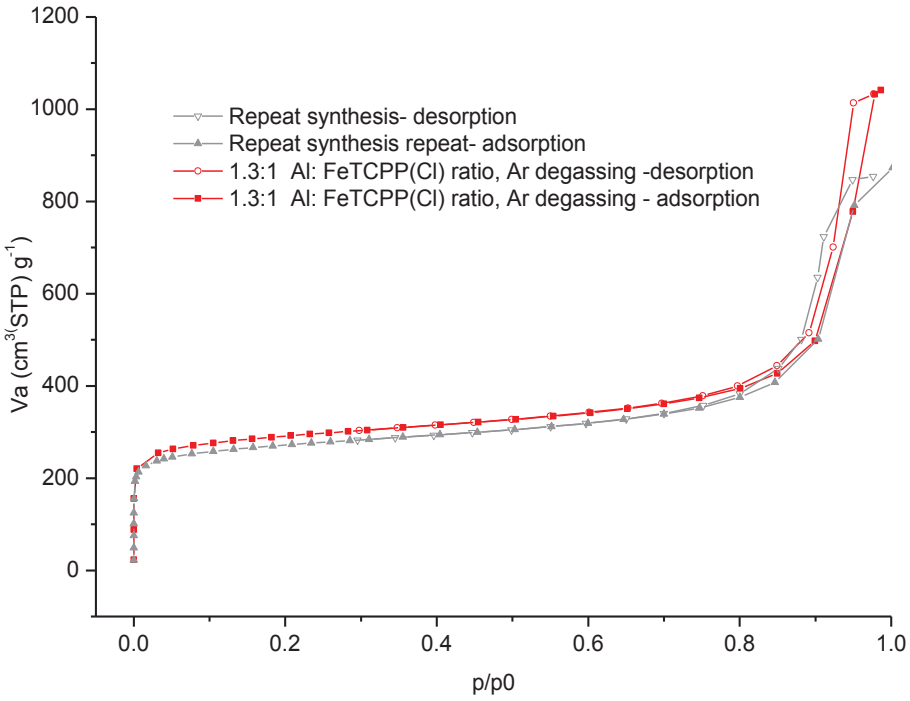

Figure B-14 N_2 adsorption/desorption isotherms at 77K for two different batches of Fe-Al-PMOF obtained from the synthesis performed with a 1.3:1 Al to FeTCPP(Cl) ratio and with Ar degassing (190 °C, 3h-16h-4h, solvent: 50%/50% DMF-water).

Table B-10 BET surface areas calculated for selected Fe-Al-PMOF samples

Synthesis	BET surface area (m^2g^{-1})
2:1 Al:FeTCPP(Cl), 190 °C, 3h-16h-4h,	980
2:1 Al:FeTCPP(Cl), 190 °C, 3h-16h-4h, repeat synthesis which showed increased presence of boehmite	812
1.3:1 Al:FeTCPP(Cl), 190 °C, 3h-16h-4h, Ar degassing	1090
1.3:1 Al:FeTCPP(Cl), 190 °C, 3h-16h-4h, Ar degassing-repeat synthesis	1033

Solvent used: 50%/50% DMF-water

B.6. Catalysis work with Fe-Al-PMOF

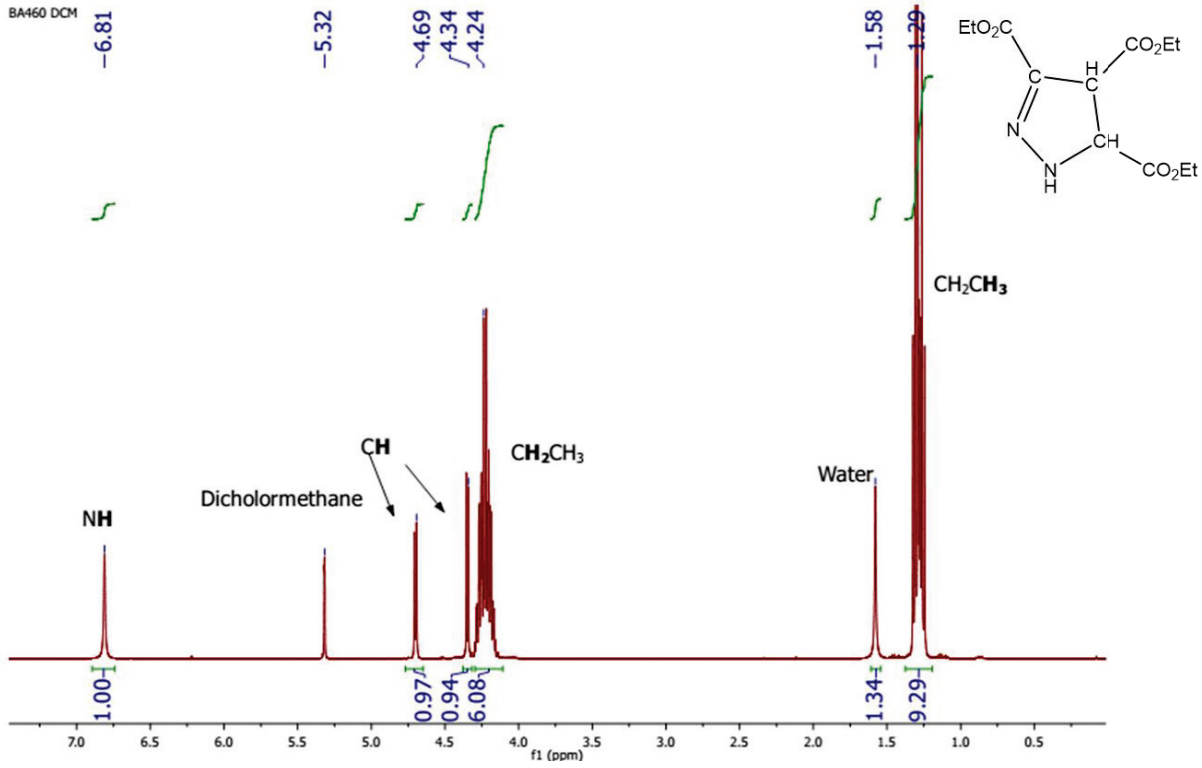

Figure B-15 ^1H NMR spectrum (CD_2Cl_2) of the reaction mixture after all the EDA has been consumed indicating the presence of the 3,4,5-triethyl-4,5-dihydro-1H-pyrazole-3,4,5-tricarboxylate (P1).

Reported[1] NMR $^1H(CDCl_3)$ δ/ppm: d=1.22–1.40 (3t, 9H; $CH_2C\mathbf{H_3}$), 4.15–4.38 (3q, 6H; $C\mathbf{H_2}CH_3$), 4.42 (d, 1H; CH), 4.75 (d, 1H; CH), 6.77 (s, 1H: NH).

1. Basato, M.; Tubaro, C.; Biffis, A.; Bonato, M.; Buscemi, G.; Lighezzolo, F.; Lunardi, P.; Vianini, C.; Benetollo, F.; Del Zotto, A., Reactions of Diazo Compounds with Alkenes Catalysed by [RuCl(cod)(Cp)]: Effect of the Substituents in the Formation of Cyclopropanation or Metathesis Products. *Chemistry – A European Journal* **2009,** *15* (6), 1516-1526.

C. Appendix Chapter 5

C.1. Exploratory synthesis for optimising the single crystal size for the system with hydrated $FeCl_3$, free base 5,10,15,20-tetrakis(3,4-dihydroxyphenyl)porphyrin, and pyrocatechol

Synthesis optimisation

Table C-1 Reaction conditions for the exploratory synthesis for optimising the single crystal size for the system with hydrated $FeCl_3$, free base 5,10,15,20-tetrakis(3,4-dihydroxyphenyl)porphyrin, and pyrocatechol

	L (mg)	L (mmol)	$FeCl_3.6H_2O$ (mg)	$FeCl_3.6H_2O$ (mol)	Pyrocatechol (mg)l	Pyrocatechol (mmol)	Pyrazine (mg)	Ratio (P:Fe:PyC:A)	DMF (mL)	H_2O (mL)	Temp (°C)	Heating program (h)
1	18.4	0.025	18.4	0.068	160	1.5	6	1:3:60:3	0.4	1.6	140	5-48-5
2	18.4	0.025	18.4	0.068	160	1.5	6	1:3:60:3	0.8	1.2	140	5-48-5
3	18.4	0.025	18.4	0.068	80	0.73	6	1:3:30:3	0.4	1.6	140	5-48-5
4	18.4	0.025	12.3	0.046	160	1.5	6	1:2:60:3	0.4	1.6	140	5-48-5
5	18.4	0.025	18.4	0.068	160	1.5	6	1:3:60:3	0.4	1.6	150	5.5-48-5.5
6	18.4	0.025	18.4	0.068	80	0.73	6	1:3:30:3	0.4	1.6	150	5.5-48-5.5
7	18.4	0.025	18.4	0.068	40	0.36	6	1:3:15:3	0.4	1.6	150	5.5-48-5.5
8	46.0	0.062	46.0	0.170	400	3.6	15	1:3:60:3	3	2	160	6-48-6
9	46.0	0.062	46.0	0.170	400	3.6	15	1:3:60:3	1	4	160	6-48-6
10	46.0	0.062	46.0	0.170	400	3.6	15	1:3:60:3	4	1	160	6-48-6
11	46.0	0.062	46.0	0.170	400	3.6	15	1:3:60:3	0.75	3	160	6-48-6
12	46.0	0.062	46.0	0.170	400	3.6	15	1:3:60:3	0.75	4.25	160	6-48-6
13	46.0	0.062	46.0	0.170	660	6.0	15	1:3:100:3	3	2	160	6-48-6
14	46.0	0.062	46.0	0.170	400	3.6	20	1:3:60:3	3	2	160	6-48-6
15	46.0	0.062	92.0	0.340	400	3.6	15	1:6:60:3	1	4	160	6-48-6
16	18.4	0.025	18.4	0.068	80	0.73	6	1:3:30:3	0.4	1.6	160	6-48-6
17	18.4	0.025	18.4	0.068	40	0.36	6	1:3:15:3	0.4	1.6	160	6-48-6
18	46.0	0.062	46.0	0.170	400	3.6	15	1:3:60:3	1	4	180	6-48-6

L= H_{10}-PorphCat (molar mass used for calculations 742.74 $gmol^{-1}$)

Legend = | 140 °C | 150 °C | 160 °C | 180 °C |

C.2. Exploratory synthesis with the trihydroxy phenyl porphyrin (H_{14}-PorphGal) ligand

Reactivity of RE metals and H_{14}-PorphGal

Table C-2 Conditions for high throughput synthesis with $Gd(NO_3)_3.6H_2O$ where different solvent conditions were investigated. Concentration of HCl solution used was 1 mol/L. Temperature 120 °C, heating program 2h-12h-4h. M:L ratio 3.6:1.

	L (mg)	L (mmol)	$Gd(NO_3)_3.6H_2O$ (mg)	$Gd(NO_3)_3.6H_2O$ (mmol)	HCl (mL)	DMF (mL)	H_2O (mL)	Methanol (mL)	result
1	5.0	0.0052	8.4	0.0186	0.00	0.50	0.00	0.00	MIL-173(Zr) phase low crystallinity
2	5.0	0.0052	8.4	0.0186	0.10	0.40	0.00	0.00	MIL-173(Zr) phase
3	5.0	0.0052	8.4	0.0186	0.00	0.25	0.25	0.00	MIL-173(Zr) phase
4	5.0	0.0052	8.4	0.0186	0.10	0.25	0.15	0.00	MIL-173(Zr) phase
5	5.0	0.0052	8.4	0.0186	0.00	0.00	0.50	0.00	Unknown phase
6	5.0	0.0052	8.4	0.0186	0.10	0.00	0.40	0.00	amorphous
7	5.0	0.0052	8.4	0.0186	0.00	0.00	0.00	0.50	amorphous
8	5.0	0.0052	8.4	0.0186	0.10	0.00	0.00	0.40	amorphous

L= H_{14}-PorphGal (molar mass for $C_{44}H_{32}N_4O_{12}Br_2$ 968.55 $gmol^{-1}$)

Table C-3 Syntheses with La, Y, Gd to investigate the formation of the MIL-173 phase with rare earth metals

L (mg)	L (mmol)	Metal salt	Metal salt (mg)	Metal salt (mmol)	M:L	Solvent/ Total volume	Temp (°)	Heating program (h)
5.0	0.0052	$Gd(NO_3)_3.6H_2O$	8.4	0.0186	3.6:1	DMF/H_2O (1:1) 0.5mL	120	2-12-4
5.0	0.0052	$LaCl_3.6H_2O$	6.6	0.0187	3.6:1	DMF/H_2O (1:1) 0.5mL	120	2-12-4
5.0	0.0052	$YCl_3.6H_2O$	5.6	0.0185	3.6:1	DMF/H_2O (1:1) 0.5mL	120	2-12-4

L= H_{14}-PorphGal (molar mass for $C_{44}H_{32}N_4O_{12}Br_2$ 968.55 $gmol^{-1}$)

Table C-4 Syntheses of MIL-173(La) to prevent the formation of the La-formate impurity.

L (mg)	L (mmol)	$LaCl_3.6H_2O$ (mg)	$LaCl_3.6H_2O$ (mmol)	Ratio (P:M:A)	DMF (mL)	H_2O (mL)	Temp (°C)	Heating Program (h)
20	0.021	26.3	0.074	1:3.6	1	1	120	2-12-4
20	0.021	21.9	0.062	1:3	1	1	120	2-12-4
20	0.021	15.3	0.043	1:2	1	1	120	2-12-4
20	0.021	13.1	0.037	1:1.8	1	1	120	2-12-4

L= H_{14}-PorphGal (molar mass for $C_{44}H_{32}N_4O_{12}Br_2$ 968.55 $gmol^{-1}$)

Reactivity of other trivalent metal ions and H_{14}-PorphGal

Table C-5 The high throughput syntheses exploring the reactivity of Fe^{3+}, Al^{3+} and In^{3+} with H_{14}-PorphGal. Concentration of HCl solution used was 1 mol/L. Temperature 120 °C, heating program 2h-48h-4h.

	L (mg)	M/L	Fe (mg)	Al (mg)	In (mg)	HCl (mL)	DMF (mL)	H_2O (mL)	Result
1	5.0	3.6	5.0			0.000	0.250	0.250	Amorphous
2	5.0	3.6	5.0			0.250	0.250	0.000	Amorphous
3	5.0	3.6	5.0			0.125	0.250	0.125	Amorphous
4	5.0	3.6	5.0			0.000	0.167	0.333	Amorphous
5	5.0	7.2	10.1			0.000	0.250	0.250	Amorphous
6	5.0	7.2	10.1			0.250	0.250	0.000	Amorphous
7	5.0	7.2	10.1			0.125	0.250	0.125	Amorphous
8	5.0	7.2	10.1			0.000	0.167	0.333	Amorphous
9	5.0	3.6		4.5		0.000	0.250	0.250	Al/In-PorphGal phase
10	5.0	3.6		4.5		0.250	0.250	0.000	Amorphous
11	5.0	3.6		4.5		0.125	0.250	0.125	Amorphous
12	5.0	3.6		4.5		0.000	0.167	0.333	Amorphous
13	5.0	7.2		9.0		0.000	0.250	0.250	Al/In- PorphGal phase less crystalline
14	5.0	7.2		9.0		0.250	0.250	0.000	Amorphous
15	5.0	7.2		9.0		0.125	0.250	0.125	Amorphous
16	5.0	7.2		9.0		0.000	0.167	0.333	Amorphous
17	5.0	3.6			5.6	0.000	0.250	0.250	Al/In- PorphGal phase
18	5.0	3.6			5.6	0.250	0.250	0.000	Amorphous
19	5.0	3.6			5.6	0.125	0.250	0.125	Amorphous
20	5.0	3.6			5.6	0.000	0.167	0.333	Al/In- PorphGal phase more crystalline
21	5.0	7.2			11.2	0.000	0.250	0.250	Al/In- PorphGal phase very low crystallinity
22	5.0	7.2			11.2	0.250	0.250	0.000	amorphous
23	5.0	7.2			11.2	0.125	0.250	0.125	amorphous
24	5.0	7.2			11.2	0.000	0.167	0.333	amorphous

L= H_{14}-PorphGal (molar mass for $C_{44}H_{32}N_4O_{12}Br_2$ 968.55 $gmol^{-1}$)
M/L= Metal / ligand ratio
Fe source = $FeCl_3.6H_2O$
Al source = $AlCl_3.6H_2O$
In source = $In(NO_3)_3.xH_2O$

Legend =

Fe	Al	In

Figure C-6 The high throughput syntheses exploring effect of different indium metal salts to the phase obtained with H_{14}-PorphGal. Concentration of HCl and KOH solutions used was 1 mol/L. Temperature 120 °C, heating program 2h-48h-4h.

	L (mg)	M/L	Anhydrous $InCl_3$ (mg)	Hydrated $In_2(SO_4)_3$ (mg)	Hydrated $In(NO_3)_3$ (mg)	DMF (mL)	H_2O (mL)	HCl (mL)	KOH (mL)	result
1	5.0	3.6	4.1			0.167	0.333			In-PorphGal phase best crystallinity
2	5.0	3.6	4.1			0.167	0.283	0.050		Very low crystallinity
3	5.0	3.6	4.1			0.167	0.233	0.100		Very low crystallinity
4	5.0	3.6	4.1			0.167	0.283		0.050	In-PorphGal phase
5	5.0	3.6		9.6		0.167	0.333			Very low crystallinity
6	5.0	3.6		9.6		0.167	0.283	0.050		Very low crystallinity
7	5.0	3.6		9.6		0.167	0.233	0.100		amorphous
8	5.0	3.6		9.6		0.167	0.283		0.050	amorphous
9	5.0	3.6			5.6	0.167	0.333			In-PorphGal
10	5.0	3.6			5.6	0.167	0.283	0.050		In-PorphGal
11	5.0	3.6			5.6	0.167	0.233	0.100		Very low crystallinity
12	5.0	3.6			5.6	0.167	0.283		0.050	Very low crystallinity

L= H_{14}-PorphGal (molar mass for $C_{44}H_{32}N_4O_{12}Br_2$ 968.55 $gmol^{-1}$)
M/L= Metal / ligand ratio

Legend =

Anhydrous $InCl_3$	Hydrated $In_2(SO_4)_3$	Hydrated $In(NO_3)_3$